
WESTINGHOUSE NON-PROPRIETARY CLASS 3

WCAP-14936-NP
Volume 3, Rev. 0
Sections 24-28

**Code Qualification Document
for Best Estimate Small Break LOCA Analysis**

**Volume 3:
PWR Uncertainties and Sensitivities
for Small Break LOCA**

R. M. Kemper
K. Ohkawa
N. Petkov

April 2003

Westinghouse Electric Company LLC
P.O. Box 355
Pittsburgh, PA 15230-0355

© 2003 Westinghouse Electric Company LLC
All Rights Reserved

J

J

J

ABSTRACT

The document "Code Qualification Document for Best Estimate Loss of Coolant Accident Analysis" (WCAP-12945-P-A) discussed the WCOBRA/TRAC computer code and the methodology used to determine the 95th percentile peak cladding temperature (PCT) for a large break loss of coolant accident (LOCA) scenario. Westinghouse has reviewed the large break code and methodology to determine if the same principles could be adapted to reliably predict the processes that occur in a small break LOCA lasting from several hundred to several thousand seconds. This document, "Code Qualification Document for Best Estimate Small Break LOCA Analysis," (WCAP-14936), describes the WCOBRA/TRAC small break LOCA code version, the code validation performed, and a methodology to determine the 95th percentile PCT for small break LOCA transients.

Volume 1 describes the features, models and correlations contained in the small break LOCA version of the WCOBRA/TRAC computer code. First, the small break processes considered to have the greatest effect during a small LOCA event are identified and ranked in the phenomena identification and ranking table (PIRT). The sufficiency of the large break WCORBA/TRAC models and correlations for small LOCA analysis is then evaluated. A comprehensive presentation of the WCORBA/TRAC-SB models and correlations follows.

Volume 2 documents simulations of a large number of separate and integral effects tests using this small break version of the code. The simulations provide, at different scales, predicted transients in which all of the important processes are compared with experimental data. The information obtained from the simulations is used to assess errors within the code. The test simulations and subsequent comparison to experimental data determine the bias and uncertainty of major model packages as they apply to small break LOCA thermal-hydraulic conditions.

Volume 3 reviews the operator actions pertinent to a small break loss-of-coolant accident (LOCA) event using Indian Point Unit 2, a four-loop pressurized water reactor (PWR), as the reference. Sources of uncertainty in the plant condition and the limiting accident analysis assumptions are identified. The effects of various assumptions on small break LOCA transient behavior are investigated through numerous calculations using WCORBA/TRAC-SB. The calculations examine the sensitivity of the results to the break size, location, orientation, and offsite power availability.

Volume 4 presents calculations that are performed to determine the sensitivity of results to the plant core power distribution, the initial and boundary conditions, and code modelling assumptions. These studies, in which parameters are varied one at a time, are performed for Indian Point Unit 2 to quantify the sensitivity of plant behavior to changes in plant initial conditions and accident modelling. An uncertainty methodology consistent with the application of the Code Scaling, Applicability, and Uncertainty (CSAU) methodology is identified to define the overall plant analysis uncertainty and is applied to determine the 95th percentile PCT for the Indian Point Unit 2 small break LOCA analysis. Volume 4 also demonstrates the compliance of the Westinghouse best estimate large break LOCA methodology with U.S. Nuclear Regulatory Commission (NRC) Regulatory Guide 1.157 and with 10CFR50.46.

TABLE OF CONTENTS

Volume 1	Models and Correlations
Volume 2	Small Break Code Validation
Volume 3	PWR Uncertainties and Sensitivities for Small Break LOCA
Volume 4	Small Break Uncertainty Methodology

<u>Section</u>	<u>Title</u>	<u>Page</u>
ABSTRACT	iii
LIST OF TABLES	ix
LIST OF FIGURES	xi
LIST OF ACRONYMS	xvii
COMMONLY USED EQUATION NOMENCLATURE	xxi

24 PLANT SOURCES OF UNCERTAINTY

24-1	Introduction	24-1
24-2	Plant Physical Configuration	24-1
24-3	Plant Initial Operating Conditions:	
	Core Power Parameters	24-5
24-4	Plant Fluid Conditions	24-11
24-5	Reactor Accident Boundary Conditions	24-14
24-6	Global Model Parameters	24-19
24-7	Overview of the Plant Analysis Methodology	24-25
24-8	References	24-27

25 OPERATOR INTERACTIONS

25-1	Introduction	25-1
25-2	EOP Sequences for a Small Break LOCA	25-2
	25-2-1 Adverse Containment Conditions	25-2
	25-2-2 Continuously Monitored Conditions	25-2
	25-2-3 Inadequate Core Cooling	25-3
25-3	Variability of Plant Conditions Due to Operator Actions	25-4

TABLE OF CONTENTS (Cont'd)

<u>Section</u>	<u>Title</u>	<u>Page</u>
26	<u>WCOBRA/TRAC-SB MODEL OF INDIAN POINT UNIT 2</u>	
26-1	<u>WCOBRA/TRAC-SB Nodalization</u>	26-1
26-2	Reference Case Conditions and Steady-State	26-3
26-2-1	Reference Case Conditions	26-3
26-2-2	Steady-State Calculation	26-4
26-3	Cold Leg Break Transient Calculation	26-6
26-4	References	26-7
27	INDIAN POINT UNIT 2 REFERENCE TRANSIENTS	
27-1	Break Spectrum With LOOP Scenario	27-1
27-2	3-Inch Cold Leg Break With LOOP	27-3
27-3	4-Inch Cold Leg Break With LOOP	27-12
27-4	6-Inch Cold Leg Break With LOOP	27-20
27-5	10-Inch Cold Leg Break With LOOP	27-28
27-6	2.5-Inch Cold Leg Break With LOOP	27-36
27-7	3.5-Inch Cold Leg Break With LOOP	27-44
27-8	Summary of LOOP Reference Cases	27-52
27-9	Break Spectrum With OPA Scenario	27-57
27-10	3-Inch Cold Leg Break With OPA	27-59
27-11	4-Inch Cold Leg Break With OPA	27-67
27-12	6-Inch Cold Leg Break With OPA	27-75
27-13	10-Inch Cold Leg Break With OPA	27-83
27-14	Summary of OPA Cases	27-91
27-15	Conclusions	27-93
27-16	References	27-93
28	PWR SCOPING STUDIES FOR GEOMETRIC CONFIGURATION	
28-1	Introduction	28-1
28-2	Break Location Study	28-6

TABLE OF CONTENTS (Cont'd)

<u>Section</u>	<u>Title</u>	<u>Page</u>
28-2-1	Cold Leg Break in a Nonpressurizer Loop	28-6
28-2-1-1	Model Description	28-6
28-2-1-2	Description of Transient (Figures 28-2-1 through 28-2-5)	28-6
28-2-1-3	Comparison to Reference Case	28-7
28-2-2	Break at Pump Suction	28-8
28-2-2-1	Model Description	28-8
28-2-2-2	Description of Transient (Figures 28-2-6 through 28-2-10)	28-8
28-2-2-3	Comparison to Reference Case	28-9
28-2-3	Break at Hot Leg	28-9
28-2-3-1	Description of Model	28-9
28-2-3-2	Description of Transient (Figures 28-2-11 through 28-2-15)	28-9
28-2-3-3	Comparison to Reference Case	28-10
28-3	Break Orientation Study	28-27
28-3-1	Top Break With SI Into Broken Loop	28-27
28-3-1-1	Model Description	28-27
28-3-1-2	Description of Transient (Figures 28-3-1 through Figures 28-3-6)	28-27
28-3-1-3	Comparison to Reference Case	28-28
28-3-2	Side Break	28-29
28-3-2-1	Description of Model	28-29
28-3-2-2	Description of Transient (Figures 28-3-7 through 28-3-12)	28-29
28-3-2-3	Comparison to Reference Case	28-30
28-3-3	Bottom Break	28-30
28-3-3-1	Description of Model	28-30
28-3-3-2	Description of Transient (Figures 28-3-13 through 28-3-18)	28-30
28-3-3-3	Comparison to Reference Case	28-32

TABLE OF CONTENTS (Cont'd)

<u>Section</u>	<u>Title</u>	<u>Page</u>
28-4	Effect of SGTP Level	28-51
28-4-1	Associated Phenomena	28-51
28-4-2	Results	28-51
28-4-3	Conclusions	28-55
28-5	Summary and Conclusions	28-67
28-5-1	Worst Break Location	28-67
28-5-2	Worst Break Orientation	28-67
28-6	References	28-70

LIST OF TABLES

<u>Table</u>	<u>Title</u>	<u>Page</u>
24-1	Key Small Break LOCA Parameters and Analysis Basis Values	24-28
25-1	Condensed EOPs for Indian Point Unit 2 Small Break LOCA: Short-Term Portion	25-7
26-1	Plant Steady-State Parameters in <u>WCOBRA/TRAC-SB</u>	26-8
27-8-1	Summary of LOOP Reference Cases	27-55
27-14-1	OPA Transient Summary	27-92
28-1-1	Time Sequence of Events for 3-Inch Sensitivity Cases	28-3

1

1

1

LIST OF FIGURES

<u>Figure</u>	<u>Title</u>	<u>Page</u>
24-1	Uncertainty Parameters in Best Estimate Small Break LOCA Methodology	24-31
24-2	Flowchart of the Best Estimate Small Break LOCA Analysis Methodology Presentation	24-32
24-3	Flowchart of the Best Estimate Small Break LOCA Analysis Methodology Application to Indian Point Unit 2	24-33
26-1	Indian Point Unit 2 Reactor Vessel Nodalization	26-9
26-2	Indian Point Unit 2 Loop 21 Hot Leg and Steam Generator Nodalization	26-10
26-3	Indian Point Unit 2 Loop 22 Hot Leg and Steam Generator Nodalization	26-11
26-4	Indian Point Unit 2 Loop 23 Hot Leg and Steam Generator Nodalization	26-12
26-5	Indian Point Unit 2 Loop 24 Hot Leg and Steam Generator Nodalization	26-13
26-6	Loop 21 Loop Seal, Cold Leg, and Safety Injection Noding	26-14
26-7	Loop 22 Loop Seal, Cold Leg, and Safety Injection Noding	26-14
26-8	Loop 23 Loop Seal, Cold Leg, and Safety Injection Noding	26-15
26-9	Loop 24 Loop Seal, Cold Leg, and Safety Injection Noding	26-15
27-2-1	Primary and Secondary System Pressures, 3-Inch Break With LOOP	27-5
27-2-2	Core Collapsed Liquid Level, 3-Inch Break With LOOP	27-6
27-2-3	Break Flowrate and Void Fraction, 3-Inch Break With LOOP	27-7
27-2-4	Loop Seal Steam Flows, 3-Inch Break With LOOP	27-8
27-2-5	Reactor Vessel Mass, 3-Inch Break With LOOP	27-9
27-2-6	PCT, 3-Inch Break With LOOP	27-10
27-2-7	Total Safety Injection Flow to RCS, 3-Inch Break With LOOP	27-11
27-3-1	Primary and Secondary System Pressures, 4-Inch Break With LOOP	27-13
27-3-2	Core Collapsed Liquid Level, 4-Inch Break With LOOP	27-14
27-3-3	Break Flowrate and Void Fraction, 4-Inch Break With LOOP	27-15
27-3-4	Loop Seal Steam Flows, 4-Inch Break With LOOP	27-16
27-3-5	Reactor Vessel Mass, 4-Inch Break With LOOP	27-17
27-3-6	PCT, 4-Inch Break With LOOP	27-18
27-3-7	Total Safety Injection Flow to RCS, 4-Inch Break With LOOP	27-19
27-4-1	Primary and Secondary System Pressures, 6-Inch Break With LOOP	27-21
27-4-2	Core Collapsed Liquid Level, 6-Inch Break With LOOP	27-22

LIST OF FIGURES (Cont'd)

<u>Figure</u>	<u>Title</u>	<u>Page</u>
27-4-3	Break Flowrate and Void Fraction, 6-Inch Break With LOOP	27-23
27-4-4	Loop Seal Steam Flows, 6-Inch Break With LOOP	27-24
27-4-5	Reactor Vessel Mass, 6-Inch Break With LOOP	27-25
27-4-6	PCT, 6-Inch Break With LOOP	27-26
27-4-7	Total Safety Injection Flow to RCS, 6-Inch Break With LOOP	27-27
27-5-1	Primary and Secondary System Pressures, 10-Inch Break With LOOP	27-29
27-5-2	Core Collapsed Liquid Level, 10-Inch Break With LOOP	27-30
27-5-3	Break Flowrate and Void Fraction, 10-Inch Break With LOOP	27-31
27-5-4	Loop Seal Steam Flows, 10-Inch Break With LOOP	27-32
27-5-5	Reactor Vessel Mass, 10-Inch Break With LOOP	27-33
27-5-6	PCT, 10-Inch Break With LOOP	27-34
27-5-7	Total Safety Injection Flow to RCS, 10-Inch Break With LOOP	27-35
27-6-1	Primary and Secondary System Pressures, 2.5-Inch Break With LOOP	27-37
27-6-2	Core Collapsed Liquid Level, 2.5-Inch Break With LOOP	27-38
27-6-3	Break Flowrate and Void Fraction, 2.5-Inch Break With LOOP	27-39
27-6-4	Loop Seal Steam Flows, 2.5-Inch Break With LOOP	27-40
27-6-5	Reactor Vessel Mass, 2.5-Inch Break With LOOP	27-41
27-6-6	PCT, 2.5-Inch Break With LOOP	27-42
27-6-7	Total Safety Injection Flow to RCS, 2.5-Inch Break With LOOP	27-43
27-7-1	Primary and Secondary System Pressures, 3.5-Inch Break with LOOP	27-45
27-7-2	Core Collapsed Liquid Level, 3.5-Inch Break With LOOP	27-46
27-7-3	Break Flowrate and Void Fraction, 3.5-Inch Break With LOOP	27-47
27-7-4	Loop Seal Steam Flows, 3.5-Inch Break With LOOP	27-48
27-7-5	Reactor Vessel Mass, 3.5-Inch Break With LOOP	27-49
27-7-6	PCT, 3.5-Inch Break With LOOP	27-50
27-7-7	Total Safety Injection Flow to RCS, 3.5-Inch Break With LOOP	27-51
27-8-1	Loop Seal Steam Venting as a Function of Break Size	27-56
27-10-1	Primary and Secondary System Pressures, 3-Inch Break With OPA	27-60
27-10-2	Core Collapsed Liquid Level, 3-Inch Break With OPA	27-61
27-10-3	Break Flowrate and Void Fraction, 3-Inch Break With OPA	27-62
27-10-4	Loop Seal Steam Flows, 3-Inch Break With OPA	27-63
27-10-5	Reactor Vessel Mass, 3-Inch Break With OPA	27-64

LIST OF FIGURES (Cont'd)

<u>Figure</u>	<u>Title</u>	<u>Page</u>
27-10-6	PCT, 3-Inch Break With OPA	27-65
27-10-7	Total Safety Injection Flow to RCS, 3-Inch Break With OPA	27-66
27-11-1	Primary and Secondary System Pressures, 4-Inch Break With OPA	27-68
27-11-2	Core Collapsed Liquid Level, 4-Inch Break With OPA	27-69
27-11-3	Break Flowrate and Void Fraction, 4-Inch Break With OPA	27-70
27-11-4	Loop Seal Steam Flows, 4-Inch Break With OPA	27-71
27-11-5	Reactor Vessel Mass, 4-Inch Break With OPA	27-72
27-11-6	PCT, 4-Inch Break With OPA	27-73
27-11-7	Total Safety Injection Flow to RCS, 4-Inch Break With OPA	27-74
27-12-1	Primary and Secondary System Pressures, 6-Inch Break With OPA	27-76
27-12-2	Core Collapsed Liquid Level, 6-Inch Break With OPA	27-77
27-12-3	Break Flowrate and Void Fraction, 6-Inch Break With OPA	27-78
27-12-4	Loop Seal Steam Flows, 6-Inch Break With OPA	27-79
27-12-5	Reactor Vessel Mass, 6-Inch Break With OPA	27-80
27-12-6	PCT, 6-Inch Break With OPA	27-81
27-12-7	Total Safety Injection Flow to RCS, 6-Inch Break With OPA	27-82
27-13-1	Primary and Secondary System Pressures, 10-Inch Break With OPA	27-84
27-13-2	Core Collapsed Liquid Level, 10-Inch Break With OPA	27-85
27-13-3	Break Flowrate and Void Fraction, 10-Inch Break With OPA	27-86
27-13-4	Loop Seal Steam Flows, 10-Inch Break With OPA	27-87
27-13-5	Reactor Vessel Mass, 10-Inch Break With OPA	27-88
27-13-6	PCT, 10-Inch Break With OPA	27-89
27-13-7	Total Safety Injection Flow to RCS, 10-Inch Break With OPA	27-90
27-15-1	Peak Cladding Temperature as a Function of Break Area, Loop Cases	27-94
28-1-1	Indian Point Unit 2 NSSS Schematic Diagram With <u>WCOBRA/TRAC</u> Loop Designations	28-4
28-1-2	Modelling Used for Break Orientation Study	28-5
28-2-1	Break Location - RCS Pressure Comparison, Break in Nonpressurizer Loop ..	28-12
28-2-2	Break Location - Integrated Break Flow Comparison, Break in Nonpressurizer Loop	28-13

LIST OF FIGURES (Cont'd)

<u>Figure</u>	<u>Title</u>	<u>Page</u>
28-2-3	Break Location - Downcomer Collapsed Liquid Level Comparison, Break in Nonpressurizer Loop	28-14
28-2-4	Break Location - Inner Vessel Collapsed Liquid Level Comparison, Break in Nonpressurizer Loop	28-15
28-2-5	Break Location - PCT Comparison - Break in Nonpressurizer Loop	28-16
28-2-6	Break Location - RCS Pressure Comparison, Break in Pump Suction	28-17
28-2-7	Break Location - Integrated Break Flow Comparison, Break in Pump Suction	28-18
28-2-8	Break Location - Downcomer Collapsed Liquid Level Comparison, Break in Pump Suction	28-19
28-2-9	Break Location - Inner Vessel Collapsed Liquid Level Comparison, Break in Pump Suction	28-20
28-2-10	Break Location - PCT Comparison, Break in Pump Section	28-21
28-2-11	Break Location - RCS Pressure Comparison, Break in Hot Leg	28-22
28-2-12	Break Location - Integrated Break Flow Comparison, Break in Hot Leg	28-23
28-2-13	Break Location - Downcomer Collapsed Liquid Level Comparison, Break in Hot Leg	28-24
28-2-14	Break Location - Inner Vessel Collapsed Liquid Level Comparison, Break in Hot Leg	28-25
28-2-15	Break Location - PCT Comparison, Break in Hot Leg	28-26
28-3-1	Break Orientation - RCS Pressure Comparison, Top Break With Full SI	28-33
28-3-2	Break Orientation - Integrated Break Flow Comparison, Top Break With Full SI	28-34
28-3-3	Break Orientation - Downcomer Collapsed Liquid Level Comparison, Top Break With Full SI	28-35
28-3-4	Break Orientation - Inner Vessel Collapsed Liquid Level Comparison, Top Break With Full SI	28-36
28-3-5	Break Orientation - PCT Comparison, Top Break With Full SI	28-37
28-3-6	Break Orientation - Void Fraction Comparison at Break, Top Break With Full SI	28-38
28-3-7	Break Orientation - RCS Pressure Comparison, Side Break	28-39
28-3-8	Break Orientation - Integrated Break Flow Comparison, Side Break	28-40

LIST OF FIGURES (Cont'd)

<u>Figure</u>	<u>Title</u>	<u>Page</u>
28-3-9	Break Orientation - Downcomer Collapsed Liquid Level Comparison, Side Break	28-41
28-3-10	Break Orientation - Inner Vessel Collapsed Liquid Level Comparison, Side Break	28-42
28-3-11	Break Orientation - PCT Comparison, Side Break	28-43
28-3-12	Break Orientation - Comparison of Void Fraction at Break, Side Break	28-44
28-3-13	Break Orientation - RCS Pressure Comparison, Bottom Break	28-45
28-3-14	Break Orientation - Integrated Break Flow Comparison, Bottom Break	28-46
28-3-15	Break Orientation - Downcomer Collapsed Liquid Level Comparison, Bottom Break	28-47
28-3-16	Break Orientation - Inner Vessel Collapsed Liquid Level Comparison, Bottom Break	28-48
28-3-17	Break Orientation - PCT Comparison, Bottom Break	28-49
28-3-18	Break Orientation - Void Fraction Comparison at Break	28-50
28-4-1	PCT, SGTP Sensitivity	28-56
28-4-2	Inner Vessel (Core to Upper Plenum) Collapsed Liquid Levels, SGTP Sensitivity	28-57
28-4-3	Break Flowrates, SGTP Sensitivity	28-58
28-4-4	Integrated Break Flow, SGTP Sensitivity	28-59
28-4-5	Total RCS Primary Mass, SGTP Sensitivity	28-60
28-4-6	RCS Primary Pressures, SGTP Sensitivity	28-61
28-4-7	Pump Suction Vapor Flowrates, SGTP Sensitivity	28-62
28-4-8	Total Pump Suction Vapor Flowrates for Four Loops, SGTP Sensitivity	28-63
28-4-9	Loop Seal Steam Venting as a Function of Break Size	28-64
28-4-10	Steam Generator Uphill Side Tube Collapsed Liquid Levels, SGTP Sensitivity	28-65
28-4-11	Pump Suction Downflow Piping Collapsed Liquid Levels, SGTP Sensitivity	28-66
28-5-1	Integrated Break Flow Comparison for Break Location Study	28-68
28-5-2	Integrated Break Flow Comparison for Break Orientation Study	28-69

1

1

1

LIST OF ACRONYMS AND ABBREVIATIONS

A. O.	Axial Offset
ACRS	Advisory Committee on Reactor Safeguards
AFLUX	Core Average Heat Flux
ANS	American Nuclear Society
ANSI	American National Standards Institute
BE-SBLOCA	Best Estimate Small Break LOCA
BLD	Blowdown
BO	Boil-off
BOL	Beginning of Life
CAOC	Constant Axial Offset Control
CCFL	Counter-current Flow Limitation
CD	Discharge Coefficient for Two-phase Break Flow
CE	Combustion Engineering
CHF	Critical Heat Flux
COLR	Core Operating Limits Report
COSI	Condensation On Safety Injection
CP	Conditional Probability
CQD	Code Qualification Document
CSAU	Code Scaling Applicability and Uncertainty
DFFB	Dispersed Flow Film Boiling
DNB	Departure from Nucleate Boiling
ECCS	Emergency Core Cooling System
EOP	Emergency Operating Procedure
FAC	Final Acceptance Criteria
FEM	Entrained Droplet Flowrate
FLM	Continuous Liquid Flowrate
GEDM	Generalized Energy Deposition Model
H	High (Importance Level in Los Alamos PIRT Ranking Scheme)
HAFLUX	Hot Assembly Average Power
HAPHR	Hot Assembly Peak Heat Rate
HHSI	High Head Safety Injection
HRFLUX	Hot Rod Average Power
HTC	Heat Transfer Coefficient

LIST OF ACRONYMS AND ABBREVIATIONS (Cont'd)

IADF	Inverted Annular Dispersed Flow
IAFB	Inverted Annular Film Boiling
INEL	Idaho National Engineering Laboratory
IP2	Indian Point Unit 2
JAERI	Japan Atomic Energy Research Institute
L	Low (Importance Level in Los Alamos PIRT ranking scheme)
LOCA	Loss of Coolant Accident
LOCE	Loss of Coolant Experiment
LOFT	Loss of Fluid Test
LOOP	Loss of Offsite Power
LSC	Loop Seal Clearance
LSTF	Large Scale Test Facility
M	Medium (Importance Level in Los Alamos PIRT ranking scheme)
MSSV	Main Steam Safety Valve
MSIV	Main Steam Isolation Valve
MTC	Moderator Temperature Coefficient
N/A	Not Applicable
NC	Natural Circulation
NPP	Nuclear Power Plant
NRC	Nuclear Regulatory Commission
NRU	National Research Universal
NSSS	Nuclear Steam Supply System
NUCL	Saturated Nucleate Boiling
OPA	Offsite Power Available
ORNL	Oak Ridge National Laboratory
PCT	Peak Cladding Temperature
PIRT	Phenomena Identification and Ranking Table
PLHGR	Peak Linear Heat Generation Rate
PLHR	Peak Linear Heat Rate
PLOW	Low Power Region Relative Power
PORV	Pressure-operated Relief Valve
PWR	Pressurized Water Reactor
RABL	Reflood Assist Bypass Line
RAI	Request for Additional Information

LIST OF ACRONYMS AND ABBREVIATIONS (Cont'd)

RAOC	Relaxed Axial Offset Control
RCP	Reactor Coolant Pump
RCS	Reactor Coolant System
REC	Core Recovery
RHR	Residual Heat Removal
ROSA	Rig-of-Safety Assessment
RSIC	Radiation Shielding Information Center
RWST	Refueling Water Storage Tank
SBLOCA	Small Break Loss of Coolant Accident
SCNB	Subcooled Nucleate Boiling
SG	Steam Generator
SGTP	Steam Generator Tube Plugging
SI	Safety Injection
SIS	Safety Injection Systems
SPL	Single-phase Liquid Convection
SPV	Single-phase Vapor Convection
SPV	Single-Phase Vapor
THTF	Thermal Hydraulic Test Facility
TPFL	Two-Phase Flow Loop
TRAN	Transition Boiling
TS	Technical Specifications
TSI	Safety Injection Water Temperature
UHI	Upper Head Injection
UPTF	Upper Plenum Test Facility

COMMONLY USED EQUATION NOMENCLATURE

a	sonic velocity	h	heat transfer coefficient
a_r	grid blockage ratio	h	normalized pump head (Ch. 9)
a_v	vapor absorption coefficient	h_i	interfacial heat transfer coefficient
a_l	liquid absorption coefficient	H	enthalpy
A	area	H_{fg}	enthalpy of vaporization
A_x	axial flow area	H_m	Meyer hardness
A_z	lateral flow area	I	grid rewet index (Ch. 5,6)
A_w	wall heat transfer area	I	pump moment of inertia (Ch. 9)
A_f	intercell friction area	k	thermal conductivity
A_i	interfacial area	K	loss coefficient (Ch. 2,4)
B	mass transfer number	K	conductance (Ch. 7)
C_o	slip distribution parameter	K_{ix}	vertical interfacial drag coefficient
C_D	drag coefficient	K_{iz}	transverse interfacial drag coefficient
C_p	specific heat at constant pressure	K_{wx}	vertical wall drag coefficient
C_v	specific heat at constant volume	K_{wz}	transverse wall drag coefficient
D	diameter	K_x	axial flow form loss coefficient
D_h	hydraulic diameter	K_z	transverse flow form loss coefficient
\underline{D}	deformation tensor	L	length
e	specific energy	L_g	gap width
f_w	wall friction factor	L_g^o	orthogonal gap width
f_i	interfacial friction factor	L_b	mean beam length
f	theoretical density fraction (Ch. 7)	ℓ_m	momentum mixing length
F	ramping function	ℓ_H	energy mixing length
\underline{F}	turbulence anisotropy tensor	\dot{m}	mass flowrate
F	gray body factor (Ch. 6)	M	momentum (Ch. 2)
F_{CHEN}	Chen convective boiling multiplier	M	molecular weight (Ch. 7)
\mathcal{F}	force	n	pump head multiplier (Ch. 9)
g	gravitational acceleration	N	mole fraction
g_c	gravitational conversion constant	N	number density
\underline{g}	gravitational acceleration vector	N_μ	pump torque multiplier (Ch. 9)
G	mass flux	P	viscosity number
G_x	axial mass flux	P	pressure
G_z	transverse mass flux	P_w	wetted perimeter

Pr	Prandtl number	w	transverse velocity component, Cartesian coordinates
P_{rod}	fuel rod pitch	W	transverse velocity, subchannel coordinates
q_{wl}	wall-liquid heat transfer rate	W'	orthogonal transverse velocity, subchannel coordinates
q_{vv}	wall-vapor heat transfer rate	We	Weber number
q_{il}	interface-liquid heat transfer rate	x	quality
q_{iv}	interface-vapor heat transfer rate	x	vertical direction, Cartesian coordinates (Ch. 2)
Q_{wl}	wall-liquid heat transfer	X	vertical direction, subchannel coordinates
Q_{vv}	wall-vapor heat transfer	X'	axial direction, 1D components
r	bubble/drop radius	y	transverse direction, Cartesian coordinates
r	radial coordinate	z	transverse direction, Cartesian coordinates
R	internode resistance (Ch. 7)	Z	transverse direction, subchannel coordinates
R	radiation resistance (Ch. 6)		
R	gas constant (Ch. 10)		
R_o	orifice hole radius		
Re	Reynolds number		
s	specific entropy		
S	net rate of entrainment		
S_{CHEN}	Chen building suppression factor		
S_E	rate of entrainment		
S_{DE}	rate of de-entrainment		
St	Stanton number		Greek
t	time	α	void fraction
T	temperature	α_N	normalized pump speed
T	pump torque (Ch. 9)	β	volumetric coefficient of expansion
$\underline{\underline{T}}$	stress tensor	Γ	net rate of mass transfer
$\underline{\underline{T}}^T$	Reynold stress tensor	δ	film thickness
u	vertical velocity component, Cartesian coordinates	δ_{ij}	Kronecker delta
U	vertical velocity component, subchannel coordinates	ϵ	thermal emissivity
v	transverse velocity component, Cartesian coordinates	ϵ	strain
V	volume	η	fraction of vapor generation coming from entrained liquid
V_c	mesh cell volume	η_{NR}	de-entrainment efficiency
		κ	thermal diffusivity

λ	characteristic wave length	<i>dcht</i>	direct contact heat transfer
μ	viscosity	<i>DD</i>	dispersed droplet flow regime
μ^T	turbulent viscosity	<i>DE</i>	de-entrainment
ρ	density	<i>dffb</i>	dispersed flow film boiling
Σ	absorption cross section	<i>DFFB</i>	dispersed flow film boiling
σ	surface tension	<i>e</i>	entrained field
σ	stress (Ch. 2, 7)	<i>E</i>	entrainment
$\underline{\sigma}$	fluid-fluid stress tensor	<i>f</i>	saturated liquid
σ_{SB}	Stephan-Boltzmann constant	<i>fb</i>	film boiling
τ	shear stress	<i>fr</i>	flow regime
$\underline{\tau}$	viscous drag force	<i>fric</i>	friction loss
τ_i	interfacial drag force	<i>form</i>	form loss
ν	specific volume	<i>FC</i>	forced convection
ν	normalized pump volumetric flow	<i>FD</i>	film/drop flow regime
χ	Martinelli-Nelson factor	<i>FF</i>	falling film flow regime
Ψ_a	absorption efficiency	<i>g</i>	saturated vapor
Ω	source term	<i>gas</i>	gas
ω	specific speed	<i>gv</i>	grid to vapor
		<i>Gr</i>	Grashof number
		<i>h</i>	hydraulic
		<i>Henry</i>	Henry correlation
		<i>I</i>	interfacial
		<i>IVA</i>	inverted annular flow regime
		<i>IVS</i>	inverted liquid slug flow regime
		<i>k</i>	phase k
		<i>l</i>	liquid field
		<i>liq</i>	liquid
		<i>LB</i>	large bubble
		<i>m</i>	mixture
		<i>MIN</i>	minimum film boiling point
		<i>nc</i>	natural convection
		<i>lnc</i>	laminar natural convection
		<i>lfc</i>	laminar forced convection
		<i>N</i>	normalized
		<i>NB</i>	nucleate boiling
		<i>o</i>	orifice

Subscripts

<i>am</i>	annular-mist flow regime
<i>ACC</i>	accumulator
<i>b</i>	bubble
<i>br</i>	bubble rise
<i>bubbly</i>	bubbly flow regime
<i>Brom</i>	Bromley correlation
<i>crit</i>	critical
<i>cwv</i>	convection wall-vapor
<i>CHEN</i>	Chen correlation
<i>CHF</i>	critical heat flux
<i>churn</i>	churn flow regime
<i>CT</i>	churn-turbulent flow regime
<i>d</i>	drop

<i>p</i>	pipe	<i>x</i>	vertical direction, Cartesian coordinates
<i>QF</i>	quench front	<i>X</i>	vertical direction, subchannel coordinates
<i>r</i>	relative	<i>X</i>	axial direction, 1D components
<i>r</i>	radial (Ch. 7)	<i>y</i>	transverse direction, Cartesian coordinates
<i>rwe</i>	radiation wall-entrained field	<i>z</i>	transverse direction, Cartesian coordinates
<i>rwg</i>	radiation wall to grid	<i>Z</i>	transverse direction, subchannel coordinates
<i>rw\ell</i>	radiation wall-liquid field	<i>Zr</i>	Zirconium
<i>rwv</i>	radiation wall-vapor field	<i>2\phi</i>	two-phase
<i>s</i>	drop formation	Γ	phase change
<i>sat</i>	saturation		
<i>slug</i>	slug flow regime		
<i>s</i>	slug		
<i>SB</i>	small bubble flow regime		
<i>SCL</i>	subcooled liquid		
<i>SCNB</i>	subcooled nucleate boiling		
<i>SCV</i>	subcooled vapor		
<i>SNL</i>	superheated liquid		
<i>SLV</i>	superheated vapor	<i>I</i>	interfacial surface average
<i>SLB</i>	small to large bubble flow regime	<i>n</i>	old time value
<i>SPL</i>	single-phase liquid	\tilde{n}	donor cell old time value
<i>SPV</i>	single-phase vapor	<i>T</i>	turbulent
<i>sup</i>	suppression	<i>t</i>	transpose
<i>TB</i>	transition boiling	"	per unit area
<i>TD</i>	top deluge flow regime	""	per unit volume
<i>tnc</i>	turbulent natural convection		
<i>TQ</i>	top quench		
<i>UO₂</i>	uranium dioxide		
<i>v</i>	vapor field		
<i>vap</i>	vapor		
<i>ve</i>	between vapor and entrained fields		
<i>v\ell</i>	between vapor and liquid fields		
<i>w</i>	wall		
<i>wb</i>	wall to fluid as latent heat		
<i>w\ell</i>	wall to liquid		
<i>wv</i>	wall to vapor		

Superscripts

<i>I</i>	interfacial surface average
<i>n</i>	old time value
\tilde{n}	donor cell old time value
<i>T</i>	turbulent
<i>t</i>	transpose
"	per unit area
""	per unit volume

SECTION 24

PLANT SOURCES OF UNCERTAINTY

24-1 Introduction

If the initial and boundary conditions were known exactly, then the uncertainty in a small break LOCA calculation would depend only on the uncertainty in the code models and correlations, plus the uncertainty of these models as they are applied at full-scale. The code validation using separate effects tests identifies the code bias and uncertainty in the most important small break processes. Variability in the plant initial and boundary conditions, however, introduces additional uncertainty into the calculation. Section 21 of WCAP-12945-P-A (Bajorek, et al., 1998) discusses the plant uncertainties important in a large break LOCA. For small break LOCA, some additional plant uncertainties must be considered; these are discussed in this section. The objective of this section is to define the PWR conditions that should be assumed and ranged in scoping studies to determine the effect of these various parameters in a small break LOCA event.

The sources of uncertainty are categorized into five separate groups. Section 24-2 discusses uncertainty due to the plant physical configuration, and Section 24-3 discusses variability in the core initial operating conditions. Section 24-4 describes uncertainties in plant fluid conditions, Section 24-5 discusses reactor accident boundary conditions, and Section 24-6 discusses uncertainties in modelling the dominant small break LOCA processes.

24-2 Plant Physical Configuration

The plant physical configuration consists of those parameters that define the geometric and hydraulic condition of the reactor at the time the LOCA occurs. These parameters are listed below and then defined:

- a) Dimensions
- b) Flow resistance
- c) Pressurizer location, relative to broken loop
- d) Hot assembly location, relative to vessel upper internals
- e) Hot assembly type
- f) Steam generator tube plugging level

Table 24-1 summarizes the analysis basis for values of these parameters and the parameters in the other categories.

a) Dimensions

Section 21 of WCAP-12945-P-A (Bajorek, et al., 1998) discusses variability in PWR dimensions. For small break LOCA analysis, as in large break analysis, reactor dimensions, volumes, and surface areas are obtained directly from component drawings. Some variability exists in these dimensions due to tolerances and to approximations that may have been made in geometrical calculations. Dimensions also vary from nominal due to thermal expansion. Uncertainty in the volume and dimensions of the reactor is most likely to affect the blowdown period of the small break LOCA transient because mass depletion occurs much more rapidly in blowdown than during the other periods.

For small breaks, LOCA loads are not sufficient to cause deformation of fuel assembly grids, control rod guide tubes, or steam generator tubes. A dynamic analysis of the Reactor Coolant System (RCS) performed under combined seismic and LOCA loads demonstrates that key RCS components will continue to perform their safety functions. Control rod guide tubes are not displaced from their nominal positions, and control rod insertion will occur until the break area is greater than 1.0 square foot in the hot leg. Control rod guide tube forces are much less for a cold leg break.

Modelling Approach: [

]^{a,c}

b) Flow Resistance

The flow resistance in the vessel and loops during a small break LOCA calculation is a function of the models used to calculate the friction and form loss coefficient factors in the plant configuration. The accuracy of the loss coefficients

is confirmed by the prediction of steady-state flow and temperature conditions of the operating reactors. While the accuracy of these predictions using loss coefficients can be subject to large uncertainties, the flowrates and hydraulic losses are low in a small break LOCA. Flows are driven primarily by natural circulation and hydrostatic differences after reactor coolant pump (RCP) trip. Unlike a large break LOCA, friction losses and form losses in the loops in a small break LOCA do not constitute a major uncertainty.

Several integral effects tests, however, have indicated that the amount of steam bypass through the upper head spray nozzles can have a strong effect on a small break LOCA. A higher upper head bypass was found to result in a less severe core uncoverage.

In a Westinghouse PWR, bypass from the upper head and upper plenum can occur through two flow paths. Steam can reach a cold leg break by passing through the upper head spray nozzles. Steam can also leak from the upper plenum to the downcomer through the small gap between mating surfaces of the hot leg outlet nozzle and the reactor vessel wall.

Modelling Approach: [

]^{a,c}

c) Pressurizer Location, Relative to Broken Loop

The pressurizer may be on the broken loop or one of the unbroken loops. Its location is a source of uncertainty because it may introduce some asymmetry into the LOCA transient.

Modelling Approach: The effect of pressurizer location on the calculated LOCA results will be examined during the scoping studies.

d) Hot Assembly Location, Relative to Vessel Upper Internals

In a large break LOCA, the relative location of the hot assembly introduces uncertainty into transient results because the variation of upper head and upper plenum flow depending on position can significantly affect blowdown cooling. This is discussed in Section 21 of WCAP-12945-P-A (Bajorek, et al., 1998). In a small break LOCA, the overall system drain is slow and water that falls into the core is redistributed within the two-phase mixture present below the upper core plate. The dynamic behaviors associated with flow through the core to the break location that characterize a large cold leg break LOCA do not occur in small breaks.

Modelling Approach: The limiting position established by varying the hot assembly location in the plant large break LOCA scoping studies (locations beneath a guide tube and beneath an upper core plate open hole are analyzed) is adopted for small break LOCA analysis.

e) Hot Assembly Type

Uncertainties due to hot assembly design are discussed in Section 21 of WCAP-12945-P-A.

Modelling Approach: [

]^{a,c}

f) Steam Generator Tube Plugging Level

The steam generator tube plugging level affects a small break LOCA transient through its effect on liquid holdup in the uphill tubes and on the primary to secondary heat transfer. Plugging a steam generator tube removes the tube completely from the RCS volume and reduces the total flow area and heat transfer area through the steam generator. The increased potential for liquid holdup and

reduced heat transfer area is a variation that must be considered in the LOCA analysis.

Modelling Approach: The PWR is modelled with a level of tube plugging typical of the level expected over subsequent cycles. Once the effect of this parameter is determined, a conservative value will be used. [

]^{a,c}

24-3 Plant Initial Operating Conditions: Core Power Parameters

Core power parameters are those which define the core power distribution and fuel stored energy at the time of the LOCA. Considered under this category are the following:

- a) Core average linear heat rate
- b) Peak linear heat rate
- c) Hot rod average power
- d) Hot assembly average power
- e) Hot assembly peak heat rate
- f) Axial power distribution
- g) Low power region relative power
- h) Hot assembly burnup
- I) Reactor operating power history
- j) Moderator temperature coefficient
- k) Hot full power boron concentration

Core modelling using WCOBRA/TRAC is discussed in Section 20-1 of WCAP-12945-P-A (Bajorek, et al., 1998). The core modelling guidelines originally used for large break LOCA are retained for the small break model. As in the large break model, there are four core channels and five fuel rods in the PWR model where the fuel rods are defined as:

Rod 1: The rod in the core with the highest linear heat rate, assumed to also have the highest average power and to reside in the assembly with the highest average power

Rod 2: An average rod in the highest power assembly

Rod 3: An average rod in the assemblies residing under support columns

Rod 4: An average rod in the assemblies residing under guide tubes

Rod 5: An average rod in the assemblies residing on the periphery of the core

There are three distinct regions (the hot assembly, the two average channels, and the low power channel) which serve to resolve the radial power distribution in the core. Each fuel rod group has parameters describing the peak linear heat rate, the average linear heat rate, and the axial distribution of power. [

]^{a,c} The axial and radial core power distribution is of basic importance to both the peak cladding temperature (PCT) uncertainty and the absolute value of the PCT.

The U.S. Nuclear Regulatory Commission (NRC) has approved the Westinghouse methodology for the treatment of uncertainties to identify the 95-percent PCT value for application of the WCOBRA/TRAC best estimate large break LOCA model to Westinghouse three- and four-loop plants. For the small break LOCA case, this methodology has been simplified to reduce the analytical effort required. The following paragraphs discuss the bounding of certain parameters in the best estimate small break LOCA treatment of analysis uncertainties.

a) Core Average Linear Heat Rate

The only uncertainty affecting the initial core average linear heat rate (AFLUX) is the core power measurement uncertainty. The range of this uncertainty was estimated in the Westinghouse large break LOCA methodology as [

]^{a,c}

Modelling Approach: [

]^{a,c}

b) Peak Linear Heat Rate

The hot rod peak linear heat rate has an uncertainty that is [

]^{a,c}

Modelling Approach: [

]^{a,c}

c) Hot Rod Average Power

The hot rod has only a minor effect on the hot assembly fluid conditions, but uncertainties in the hot rod power affect the rod internal gap pressure and cladding burst time. In realistic small break LOCAs, cladding temperatures are low and burst is unlikely.

Modelling Approach: [

]^{a,c}

d) Hot Assembly Average Power

The hot assembly average linear heat rate is important because it affects fluid conditions in the hot assembly channel and around the hot rod.

Modelling Approach: The small break modelling approach will remain consistent with the large break approach. A review of numerous plant designs showed that the average rod in the hot assembly is typically []^{a,c} lower than the hot rod. Therefore, the relative nuclear power generated in the hot assembly average rod is assumed to be []^{a,c} lower than the hot rod relative nuclear power (F_{AH}).

e) Hot Assembly Peak Heat Rate

The relationship in power of the hot rod in an assembly to an average rod in the assembly depends on the assembly design and on the location of the hot rod within the assembly.

Modelling Approach: It is conservatively assumed [

]^{a,c}

f) Axial Power Distribution

The axial power distribution can vary considerably due to burnup and transient operation. Distributions can be characterized and correlated with PCT [

]^{a,c} The axial offset (A.O.) Technical Specification limits the skewness of power distributions that can occur.

Modelling Approach: Plant-specific calculations will be performed in which [

]^{a,c}

g) Low Power Region Relative Power

The power in the average rod (rod 5) of the low power region of assemblies is determined from the core design and usually varies from []^{a,c}

If this region has a low power, the interior channels (rods 3 and 4) have a higher power. However, the two-phase mixture level in the interior channel during a small break LOCA is negligibly affected by this small power change.

Modelling Approach: A relative power []^{a,c} of the core average is assumed for the reference case. This value is typical of current and future low leakage loading patterns and is used in the WCOBRA/TRAC-SB cases to determine the 95-percent PCT.

h) Hot Assembly Burnup

Hot assembly burnup affects fuel average temperature during normal operation. Fuel temperatures and steady-state peaking factors are typically highest early in the fuel cycle. This results in higher calculated PCT during the large break LOCA. Later in life, the higher fuel rod pressures may cause greater flow blockage should burst occur.

Modelling Approach: Beginning of life (BOL) conditions in the hot assembly are assumed for consistency with the time in life at which core peaking factors are limiting. The core average rods are assumed to be at an average burnup representative of typical reload cycles.

i) Reactor Operating Power History

The power distributions that generate high peaking factors are relatively short lived. A detailed accounting of the buildup of fission products shows that after shutdown the axial power distribution will revert back to the original, steady-state distribution. This effect is []^{a,c}

Modelling Approach: [

]^{a,c}

j) Moderator Temperature Coefficient

The moderator temperature coefficient (MTC) affects reactor shutdown during the first few seconds of the small break LOCA blowdown period. The larger (less negative) this value, the less responsive the reactor is to the increased fluid temperature, which occurs in the first seconds of the LOCA event.

Modelling Approach: The maximum value specified in the Technical Specifications is assumed to conservatively estimate core reactivity.

k) Hot Full Power Boron Concentration

A low initial primary fluid boron concentration slightly increases the total power generated in the core during the first seconds of the blowdown period.

Modelling Approach: A typical low value consistent with BOL conditions is assumed.

In reducing the total number of required WCOBRA/TRAC-SB cases, bounding values of [

]^{a,c}

For the methodology used in small break LOCA, the maximum nominal linear heat rate is the [

]^{a,c}. Defining the core average linear heat rate at 100-percent power as AFLUX gives for example; if $F_Q \leq 2.65$:

[

]^{a,c}

As in the large break LOCA best estimate methodology, an additional [

]^{a,c}.

24-4 Plant Fluid Conditions

The reactor primary fluid conditions are those parameters that describe the primary fluid thermodynamic state at the time of the LOCA. Included in this category are the following:

- a) Core average fluid temperature
- b) Pressurizer pressure
- c) Loop flowrate
- d) Upper head fluid temperature
- e) Pressurizer level
- f) Accumulator water temperature
- g) Accumulator pressure
- h) Accumulator water volume
- I) Accumulator line resistance
- j) Accumulator boron concentration

Because WCOBRA/TRAC-SB calculates a steady-state condition prior to the LOCA, the thermodynamic state cannot be overspecified. Thus, four basic quantities are defined for the primary fluid: its average temperature, pressure, volume, and flowrate. Defined are the states of significant fluid regions, which are isolated from the RCS during steady-state but become part of the RCS during the LOCA, such as the reactor vessel upper head and the accumulator.

Not all of the parameters in the above list are independent. Typically, if core power, primary flow, and secondary temperature and pressure are specified, the primary fluid temperature and pressure will seek appropriate levels consistent with these boundary conditions. In the modelling

of these parameters, the secondary side conditions are adjusted as required to obtain primary side conditions consistent with the Technical Specifications and planned operation.

In small break LOCA analysis using WCOBRA/TRAC-SB, a detailed model of the secondary side is used. Actual plant values are used in acceptance criteria for the secondary side conditions as modelled. Included in the secondary side modelling are the secondary side pressure, initial mass, feedwater flowrate and temperature, and steam flow and exit quality.

Although the accumulator is isolated from the RCS by a check valve during normal operation, it is considered part of the RCS and can inject for some small LOCA break sizes. The performance of the accumulator during a LOCA depends on several factors including the water and cover gas initial pressure, temperature, and volume. These are all subject to some variation. Typically, pressure and volume are controlled to within plus or minus 10 percent. Because the accumulators reside within containment, the long-term temperature of the containment atmosphere will affect the accumulator water temperature.

Modelling Approach: Because of the length of a small break transient, variations in several of the initial fluid conditions having uncertainty have minimal effect. The modelling approach for small break LOCA analysis is as follows:

a) Core Average Fluid Temperature (T_{avg}), degrees F

[

]^{a,c}

b) Pressurizer Pressure (P_{RCS}), psia

[

]^{a,c}

c) Loop Flowrate (W_{loop}), gpm per loop

[

]^{a,c}

d) Upper Head (UH) Fluid Temperature (T_{UH}), degrees F

[
]^{a,c}

e) Pressurizer Level (L_p), percent of full span

[
]^{a,c}

f) Accumulator Water Temperature (T_{ACC}), degrees F

[
]^{a,c}

g) Accumulator Pressure (P_{ACC}), psia

[
]^{a,c}

h) Accumulator Water Volume (V_{ACC}), cubic feet

[
]^{a,c}

i) Accumulator Line Resistance $f\frac{L}{D}$ (K_{ACC})

[
]^{a,c}

j) Accumulator Boron Concentration (C_{ACC}), ppm

[
]^{a,c}

24-5 Reactor Accident Boundary Conditions

The reactor accident boundary conditions are defined as those conditions outside the RCS pressure boundary that affect the LOCA transient. The break itself is considered a boundary condition. The following parameters are included in this category:

- a) Break location
- b) Break orientation
- c) Break size
- d) Offsite power availability
- e) Safety injection flow
- f) Safety injection temperature
- g) Safety injection delay
- h) Containment pressure
- I) Single failure assumption
- j) Control rod drop time
- k) Main steam safety valve performance
- l) Auxiliary feedwater flowrate
- m) Auxiliary feedwater temperature
- n) Operator action

Items a through j listed above were identified as contributors to uncertainty in a large break LOCA. These need to be reconsidered for small break LOCA.

Items k through n are contributors to uncertainty in a small break LOCA. Items k through m affect conditions on the secondary side, which acts as a heat sink/source to the primary. Operator action can impact the conditions on either the primary or the secondary.

The most important accident boundary condition is the postulated break. The break parameters are discussed below first.

- a) Break Location

Once it is postulated that the primary reactor coolant piping can fail, then all points in the RCS can be assumed to be possible break locations. Previous small LOCA break location studies have concluded that a break in one of the cold legs

produces the most severe transient because of the relative ease by which safety injection flow can be lost to the break. Other break locations in the RCS piping, however, have the potential to cause deep core uncover. Breaks at the bottom of the loop seal or at the bottom of the hot leg occur at a lower elevation than a break at the bottom of the cold leg. Thus, breaks at these locations can drain the primary RCS to a lower level.

Modelling Approach: Scoping studies are performed to identify the most limiting location in the RCS for a small break LOCA. Breaks in the cold leg, hot leg, and at the bottom of the loop seal are considered.

b) Break Orientation

The break can be located at any circumferential location around the RCS pipe. Other things being equal, a break located at the bottom of a pipe is generally expected to result in a more severe small break transient because the break flow quality will remain low for a longer period of time, which depletes the primary system of a greater amount of inventory. Breaks located at the top or side of a pipe do not have to drain to as low a level before the break flow transitions to two-phase. However, the postulated break of a safety injection delivery line may possibly penalize the pumped safety injection severely enough that this specific break at the top of the cold leg is limiting.

Modelling Approach: Scoping studies are performed to determine the most limiting break orientation. Breaks located at the top, side, and bottom of the specific pipe (cold leg, hot leg, and loop seal) identified as being the most limiting RCS location for a small break LOCA are examined.

c) Break Size

The size and shape of the break determines the rate at which the primary RCS depressurizes and the rate at which inventory is lost from the system. Breaks of relatively small size do not cause as much inventory depletion as larger breaks; however, for the smaller breaks, the RCS depressurizes slowly, safety injection flows are low, and the accumulators may not inject. Breaks with relatively large

size depressurize quickly, but can have much greater total loss of inventory and a deep core uncover. L

Modelling Approach: A range of break sizes is considered. Scoping studies consider a range of break sizes for the same set of plant initial and boundary conditions to determine the most limiting break size(s). [

]^{a,c}

d) Offsite Power Availability

Offsite power determines whether RCS pumps continue to run during the LOCA and whether pumped safety injection comes on with only valve opening and alignment delays. The effect of the RCS pumps on the LOCA transient may be significant, depending on whether the pumps are assumed to coast down or to continue running until they are tripped by the operator.

Modelling Approach: The initial scoping analysis will identify the bounding assumption regarding offsite power, as required by General Design Criteria (GDC) 17. L

e) Safety Injection Flow

The safety injection flow varies depending on the single failure assumed and on the specific plant pump and injection line configuration. Current methods, which are also used in currently accepted evaluation models, provide estimates of minimum and maximum flow, which take into account several uncertainties.

Modelling Approach: Variations in safety injection flow delivery as a function of break location will be examined in the scoping studies. Conservatively low SI flow rates are used in all instances. L

f) Safety Injection Temperature

The safety injection temperature may vary. This depends on the location of the refueling water storage tank and on controls imposed by the Technical Specifications.

Modelling Approach: An intermediate value between the Technical Specification maximum value and a minimum temperature is assumed, with variations examined in the sensitivity analysis.

g) Safety Injection Delay

The safety injection delays vary depending on whether loss of offsite power (LOOP) is assumed to occur and on the electrical design of the plant being analyzed.

Modelling Approach: Maximum delay times are assumed.

h) Containment Pressure

The containment pressure is dependent on the mass and energy release from the RCS during the LOCA.

Modelling Approach: A constant containment atmospheric pressure of 14.7 psia is assumed for the small break LOCA calculations.

i) Single Failure Assumption

For the Indian Point Unit 2 Emergency Core Cooling System (ECCS) design, no more than one of three high head safety injection (HHSI) pumps can be postulated to fail by the GDC35 criterion whether offsite power is available or not. If power is assumed to be lost, the most limiting single failure for a small break LOCA may be the loss of a diesel generator, which also prevents an auxiliary feedwater pump from starting. This in turn can cause asymmetry in the auxiliary feedwater delivery to the loops.

Modelling Approach: Generically, scoping studies will investigate the effect on the small LOCA transient of different single failure assumptions in conjunction with the offsite power availability. For the Indian Point Unit 2 analysis herein, in offsite power available cases one HHSI pump is assumed to fail, and one diesel generator is assumed to fail in LOOP cases.

j) Control Rod Drop Time

In small breaks, loads are not sufficient to prevent control rod drop. Therefore, control rod insertion is modelled in best estimate small break LOCA analyses.

Modelling Approach: Consistent with the current design basis for PWR plants, control rods are assumed to drop during a small break LOCA. [

]^{a,c}

k) Main Steam Safety Valve Performance

The secondary side safety valve setpoints are important in a small break LOCA because they determine the RCS pressure during the natural circulation period.

The higher the main steam safety valve (MSSV) performance setpoints are, the higher the primary pressure during this period; higher primary pressure translates into higher break flow and less total pumped safety injection. The valves have an uncertainty in the pressure differential required to fully open them.

Modelling Approach: Sensitivity calculations consider uncertainties in the MSSV setpoints.

l) Auxiliary Feedwater Flowrate

The auxiliary feedwater flowrate affects the fluid conditions on the steam generator secondary side and the effectiveness of the steam generator as a heat sink.

Modelling Approach: The minimum auxiliary feedwater flow is assumed, according to the Technical Specifications.

m) Auxiliary Feedwater Temperature

The auxiliary feedwater temperature also affects the fluid conditions on the secondary side of the steam generator.

Modelling Approach: A maximum value of auxiliary feedwater temperature is considered, consistent with the Technical Specifications.

n) Operator Action

Unlike a large break LOCA scenario, a small break LOCA proceeds at a slow enough rate that the reactor operator(s) can take action during the course of the transient, consistent with plant Emergency Operating Procedures (EOPs).

Depending on the action, the severity of the core uncover and cladding temperature heatup can be significantly impacted.

Modelling Approach: The methodology considers the effect of operator action on small break LOCA transients. While the principal action affecting the transient is tripping per EOPs of the RCPs, the operator may also initiate charging pump flow, start turbine-driven auxiliary feedwater pumps to maintain secondary side water levels, and depressurize the secondary side system.

24-6 Global Model Parameters

The Phenomena Identification and Ranking Table (PIRT) in Volume 1 of this document lists the small break processes expected to be dominant during a transient. The processes that received the highest rankings in the small break PIRT were summarized as follows:

- a) Break flow
- b) Mixture level
- c) Horizontal flow regimes
- d) Loop seal clearance
- e) Fuel rod model

- f) Steam generator hydraulics
- g) Condensation

The models and correlations in WCOBRA/TRAC-SB representing these processes are examined in the code assessment studies in Volume 2 of this document. Most of the experimental data used in these assessments were obtained from scaled test facilities. The code simulations and comparisons to data identified the accuracy of various models and correlations in WCOBRA/TRAC-SB, and in some cases represents these processes through a bias and uncertainty.

Two aspects of the WCOBRA/TRAC-SB models should be considered further as follows:

- Processes where modelling has been simplified, or where the basic fundamental physics of the process is not well understood and is thus subject to a large uncertainty
- Phenomena that may have a more important effect on the PWR transient than in the scaled experiment

Some models, although previously verified against nearly prototypical tests, should be re-examined when being applied to the PWR. There are several reasons for this, the most important being the difference in transient timescales resulting from the large increase in scale involved in the application of the models to the PWR. Other reasons are relative lack of data for verification of a specific model, model simplicity, and models judged to be of high importance for the PWR relative to experiments.

The approach is to examine the models at full PWR scale using the bias and uncertainty identified in the code validation studies, and in some cases, perform sensitivity studies on these models using the PWR model. This identifies which model uncertainties have a global, or system wide, effect on the PWR transient.

- a) Break Flow

The calculated break flow in WCOBRA/TRAC-SB depends substantially on the critical flow model. Section 13 in Volume 2 of this document shows that the model performed well in predicting the subcooled and two-phase critical flowrates

of a number of small break tests. The model exhibits little bias and uncertainty for the subcooled breakflow condition, and also predicts the saturated and the two-phase flow regions with an acceptable standard deviation. The calculated break flow also depends on other factors such as break geometry, orientation, and losses in the piping leading to the break.

Modelling Approach: The break flow is ranged by varying the break size. The best estimate value of the break flow model is used without bias, and the ranging of the break size identifies the most limiting transient. [

]^{a,c}

b) Mixture Level

The inner vessel mixture level swell depends on the WCOBRA/TRAC-SB models and correlations for vertical interfacial drag. Section 15 in Volume 2 of this document examines the code predictions of level swell tests in full-scale height bundles. This includes the Oak Ridge National Laboratory Thermal Hydraulic Test Facility (ORNL-THTF) and the Westinghouse G-1 Core Uncovery Tests. A bias was identified in the WCOBRA/TRAC-SB model due to an overprediction of the vertical interfacial drag in the low void fraction flow regimes (small bubble and large bubble).

Modelling Approach: A bias is applied in the core in PWR calculations to account for this model deficiency. [

]^{a,c}

c) Horizontal Flow Regimes

The horizontal flow regimes and the transition between regimes affects the flow in hot and cold legs, and in the loop seal. During a small break LOCA, transient levels form in the hot and cold legs, and for most of the transient, the horizontal stratified and slug flow regimes occur. The interfacial drag between the vapor and the liquid phases determines their relative motions. The interfacial drag is important during the natural circulation period because reflux from the steam

generator may drain back to the upper plenum through the hot leg; the rate at which reflux reaches the upper plenum partly depends on the interfacial drag in the horizontal stratified flow regime. For larger sized small breaks, the vapor flowrate in the hot leg may be sufficient to entrain droplets from the horizontal interface at some point during the LOCA. This process limits the backflow of reflux to the upper plenum from the steam generators and also increases the sweepout of water from the loop seal during the loop seal clearance period.

Modelling Approach: WCOBRA/TRAC-SB includes separate correlations for interfacial drag and entrainment that are used in the horizontal stratified and slug flow regimes. [

]^{a,c}

d) Loop Seal Clearance

The severity of a small break LOCA, in terms of core uncover and overall vessel inventory, depends somewhat on the loop seal clearing process. As described in Section 16 in Volume 2 of this document, the loop seal clearing process is complex. The physical process itself depends on interfacial drag between the vapor slipping through the loop seal horizontal section and the water remaining in that region. At high gas flows, the interfacial drag is sufficient to "push" water toward the elbow leading to the pump suction. This causes a transition from stratified to slug flow and leads to larger amounts of water in the uphill pump suction leg. Countercurrent flow limits (CCFL) in the uphill pump suction leg can become an important factor in determining the amount of water that flows back into the loop seal horizontal section, or alternatively is swept out through the pump.

Modelling Approach: [

]^{a,c}

e) Fuel Rod Model

The fuel rod model contains several models for processes that have considerable uncertainty. The models and processes that must be considered are:

- Decay heat
- Fuel conductivity
- Fuel heat capacity
- Fuel-clad gap heat transfer coefficient
- Fuel rod internal pressure
- Cladding burst temperature
- Cladding burst strain
- Metal-water reaction rate
- Minimum film boiling temperature
- Clad-fluid heat transfer coefficient

Section 21 of WCAP-12945-P-A (Bajorek, et al., 1998) discusses the uncertainty related to each of these models.

In a realistic small break LOCA calculation, PCTs are generally low. Clad-burst and high metal-water reaction rates are therefore not likely.

Modelling Approach: Models that affect the global hydraulics are ranged in WCORBA/TRAC-SB simulations. Calculations that exhibit significant impact on PCTs are [

]^{a,c}

f) Steam Generator Hydraulics

The steam generator processes that potentially have a large effect on a small break transient are flooding in the steam generator tubes and condensation heat transfer. Flooding and CCFL in the steam generator tubes reduces the amount of water available to reflux back to the upper plenum. Condensate that is held up in the

tubes creates a two-phase head, which can cause deeper core uncoveries than when there is no liquid holdup in the tubes.

Condensation in the tubes generates water that can drain back into the hot legs and vessel. High condensation, however, may lead to a large amount of water becoming held up on the uphill side of the steam generator tubes (causing a higher resistance and deeper core uncover). High condensation can also result in a greater amount of condensate draining into the loop seal region, which causes the loop seals to clear later in time.

Modelling Approach: Simulations of flooding and CCFL in steam generator tubes showed that WCOBRA/TRAC-SB tends to calculate flooding at a lower gas velocity than the gas velocity from the Wallis correlation. Because this represents a conservative bias in the code, the models for flooding in the steam generator tubes are not ranged.

[

]^{a,c}

g) Condensation

Condensation in the cold legs reduces the steam flow to the break and helps to retain more inventory in the RCS. High condensation, however, can cause a higher resistance to two-phase flow through the loops and can accelerate the rate at which a clear loop seal might replug due to backflow (over the weir) through the pump.

Modelling Approach: [

]^{a,c}

24-7 Overview of the Plant Analysis Methodology

Sections 24-2 through 24-6 discuss the parameters and models that can generate uncertainties in small break LOCA performance predictions. Table 24-1 lists these parameters and models, and the values adopted as the analysis basis values. In general, nominal plant conditions are assumed [

]^{a,c}

The modelling approaches used to consider the plant physical configuration, plant initial and boundary conditions, and global model parameters have been described in this section. The process by which the sources of uncertainty are considered for a plant application defines the best estimate small break LOCA evaluation methodology. This methodology, which is applicable to Westinghouse two-, three-, and four-loop plants, is summarized in this subsection.

In a small break LOCA methodology, both the initial plant conditions and model effects are important factors to consider in evaluating uncertainty to establish the PCT with 95% probability. The plant conditions may be subdivided into initial operating conditions and core power parameters, with []^{a,c}. In addition, a model or a parameter may be global or local in its effect. A parameter has a global effect if it can affect the entire thermal and hydraulic transient. It has a local effect if it only affects the local conditions at the PCT location. This is shown in Figure 24-1.

The Westinghouse realistic small break LOCA methodology to determine the 95th percentile PCT consists of several steps. The WCORBA/TRAC-SB code as documented in Volume 1 and validated in Volume 2 is used to perform a number of plant runs. This is followed by the analysis to determine the 95th percentile PCT. Figure 24-2 summarizes the methodology steps and provides a roadmap to where they are presented in this document.

The initial task is to perform a cold leg break spectrum analysis for both the case of offsite power lost and the case of offsite power available; the limiting case break thus identified is the basis for scoping studies that investigate whether another break location, break orientation, or steam generator tube plugging condition is more limiting. The limiting case break from the scoping studies is then further analyzed with WCORBA/TRAC-SB to determine the plant's response to changes in initial conditions through one-at-a-time sensitivity studies. The sensitivity studies are used to develop the initial conditions bias and uncertainty.

The development of a 95th percentile PCT includes investigating many different combinations of variables, and [

]^{a,c}

]^{a,c}

The best estimate small break LOCA methodology is applied to Indian Point Unit 2 in Volumes 3 and 4 of this document. Figure 24-2 is a flowchart showing the sections in this document discussing the general small break LOCA analysis methodology; Figure 24-3 is the same chart but is specific to the Indian Point Unit 2 application.

24-8 References

Bajorek, S. M., et al., 1998, "Code Qualification Document for Best Estimate LOCA Analysis Volume IV: Assessment of Uncertainty," WCAP-12945-P-A, Vol. 4.

Bajorek, S. M., et al., 1998a, "Code Qualification Document for Best Estimate LOCA Analysis Volume V: Quantification of Uncertainty," WCAP-12945-P-A, Vol. 5.

Stucker, D. L., et al., 1991, "Westinghouse ECCS Evaluation Model: Revised Large Break LOCA Power Distribution Methodology," WCAP-12909-P, Proprietary.

Table 24-1
Key Small Break LOCA Parameters and Analysis Basis Values

[]	
] ^{a,c}

Table 24-1 (Cont'd)
Key Small Break LOCA Parameters and Analysis Basis Values

[
	J ^{a,c}

Table 24-1 (Cont'd)
Key Small Break LOCA Parameters and Analysis Basis Values

[
] ^{a,c}

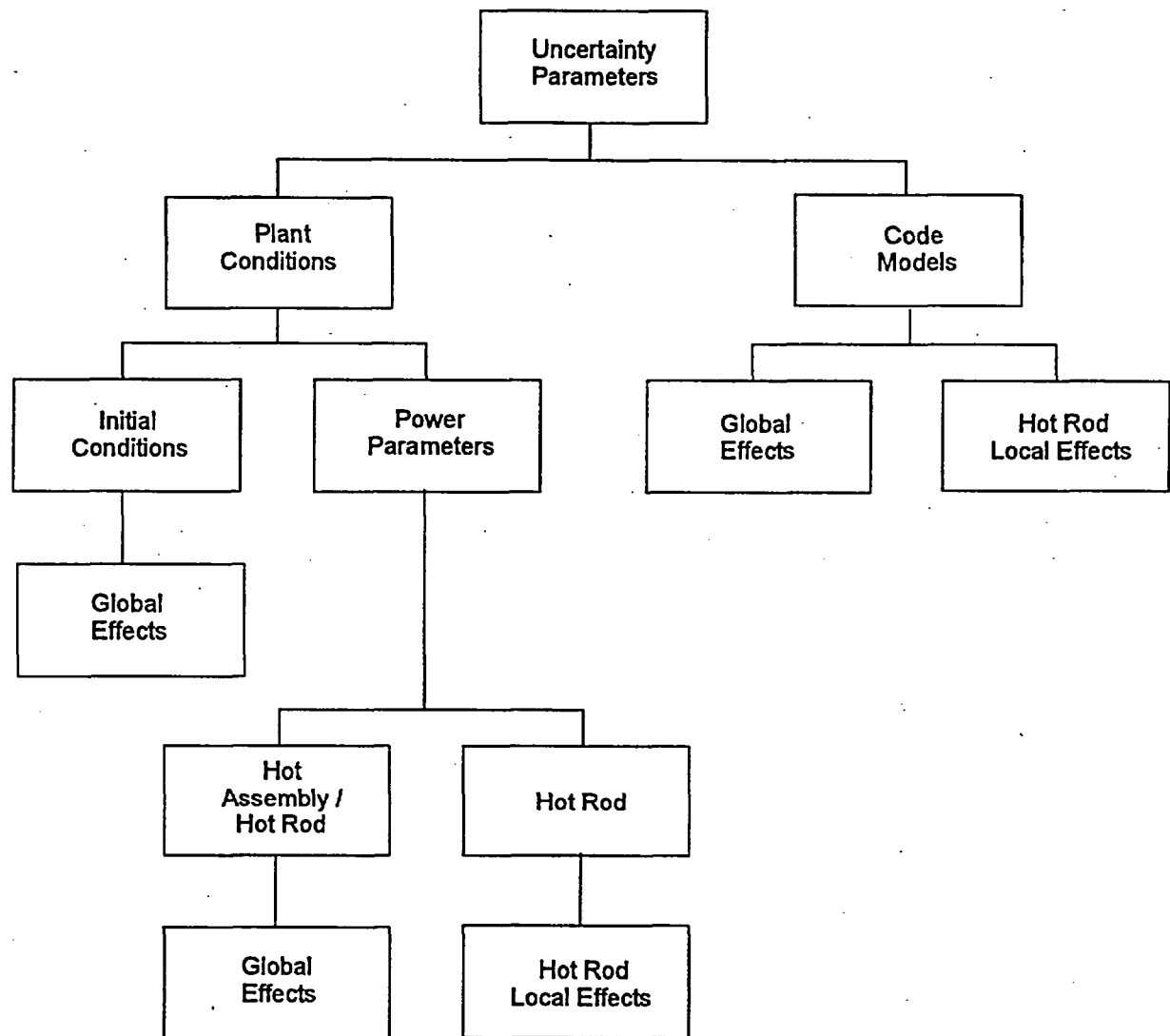


Figure 24-1. Uncertainty Parameters in Best Estimate Small Break LOCA Methodology

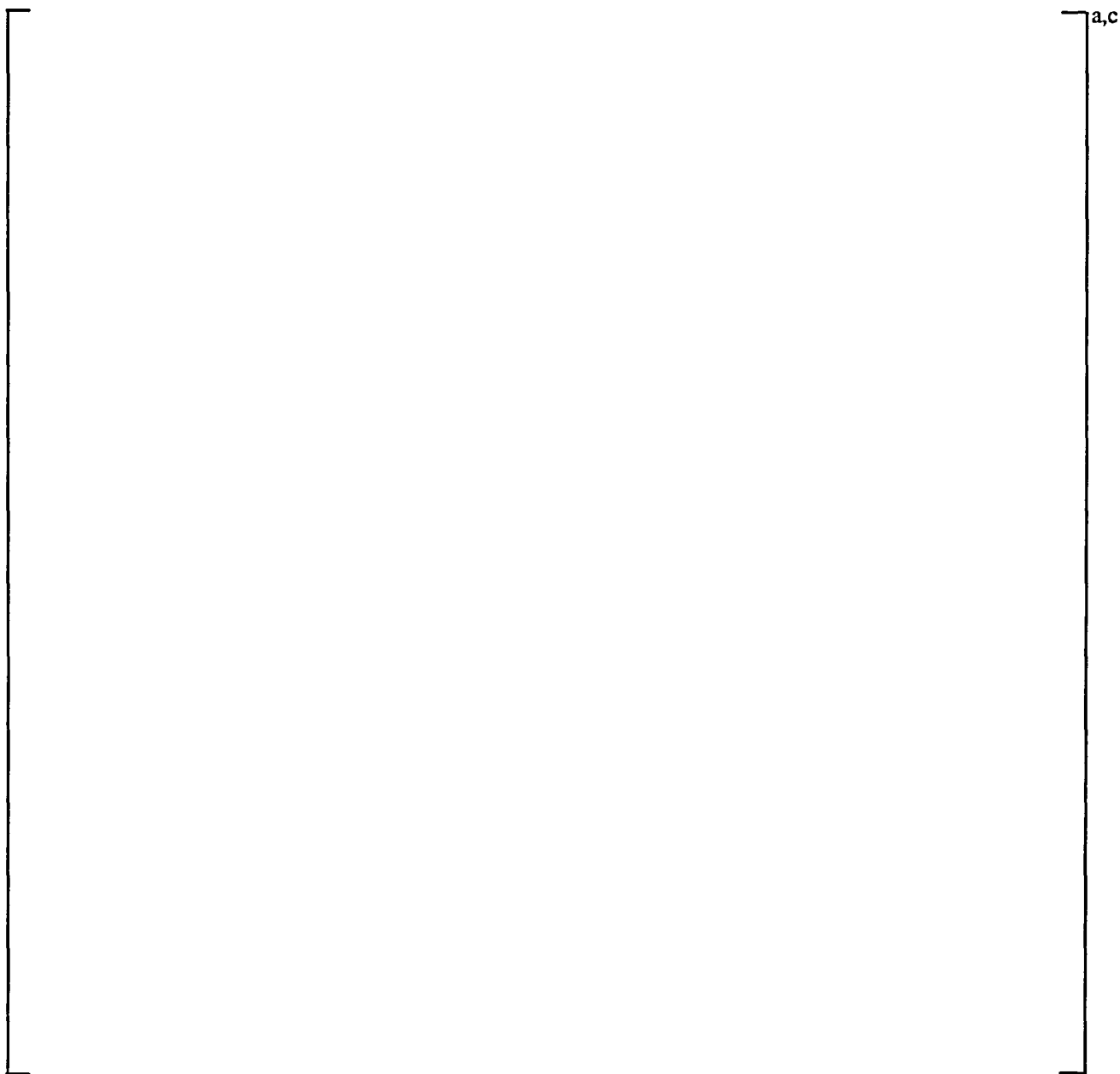


Figure 24-2. Flowchart of the Best Estimate Small Break LOCA Analysis Methodology Presentation

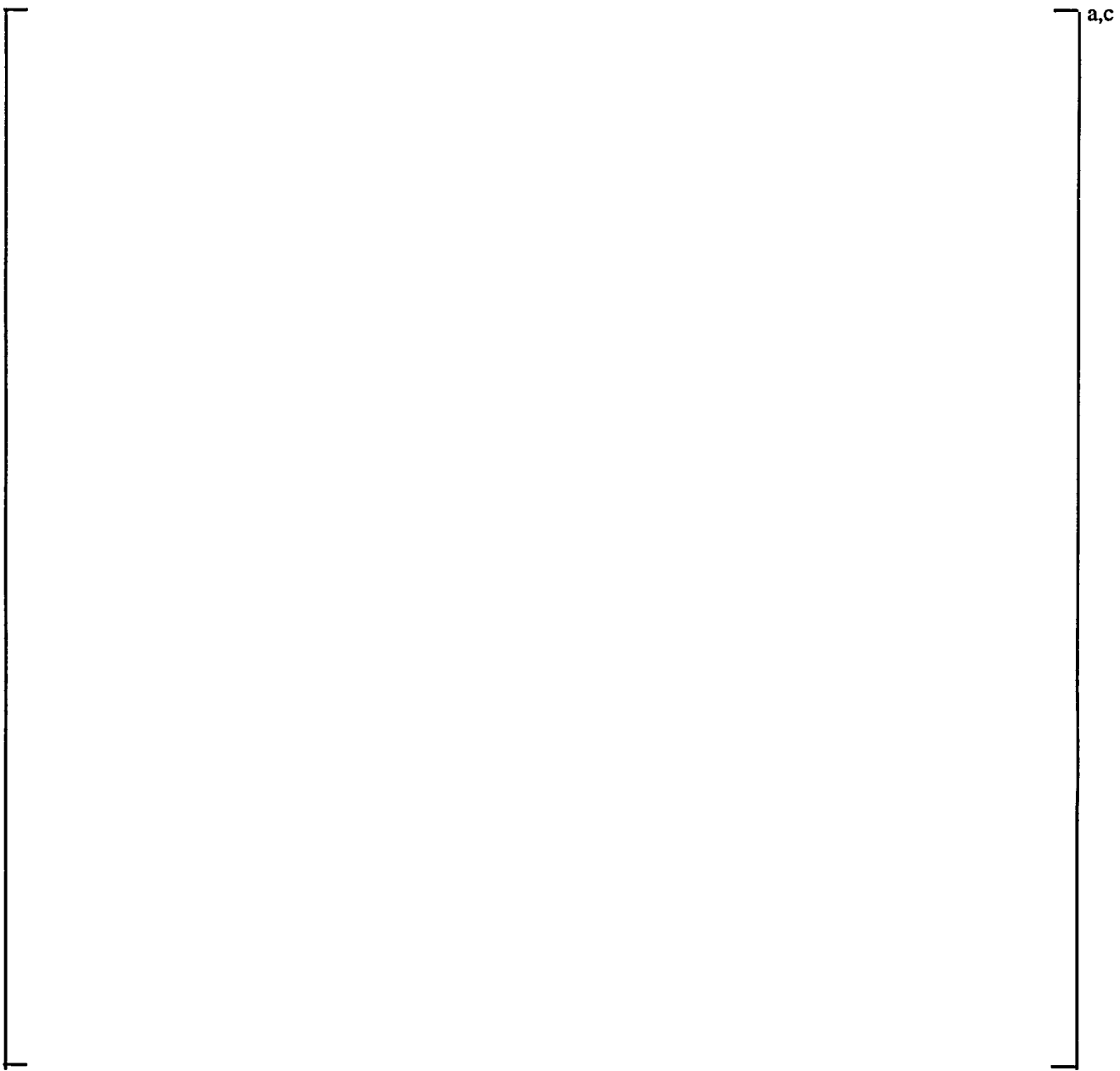


Figure 24-3. Flowchart of the Best Estimate Small Break LOCA Analysis Methodology Application to Indian Point Unit 2

SECTION 25

OPERATOR INTERACTIONS

25-1 Introduction

Upon the initiation of a transient in a plant, the operators use the plant EOPs to sequentially verify that automatic safeguards features are functioning correctly and follow prescribed operations to restore any malfunctioning systems. Eventually, the EOPs are used to begin plant recovery or to secure operations. Operator actions must be examined to determine the different transient scenarios that could develop and affect the severity of a small break LOCA transient and/or challenge the assumptions made in the LOCA analysis calculations.

The EOPs have been developed to direct the operators to analyze and respond to symptoms ascertained from measured plant parameters or trends of those parameters. During the initial stages of an accident or transient, the plant response can be similar for different events. The large number of changing parameters and their rates of change may prevent immediate diagnosis of the exact type of event; for example, LOCA, steam generator tube rupture, and steam line breaks. Therefore, the EOPs are based upon a hierarchy directing that important, common actions are performed early, based upon the symptoms observed; eventually, the EOPs branch to increasingly specific categories of accidents or transients.

The EOPs are formulated to handle many different events, including beyond design basis accident scenarios involving multiple failures. Upon first review, there appear to be numerous actions that could be followed leading to a variety of outcomes. However, after a review of the EOPs indicates the event is a design basis small break LOCA event involving no more than the limiting single failure, implementation of the EOPs can be significantly streamlined because certain actions, verifications, or branch points and their outcomes are already known. The EOPs can then be further streamlined for specific small break LOCA scenarios. For example, when analyzing a given case for an assumed failure of a diesel generator or a train of safety injection, the symptoms that the operator will observe, and the system responses to the operator's actions, will be already be known. The EOPs, which consist of dozens of pages, can be reduced to only a few pages when operations that are unnecessary for the specific small break LOCA scenario are eliminated because key plant symptoms are known a priori.

Section 25-2 describes an EOP sequence of events for a small break LOCA.

25-2 EOP Sequences for a Small Break LOCA

Table 25-1 is a condensation of the EOPs relevant to the short-term portion of a small break LOCA at the Indian Point Unit 2 plant. The procedures are contained in two major sections:

- E-0 Reactor trip or safety injection
- E-1 Loss of reactor or secondary coolant

Examination of the procedures shows that E-0 will be entered automatically when the reactor is tripped after the accident initiates. E-0 will always lead into procedure E-1.

25-2-1 Adverse Containment Conditions

In adverse containment conditions, a few parameters are evaluated against specifications that are dependent upon containment conditions. The values to use when adverse containment conditions exist are given in parentheses throughout the rest of this section. Adverse containment conditions are defined as:

$$P_{CONT} > 4 \text{ psig}$$

or

$$\text{Containment radiation level} > 10^5 \text{ R/hr}$$

Either or both of these conditions would probably be met at some time during the small break LOCA transients of interest. Actions are based upon measurement comparisons against the adverse conditions criteria.

25-2-2 Continuously Monitored Conditions

In addition to the sequential steps prescribed in the EOPs, there are a few key items continuously monitored as the procedures are followed. These are listed in "Foldouts" to a given procedure where they apply. Two of these items, both of which are in procedure E-0 of Table 25-1, are

important to the boundary conditions assumed for small break LOCA analysis calculations. They are:

- RCP trip criteria
 - At least one safety injection pump running
 - RCS subcooling < 24 (31)^(a)°F
- Safety injection actuation criteria
 - RCS subcooling < [RCS pressure-dependent table]
 - Pressurizer level cannot be maintained > 11 (33)^(a)%

Because these criteria are continuously monitored, safety injection actuation and RCP trip will occur, but not necessarily in a specifically defined sequence. This is discussed further in Section 25-3.

25-2-3 Inadequate Core Cooling

Another condition the operator will monitor following a small break LOCA event is to verify that the core is being adequately cooled. To establish that adequate core cooling exists, the EOPs require that the temperature readings of the core exit thermocouples do not exceed 1200°F. If this criterion is not met, the operator will enter the Inadequate Core Cooling Procedure FR-C.1, which directs the operator to depressurize the steam generator secondary side. If this depressurization is performed, it may significantly affect the small break LOCA transient. However, for best estimate small break LOCA analysis, it is anticipated that the steam temperature exiting the core will remain below 1200°F and procedure FR-C.1 will never be invoked.

a. Values in parentheses are typical values for adverse containment conditions.

25-3 Variability of Plant Conditions Due to Operator Actions

The condensed procedures in Table 25-1 show the importance of operator actions in defining the conditions during the short-term phases of a small break LOCA. The process is summarized chronologically as follows:

1. Verify that automatic safeguards features are functioning; identify and attempt to correct equipment malfunctions per prescribed procedures.
2. Analyze and respond to equipment status.
 - If no loss-of-offsite power (LOOP) occurs, stop RCPs when subcooling < 24 (31)^(a)°F (E-0, continuously checked) and at least one safety injection pump is injecting.
 - Start one charging pump (E-0, step 5).
 - Isolate unnecessary secondary side equipment steam loads (E-0, step 24).
3. Continue to monitor system conditions.
 - Check core exit thermocouples for indication of an inadequate core cooling condition.
 - Throttle auxiliary feedwater if narrow range level > 9 (26)^(a)% (E-0, step 24, E-1, step 3).

A review of the operations in Table 25-1 shows that the majority of the efforts undertaken by the operators are categorized as "verify operation or status." Although the operators continuously analyze equipment status and respond to failures throughout the entire operation, selected equipment failures are prescribed as boundary conditions to any given LOCA analysis calculation and the responses may, therefore, be defined a priori for an analysis. It may be assumed that an operator will spend more or less time on a given EOP step attempting to remedy an equipment failure. However, given an assumption concerning the failure of certain equipment for a defined analysis scenario, that equipment will still be unavailable as far as the LOCA

a. Adverse containment conditions typical value.

analysis boundary conditions are concerned. Furthermore, the operators have little latitude in the operations that may be attempted while working through the EOPs during the response to an accident. The possibility of various equipment failures is addressed within the procedures. When a failure is noted during a given step in the EOPs, the operators are directed immediately to an alternate action under a "Response Not Obtained" column. There, specific actions such as verifying or cycling a switch position or sending an operator into the field to perform a manual action are listed to attempt to remedy the failure. If the failure remains after the alternate action is taken, the operators note the failure and return to the subsequent actions directed by the EOPs.

Although some variability in the overall response times may occur from the operators spending time attempting to rectify individual failures – for example, time spent attempting to restart a failed safety injection pump – the net result is manifested only in terms of a few boundary conditions to a LOCA analysis. The only ones with potentially significant variability that could affect the ECCS performance prior to the time of PCT during a given small break LOCA calculation, are as follows:

- RCP trip
- Charging pump start time
- Shedding of unnecessary steam loads

All of the conditions required to allow RCP trip occur relatively early in a small break LOCA transient. The time at which the RCPs are tripped can have a potentially significant effect on the transient response. As explained in the procedures, the RCP trip criteria are continuously (periodically) reviewed throughout the transient. Given that at least one safety injection pump is probably functioning, the remaining RCP trip criterion to be met is that the RCS subcooling margin decreases below 24°F, or 31°F^(a) for adverse containment conditions. The RCP trip time variability is caused by the time the operators take to identify that the trip conditions exist during their periodic scan of system parameters, and the small increment required to actually perform the trip.

The startup of a charging pump is performed early in the EOPs (E-0, step 5 or 21). Therefore, little variation is caused by the possible cumulative effects of other operator action time variances prior to reaching this step. Additionally, because it is performed early, the effects of small differences in charging pump start time are further eliminated due to the high RCS

a. Adverse containment conditions typical value.

backpressure during these time periods. Therefore, the difference in injection will be small relative to the integral mass injected over the course of the transient.

Shedding unnecessary steam loads, prescribed in response to the continued cooldown of the primary, has a negligible effect on the boundary conditions for a small break LOCA because the steam loads in question are not significant relative to the large capacity of the secondaries. Because the impact of considering operator action to shed unnecessary steam loads and to initiate charging pump flow is minimal, and ignoring these actions is conservative, neither action is considered in the best estimate small break LOCA methodology.

Therefore, of the three operator actions identified as having potential effects on the small break LOCA behavior due to timing, only RCP trip time is significant. As discussed earlier, the variability in RCP trip time is not large because it is a continuously monitored parameter. Based upon studies conducted during operator training in plant simulators, a range of less than 60 seconds is expected in operator action to trip the RCP for small break LOCAs from the time at which the trip criteria physically occur in the plant. The database of studies includes a special session at the Indian Point Unit 2 simulator in which personnel performing the small break LOCA model development presented herein simulated LOCA events and observed the response of licensed plant operators. Various scenarios were run, and the operator actions were timed.

This range is considered in the uncertainty methodology; the upper bound to operator action time to trip the RCPs is 32 seconds and this time is used in the reference break spectrum with offsite power available in Section 27 of this document. The impact on the small break LOCA transient of operator actions upon entering the inadequate core cooling EOP is considered only if the core exit steam temperature is high enough for the core exit thermocouple readings to exceed 1200°F.

Table 25-1
Condensed EOPs for Indian Point Unit 2 Small Break LOCA: Short-Term Portion

Procedure E-0: Reactor Trip or Safety Injection	
Event/Response	Notes
1. Verify reactor trip. <ul style="list-style-type: none">• Rod bottom lights• Neutron flux decreasing	Normal rod insertion is assumed. Flux decrease occurs even if rods stuck.
2. Verify turbine trip.	Turbine stop valves will have closed.
3. Verify SI annunciator lights or SI pump running indications.	-
4. Verify power to 480 V bus.	Either offsite lines or diesels supply power.
5. Verify one charging pump running for seal injection.	-
6. Verify power to lighting and MCCs.	-
7. Verify component cooling water (CCW).	If CCW failure, use one charging pump to supply RCP seal cooling.
8. Verify FW isolation.	Standard assumptions
9. Verify SI valve alignment.	Standard assumptions
10. Verify AFW pumps running: one motor-driven (MD) pump is running.	One MD pump is lost. One MD pump supplies a minimum of 380 gpm in the current analysis.
11. Verify SI pumps running. <ul style="list-style-type: none">• Are all three pumps running?• Verify valve alignment.	Train failure is noted here. Valves are normally open.
12. Verify service water system.	Standard assumptions
13. Verify containment fan coolers running.	Standard assumptions

Table 25-1 (Cont'd)
Condensed EOPs for Indian Point Unit 2 Small Break LOCA: Short-Term Portion

Procedure E-0: Reactor Trip or Safety Injection (Cont'd)	
Event/Response	Notes
14. Verify containment ventilation isolation.	Standard assumptions
15. Verify containment isolation, Phase A.	Standard assumptions
16. Verify air conditioners operating.	Standard assumptions
17. Check main steam line isolation.	Close MSIVs Only if $P_{CONT} > 24$ psig - OR - Hi steam flow with either $T_{AVE} < 541^{\circ}\text{F}$ or steamline pressure < 525 psig
18. Verify containment spray if $P_{CONT} > 24$ psig.	Conditions may be met for larger small break LOCAs.
19. Verify SI flow. <ul style="list-style-type: none">• $P_{RCS} < 1660$ (1690)^(a) psig• Check flow indicators.• Attempt manual start.	Condition will be met. Train failure noted in step 11. Failed trains are assumed not to start. Continue on to step 20.
20. Verify RHR flow. $P_{RCS} < 320$ (340) ^(a) psig	Conditions will not be met at this time for most small break LOCAs.
21. Verify AFW flow > 400 gpm.	AFW verified previously, step 10, one MD pump will supply 380 gpm minimum.
22. Verify AFW flow to all SGs.	-
23. Align service water system.	Standard assumptions

a. Adverse containment conditions

Table 25-1 (Cont'd)
Condensed EOPs for Indian Point Unit 2 Small Break LOCA: Short-Term Portion

Procedure E-0: Reactor Trip or Safety Injection (Cont'd)	
Event/Response	Notes
24. Check RCS temperature. <ul style="list-style-type: none"> • T_{RCS} stable at or trending to 547°F? Stop dumping steam. • Isolate unnecessary steam loads. If cooldown continues: <ul style="list-style-type: none"> • Maintain AFW > 400 gpm. • Close MSIVs. 	No. It will be decreasing. Yes SG narrow range is still not to 9 (26) ^(a) %.
25. Verify pressurizer PORV and spray valves closed.	-
26. Check if RCPs should be stopped. <ul style="list-style-type: none"> • SI pump – at least one running • $\Delta T_{SUB}(\text{RCS}) < 24 (31)^{(a)} \text{ }^{\circ}\text{F}$ 	If LOOP, RCPs have already tripped. If no LOOP, RCP trip criteria have been continuously monitored and trip would have occurred sooner than this.
27. Check for faulted secondary boundaries.	Conditions will not be met.
28. Check for SGTR.	Conditions will not be met.
29. Check for LOCA.	Conditions are met.

a. Adverse containment conditions

Table 25-1 (Cont'd)

Condensed EOPs for Indian Point Unit 2 Small Break LOCA: Short-Term Portion

Procedure E-1: Loss of Reactor or Secondary Coolant (Entered from E-0, Step 29)	
Event/Response	Notes
1. Check if RCPs should be tripped.	Already tripped in E-0.
2. Check for SG secondary boundary failure.	No. This was already verified in E-0, Step 27.
3. Check SG levels. Maintain narrow range > 9 (26) ^(a) %.	Probably no throttling needed yet.
4. Verify pressurizer PORV/block valve closed.	Yes. This is not a PORV break. Already verified in E-0, step 25.
5. Reset SI.	This is not necessary; only for LOOP after initial SI.
6. Reset containment isolation.	-
7. Establish instrument air to containment.	No failure is assumed.
8. Check for secondary radiation.	No SGTR has occurred.
9. Check if charging flow is established. <ul style="list-style-type: none"> • At least one charging pump is running. • Adjust pump speed control. 	Already done in E-0, step 5. Pump is turned on at maximum flow.
10. Check if SI is to be terminated. <ul style="list-style-type: none"> • $\Delta T_{SUB}(\text{RCS}) > 19$ (26)^(a) °F • SG AFW > 400 gpm • PRCS > 1660 (1690)^(a) psig • $LL_{PRZ} > 11$ (33)^(a) % 	Condition not met - Condition not met Condition not met

a. Adverse containment conditions

Table 25-1 (Cont'd)

Condensed EOPs for Indian Point Unit 2 Small Break LOCA: Short-Term Portion

Procedure E-1: Loss of Reactor or Secondary Coolant (Cont'd) (Entered from E-0, Step 29)	
Event/Response	Notes
11. Proceed to SI termination (ES-1.1)	No. Conditions have not been met.
12. Check if containment spray should be stopped. $P_{CONT} < 17$ psig	If P_{CONT} was never > 24 psig, the sprays were never started.
13. Check if RHR is to be stopped. Check if $P_{RCS} > 320$ (340) psig and P_{RCS} stable or increasing.	Condition not met
14. Check RCS and SG pressures. Pressures stable? No? Yes?	If no, return to Step 1. If pressure is stable, the operator will move forward in the EOPs at this point. A return to Step 1 occurs only if the SG pressure is decreasing or the RCS pressure is increasing.

SECTION 26

WCOBRA/TRAC-SB MODEL OF INDIAN POINT UNIT 2

26-1 WCOBRA/TRAC-SB Nodalization

The nodalization for small break LOCA analysis of a PWR using WCOBRA/TRAC-SB must provide sufficient detail to model all design features of the PWR that might influence a small break transient, while allowing for an accurate modelling of physical processes important in a small break LOCA. This requirement for detail must be balanced with the need to keep the model small enough so that CPU times do not become excessively large. The WCOBRA/TRAC-SB model for Indian Point Unit 2 was developed based on a set of common modelling guidelines used for integral effects tests and separate effects tests. This ensures that the nodalization necessary to capture essential processes in the validation tests is included in the PWR model. The following are of particular note for the PWR model:

- The reactor vessel model is similar to the model used for large break LOCA analysis at Indian Point Unit 2 and other three- and four-loop plants as well. As in the large break model, the downcomer is modelled [

]^{a,c} to allow more accurate tracking of two-phase levels in the vessel. Section 20-2 of WCAP-12945-P-A (Bajorek, et al., 1998) describes the Indian Point Unit 2 vessel model for large break LOCA.

- The steam generators are modelled [

]^{a,c}

- The hot leg and cold leg horizontal pipes are modelled [

]^{a,c}

Figure 26-1 shows the reactor vessel nodalization. Compared to the large break LOCA model (Figure 20-2-2 in WCAP-12945-P-A), [

]^{a,c}.

Figures 26-2 through 26-5 show the Indian Point Unit 2 hot leg and steam generator nodalizations for small break LOCA calculations. [

]^{a,c} The TRAC 1-D components

are used to model the feedwater and steam line piping systems.

Figures 26-6 through 26-9 show the loop seals and cold legs. [

]^{a,c}

The safety injection system is modelled using FILL and ACCUM components attached to the cold legs by TEE and PIPE components.

26-2 Reference Case Conditions and Steady-State

26-2-1 Reference Case Conditions

Break spectrum scoping studies to determine the effect of various assumptions and initial conditions on a small break LOCA should be based on a reference set of conditions that are expected to produce a relatively severe transient. For a small break LOCA, a severe transient is generally expected to be one producing low vessel inventories, and deep or prolonged core uncoveries. A severe small break transient is expected to generate a significant PCT and maximize the sensitivities of the parameters examined. Assumptions that affect the severity of the small break transient can be categorized in terms of power-related parameters, break flow, primary-to-secondary heat transfer, and safety injection system performance. The following paragraphs discuss each parameter:

- **Power-Related Parameters**

Previous (Appendix K, 10 CFR 50) small break LOCA calculations generally indicate that PCTs increase with hot assembly power and that top-skewed power shapes are more limiting. Therefore, for the Indian Point Unit 2 break spectrum scoping study reference case, the peaking factors are assumed at [

]^{a,c}. Because partial core uncover occurs during a small break LOCA, a top-skewed power shape is assumed to result in high PCTs, based on Appendix K studies. Thus, [

]^{a,c}. This shape is peaked at the 9-foot elevation and has a relatively high amount of power in the top one-third of the core compared to other possible power shapes. [

.] ^{a,c}

- **Break Flow**

The reference case assumes that the most conservative location for the break is at the top of one of the cold legs. This assumption is based on the fact that locating the break at the top of the cold leg and presuming that the broken pipe is the safety injection delivery line severely penalizes the pumped safety injection flow entering

the RCS. The sensitivity studies of Section 28 of this document confirm that this is the limiting break location/orientation for a postulated small break LOCA event.

- Primary-to-Secondary Heat Transfer

[

]^{a,c}

- Safety Injection System Performance

Minimum pumped safety injection flows, consistent with the postulated break location, are assumed in the model. The closing of valves that diminish pumped injection is conservatively represented in the FILL tables for the safety injection system.

26-2-2 Steady-State Calculation

A WCOBRA/TRAC-SB PWR LOCA calculation is initialized when the RCS flows, RCS temperatures, core power, and steam generator pressures are at approximately the intended steady-state values before the postulated break occurs. Consequently, steady-state WCOBRA/TRAC calculations that establish the desired steady-state reactor conditions are performed prior to the transient calculations.

Steady-state plant pressure drop conditions are obtained from data generated by the Westinghouse Mechanical Equipment Design group. These calculated plant conditions reflect input parameters such as RCP flows, core power, steam generator tube plugging levels, system pressures, and fluid temperatures. The steam generator pressure drop and secondary side data are obtained from data generated by the Westinghouse Steam Generator Mechanical Development group.

Fuel parameters are obtained from the Westinghouse Commercial Nuclear Fuel Division PAD code (Weiner, et al., 1988), which provides the steady-state fuel pellet average temperatures as a function of fuel burnup and linear power, the fuel rod gas pressure, the gap conductance, and the like.

The calculated flowrate, pressure distribution, and fluid and fuel temperatures are adjusted to closely match the above data. This can be achieved by adjusting some of the axial or lateral flow loss coefficients, the initial vessel pressure level, the steam generator secondary fill conditions, and the initial cold gap widths between the pellet and the cladding. This typically requires a number of shakedown test runs.

While the fluid and core conditions discussed above are likely to differ somewhat from plant to plant, the degree to which these parameters are matched in the WCOBRA/TRAC-SB simulation must be consistent. A 100-second steady-state calculation is performed, and the results are checked for the acceptance criteria listed below. Table 26-1 compares the desired nominal and WCOBRA/TRAC-SB-predicted values for Indian Point Unit 2.

- Core power and peak linear heat rate are matched exactly.
- Integrals of rod power represent the radial peaking parameters ($F_{\Delta H}$). Integrals of the input power are calculated and normalized by the code to given $F_{\Delta H}$ values for the hot rod, the hot assembly rod, and the core average rod. These values must agree with their intended values.
- The maximum fuel average temperatures for the hot rod, the hot assembly rod, the average rods, and the low power rod must agree with the desired values from the PAD data.
- Vessel inlet, outlet, and upper head fluid temperatures define the fluid temperature distribution in the reactor vessel. The average RCS cold leg temperature (T_{cold}) at the vessel inlet should be within ± 1.0 percent of the intended value.
- Pump flow must be kept within a tight tolerance to ensure that the overall vessel/loop pressure drop is balanced by the pump head and the desired flowrate through the vessel has been approached.
- System pressure (pressure in the top cell of the pressurizer) and the water level in the pressurizer must be kept within a close tolerance, as shown in Table 26-1, to ensure that the steady-state pressurizer condition is closely simulated.

- Pressure drops across the vessel and through the core must agree closely with the values provided by the mechanical design data.
- Core bypass flow (including the thimble bypass flow and the spray nozzle flow) should closely match that provided by the mechanical design data.
- When identical loops are used to simulate the reactor system, the calculated results should be symmetrical with respect to each loop. Minimal crossflow (lateral gap flow) is to occur in the downcomer and in the lower plenum.
- Losses through the steam generator should closely match design data.
- The steam generator secondary pressure and initial mass should approximate the steam generator design values for the intended level of tube plugging. The reference calculations model 15-percent uniform steam generator tube plugging.

Once the fuel and fluid temperatures, vessel and loop pressure drop, and flow distributions are in agreement with the desired input parameters and conditions are steady, it is assumed that a suitable initial condition has been achieved for the LOCA transient simulation.

Table 26-1 shows the important plant steady-state parameters for the small break LOCA transient reference calculations for Indian Point Unit 2.

26-3 Cold Leg Break Transient Calculation

Once the steady-state calculation is executed and found to be acceptable, the transient calculation is initialized. To begin the transient, a small break is assumed to occur in the loop 24 cold leg (Figure 26-9). The accumulator and the safety injection lines of each loop are modelled explicitly. Valves are used in the intact accumulator/safety injection lines. Check valves 61, 71, 81, and 91 open the safety injection lines when the RCS pressure drops below the maximum pressure of the high head safety injection pumps after activation. Check valves 64, 74, 84, and 94 open the accumulator lines once the RCS pressure reaches the accumulator setpoint. Components 63, 73, 83, and 93 are FILL components which use pressure versus flow tables for the desired pumped safety injection flow. The steam generators are isolated by replacing the main feedwater FILL components (69, 79, 89, and 99) with zero-flow FILL components at the proper time; auxiliary feedwater is modelled through FILL components actuated by trips on a

safety injection signal after the appropriate delay time has elapsed. Closing of the steam isolation valve components 111, 121, 131, and 141 occurs at the proper time. The containment back pressure is assumed to be atmospheric pressure for the entire transient. The break orientation at the bottom of the cold leg is shown in Figure 26-9.

The primary heat sources during any LOCA are fission product decay heat, fission heat, and actinide decay heat. The WCOBRA/TRAC-MOD7A code version provides an option to calculate these three heat sources via the LUCIFER subroutine. The code logic associated with this option has been specifically developed for the needs of large break LOCA analysis. As discussed in Section 11, Volume 2, a specific option to model the control rod insertion was implemented in WCOBRA/TRAC-SB, which allows a negative reactivity to be introduced into the core using an appropriate time function. The moderator density reduction due to core voiding that occurs after the break and prior to the reactor trip is modelled.

Transient calculations may be done under either offsite power available (RCPs on) or offsite power off (RCPs tripped) conditions. The WCOBRA/TRAC-SB version contains code logic to activate the safety injection pumps and delay RCP trip by an appropriate delay time. The calculation is performed beyond the time when PCT is reached, until it becomes clear that no further cladding heatup will occur based on the core inventory and the comparative magnitudes of the safety injection delivery and the break flowrate.

26-4 References

Bajorek, S. M., et al., 1998, "Code Qualification Document for Best Estimate LOCA Analysis Volume IV: Assessment of Uncertainty," WCAP-12945-P-A, Vol. 4.

Bajorek, S. M., et al., 1998a, "Code Qualification Document for Best Estimate LOCA Analysis Volume V: Quantification of Uncertainty," WCAP-12945-P-A, Vol. 5.

Weiner, R. A., et al., 1988, "Improved Fuel Performance Models for Westinghouse Fuel Rod Design and Safety Evaluations," WCAP-10851-A (Proprietary), WCAP-11873-A (Nonproprietary).

Table 26-1
Plant Steady-State Parameters in WCOBRA/TRAC-SB

Parameter	Nominal Value	Steady-State Value
Initial reactor power (MWt)	3216	3216
RCS loop flow (gpm)	83,000	84,300
Total core bypass flow (% of vessel)	7.1	7.4
Upper head bypass flow (% of vessel)	0.17	0.17
T_{COLD} (°F)	552.9	548.5
Initial pressurizer pressure (psia)	2310	2311
Initial pressurizer water level (% of span)	60	61.8
Secondary side pressure (psia)	710	718

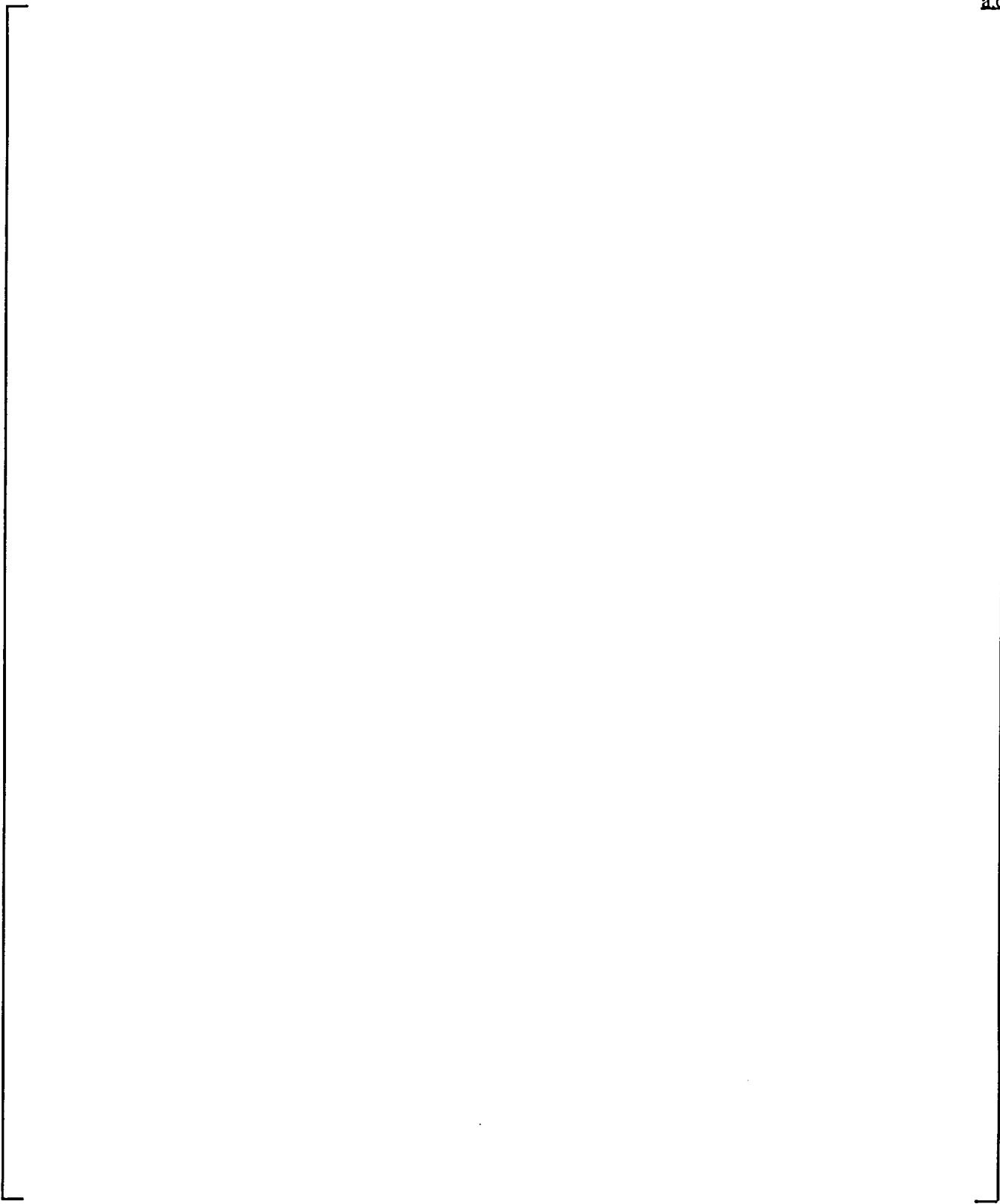


Figure 26-1. Indian Point Unit 2 Reactor Vessel Nodalization

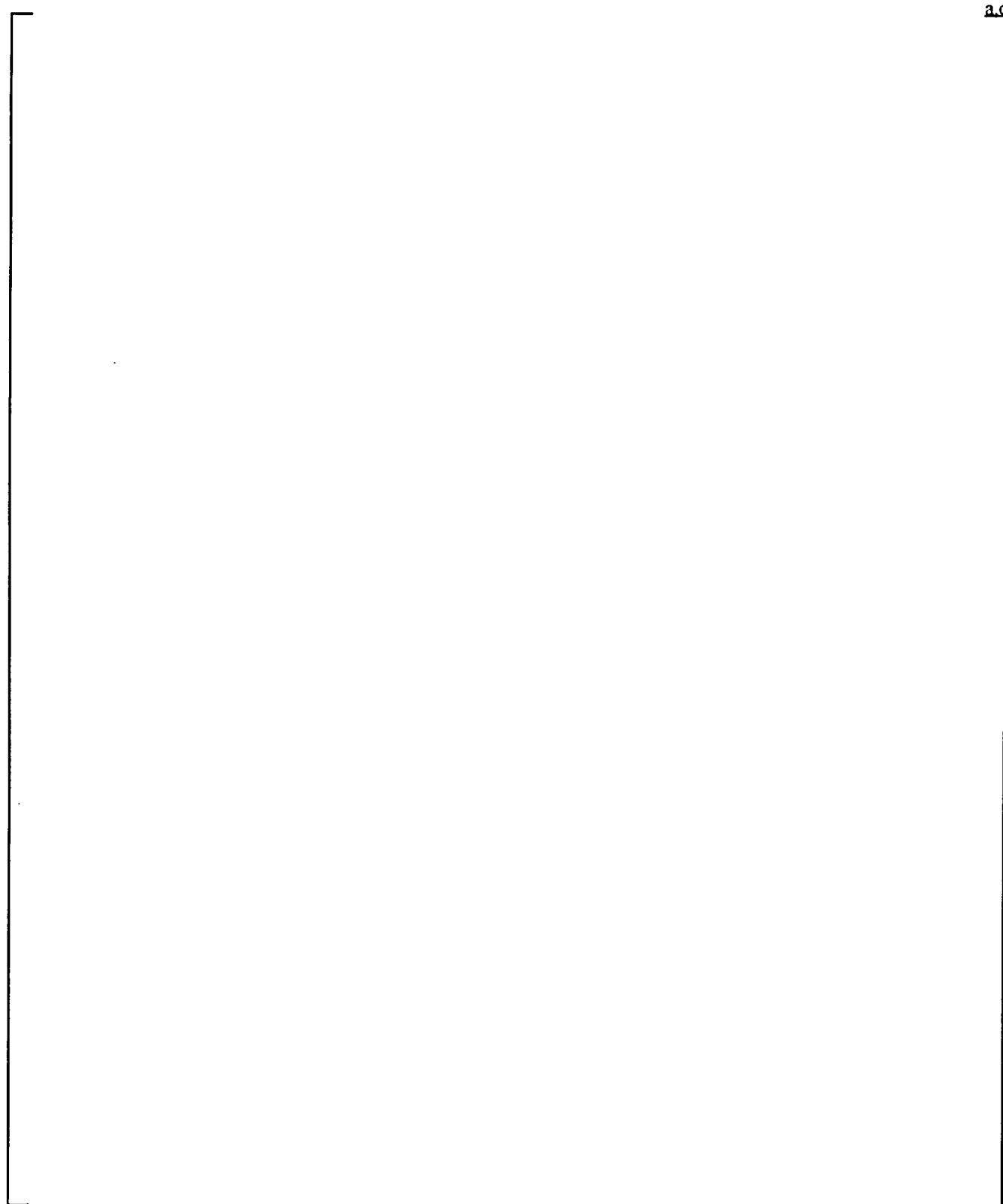


Figure 26-2. Indian Point Unit 2 Loop 21 Hot Leg and Steam Generator Nodalization

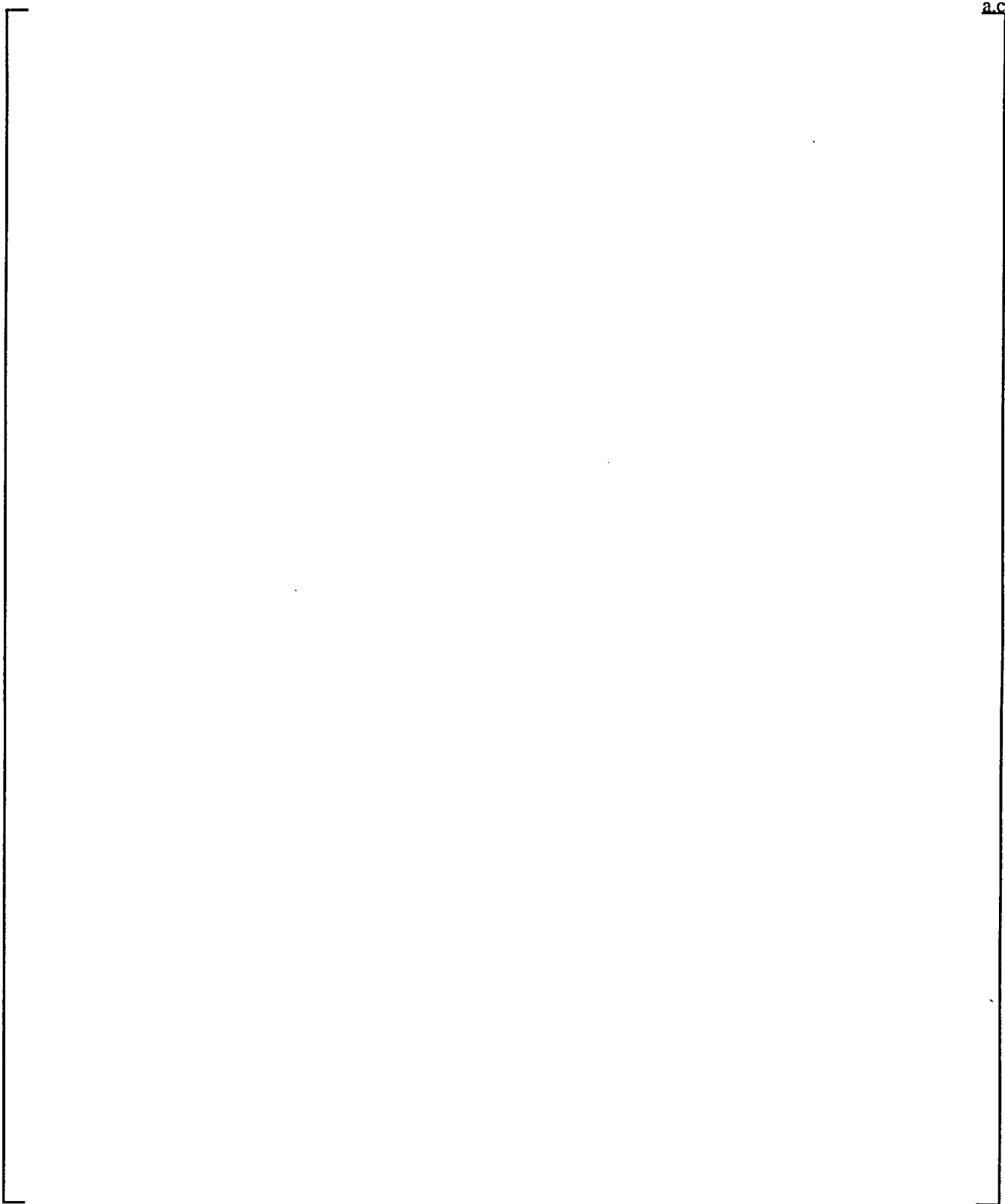


Figure 26-3. Indian Point Unit 2 Loop 22 Hot Leg and Steam Generator Nodalization

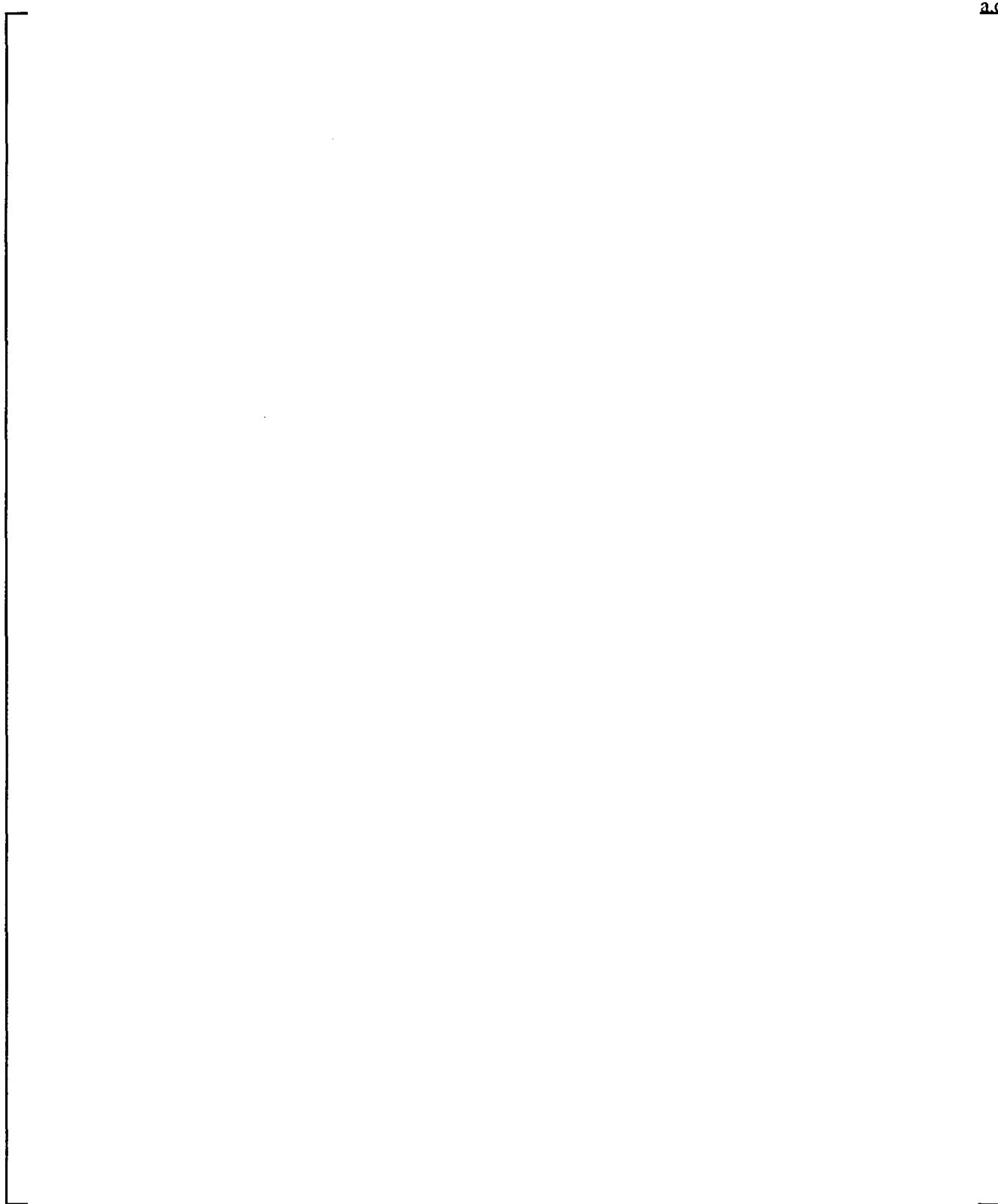


Figure 26-4. Indian Point Unit 2 Loop 23 Hot Leg and Steam Generator Nodalization

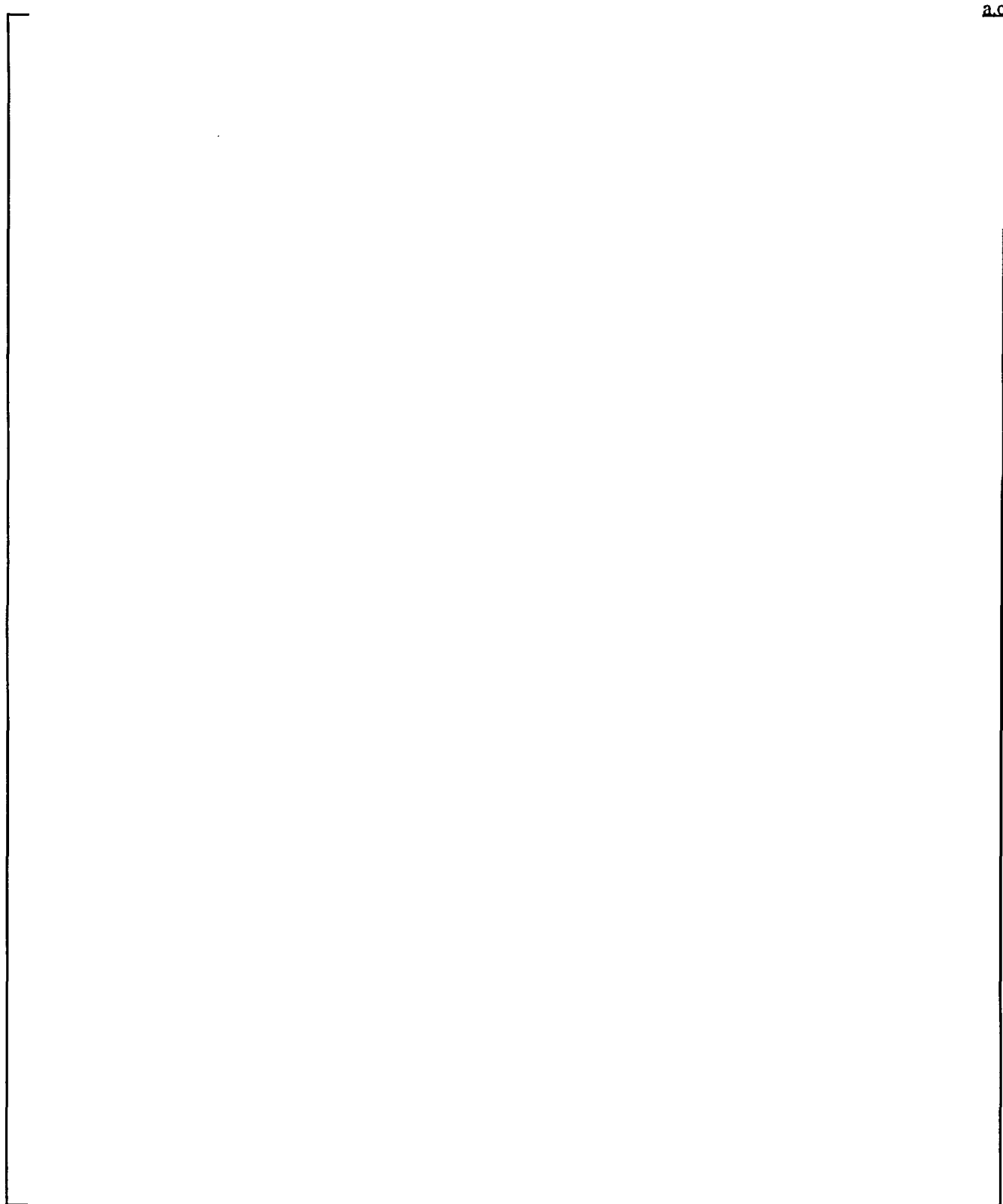


Figure 26-5. Indian Point Unit 2 Loop 24 Hot Leg and Steam Generator Nodalization



Figure 26-6. Loop 21 Loop Seal, Cold Leg, and Safety Injection Noding



Figure 26-7. Loop 22 Loop Seal, Cold Leg, and Safety Injection Noding

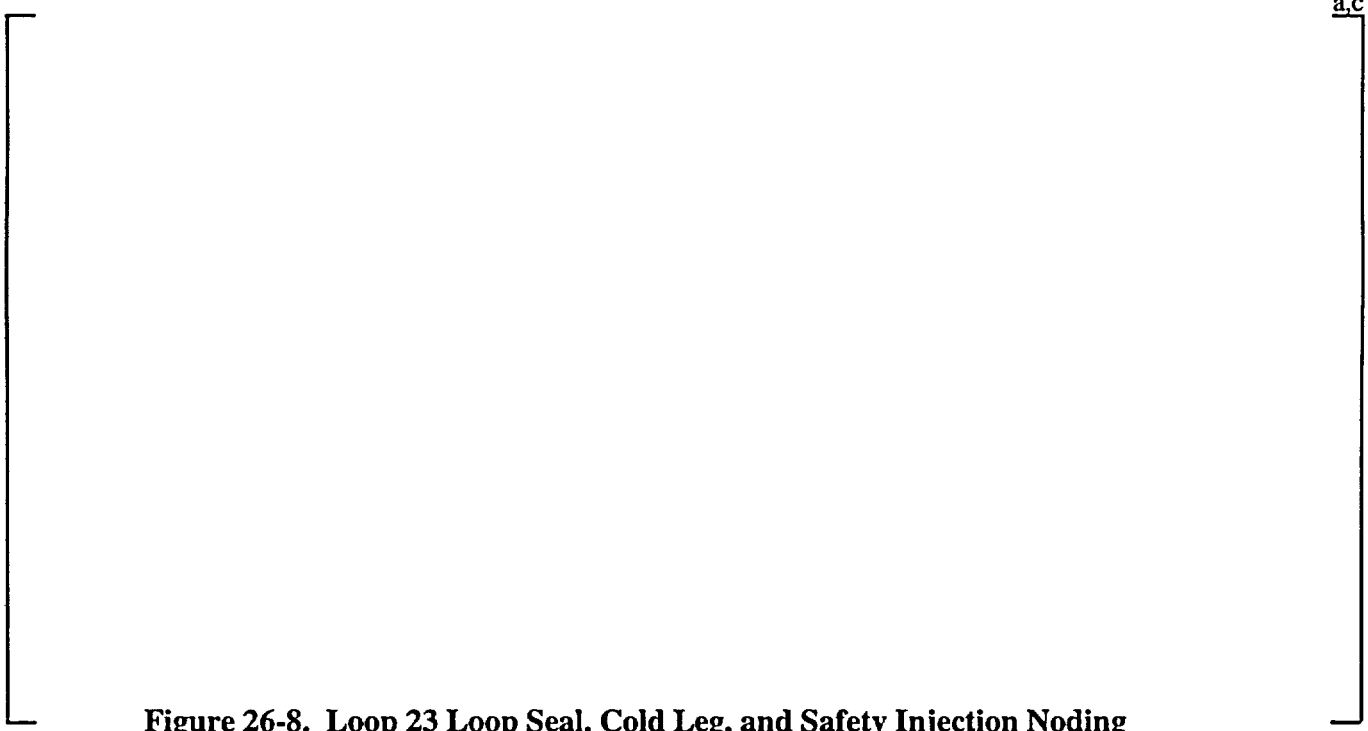


Figure 26-8. Loop 23 Loop Seal, Cold Leg, and Safety Injection Noding



Figure 26-9. Loop 24 Loop Seal, Cold Leg, and Safety Injection Noding

SECTION 27

INDIAN POINT UNIT 2 REFERENCE TRANSIENTS

27-1 Break Spectrum With LOOP Scenario

The worst single active failure in the current Westinghouse small break LOCA ECCS evaluation model analyses depends on the availability of offsite power. Appendix A of 10 CFR 50, criterion 17, requires that an onsite electric power system be available in case the offsite power is assumed lost. In the loss of offsite power (LOOP) assumption, the worst single active failure is the loss of one entire train of pumped ECCS because of a diesel generator failing to start. This results in the minimum safeguards safety injection flow, which provides the minimum replacement of mass lost from the RCS. The LOOP assumption also results in a significant delay in the time of pumped ECCS delivery. In addition to losing power to the reactor pumps, pressurizer heaters, and steam dump secondary pressure control system, the LOOP assumption minimizes the amount of pumped safety injection flow delivery. The LOOP requires that the safety injection train be loaded onto the emergency diesel power bus. The emergency diesel generator must be brought up to speed before flow delivery can occur, delaying safety injection flow delivery once an S-signal has been generated.

The minimum safeguards assumption also stipulates that minimum auxiliary feedwater flow be provided to the steam generator secondaries. With the LOOP assumption, auxiliary feedwater is delayed while the pumps are loaded onto the power bus and brought up to speed. Under the LOOP assumption, the single failure of a diesel generator also means that one motor-driven auxiliary feedwater pump fails to start. This minimizes the amount of decay heat removal to the secondary side. In the Indian Point Unit 2 design, two steam generators do not receive auxiliary feedwater flow when a pump fails to start.

A spectrum of cold leg break sizes is analyzed to cover the range of small break LOCAs with the WCOPRA/TRAC-SB break flow model. Sections 27-2 to 27-7 describe a set of calculations assuming LOOP occurs at the time of reactor trip for a postulated break in the cold leg of the loop that contains the pressurizer.

Section 24 of this volume describes the initial PWR conditions assumed for these calculations. The values were selected to establish a nominal plant reference condition in the calculations reported in this section. The break orientation is at the top of the pipe with no injection modeled

into the broken loop from either the safety injection pump or accumulator. This assumption is consistent with a rupture in the safety injection supply line. The piping design of Indian Point Unit 2 permits LOCA break sizes as low as 2-inches in diameter to be postulated as double-ended pipe severances in which the pumped SI spills into the containment. The YDRAG multiplier is set at a value of 0.8 in the core for the PWR analysis. This will reduce the interfacial drag in the core region, which will likely result in a deeper core uncover. The value of 0.8 was identified in Volume 2, Section 15, as the YDRAG multiplier that gives the best agreement with uncovered rod bundle test data.

Once the break occurs, the RCS primary rapidly depressurizes to the saturation pressure of the hot leg fluid. As flashing occurs, the rate of depressurization decreases. A reactor trip signal is generated by low pressurizer pressure and results in closure of the turbine stop valves on the steam generator secondary side, which then pressurizes, possibly to the steam generator secondary safety valve pressure setpoint. In that event, some steam relief through the steam generator secondary safety valves occurs, and the primary pressure is governed by the steam generator secondary conditions and primary to secondary heat transfer. The primary pressure equilibrates at a pressure where the primary to secondary heat transfer compensates for the volume expansion due to safety injection and core decay heat not removed by the break in the primary RCS. The postulated small LOCA also generates an "S" signal which, after a time delay, leads to isolation of the SG main feedwater and to pumped safety injection delivery to the RCS.

For breaks in the cold leg of the RCS, the primary pressure decreases below the secondary pressure when loop seal steam venting occurs. Loop seal steam venting is the process where steam produced by decay heat in the core flows through the hot legs and steam generators, and eventually passes through the inverted U-bend region of the pump suction (crossover leg) piping to reach the break. In order to accomplish this venting, the inner vessel pressure increases, which depresses the two-phase mixture level in the upper plenum.

The venting of steam through the loop seal allows the steam produced by the core decay heat to exit through the break. Once steam passes through the loop seal, the inner vessel pressure decreases relative to the downcomer pressure, and the hydrostatic head in the downcomer increases the inner vessel mixture level. This phenomenon is highly dependent on hydrostatic balances throughout the system. Additional system perturbations resulting from the loop seal venting, and from condensation caused by nonequilibrium effects, may result in steam venting through a different loop seal while the previously cleared loop seal plugs with liquid. Liquid

forced out of the loops as they clear can increase the liquid mass inventory in the core. These perturbations can change which loop seals vent steam and to what extent they vent steam. The magnitude of these perturbations and the nature of loop-to-loop interactions depend on the break size. Smaller breaks tend to have smaller system perturbations and are less influenced by loop-to-loop inertial effects. In larger small breaks, the loop-to-loop perturbations are more prevalent. This phenomenon was discussed by Lee (Lee, et al., 1983). The PWR calculations in this report are biased to minimize the number of loop seals that are predicted to clear. This is discussed further in Subsection 27-8.

After the loop seal(s) vents, the steam generator secondaries become an additional heat source to the primary fluid. After loop seal clearance, the break flow quality makes a transition to predominantly steam, and the volume removed by the break exceeds volume swell. However, the mass removal exceeds the mass input due to safety injection, and a core uncover may result. Eventually, the primary RCS pressure will decrease to the point where the break mass flow will decrease below the mass flow entering the RCS by safety injection and/or accumulator injection, and the system mass inventory will begin to increase.

Eventually, the system will reach a stable equilibrium pressure where the mass flow through the break equals the mass flow into the RCS. Stable decay heat removal and long-term pressure decay results from this condition.

27-2 3-Inch Cold Leg Break With LOOP

Figures 27-2-1 to 27-2-7 provide a summary of the 3-inch cold leg break transient. The RCPs continue to be powered from the generator until 30 seconds have elapsed after reactor trip; at that time, the RCPs begin to coast down.

During the blowdown phase, the 3-inch break depressurizes to the saturation pressure corresponding to the core outlet temperature. A reactor trip signal occurs at 35.5 seconds as the pressurizer pressure reaches the setpoint; a safety injection signal occurs at 39.7 seconds. Steam generator isolation occurs following reactor trip, and the steam generator secondary pressure increases rapidly to the MSSV setpoint. After the MSSVs open, steam flow through the safety valves maintains the secondary pressure near the MSSV setpoint. The primary side continues to depressurize rapidly after core shutdown to a pressure approximately 40 to 80 psi higher than the MSSV setpoint.

The loop seals attempt to clear beginning at 724 seconds, and the break flow quality increases thereafter. Only loop 22 clears and has a continuous steam flow as shown in Figure 27-2-4. The steam flow through that loop seal reaches a maximum flowrate of approximately 120 lbm/s shortly after loop seal clearance.

Figure 27-2-2 shows the core collapsed liquid level. The level exhibits close to a 1-foot increase at the time of loop seal clearance. This occurs because, during the loop seal clearance, liquid that has been held in the loop seals and cold legs flows into the reactor vessel, decreasing the core void fraction.

Following loop seal clearance, the pumped safety injection flow is not sufficient to make up for the break flow and the vessel mass inventory continues to decrease. Core uncover and heatup begin at approximately 1372 seconds, and the hot rod cladding temperature increases slowly to a peak of 964°F at 1948 seconds. The collapsed liquid level in the core reaches a minimum immediately before the PCT and begins to recover as the accumulators begin to inject. While accumulator flow is responsible for the core recovery, the minimum inventory is established by the pumped safety injection flow. Following accumulator injection, the collapsed level in the core increases steadily and the entire core quenches.

The transient calculation was ended prior to 2400 seconds because the core was quenched and the total safety injection flow exceeded the break flow.

Indian Point 2 BE SBLOCA Analysis
3-INCH CL BREAK WITH LOOP
Primary and Secondary System Pressures

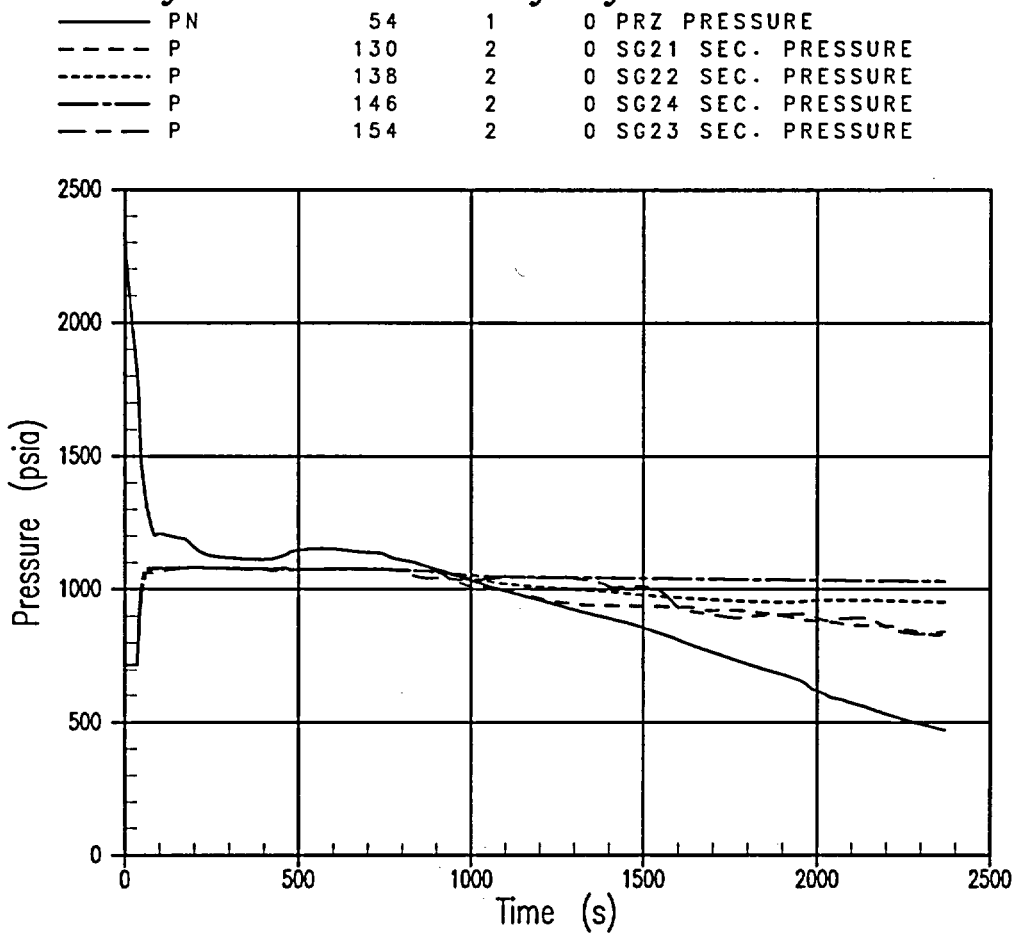


Figure 27-2-1. Primary and Secondary System Pressures, 3-Inch Break With LOOP

Indian Point 2 BE SBLOCA Analysis
3-INCH CL BREAK WITH LOOP
Core Collapsed Liquid Levels

— LQ-LEVEL 5 0 0 HOT ASSY
- - - LQ-LEVEL 4 0 0 CORE AVERAGE

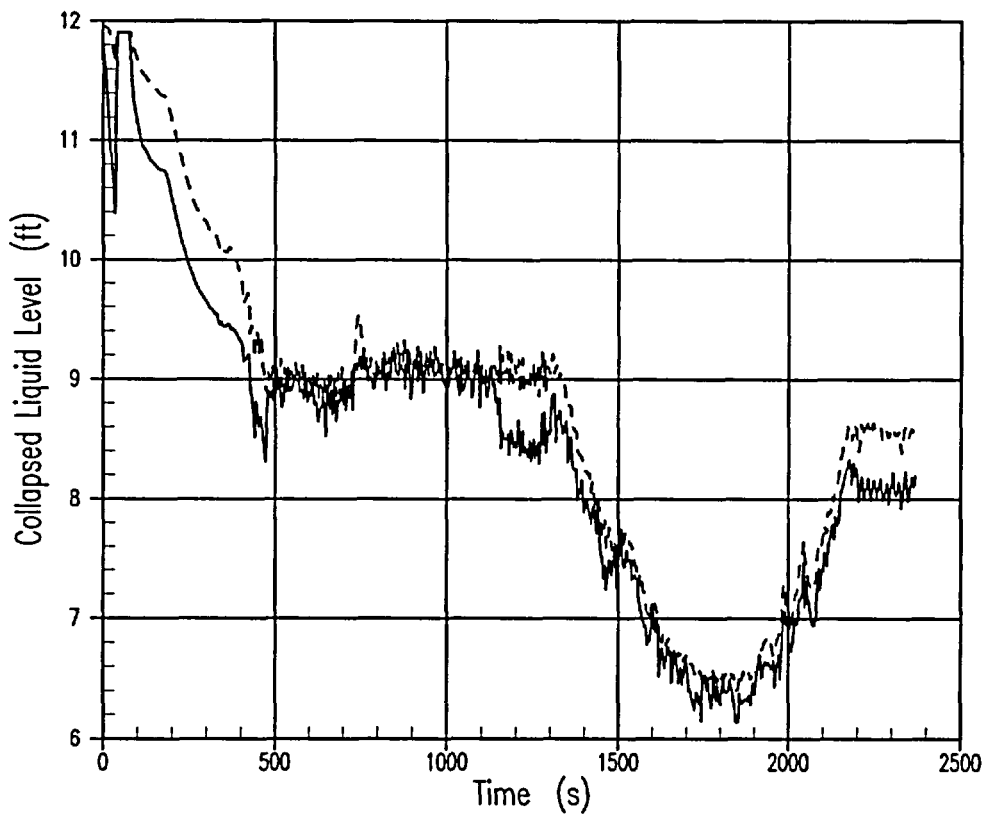


Figure 27-2-2. Core Collapsed Liquid Level, 3-Inch Break With LOOP

Indian Point 2 BE SBLOCA Analysis 3-INCH CL BREAK WITH LOOP Break Flowrate and Void Fraction

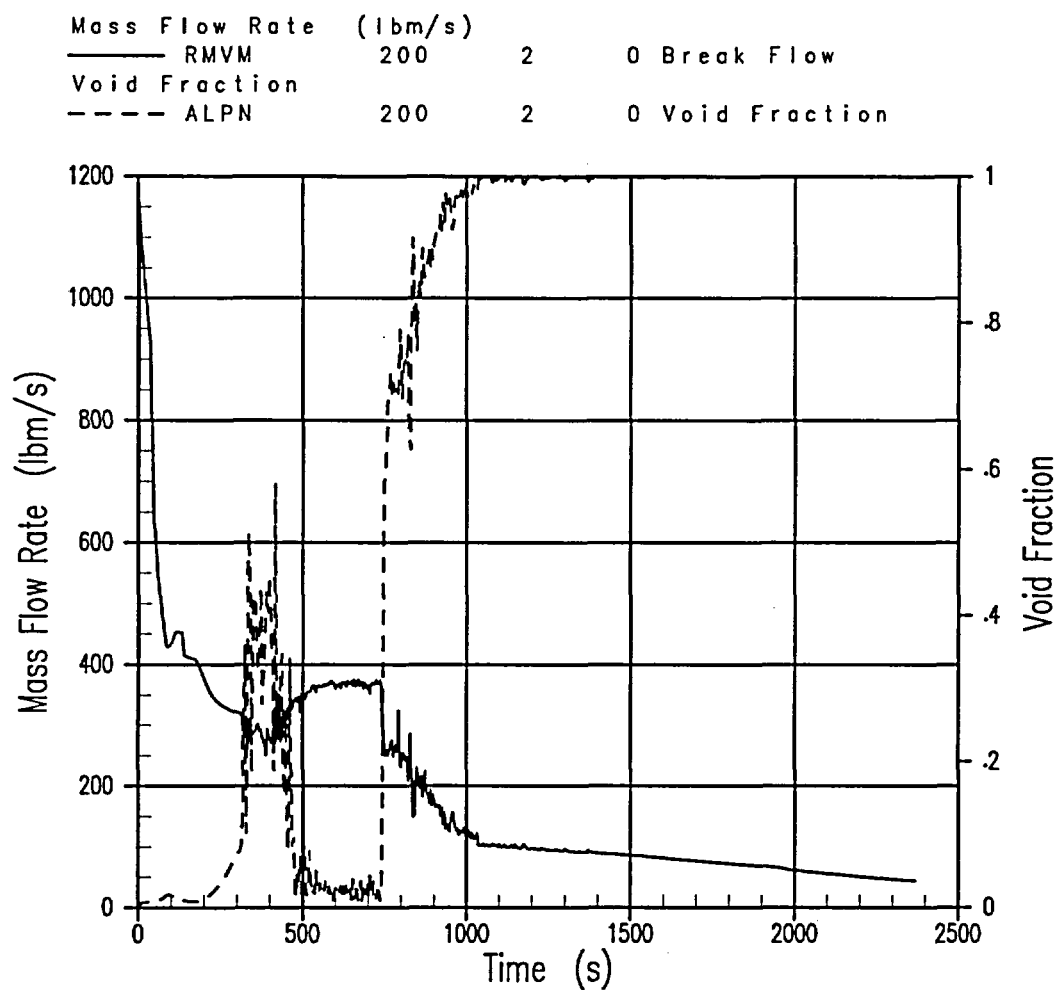
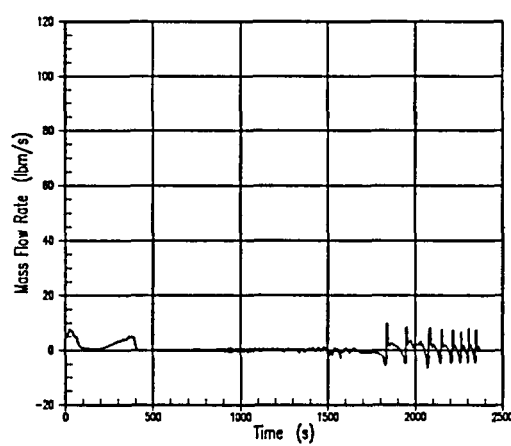


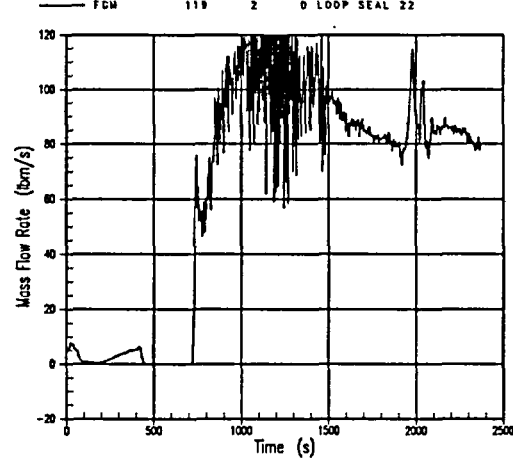
Figure 27-2-3. Break Flowrate and Void Fraction, 3-Inch Break With LOOP

Indian Point 2 BE SBLOCA Analysis
3-INCH CL BREAK WITH LOOP
Loop 21 Steam Flow



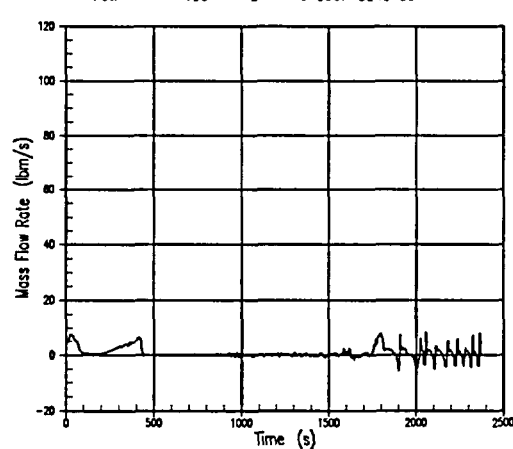
A. Loop 21 Loop Seal Steam Flow

Indian Point 2 BE SBLOCA Analysis
3-INCH CL BREAK WITH LOOP
Loop 22 Steam Flow



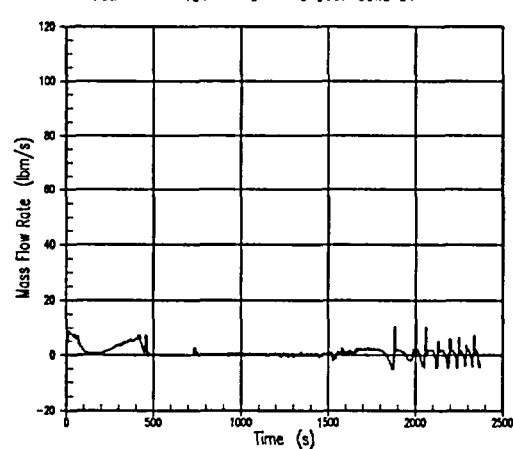
B. Loop 22 Loop Seal Steam Flow

Indian Point 2 BE SBLOCA Analysis
3-INCH CL BREAK WITH LOOP
Loop 23 Steam Flow



C. Loop 23 Loop Seal Steam Flow

Indian Point 2 BE SBLOCA Analysis
3-INCH CL BREAK WITH LOOP
Loop 24 Steam Flow



D. Loop 24 Loop Seal Steam Flow

Figure 27-2-4. Loop Seal Steam Flows, 3-Inch Break With LOOP

Indian Point 2 : BE SBLOCA Analysis
3-INCH CL BREAK WITH LOOP
Reactor Vessel Mass

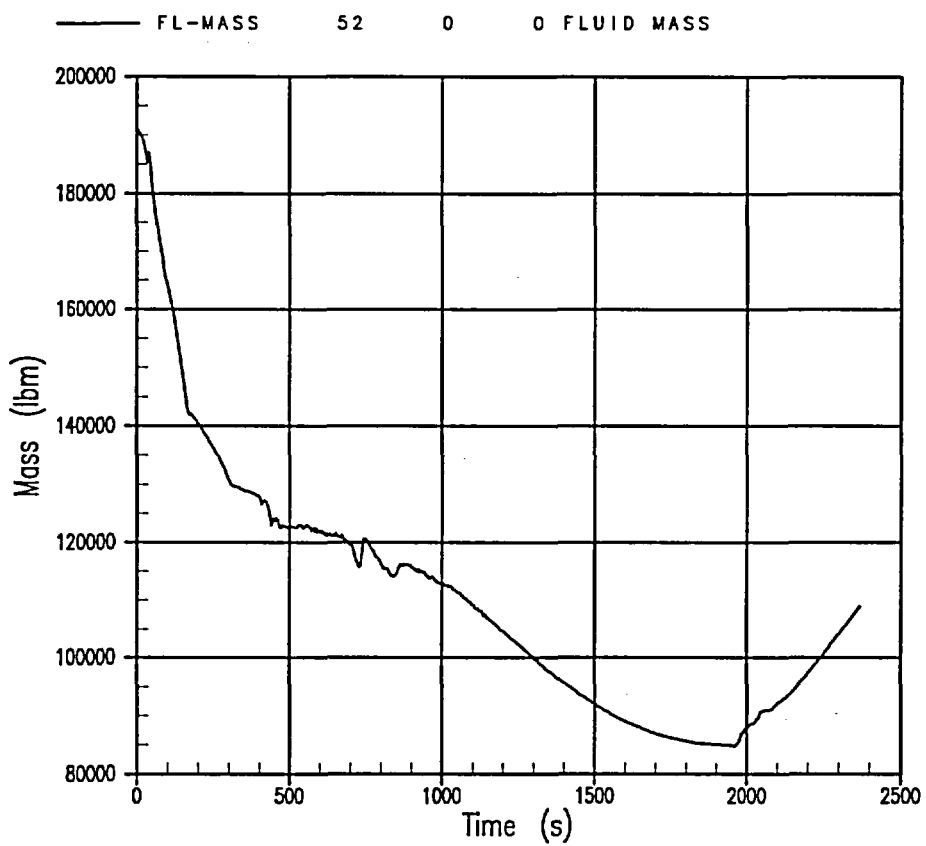


Figure 27-2-5. Reactor Vessel Mass, 3-Inch Break With LOOP

Indian Point 2 BE SBLOCA Analysis
3-INCH CL BREAK WITH LOOP
Peak Cladding Temperature

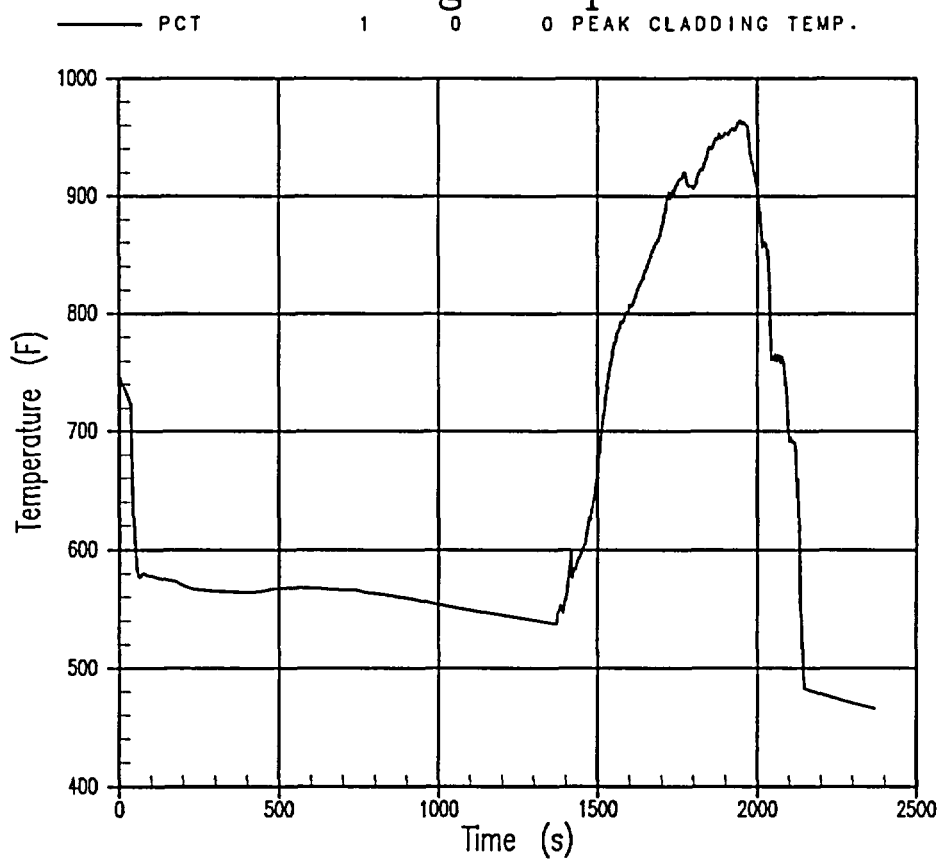


Figure 27-2-6. PCT, 3-Inch Break With LOOP

Indian Point 2 BE SBLOCA Analysis
3-INCH CL BREAK WITH LOOP
Total Safety Injection Flow

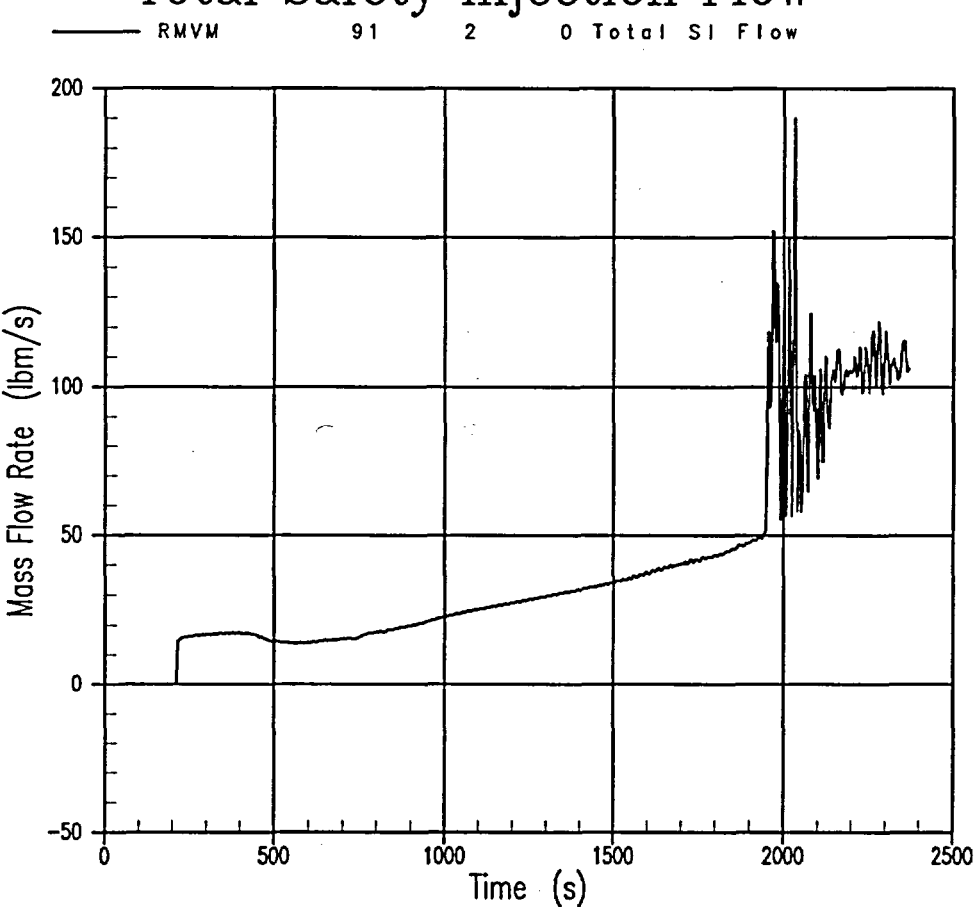


Figure 27-2-7. Total Safety Injection Flow to RCS, 3-Inch Break With LOOP

27-3 4-Inch Cold Leg Break With LOOP

The sequence of events for the 4-inch equivalent diameter cold leg break are similar to the events and behavior of the 3-inch break discussed in Section 27-2. In the 4-inch break, events occur earlier and the transient is more rapid. Figures 27-3-1 to 27-3-7 provide a summary of the transient.

The 4-inch break quickly depressurizes to the saturation pressure corresponding to the core outlet temperature. A reactor trip signal occurs at 20.7 seconds. The steam generator secondaries are isolated shortly following reactor trip, and the steam generator secondary pressure increases rapidly to the MSSV setpoint. After the MSSVs open, steam flow through the safety valves maintains the secondary pressure near the MSSV setpoint. The primary side continues to depressurize to a pressure approximately 40 to 80 psi higher than the MSSV setpoint and remains in that pressure range until the loop seals begin to clear.

The loop seals begin to clear at 404 seconds. The break flow quality increases and becomes primarily steam flow. In the 4-inch break, two loop seals (loop 24 and loop 23) have sustained venting for most of the remainder of the transient. Venting occurs later in the pressurizer loop 24, and loop 24 vents continuously after initial clearance. With the loop seal clearance, the primary pressure continuously decreases and the accumulator setpoint pressure is reached at 943 seconds.

Core heatup in the 4-inch break begins at 818 seconds. The heatup rate is more rapid than in the 3-inch break; however, the heatup is terminated by accumulator injection at 960 seconds, and the core quenches shortly thereafter. The heatup is so minor that the PCT barely exceeds the steady-state fuel cladding temperature.

The transient calculation was ended when the total safety injection flow exceeded the break flow and the relatively minor PCT excursion had terminated.

Indian Point 2 BE SBLOCA Analysis
4-INCH CL BREAK WITH LOOP
Primary and Secondary System Pressures

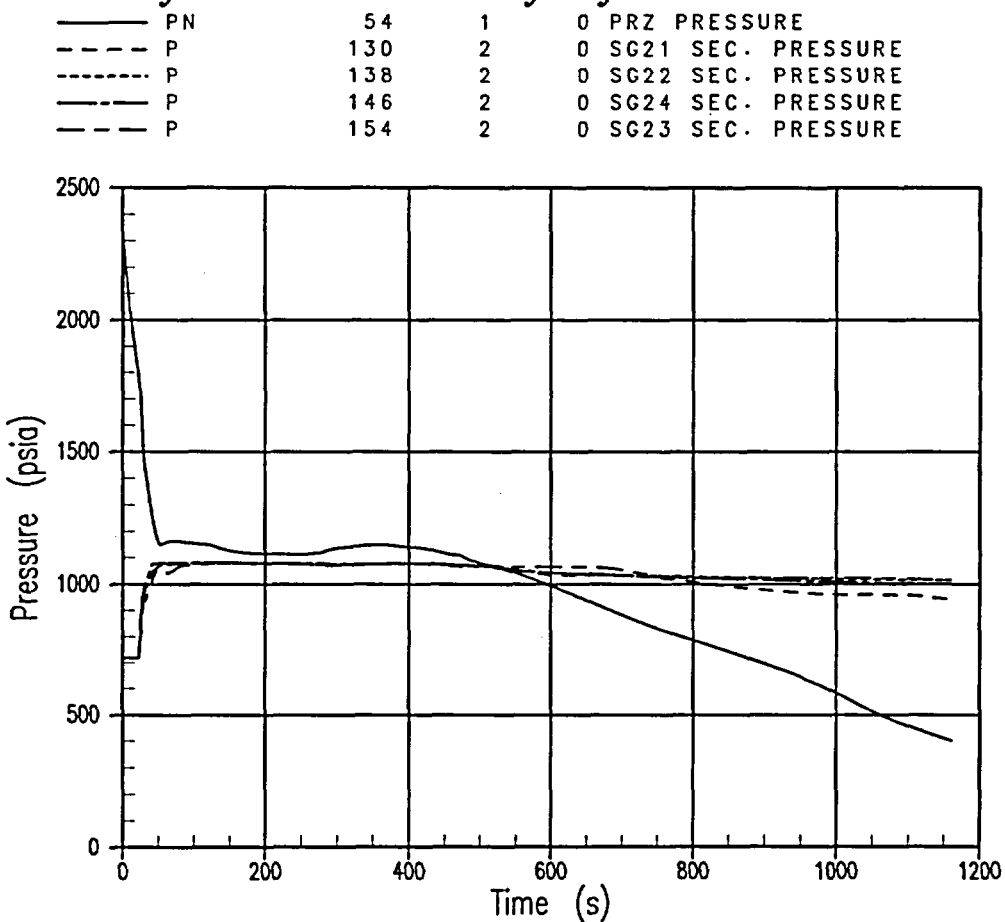


Figure 27-3-1. Primary and Secondary System Pressures, 4-Inch Break With LOOP

Indian Point 2 BE SBLOCA Analysis
4-INCH CL BREAK WITH LOOP
Core Collapsed Liquid Levels

— LQ-LEVEL 5 0 0 HOT ASSY
- - - LQ-LEVEL 4 0 0 CORE AVERAGE

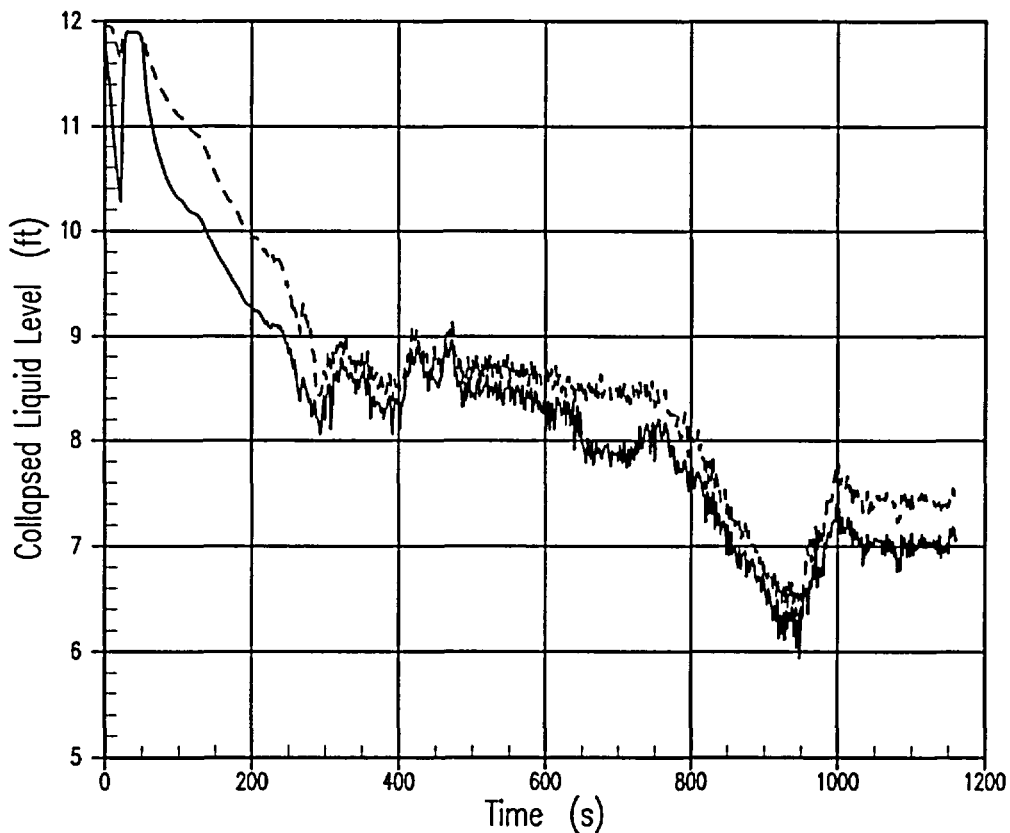


Figure 27-3-2. Core Collapsed Liquid Level, 4-Inch Break With LOOP

Indian Point 2 BE SBLOCA Analysis
4-INCH CL BREAK WITH LOOP
Break Flowrate and Void Fraction

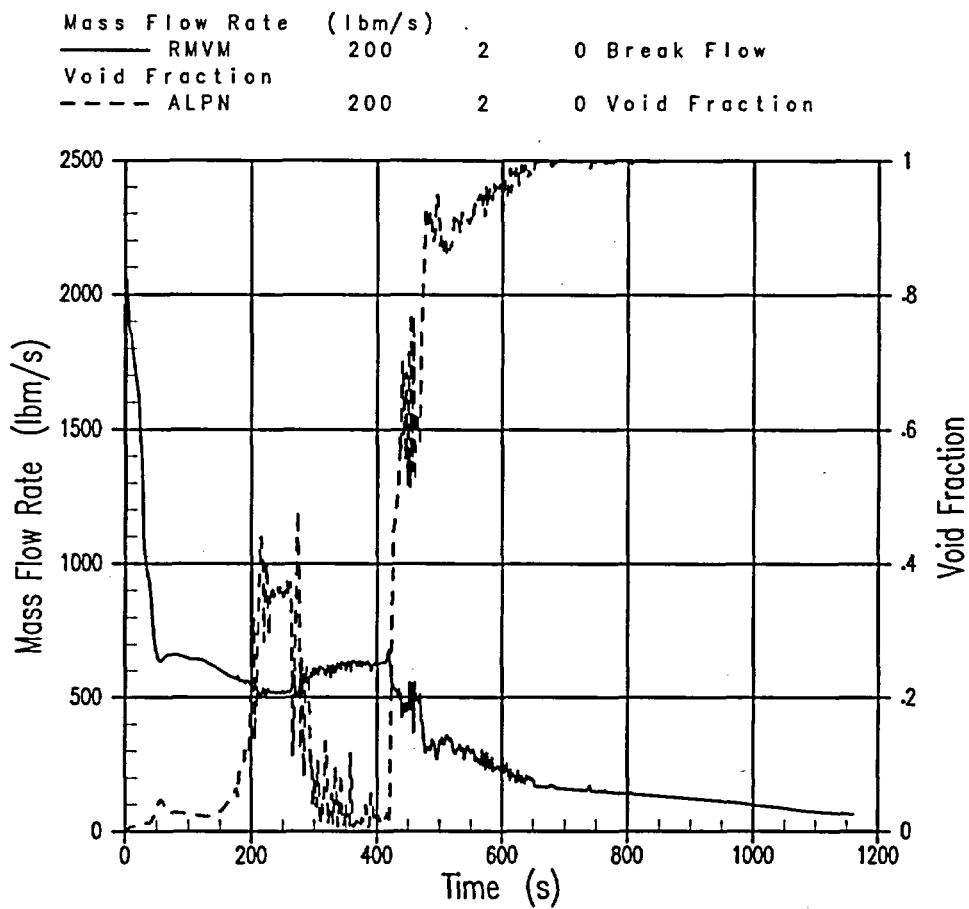
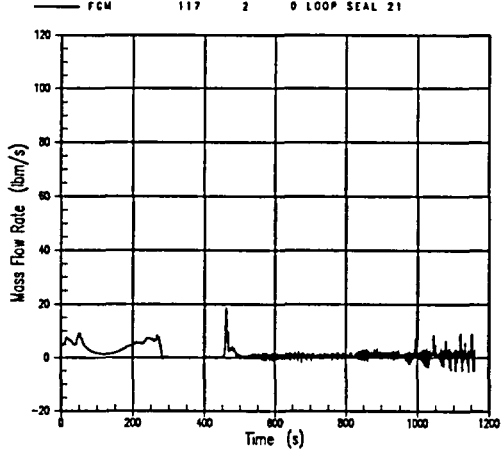


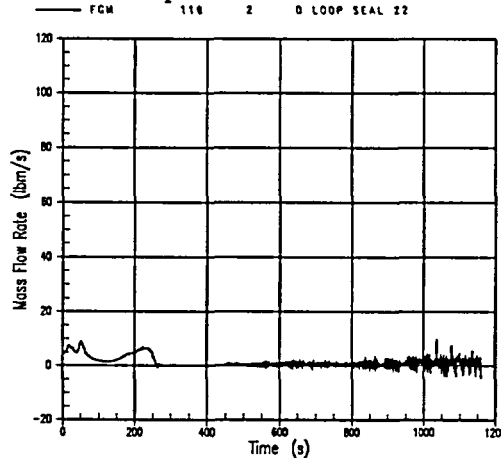
Figure 27-3-3. Break Flowrate and Void Fraction, 4-Inch Break With LOOP

Indian Point 2 BE SBLOCA Analysis
4-INCH CL BREAK WITH LOOP
Loop 21 Steam Flow



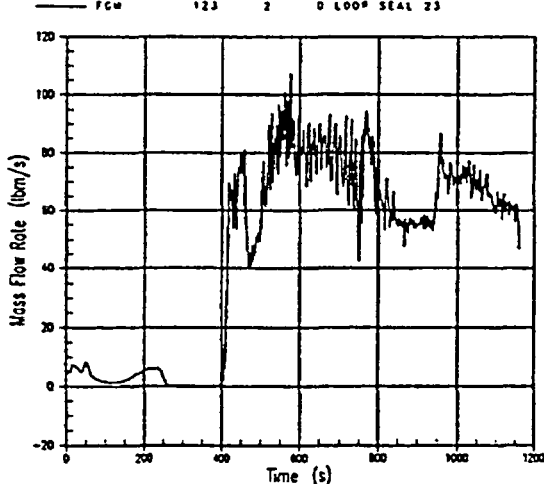
A. Loop 21 Seal Steam Flow

Indian Point 2 BE SBLOCA Analysis
4-INCH CL BREAK WITH LOOP
Loop 22 Steam Flow



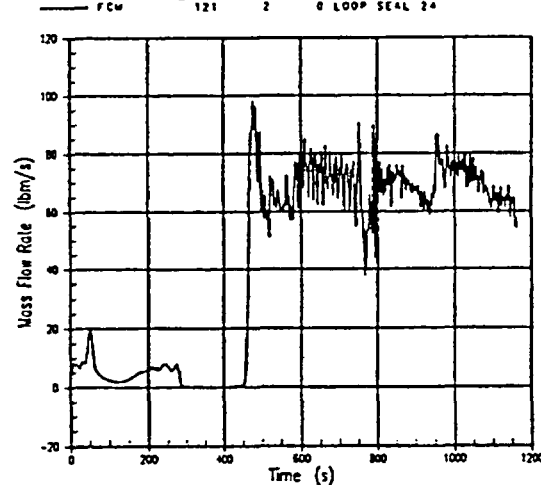
B. Loop 22 Loop Seal Steam Flow

Indian Point 2 BE SBLOCA Analysis
4-INCH CL BREAK WITH LOOP
Loop 23 Steam Flow



C. Loop 23 Seal Steam Flow

Indian Point 2 BE SBLOCA Analysis
4-INCH CL BREAK WITH LOOP
Loop 24 Steam Flow



D. Loop 24 Loop Seal Steam Flow

Figure 27-3-4. Loop Seal Steam Flows, 4-Inch Break With LOOP

Indian Point 2 BE SBLOCA Analysis
4-INCH CL BREAK WITH LOOP
Reactor Vessel Mass

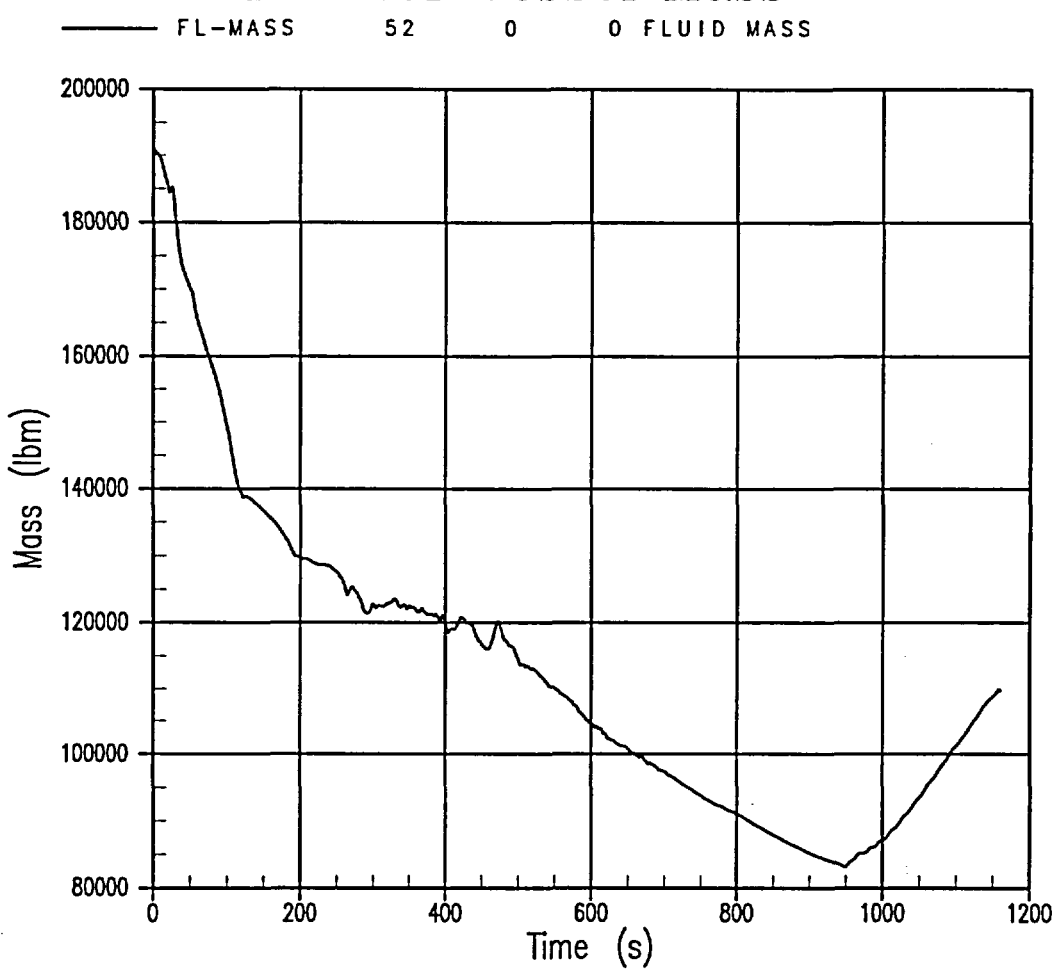


Figure 27-3-5. Reactor Vessel Mass, 4-Inch Break With LOOP

Indian Point 2 BE SBLOCA Analysis
4-INCH CL BREAK WITH LOOP
Peak Cladding Temperature

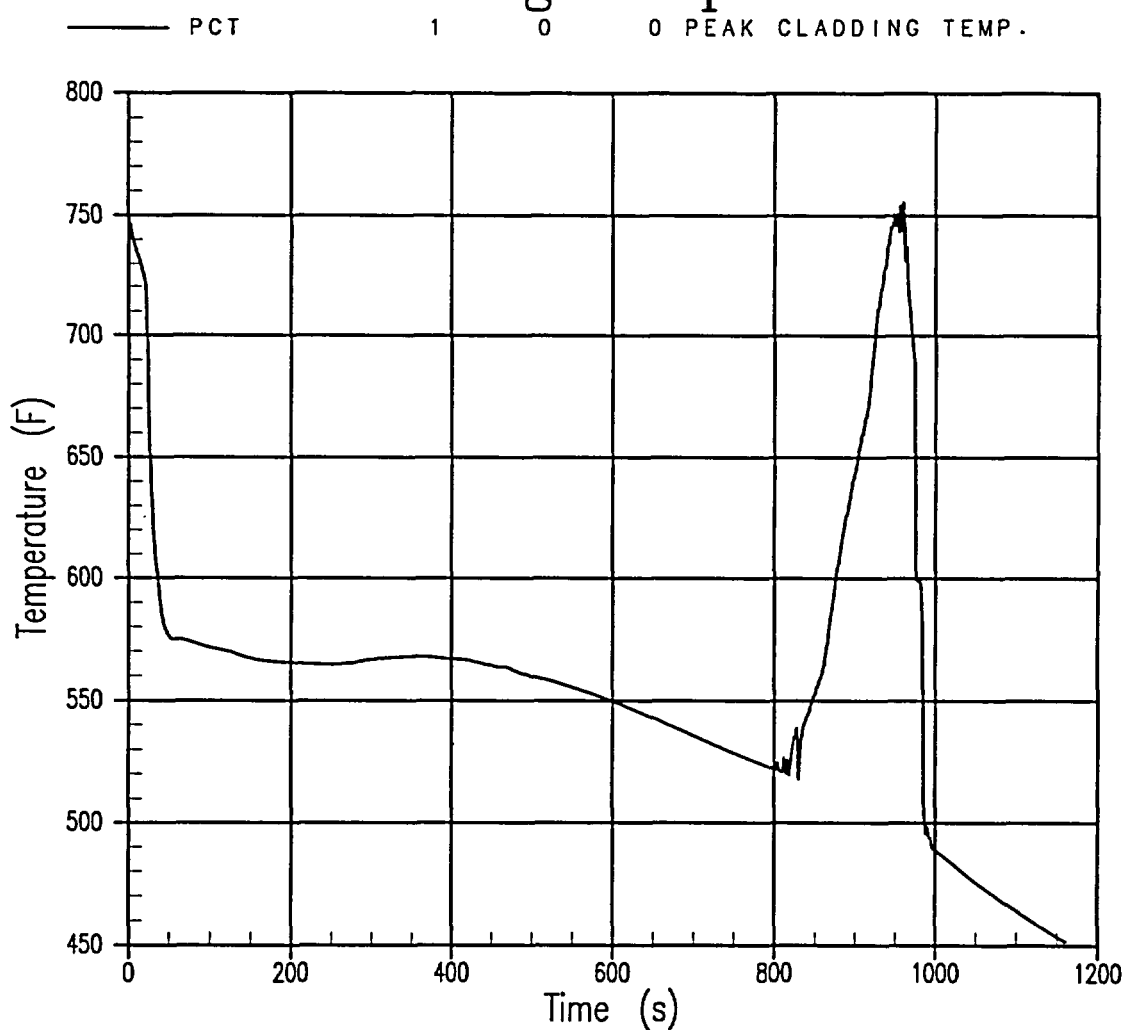


Figure 27-3-6. PCT, 4-Inch Break With LOOP

Indian Point 2 BE SBLOCA Analysis
4-INCH CL BREAK WITH LOOP
Total Safety Injection Flow

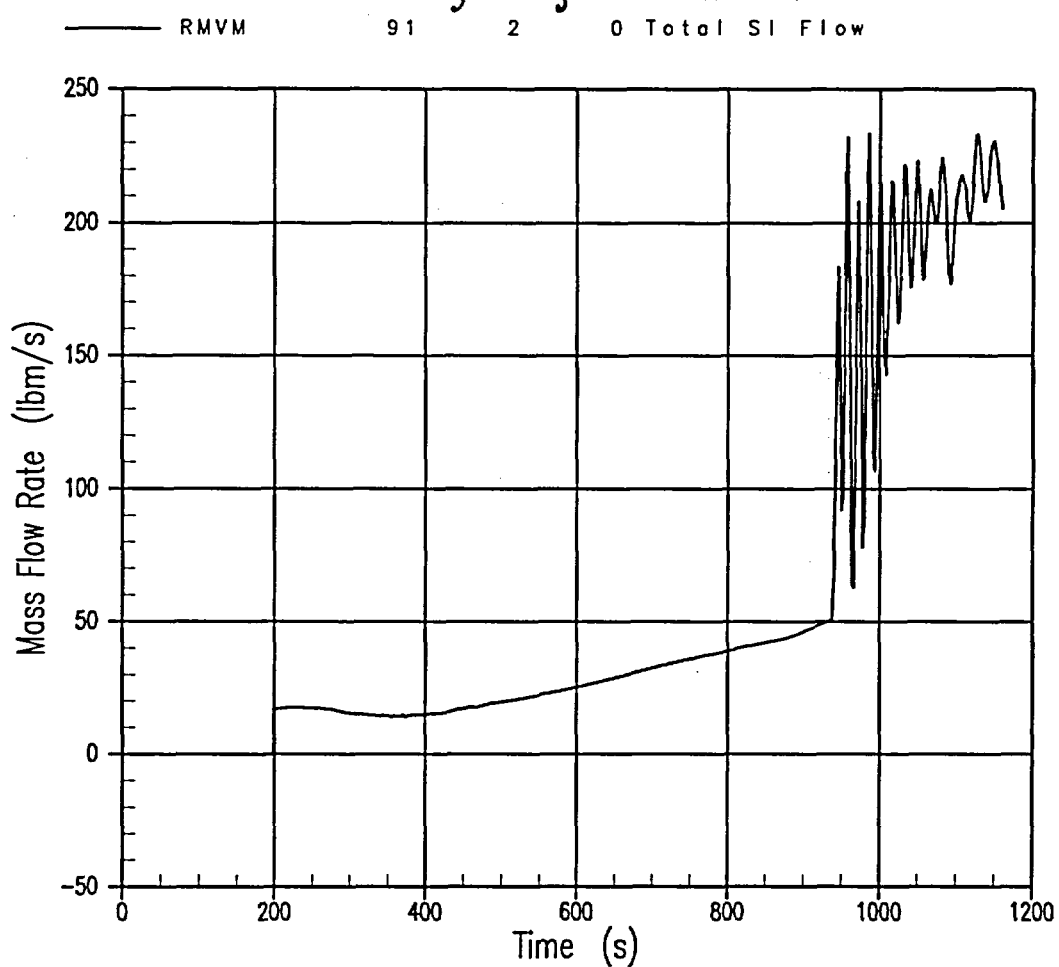


Figure 27-3-7. Total Safety Injection Flow to RCS, 4-Inch Break With LOOP

27-4 6-Inch Cold Leg Break With LOOP

The sequence of events and overall behavior for the 6-inch equivalent diameter cold leg break begins to depart from that observed in the breaks of smaller size (3- and 4-inch). In the 6-inch break, events occur earlier, the transient is more rapid, and no core uncover is observed. As in the 4-inch break, the core collapsed level moves upward by approximately 1 foot after loop seal clearance (Figure 27-4-2). No boiloff uncover occurs later in the transient before accumulator injection begins. Figures 27-4-1 to 27-4-7 provide a summary of the transient.

The 6-inch break quickly depressurizes past the saturation pressure corresponding to the core outlet temperature and holds briefly at a pressure about 40 to 50 psi higher than the MSSV setpoint. The reactor trip signal occurs at 10.2 seconds. After isolation, the steam generator secondary pressure increases rapidly to the MSSV setpoint. After the MSSVs open, steam flow through the safety valves maintains the secondary pressure near the MSSV setpoint. This occurs for a relatively short time before the break depressurizes the primary below the steam generator secondary pressure.

The loop seals begin to clear at 175 seconds. The steam production in the core is high at this time and is sufficient to initially clear three of the four loop seals. After venting begins, the break flow quality increases and becomes primarily steam flow. Three of the loop seals (loops 21, 22, and 24) vent steam continuously. After loop seal clearance, the primary pressure rapidly decreases and the accumulator setpoint pressure is reached at 308 seconds.

No core heatup occurs due to a boiloff uncover. Following accumulator injection, the vessel mass inventory begins to increase.

The transient calculation was ended at 500 seconds because the total safety injection flow exceeded the break flow.

Indian Point 2 BE SBLOCA Analysis
6-INCH CL BREAK WITH LOOP
Primary and Secondary System Pressures

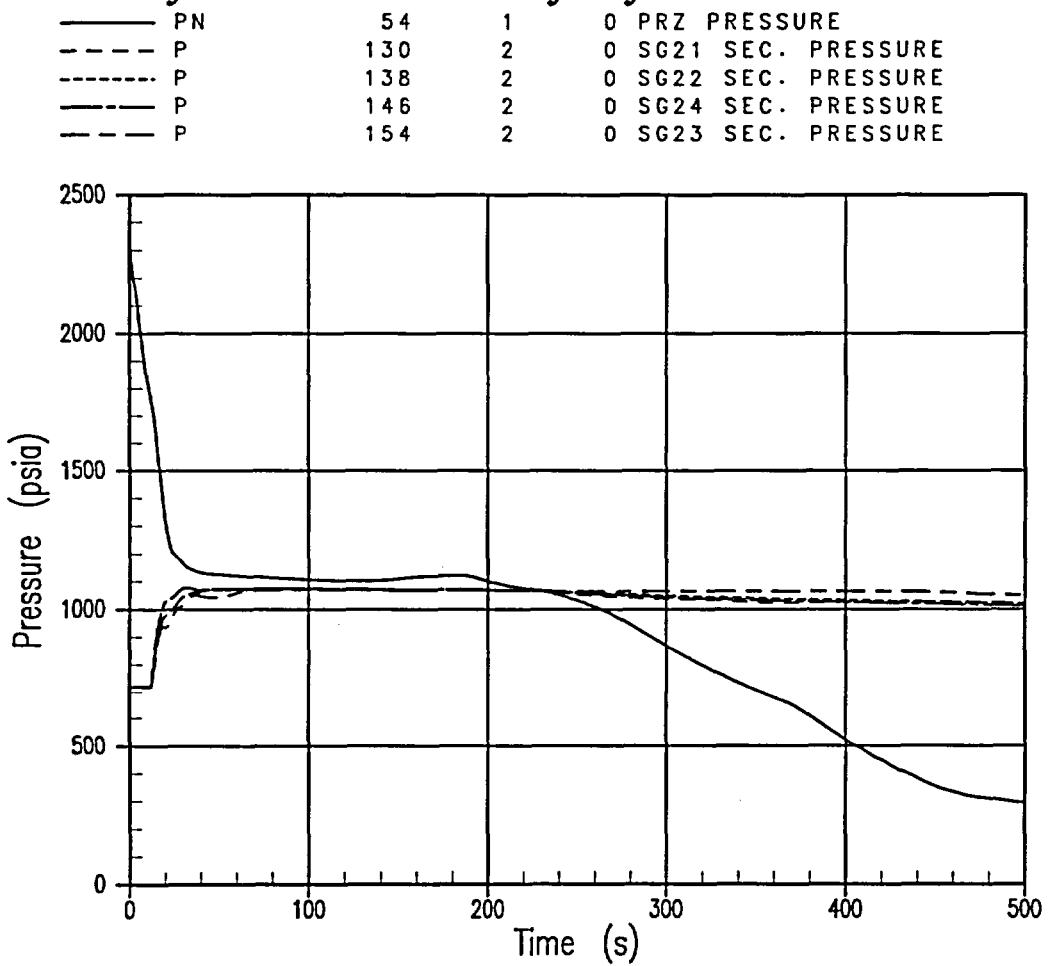


Figure 27-4-1. Primary and Secondary System Pressures, 6-Inch Break With LOOP

Indian Point 2 BE SBLOCA Analysis
6-INCH CL BREAK WITH LOOP
Core Collapsed Liquid Levels

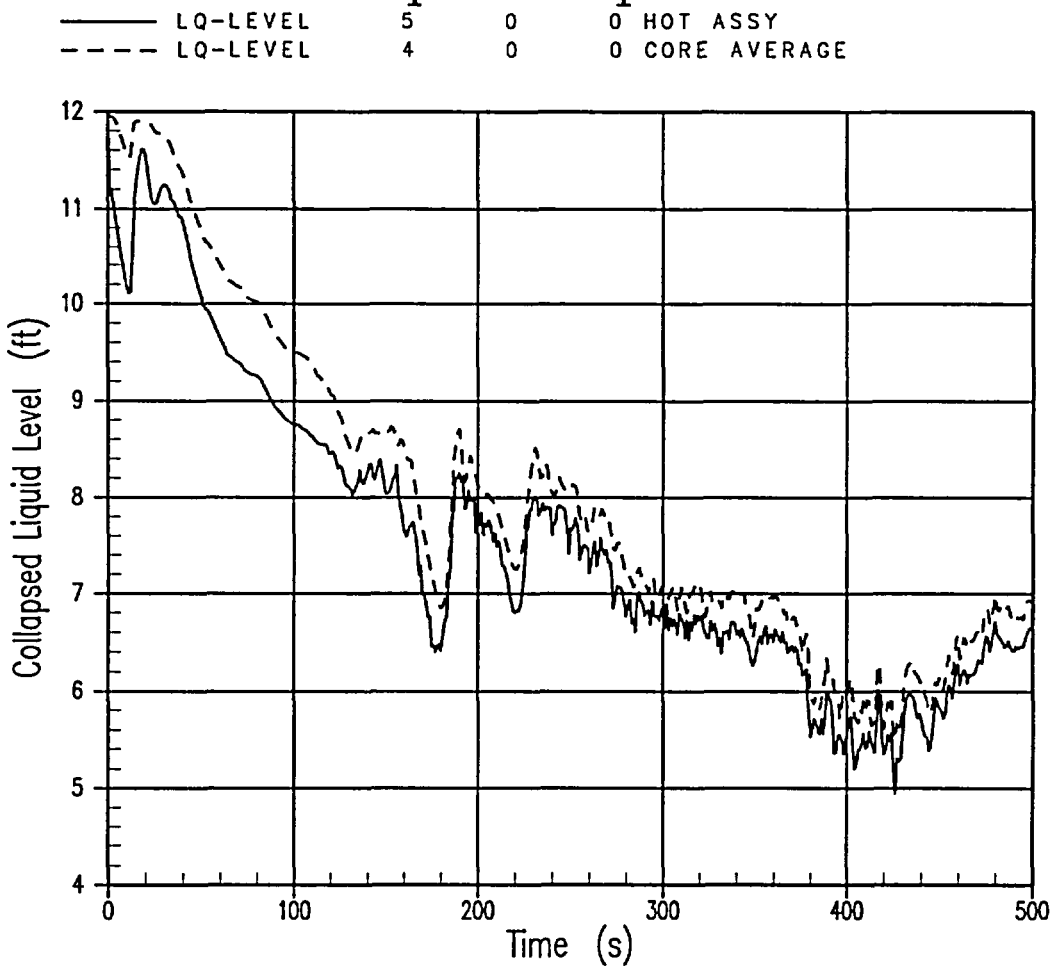


Figure 27-4-2. Core Collapsed Liquid Level, 6-Inch Break With LOOP

Indian Point 2 BE SBLOCA Analysis
 6-INCH CL BREAK WITH LOOP
 Break Flowrate and Void Fraction

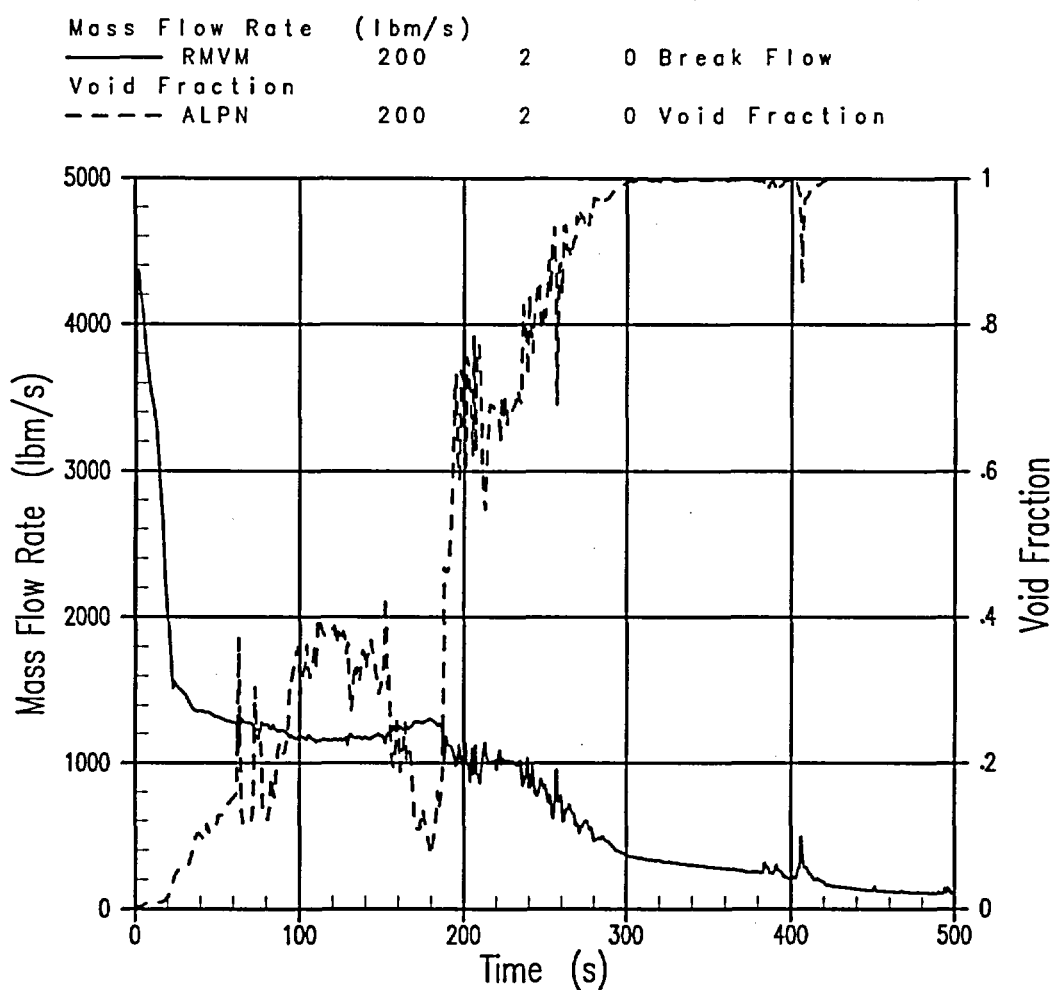
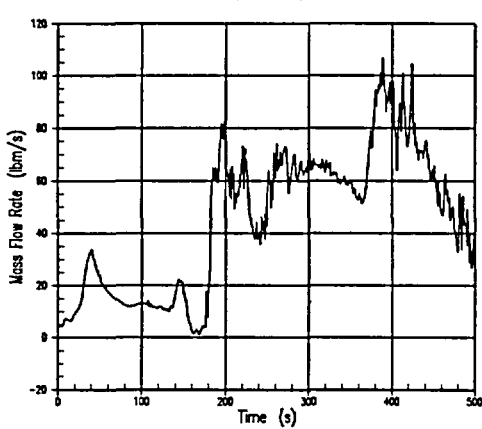


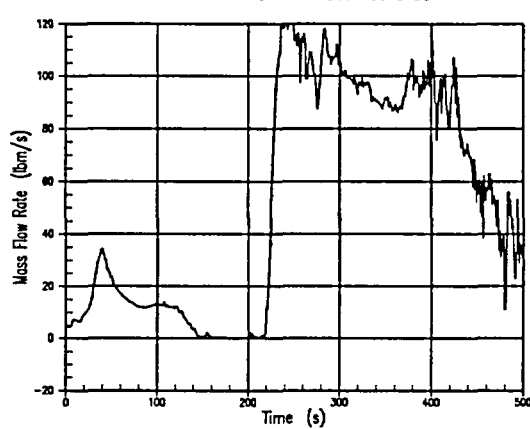
Figure 27-4-3. Break Flowrate and Void Fraction, 6-Inch Break With LOOP

Indian Point 2 BE SBLOCA Analysis
6-INCH CL BREAK WITH LOOP
Loop 21 Steam Flow



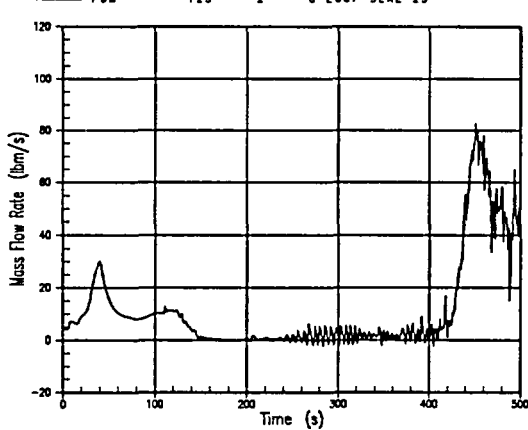
A. Loop 21 Loop Seal Steam Flow

Indian Point 2 BE SBLOCA Analysis
6-INCH CL BREAK WITH LOOP
Loop 22 Steam Flow



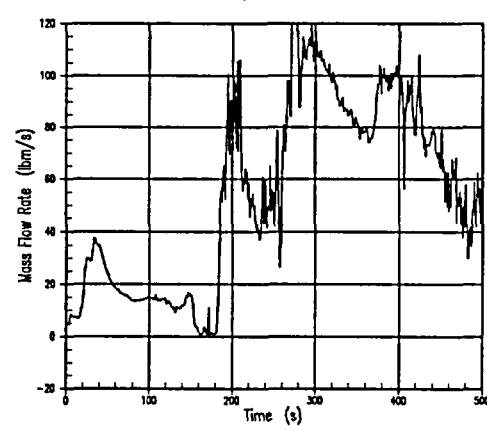
B. Loop 22 Loop Seal Steam Flow

Indian Point 2 BE SBLOCA Analysis
6-INCH CL BREAK WITH LOOP
Loop 23 Steam Flow



C. Loop 23 Loop Seal Steam Flow

Indian Point 2 BE SBLOCA Analysis
6-INCH CL BREAK WITH LOOP
Loop 24 Steam Flow



D. Loop 24 Loop Seal Steam Flow

Figure 27-4-4. Loop Seal Steam Flows, 6-Inch Break With LOOP

Indian Point 2 BE SBLOCA Analysis
6-INCH CL BREAK WITH LOOP
Reactor Vessel Mass

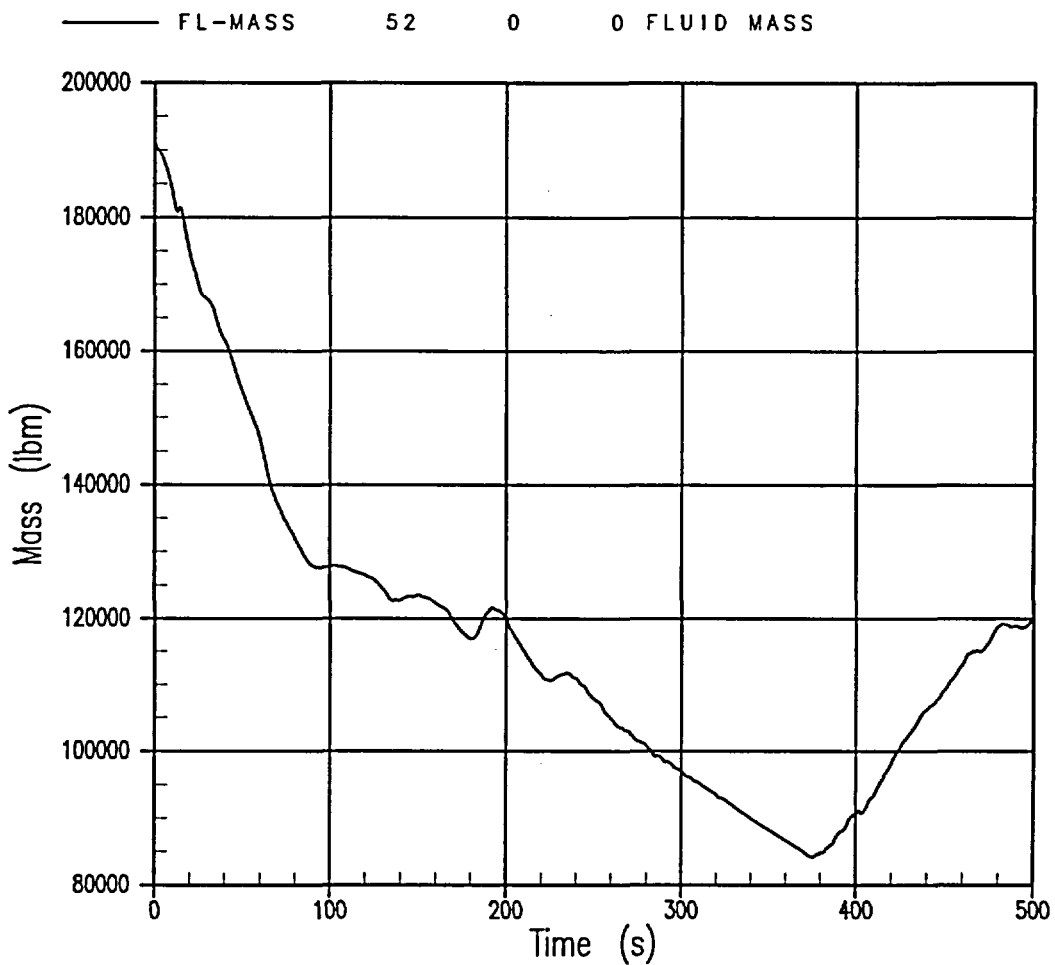


Figure 27-4-5. Reactor Vessel Mass, 6-Inch Break with LOOP

Indian Point 2 BE SBLOCA Analysis
6-INCH CL BREAK WITH LOOP
Peak Cladding Temperature

— PCT 1 0 0 PEAK CLADDING TEMP.

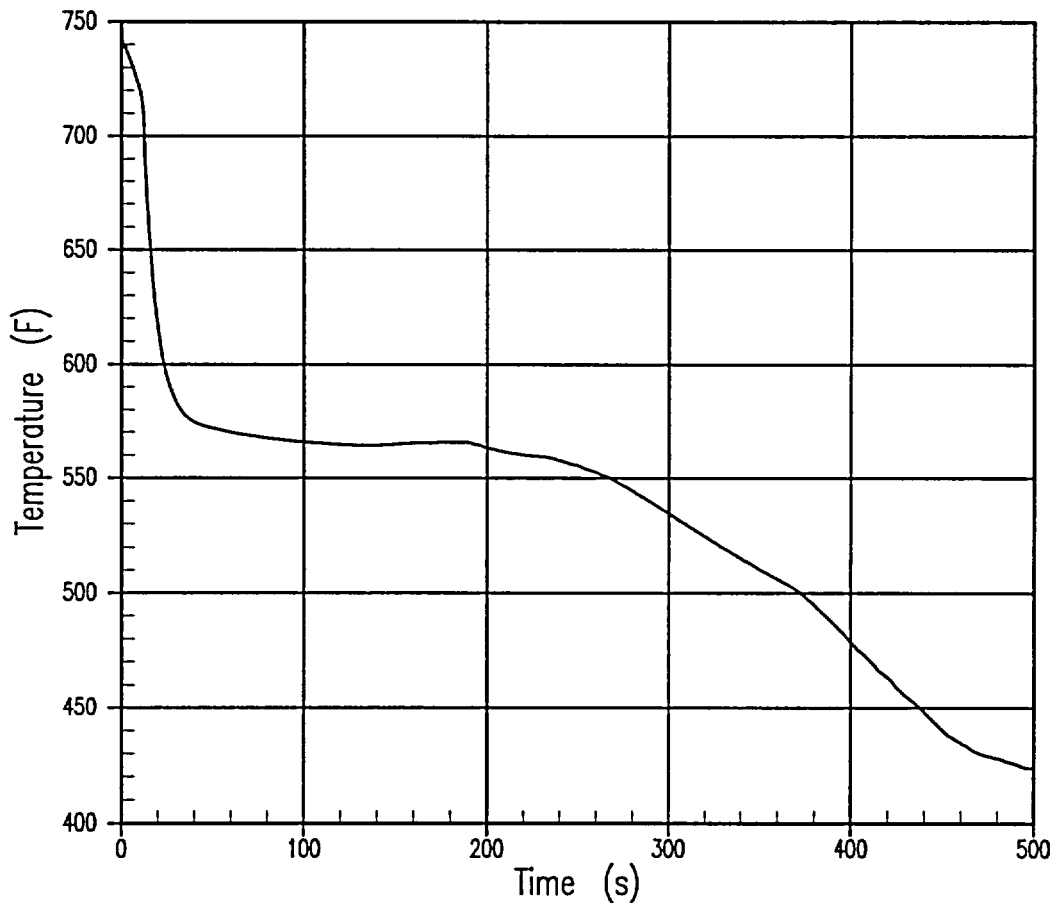


Figure 27-4-6. PCT, 6-Inch Break With LOOP

Indian Point 2 BE SBLOCA Analysis
6-INCH CL BREAK WITH LOOP
Total Safety Injection Flow

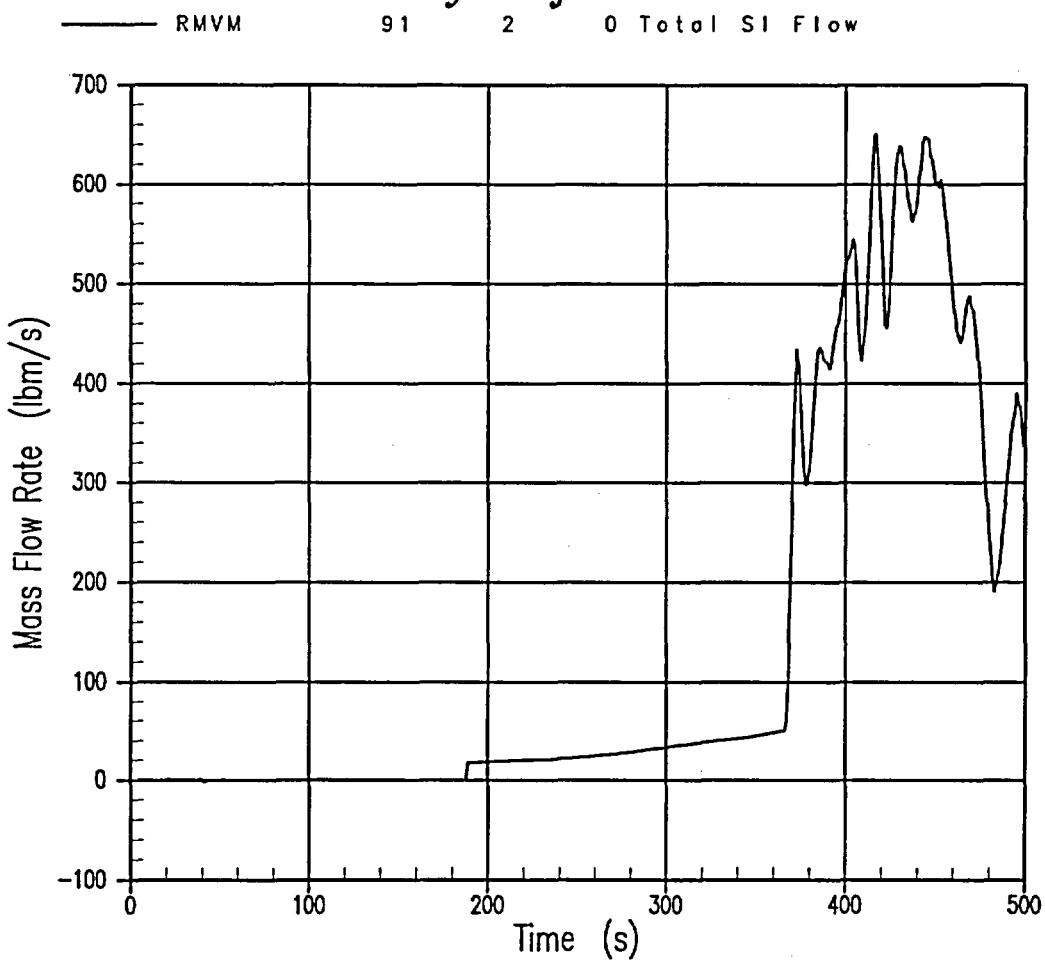


Figure 27-4-7. Total Safety Injection Flow to RCS, 6-Inch Break With LOOP

27-5 10-Inch Cold Leg Break With LOOP

The sequence of events and overall behavior for the 10-inch equivalent diameter cold leg break departs from that observed in the smaller breaks. In the 10-inch break, the core uncover follows a continuous depressurization of the primary side, and loop seal clearance is not as distinct an event as for smaller breaks. For the 10-inch and larger sized breaks, the break is of sufficient size that the core becomes almost completely uncovered. Figures 27-5-1 to 27-5-7 provide a summary of the transient.

The 10-inch break rapidly depressurizes to a pressure near the MSSV setpoint, and the depressurization rate then slows for approximately 60 seconds. The reactor trip signal occurs at 6.3 seconds. The steam generator secondaries are isolated shortly following reactor trip, and the steam generator secondary pressure increases but does not reach the MSSV setpoint.

Loop seal clearance is not as distinctive in the 10-inch break as in smaller breaks because of flashing in the RCS. The loop seal flow includes a significant vapor component from nearly the start of the transient. The loop seal steam flow through the broken loop begins to increase rapidly at 67 seconds. At this time, the collapsed liquid level in the loop seal has dropped to the elevation of the top of the horizontal section. The other three loop seals begin to clear fully 10 to 15 seconds later, and all remain clear for the remainder of the transient. The break flow quality increases and becomes primarily steam flow.

A single core heatup is observed in the 10-inch break, which begins at 136 seconds. The heatup rate is rapid and reaches a PCT of 652°F at 154 seconds. The core heatup turns around after the accumulators begin to inject; it is terminated by accumulator injection, although there is a longer delay between the start of accumulator injection and the core temperature maximum than for the smaller breaks. This is due to the additional time required to fill the downcomer, which becomes largely voided at this break size.

The transient calculation was ended at 198 seconds. At this time, the total safety injection flow exceeded the break flow and the accumulators continued to inject.

Indian Point 2 BE SBLOCA Analysis
10-INCH CL BREAK WITH LOOP
Primary and Secondary System Pressures

— PN	54	1	0 PRZ PRESSURE
- - - P	130	2	0 SG21 SEC. PRESSURE
- - - P	138	2	0 SG22 SEC. PRESSURE
- - - P	146	2	0 SG24 SEC. PRESSURE
- - - P	154	2	0 SG23 SEC. PRESSURE

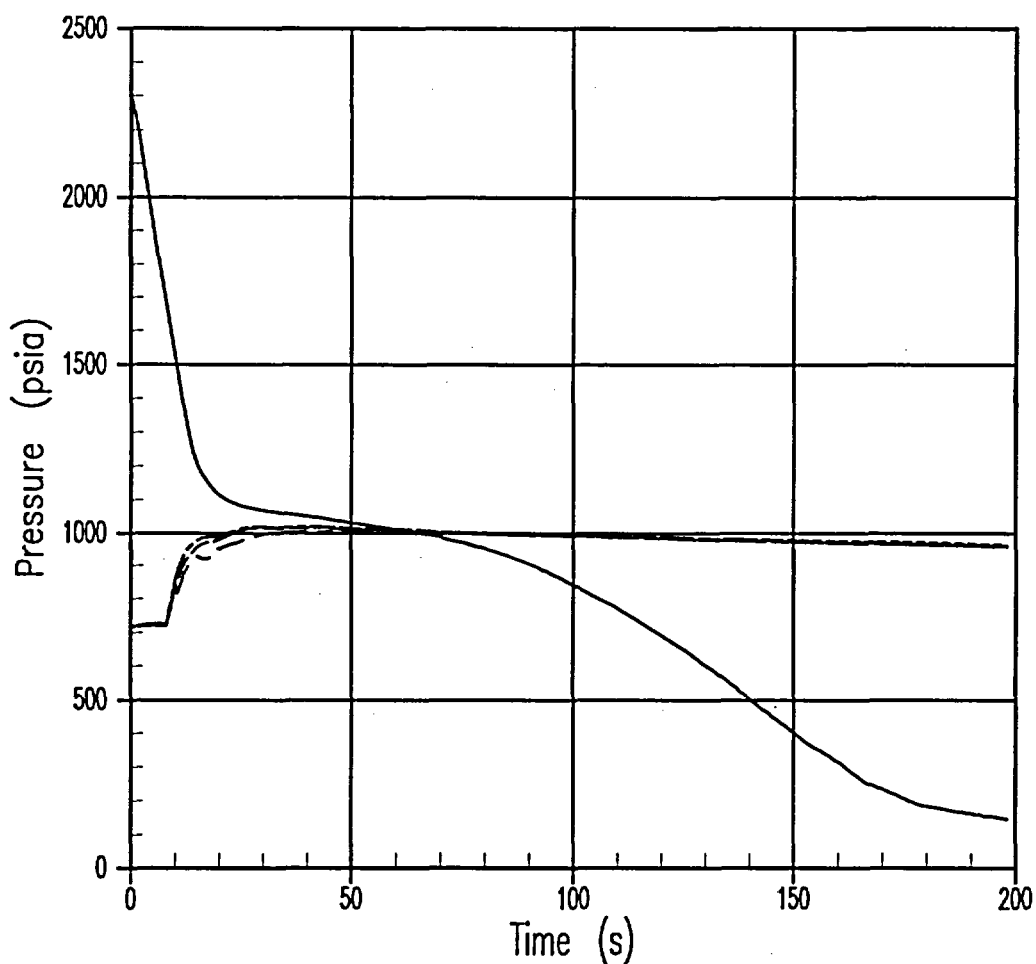


Figure 27-5-1. Primary and Secondary System Pressures, 10-Inch Break With LOOP

Indian Point 2 BE SBLOCA Analysis
10-INCH CL BREAK WITH LOOP
Core Collapsed Liquid Levels

— LQ-LEVEL 5 0 0 HOT ASSY
---- LQ-LEVEL 4 0 0 CORE AVERAGE

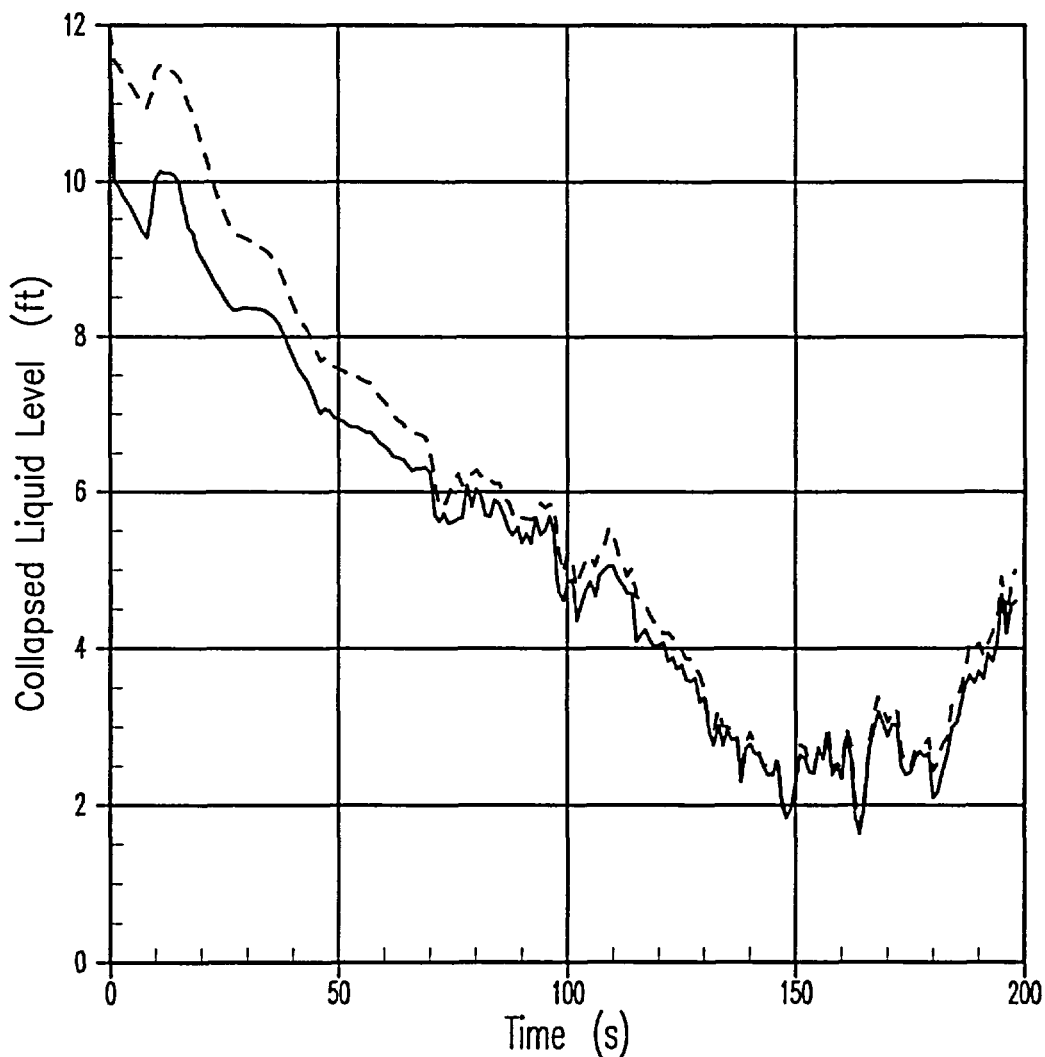


Figure 27-5-2. Core Collapsed Liquid Level, 10-Inch Break With LOOP

Indian Point 2 BE SBLOCA Analysis
 10-INCH CL BREAK WITH LOOP
 Break Flowrate and Void Fraction

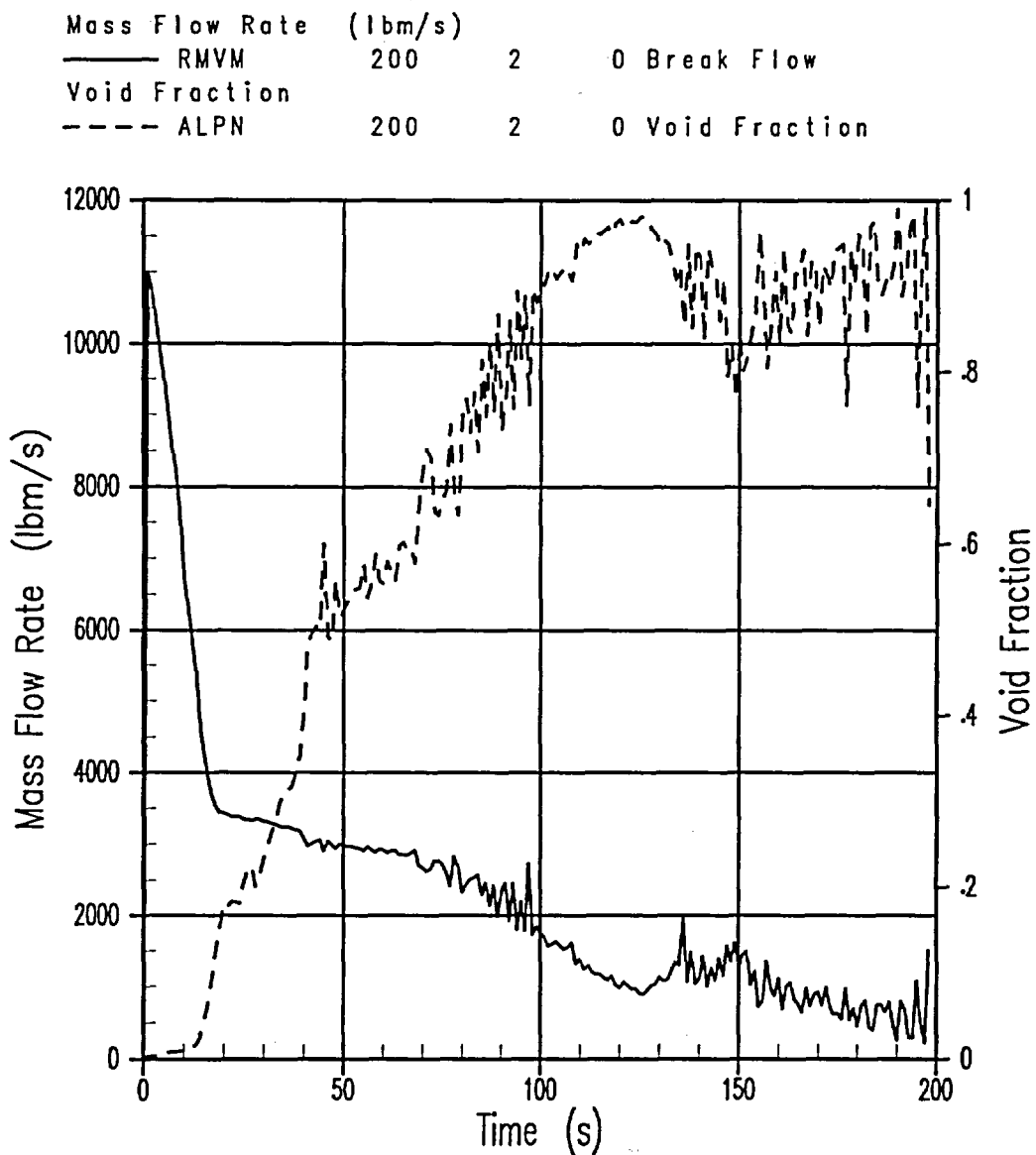
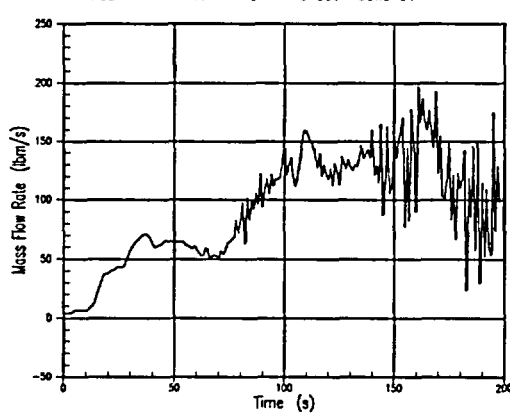


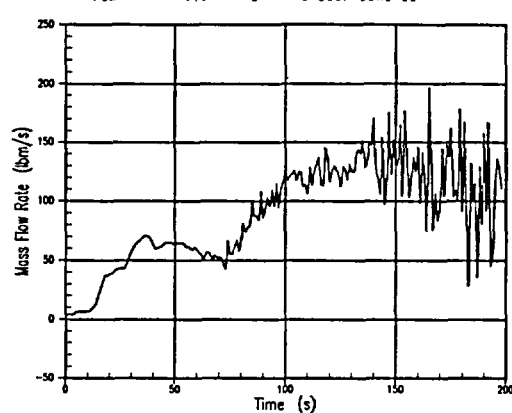
Figure 27-5-3. Break Flowrate and Void Fraction, 10-Inch Break With LOOP

Indian Point 2 BE SBLOCA Analysis
10-INCH CL BREAK WITH LOOP
Loop 21 Steam Flow



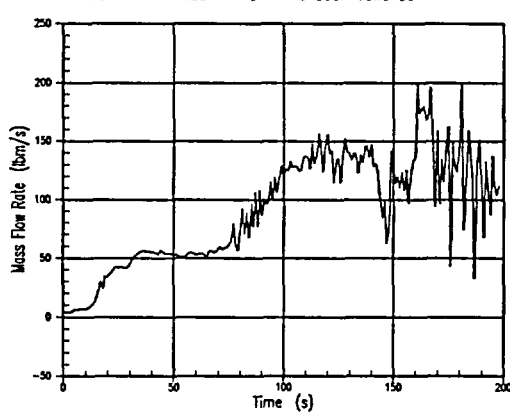
A. Loop 21 Loop Seal Steam Flow

Indian Point 2 BE SBLOCA Analysis
10-INCH CL BREAK WITH LOOP
Loop 22 Steam Flow



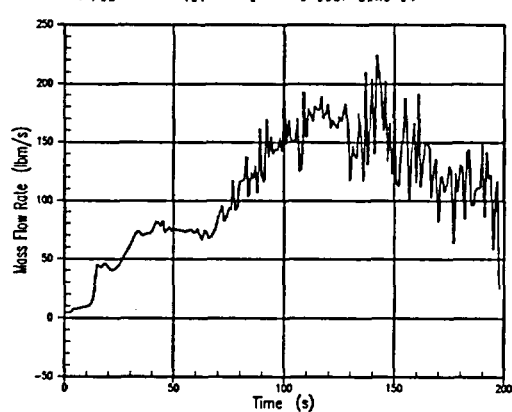
B. Loop 22 Loop Seal Steam Flow

Indian Point 2 BE SBLOCA Analysis
10-INCH CL BREAK WITH LOOP
Loop 23 Steam Flow



C. Loop 23 Seal Steam Flow

Indian Point 2 BE SBLOCA Analysis
10-INCH CL BREAK WITH LOOP
Loop 24 Steam Flow



D. Loop 24 Loop Seal Steam Flow

Figure 27-5-4. Loop Seal Steam Flows, 10-Inch Break With LOOP

Indian Point 2 BE SBLOCA Analysis
10-INCH CL BREAK WITH LOOP
Peak Cladding Temperature

— PCT 1 0 0 PEAK CLADDING TEMP.

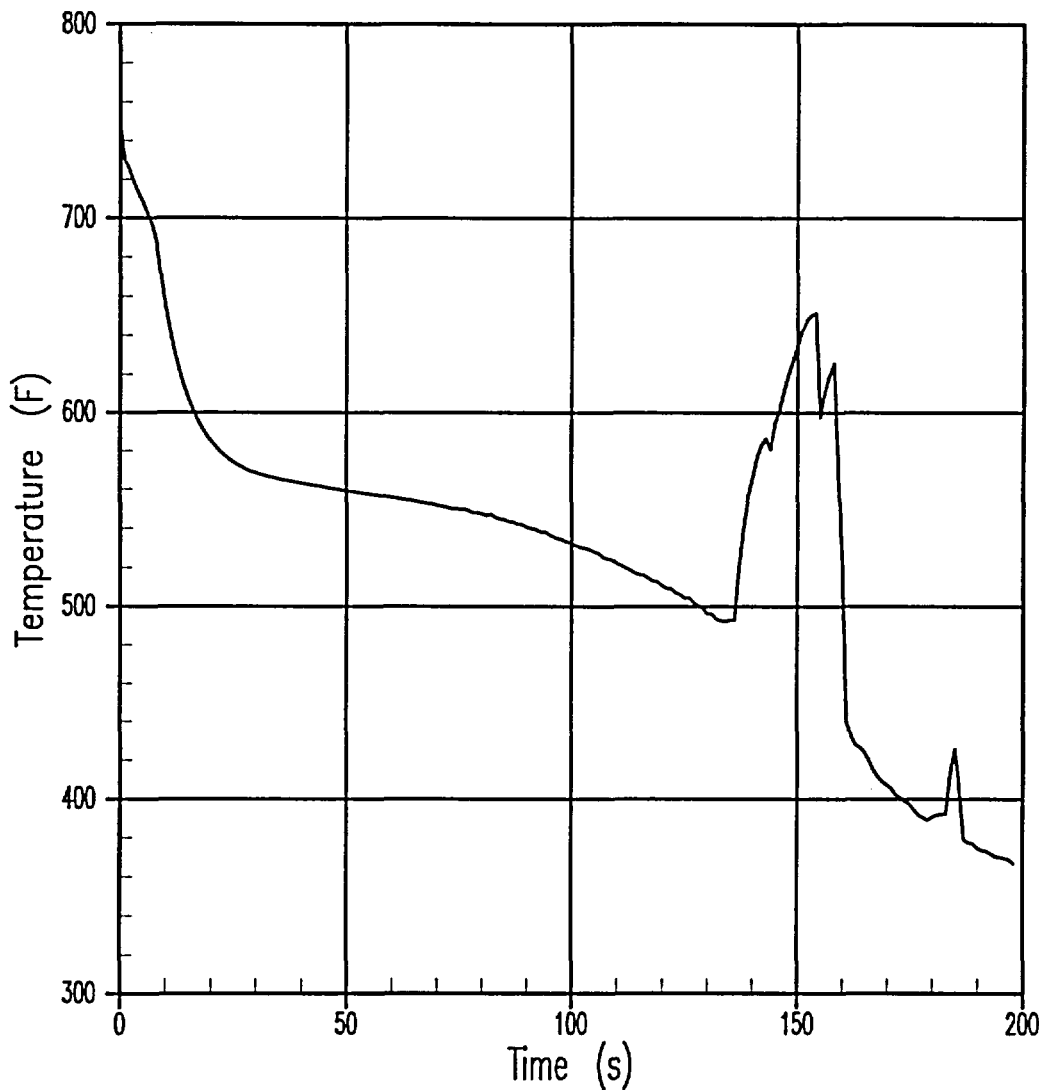


Figure 27-5-5. Reactor Vessel Mass, 10-Inch Break With LOOP

Indian Point 2 BE SBLOCA Analysis
10-INCH CL BREAK WITH LOOP
Reactor Vessel Mass

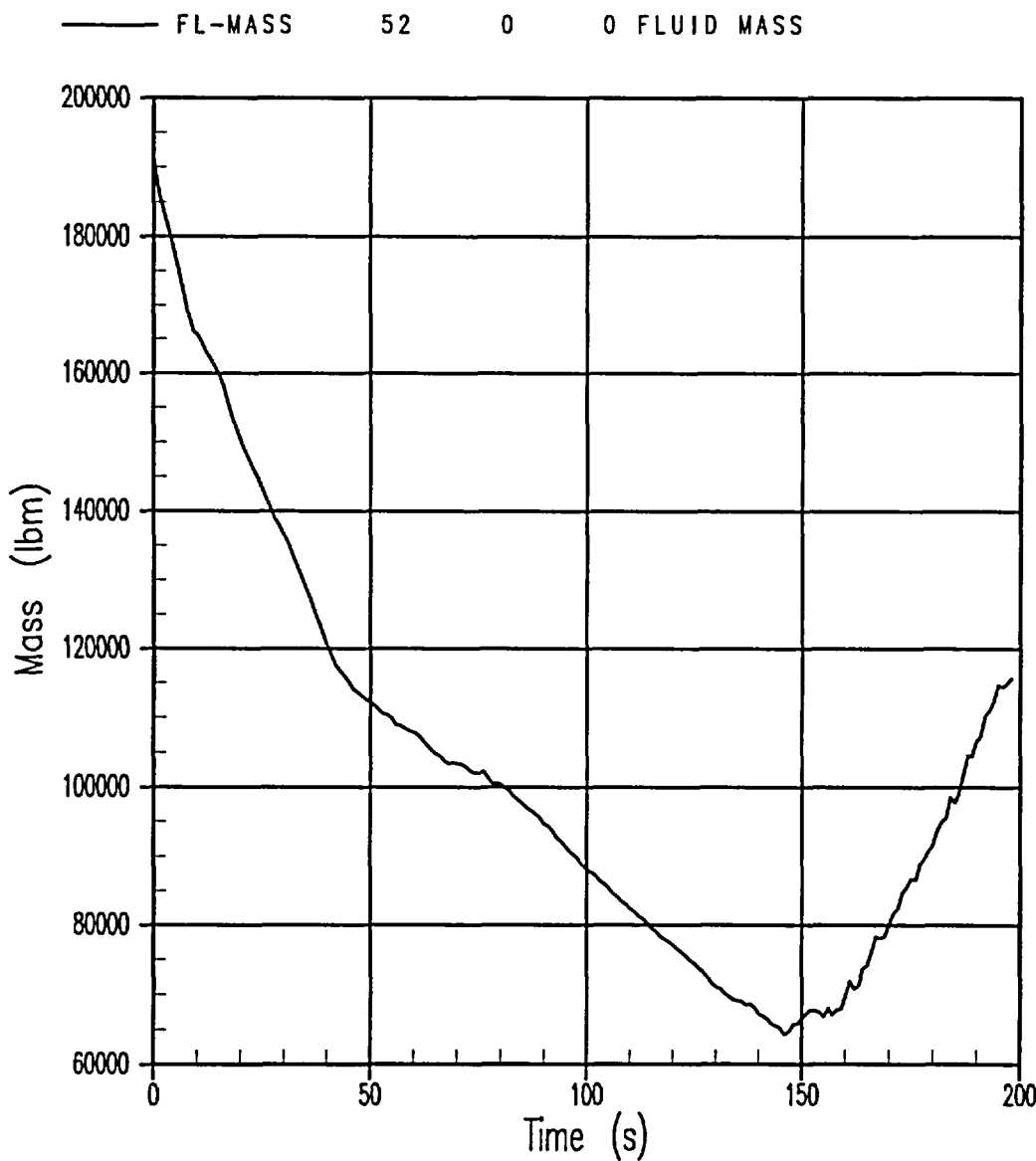


Figure 27-5-6. PCT, 10-Inch Break With LOOP

Indian Point 2 BE SBLOCA Analysis
10-INCH CL BREAK WITH LOOP
Total Safety Injection Flow

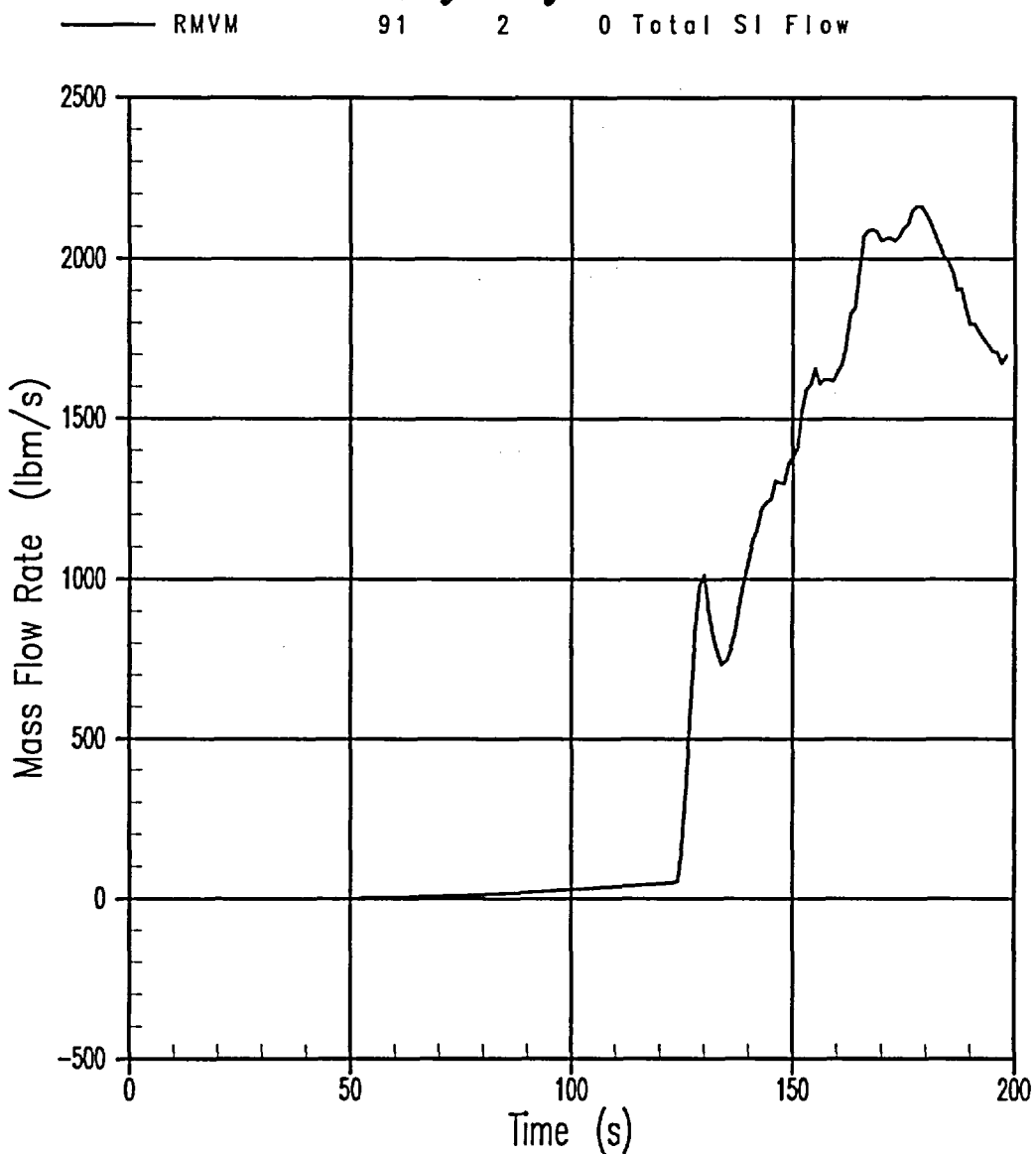


Figure 27-5-7. Total Safety Injection Flow to RCS, 10-Inch Break With LOOP

27-6 2.5-Inch Cold Leg Break with LOOP

The sequence of events and overall behavior for the 2.5-inch equivalent diameter cold leg break is similar to that observed in the 3-inch break. The 2.5-inch break is a relatively slow transient and is similar to the 3-inch break as it has a core uncover with significant heatup.

Figures 27-6-1 to 27-6-7 provide a summary of the transient.

The 2.5-inch break depressurizes to the reactor trip setpoint, and then to the "S" signal setpoint. The depressurization rate slows when the hot leg saturation pressure is reached. The reactor trip signal occurs at 50.4 seconds. After isolation, the steam generator secondary pressure increases rapidly until it reaches the MSSV setpoint.

Similar to the 3-inch break, loop seal clearance occurs in only one loop in the 2.5 inch break. The steam flow through the cleared loop is adequate to maintain a relatively low pressure above the core. The loop seal remains clear for the remainder of the transient; the break flow quality increases and becomes primarily steam flow, as shown in Figure 27-6-3.

A single core heatup is observed in the 2.5-inch break, which begins at 2080 seconds. The heatup rate is relatively slow until a PCT of 832°F is reached at 2600 seconds. The SI flow exceeds break flow prior to accumulator injection, solely due to the pumped SI flow. Core quench is complete by 2977 seconds.

Indian Point 2 BE SBLOCA Analysis

2.5-IN CL BREAK WITH LOOP

Primary and Secondary System Pressures

— PN	54	1	0 PRZ PRESSURE
- - - P	130	2	0 SG21 SEC. PRESSURE
- - - P	138	2	0 SG22 SEC. PRESSURE
- - - P	146	2	0 SG24 SEC. PRESSURE
- - - P	154	2	0 SG23 SEC. PRESSURE

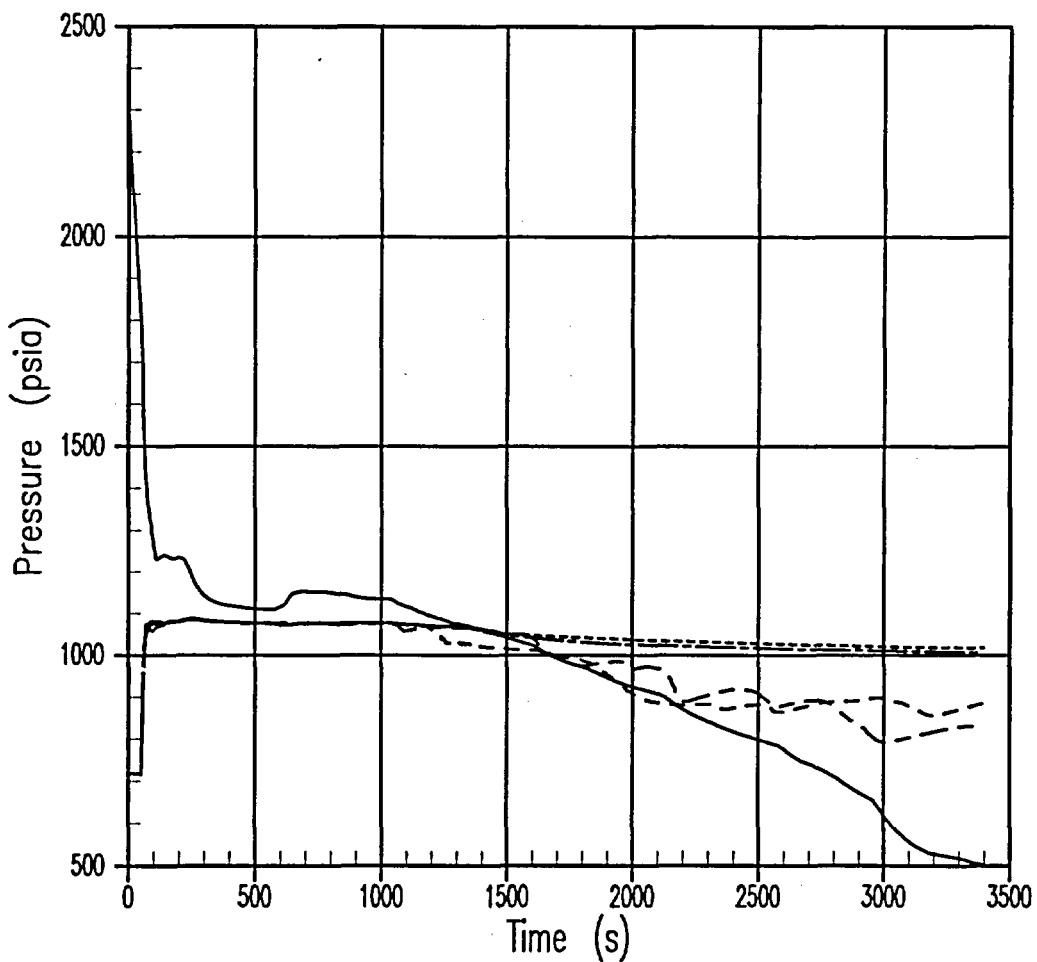


Figure 27-6-1. Primary and Secondary System Pressures, 2.5-Inch Break With LOOP

Indian Point 2 BE SBLOCA Analysis

2.5-IN CL BREAK WITH LOOP

Core Collapsed Liquid Levels

— LQ-LEVEL 5 0 0 HOT ASSY
- - - LQ-LEVEL 4 0 0 CORE AVERAGE

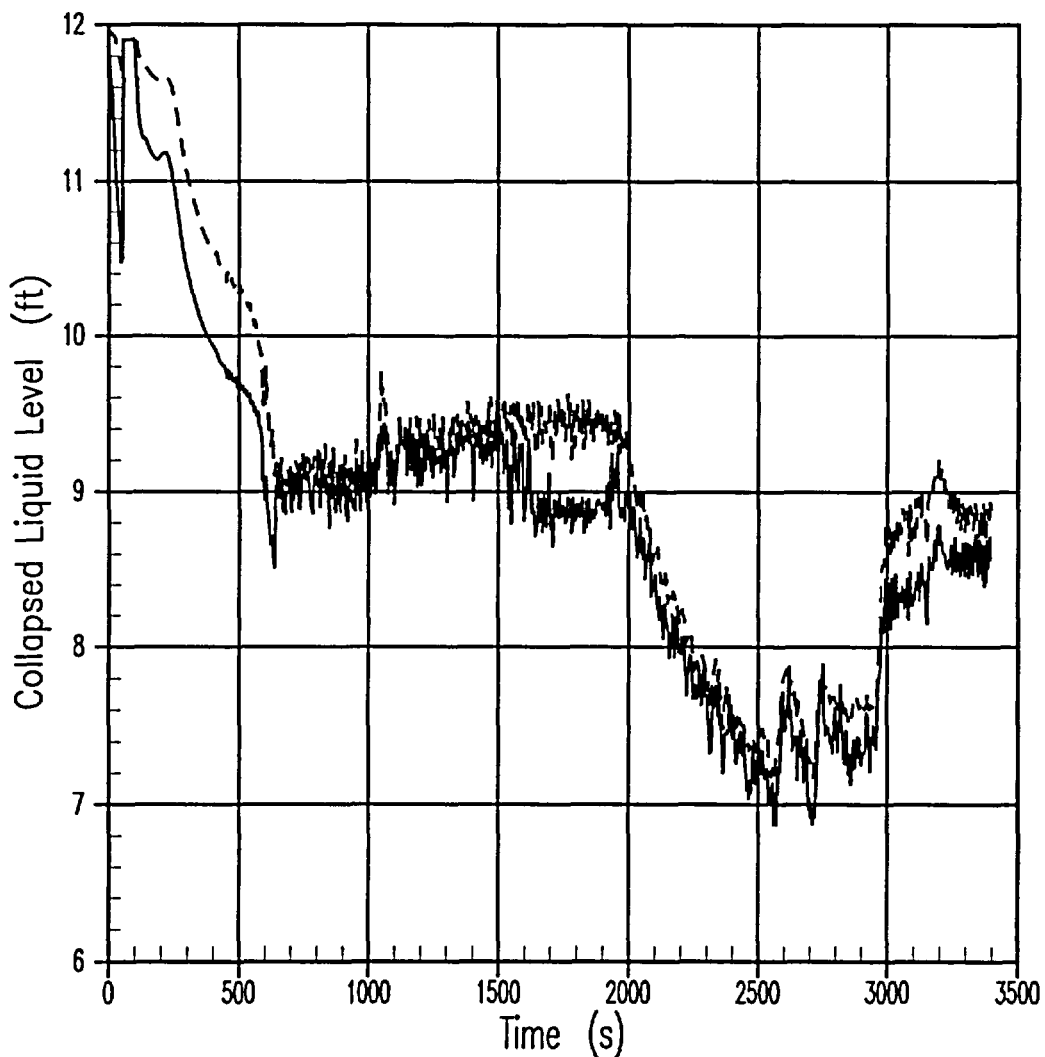


Figure 27-6-2. Core Collapsed Liquid Level, 2.5-Inch Break With LOOP

Indian Point 2 BE SBLOCA Analysis
2.5-IN CL BREAK WITH LOOP
Break Flowrate and Void Fraction

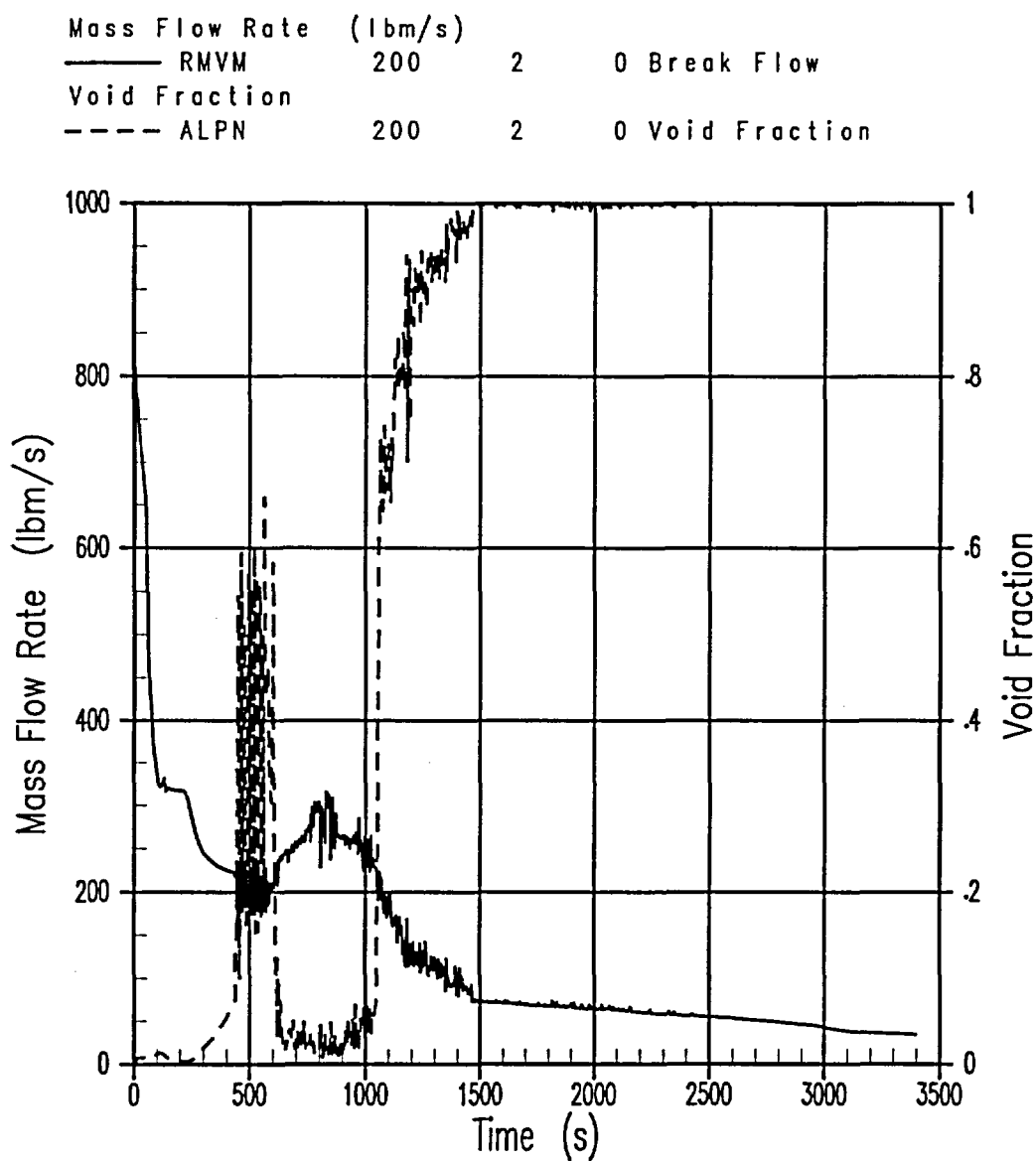
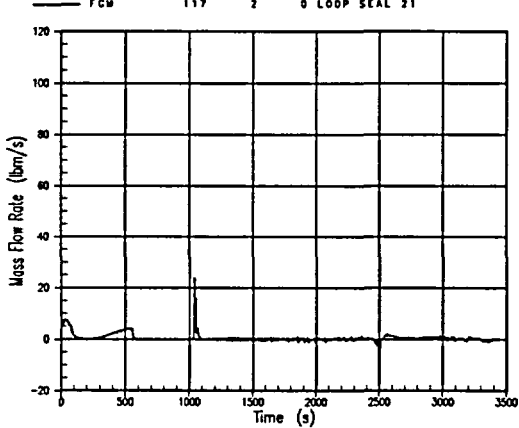


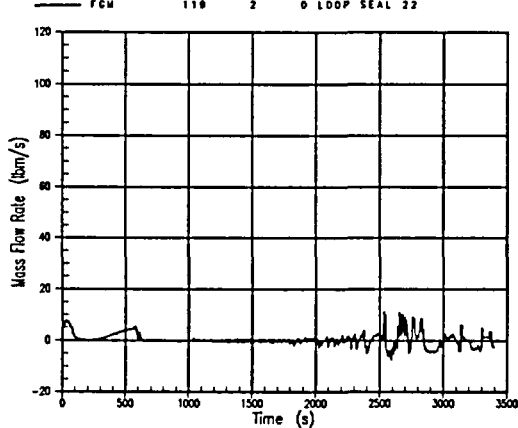
Figure 27-6-3. Break Flowrate and Void Fraction, 2.5-Inch Break With LOOP

Indian Point 2 BE SBLOCA Analysis
2.5-IN CL BREAK WITH LOOP
Loop 21 Steam Flow



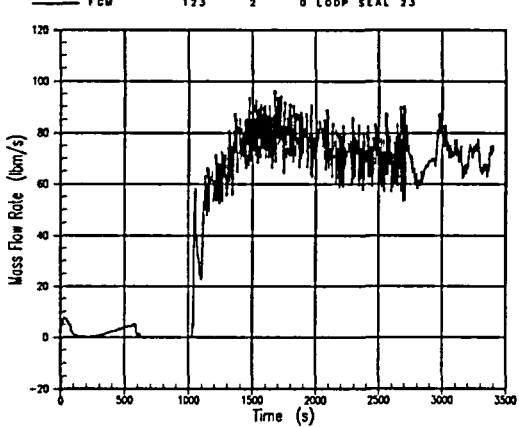
A. Loop 21 Loop Seal Steam Flow

Indian Point 2 BE SBLOCA Analysis
2.5-IN CL BREAK WITH LOOP
Loop 22 Steam Flow



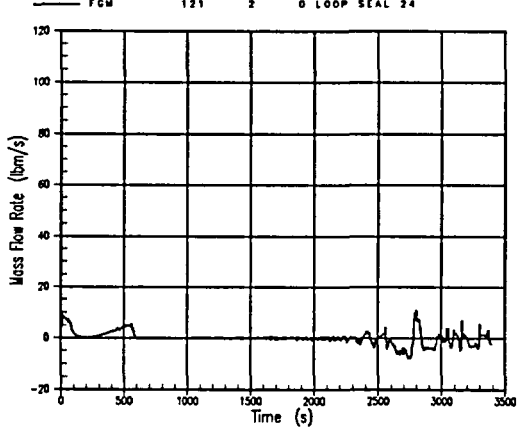
B. Loop 22 Loop Seal Steam Flow

Indian Point 2 BE SBLOCA Analysis
2.5-IN CL BREAK WITH LOOP
Loop 23 Steam Flow



C. Loop 23 Loop Seal Steam Flow

Indian Point 2 BE SBLOCA Analysis
2.5-IN CL BREAK WITH LOOP
Loop 24 Steam Flow



D. Loop 24 Loop Seal Steam Flow

Figure 27-6-4. Loop Seal Steam Flows, 2.5-Inch Break With LOOP

Indian Point 2 BE SBLOCA Analysis
2.5-IN CL BREAK WITH LOOP
Reactor Vessel Mass

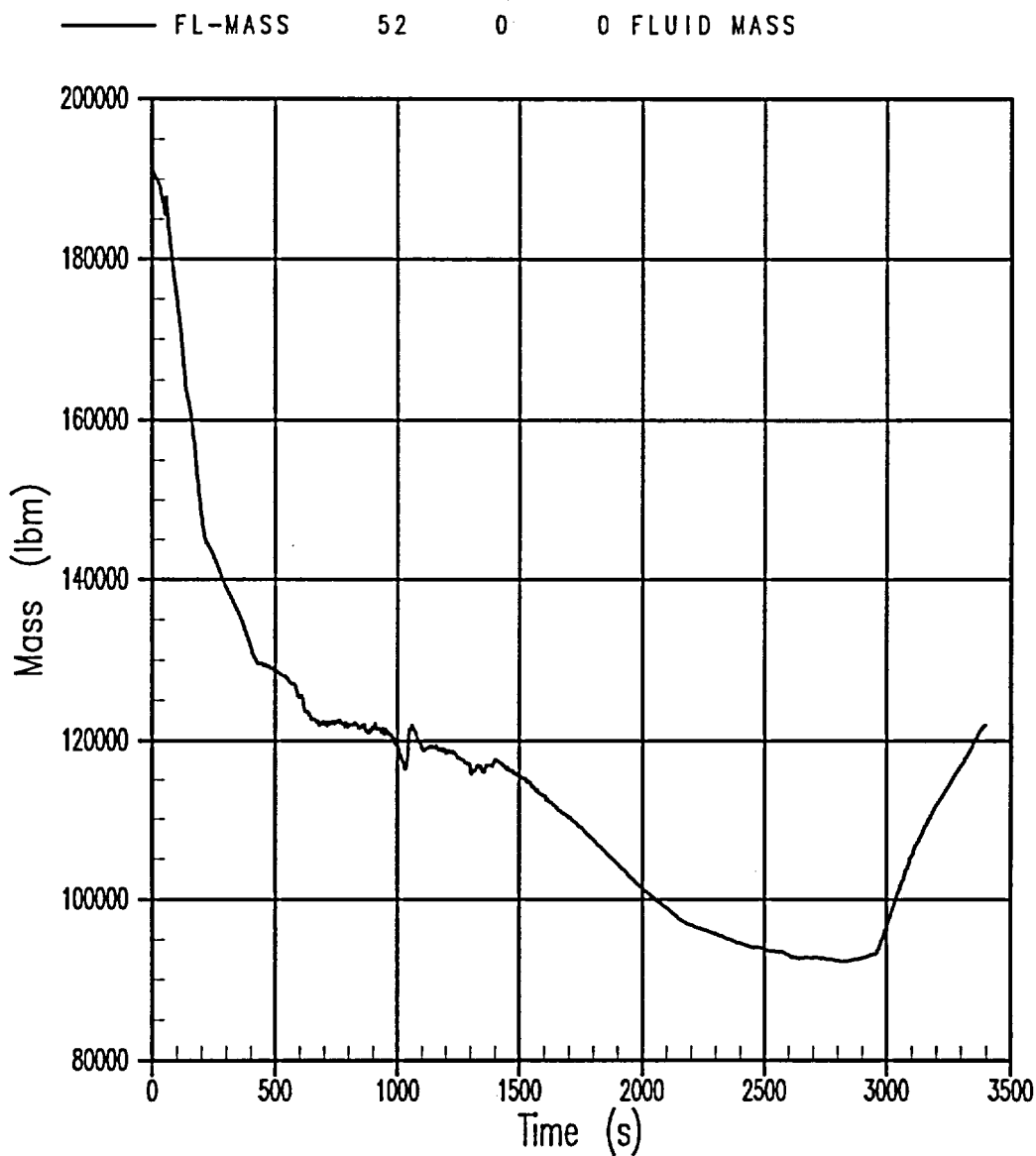


Figure 27-6-5. Reactor Vessel Mass, 2.5-Inch Break With LOOP

Indian Point 2 BE SBLOCA Analysis
2.5-IN CL BREAK WITH LOOP
Peak Cladding Temperature

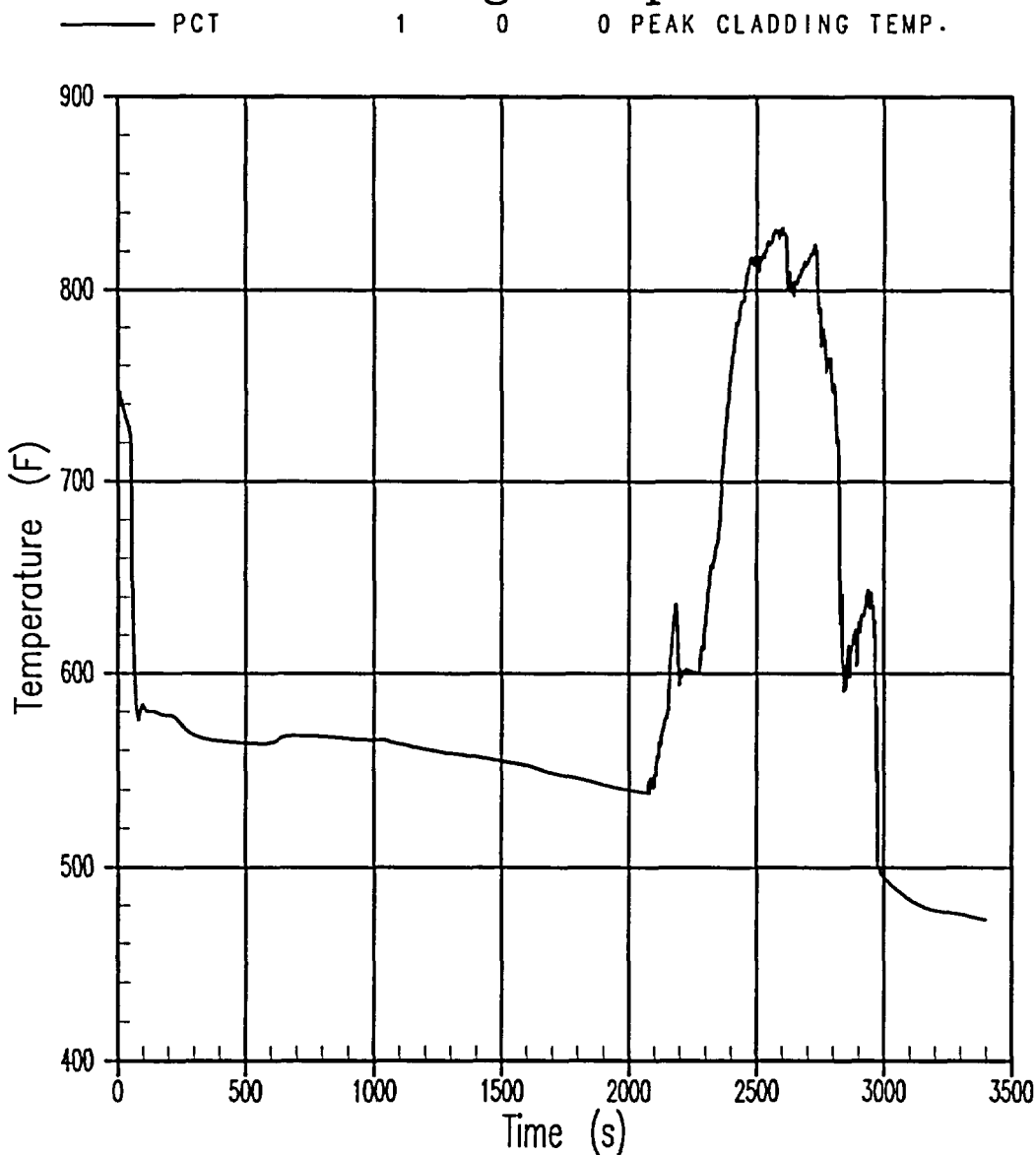


Figure 27-6-6. PCT, 2.5-Inch Break With LOOP

Indian Point 2 BE SBLOCA Analysis

2.5-IN CL BREAK WITH LOOP

Total Safety Injection Flow

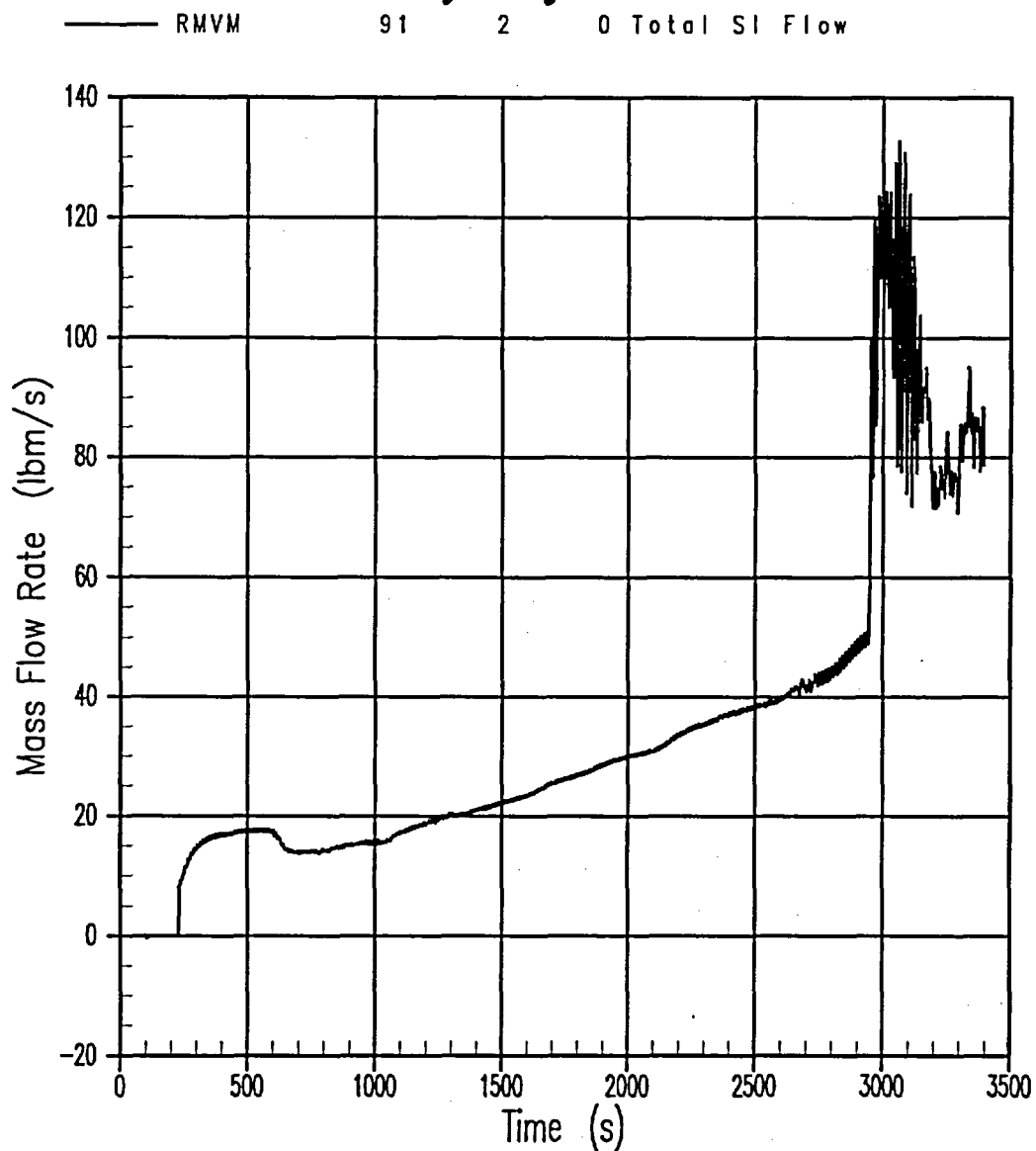


Figure 27-6-7. Total Safety Injection Flow to RCS, 2.5-Inch Break With LOOP

27-7 3.5-Inch Cold Leg Break With LOOP

Figures 27-7-1 to 27-7-7 provide a summary of the 3.5-inch cold leg break transient. The RCPs continue to be powered from the generator until 30 seconds have elapsed after reactor trip; at that time, the RCPs begin to coast down.

During the blowdown phase, the 3.5-inch break depressurizes to the saturation pressure corresponding to the core outlet temperature. A reactor trip signal occurs at 26.5 seconds as the pressurizer pressure reaches the setpoint. A safety injection signal occurs at 30.6 seconds. Steam generator isolation occurs following reactor trip, and the steam generator secondary pressure increases rapidly to the MSSV setpoint. After the MSSVs open, steam flow through the safety valves maintains the secondary pressure near the MSSV setpoint. The primary side continues to depressurize rapidly after core shutdown to a pressure approximately 40 to 80 psi higher than the MSSV setpoint.

The loop seals begin to clear at 536 seconds, and the break flow quality increases thereafter. Both Loop 21 and Loop 22 clear and provide a continuous steam flow to the break as illustrated in Figure 27-7-4. The steam flow through each loop seal reaches a maximum flowrate of approximately 70 lbm/s shortly after loop seal clearance.

Figure 27-7-2 shows the core collapsed liquid level. The level exhibits close to a 1-foot increase at the time of loop seal clearance. This occurs because during the loop seal clearance, liquid that has been held in the loop seals and cold legs flows into the reactor vessel, decreasing the core void fraction.

Following loop seal clearance, the pumped safety injection flow is not sufficient to make up for the break flow and the vessel mass inventory continues to decrease. Core uncover and heatup begin at approximately 1096 seconds, and the hot rod cladding temperature increases slowly to a peak of 828 °F at 1312 seconds. The collapsed liquid level in the core reaches a minimum immediately before the PCT and begins to recover as the accumulators begin to inject. While accumulator flow is responsible for the core recovery, the minimum inventory is established by the pumped safety injection. Following accumulator injection, the collapsed level in the core increases steadily and the entire core quenches.

The transient calculation was ended when the core was quenched and the total safety injection flow exceeded the break flow.

Indian Point 2 BE SBLOCA Analysis

3.5-INCH CL BREAK WITH LOOP

Primary and Secondary System Pressures

— PN	54	1	0 PRZ PRESSURE
- - - P	130	2	0 SG21 SEC. PRESSURE
- - - P	138	2	0 SG22 SEC. PRESSURE
- - - P	146	2	0 SG24 SEC. PRESSURE
- - - P	154	2	0 SG23 SEC. PRESSURE

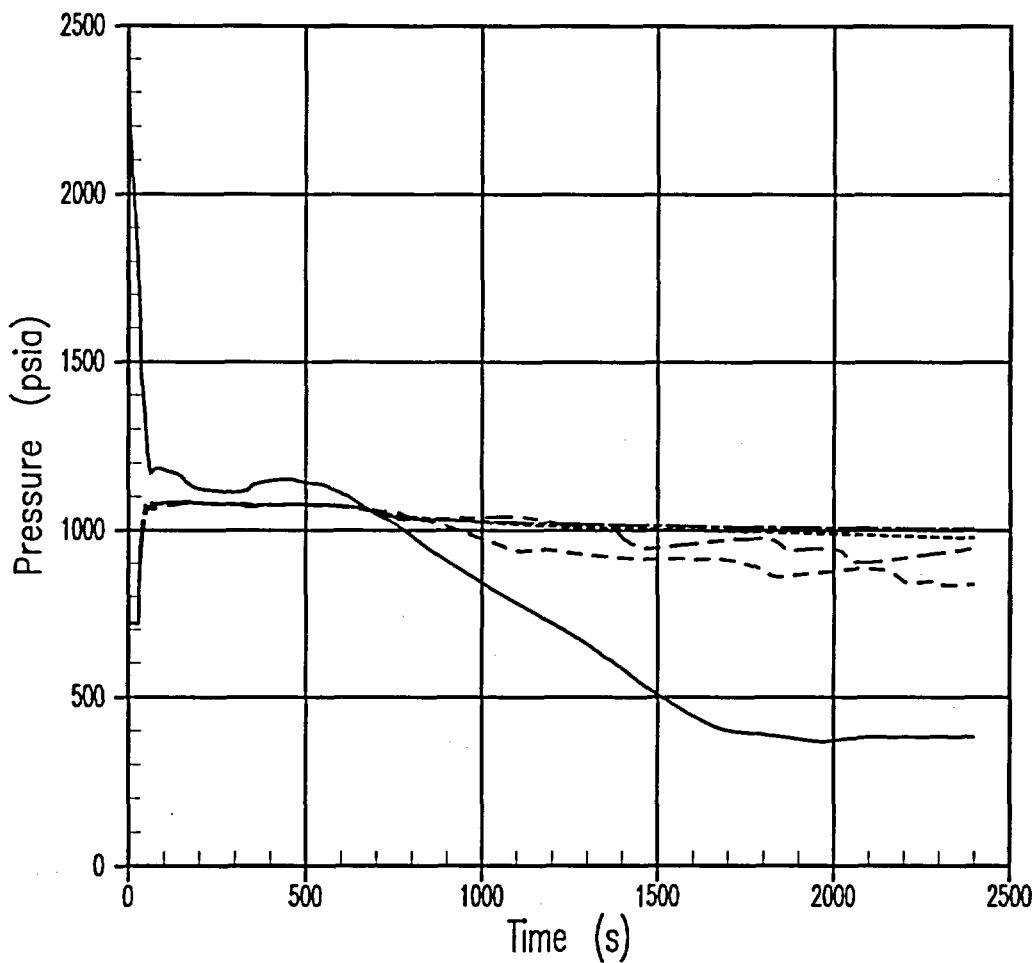


Figure 27-7-1. Primary and Secondary System Pressures, 3.5-Inch Break With LOOP

Indian Point 2 BE SBLOCA Analysis
3.5-INCH CL BREAK WITH LOOP
Core Collapsed Liquid Levels

— LQ-LEVEL 5 0 0 HOT ASSY
- - - LQ-LEVEL 4 0 0 CORE AVERAGE

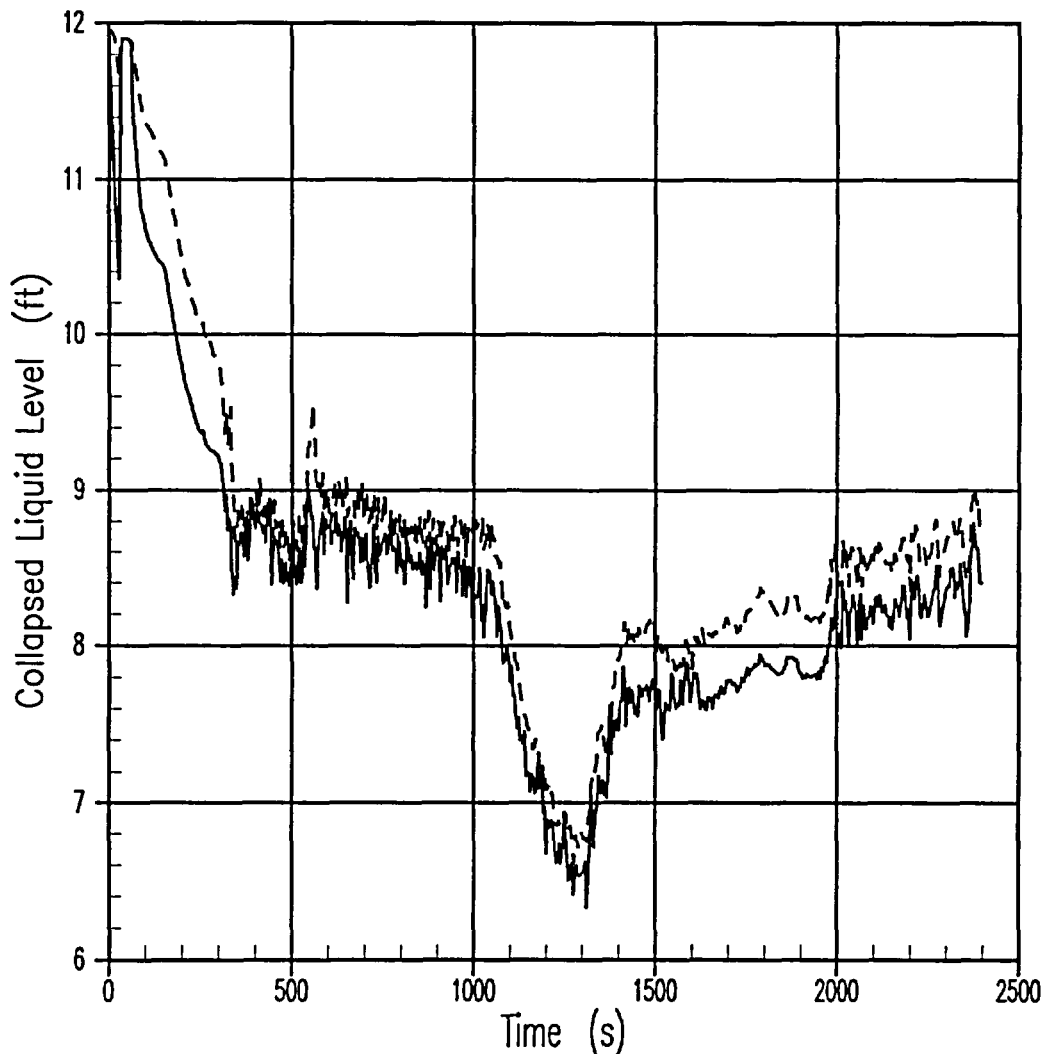


Figure 27-7-2. Core Collapsed Liquid Level, 3.5-Inch Break With LOOP

Indian Point 2 BE SBLOCA Analysis

3.5-INCH CL BREAK WITH LOOP

Break Flowrate and Void Fraction

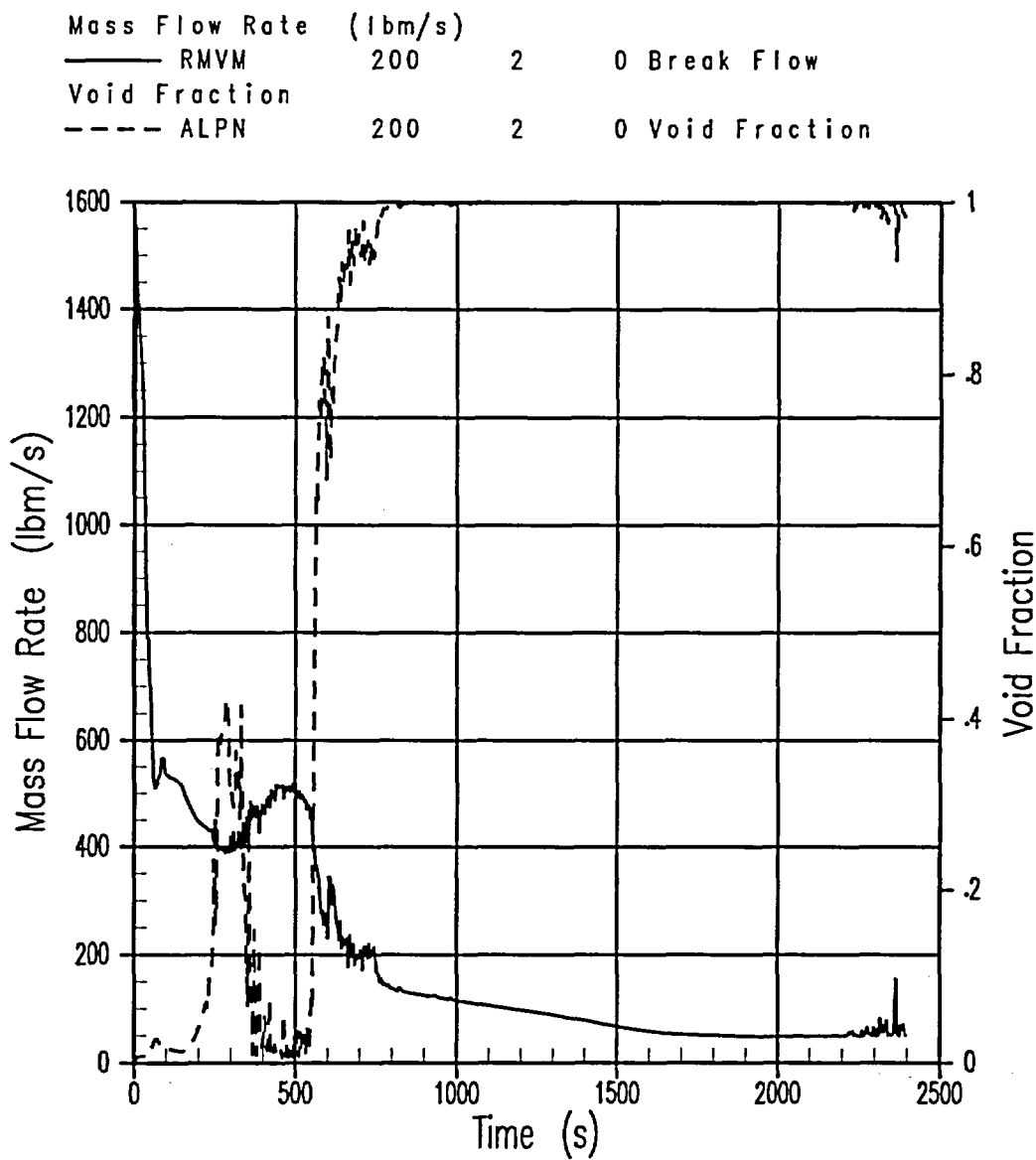
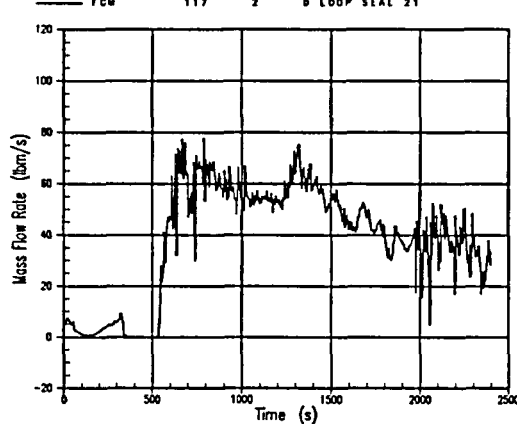


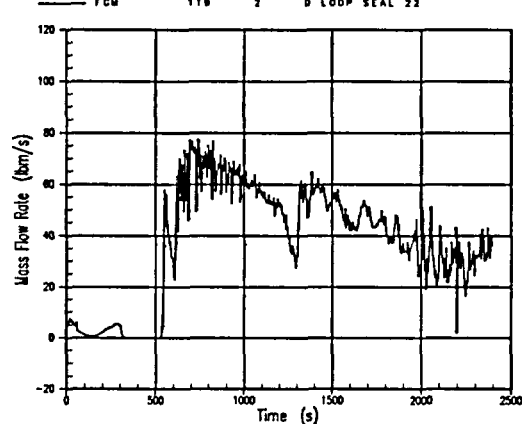
Figure 27-7-3. Break Flowrate and Void Fraction, 3.5-Inch Break With LOOP

Indian Point 2 BE SBLOCA Analysis
3.5-INCH CL BREAK WITH LOOP
Loop 21 Steam Flow



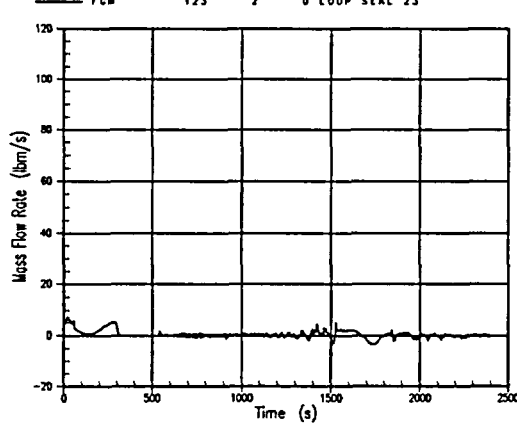
A. Loop 21 Seal Steam Flow

Indian Point 2 BE SBLOCA Analysis
3.5-INCH CL BREAK WITH LOOP
Loop 22 Steam Flow



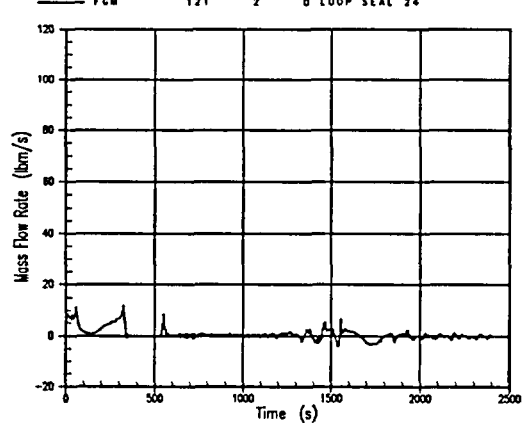
B. Loop 22 Seal Steam Flow

Indian Point 2 BE SBLOCA Analysis
3.5-INCH CL BREAK WITH LOOP
Loop 23 Steam Flow



C. Loop 23 Seal Steam Flow

Indian Point 2 BE SBLOCA Analysis
3.5-INCH CL BREAK WITH LOOP
Loop 24 Steam Flow



D. Loop 24 Seal Steam Flow

Figure 27-7-4. Loop Seal Steam Flows, 3.5-Inch Break With LOOP

Indian Point 2 BE SBLOCA Analysis
3.5-INCH CL BREAK WITH LOOP
Reactor Vessel Mass

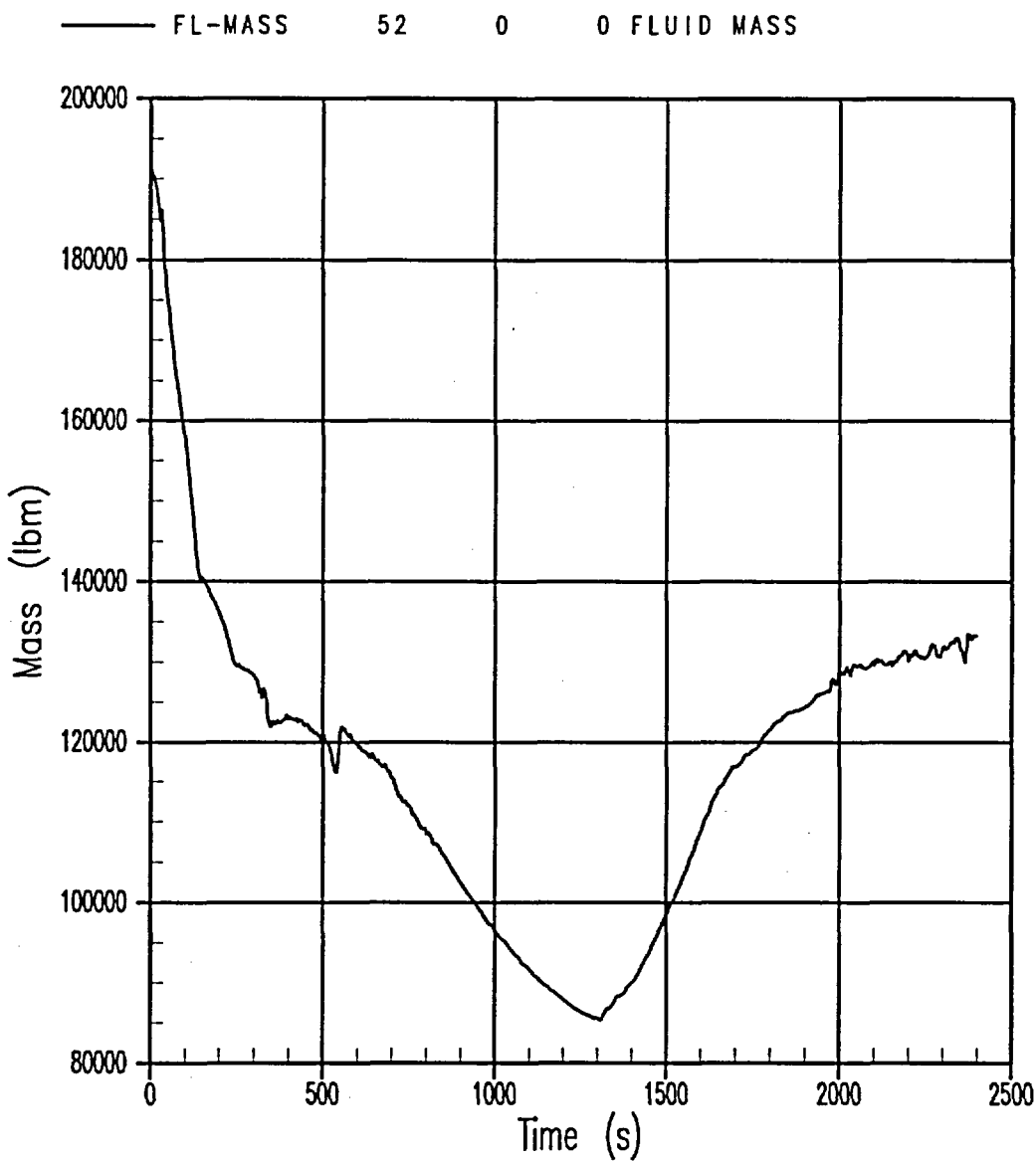


Figure 27-7-5. Reactor Vessel Mass, 3.5-Inch Break With LOOP

Indian Point 2 BE SBLOCA Analysis
3.5-INCH CL BREAK WITH LOOP
Peak Cladding Temperature

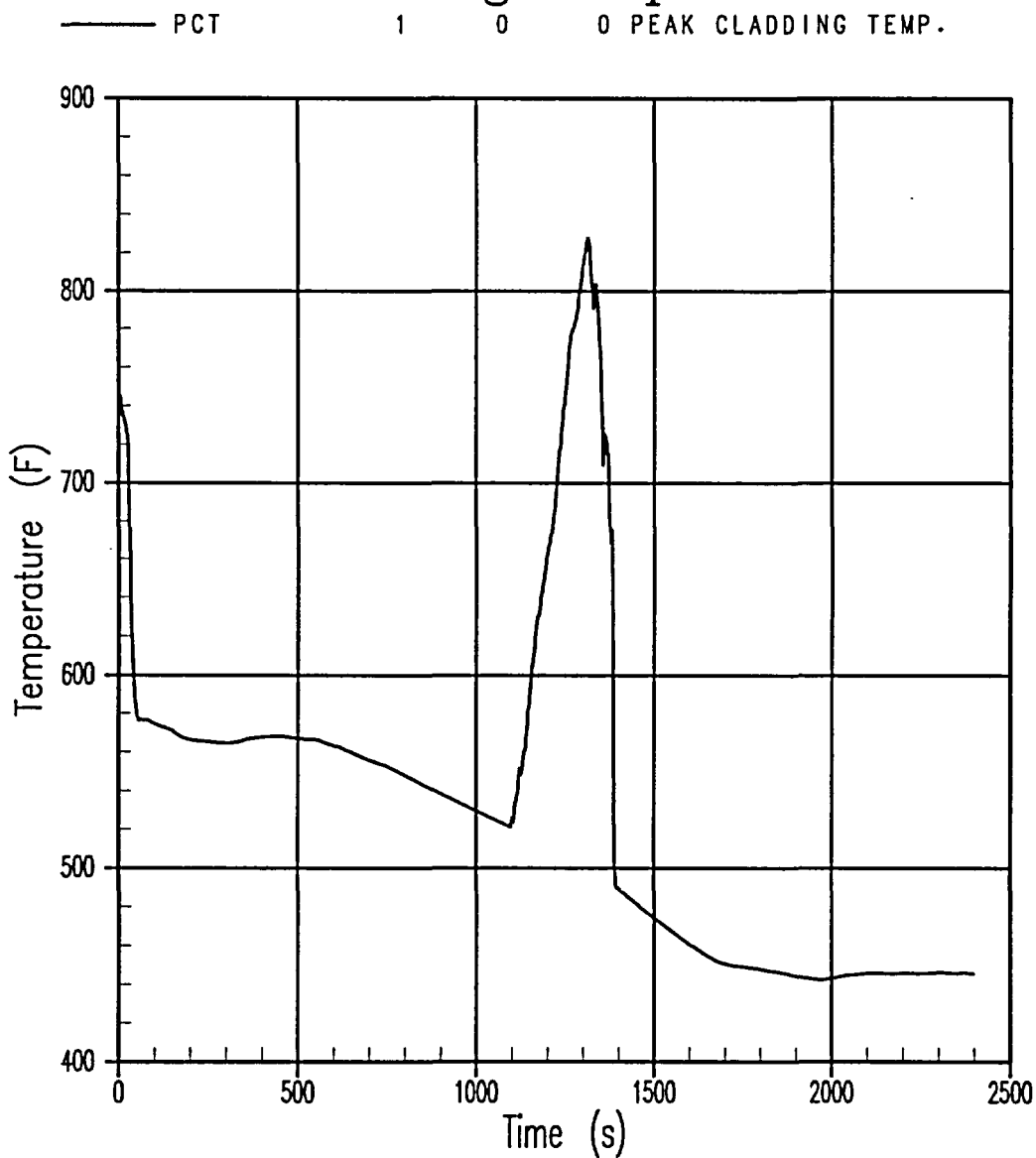


Figure 27-7-6. PCT, 3.5-Inch Break With LOOP

Indian Point 2 BE SBLOCA Analysis
3.5-INCH CL BREAK WITH LOOP
Total Safety Injection Flow

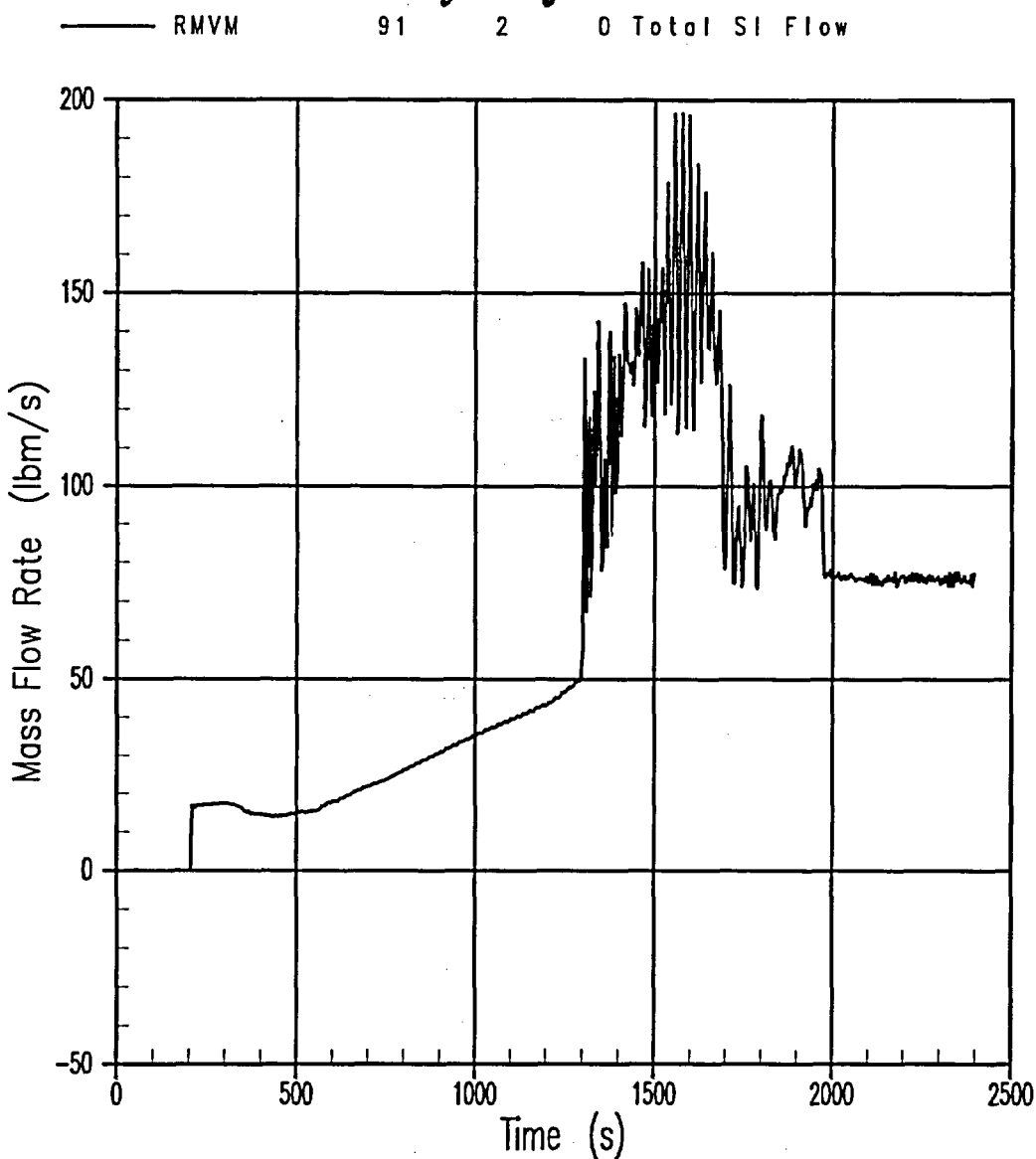


Figure 27-7-7. Total Safety Injection Flow to RCS, 3.5-Inch Break With LOOP

27-8 Summary of LOOP Reference Cases

The series of calculations assuming that offsite power is lost coincident with the inception of the small break LOCA event has identified the 3-inch equivalent diameter cold leg break as the size that produces the highest PCT. Breaks greater than 10-inches equivalent diameter can be characterized as "intermediate" breaks, breaks that have characteristics of both small and large break LOCAs. The 10-inch break exhibits a short-lived core uncover and heatup in which the collapsed liquid level in the core as a whole and in the hot assembly drops to nearly the bottom of the core; that is, almost the entire core voids. The major difference between the 10-inch and larger (12-inch equivalent diameter break) LOCAs is that in the 10-inch break, water remains in the lower part of the core during blowdown. Breaks in which the core is predicted to uncover completely (such as the 12-inch break) are considered to be intermediate break LOCAs.

All four loop seals clear in the 10-inch break; however, it is more difficult to identify the initialization of loop seal clearing than for the smaller breaks. The primary RCS depressurization is rapid, and flashing in the loops causes steam flow through all of the loop seals nearly from the start of the transient. Core recovery in the 10-inch break is slower than the recoveries in the smaller breaks because it requires more accumulator water to fill the downcomer and core. Core recovery, as defined in Table 27-8-1, refers to the quenching of the fuel due to heat transfer to the two-phase mixture present in the inner vessel region. The PCT calculated during the 10-inch break transient remains below the initial normal operation clad temperature.

The 2.5-inch, 3-inch, 3.5-inch, and 4-inch breaks feature a slow, top-down drain of the RCS, and a natural circulation period in which the primary pressure equilibrates just above the secondary side pressure for several hundred seconds. System-wide loop seal clearance was incomplete. That is, loop seal clearance was a function of the break size. In the 2.5 inch and 3-inch breaks, only one loop seal cleared and remained clear. In the 3.5-inch and 4-inch breaks, two loop seals cleared and had sustained steam venting for the rest of the transient. Core uncover was due to a prolonged boiloff period, and the PCT transient was limited primarily due to pumped safety injection before terminating when the accumulators inject.

The 6-inch break can be characterized as a medium-size small break LOCA; however, its characteristics are less similar to the 3-inch break than are the 4-inch break results. In the 6-inch break, the transient is significantly more rapid and there is no core uncover and heatup. All four loop seals clear initially in this break and vent thereafter. In comparison to the smaller breaks,

the accumulator setpoint pressure is reached early; the mass inventory depletion is terminated by accumulator injection in the 6-inch break before any core uncover occurs.

Table 27-8-1 summarizes events in the reference case break spectrum assuming LOOP. In the variation of PCT with break size, the depth of core uncover varies as the break size increases. The 3-inch break exhibits a much longer core uncover interval than any larger size break, and its core mixture level is low enough that it is limiting in calculated PCT. For break sizes larger than the 10-inch LOCA, it is apparent that the entire core will become voided and the transients become intermediate or large break LOCA events. The PCTs for all of the breaks are low relative to the 2200°F licensing limit. A maximum PCT of 964°F was predicted to occur for the 3-inch break.

The loop seal steam venting behavior plays a major role in the outcome of the LOOP reference cases. Lee, et al. (1983) identified that phenomenological uncertainties associated with the loop seal steam venting make it impossible to predict which loop seal(s) will clear deterministically and that the loop seal steam venting performance is dependent upon the size of a cold leg small break LOCA. Since each loop has essentially the same flow resistance, each of the loop seals is poised to clear to vent steam generated in the core to the break at the same time. Small perturbations within the RCS loops determine which loop seal(s) clear.

Because of the uncertainty in loop seal steam venting capability caused by system perturbations, there exists a range of loop seal behaviors that can result in no loop seals venting steam, a single loop seal venting steam, or multiple loop seals venting steam depending upon the break size.

A threshold break size exists for which more than one loop seal will vent steam for an extended period of time. A threshold break size can be defined as the break size whose transient loop seal perturbations are large enough to always result in more than one loop seal venting steam for some period of time. Break sizes below this threshold break size tend to vent steam through only one loop seal. Lee, et al. (1983) provided a qualitative map of loop seal steam venting behavior for cold leg breaks as a function of break size as shown in Figure 27-8-1. Because actual transients depend on several parameters, a general quantitative map cannot be generated. Still, this map can provide a framework for understanding the loop seal steam venting behavior. As shown in Figure 27-8-1, neighboring regions may overlap each other as indicated by the shaded regions. Explanations for each region follows:

Region A - The break size is not large enough to result in sufficient reactor coolant depletion for loop seal steam venting to occur given the associated safeguards systems and secondary decay heat removal capability.

Region B - There is a narrow range of break size where the broken loop is preferentially cleared due to its proximity to the break. In this region, the influence of the break outweighs system perturbations.

Region C - This break is small enough to vent steam through only one loop. Each loop has the same probability of steam venting.

Region D - Break sizes in this region are large enough so that attendant loop seal oscillations will cause multiple loop seals to vent steam. The resulting set of loop seals venting steam is random.

Region E - The break size is large enough to result in all loop seals venting steam.

In the Indian Point Unit 2 LOOP break spectrum, the threshold break size is approximately 3-inches in equivalent diameter. In order to conservatively bound the phenomenological uncertainties associated with the loop seal steam venting behavior in the Indian Point Unit 2 analysis, the calculational technique is biased so as to predict the clearing of no more than one loop seal during the LOOP 3-inch cold leg break reference transient. This is discussed further in Section 28 and Section 34.

Table 27-8-1
Summary of LOOP Reference Cases

Event	2.5-Inch	3-Inch	3.5-Inch	4-Inch	6-Inch	10-Inch
Break opens (s)	0.0	0.0	0.0	0.0	0.0	0.0
Reactor trip signal (s) at 1800 psig pressurizer pressure	50.4	35.5	26.5	20.7	10.2	6.3
S-signal (s) at 1700 psig	54.9	39.7	30.6	24.6	13.1	7.6
Loop seal clearance begins (s)	1030	724	536	404	175	13
Loop 21 steam venting	No	No	Yes	No	Yes	Yes
Loop 22 steam venting	No	Yes	Yes	No	Yes	Yes
Loop 23 steam venting	Yes	No	No	Yes	No	Yes
Pressurizer loop 24 steam venting	No	No	No	Yes	Yes	Yes
Boiloff core uncover begins (s)	2080	1372	1096	818	N/A ^(a)	136
Minimum core collapsed level (ft)	7.2	6.4	6.6	6.2	5.5	1.7
Boiloff core uncover PCT (°F)	832	964	828	756	N/A	652
Boiloff core uncover PCT time (s)	2600	1948	1312	960	N/A	154
Accumulator injection begins (s)	2957	1957	1305	943	368	125
Core recovery (s)	2977	2147	1392	986	N/A	161
Safety injection exceeds break flow(s)	2875	1957	1305	943	380	152

a. N/A = not applicable

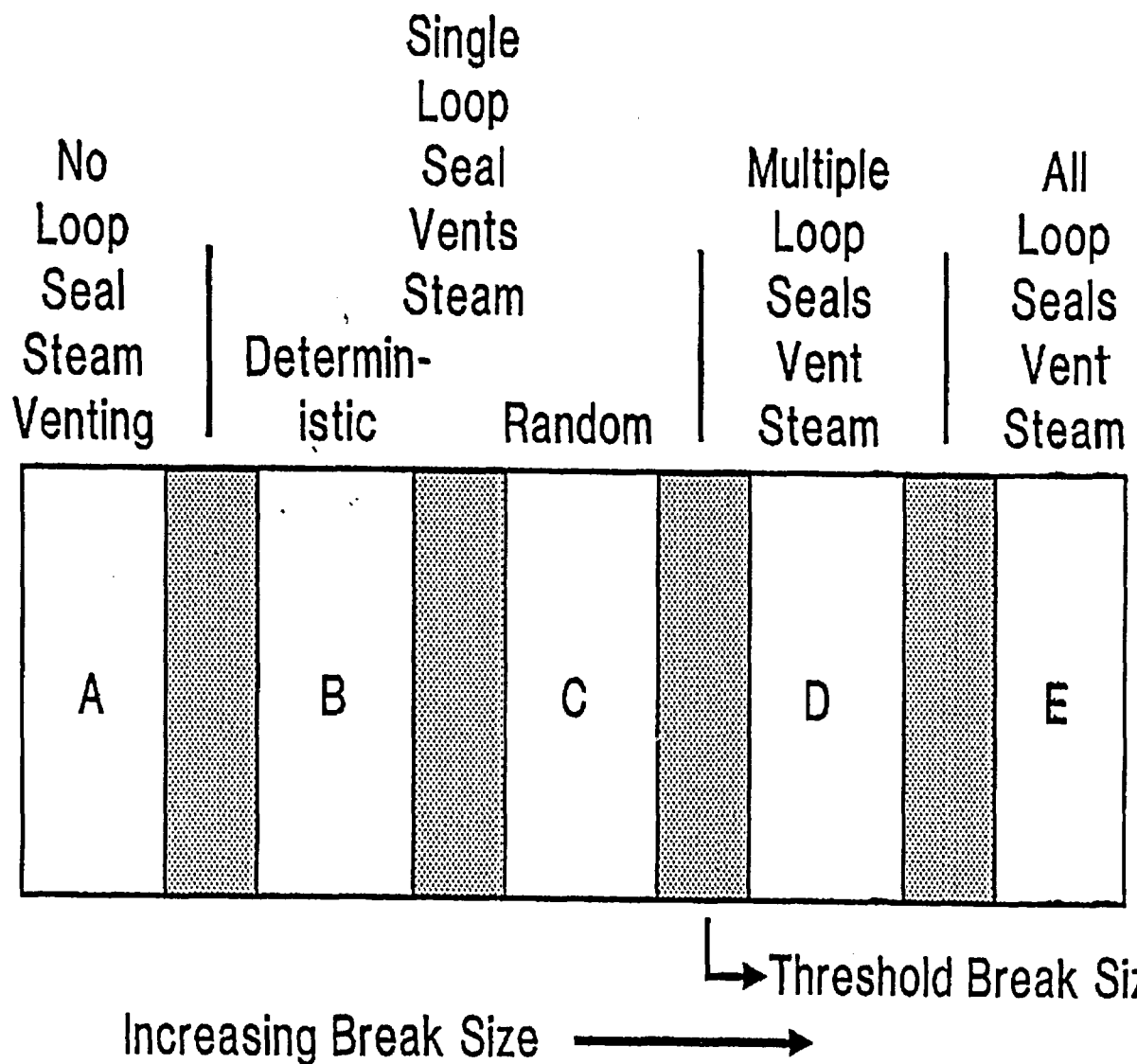


Figure 27-8-1. Loop Seal Steam Venting as a Function of Break Size

27-9 Break Spectrum With OPA Scenario

The calculations reported in Sections 27-1 through 27-7 were based on the assumption that offsite power was lost coincident with the time of reactor trip during the break transient. It has been shown that the LOOP assumption generally leads to the most conservative small break PCTs. Studies reported by Lee (Lee, et al., 1983) have confirmed this.

If offsite power is available following the initiation of the break and reactor trip, the scenario for the small break transient changes. The most significant difference between LOOP and offsite power available (OPA) scenarios is the time of RCP trip. In the LOOP scenario, the RCPs trip due to the loss of ac power after running for 30 seconds on the plant generator. If offsite power remains available, however, RCP trip does not occur and the RCPs must be tripped by the reactor operators. As discussed in Sections 24 and 25 in this volume, this creates an additional uncertainty in the small break analysis. The RCP trip criteria, described in Section 25, are defined in the plant EOPs. The actual time of RCP trip depends on three things that must take place:

- The EOPs must be followed to the point at which an RCP trip decision is made.
- The RCP trip criteria, based on various instrument signals, must be recognized by the reactor operating crew.
- The physical time that it takes the operator(s) to reach the RCP switch and deactivate the RCPs must be considered.

In the small break LOCA analysis, the time of RCP trip can have an important consequence on the transient. Leaving the RCP running is not necessarily a PCT benefit. While the pumps are on, convective heat transfer in the core is improved, and the pumps help to supply the core with water from the loops. However, with the pumps running, it is possible to pump more mass out of the break than otherwise would have been lost.

In addition, the most limiting failure is different in the OPA scenario. The diesel generators are not needed with OPA to run the safety injection pumps. Rather than an entire train of safety injection being lost due to the failure of a diesel to start, the most limiting single failure in the OPA scenario is the failure of one of the high head safety injection pumps to start. Also, the

surviving safety injection pumps start with slightly less delay in the OPA scenario than in the LOOP scenario.

Therefore, a series of Indian Point Unit 2 simulations were run to investigate the effect that a delay in RCP trip time has on the small break transient. For these cases, the following assumptions were made:

- The RCPs continue to run following a reactor trip signal. Trip occurs by operator action. Based on the operator timing study documented in Section 25, RCP trip is expected to occur nominally within 25 seconds following the time of the pump trip criteria being satisfied. This operator action delay time is largely a function of the EOPs and how quickly a reactor operator team can proceed through them. This delay time is considered to be independent of break size. A 32-second delay for operator action is assumed in these simulations as an upper-bound delay time. Combined with an assumed delay of 38 seconds in safety injection actuation, the RCPs are tripped 70 seconds after the safety injection signal. The upper-bound value is assumed so that the maximum difference in RCP trip time is considered in the LOOP/OPA comparisons.
- No credit is assumed for injection from the charging pump. As described in Section 3 of Volume 1 of this document, one of the operator actions taken early enough in the EOPs to affect a small break LOCA is the action to energize one high head charging pump. (This is a Class A system in Indian Point Unit 2.) While including this flow will lead to lower PCTs, the action is not assumed to take place.
- Safety injection delay time is assumed to be 38 seconds, versus 45 seconds in the LOOP study. The delay time will be less when offsite power is available because diesel generator startup is not required.

Calculations were performed for breaks ranging from a 3-inch equivalent diameter break to a 10-inch break. All of the breaks were located at the top of the pressurizer loop cold leg, the same location and orientation as in the LOOP break spectrum. The following sections discuss the OPA breaks and compare them to the corresponding LOOP breaks.

27-10 3-Inch Cold Leg Break with OPA

The sequence of events and overall behavior for the 3-inch equivalent diameter cold leg break with OPA is presented in Figures 27-10-1 to 27-10-7. In general, the 3-inch break with LOOP and OPA (delayed pump trip) transients are similar. Reactor trip occurs at 35.5 seconds in the OPA case, and the pumps continue to run until 109.7 seconds before they begin to coast down. Following reactor trip, the RCS pressure decreases rapidly and voids begin to form in the upper head and upper plenum. In the LOOP case, these voids begin to collect in the upper plenum and at the top of the steam generator tubes. With the RCPs running, the system tends to be more homogeneous because the pumps distribute the voids throughout the RCS.

In the OPA case, some of the vapor is swept through the RCS to the break. This reduces the total break flow, as seen in Figures 27-10-3 and 27-10-5. Most of the difference occurs during the period in which the pumps are running in the OPA case, but coasting down in the LOOP case. The small reduction in break flow results in more inventory retained in the RCS.

The other difference between the OPA and LOOP cases is the loop seal venting. The LOOP case clears only one loop seal for the duration of the transient; in the OPA scenario, two loop seals clear and remain clear after the initial clearing almost until accumulator injection.

Depressurization following loop seal clearing is similar in the two cases, which reach the accumulator pressure at virtually the same time. Because additional mass from the loop seal region is delivered into the reactor vessel, the collapsed liquid level in the core remains higher in the OPA case. The PCT in the OPA case is the initial normal operation cladding temperature. The two-phase mixture level is close to the top of the core in the OPA case, and only a small length of uncovered fuel exists for a short period of time. Steam cooling is able to limit the excursion in cladding temperature.

Indian Point 2 BE SBLOCA Analysis 3-INCH CL BREAK WITH OPA

Primary and Secondary System Pressures

— P N	54	1	0 PRZ PRESSURE
- - - P	130	2	0 SG21 SEC. PRESSURE
- - - P	138	2	0 SG22 SEC. PRESSURE
- - - P	146	2	0 SG24 SEC. PRESSURE
- - - P	154	2	0 SG23 SEC. PRESSURE

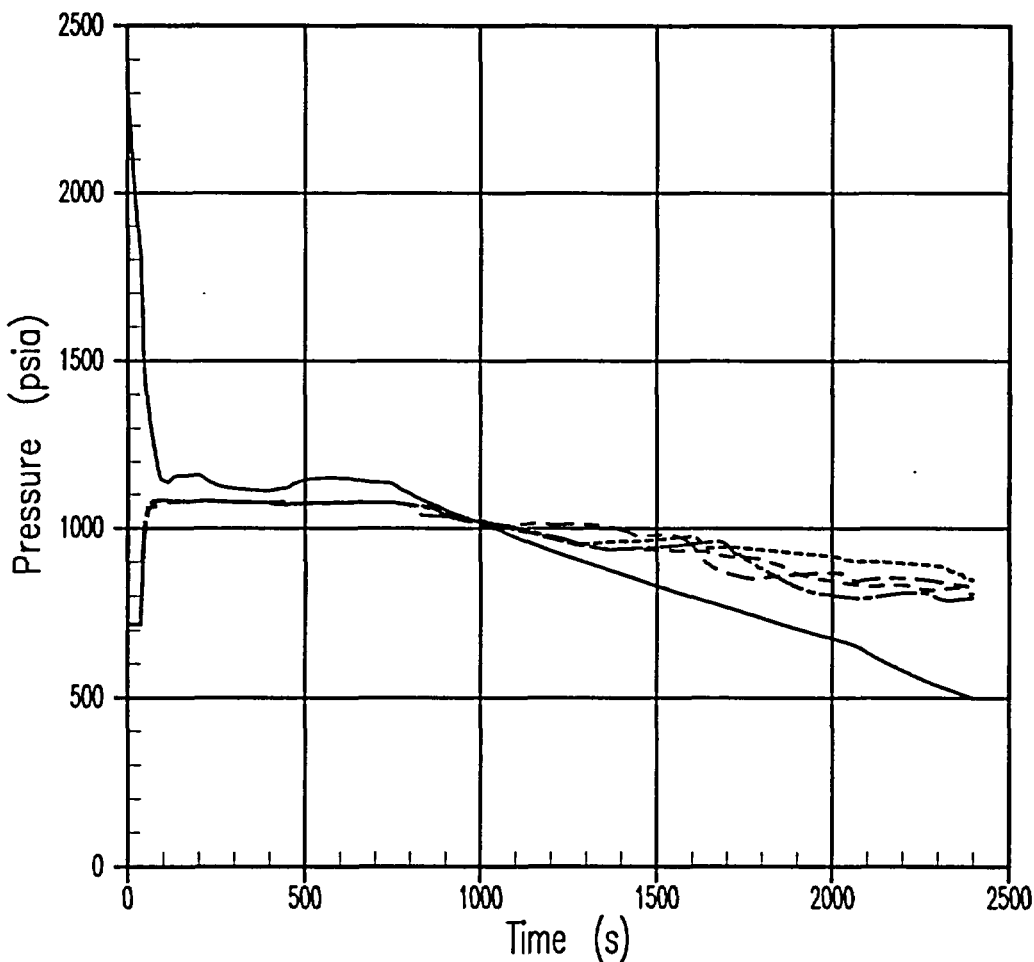


Figure 27-10-1. Primary and Secondary System Pressures, 3-Inch Break With OPA

Indian Point 2 BE SBLOCA Analysis
3-INCH CL BREAK WITH OPA
Core Collapsed Liquid Levels

— LQ-LEVEL 5 0 0 HOT ASSY
- - - LQ-LEVEL 4 0 0 CORE AVERAGE

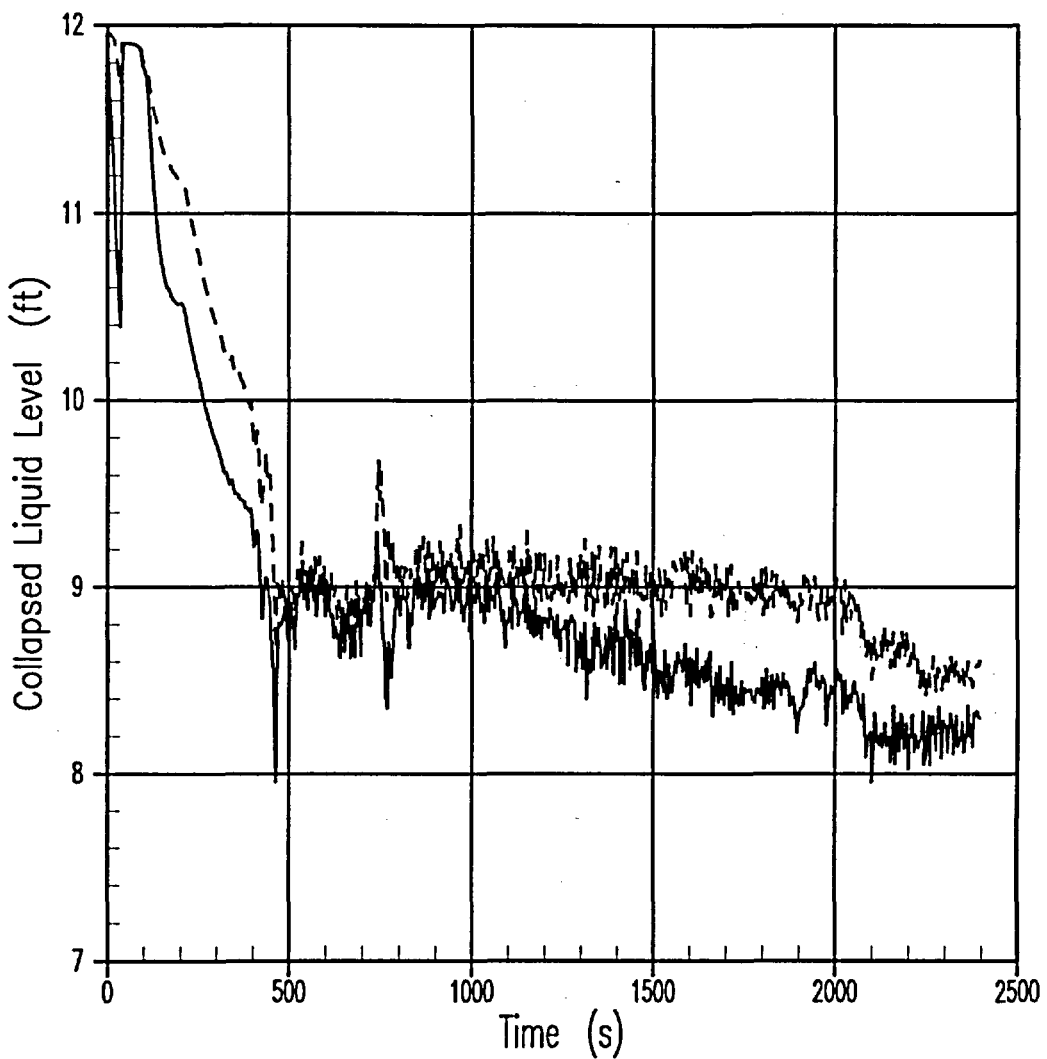


Figure 27-10-2. Core Collapsed Liquid Level, 3-Inch Break With OPA

Indian Point 2 BE SBLOCA Analysis 3-INCH CL BREAK WITH OPA Break Flowrate and Void Fraction

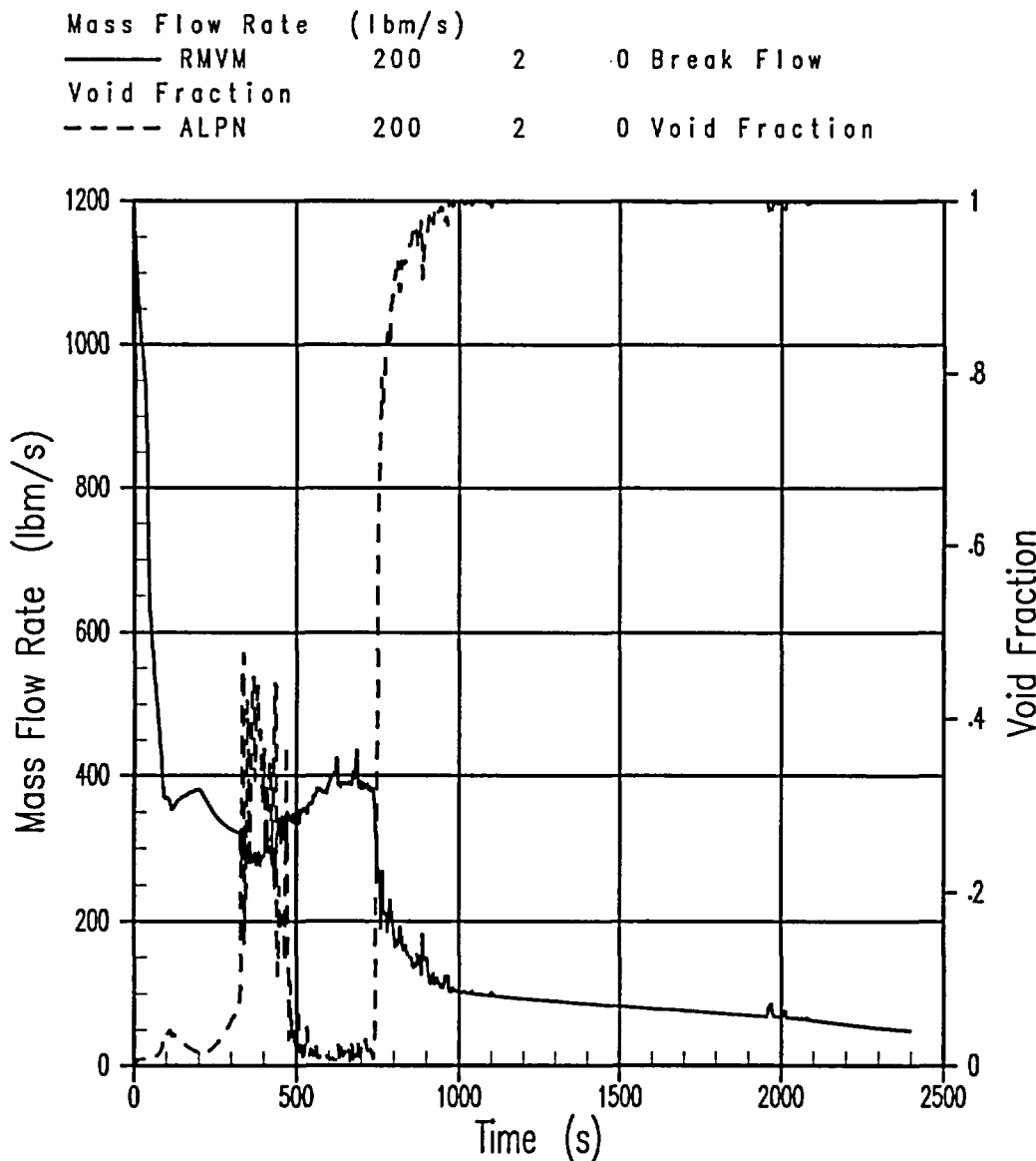
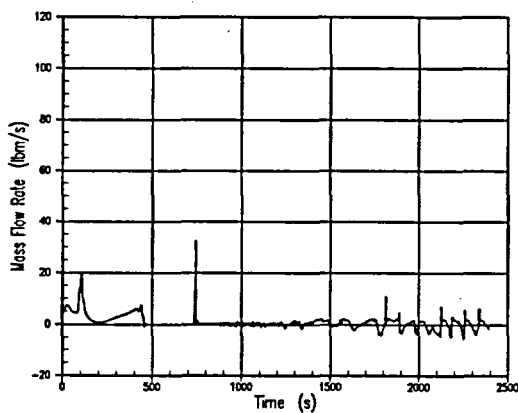


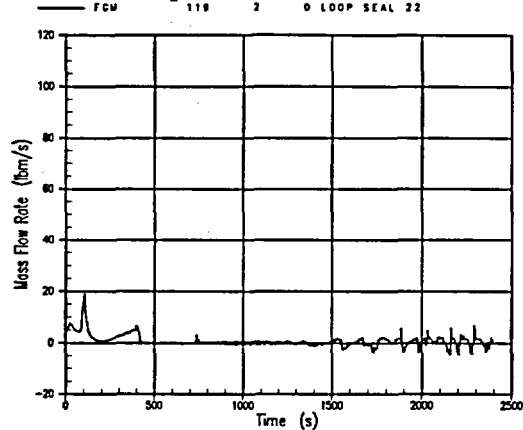
Figure 27-10-3. Break Flowrate and Void Fraction, 3-Inch Break With OPA

Indian Point 2 BE SBLOCA Analysis
3-INCH CL BREAK WITH OPA
Loop 21 Steam Flow



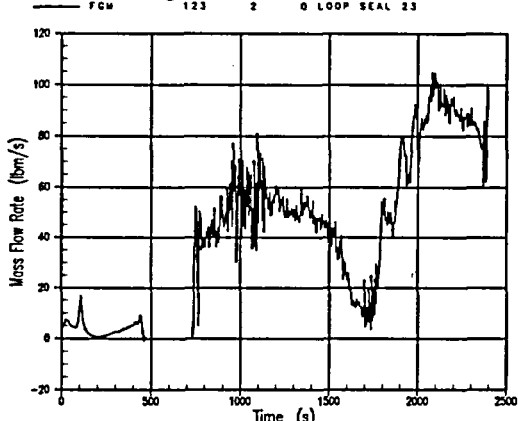
A. Loop 21 Loop Seal Steam Flow

Indian Point 2 BE SBLOCA Analysis
3-INCH CL BREAK WITH OPA
Loop 22 Steam Flow



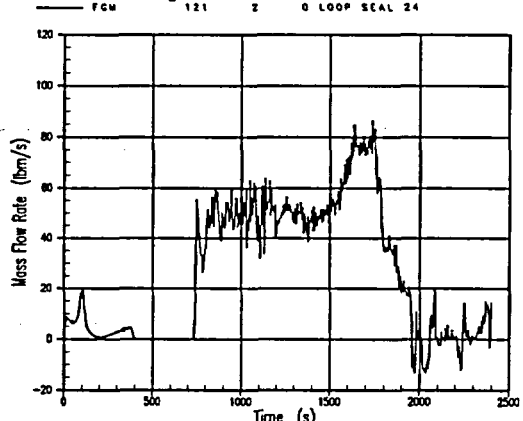
B. Loop 22 Loop Seal Steam Flow

Indian Point 2 BE SBLOCA Analysis
3-INCH CL BREAK WITH OPA
Loop 23 Steam Flow



C. Loop 23 Loop Seal Steam Flow

Indian Point 2 BE SBLOCA Analysis
3-INCH CL BREAK WITH OPA
Loop 24 Steam Flow



D. Loop 24 Loop Seal Steam Flow

Figure 27-10-4. Loop Seal Steam Flows, 3-Inch Break With OPA

Indian Point 2 BE SBLOCA Analysis
3-INCH CL BREAK WITH OPA
Reactor Vessel Mass

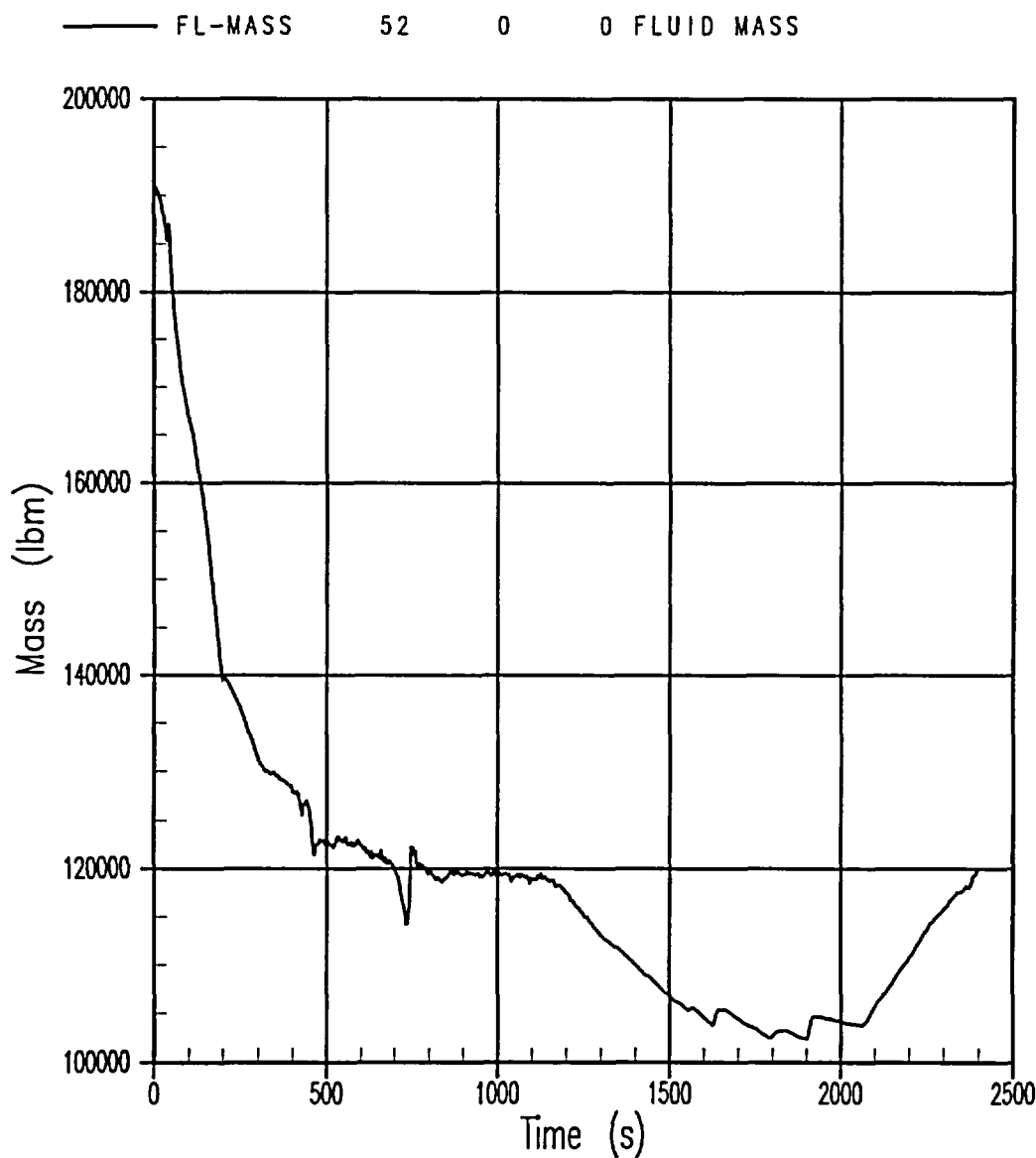


Figure 27-10-5. Reactor Vessel Mass, 3-Inch Break With OPA

Indian Point 2 BE SBLOCA Analysis
3-INCH CL BREAK WITH OPA
Peak Cladding Temperature

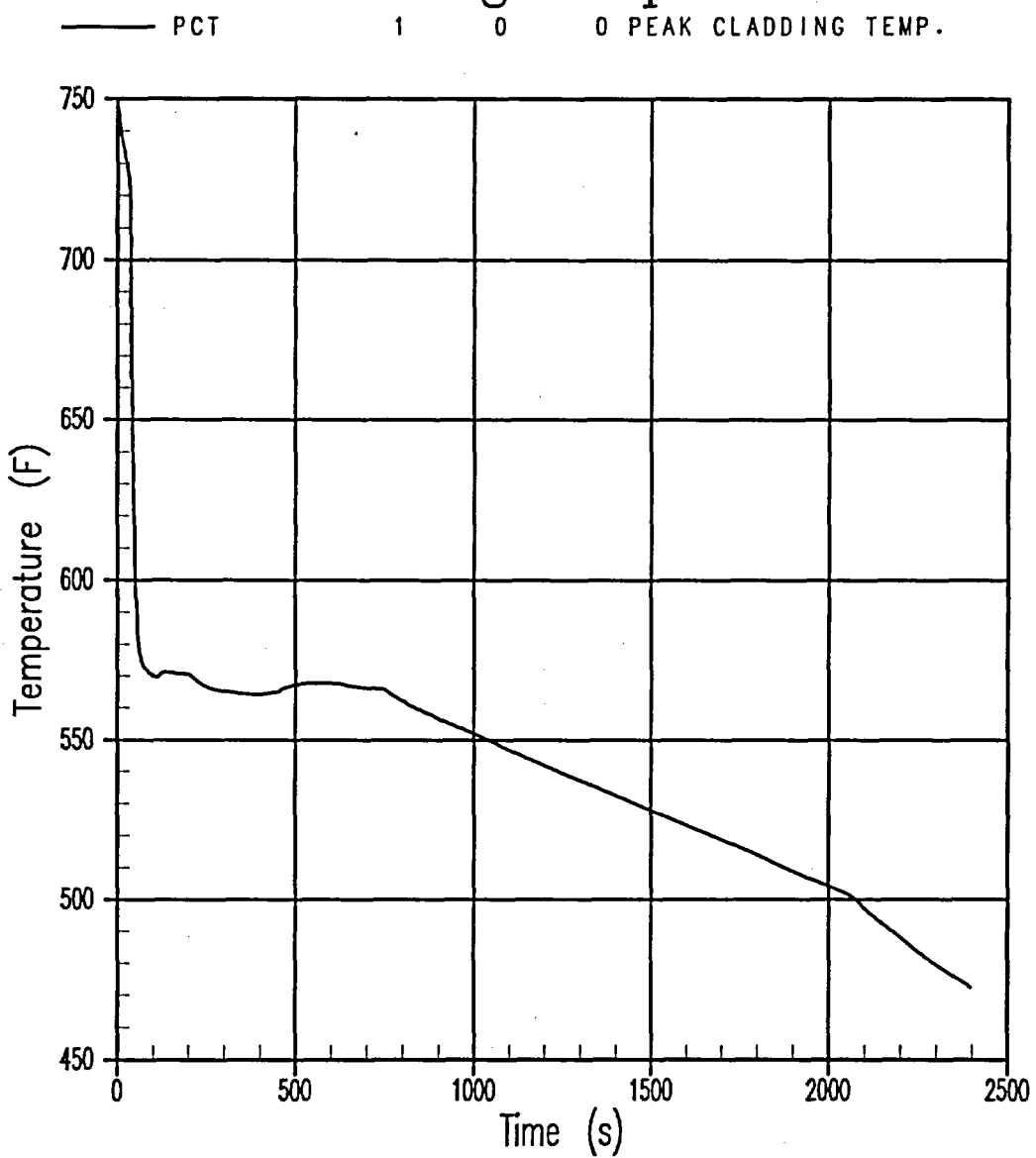


Figure 27-10-6. PCT, 3-Inch Break With OPA

Indian Point 2 BE SBLOCA Analysis
3-INCH CL BREAK WITH OPA
Total Safety Injection Flow

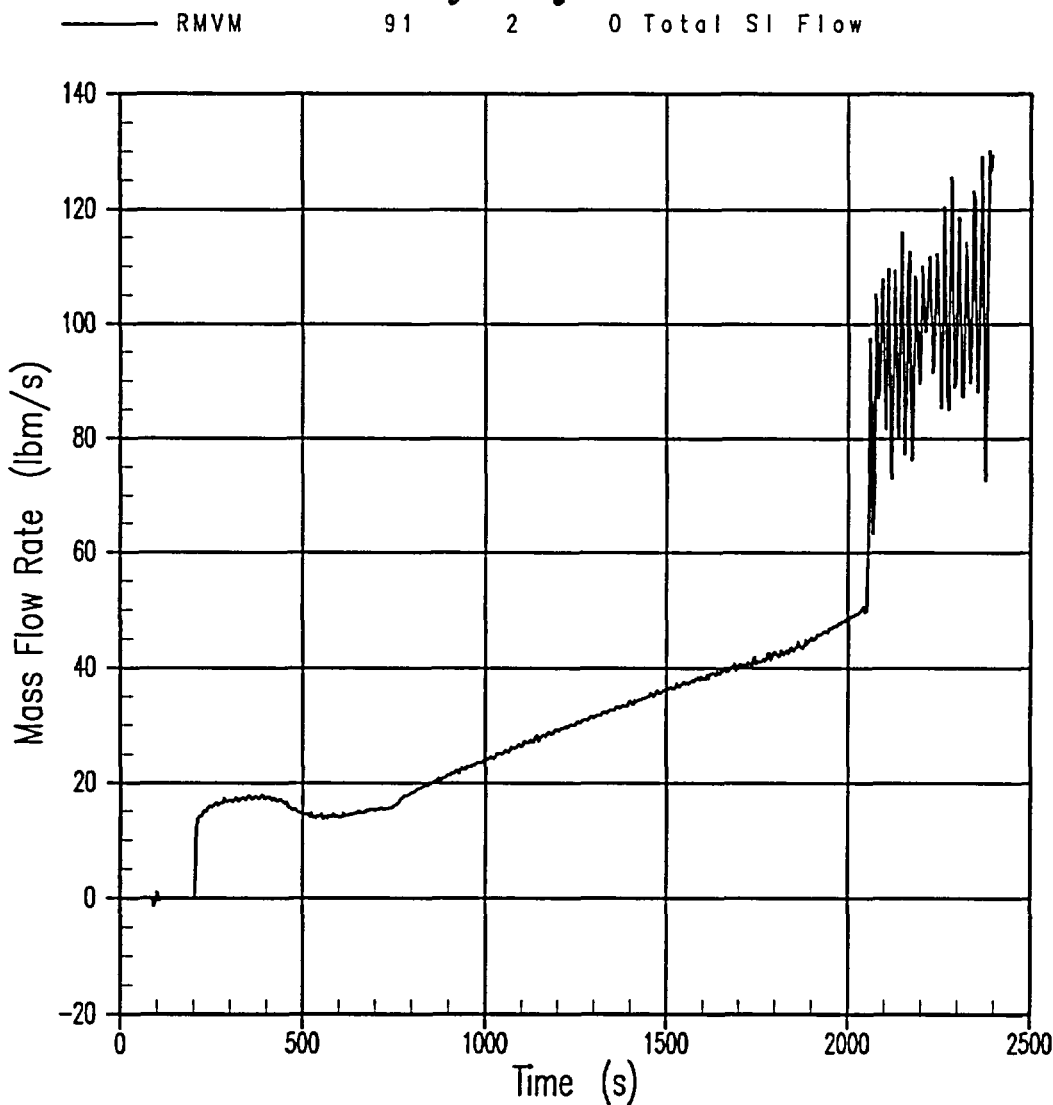


Figure 27-10-7. Total Safety Injection Flow to RCS, 3-Inch Break With OPA

27-11 4-Inch Cold Leg Break With OPA

The sequence of events and overall behavior for the 4-inch equivalent diameter cold leg break with OPA are illustrated in Figures 27-11-1 to 27-11-7. In general, the LOOP (pump trip on reactor trip) and OPA (delayed pump trip) transients are similar. Reactor trip occurs at 20.7 seconds in the OPA case, and the pumps continue to run for 94.6 seconds when they are tripped and begin to coast down. During the blowdown period, flashing occurs in the reactor vessel and loops. As the pumps continue to run in the OPA case, the pumps tend to homogenize the RCS. Within the initial 40 seconds of blowdown, because there are some voids pumped into the broken cold leg in the OPA case, the break flow becomes less than the break flow in the LOOP case as shown in Figure 27-11-3. When the pumps are tripped and have coasted down, the voids in the cold leg collect near the break as the loop seals replug, and the break flowrate in the OPA case becomes similar to the LOOP case from 160 seconds onward. After that time in both cases, the voids are swept from the broken cold leg and a low void fraction critical flow exists until the loop seal begins to clear. The three loop seals that clear in this case (Figure 27-11-4) clear at different times over a 70 second interval. Eventually, the masses in the reactor vessel become nearly equal, however, as shown in Figure 27-11-5 (versus Figure 27-3-5) shortly after loop seal clearance. This shows that the change in critical flow at the break, from single-phase to two-phase and back to single-phase, during the extended pump operation has limited overall effect for this break size.

The impact of the delayed pump trip on core heatup is seen in Figures 27-11-2 and 27-11-6. Operation of the pump following reactor trip during the early part of the transient results in a small, but important redistribution of mass in the RCS. Figure 27-11-2 shows that the inner vessel collapsed level in the OPA case is greater than that in the LOOP case from just before 800 seconds onward. The OPA collapsed level in the hot assembly and in the core as a whole, as seen in Figure 27-11-2, exceeds that of the LOOP case. The RCS depressurization in the OPA case trails that in the LOOP case because liquid retained in the cold legs passes out the break, decreasing break quality relative to the LOOP 4-inch cold leg break. The higher pressure present in the OPA case leads to less pumped injection, but it exhibits a larger mass inventory at the time of accumulator injection than the LOOP case. The boiloff begins earlier and is more prolonged in the LOOP case. The PCT in the 4-inch break with OPA occurs at the inception of the transient (Figure 27-11-6) and equals the initial, normal operation cladding temperature.

Indian Point 2 BE SBLOCA Analysis 4-INCH CL BREAK WITH OPA

Primary and Secondary System Pressures

— PN	54	1	0 PRZ PRESSURE
- - - P	130	2	0 SG21 SEC. PRESSURE
- - - P	138	2	0 SG22 SEC. PRESSURE
- - - P	146	2	0 SG24 SEC. PRESSURE
- - - P	154	2	0 SG23 SEC. PRESSURE

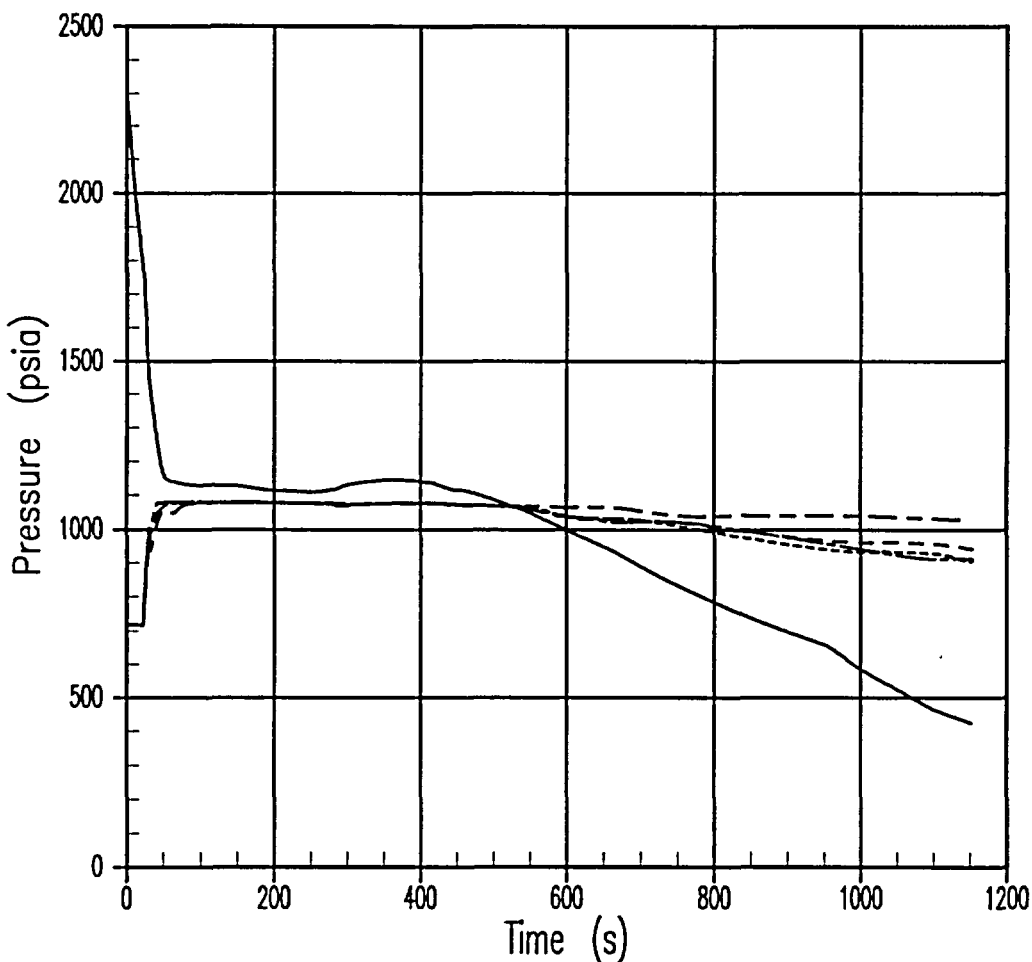


Figure 27-11-1. Primary and Secondary System Pressures, 4-Inch Break With OPA

Indian Point 2 BE SBLOCA Analysis
4-INCH CL BREAK WITH OPA
Core Collapsed Liquid Levels

— LQ-LEVEL 5 0 0 HOT ASSY
- - - LQ-LEVEL 4 0 0 CORE AVERAGE

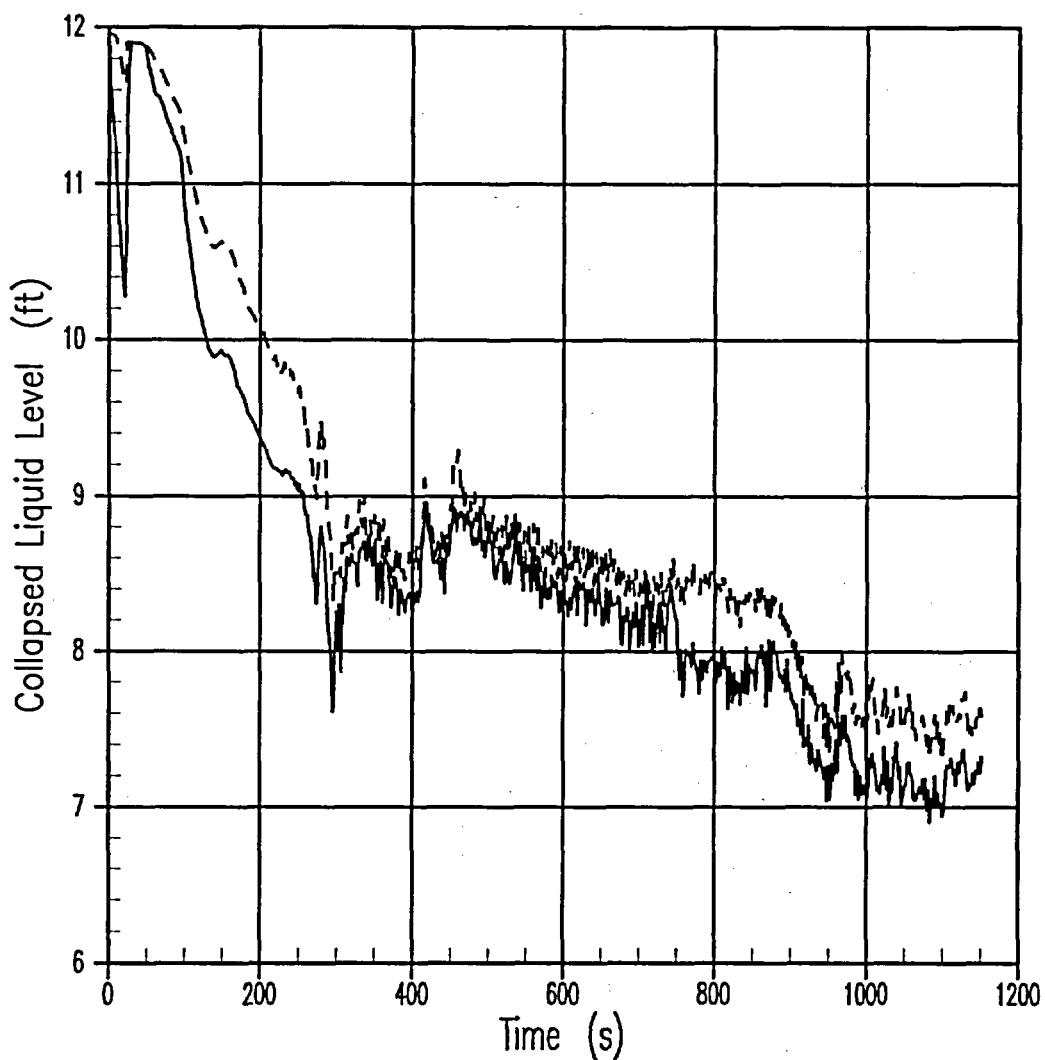


Figure 27-11-2. Core Collapsed Liquid Level, 4-Inch Break With OPA

Indian Point 2 BE SBLOCA Analysis 4-INCH CL BREAK WITH OPA Break Flowrate and Void Fraction

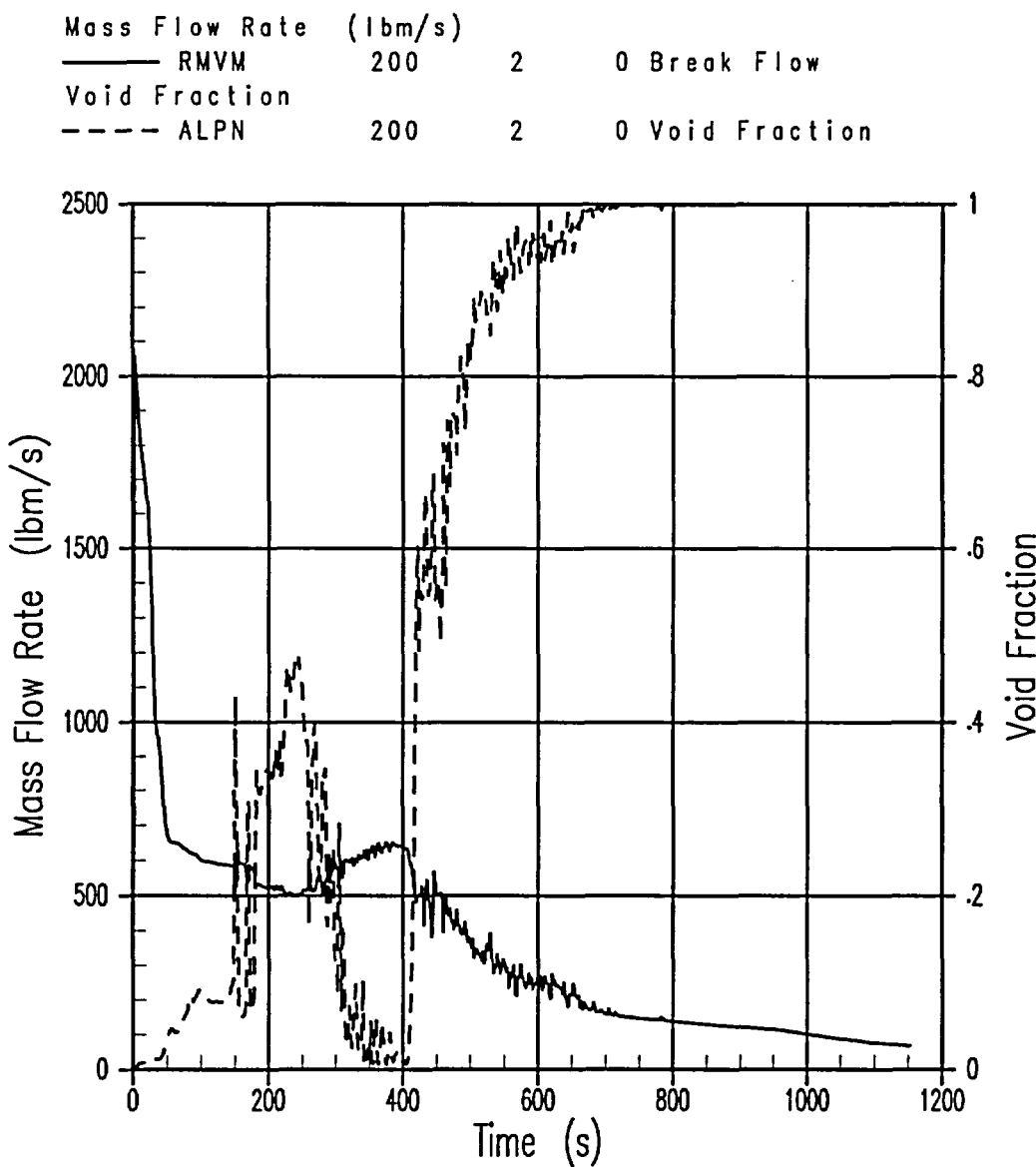
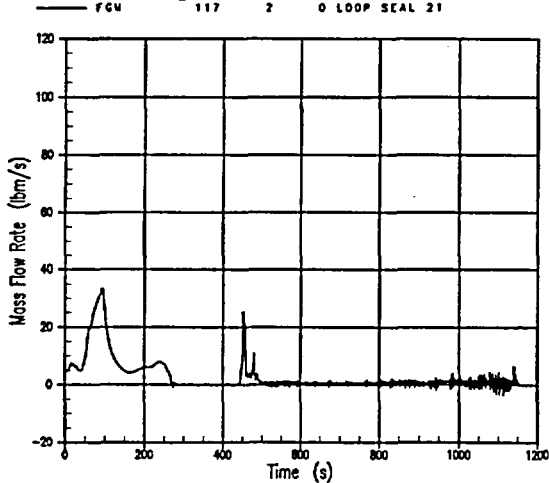


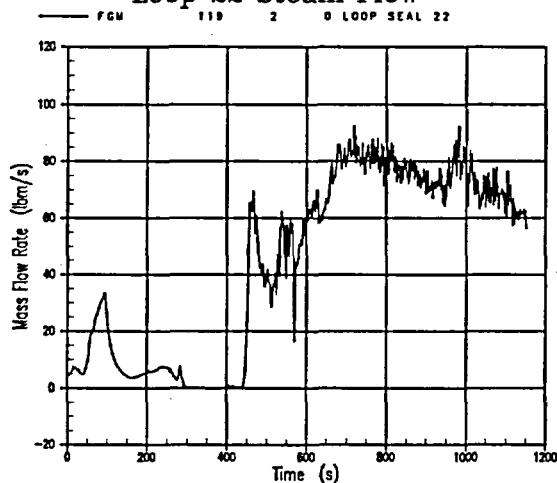
Figure 27-11-3. Break Flowrate and Void Fraction, 4-Inch Break With OPA

Indian Point 2 BE SBLOCA Analysis
4-INCH CL BREAK WITH OPA
Loop 21 Steam Flow



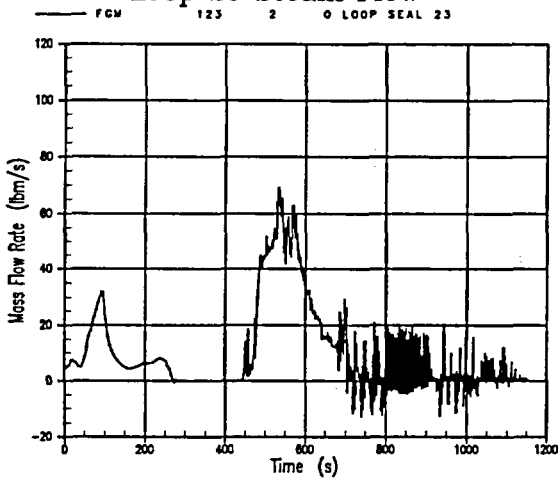
A. Loop 21 Seal Steam Flow

Indian Point 2 BE SBLOCA Analysis
4-INCH CL BREAK WITH OPA
Loop 22 Steam Flow



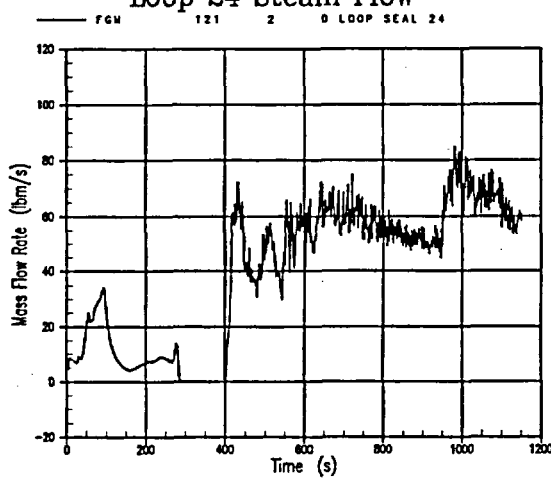
B. Loop 22 Loop Seal Steam Flow

Indian Point 2 BE SBLOCA Analysis
4-INCH CL BREAK WITH OPA
Loop 23 Steam Flow



C. Loop 23 Seal Steam Flow

Indian Point 2 BE SBLOCA Analysis
4-INCH CL BREAK WITH OPA
Loop 24 Steam Flow



D. Loop 24 Loop Seal Steam Flow

Figure 27-11-4. Loop Seal Steam Flows, 4-Inch Break With OPA

Indian Point 2 BE SBLOCA Analysis
4-INCH CL BREAK WITH OPA
Reactor Vessel Mass

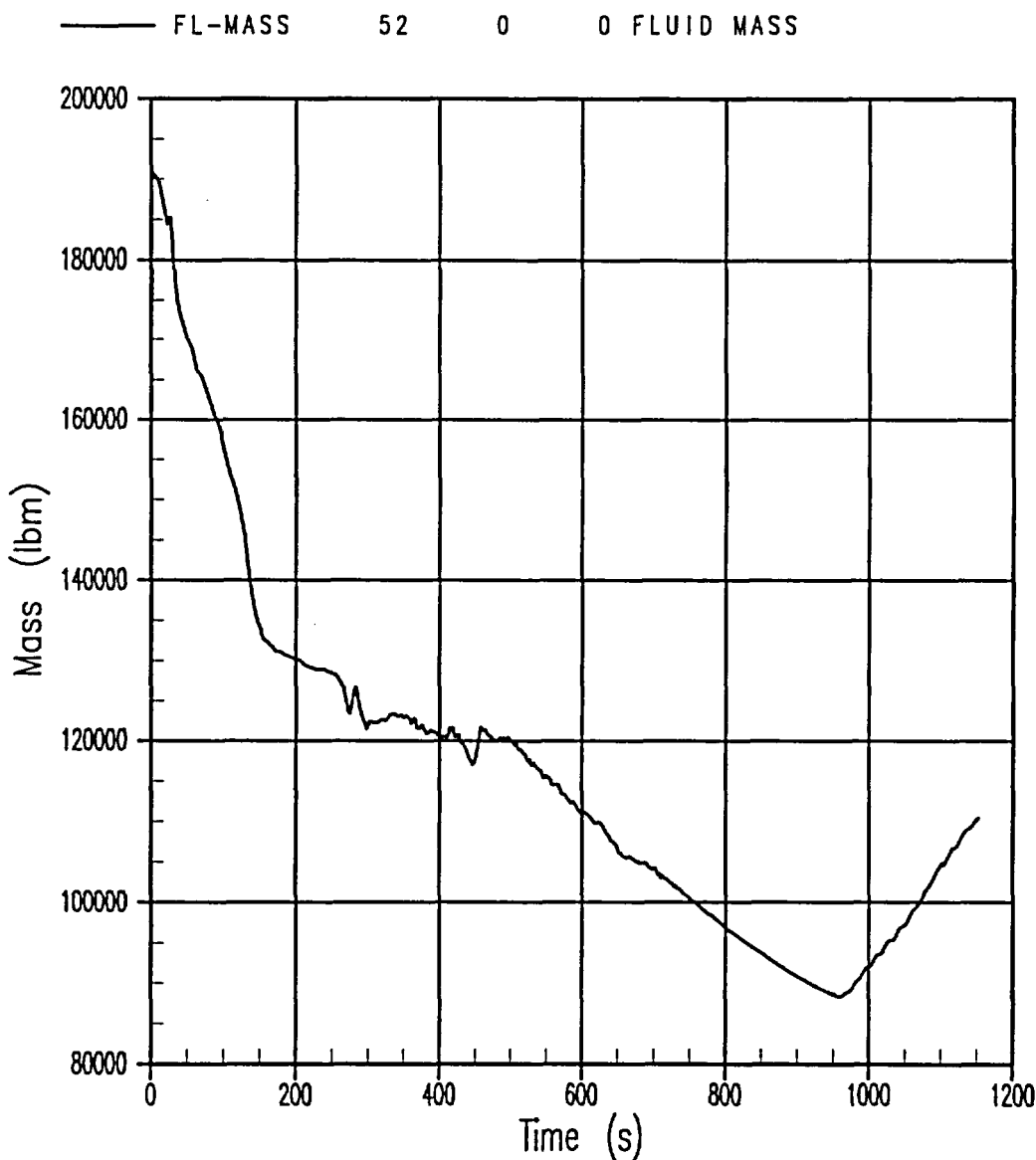


Figure 27-11-5. Reactor Vessel Mass, 4-Inch Break With OPA

Indian Point 2 BE SBLOCA Analysis
4-INCH CL BREAK WITH OPA
Peak Cladding Temperature

— PCT 1 0 0 PEAK CLADDING TEMP.

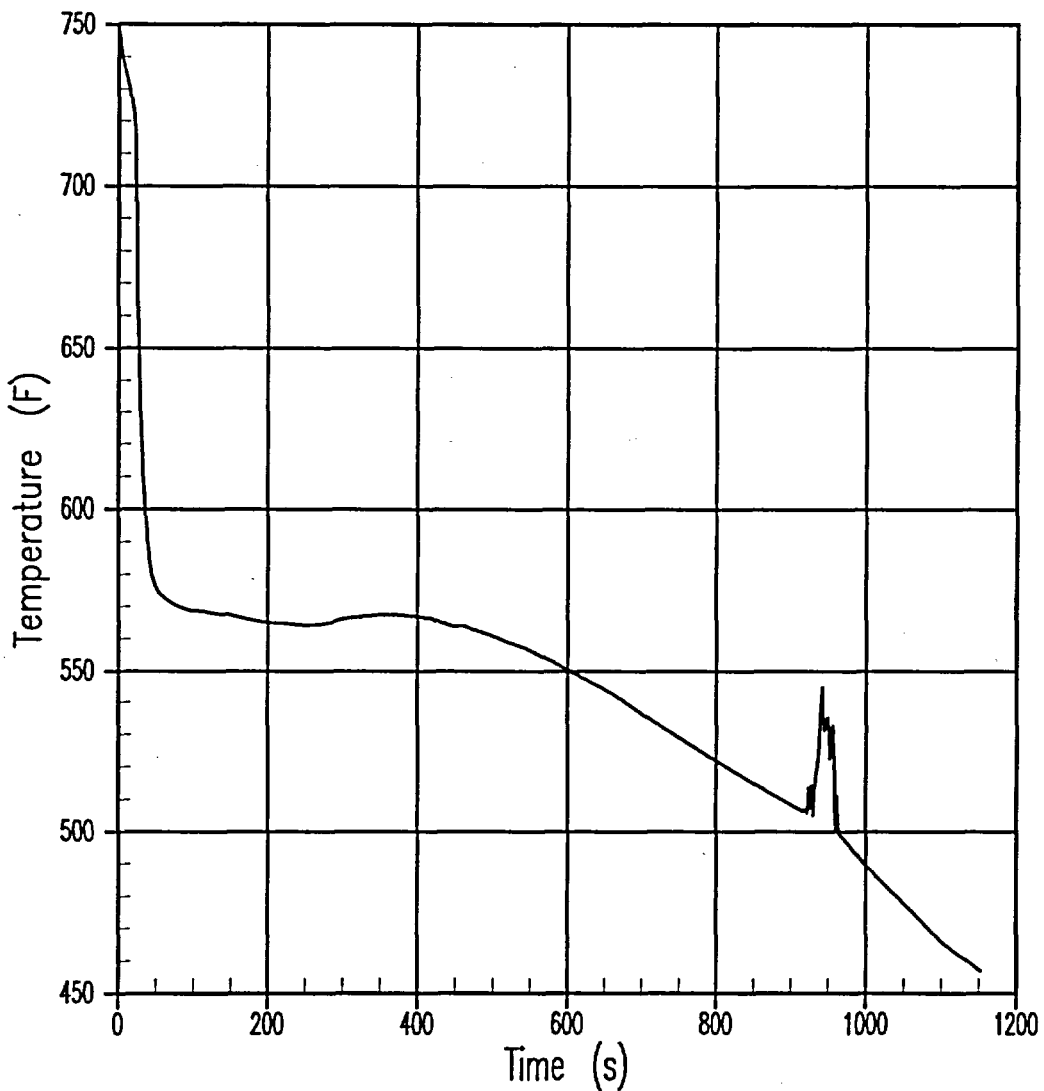


Figure 27-11-6. PCT, 4-Inch Break With OPA

Indian Point 2 BE SBLOCA Analysis
4-INCH CL BREAK WITH OPA
Total Safety Injection Flow

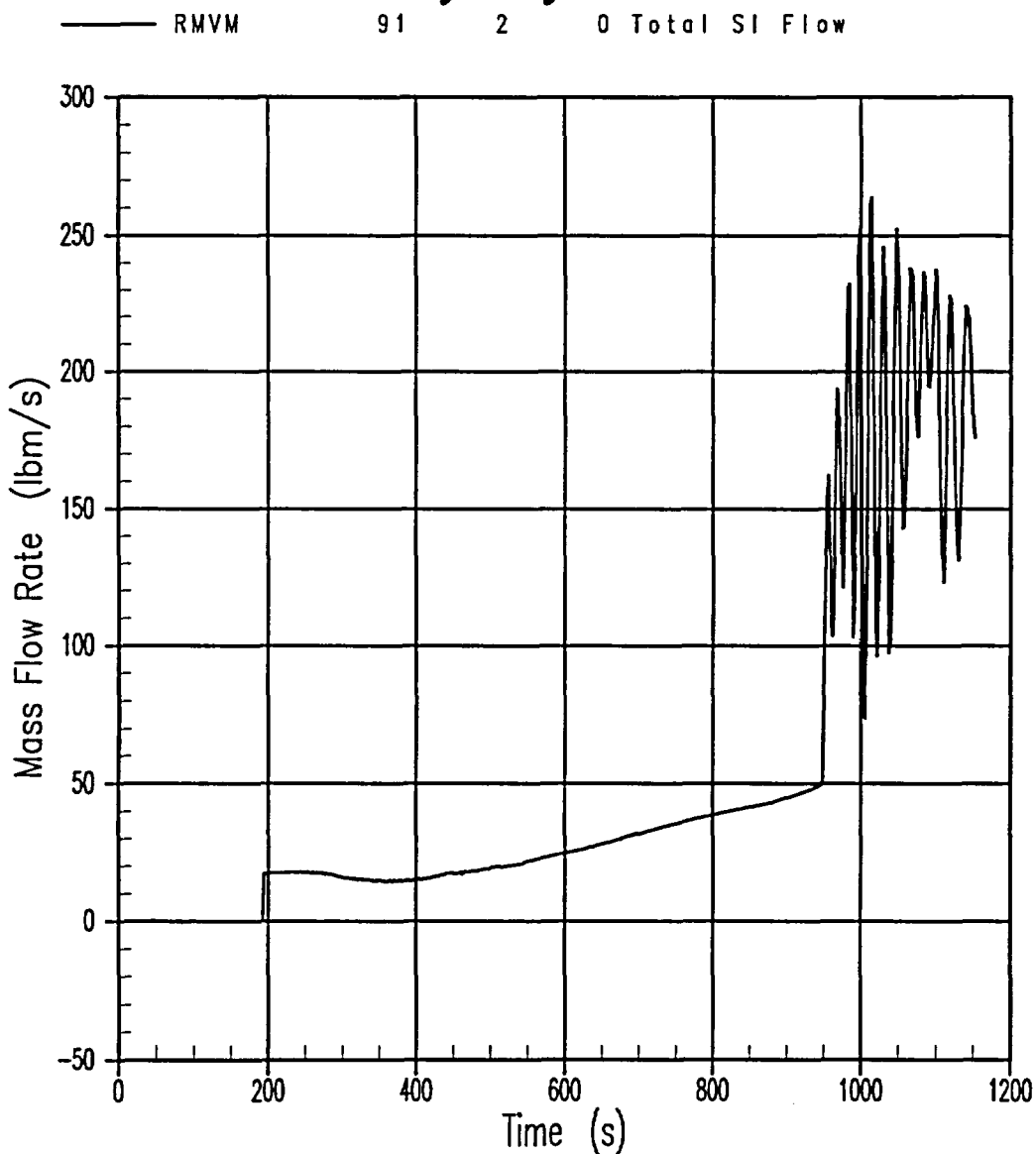


Figure 27-11-7. Total Safety Injection Flow to RCS, 4-Inch Break With OPA

27-12 6-Inch Cold Leg Break With OPA

The 6-inch break with OPA was simulated assuming the pump trip to occur 70 seconds after the S-signal setpoint is reached. This is consistent with the RCP trip assumption in the 3- and 4-inch breaks.

The sequence of events and overall behavior for the 6-inch equivalent diameter cold leg break with OPA and a 70-second RCP trip delay is illustrated in Figures 27-12-1 to 27-12-7. As with the smaller breaks, the LOOP (pump trip 30 seconds after the break) and OPA (delayed pump trip) transients are similar. Reactor trip occurs at 10.2 seconds. In the OPA case, the pumps continue to run until 83.1 seconds and then are tripped and begin to coast down. Because the 6-inch break is a relatively large break size, there is significant flashing during blowdown and a rapid depletion of the initial inventory. In the OPA case, as the pumps continue to run, steam is pumped into the broken cold leg early in the transient through partially voided loop seals. This reduces the break flow in the OPA case compared to the LOOP case. As the transient progresses, all of the loop seals refill with liquid, and Loop 23 replugs; the other loops do not totally replug, although they come close to doing so. The final clearance of the loop seals in Loops 22 and 24 begins at 192 seconds (Figure 27-12-4), while the final clearance of Loop 23 begins at 400 seconds. Although the minimum reactor vessel mass is not quite as low for the OPA case as in the LOOP case, the difference is not significant in the sense that neither of the 6-inch break cases has enough core uncoverage to enable the transient cladding temperature to reach the initial, normal operation value.

In comparing the primary pressures (Figure 27-12-1), it is seen that the delayed pump trip case depressurizes to the accumulator pressure at approximately the same time as the corresponding LOOP case. The PCT excursion is short-lived in the 6-inch case, as the cladding temperature peaks and then drops when accumulator injection begins. The loop seal clearing is characterized by oscillations in which multiple loop seals vent steam, then plug once again, then alternately clear again. This behavior is consistent with the assessment of Lee, et al. (1983) for break sizes greater than the threshold break size.

Indian Point 2 BE SBLOCA Analysis

6-INCH CL BREAK WITH OPA

Primary and Secondary System Pressures

— PN	54	1	0 PRZ PRESSURE
- - - P	130	2	0 SG21 SEC. PRESSURE
- - - P	138	2	0 SG22 SEC. PRESSURE
- - - P	146	2	0 SG24 SEC. PRESSURE
- - - P	154	2	0 SG23 SEC. PRESSURE

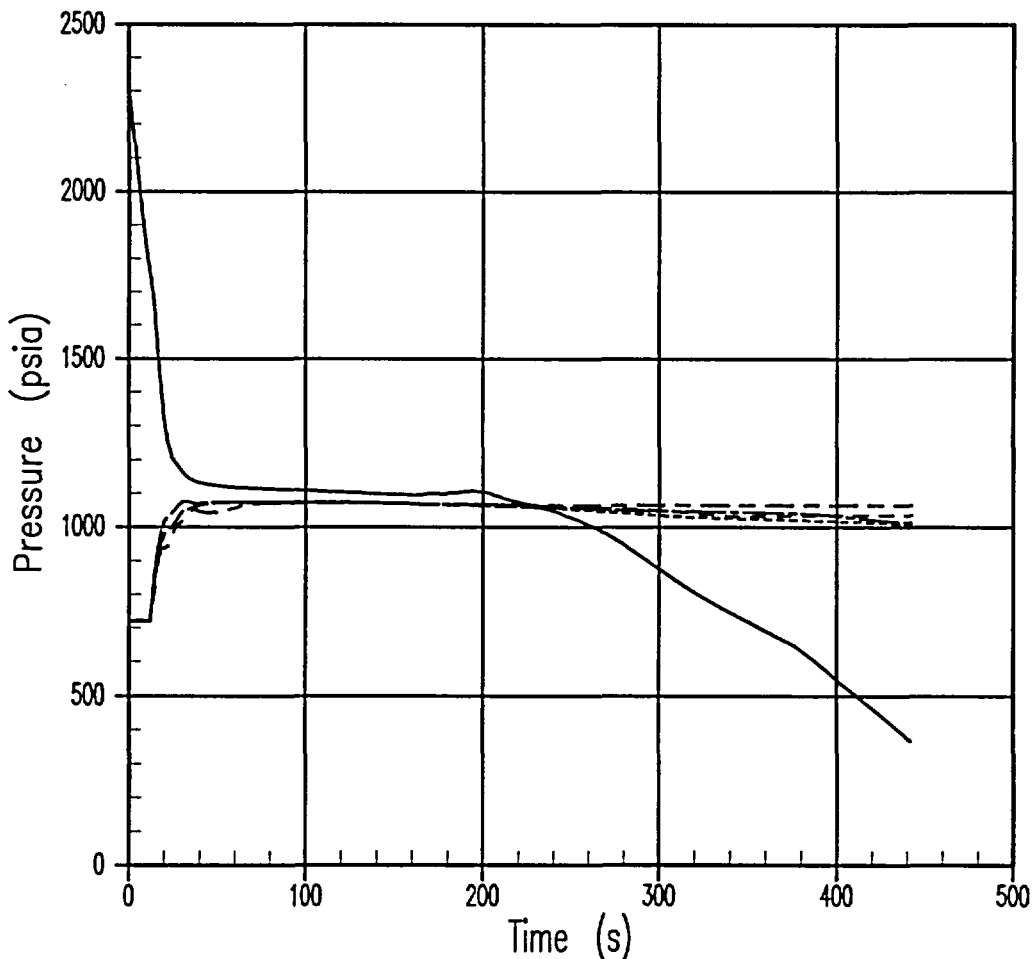


Figure 27-12-1. Primary and Secondary System Pressures, 6-Inch Break With OPA

Indian Point 2 BE SBLOCA Analysis
6-INCH CL BREAK WITH OPA
Core Collapsed Liquid Levels

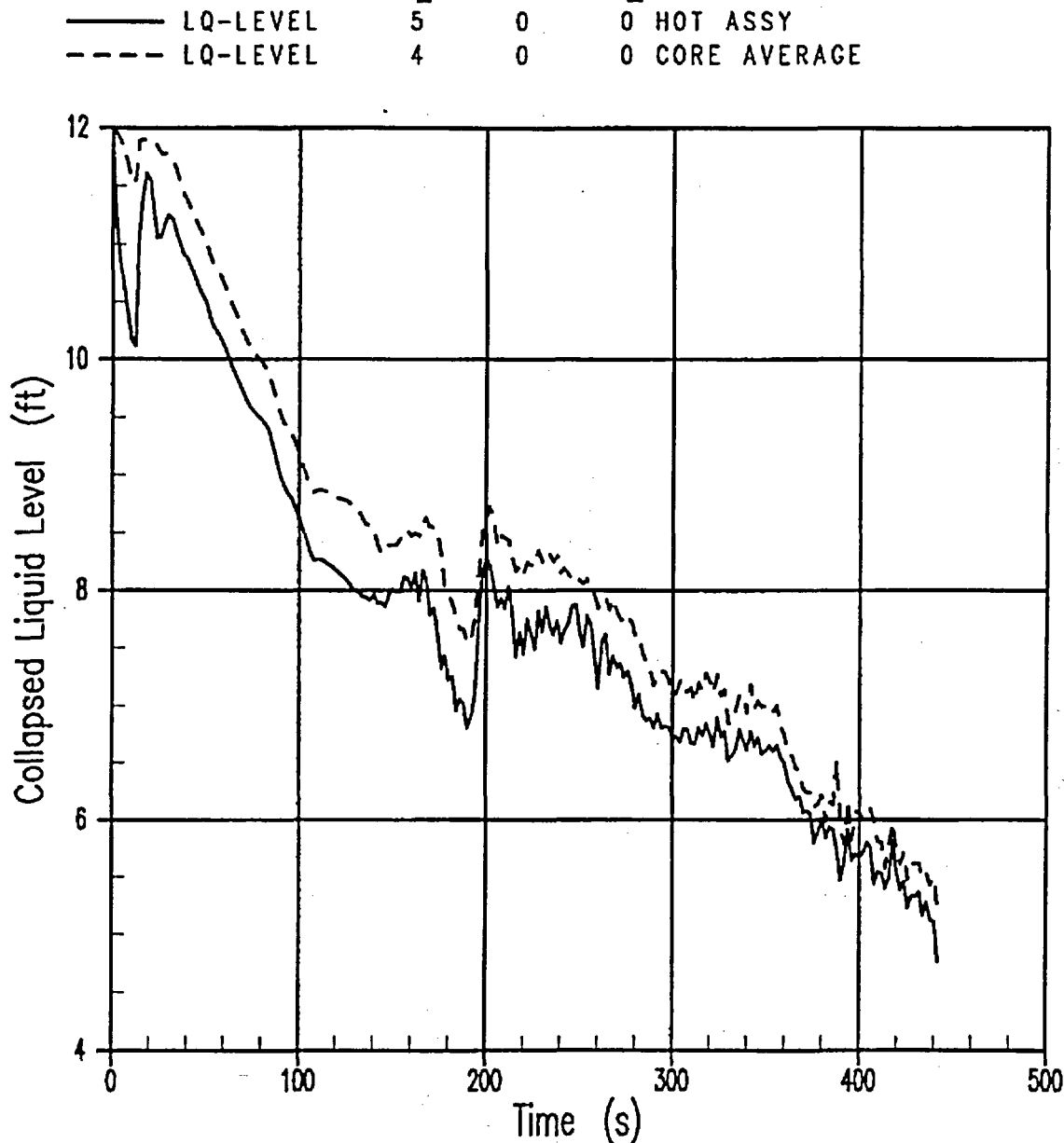


Figure 27-12-2. Core Collapsed Liquid Level, 6-Inch Break With OPA

Indian Point 2 BE SBLOCA Analysis
6-INCH CL BREAK WITH OPA
Break Flowrate and Void Fraction

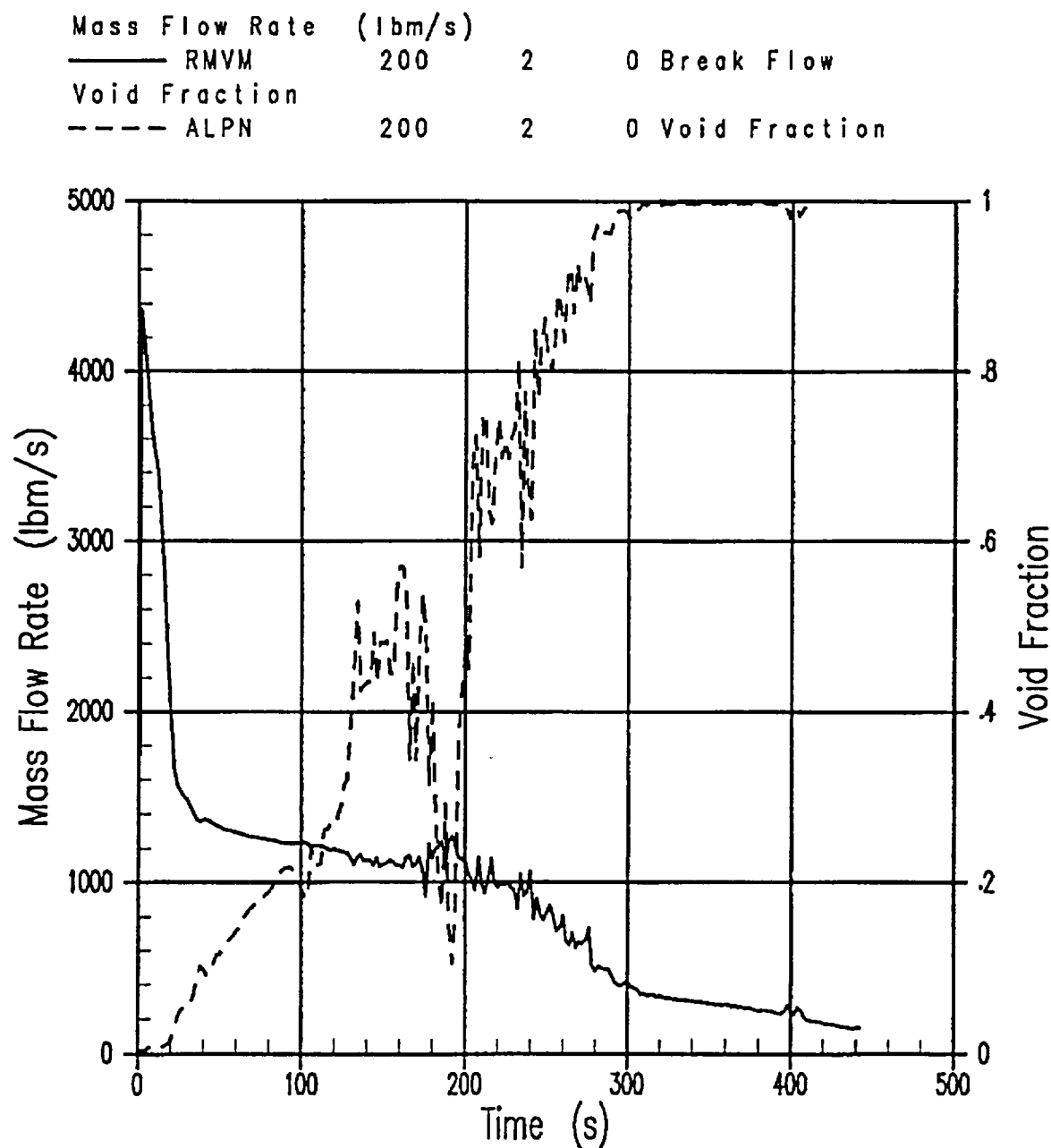
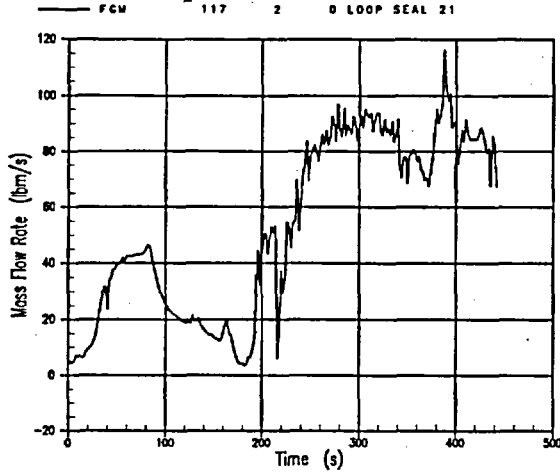


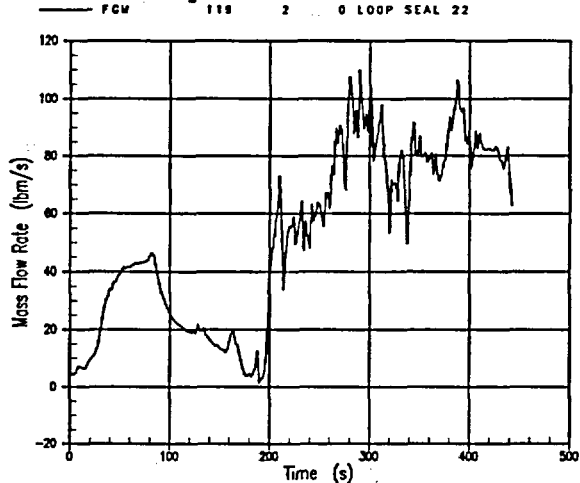
Figure 27-12-3. Break Flowrate and Void Fraction, 6-Inch Break With OPA

Indian Point 2 BE SBLOCA Analysis
6-INCH CL BREAK WITH OPA
Loop 21 Steam Flow



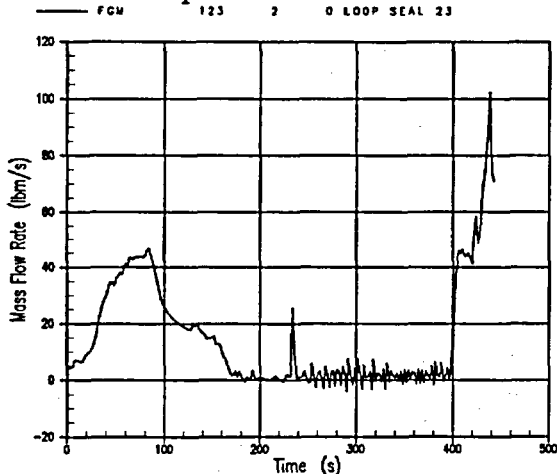
A. Loop 21 Loop Seal Steam Flow

Indian Point 2 BE SBLOCA Analysis
6-INCH CL BREAK WITH OPA
Loop 22 Steam Flow



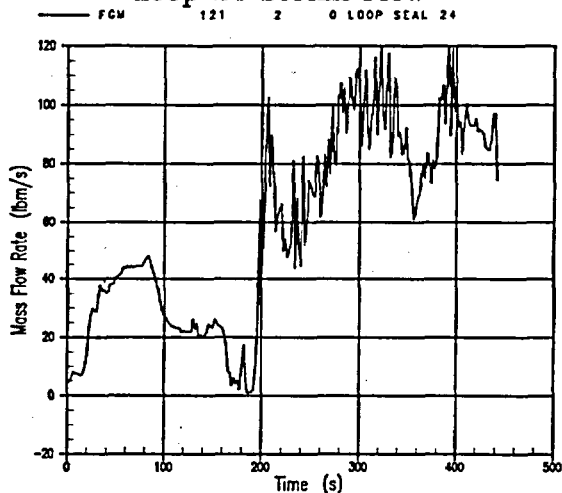
B. Loop 22 Loop Seal Steam Flow

Indian Point 2 BE SBLOCA Analysis
6-INCH CL BREAK WITH OPA
Loop 23 Steam Flow



C. Loop 23 Loop Seal Steam Flow

Indian Point 2 BE SBLOCA Analysis
6-INCH CL BREAK WITH OPA
Loop 24 Steam Flow



D. Loop 24 Loop Seal Steam Flow

Figure 27-12-4. Loop Seal Steam Flows, 6-Inch Break With OPA

Indian Point 2 BE SBLOCA Analysis
6-INCH CL BREAK WITH OPA
Reactor Vessel Mass

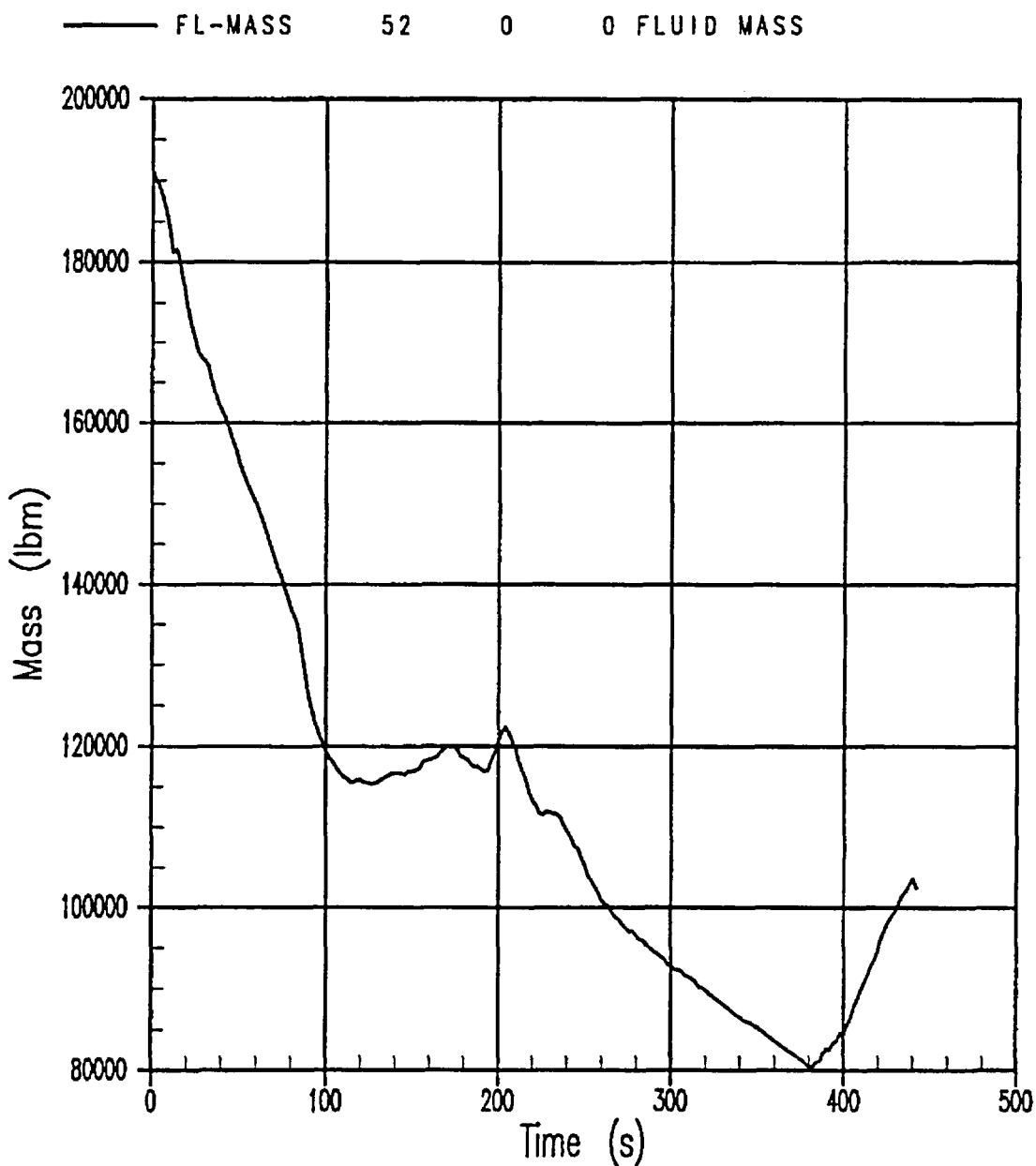


Figure 27-12-5. Reactor Vessel Mass, 6-Inch Break With OPA

Indian Point 2 BE SBLOCA Analysis
6-INCH CL BREAK WITH OPA
Peak Cladding Temperature

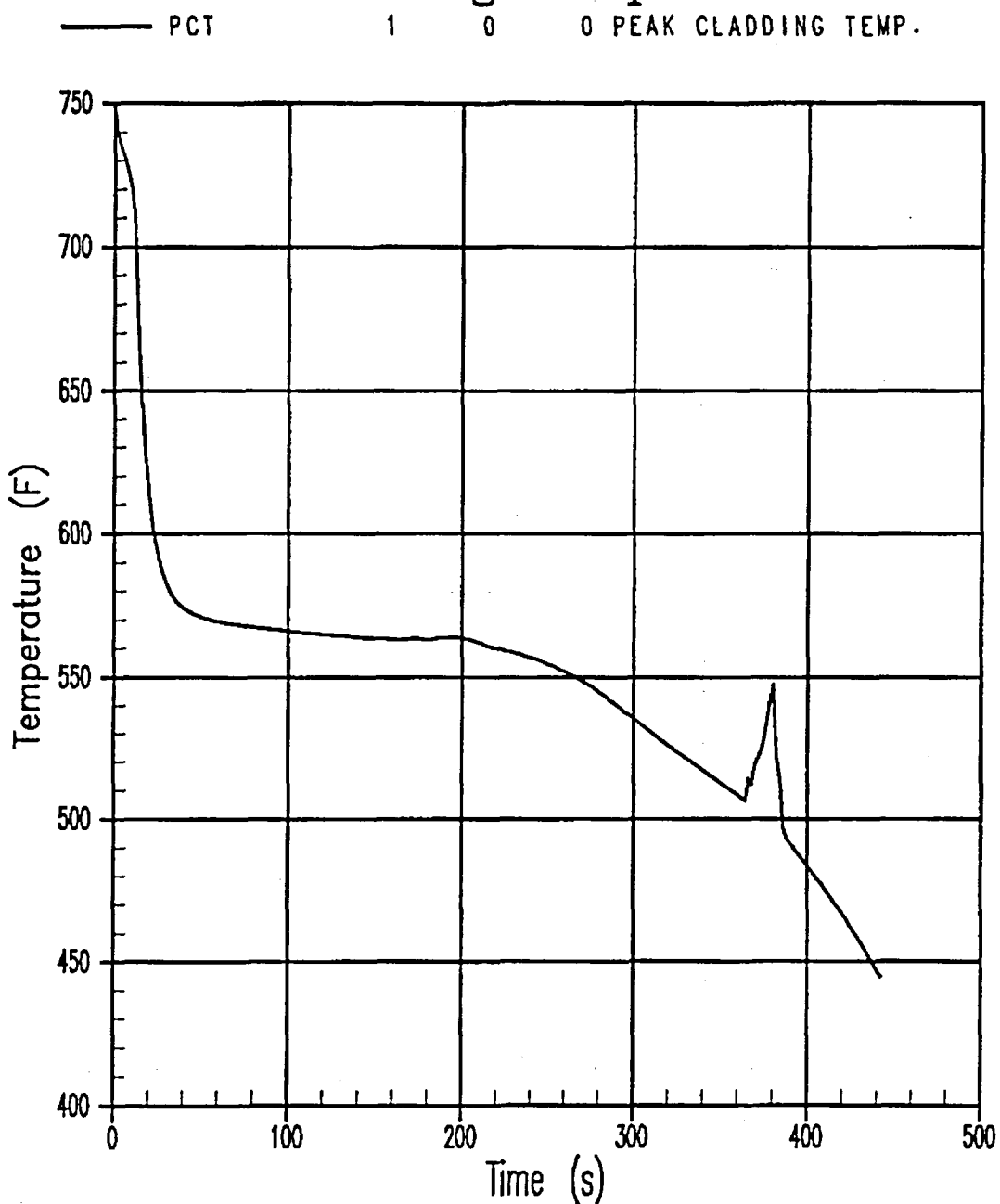


Figure 27-12-6. PCT, 6-Inch Break With OPA

Indian Point 2 BE SBLOCA Analysis
6-INCH CL BREAK WITH OPA
Total Safety Injection Flow

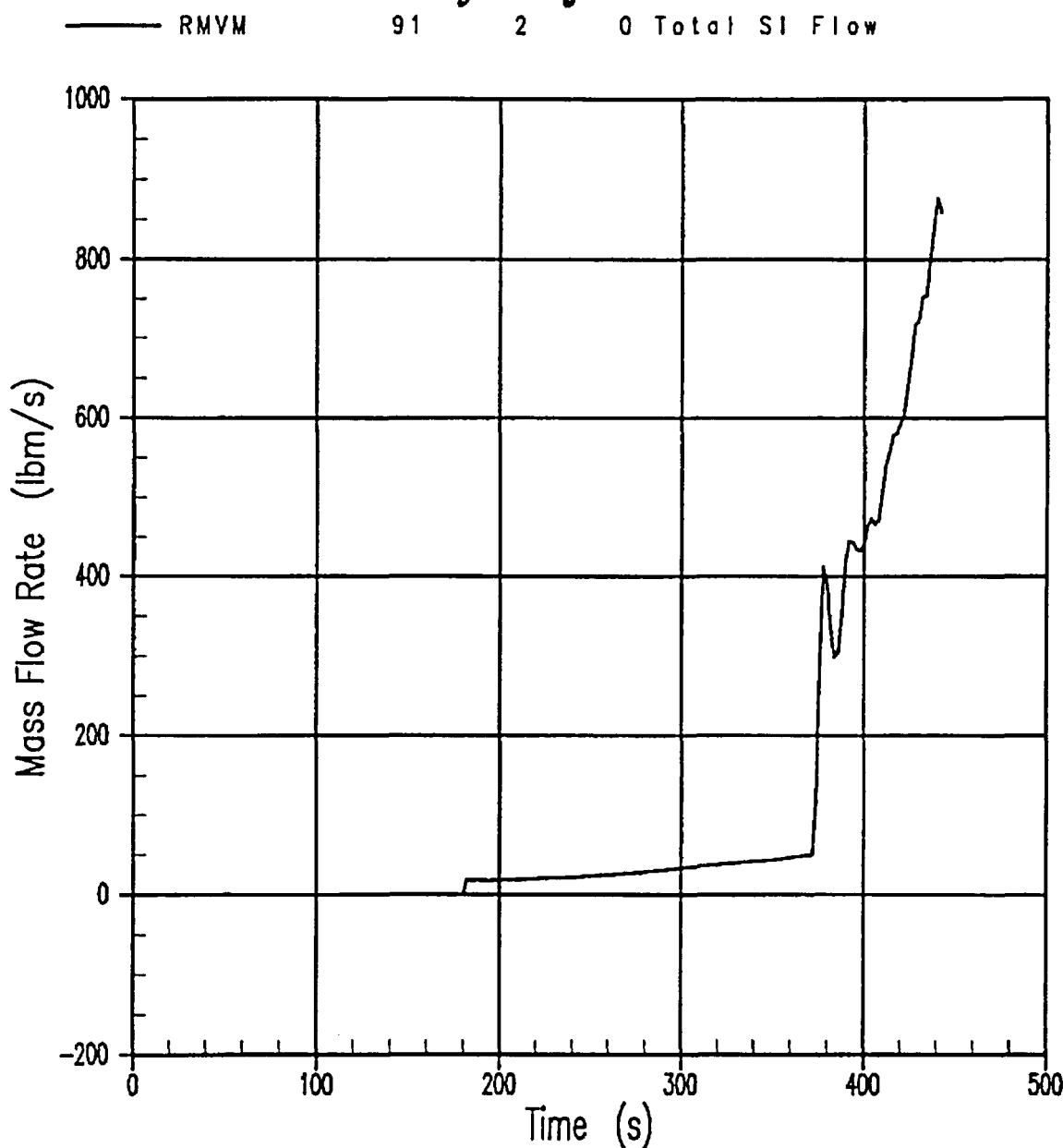


Figure 27-12-7. Total Safety Injection Flow to RCS, 6-Inch Break With OPA

27-13 10-Inch Cold Leg Break With OPA

The sequence of events and overall behavior for the 10-inch equivalent diameter cold leg break with OPA at a 70-second RCP trip delay is illustrated in Figures 27-13-1 to 27-13-7. Reactor trip occurs at 6.3 seconds. In the OPA case, the pumps continue to run until 77.5 seconds and then are tripped and begin to coast down. In comparison to the LOOP case, there is a significant redistribution of mass in the OPA case after 50 seconds while the pumps remain running. Mass from the downcomer is displaced from the inner vessel into the loops, as the pumps tend to make the system more homogeneous. As in the smaller break sizes, the running pumps in the OPA case push more steam into the broken cold leg, which reduces the break flow compared to the LOOP case as seen in Figure 27-13-3. The OPA case depressurizes to the accumulator pressure at about the same time as the LOOP case. Because of the higher mass retention, however, core uncovering does not occur; the inner vessel inventory is greater when the system mass redistributes after the RCPs are tripped (Figure 27-13-6) than in the LOOP case. Accumulator injection begins before the two-phase mixture level has decreased enough to uncover the fuel rods. No cladding heatup is observed when the core collapsed level decreases to 3 feet and below because although the core is highly voided throughout (void fraction of 0.6 at the bottom), dryout does not occur in the upper regions for a significant length of time.

Indian Point 2 BE SBLOCA Analysis

10-INCH CL BREAK WITH OPA

Primary and Secondary System Pressures

— PN	54	1	0 PRZ PRESSURE
- - - P	130	2	0 SG21 SEC. PRESSURE
- - - P	138	2	0 SG22 SEC. PRESSURE
- - - P	146	2	0 SG24 SEC. PRESSURE
- - - P	154	2	0 SG23 SEC. PRESSURE

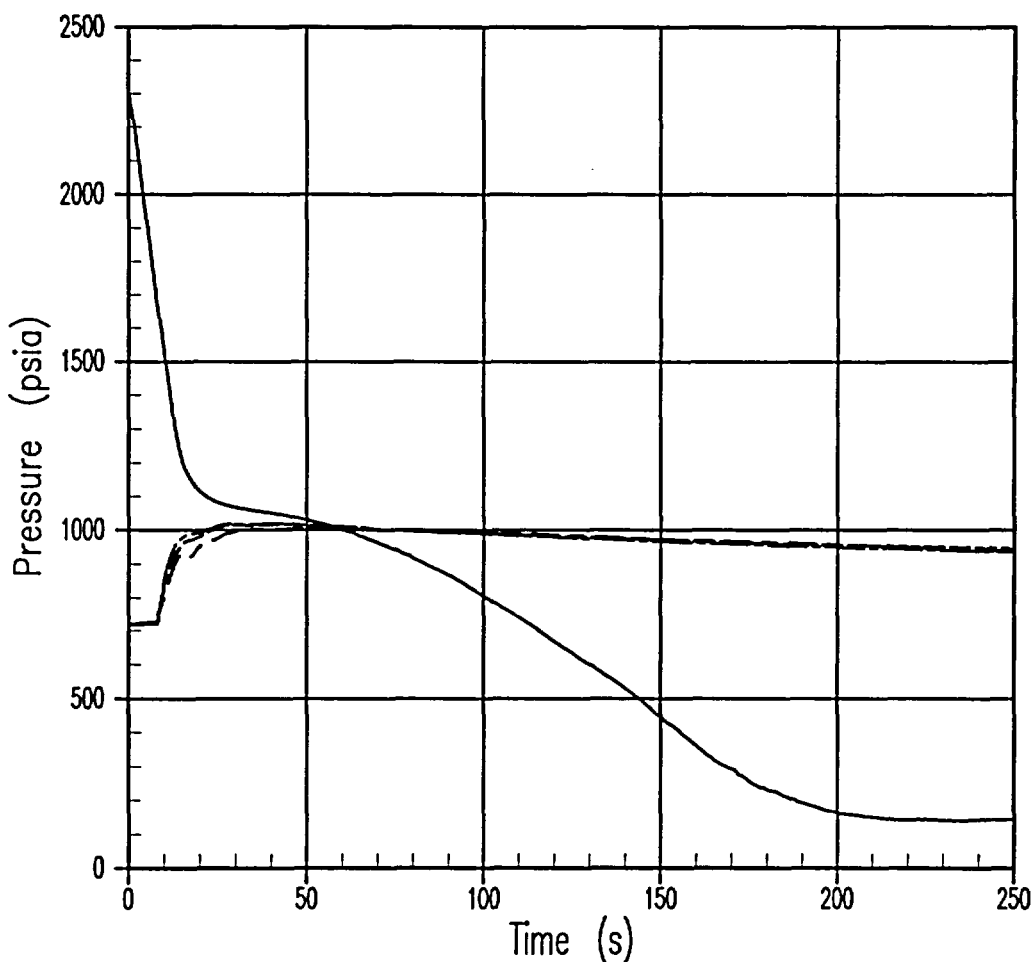


Figure 27-13-1. Primary and Secondary System Pressures, 10-Inch Break With OPA

Indian Point 2 BE SBLOCA Analysis
10-INCH CL BREAK WITH OPA
Core Collapsed Liquid Levels

— LQ-LEVEL 5 0 0 HOT ASSY
---- LQ-LEVEL 4 0 0 CORE AVERAGE

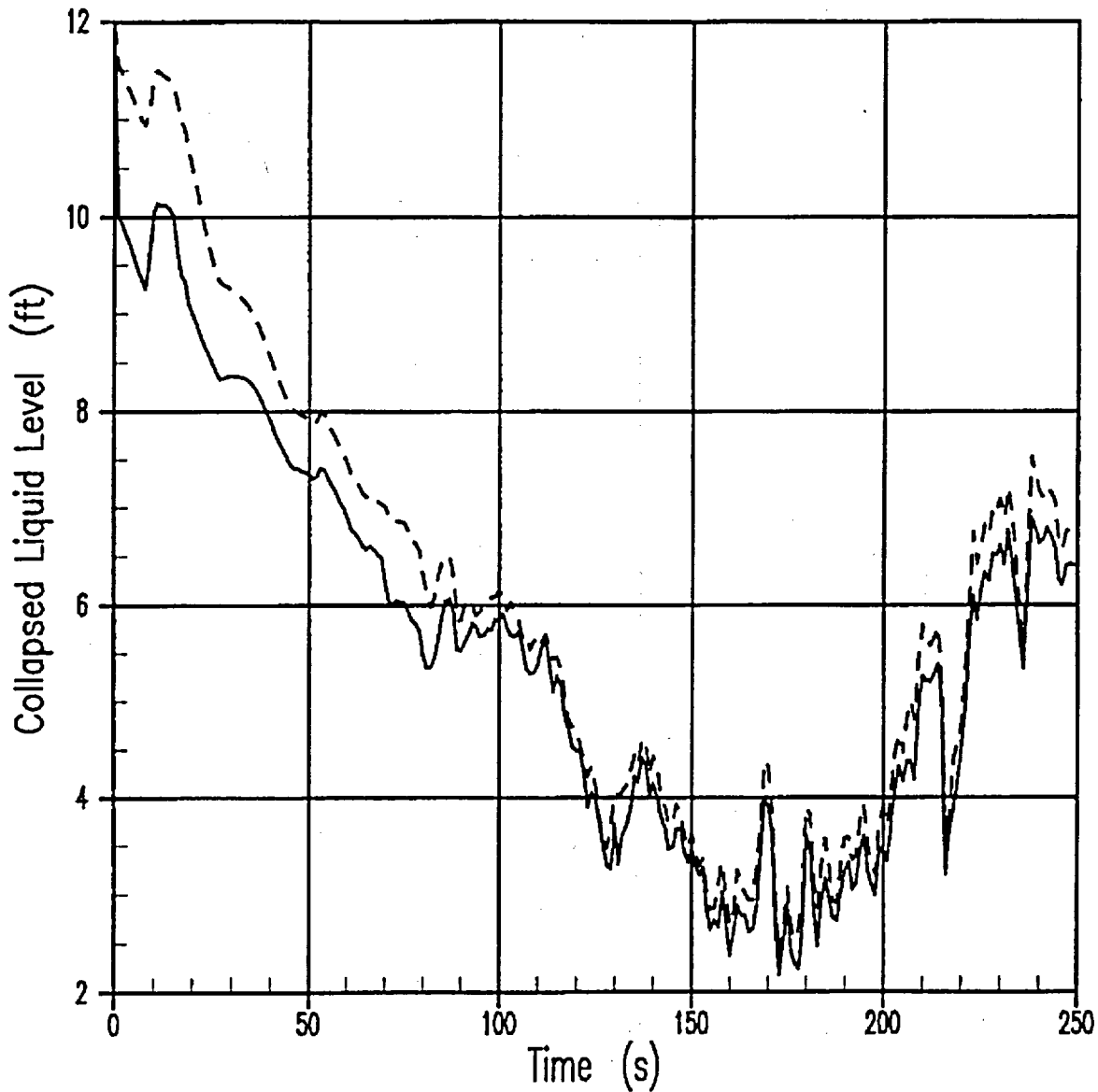


Figure 27-13-2. Core Collapsed Liquid Level, 10-Inch Break With OPA

Indian Point 2 BE SBLOCA Analysis 10-INCH CL BREAK WITH OPA Break Flowrate and Void Fraction

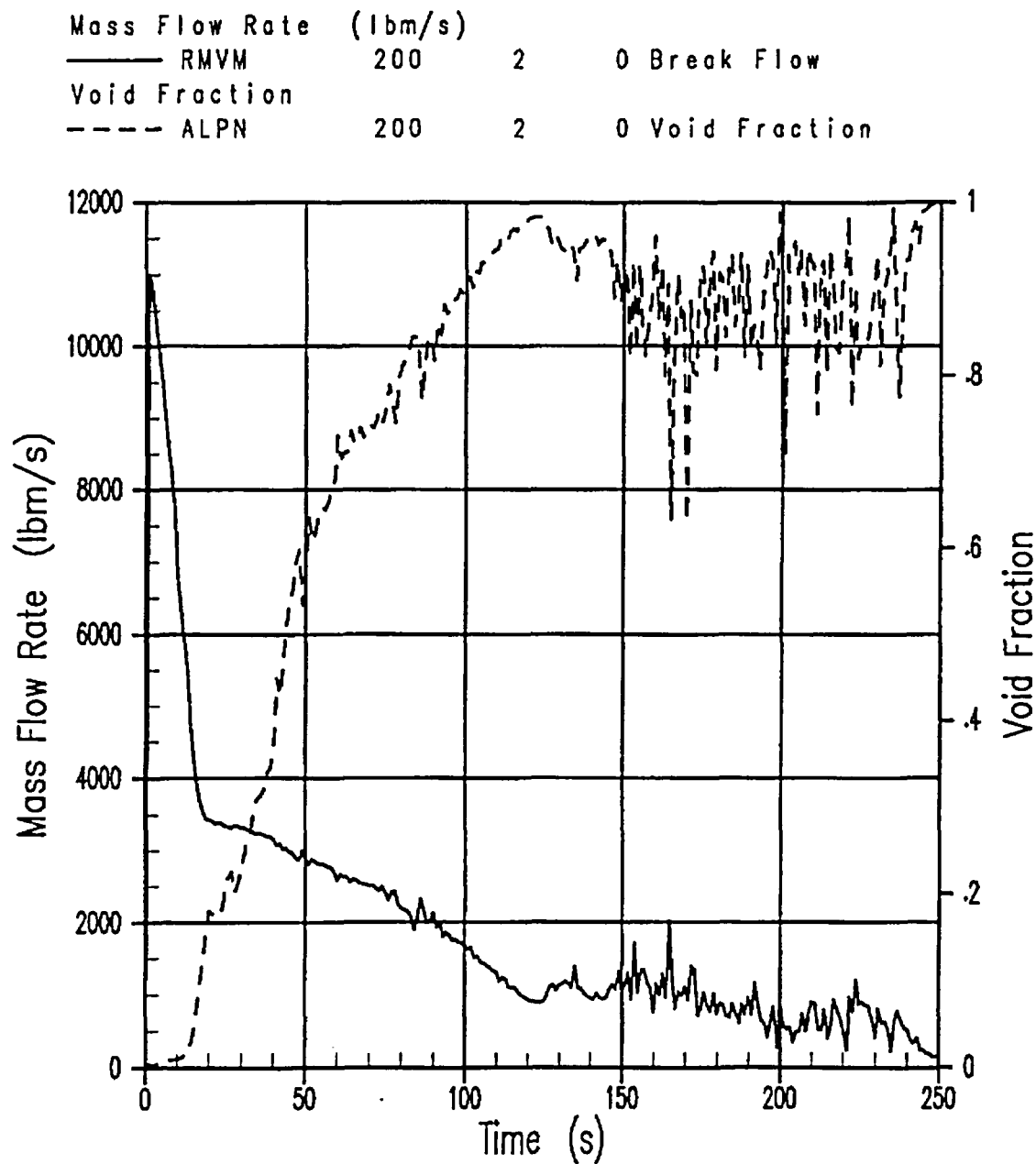
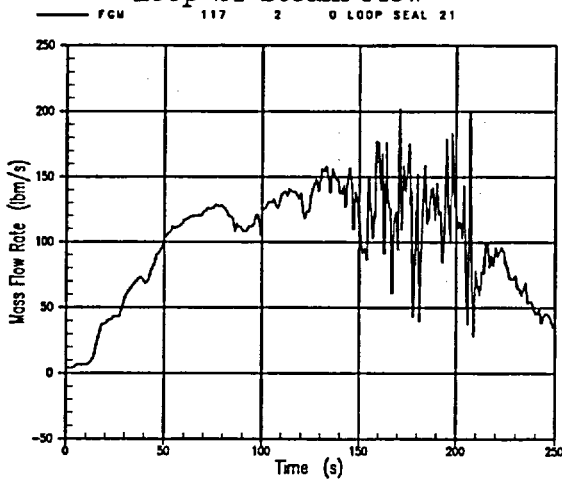


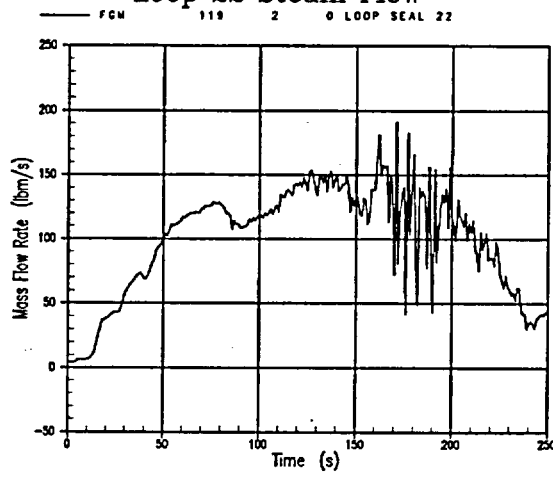
Figure 27-13-3. Break Flowrate and Void Fraction, 10-Inch Break With OPA

Indian Point 2 BE SBLOCA Analysis
10-INCH CL BREAK WITH OPA
Loop 21 Steam Flow



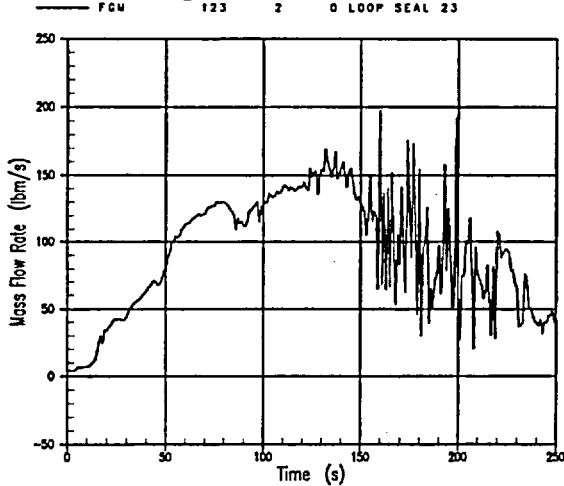
A. Loop 21 Seal Steam Flow

Indian Point 2 BE SBLOCA Analysis
10-INCH CL BREAK WITH OPA
Loop 22 Steam Flow



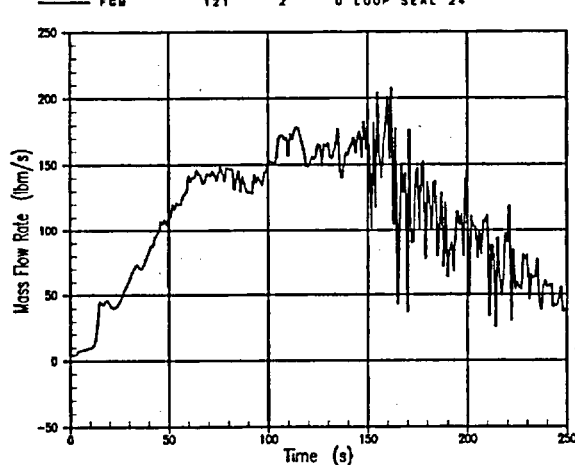
B. Loop 22 Loop Seal Steam Flow

Indian Point 2 BE SBLOCA Analysis
10-INCH CL BREAK WITH OPA
Loop 23 Steam Flow



C. Loop 23 Seal Steam Flow

Indian Point 2 BE SBLOCA Analysis
10-INCH CL BREAK WITH OPA
Loop 24 Steam Flow



D. Loop 24 Loop Seal Steam Flow

Figure 27-13-4. Loop Seal Steam Flows, 10-Inch Break With OPA

Indian Point 2 BE SBLOCA Analysis
10-INCH CL BREAK WITH OPA
Reactor Vessel Mass

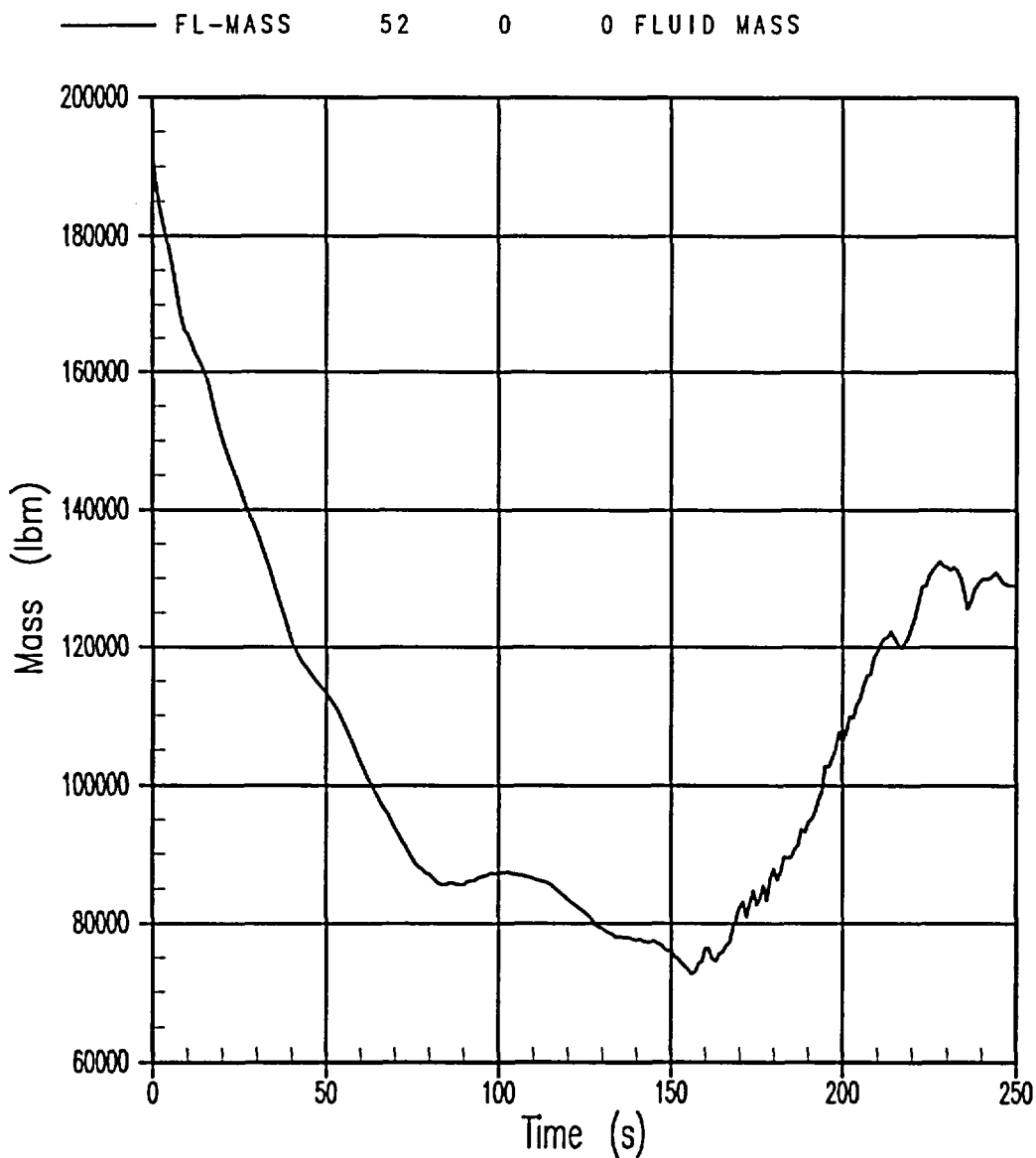


Figure 27-13-5. Reactor Vessel Mass, 10-Inch Break With OPA

Indian Point 2 BE SBLOCA Analysis
10-INCH CL BREAK WITH OPA
Peak Cladding Temperature

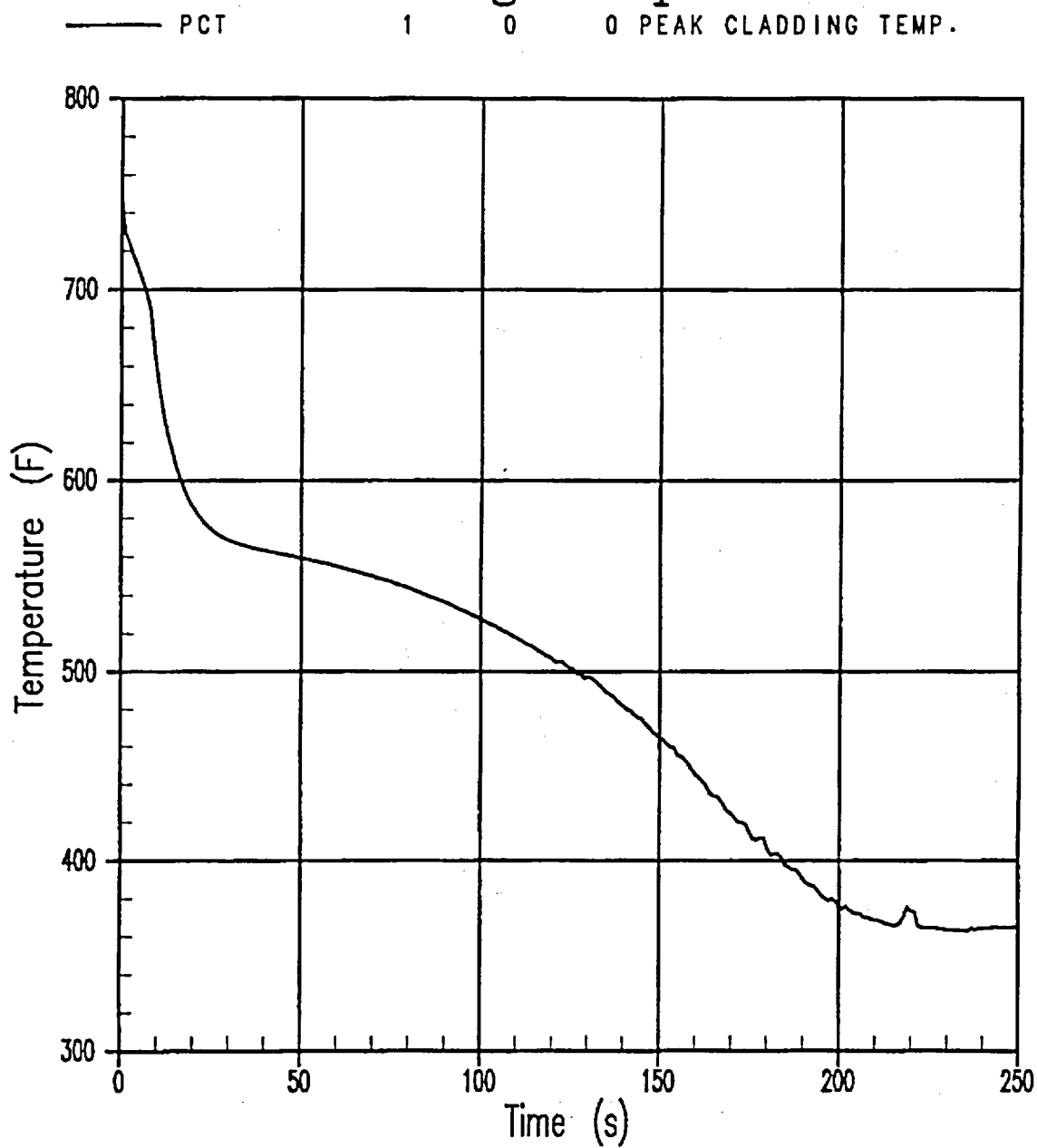


Figure 27-13-6. PCT, 10-Inch Break With OPA

Indian Point 2 BE SBLOCA Analysis
10-INCH CL BREAK WITH OPA
Total Safety Injection Flow

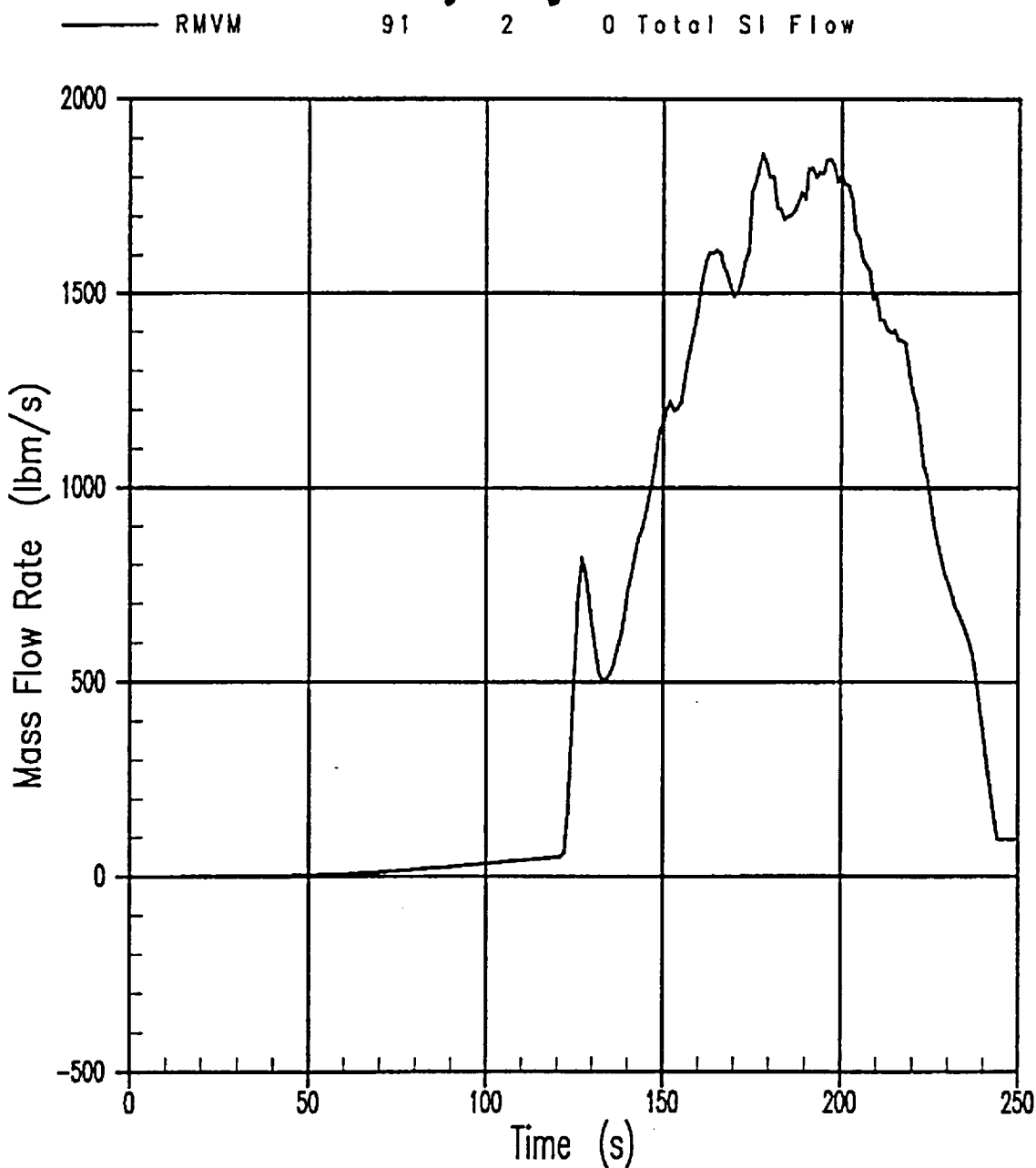


Figure 27-13-7. Total Safety Injection Flow to RCS, 10-Inch Break With OPA

27-14 Summary of OPA Cases

In the OPA scenario, the RCPs continue to run until they are manually tripped by the reactor operators. A break spectrum was executed for this scenario assuming that RCP trip occurs 70 seconds following the S-signal. In the LOOP scenario, when offsite power is assumed to be lost at the time of the reactor trip, the RCPs trip 30 seconds after reactor trip during the LOCA events.

The OPA calculations for a given break size were similar to the corresponding LOOP break of that size. Continued operation of the RCPs until manual trip at 70 seconds after the S-signal tends to homogenize the RCS inventory compared to the case when pumps trip due to LOOP. This had two effects on the transients:

- Vapor that normally became trapped in the upper plenum and at the top of the steam generator tubes early in the LOOP case transients is pumped around the loops to the cold legs in the OPA cases. Higher voiding in the broken cold leg in the OPA set of cases results in a reduction in the total break flow. The total RCS inventory is typically greater in the OPA scenarios for the assumed operator action time, which results in a net PCT benefit.
- Liquid is redistributed during the extended RCP operation compared to the LOOP scenario for a given break size. Because of the homogenization, water is moved from the downcomer and inner vessel to the loops. This liquid can drain to the reactor vessel later in the transient when the RCPs are tripped. Alternatively, extra water in the loops can decrease the depressurization rate after loop seal clearance if it passes through the break.

Table 27-14-1 provides a summary of the OPA transient results.

Table 27-14-1
OPA Transient Summary

Event	3-Inch	4-Inch	6-Inch	10-Inch
Break opens (s)	0.0	0.0	0.0	0.0
Reactor trip signal (s)	35.5	20.7	10.2	6.3
RCP delay time (operator actuated) (s)	109.7	94.6	83.1	77.6
S-signal (s)	39.7	24.6	13.1	7.6
Loop seal clearance begins (s)	732	403	174	13
Loop 21 steam venting	No	No	Yes	Yes
Loop 22 steam venting	No	Yes	Partially clears, replugs, clears	Yes
Loop 23 steam venting	Yes	Clears, replugs	Partially clears, replugs	Yes
Pressurizer loop 24 steam venting	Clears, replugs	Yes	Partially clears, replugs, clears	Yes
Boiloff core uncover begins (s)	N/A ^(a)	922	364	N/A
Minimum core collapsed liquid level during PCT excursion (ft)	N/A	7.4	5.8	N/A
Boiloff core uncover PCT (°F)	N/A	544	548	N/A
Boiloff core uncover PCT time (s)	N/A	942	380	N/A
Accumulator injection begins (s)	2063	953	376	123
Core recovery established (s)	N/A	964	386	N/A
Safety injection exceeds break flow (s)	2063	953	378	143

a. N/A = not applicable

27-15 Conclusions

This section discusses calculations of small break LOCA scenarios with and without RCP operation following reactor trip. The results of these calculations are compared to estimate the overall impact of the continued operation on the transient.

Comparing the times at which the loop seals began to clear in the LOOP and OPA cases, there is little or no difference except perhaps for the 10-inch break case. The 3- and 4-inch breaks show vapor passing through the loop seal early on in the OPA cases, but after the RCPs are tripped, the timing of the loop seal clearance event is similar in both cases. This suggests that while the continued pump operation in the OPA cases causes a mass redistribution in the RCS, the difference in total inventory resulting from extended pump operation is a consequence of the loop seal clearance prediction when comparing LOOP and OPA results for a given break size.

The minimum core collapsed liquid level times in the LOOP and OPA larger break size cases vary little because the depressurization to accumulator pressure varies little.

Figure 27-15-1 presents the PCT results calculated by WCOBRA/TRAC-SB for Indian Point Unit 2 for the LOOP cases as a function of the break area expressed as a percentage of the cold leg pipe cross-sectional area. The LOOP assumption produces a higher calculated core uncoverage PCT for every break size analyzed except the 6-inch equivalent diameter break; the core uncoverage PCT of the 6-inch OPA case is much lower than the steady-state nominal operation value. Figure 27-15-1 shows that within the range of small break LOCAs, the 3-inch equivalent diameter break is limiting for Indian Point Unit 2. With regard to the overall uncertainty in a realistic small break LOCA, the identified limiting break size (3 inches, with the LOOP assumption) is bounding for Indian Point Unit 2. The scoping studies that follow in Section 28 and the sensitivity cases in Volume 4 will, therefore, consider the 3-inch break with LOOP case to determine the 95th percentile PCT value for Indian Point Unit 2.

27-16 References

Lee, N., et al., 1983, "Phenomenological Uncertainty During Loop Seal Steam Venting in a Small Break Cold Leg LOCA of a PWR," Paper 83-HT-104, National HT Conf., Seattle, WA.

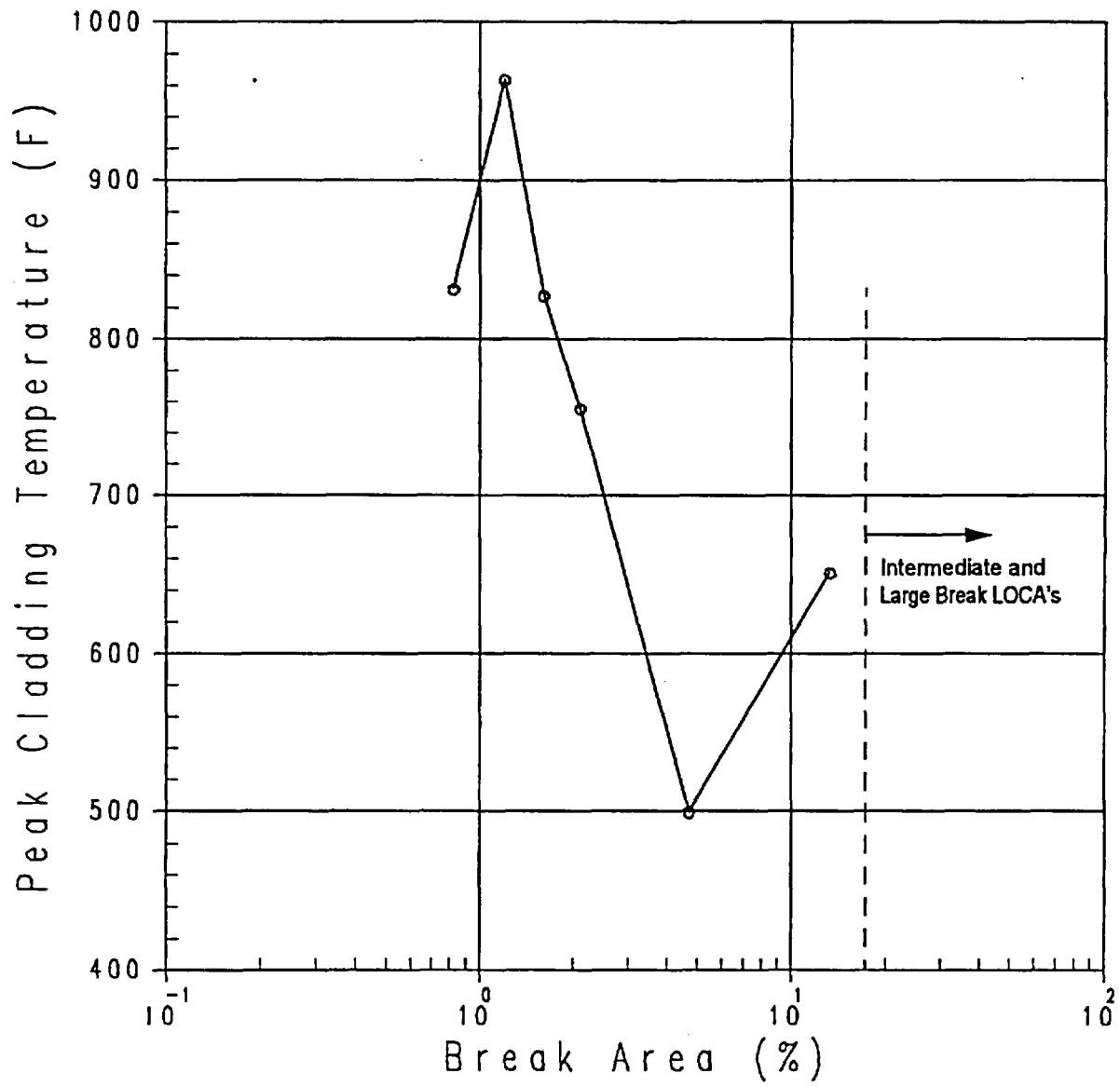


Figure 27-15-1. Peak Cladding Temperature as a Function of Break Area, LOOP Cases

SECTION 28

PWR SCOPING STUDIES FOR GEOMETRIC CONFIGURATION

28-1 Introduction

The objective of the PWR scoping studies is to examine the sensitivity of small break LOCA transients to geometric parameters: break location, break orientation, and steam generator tube plugging (SGTP). The reference case, as identified in Section 27, is a 3-inch diameter break at the top of the cold leg in loop 24, the pressurizer loop. All sensitivity cases examined in this section modelled the 3-inch equivalent diameter break. The locations examined were the hot leg, crossover leg, and cold leg in a nonpressurizer loop (loop 21). For the break orientation sensitivity study, the top, bottom, and side breaks were examined at the reference case location.

Figure 28-1-1 shows the schematic diagram of Indian Point Unit 2 Nuclear Steam Supply System (NSSS). The break locations examined consist of the reference break location in the pressurizer loop (X'); cold leg (X), hot leg (Z), and pump suction (Y) sensitivity study break locations in a non-pressurizer loop.

Figure 28-1-2 shows the conceptual basis of the break orientation study. As seen in this figure, the break is modelled by a one-dimensional (1-D) pipe component and a break component. For the top break configuration, the 1-D pipe is attached vertically at the top of the top cell of the simulated cold leg. The side break configuration is modelled by the 1-D pipe attached horizontally at the side of the middle cell among the cold leg cells. The bottom break is modelled by the 1-D pipe attached downward vertically at the bottom.

A typical small break LOCA transient is assumed to be initiated by a break in the primary system piping. Upon initiation of the break, the primary system depressurizes quickly to the saturation pressure corresponding to the hot leg liquid temperature. The system depressurizes more slowly after reaching the saturation pressure, due to flashing of hot liquid in the primary system. A reactor trip signal is generated by the low pressurizer pressure setpoint at 1815 psia, leading to turbine trip and isolation of the steam generator secondary side; it then may pressurize to the steam generator secondary safety valve setpoint pressure. Following main feedwater pump trip and isolation, the auxiliary feedwater system is automatically actuated, and it begins delivering flow to the SG secondary sides 75 seconds later.

After reactor trip the RCS continues to depressurize and reaches the pressurizer low-low pressure setpoint of 1715 psia, which generates a safety injection (SI) S-signal. The flow of SI is initiated

45 seconds after the S-signal generation in the LOOP case, 38 seconds if offsite power is available. After a time, the RCS depressurization is halted, as the RCS reaches a quasi-equilibrium pressure condition just above the steam generator secondary side pressure. During this period, the break flow is all liquid and the steam generators are active heat sinks. The vapor generated in the core is trapped within the RCS for a cold leg break because the loop seals are plugged. The pressure is maintained almost constant because the vapor generation in the core is balanced by condensation in the steam generators and the volumetric loss through the break. At the end of this period, the inner vessel liquid level depresses compared to the downcomer liquid level due to the increasing vapor volume trapped in the inner vessel.

This quasi-equilibrium state is upset when at least one loop seal clears and the vapor generated in the core can vent through the break causing the RCS to start to depressurize once again. The loop seal clearing also relieves the pressure difference that caused the liquid level difference between the inner vessel and the downcomer/cold legs, and the liquid level in the inner vessel increases.

Following the loop seal clearing event, the RCS depressurization is accompanied by a gradual decrease in the inner vessel liquid level for as long as the core boiloff rate exceeds the SI flowrate and the condensation in the system. This condition can persist until the RCS pressure falls below the accumulator cover gas pressure of 655 psia.

The PCT typically occurs when the mixture level is at its lowest in the core, before the SI/accumulator injection exceeds the boiloff rate and raises the core mixture level. As the RCS pressure decreases, the SI injection flow increases. The small break LOCA transient is considered to have terminated when the SI flow exceeds the break flow and the fuel is quenched.

Table 28-1-1 lists the timing sequence of significant small break LOCA transient events for the sensitivity cases examined in Section 28. LOOP occurs at reactor trip, and RCP coastdown begins 30 seconds after the reactor trip signal in each of these cases. The following subsections describe each individual transient in detail.

Table 28-1-1
Time Sequence of Events for 3-Inch Sensitivity Cases

Event	Bottom of Cold Leg	Top of Cold Leg	Side of Cold Leg	Hot Leg	Pump Suction Leg	Nonpressurizer Loop Cold Leg
Break (s)	0	0	0	0	0	0
Reactor trip (s)	36	35.5	36	64.3	36.8	35.4
S-signal (s)	39.8	39.8	40	69	41.1	39.6
Quasi-SS (s)	220	240	240	320	240	240
Loop seal clearing (s)	640	640	630	1115	680	720
Boiloff core uncover (s)	N/A	N/A	N/A	N/A	N/A	N/A
Accumulator injection (s)	1815	1705	>2500	1855	1870	2120
Time of PCT (s)	0	0	0	0	0	0
Beginning of core heatup (s)	N/A	N/A	N/A	N/A	N/A	N/A
PCT (°F)	748	748	748	748	748	748

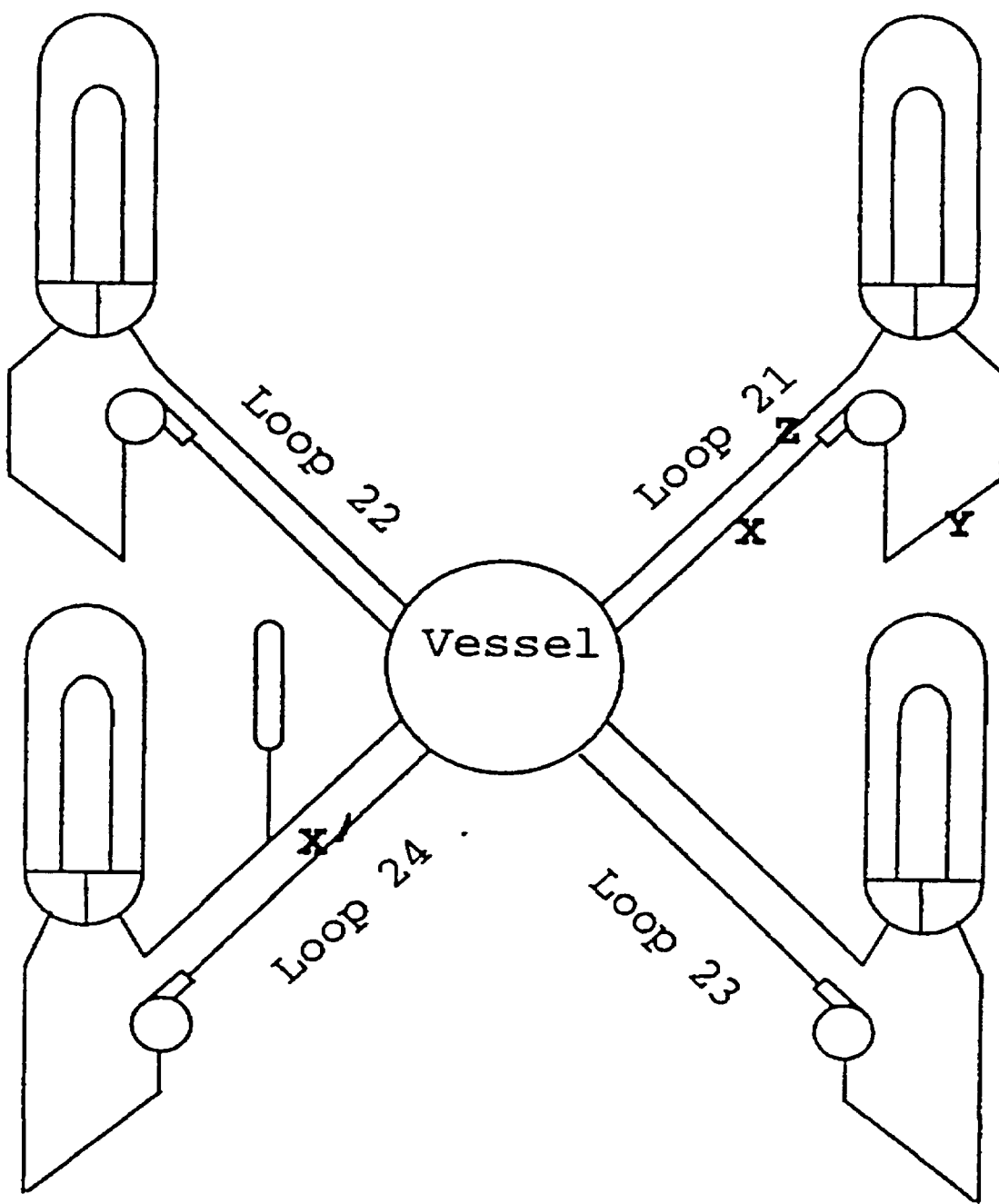


**Figure 28-1-1. Indian Point Unit 2 NSSS Schematic Diagram
With WCOBRA/TRAC Loop Designations**

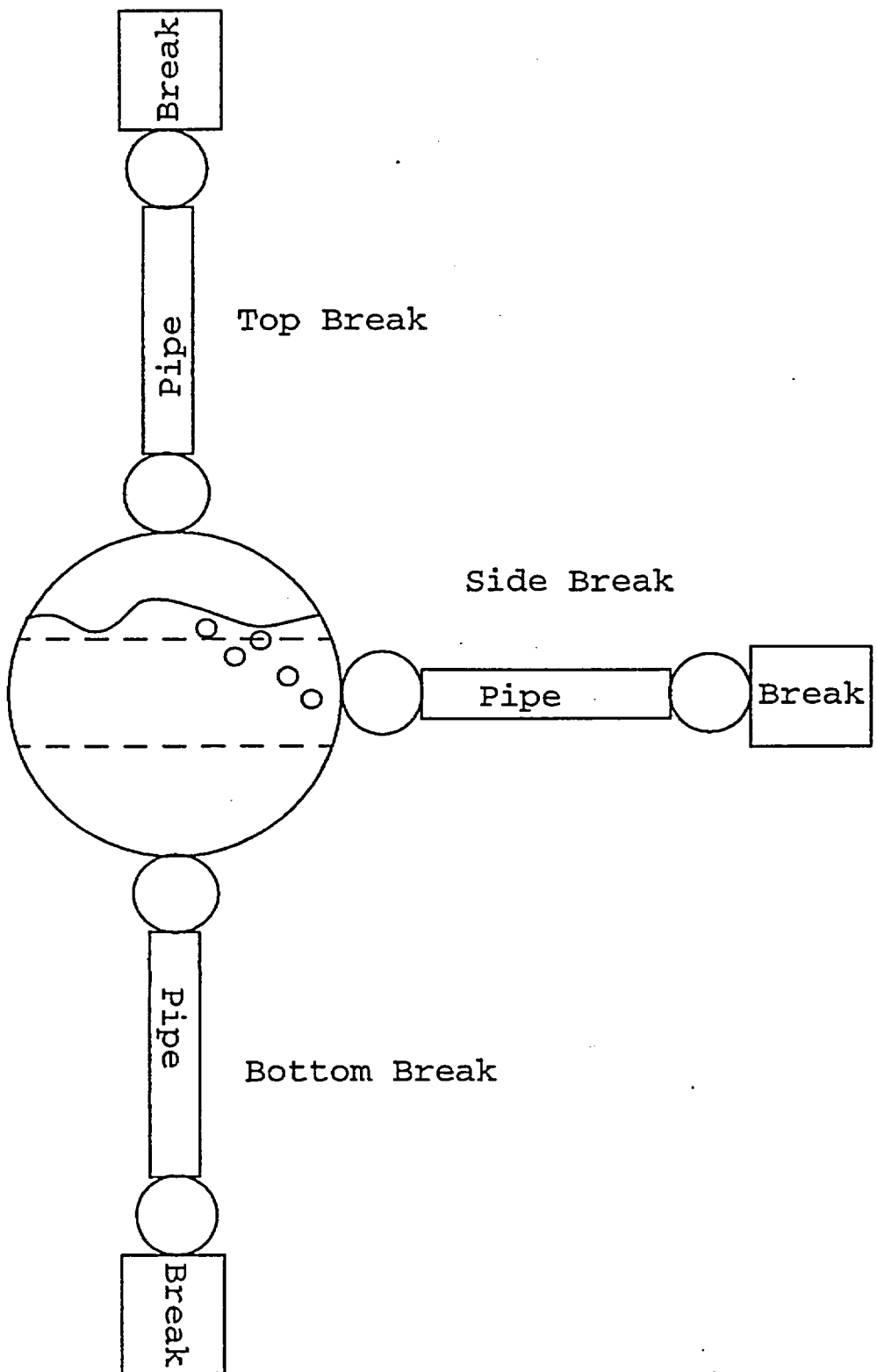


Figure 28-1-2. Modelling Used for Break Orientation Study

28-2 Break Location Study

This section describes the break location sensitivity runs. Significant parameters – such as the system pressure, the integrated break mass flow, the downcomer collapsed liquid level, the inner vessel collapsed liquid level, and the PCT – are compared against the reference case.

Figures 28-2-1 through 28-2-5 show the comparison plots for the case where the break is assumed in the nonpressurizer loop. Figures 28-2-6 through 28-2-12 show the comparison plots for the pump suction break case. Figures 28-2-13 through 28-2-17 show the plots for the hot leg break case.

28-2-1 Cold Leg Break in a Nonpressurizer Loop

28-2-1-1 Model Description

The break location was moved from the cold leg of loop 24 to the cold leg of loop 21 (marked X in Figure 28-1-1). Because all four loops are essentially identical except for the pressurizer, this modelling examines the effect of the pressurizer loop location on the small break LOCA transient.

28-2-1-2 Description of Transient (Figures 28-2-1 through 28-2-5)

Upon initiation of the break, the primary system depressurizes quickly to the saturation pressure corresponding to the hot leg liquid temperature. A reactor trip signal is generated by the low pressurizer pressure setpoint of 1815 psia at 35.4 seconds after the break. The LOOP assumption results in RCP trip 30 seconds later. Turbine trip, and isolation of the steam generator secondary side, follow reactor trip. The steam generator secondary side pressurizes to a safety valve setpoint relief pressure of 1080 psia. Following main feedwater pump trip and isolation, the auxiliary feedwater system automatically actuates and begins delivering flow to the secondary side 75 seconds later.

The RCS continues to depressurize and reaches the pressurizer low-low pressure setpoint of 1715 psia at 39.6 seconds after the break, which generates an S-signal. The SI initiates 45 seconds after the S-signal generation.

The RCS depressurization is halted, and the RCS reaches a quasi-equilibrium pressure condition at 240 seconds after the break just above the steam generator secondary side pressure. During

this period, the break flow is all liquid and the steam generators are active heat sinks. The vapor generated in the core is trapped within the RCS due to loop seal plugging. The pressure is maintained in this period because the vapor generation in the core is balanced by condensation in the steam generators and the volumetric loss through the break. During this period, the inner vessel liquid level is depressed compared to the downcomer liquid level due to the increased vapor volume in the inner vessel which is unable to vent.

This quasi-equilibrium state is upset when the loop seal clears at 720 seconds after the break and the vapor generated in the core starts to vent through the break. Consequently, the RCS depressurizes. The loop seal clearing also allows the liquid level in the inner vessel to approach the downcomer liquid level. Both the broken loop loop seal and its adjacent loop loop seal clear in this case.

Following the loop seal clearing event, as the RCS depressurization proceeds only a small decrease occurs in the inner vessel liquid level. The core boiloff rate exceeds the SI delivery rate and condensation in the system, but liquid provided to the downcomer provides enough margin so that core uncovering does not occur.

The RCS pressure falls below the accumulator cover gas pressure of 655 psia at 2120 seconds after the break. The PCT for this transient occurs at the time of the break.

28-2-1-3 Comparison to Reference Case

After the loop seal clearance, the break flow completes the transition from liquid to vapor earlier than the reference case, within 1000 seconds after the break, which results in less total break flow (Figure 28-2-2). The inner vessel collapsed liquid level (core to upper plenum) shows the effect of the second loop seal clearance compared to the reference case transient (Figure 28-2-4). This difference in loop seal clearing results in the sensitivity case having more mass in the reactor vessel at the beginning of boiloff and subsequently at the minimum liquid level. The minimum vessel collapsed liquid level calculated is high enough so that no core uncovering is predicted to occur, and no cladding temperature excursion occurs.

28-2-2 Break at Pump Suction

28-2-2-1 Model Description

The break location was moved from the bottom of the cold leg in loop 24 to the bottom of the crossover leg in loop 21 []^{a,c}. The bottom of the crossover leg is 17.5 feet above the bottom of vessel, which is 8.6 feet lower than the WCOBRA/TRAC cold leg bottom elevation. However, due to the presence of a weir at the outlet of the pump, the downcomer/cold leg liquid level is at the top of the weir.

28-2-2-2 Description of Transient (Figures 28-2-6 through 28-2-10)

Upon initiation of the break, the primary system depressurizes quickly to the saturation pressure corresponding to the hot leg liquid temperature. A reactor trip signal is generated by the low pressurizer pressure setpoint of 1815 psia at 36.8 seconds after the break. The LOOP assumption results in RCP trip 30 seconds later. Turbine trip, and isolation of the steam generator secondary side, follow reactor trip. The steam generator secondary pressurizes to a safety valve setpoint relief pressure of 1080 psia. Following main feedwater pump trip and isolation, the auxiliary feedwater system is automatically actuated and begins delivering flow to the secondary side 75 seconds later.

The RCS continues to depressurize and reaches the pressurizer low-low pressure setpoint of 1715 psia at 41.1 seconds after the break, which generates an S-signal. The SI is initiated 45 seconds after the S-signal generation.

The RCS depressurization is halted, and the RCS reaches a quasi-equilibrium pressure condition at 240 seconds after the break just above the steam generator secondary side pressure. During this period, the break flow is all liquid and the steam generators are active heat sinks. The vapor generated in the core is trapped within the RCS because the loop seals have yet to clear. The pressure is maintained in this period because the vapor generation in the core is balanced by condensation in the steam generators and the volumetric loss through the break. During this period, the inner vessel liquid level is depressed compared to the downcomer liquid level due to the increased vapor volume in the inner vessel which is unable to vent.

This quasi-equilibrium state is upset when two intact loop seals clear at 680 seconds after the break. The break itself uncovers a short time later. Thereafter, the break has the vapor flow from

both the steam generator and the pump side of the crossover leg; consequently, the RCS depressurizes rapidly. The loop seal clearing also relieves the liquid level difference between the inner vessel and the downcomer, when the liquid level in the inner vessel increases as a result of the loop seal clearance.

The increased RCS depressurization rate is accompanied by an increased break flow for the pump suction break location. However, because the SI delivery rate is much larger with all lines injecting, no core uncover occurs. The PCT occurs at the inception of the transient; no clad heatup occurs during the 3-inch pump suction small break LOCA transient. Both the downcomer and inner vessel levels remain almost constant during the core boiloff phase (Figures 28-2-9 and 28-2-10).

The RCS pressure falls below the accumulator cover gas pressure of 655 psia at 1870 seconds after the break. After an initial dip, the accumulator causes a noticeable liquid level increase (Figure 28-2-9).

28-2-2-3 Comparison to Reference Case

In this transient, the increase in SI flow is adequate to preclude core uncover because no injection line spills.

28-2-3 Break at Hot Leg

28-2-3-1 Description of Model

For this study, the break was moved to the bottom of the hot leg in loop 21. In this transient, the vapor generated in the core can vent through the break without clearing a loop seal.

28-2-3-2 Description of Transient (Figures 28-2-11 through 28-2-15)

Upon initiation of the break, the primary system depressurizes quickly to the saturation pressure corresponding to the hot leg liquid temperature. A reactor trip signal is generated by the low pressurizer pressure setpoint of 1815 psia at 64.3 seconds after the break. The LOOP assumption results in RCP trip 30 seconds later. Turbine trip, and isolation of the steam generator secondary side, follow reactor trip. The steam generator secondary pressurizes to a safety valve setpoint relief pressure of 1080 psia. Following main feedwater pump trip and isolation, the auxiliary

feedwater system is automatically actuated and begins delivering flow to the secondary side 75 seconds later.

The RCS continues to depressurize and reaches the pressurizer low-low pressure setpoint of 1715 psia 69 seconds after the break, which generates an S-signal. The SI is initiated 45 seconds after the S-signal generation.

The RCS depressurization is halted, and the RCS reaches a quasi-equilibrium pressure condition 320 seconds after the break just above the steam generator secondary side pressure. During this period, the break flow is a mixture of vapor and liquid due to the location of the break, and the steam generators are active heat sinks. The vapor generated in the core is vented through the break and also condensed by the steam generators. This results in the quasi-equilibrium condition. For a 3-inch hot leg break, the venting and condensation in the RCS are not enough to totally eliminate the volume expansion of vapor in the core. This causes the inner vessel liquid level, due to the increased vapor volume, to be depressed compared to the downcomer liquid level.

This quasi-equilibrium state is upset when the loop seal clears at 1115 seconds after the break, which relieves the liquid level difference between the inner vessel and the downcomer. By this time, cold legs are filled with liquid prior to the loop seal clearance. When the liquid level balances, it is available to fill the inner vessel. When the loop seal clears, the liquid level in the inner vessel increases by approximately 1 foot.

Following the loop seal clearing event, the RCS depressurization is accompanied by only a small decrease in the inner vessel liquid level. The SI delivery rate is much larger for the hot leg break than for the reference case because all SI lines inject into the cold legs. The slow decrease in inner vessel and downcomer collapsed liquid levels lasts until the RCS pressure falls below the accumulator cover gas pressure of 655 psia. Core heatup is not observed in this transient because the core is covered during the entire transient.

28-2-3-3 Comparison to Reference Case

Due to the location of the break, the liquid reaching the break is hotter than in the cold leg break reference case. This results in the lower initial break flow. The break flow transition from liquid to two-phase flow is much less pronounced than in the reference case (Figure 28-2-12). The ability to vent steam through the break causes loop seal clearance to be delayed relative to other break locations. The minimum inner vessel collapsed liquid level is approximately the same distance above the bottom of the vessel as in the pump suction break case. The two-phase

mixture level is above the core region; consequently, there is no heatup in this transient. This case also benefits from the increased SI flowrate associated with a break location that involves no spilling injection line.

Break Location Sensitivity Study
RCS Pressure Comparisons

— PN 54 1 0 Reference Case
--- PN 54 1 0 Break Non-PZR Loop

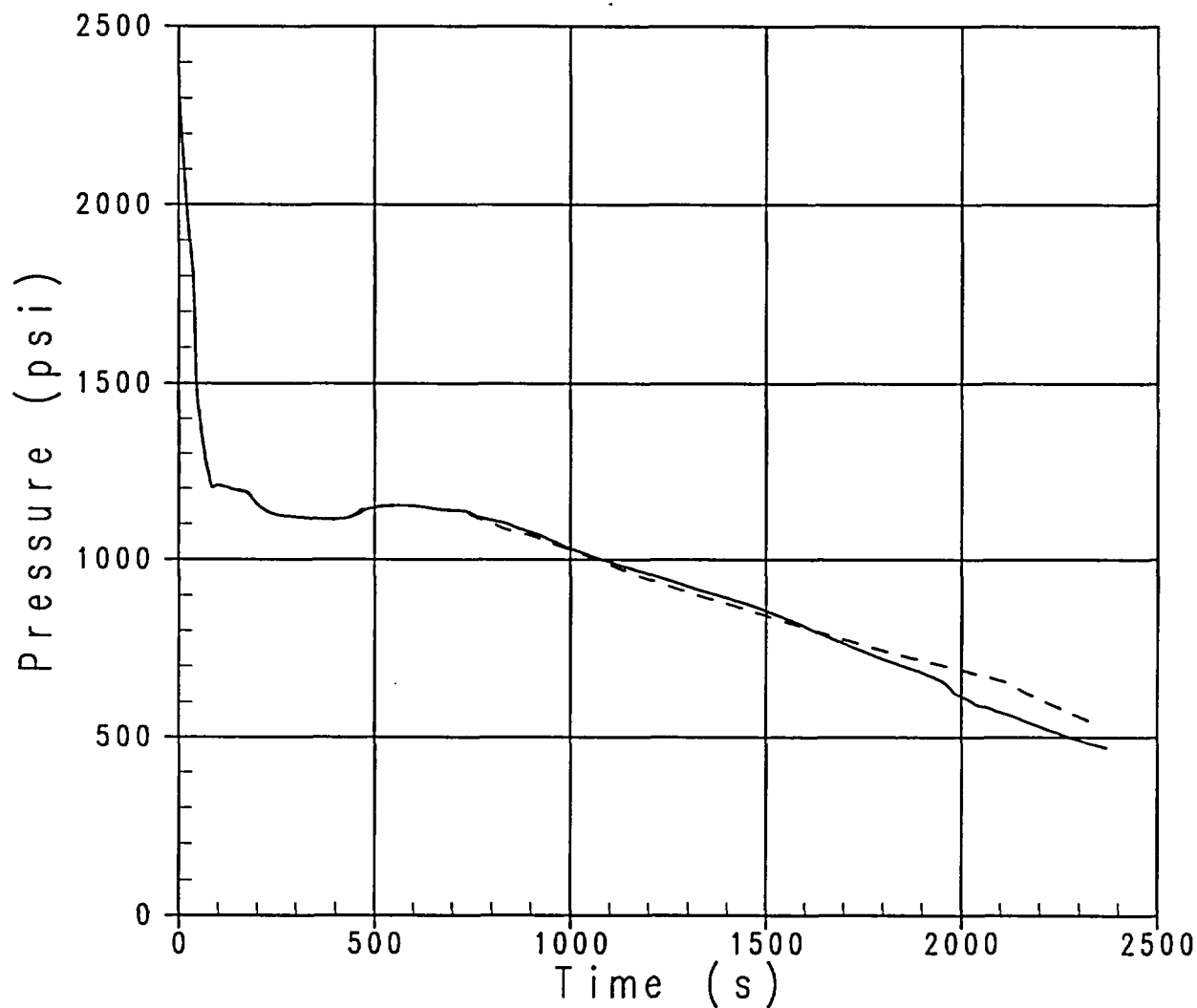


Figure 28-2-1. Break Location – RCS Pressure Comparison, Break in Nonpressurizer Loop

Break Location Sensitivity Study
Integrated Break Flow

— INTMTOT 200 2 0 Reference Case
- - - INTMTOT 200 2 0 Break Non-PZR Loop

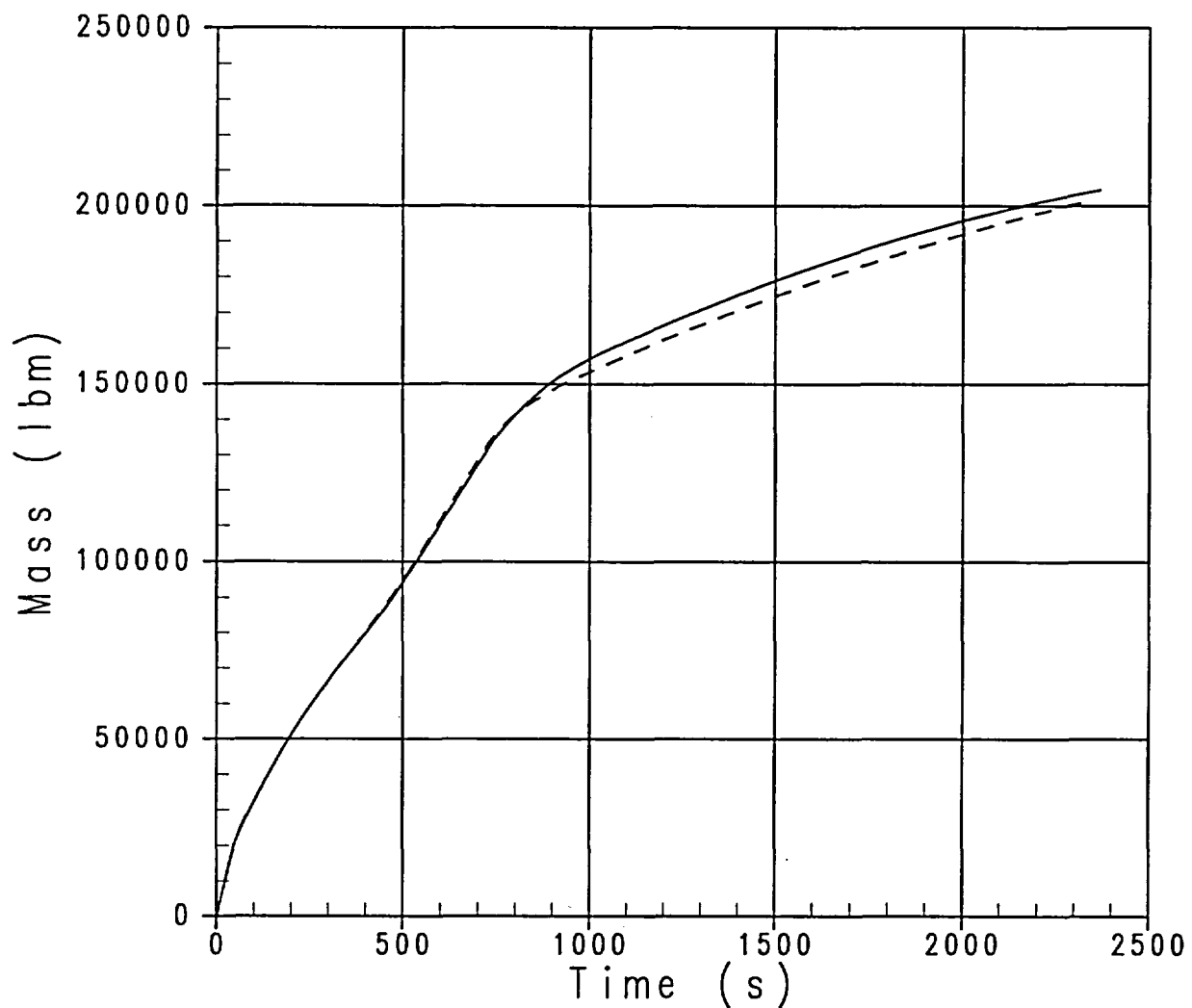


Figure 28-2-2. Break Location – Integrated Break Flow Comparison, Break in Nonpressurizer Loop

Break Location Sensitivity Study
Downcomer Collapsed Liquid Level

— LQ-LEVEL 6 0 0 Reference Case
--- LQ-LEVEL 6 0 0 Break Non-PZR Loop

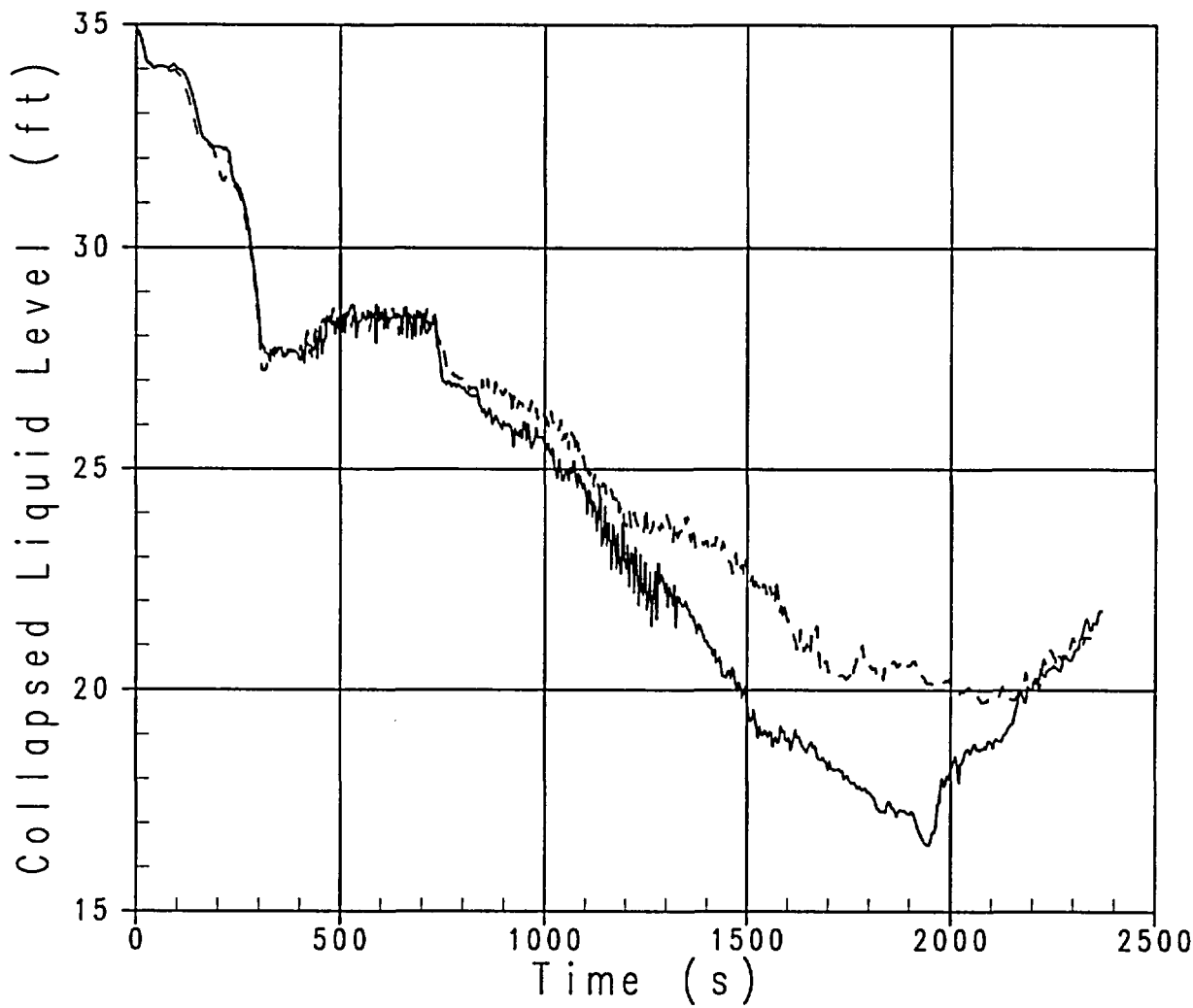


Figure 28-2-3. Break Location – Downcomer Collapsed Liquid Level Comparison, Break in Nonpressurizer Loop

Break Location Sensitivity Study
Inner Vessel Collapsed Liquid Level Comparison
 — LQ-LEVEL 1 0 0 Reference Case
 - - - LQ-LEVEL 1 0 0 Break Non-PZR Loop

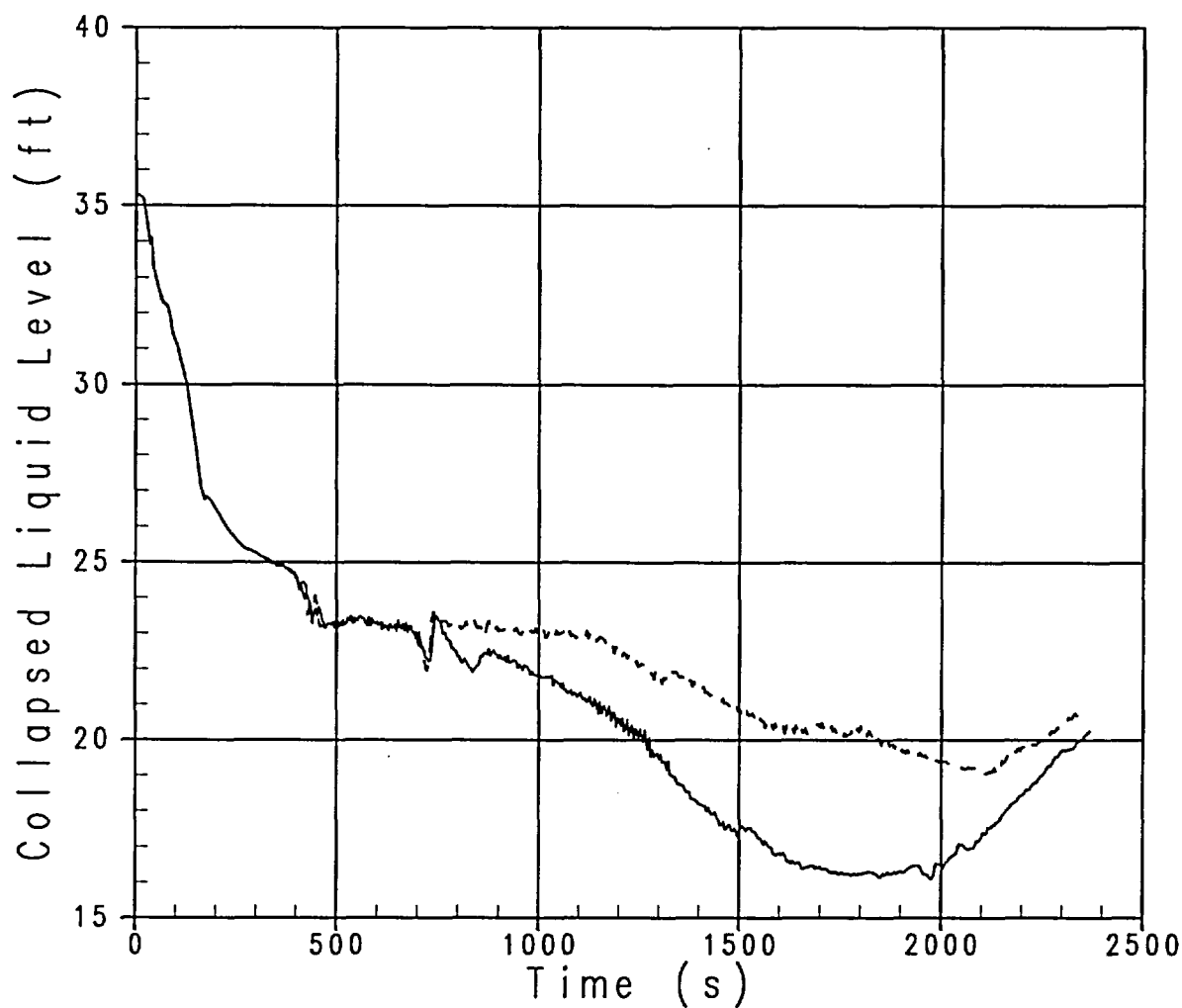


Figure 28-2-4. Break Location – Inner Vessel Collapsed Liquid Level Comparison, Break in Nonpresurizer Loop

Break Location Sensitivity Study

PCT Comparisons

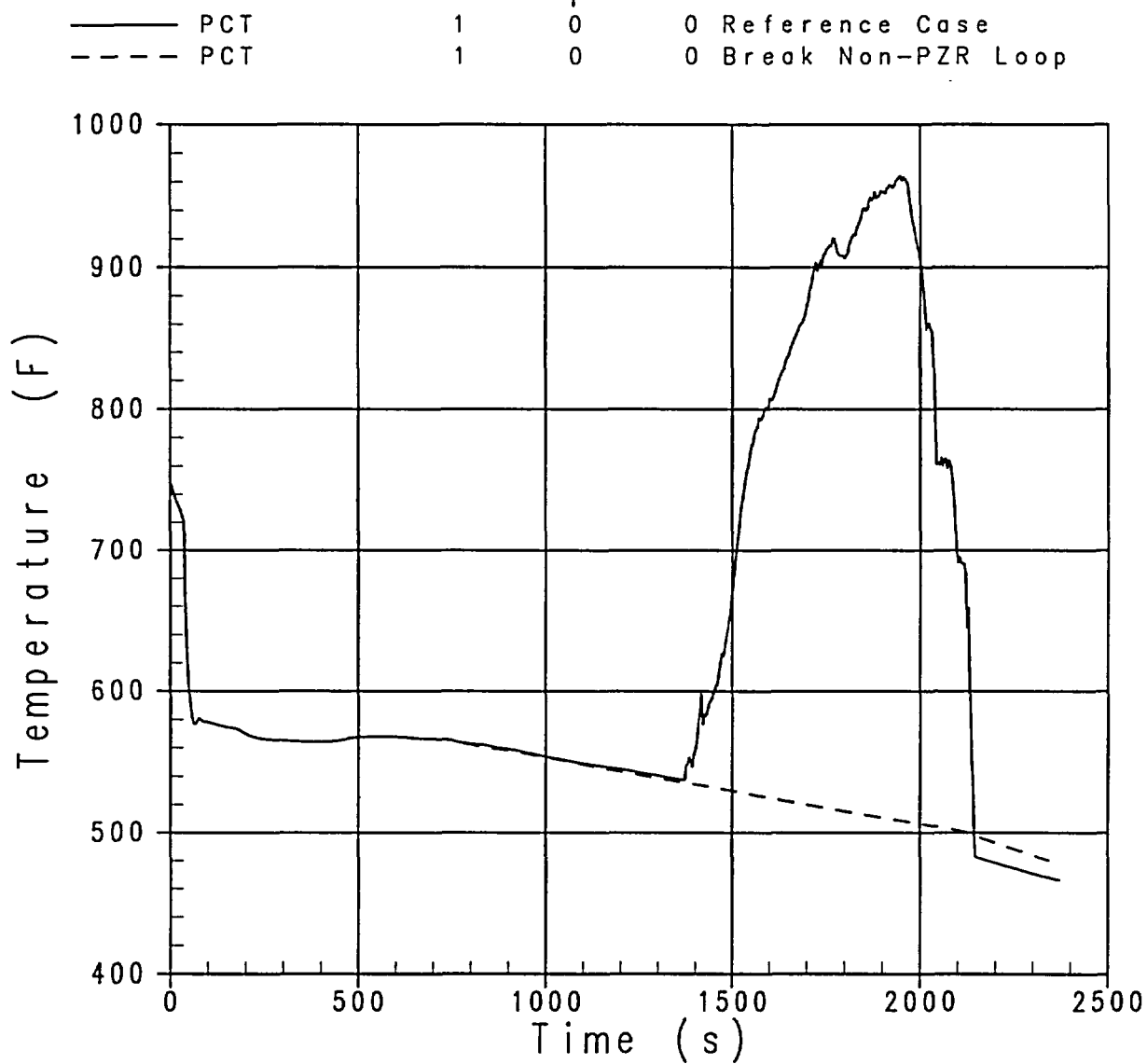


Figure 28-2-5. Break Location – PCT Comparison, Break in Nonpressurizer Loop

Break Location Sensitivity Study
RCS Pressure Comparisons

— PN 54 1 0 Reference Case
--- PN 54 1 0 Break in PS

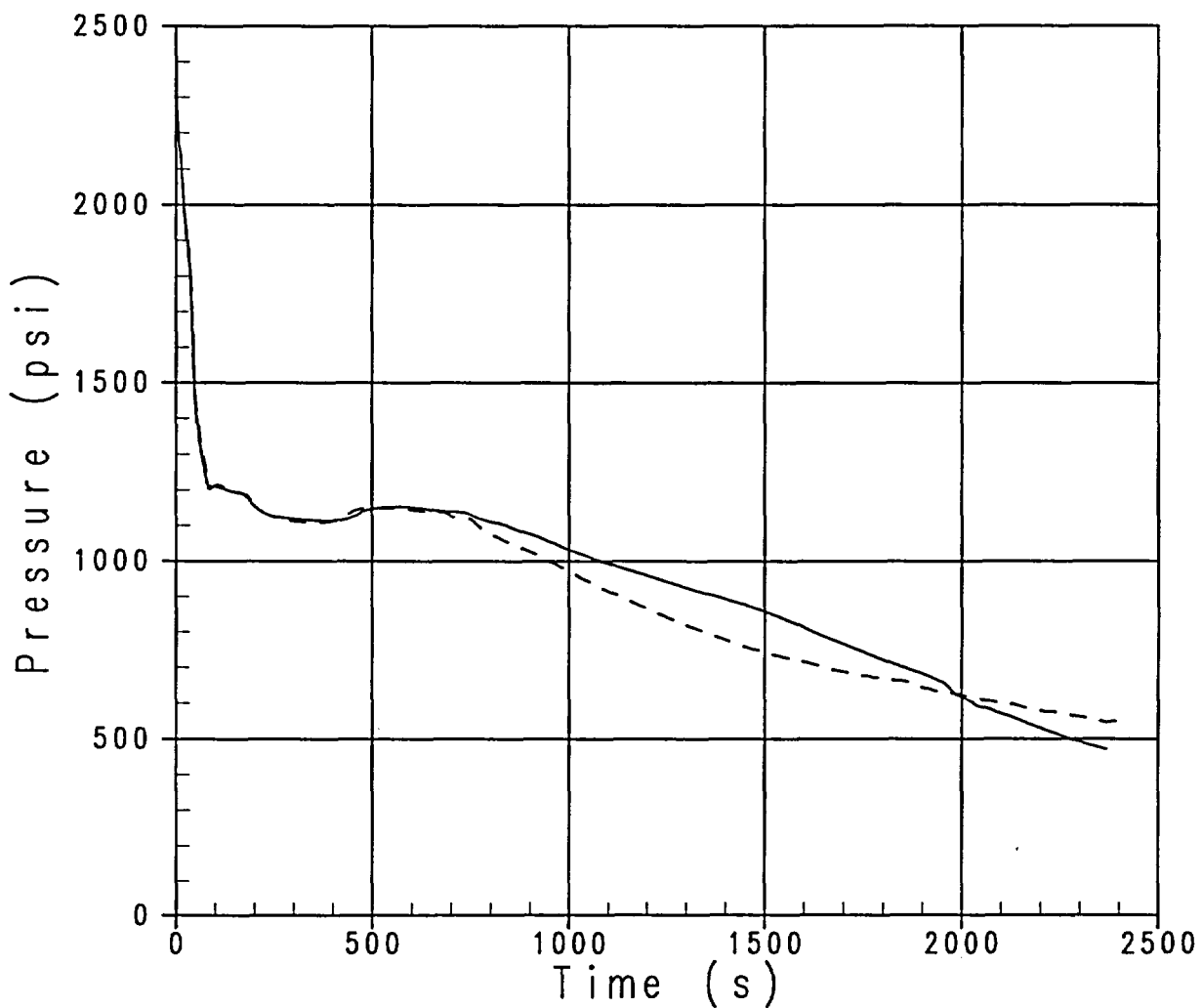


Figure 28-2-6. Break Location – RCS Pressure Comparison, Break in Pump Suction

Break Location Sensitivity Study
Integrated Break Flow

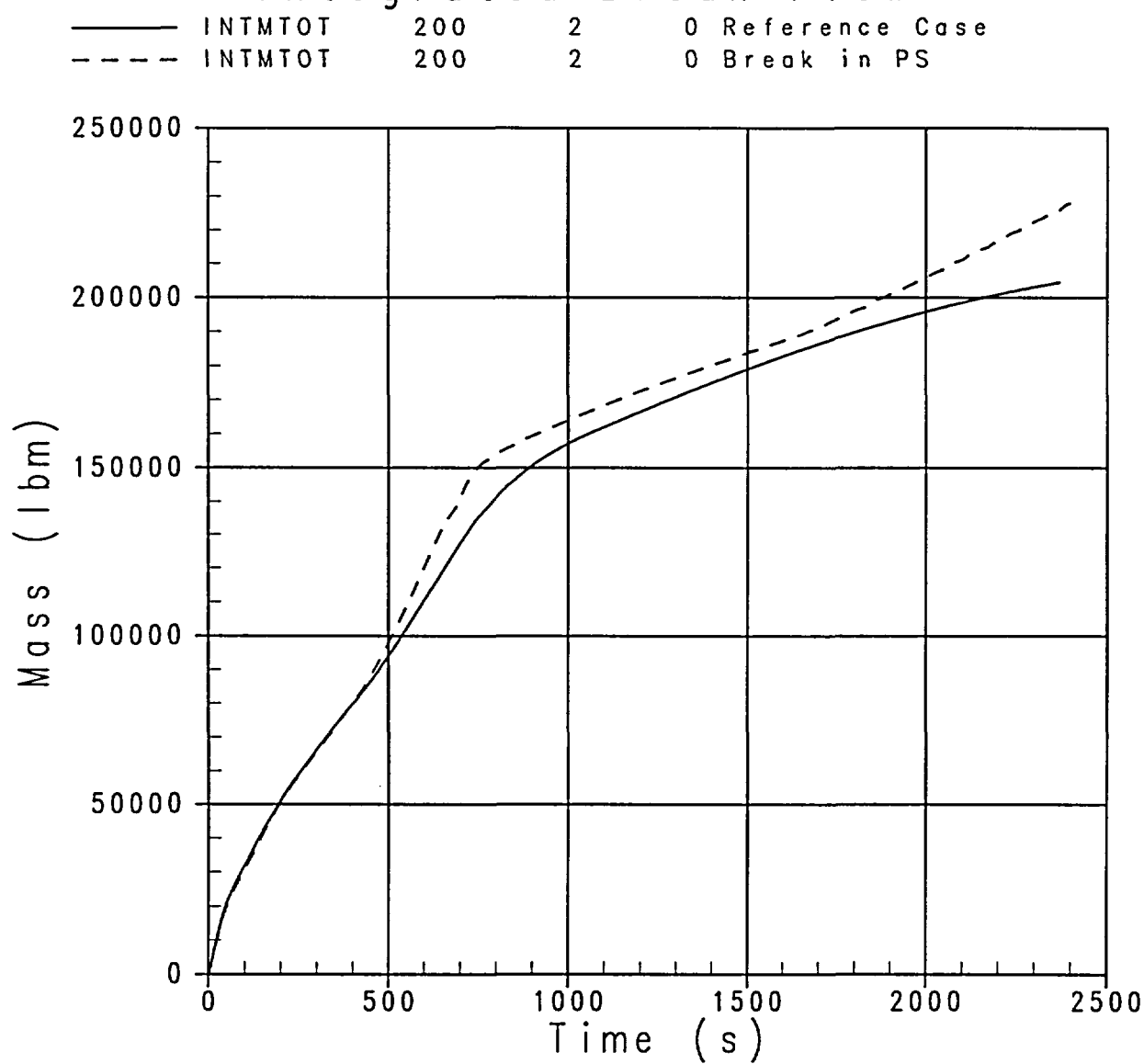


Figure 28-2-7. Break Location – Integrated Break Flow Comparison, Break in Pump Suction

Break Location Sensitivity Study
Downcomer Collapsed Liquid Level

LQ-LEVEL	6	0	0	Reference Case
LQ-LEVEL	6	0	0	Break in PS

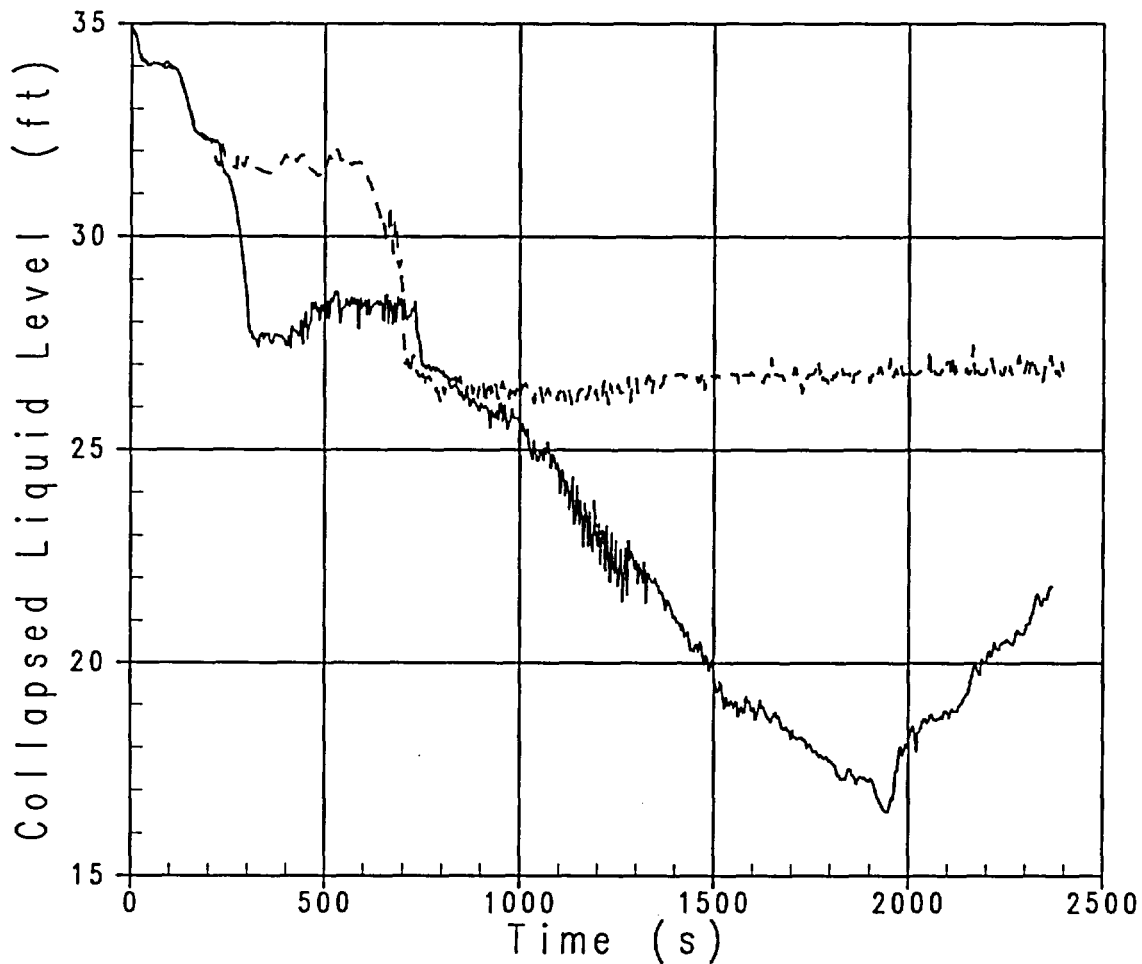


Figure 28-2-8. Break Location – Downcomer Collapsed Liquid Level Comparison, Break in Pump Suction

Break Location Sensitivity Study
Inner Vessel Collapsed Liquid Level Comparison

— LQ-LEVEL 1 0 0 Reference Case
--- LQ-LEVEL 1 0 0 Break in PS

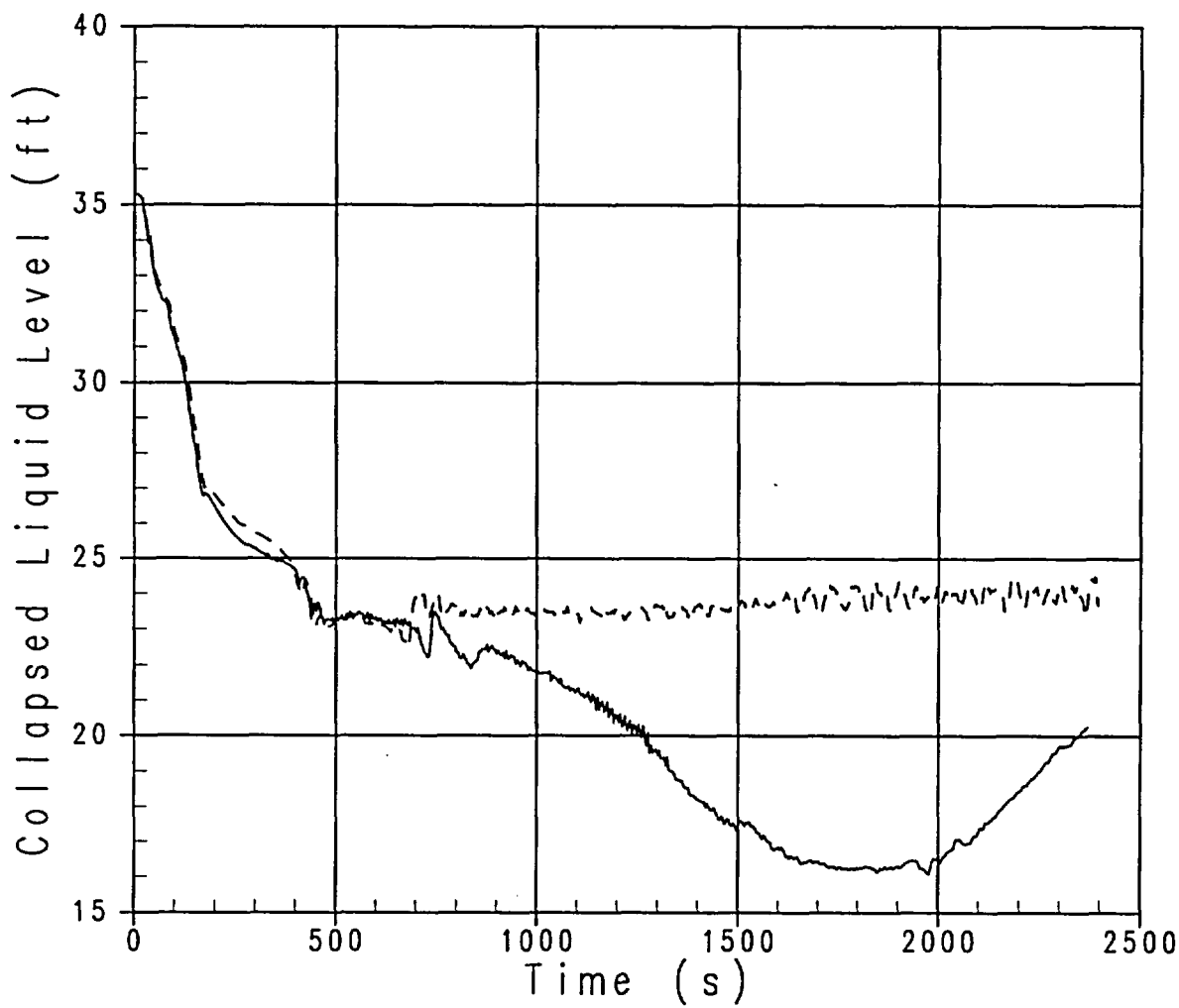


Figure 28-2-9. Break Location – Inner Vessel Collapsed Liquid Level Comparison, Break in Pump Suction

Break Location Sensitivity Study
PCT Comparisons

— PCT 1 0 0 Reference Case
- - - PCT 1 0 0 Break in PS

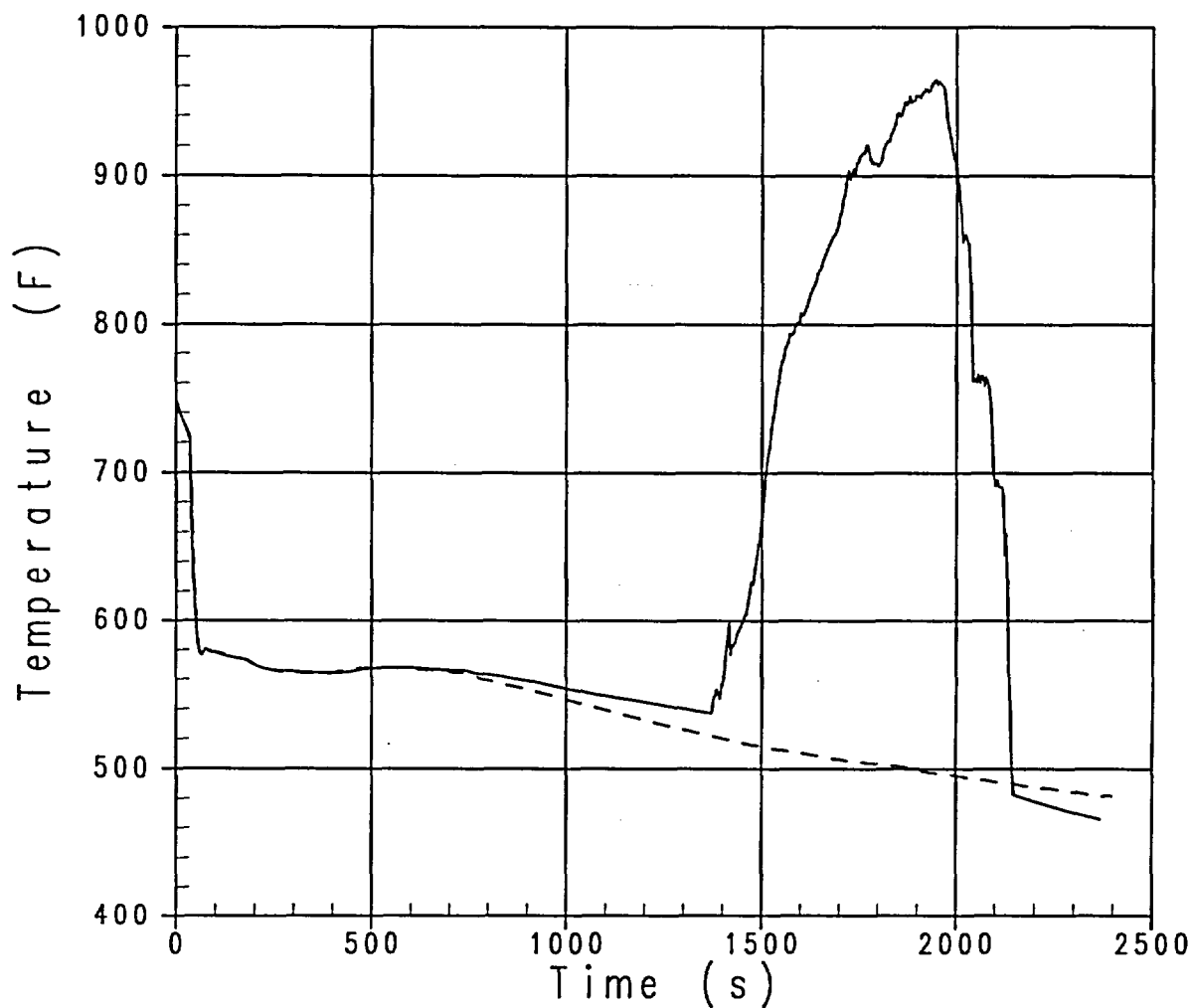


Figure 28-2-10. Break Location – PCT Comparison, Break in Pump Suction

Break Location Sensitivity Study
RCS Pressure Comparisons

— PN 54 1 0 Reference Case
--- PN 54 1 0 Break in Hot Leg

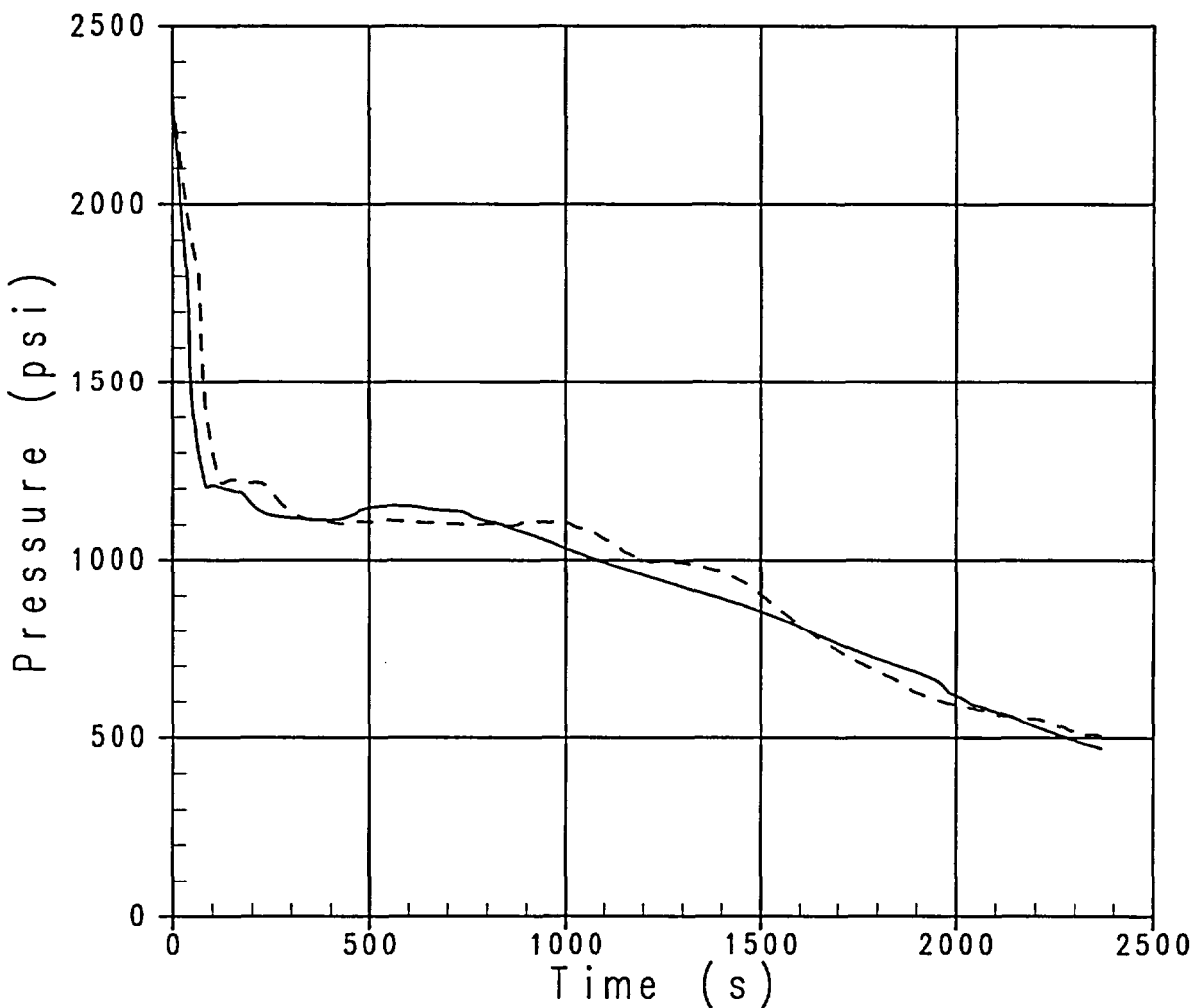


Figure 28-2-11. Break Location – RCS Pressure Comparison, Break in Hot Leg

Break Location Sensitivity Study
Integrated Break Flow

— INTMTOT 200 2 0 Reference Case
--- INTMTOT 200 2 0 Break in Hot Leg

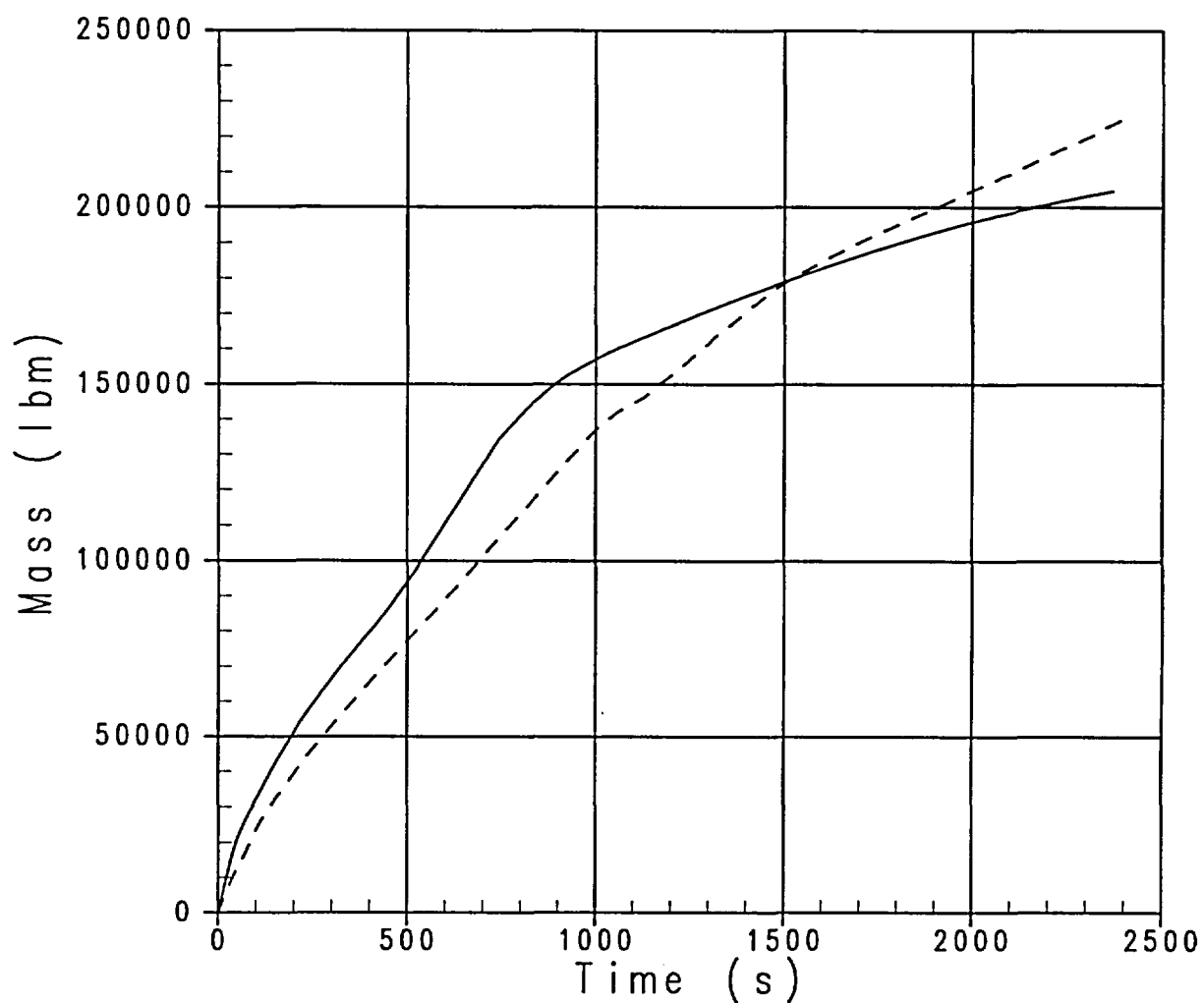


Figure 28-2-12. Break Location – Integrated Break Flow Comparison, Break in Hot Leg

Break Location Sensitivity Study
Downcomer Collapsed Liquid Level

— LQ-LEVEL 6 0 0 Reference Case
- - - LQ-LEVEL 6 0 0 Break in Hot Leg

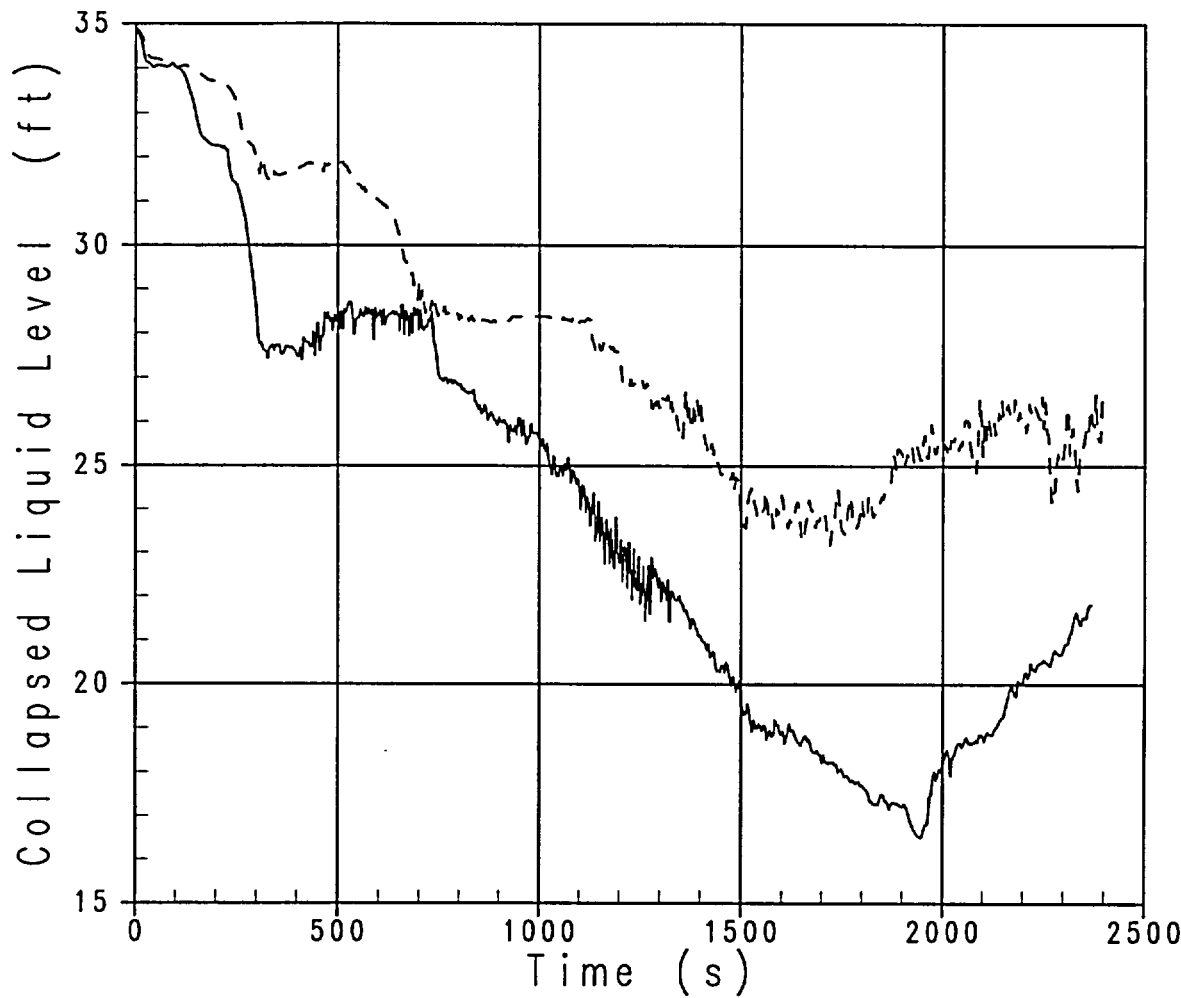


Figure 28-2-13. Break Location – Downcomer Collapsed Liquid Level Comparison, Break in Hot Leg

Break Location Sensitivity Study
Inner Vessel Collapsed Liquid Level Comparison
 _____ LQ-LEVEL 1 0 0 Reference Case
 - - - LQ-LEVEL 1 0 0 Break in Hot Leg

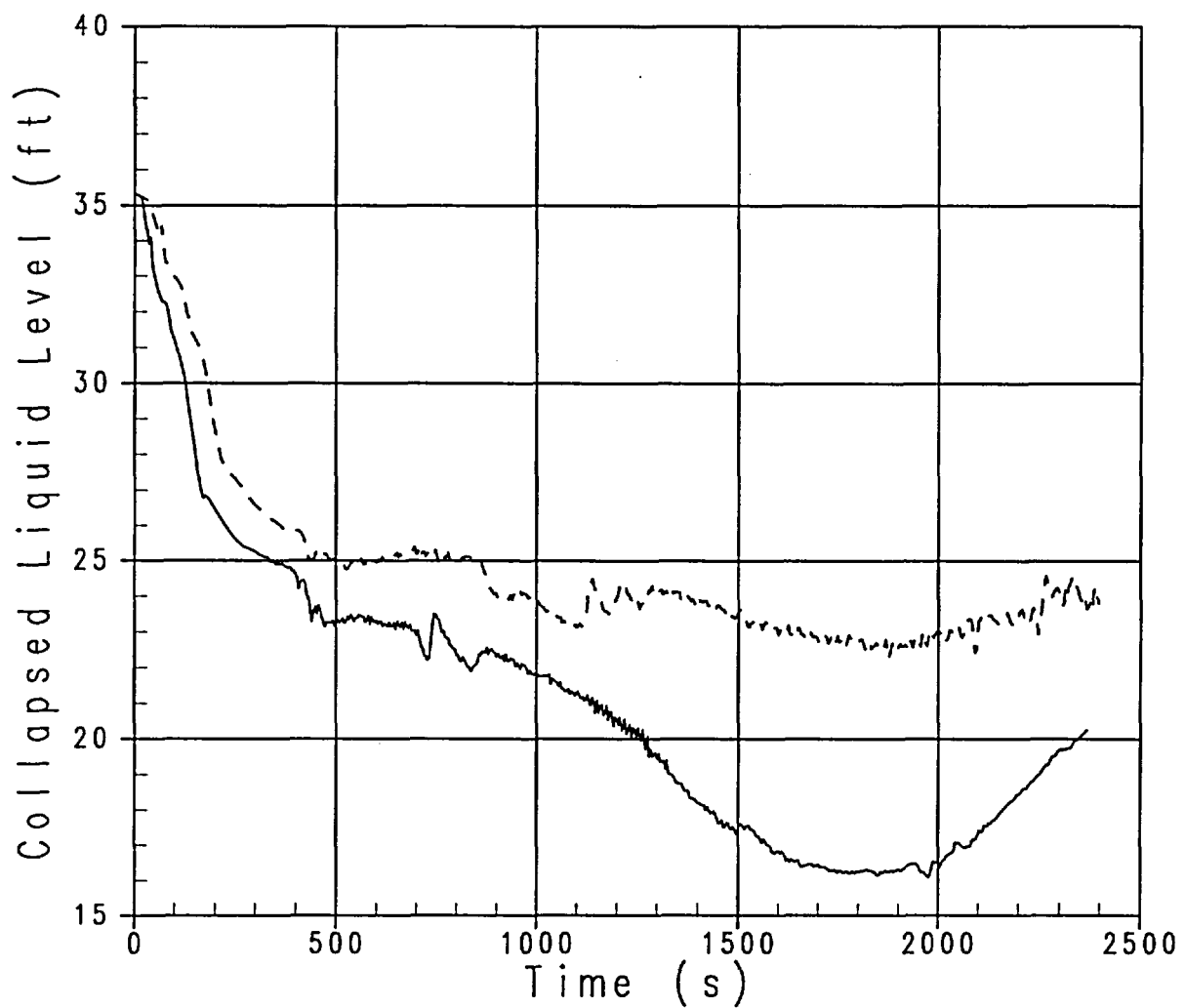


Figure 28-2-14. Break Location – Inner Vessel Collapsed Liquid Level Comparison, Break in Hot Leg

Break Location Sensitivity Study
PCT Comparisons

— PCT 1 0 0 Reference Case
- - - PCT 1 0 0 Break in Hot Leg

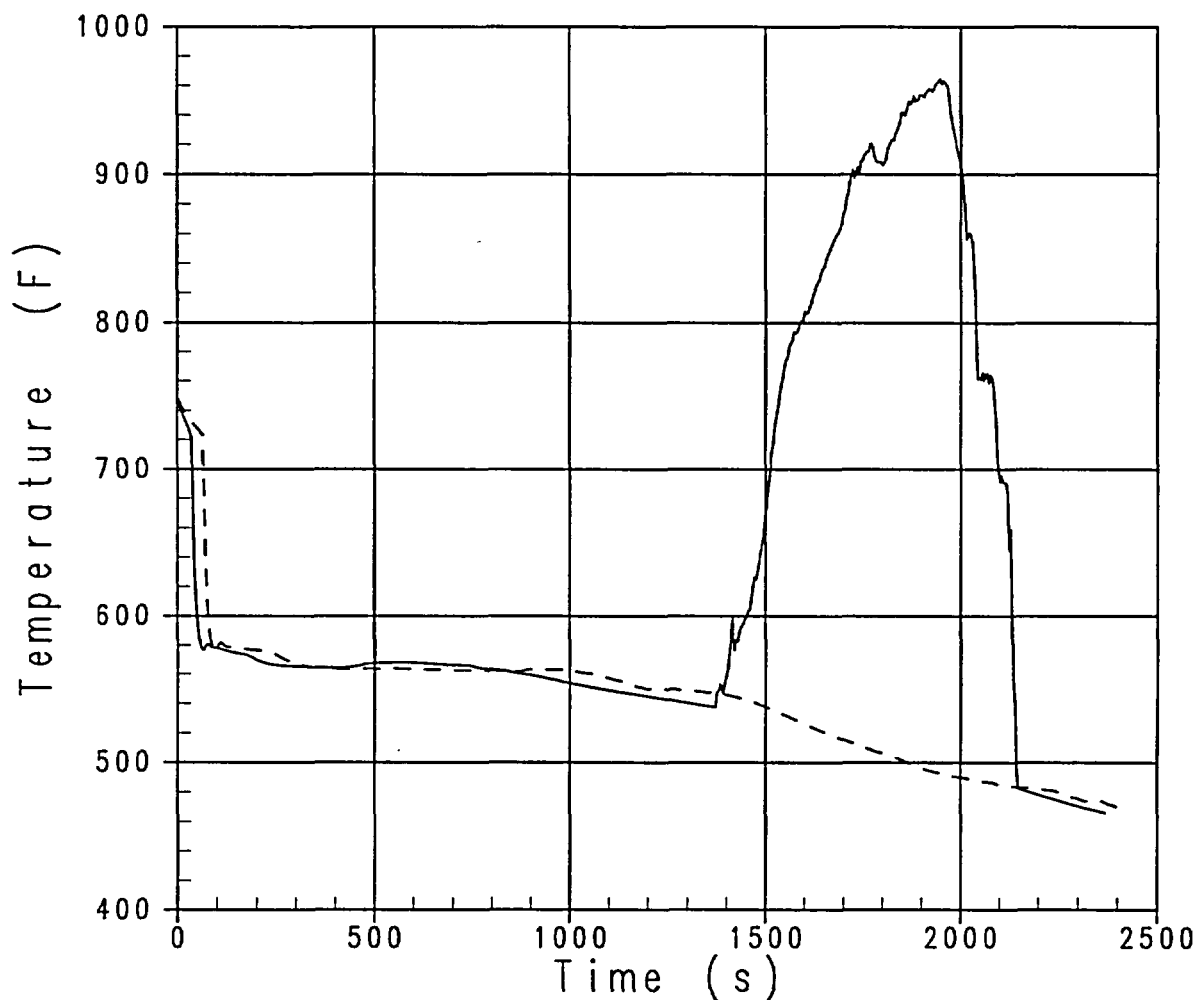


Figure 28-2-15. Break Location – PCT Comparison, Break in Hot Leg

28-3 Break Orientation Study

In Volume 2, Section 19, the ability of the code to model break orientation is demonstrated in simulations of the ROSA-IV 2.5% break tests. WCOBRA/TRAC-SB is judged to be acceptable for studying the effect of break orientation on small break LOCA transients. The simulation of the two-phase flow loop (TPFL) (EPRI, 1986) test by WCOBRA/TRAC-SB further indicates (Section 13, Volume 2) that the phase transition and the exit quality as a function of liquid level are in excellent agreement with the data for a branchline orientation.

The effect of the break orientation on the small break LOCA transient is examined in this section. In small break LOCA transients, the circumferential orientation of the break is thought to have a significant impact on the transient and PCT. The flow in the pipe is stratified so the break is adjacent to either the vapor or the liquid phase, depending on where the break is located; for stratified flow in the main pipe, the top break has the vapor phase adjacent, and the bottom break has the liquid phase. Because the volumetric break flowrate is a strong function of the quality at the break, the orientation of the break can have a significant effect both on the transient and on PCT. In the following subsections, bottom and side cold leg breaks are examined and compared against the reference case – the top break case with one SI line spilling to the containment. A top break case in which the SI line does not spill but rather injects is also analyzed.

28-3-1 Top Break With SI Into Broken Loop

28-3-1-1 Model Description

The vertically oriented top break model shown in Figure 28-1-2 is used to model the top break in the cold leg piping. Because of the break elevation, it is expected to result in the highest liquid level at the break location and in the downcomer, and consequently, in the core, other things being equal.

28-3-1-2 Description of Transient (Figures 28-3-1 through 28-3-6)

Upon initiation of the break, the primary system depressurizes quickly to the saturation pressure corresponding to the hot leg liquid temperature. A reactor trip signal is generated by the low pressurizer pressure setpoint of 1815 psia at 35.5 seconds after the break. The LOOP assumption results in an RCP trip 30 seconds later. Turbine trip, and isolation of the steam generator

secondary side, follow reactor trip. The steam generator secondary pressurizes to a safety valve setpoint relief pressure of 1080 psia. Following main feedwater pump trip and isolation, the auxiliary feedwater system is automatically actuated and begins delivering flow to the secondary side 75 seconds later.

The RCS continues to depressurize and reaches the pressurizer low-low pressure setpoint of 1715 psia at 39.8 seconds after the break, which generates an S-signal. The SI is initiated 45 seconds after the S-signal generation.

The RCS depressurization is halted, and the RCS reaches a quasi-equilibrium pressure condition at 240 seconds after the break just above the steam generator secondary side pressure. During this period, the break flow is all liquid and the steam generators are active heat sinks. The vapor generated in the core is trapped within the RCS due to loop seal plugging. The pressure is maintained in this period because the vapor generation in the core is balanced by condensation in the steam generators and the volumetric loss through the break. During this period, the inner vessel liquid level is depressed compared to the downcomer liquid level, due to the increased vapor volume in the inner vessel which is unable to vent.

This quasi-equilibrium state is upset when the loop seal clears at 640 seconds after the break and the vapor generated in the core starts to vent through the break. Consequently, the RCS once again depressurizes. The loop seal clearing also relieves the liquid level difference between the inner vessel and the downcomer. The liquid level in the inner vessel exhibits its minimum value immediately before the loop seal clearance. Two loop seals clear in this transient. Following the loop seal clearing event, the inner vessel collapsed liquid level increases. It remains steady to slightly increasing throughout the rest of the transient due to the SI delivery rate, which is much higher than in the Reference case, which assumes a spilling SI line. Eventually, the RCS pressure falls below the accumulator cover gas pressure of 655 psia. The PCT occurs at the inception of the transient. The cladding temperature during the transient follows the saturation temperature, since the vessel mixture level at its minimum value remains above the top of the active fuel.

28-3-1-3 Comparison to Reference Case

The increased SI flow has two major effects on the top break transient. First, the pressure decreases more rapidly from 900 seconds onward due to increased condensation. Second, the increase in the SI flow entering the broken loop results in more total break flow (Figure 28-3-2),

which leads to the break flow transition from liquid to vapor occurring at an earlier time than in the reference case (Figure 28-3-6). As seen in Figures 28-3-3 and 4, after transitioning to two-phase break flow, the top break with SI delivery to the broken loop exhibits much more liquid in the vessel during the boiloff phase. As a consequence, core uncover does not occur, and no heatup occurs (Figure 28-3-5).

28-3-2 Side Break

28-3-2-1 Description of Model

The side-oriented break model shown in Figure 28-1-2 is used to model a break in the center cell of the cold leg piping. Because of the break elevation, this case is not expected to be limiting among the bottom, side, and top orientation sensitivity cases.

28-3-2-2 Description of Transient (Figures 28-3-7 through 28-3-12)

Upon initiation of the break, the primary system depressurizes quickly to the saturation pressure corresponding to the hot leg liquid temperature. A reactor trip signal is generated by the low pressurizer pressure setpoint of 1815 psia at 36 seconds after the break. The LOOP assumption results in an RCP trip 30 seconds later. Turbine trip, and isolation of the steam generator secondary side, follows reactor trip. The steam generator secondary pressurizes to a safety valve setpoint relief pressure of 1080 psia. Following main feedwater pump trip and isolation, the auxiliary feedwater system is automatically actuated and begins delivering flow to the secondary side 75 seconds later.

The RCS continues to depressurize and reaches the pressurizer low-low pressure setpoint of 1715 psia at 40 seconds after the break, which generates an S-signal. The SI is initiated 45 seconds after the S-signal generation.

The RCS depressurization is halted, and the RCS reaches a quasi-equilibrium pressure condition at 200 seconds after the break just above the steam generator secondary side pressure. During this period, the break flow is all liquid and the steam generators are active heat sinks. The vapor generated in the core is trapped within the RCS due to loop seal plugging. The pressure is maintained in this period because the vapor generation in the core is balanced by condensation in the steam generators and the volumetric loss through the break. During this period, the inner

vessel liquid level is depressed compared to the downcomer liquid level due to the increased vapor volume in the inner vessel which is unable to vent.

This quasi-equilibrium state is upset when the loop seal clears at 630 seconds after the break, and the vapor generated in the core starts to vent through the break. Consequently, the RCS once again depressurizes. The loop seal clearing also relieves the liquid level difference between the inner vessel and the downcomer, when the liquid level in the inner vessel increases as a result of the loop seal clearance. Three loop seals are predicted to clear in this case.

Following the loop seal clearing event, the RCS depressurization is accompanied by the gradual increase in the downcomer and inner vessel liquid levels. The depressurization rate to the accumulator cover gas pressure is significantly slowed relative to the reference case; the 655 psia setpoint has yet to be reached more than 2500 seconds after the break. Nevertheless, the PCT during the transient remains below the initial, steady-state cladding temperature (Figure 28-3-11).

28-3-2-3 Comparison to Reference Case

The break flow transitions from liquid to vapor earlier than in the reference case. Because of the location of the break, the void fraction at the break is lower than the reference case during the natural circulation period (Figure 28-3-12). This results in more liquid discharge which results in more total break flow (Figure 28-3-8) by 500-600 seconds. The longer depressurization to accumulator injection occurs because the pumped SI, which is greater than in the reference case because all SI lines are intact and inject, closely matches the break flow. The PCT for this transient occurs at the inception of the break because the core remains covered throughout.

28-3-3 Bottom Break

28-3-3-1 Description of Model

The break model at the bottom of the cold leg pipe shown in Figure 28-1-2 is used to model a break in the lowest cell of the cold leg piping.

28-3-3-2 Description of Transient (Figures 28-3-13 through 28-3-18)

Upon initiation of the break, the primary system depressurizes quickly to the saturation pressure corresponding to the hot leg liquid temperature. A reactor trip signal is generated by the low

pressurizer pressure setpoint of 1815 psia at 36 seconds after the break. The LOOP assumption results in an RCP trip 30 seconds later. Turbine trip, and isolation of the steam generator secondary side, follow reactor trip. The steam generator secondary pressurizes to a safety valve setpoint relief pressure of 1080 psia. Following main feedwater pump trip and isolation, the auxiliary feedwater system is automatically actuated and begins delivering flow to the secondary side 75 seconds later.

The RCS continues to depressurize and reaches the pressurizer low-low pressure setpoint of 1715 psia at 39.8 seconds after the break, which generates an S-signal. The SI is initiated 45 seconds after the S-signal generation.

The RCS depressurization is halted, and the RCS reaches a quasi-equilibrium pressure condition at 220 seconds after the break just above the steam generator secondary side pressure. During this period, the break flow is all liquid and the steam generators are active heat sinks. The vapor generated in the core is trapped within the RCS due to loop seal plugging. The pressure is maintained in this period because the vapor generation in the core is balanced by condensation in the steam generators and the volumetric loss through the break. During this period, the inner vessel liquid level is depressed compared to the downcomer liquid level due to the increased vapor volume in the inner vessel which is unable to vent.

This quasi-equilibrium state is upset when the loop seal clears at 640 seconds after the break, and the vapor generated in the core starts to vent through the break. Consequently, the RCS once again depressurizes. The loop seal clearing also relieves the liquid level difference between the inner vessel and the downcomer. Three loop seals are predicted to clear. The liquid level in the inner vessel exhibits its minimum value immediately before the loop seal clearance. Following the loop seal clearing event, the inner vessel collapsed liquid level holds steady or increases throughout the rest of the transient due to the relatively high safety injection flow delivery. The depressurization continues until the RCS pressure falls below the accumulator cover gas pressure of 655 psia. The PCT during the transient remains below the initial, steady-state cladding temperature.

28-3-3-3 Comparison to Reference Case

The break flow transitions from liquid to vapor earlier than in the reference case. Because of the location of the break, the void fraction at the break is lower than the reference case during the natural circulation period (Figure 28-3-18). This results in more liquid discharge which in turn results in more total break flow (Figure 28-3-14) by 500-600 seconds. The pumped SI is greater than in the reference case, because all SI lines are intact and inject. The PCT for this transient occurs at the inception of the break because the core remains covered throughout.

Break Location Sensitivity Study
RCS Pressure Comparisons

— PN 54 1 0 Reference Case
- - - PN 54 1 0 Top Break

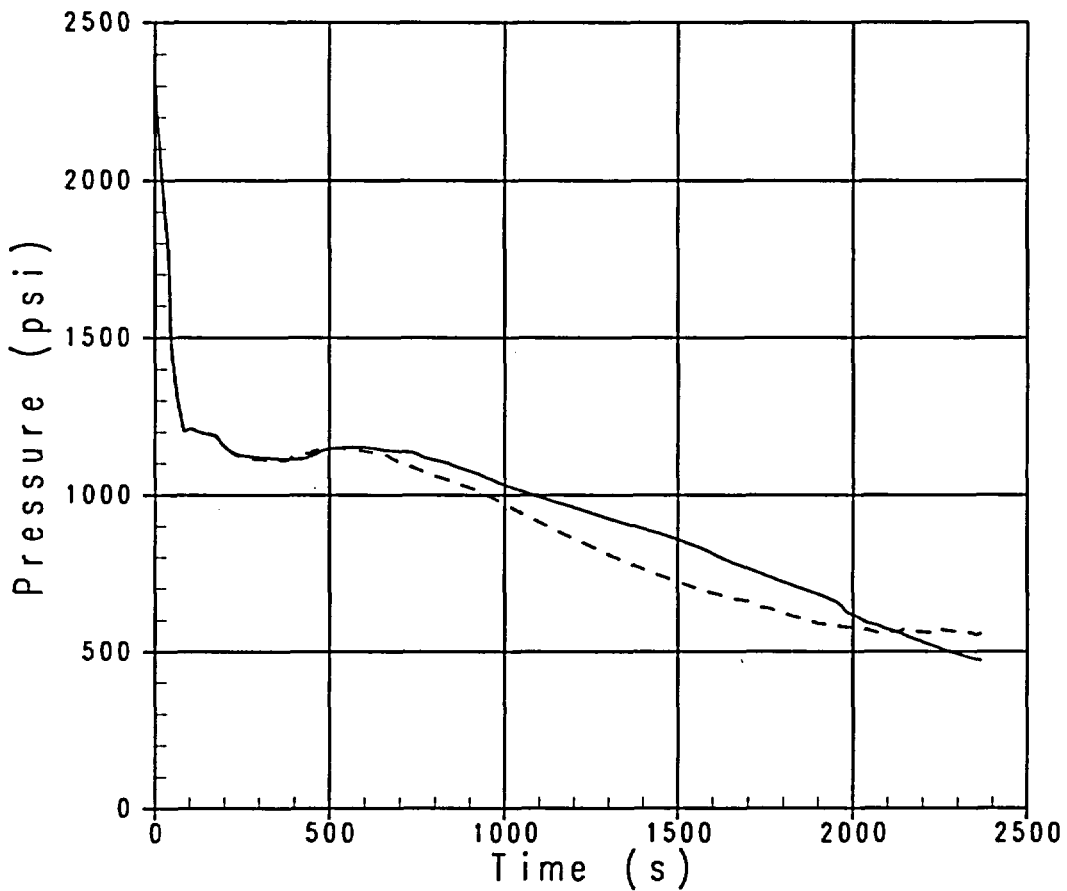


Figure 28-3-1. Break Orientation – RCS Pressure Comparison, Top Break with Full SI

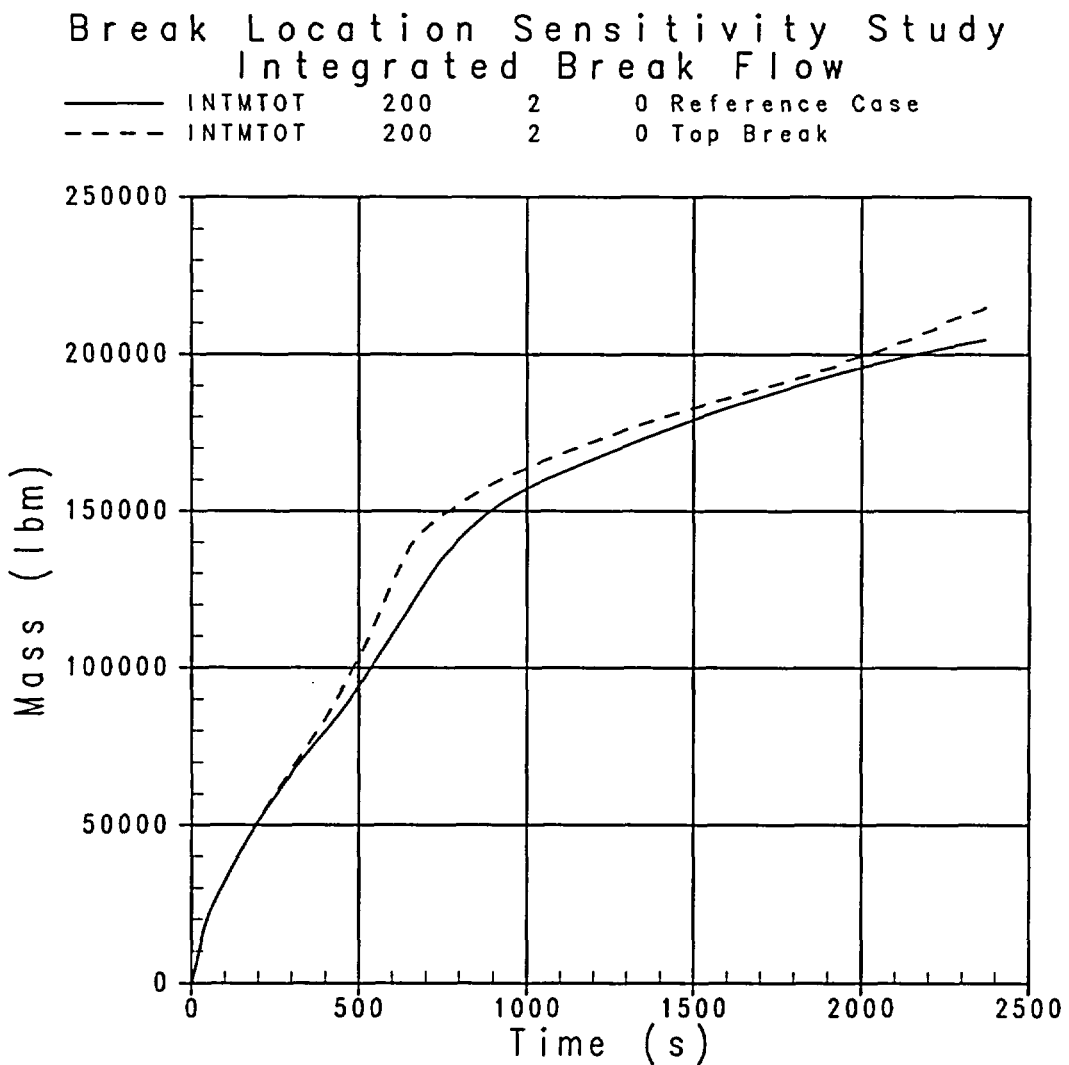


Figure 28-3-2. Break Orientation – Integrated Break Flow Comparison, Top Break with Full SI

Break Location Sensitivity Study
Downcomer Collapsed Liquid Level

LQ-LEVEL	6	0	0	Reference Case
-----------------	----------	----------	----------	-----------------------

LQ-LEVEL	6	0	0	Top Break
-----------------	----------	----------	----------	------------------

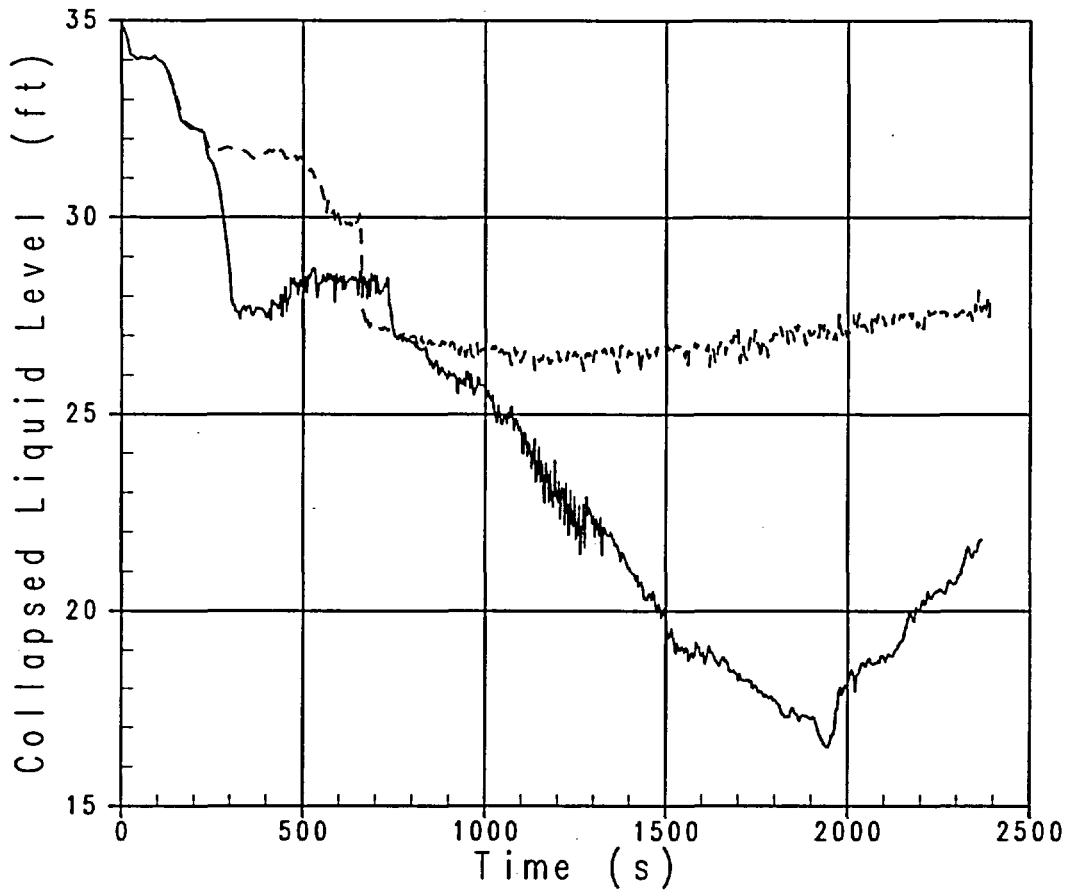


Figure 28-3-3. Break Orientation – Downcomer Collapsed Liquid Level Comparison, Top Break with Full SI

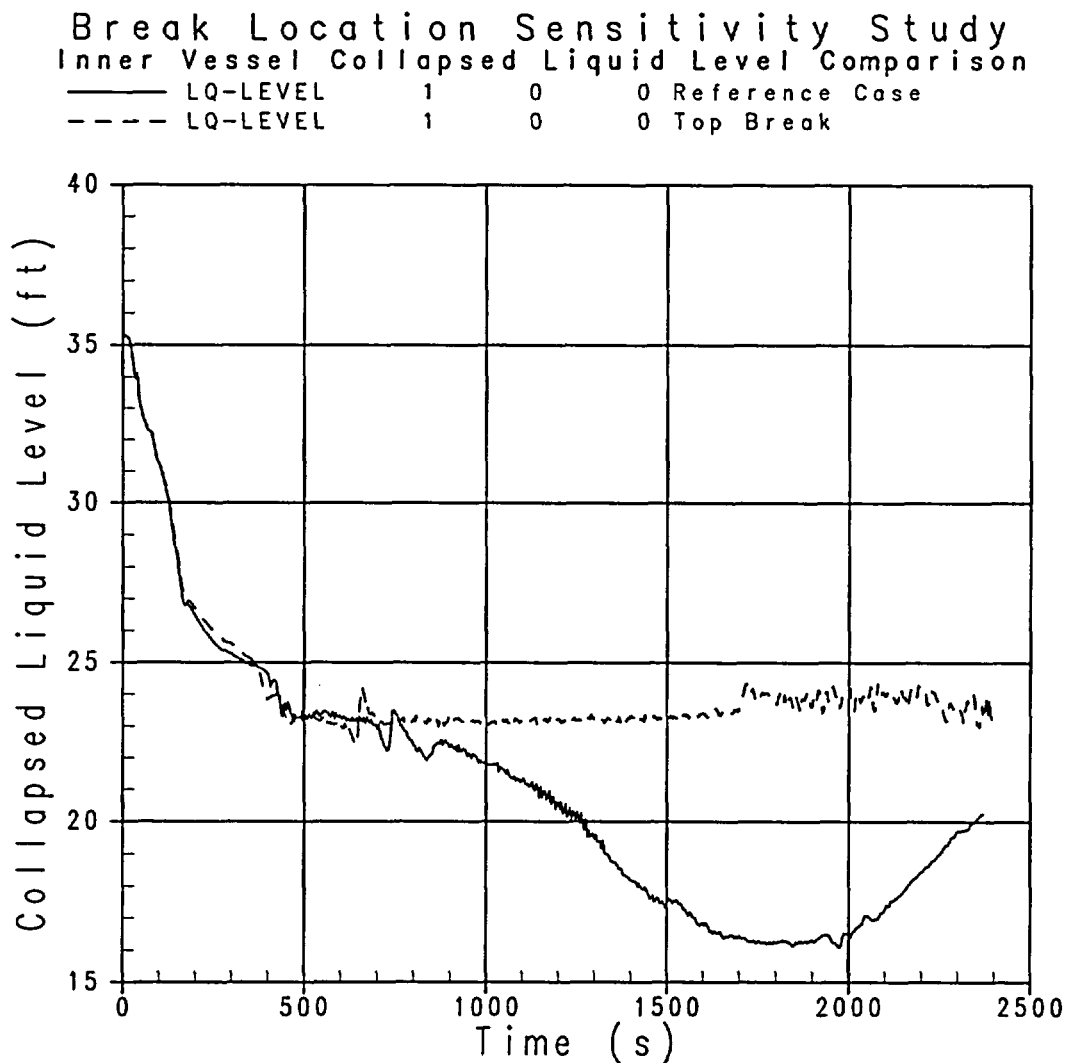


Figure 28-3-4. Break Orientation – Inner Vessel Collapsed Liquid Level Comparison, Top Break with Full SI

Break Location Sensitivity Study
PCT Comparisons

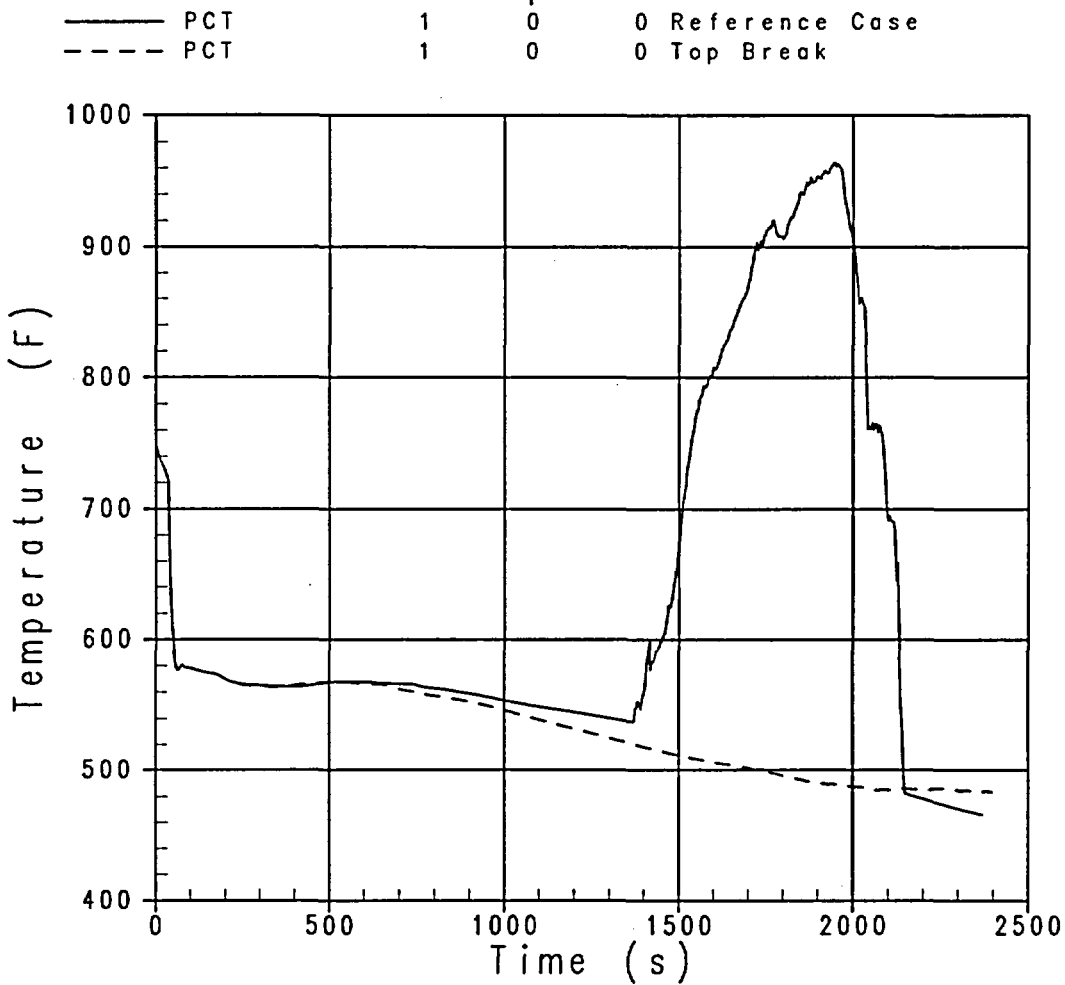


Figure 28-3-5. Break Orientation – PCT Comparison, Top Break with Full SI

Break Location Sensitivity Study
Void Fraction at Break Location

— ALPN	200	2	0	Reference Case
- - - ALPN	200	2	0	Top Break

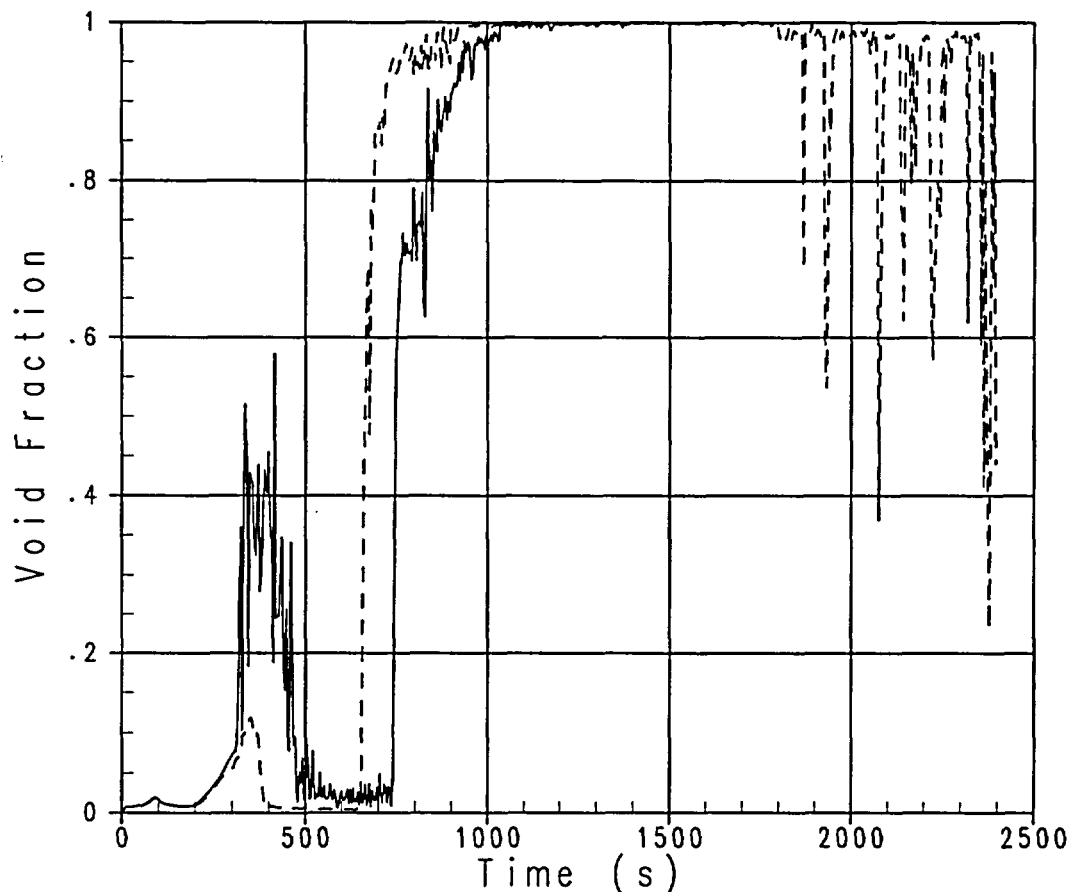


Figure 28-3-6. Break Orientation – Void Fraction Comparison at Break, Top Break with Full SI

Break Location Sensitivity Study
RCS Pressure Comparisons

— PN 54 1 0 Reference Case
- - - PN 54 1 0 Side Break

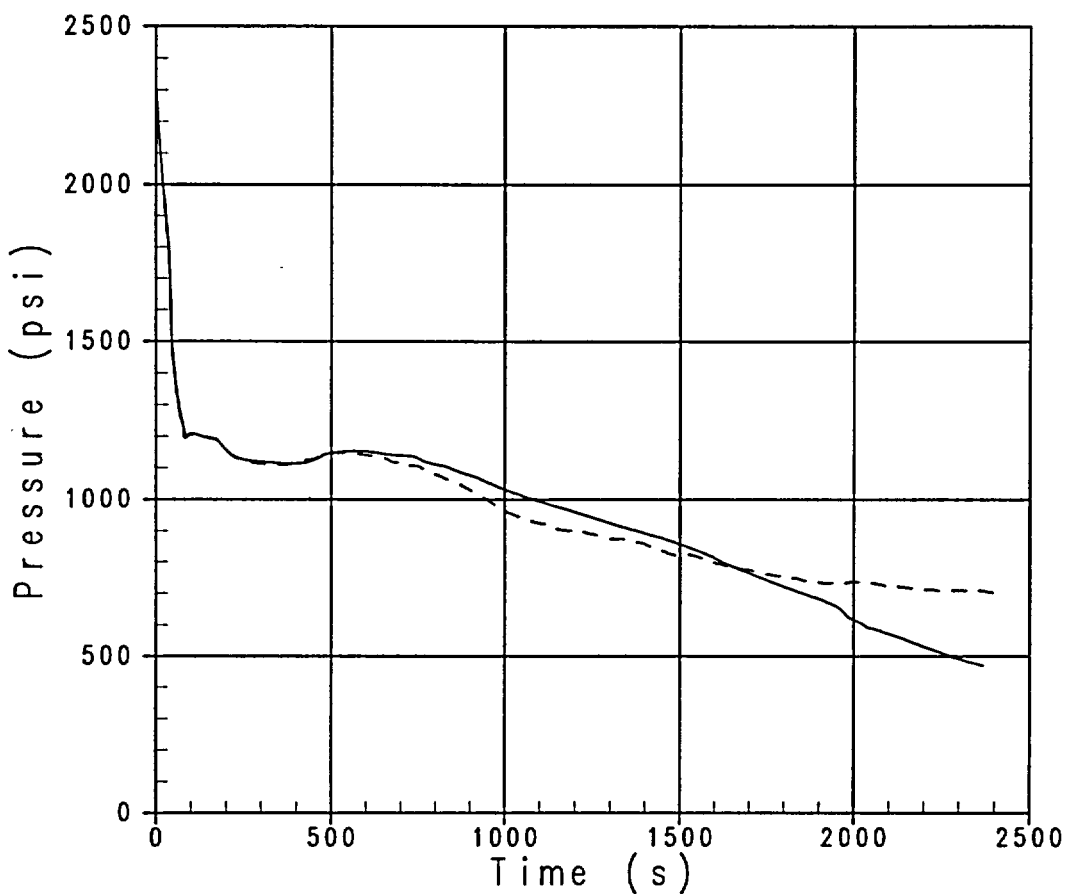


Figure 28-3-7. Break Orientation – RCS Pressure Comparison, Side Break

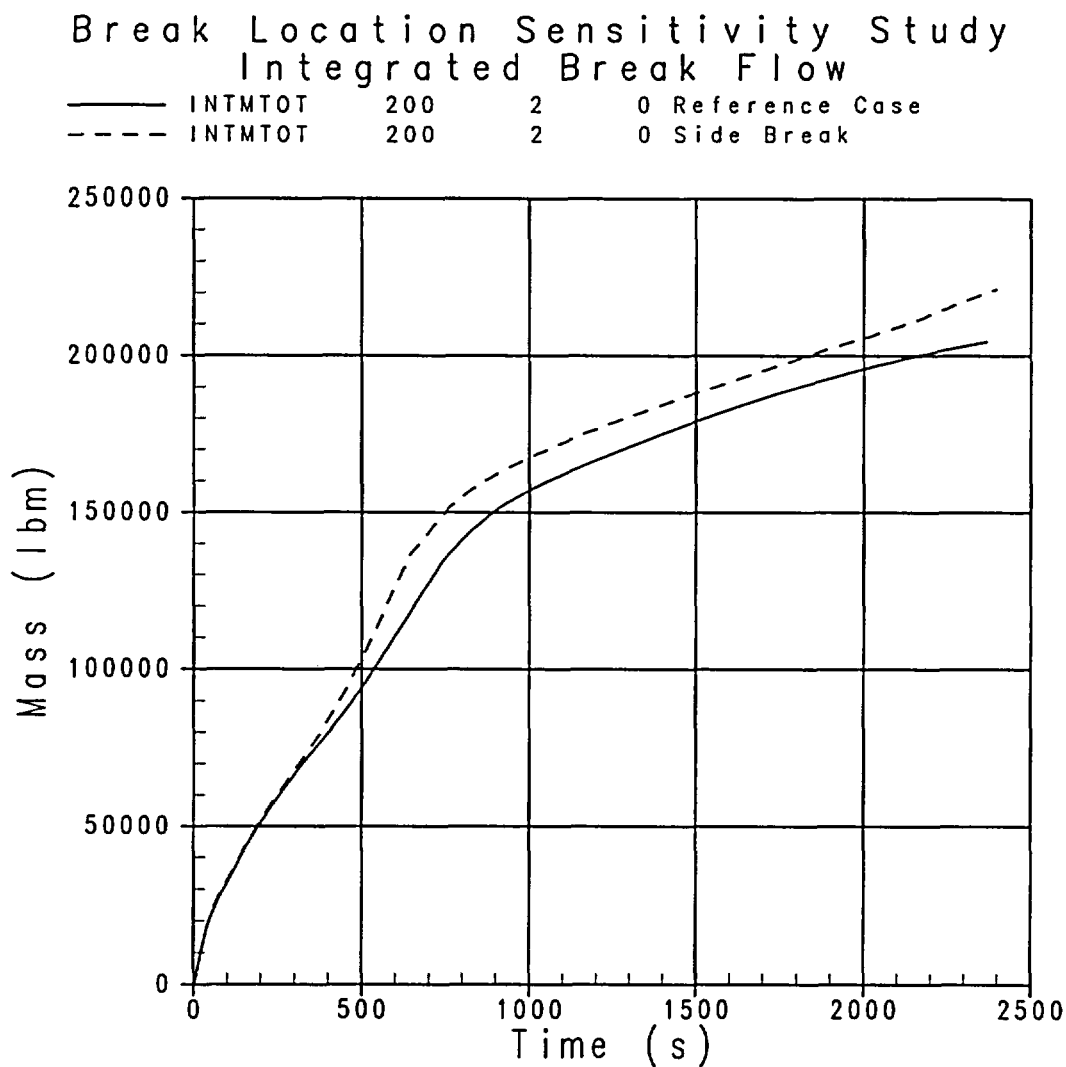


Figure 28-3-8. Break Orientation – Integrated Break Flow Comparison, Side Break

Break Location Sensitivity Study
Downcomer Collapsed Liquid Level

— LQ-LEVEL 6 0 0 Reference Case
- - - LQ-LEVEL 6 0 0 Side Break

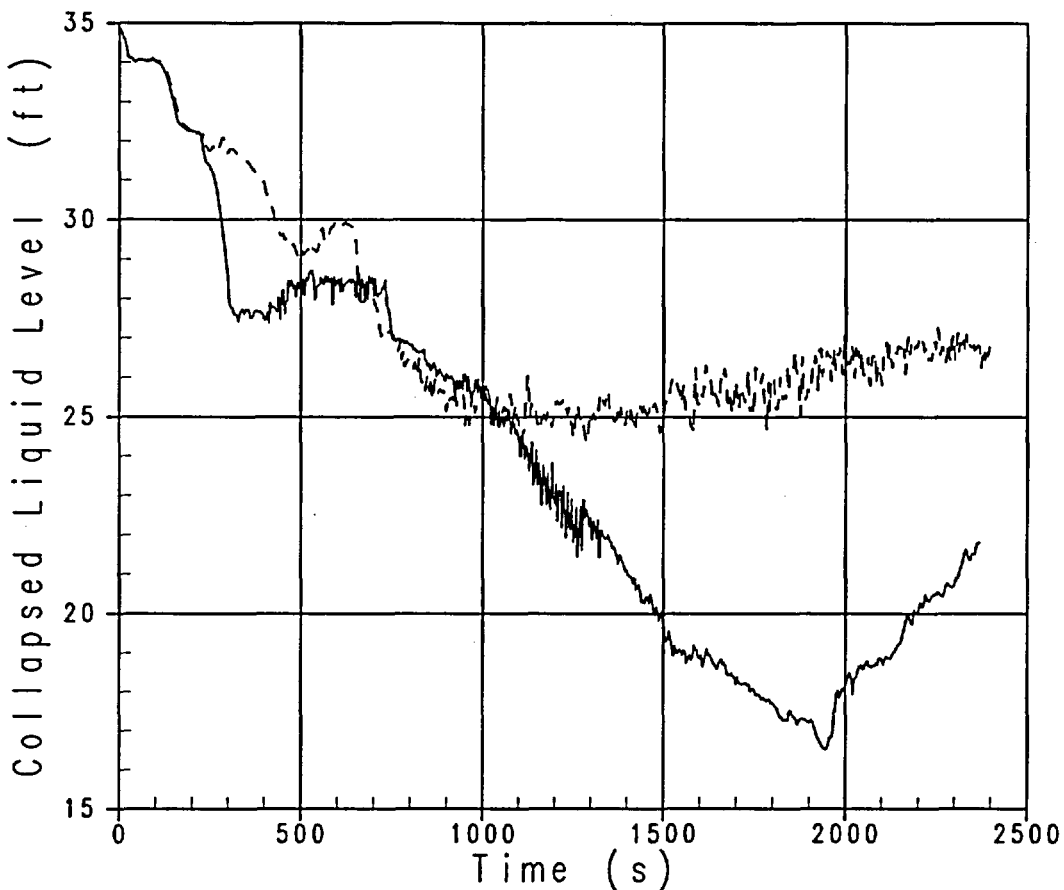


Figure 28-3-9. Break Orientation – Downcomer Collapsed Liquid Level Comparison, Side Break

Break Location Sensitivity Study
Inner Vessel Collapsed Liquid Level Comparison

— LQ-LEVEL 1 0 0 Reference Case

- - - LQ-LEVEL 1 0 0 Side Break

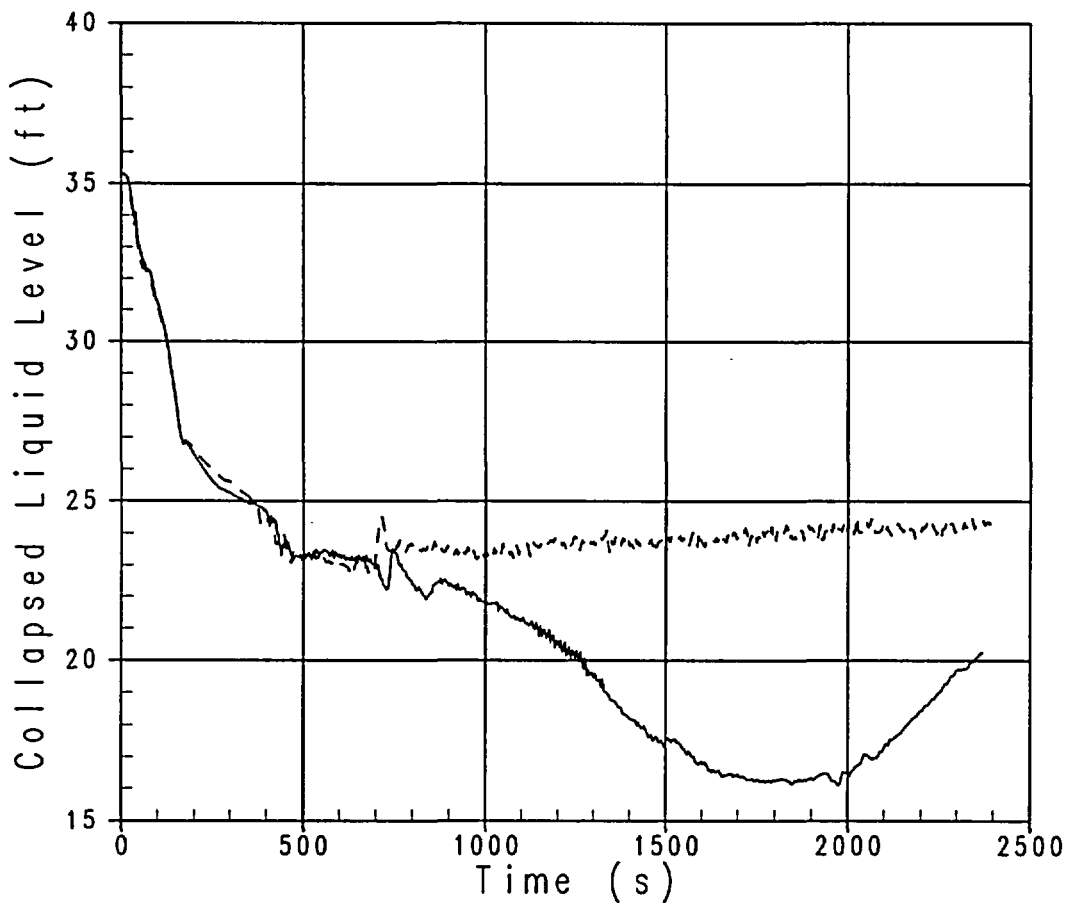


Figure 28-3-10. Break Orientation – Inner Vessel Collapsed Liquid Level Comparison, Side Break

Break Location Sensitivity Study
PCT Comparisons

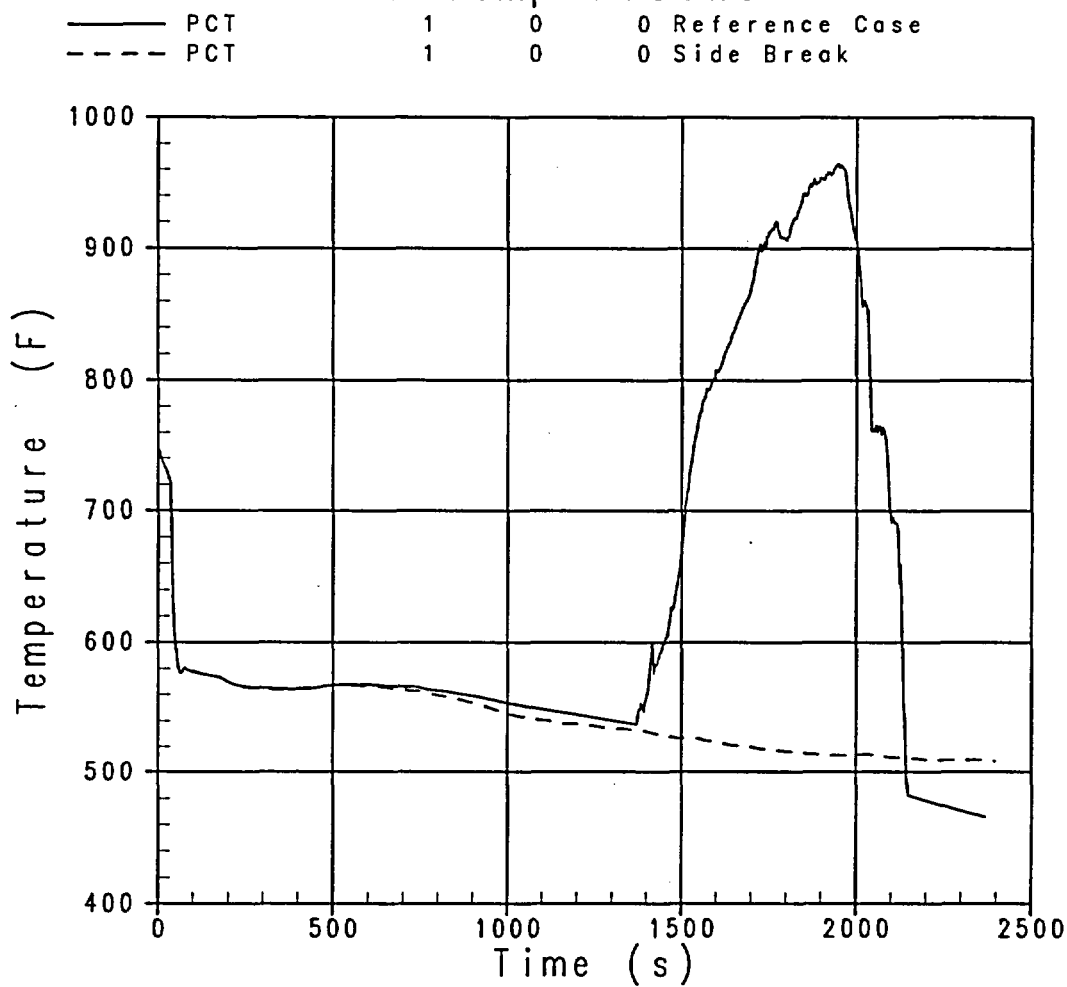


Figure 28-3-11. Break Orientation – PCT Comparison, Side Break

Break Location Sensitivity Study
Void Fraction at Break Location

— ALPN 200 2 0 Reference Case
- - - ALPN 200 2 0 Side Break

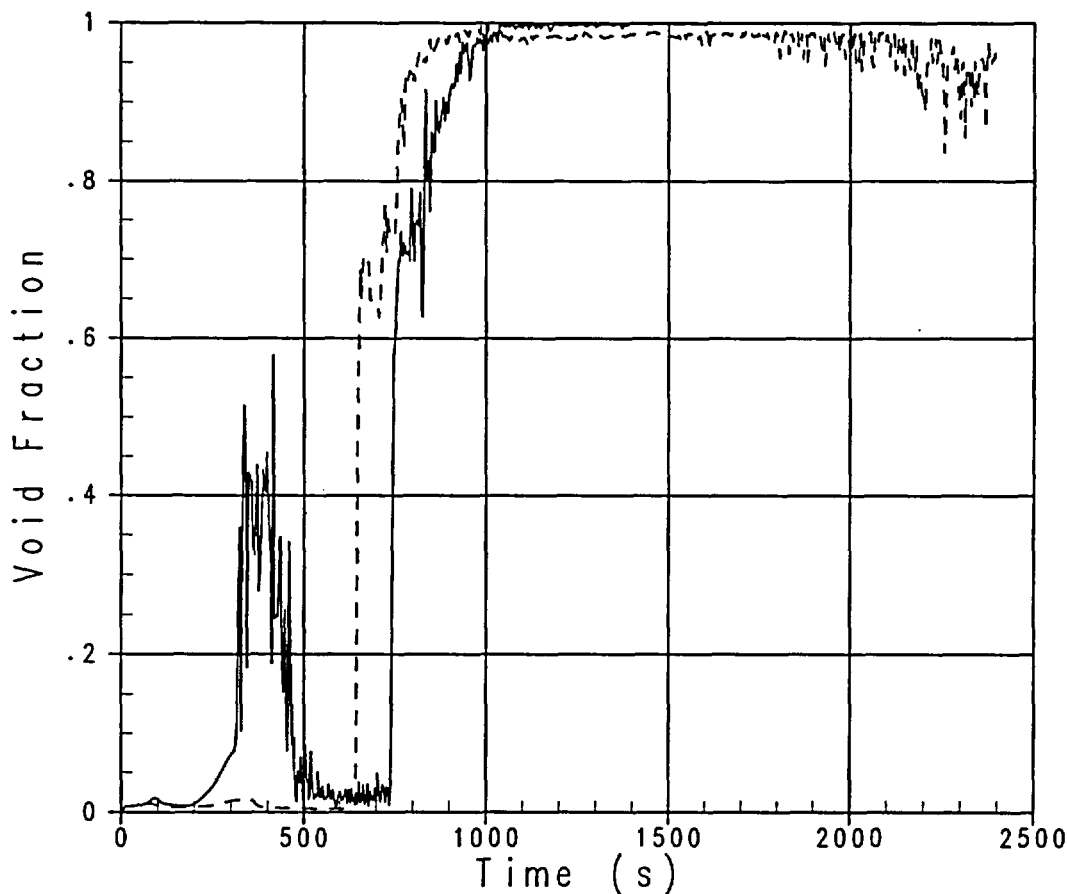


Figure 28-3-12. Break Orientation – Comparison of Void Fraction at Break, Side Break

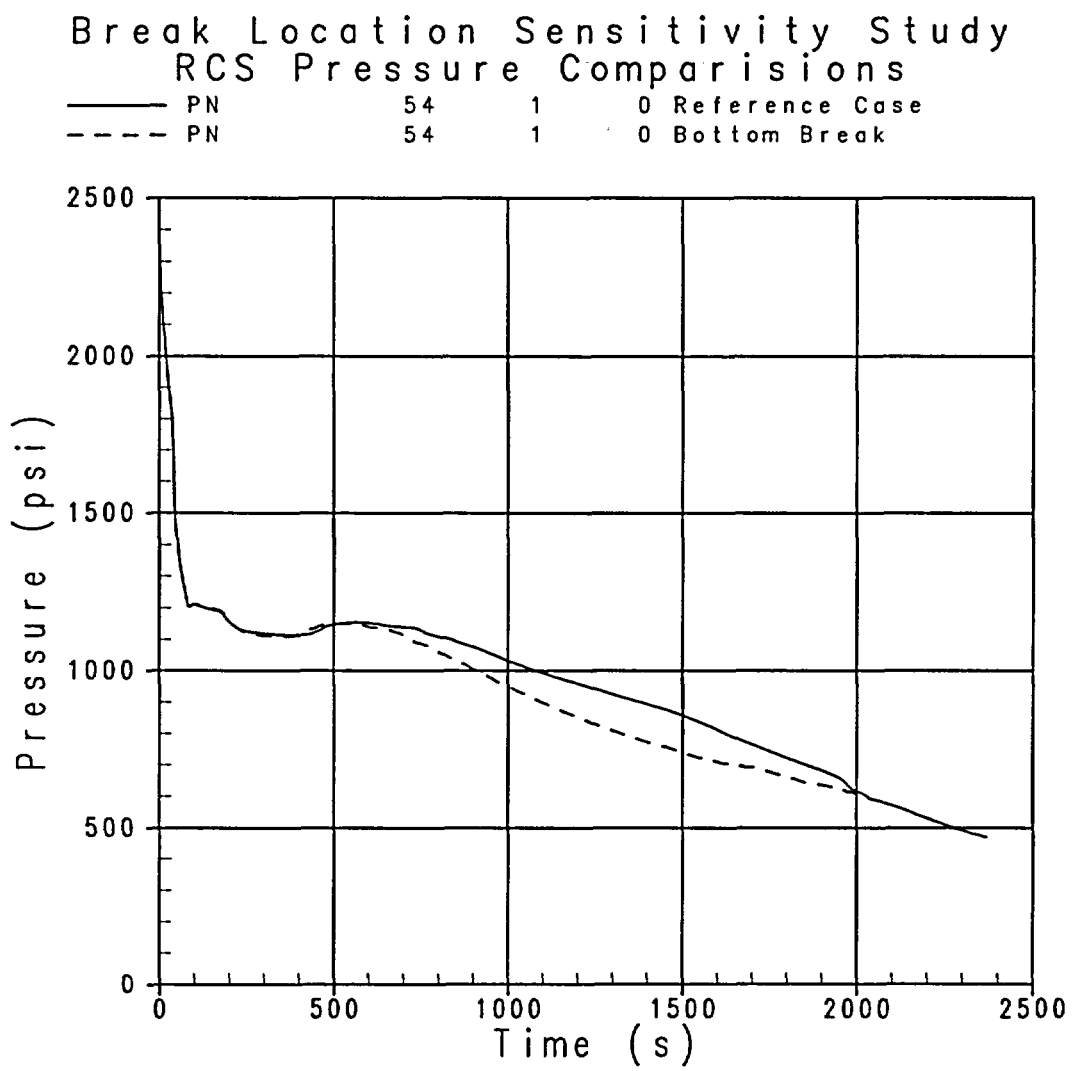


Figure 28-3-13. Break Orientation – RCS Pressure Comparison, Bottom Break

Break Location Sensitivity Study
Integrated Break Flow

— INTMTOT 200 2 0 Reference Case
- - - INTMTOT 200 2 0 Bottom Break

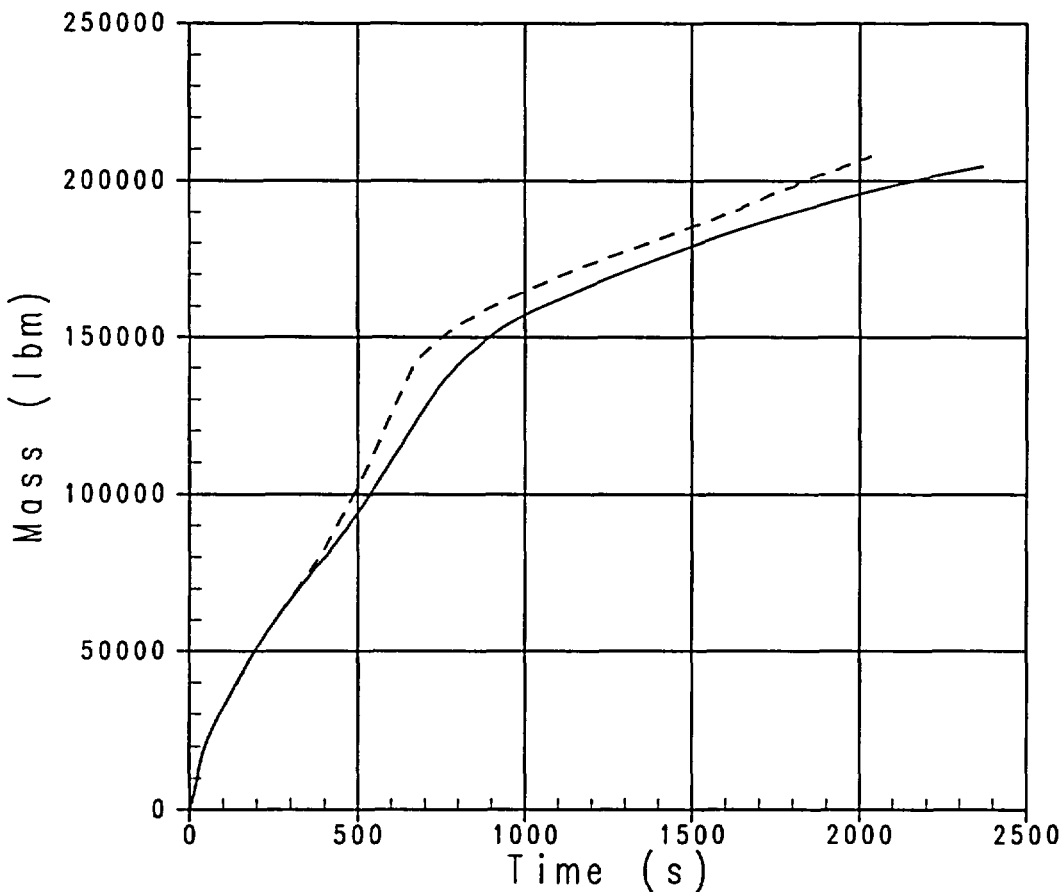


Figure 28-3-14. Break Orientation – Integrated Break Flow Comparison, Bottom Break

Break Location Sensitivity Study
Downcomer Collapsed Liquid Level

— LQ-LEVEL 6 0 0 Reference Case
--- LQ-LEVEL 6 0 0 Bottom Break

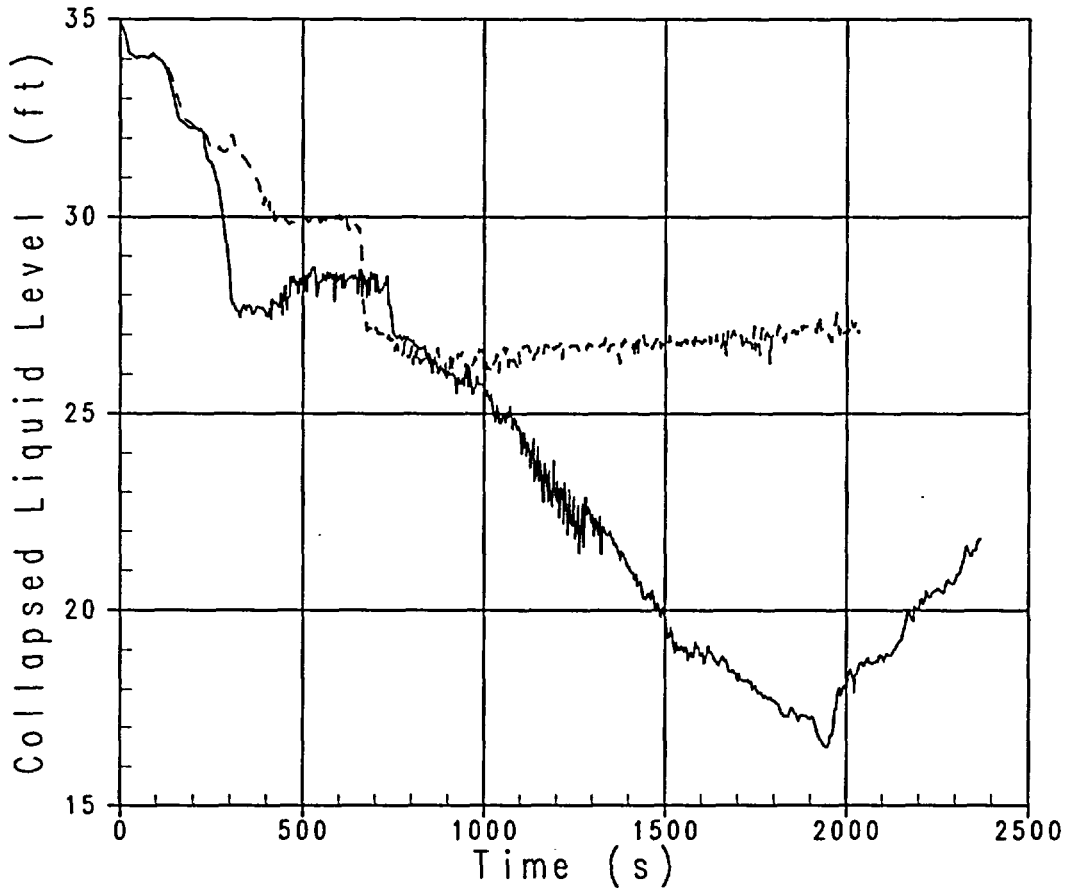


Figure 28-3-15. Break Orientation – Downcomer Collapsed Liquid Level Comparison, Bottom Break

Break Location Sensitivity Study
Inner Vessel Collapsed Liquid Level Comparison

— LQ-LEVEL	1	0	0	Reference Case
- - - LQ-LEVEL	1	0	0	Bottom Break

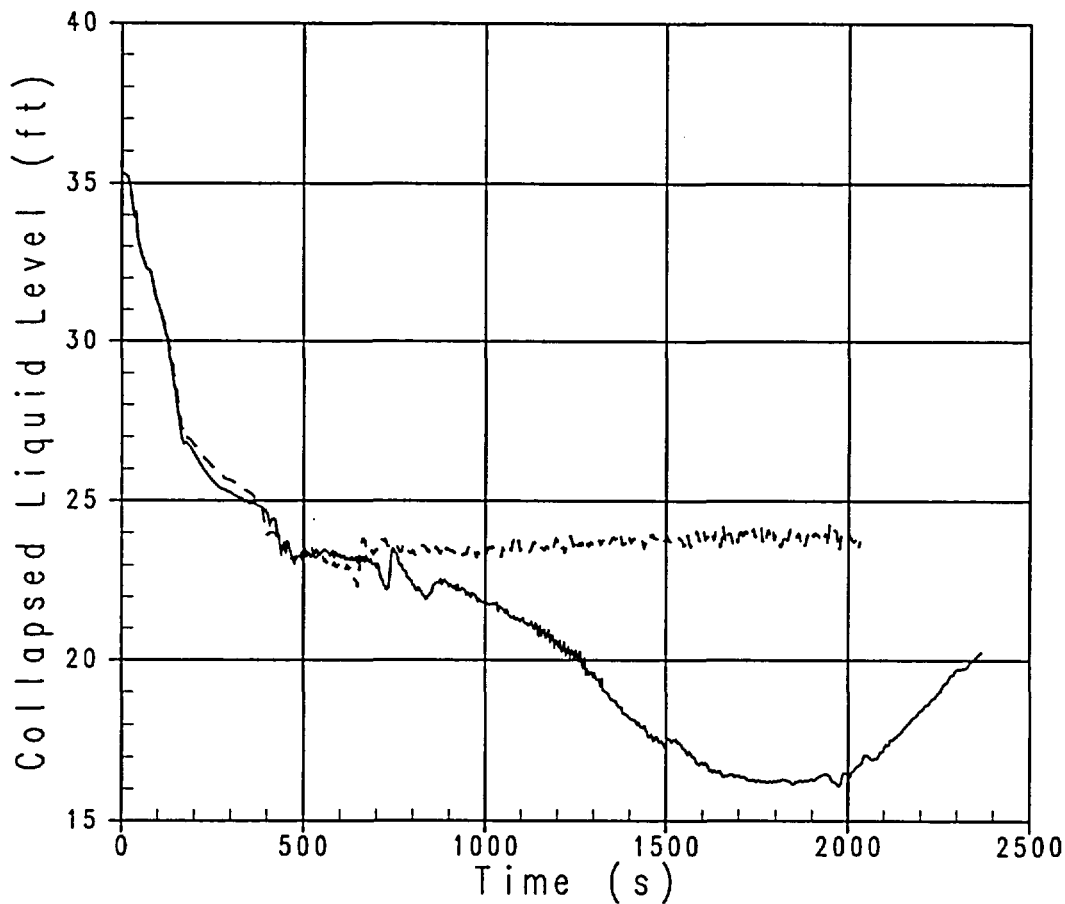


Figure 28-3-16. Break Orientation – Inner Vessel Collapsed Liquid Level Comparison, Bottom Break

Break Location Sensitivity Study
PCT Comparisons

— PCT 1 0 0 Reference Case
- - - PCT 1 0 0 Bottom Break

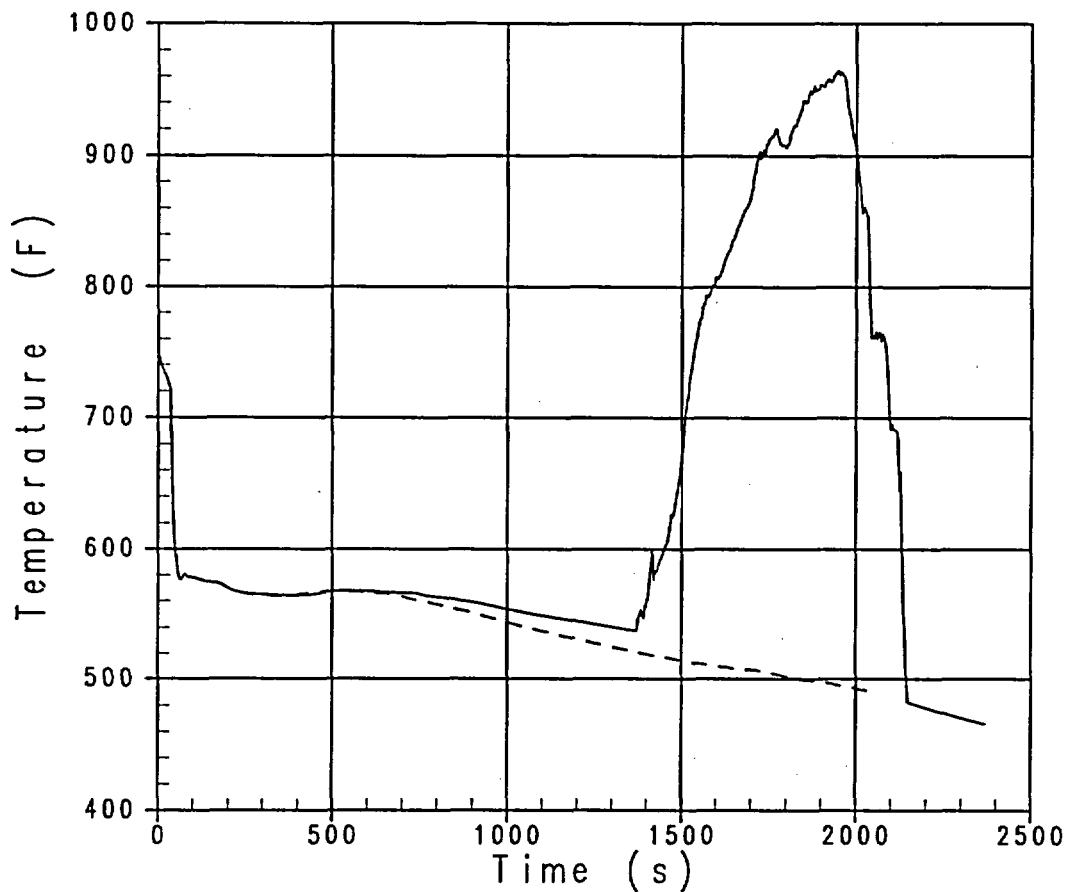


Figure 28-3-17. Break Orientation - PCT Comparison, Bottom Break

Break Location Sensitivity Study
Void Fraction at Break Location

— ALPN 200 2 0 Reference Case
- - - ALPN 200 2 0 Bottom Break

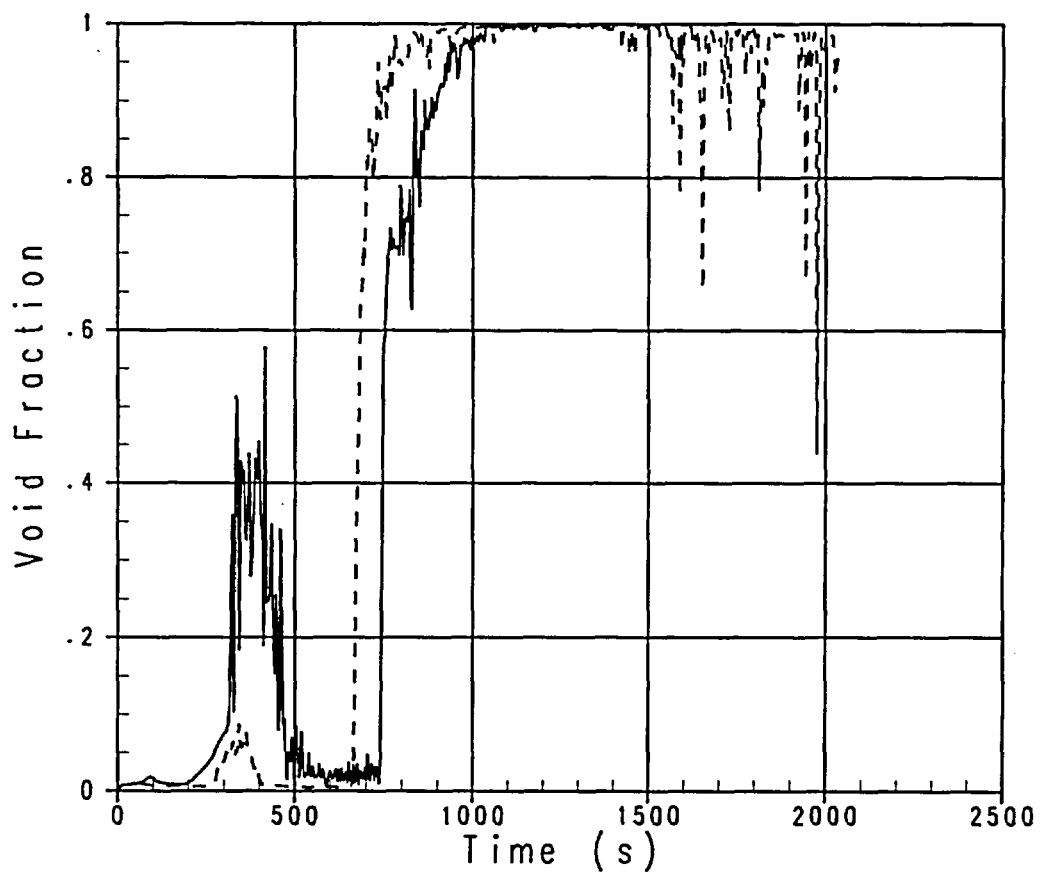


Figure 28-3-18. Break Orientation – Void Fraction Comparison at Break, Bottom Break

28-4 Effect of SGTP Level

28-4-1 Associated Phenomena

The SGTP level can affect the transient behavior through several different mechanisms. One effect arises simply from the change in the total amount of inventory in the RCS primary. The steam generator tubes and tubesheet account for approximately 13 percent of the total RCS fluid volume. Therefore, some non-inconsequential amount of mass may be removed from the primary if SGTP levels on the order of 25 percent of the tubes are modelled, as was done for this study. A uniform SGTP level of 25 percent decreases the initial primary inventory by approximately 16,500 lbm, or 3.2 percent of the total primary fluid mass at zero SGTP. SGTP also reduces the heat transfer area between the primary and secondary; a 25-percent SGTP level is equivalent to losing one entire steam generator. This loss of heat transfer area has some effect on initial, steady-state operating conditions and on heat transfer during the transient. However, in order to remove most of the effect of different initial conditions in performing SGTP sensitivities, the steady-state secondary side operating pressure was adjusted to obtain nearly the same primary side average fluid temperature for the 25% SGTP case, as in the 15% SGTP reference case. Flow resistance also increases as a function of SGTP level. As with heat transfer area, the effects of flow resistance are manifested both in initial conditions and on transient behavior.

The sensitivity to SGTP has been obtained by running two cases, varying the plugging level. The results are presented for two different SGTP levels that model overall uniform plugging in all steam generators. The base case transient selected for comparisons is one with 15-percent uniform plugging; that is, each generator has 15 percent of its tubes plugged. This approximates the actual Indian Point Unit 2 plugging level at the time the analysis was performed and was fixed in the parameter sensitivities discussed throughout this document unless otherwise noted. A case with a higher uniform SGTP level of 25 percent was run for comparison.

28-4-2 Results

The results in this section compare the transient behaviors for the two SGTP cases. The base case is a 3-inch cold leg break with 15-percent uniform SGTP. Some other significant parameters are as follows: LOOP at reactor trip, minimum SI capacity (as defined for the reference case in Section 30-3), and the same core peaking factors. The SGTP sensitivity case uses 25-percent uniform plugging. The secondary side steady-state operating pressure for the

25-percent SGTP case was retained at 718 psia, to maintain the secondary side temperatures so that they were nearly identical to those for the two cases.

Figure 28-4-1 compares the PCT for the two cases. Increasing the plugging from 15 to 25 percent results in a large reduction in the PCT, because the core inventory increases.

Figure 28-4-2 compares the inner vessel (core-to-upper plenum) collapsed liquid levels. Other figures show that there is little difference in behavior for the two cases prior to the time of loop seal clearance. Figures 28-4-3 and 28-4-4 compare the break flowrates and integrated break flow respectively. Comparison of the break flowrates in Figure 28-4-3 shows that they were close with the 15% SGTP case a bit larger for most of the early blowdown. The 25% SGTP break flow is then slightly higher for approximately 200 seconds, until loop seal clearing occurs at about 700 seconds. During this time, the average break flow in the 25-percent SGTP case is high enough to result in the 25-percent SGTP case integrated break flow drawing equal to that of the lower plugging case. The level depression caused by the loop seal clearing phenomenon at approximately 700 seconds occurs about 40 seconds later for the lower 15-percent SGTP case. Two loop seals clear in the 25-percent SGTP case, whereas only one does in the 15-percent SGTP case. Therefore, following loop seal clearing and the transition to two-phase break flow, the remaining inventory in the RCS is approximately 5000 lbm lower in the 15-percent SGTP case. This difference in core inventory increases until the RCS depressurizes to the accumulator actuation setpoint.

Figure 28-4-6 compares the RCS primary system pressures for all the cases. Overall, general differences in the system pressure trends reflect the mass inventory histories. The initial steam generator secondary side pressure is the same as for the 25-percent SGTP case, the relief valve setpoints are the same at 1080 psi, and therefore, the RCS pressure exhibits a plateau at about 1150 psi for both cases prior to loop seal clearing. Because initial loop seal clearing is delayed in the 15-percent SGTP case (Figure 28-4-6), the pressure hangs slightly longer near this plateau valve.

The predominant reason the SGTP results differ is due to the differences in the loop seal clearing behaviors. Figure 28-4-7 compares the steam flowrates in each of the loops for the 15% and 25% SGTP transients, and Figure 28-4-8 compares the sum of flow in all the loops. In the 15-percent SGTP case, only an intact loop clears, whereas in the other case, a nonbroken loop (which later replugs) and the broken loop both clear. The effect on system inventory from this difference is a significant voiding of the second loop seal and transfer of its mass into the vessel downcomer after loop seal clearing. The general trend after loop seal clearing is an equivalent

depressurization of the primary for the 15-percent SGTP case as for the higher SGTP level case, until the core uncovers. After 1500 seconds have elapsed, the reduced volumetric generation of vapor from the uncovered core causes the 15-percent SGTP case to depressurize more quickly.

There is an approximately 150-second difference in depressurizing to 655 psia where the accumulators begin to inject. The inventory in the vessel begins to recover immediately afterward (Figure 28-4-2). The fuel rod heatup in the 15% SGTP case is terminated shortly thereafter, and the cladding continues to cool down; almost no heatup is observed in the 25% SGTP case.

As the system inventory is depleted during the small break LOCA, the system will exhibit various modes of decay heat removal. When sufficient mass has been depleted, continuous two-phase natural circulation will be lost and the system will begin a top down drainage. Mixture levels in the vessel and the downhill portion of the steam generator tubes will begin to decrease to the point where steam is just able to pass through the loop seal to the reactor coolant pump inlet. It has been shown that loop seal steam venting begins soon after the water level in the steam generator side of the loop seal reaches the top of the horizontal section in the loop seal (Lee, et al., 1983).

For the Indian Point Unit 2 3-inch break transients, if only a single loop seal is predicted to clear, it apparently provides adequate steam relief to prevent the remaining loop seals from clearing. Figure 28-4-7 shows that for the 15-percent SGTP case, an unbroken loop (loop 22) experiences the clearing, while for the other case, the pressurizer loop (loop 24) preferentially clears together with an unbroken loop. As seen in Figure 28-4-8, the sum of the vapor flowrates through all four loops provides a total steam relief rate that is nearly identical for the two cases and reflects only the small differences in RCS pressure. There is an apparent lack of need for more than one loop seal to clear for the 3-inch cold leg break, although more than one may clear. The 3-inch break size appears to be the threshold break size for more than one loop seal to vent steam as indicated in Figure 28-4-9 as taken from Lee, et al. (1983), as discussed in Section 27-8.

If flow resistance were a significant contributor to governing loop seal clearing, it would be expected that although a different loop might preferentially clear for each case, the same total number of loops that cleared for the base case would also clear with 25-percent uniform SGTP. However, the friction and form loss pressure drops are small compared to the hydrostatic heads, and the pressure drop between the core and the break through each loop is the same even though each loop may have slightly different resistance factors. Figure 28-4-10 compares the collapsed

liquid levels in the uphill sides of the steam generators for the transients. Here the effect of SGTP is apparent, though small. With increased SGTP levels, there is an earlier draining, which is consistent with the reduced volume. The steam generator tubes are completely drained in both of the cases prior to the loop seal clearing. Because the loop flow is blocked by the water in the pump suction piping prior to loop seal clearing, there are generally no large loop vapor flowrates that develop significant pressure drops and strongly influence incipient loop seal clearing.

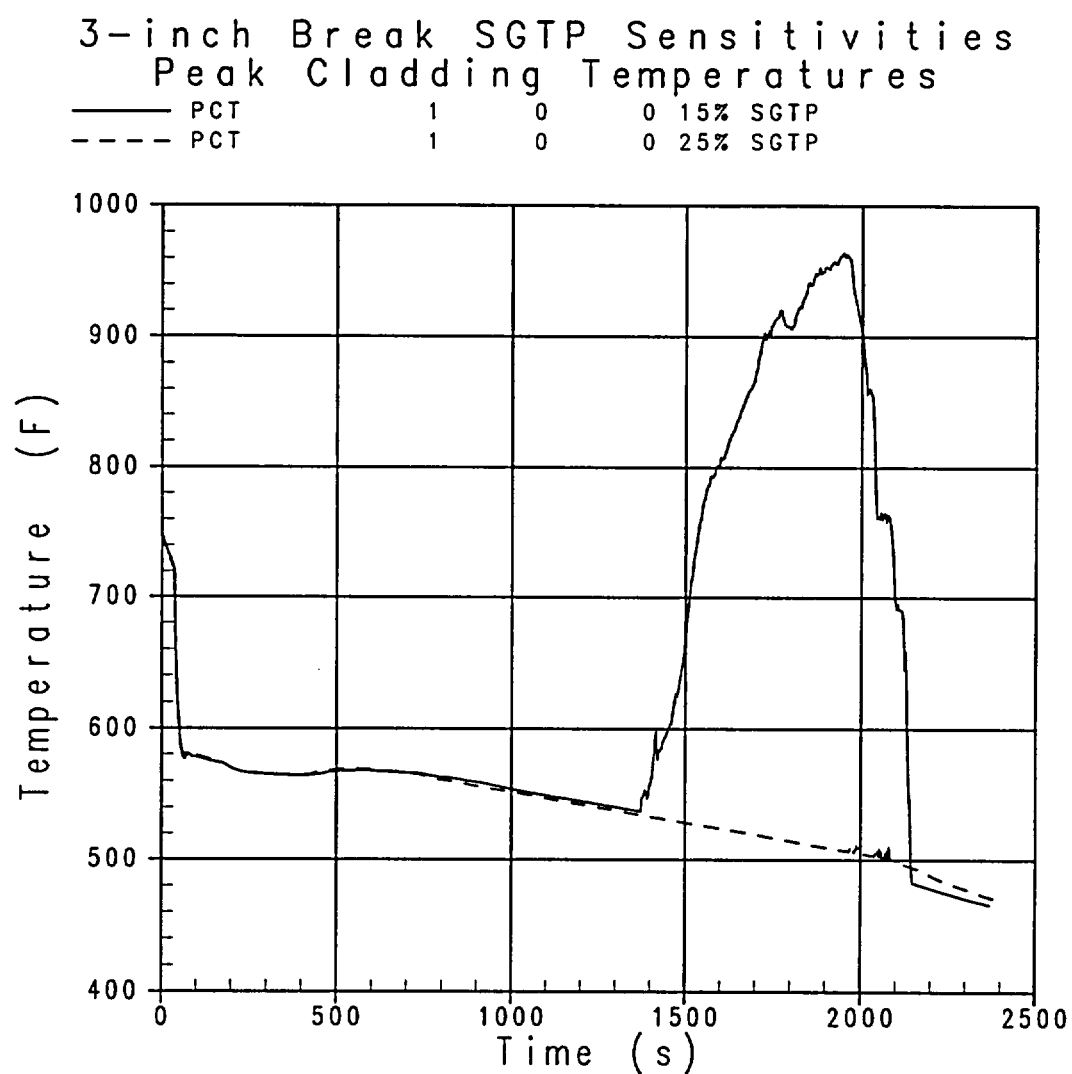
Small break LOCA's may be characterized as relatively slow system drainage transients, so the mixture level response will be similar among all of the downhill pump suction legs as controlled by the hydrostatic heads. Immediately prior to loop seal steam venting, the liquid levels in the downhill sides of all loops are about the same. Each loop is poised to potentially clear and (if the plant loops are symmetric) each has the potential to become the one(s) that does actually clear. Realistically, perturbations caused by oscillations of water levels, mechanical vibrations, pressure pulses from boiling water in the core, and momentum changes in the steam flow will result in slightly different mixture levels in the loops. Therefore, the hydrostatic heads in each of the loops may be different. The water level difference among the loops before the loop seal steam venting is affected by a combination of the several random phenomena mentioned above. This leads to uncertainty as to which loop seal will initially pass steam.

For the lower SGTP level, there is less water in the downcomer and in the inner vessel after loop seal clearance. The levels in the pump suction piping downflow legs for the cleared and uncleared loops (Figure 28-4-11) show the added vessel water in the 25% SGTP case comes from the second cleared loop seal. Immediately following initial loop seal clearing, there is a tendency to refill the seal(s) once the initial steam relief has occurred; steam flow is momentarily reduced in both cases. There is a partial replugging for both of the cases as reflected in the steam flow curves of Figure 28-4-7, but it is unclear whether this is more strongly influenced by the flow resistance of the steam generators or the RCS water mass available for refilling. Overall, no compelling reason for the clearing of a second loop seal in the 25% SGTP case can be determined. The resulting differences in system mass inventory distribution cause the collapsed liquid level difference in the core. In an actual plant 3-inch cold leg small break LOCA event, any loop(s) may actually be the one(s) to clear, consistent with the Lee, et al. (1983) reference. Furthermore, the 3-inch cold leg break is the threshold break size for the clearing of multiple loops as discussed by Lee et al. (1983) and in Section 27.

28-4-3 Conclusions

At an SGTP level of 25 percent, which is about the maximum reasonable level of average plugging for a plant, the predicted PCT for Indian Point Unit 2 is the initial, steady-state value. Increasing the SGTP level by 10 percent, from 15 to 25 percent, results in a major decrease in the calculated PCT. Although this result indicates that the sensitivity to SGTP is fairly large, it is misleading because the specific dominant phenomenon that governs the PCT sensitivity is the loop seal clearing behavior, which affects the amount of water present in the reactor vessel after the incipient loop seal clearing phase ends and the boiloff period begins.

Significant primary coolant inventory effects result from the inventory redistribution associated with the difference in loop seal clearing for the 25-percent and 15-percent SGTP cases. The primary inventory increase in the higher SGTP case reduces PCT much more than seems reasonable as a consequence of the increase in SGTP by itself. In order to obtain a conservative prediction of loop seal clearing, the 15-percent SGTP case will be the reference case for the sensitivity studies that establish the 95th percentile PCT for Indian Point Unit 2.



(L)

Figure 28-4-1. PCT, SGTP Sensitivity

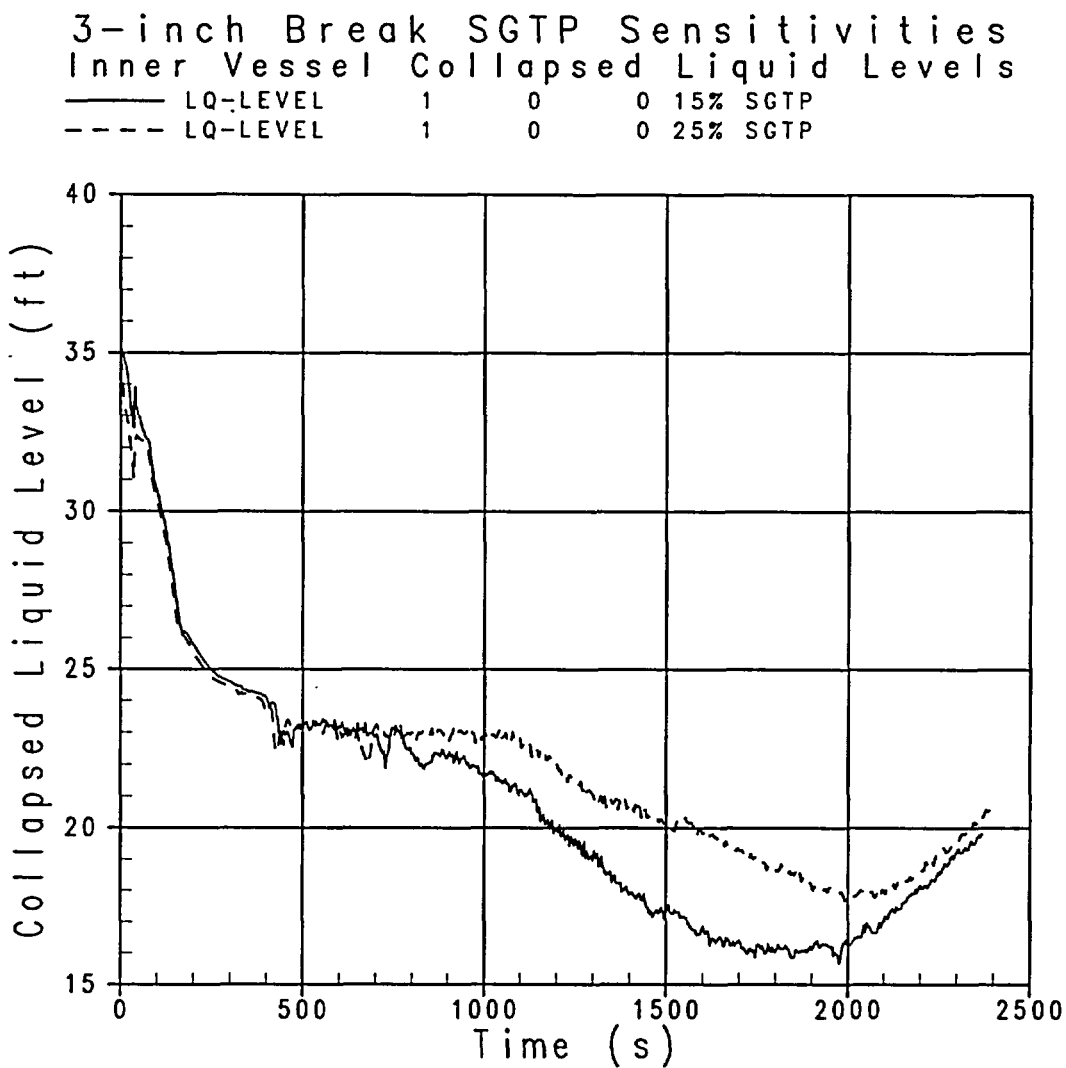


Figure 28-4-2. Inner Vessel (Core-to-Upper Plenum) Collapsed Liquid Levels, SGTP Sensitivity

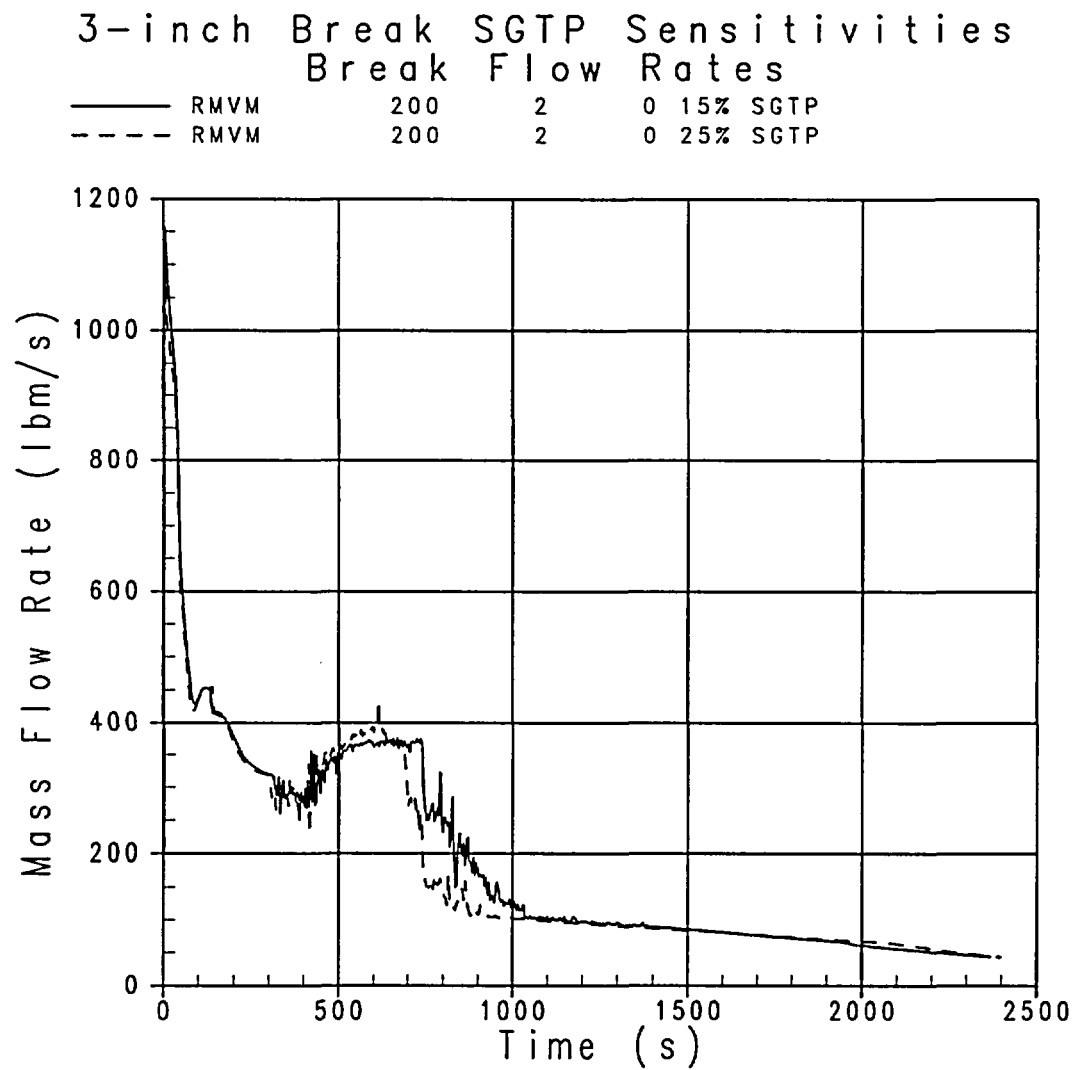


Figure 28-4-3. Break Flowrates, SGTP Sensitivity

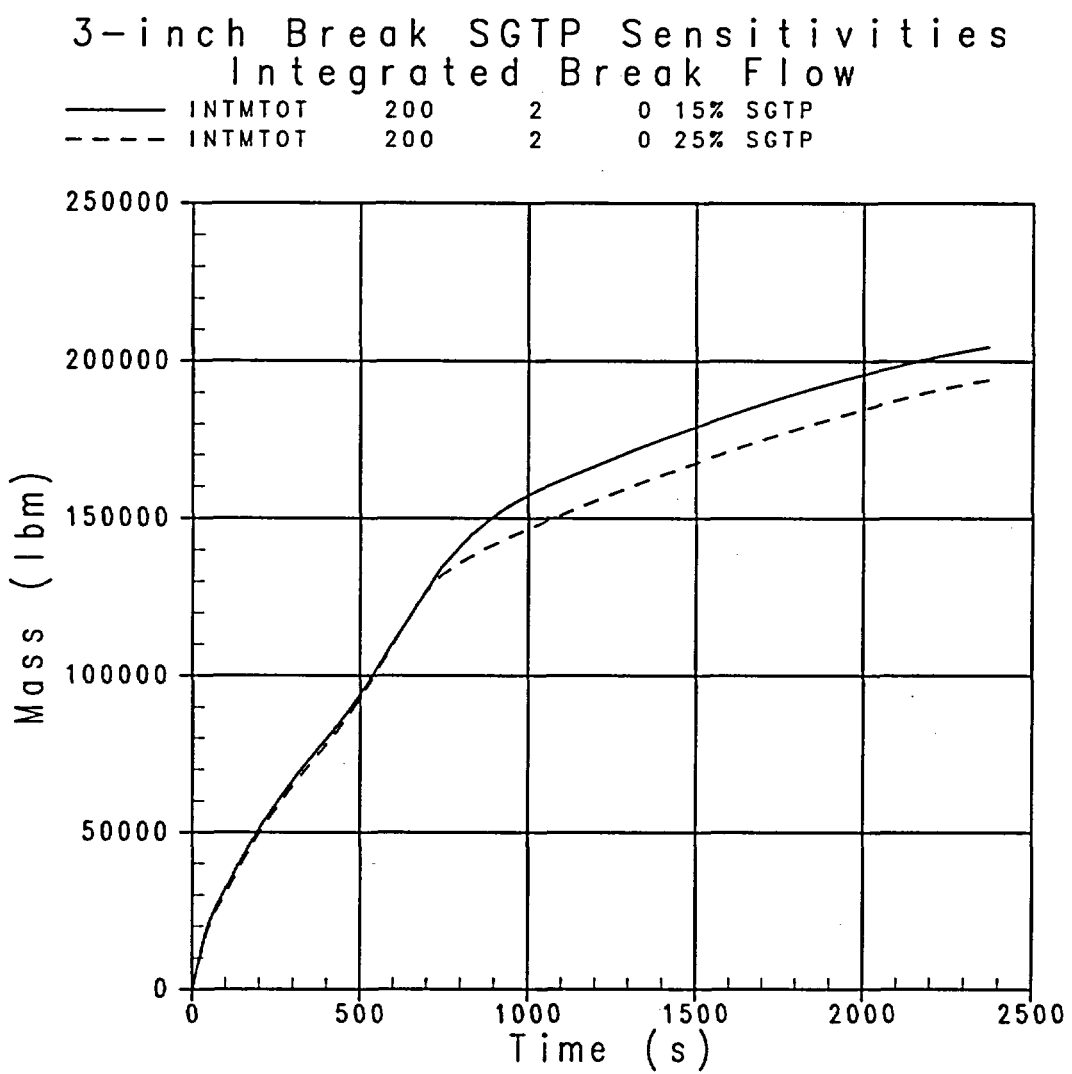


Figure 28-4-4. Integrated Break Flow, SGTP Sensitivity

3-inch Break SGTP Sensitivities
RCS Primary Mass Balance

— M(RCS) 46 0 0 15% SGTP
- - - M(RCS) 46 0 0 25% SGTP

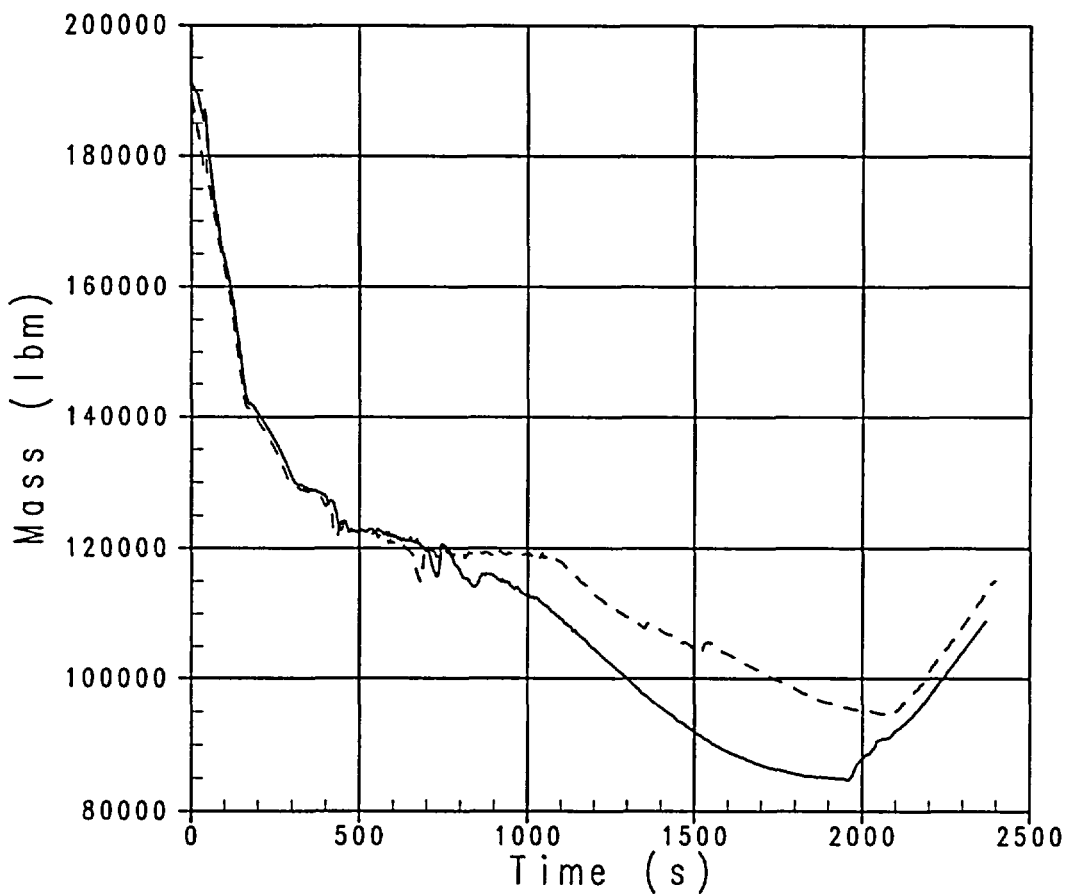


Figure 28-4-5. Total RCS Primary Mass, SGTP Sensitivity

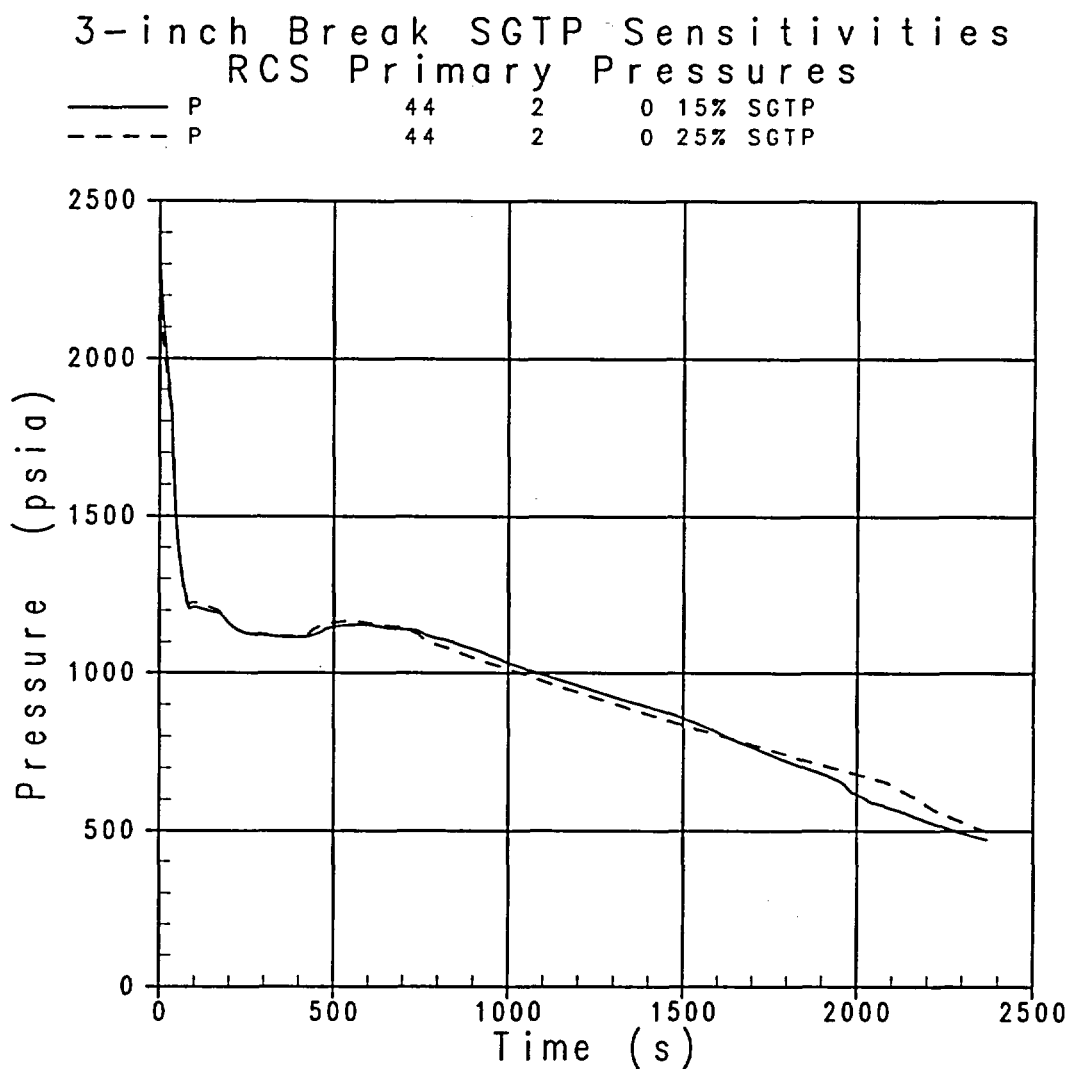


Figure 28-4-6. RCS Primary Pressures, SGTP Sensitivity

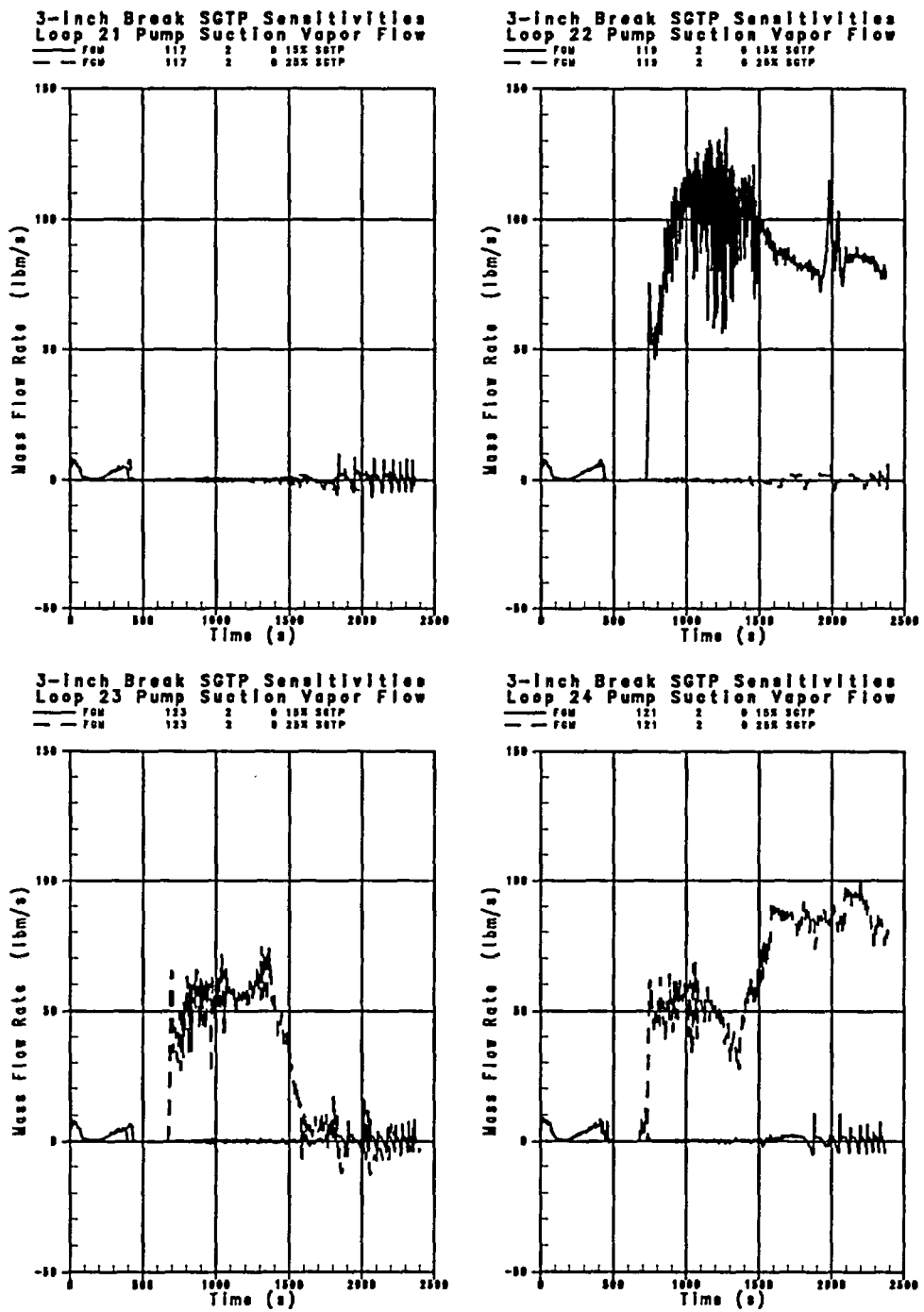


Figure 28-4-7. Pump Suction Vapor Flowrates, SGTP Sensitivity

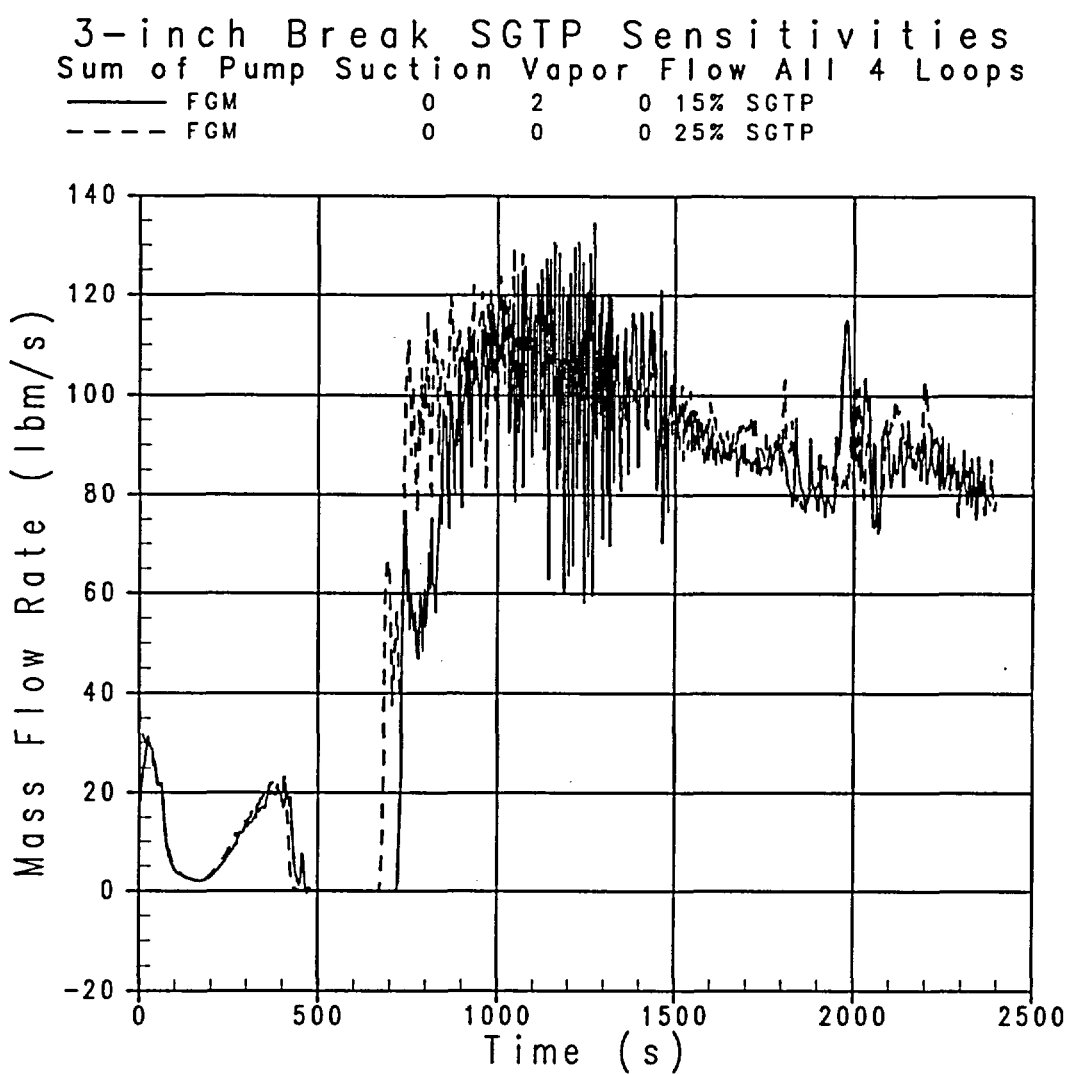


Figure 28-4-8. Total Pump Suction Vapor Flowrates for Four Loops, SGTP Sensitivity

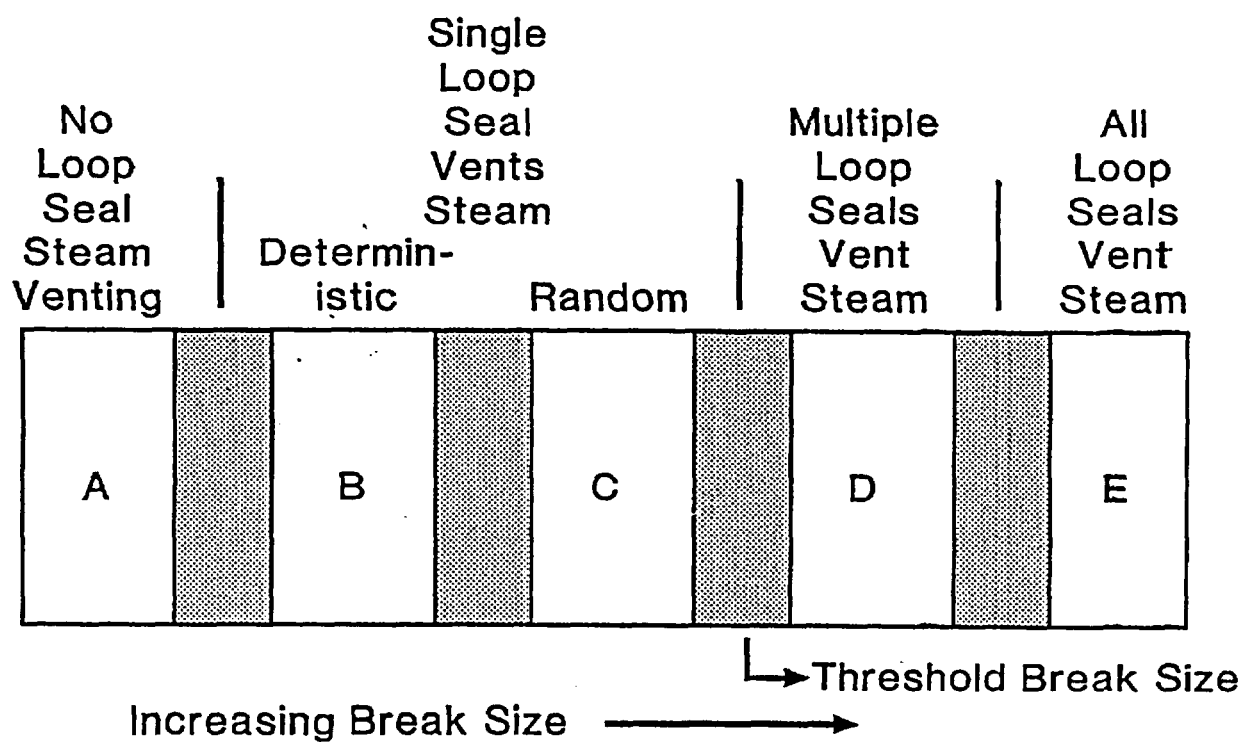


Figure 28-4-9. Loop Seal Steam Venting as a Function of Break Size

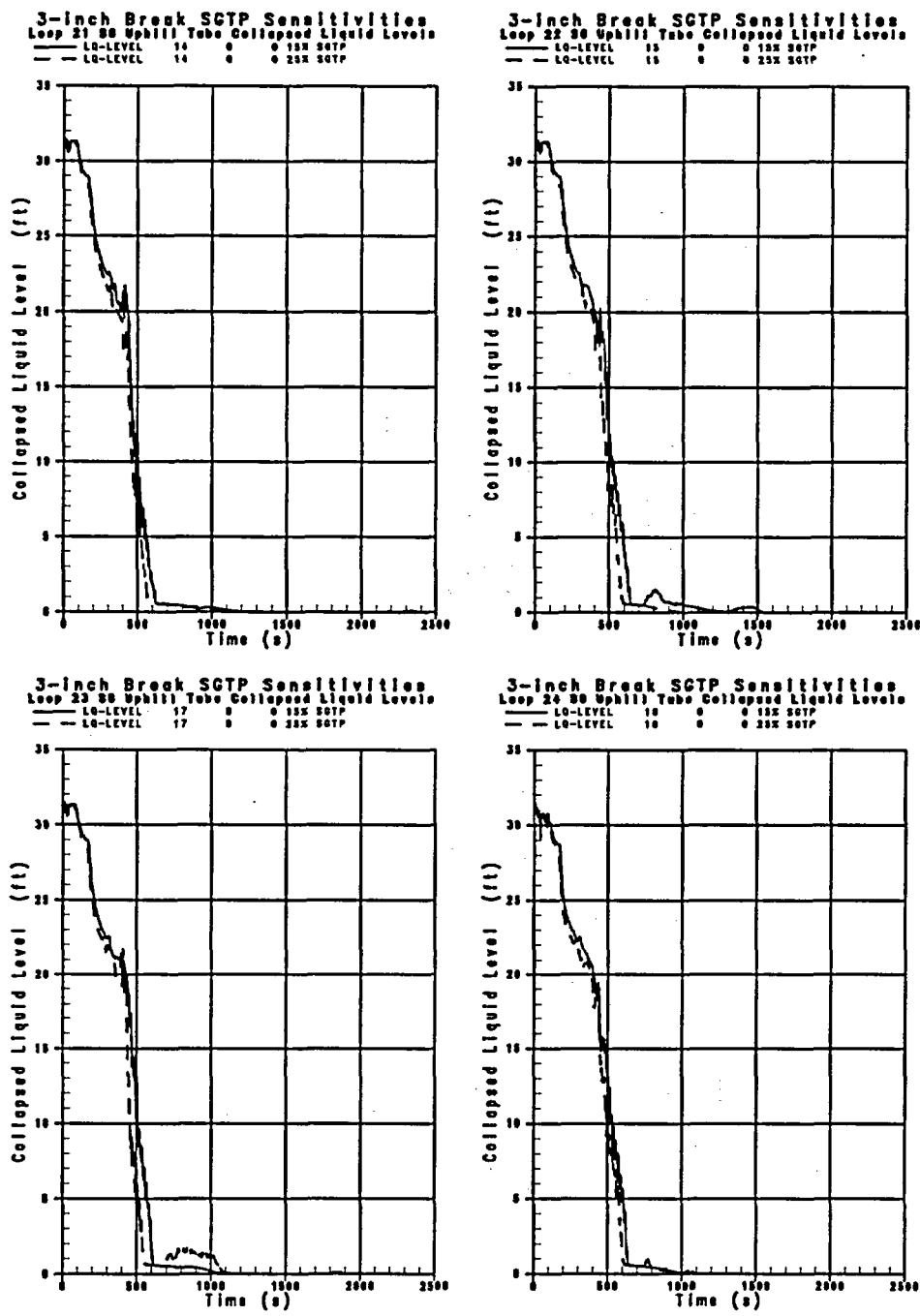


Figure 28-4-10. Steam Generator Uphill Side Tube Collapsed Liquid Levels, SGTP Sensitivity

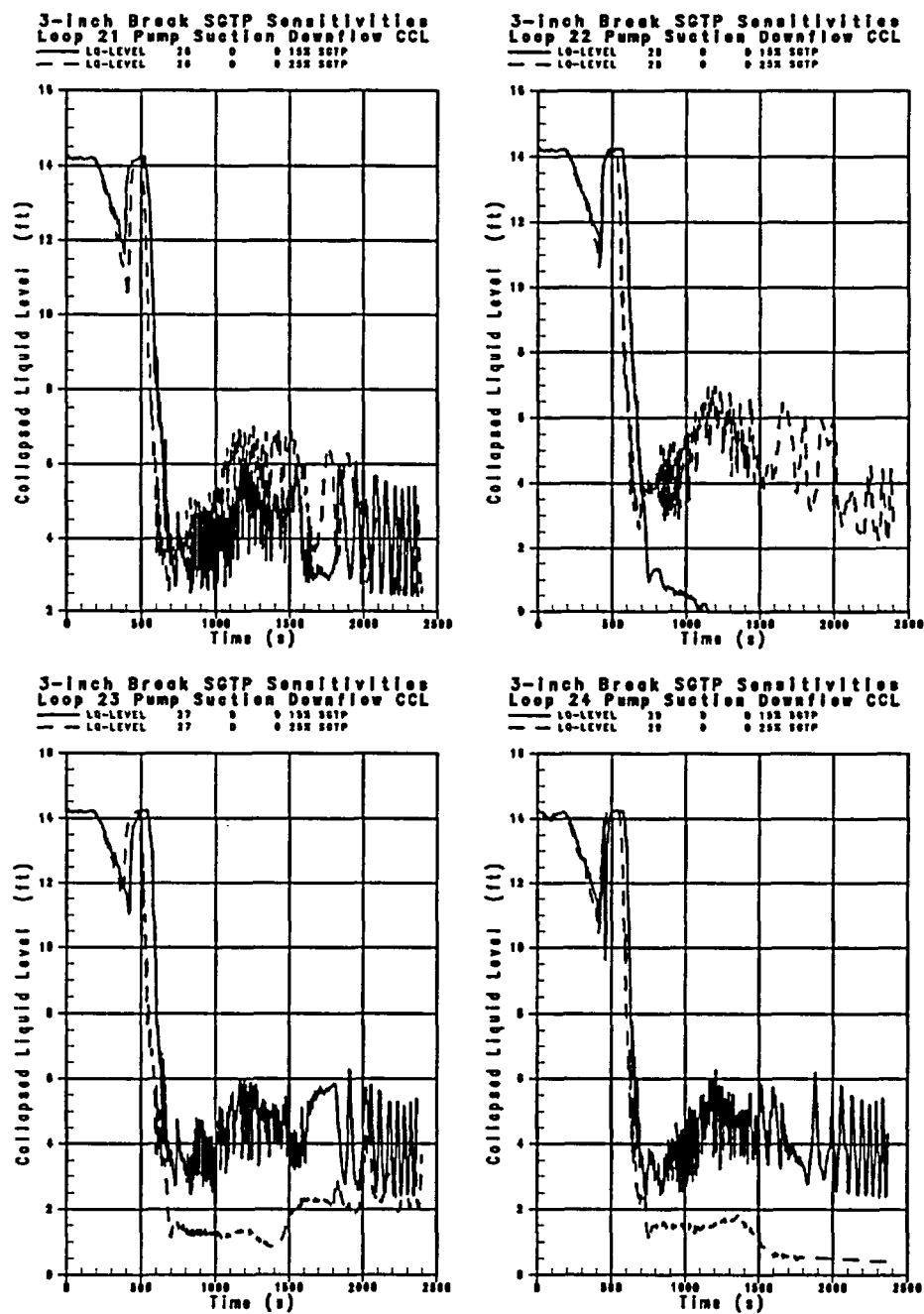


Figure 28-4-11. Pump Suction Downflow Piping Collapsed Liquid Levels, SGTP Sensitivity

28-5 Summary and Conclusions

28-5-1 Worst Break Location

For a given break size, the integrated break flow at the time the break uncovers is greater for the pump suction break than for the cold leg break. Due to location, the pump suction break loses the greatest amount of liquid inventory during the transient in draining to the break elevation. The hot leg break is initially much lower in break flow than the pump suction or cold leg breaks. Still, the integrated break flows (Figure 28-5-1) of hot leg and pump suction breaks are almost the same at accumulator actuation. This indicates a consistent behavior relative to the pumped SI flow entering the RCS. The cold leg break locations exhibit a lower integrated break flow at accumulator actuation because of lower SI flow.

28-5-2 Worst Break Orientation

For a given cold leg break size, the worst break orientation for Indian Point Unit 2 is the top break. This orientation is limiting because due to the location, the top break can be presumed to be the break of an SI delivery line. This top break case (the Reference Case) results in the spill to containment of a large fraction of the pumped SI flow; it therefore receives much less pumped SI flow (see Section 30, Volume 4 for details) than the other cases, which leads to a less favorable core inventory situation and a higher PCT prediction.

The impact of the pumped SI spill assumption is apparent in Figure 28-5-2; the "Break at Top" curve, which does credit SI flow into the broken loop, has a significantly greater integrated break flow than does the Reference Case. Among the top, bottom, and side breaks of Figure 28-5-2, each of which has the same assumption of SI injecting into all loops, the top break orientation is, as anticipated, lowest in integrated break flow. The side and bottom orientation cases are about identical at 2000 seconds; the side break orientation case is higher in integrated break flow from 750-1750 seconds because the RCS pressure is greater in the side break case.

Break Location Sensitivity Study
Integrated Break Flow

INTMTOT	200	2	0	Reference Case
INTMTOT	200	2	0	Break Non-PZR Loop
INTMTOT	200	2	0	Break in HL
INTMTOT	200	2	0	Break in PS

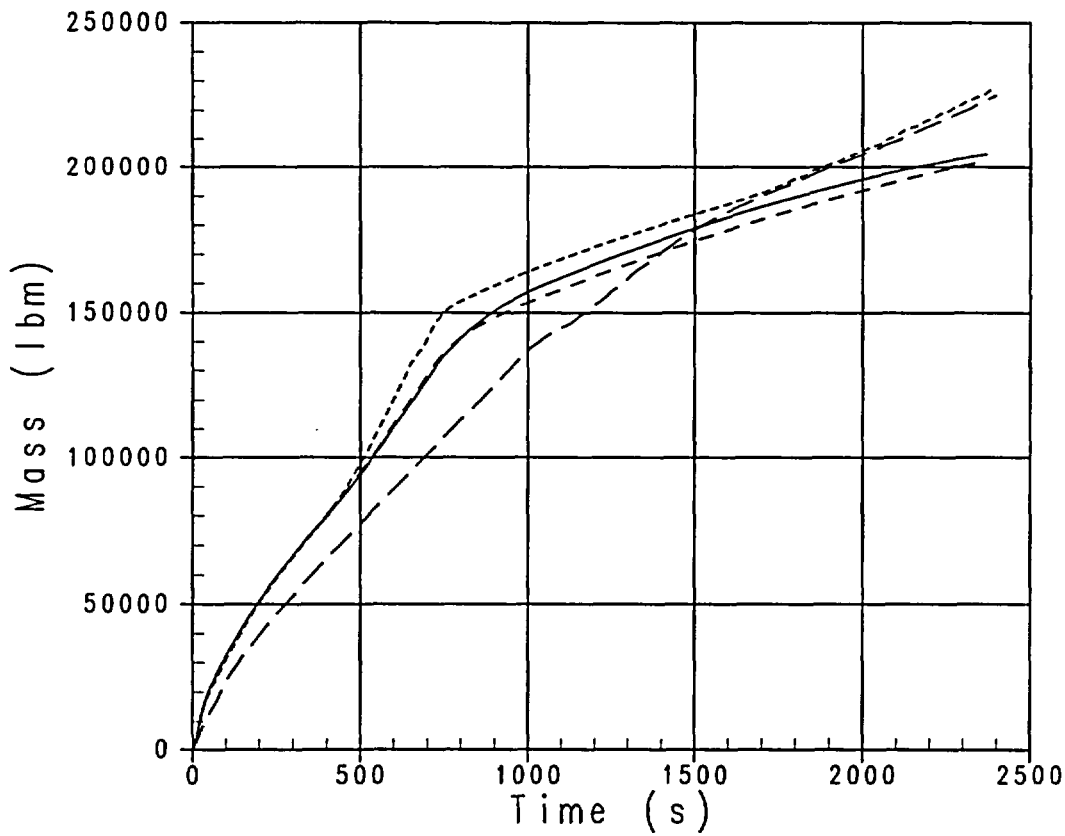


Figure 28-5-1. Integrated Break Flow Comparison for Break Location Study

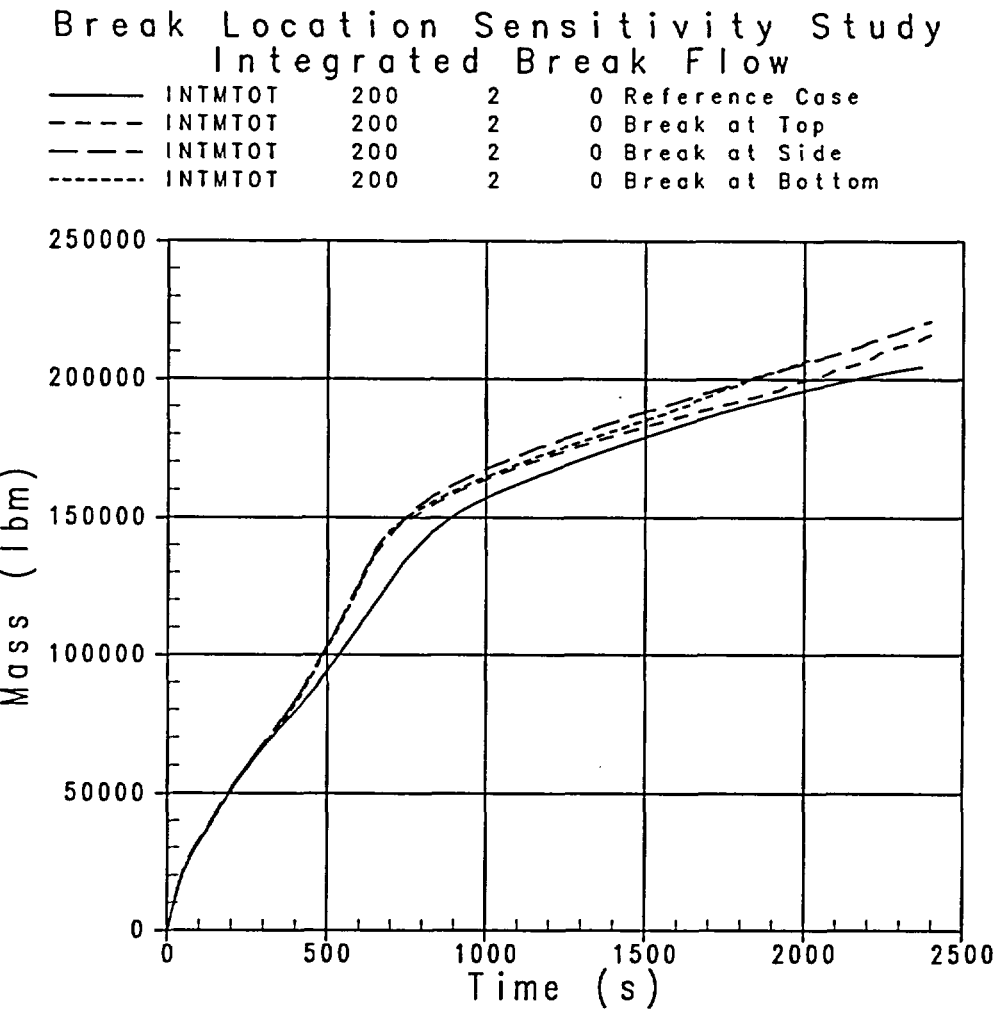


Figure 28-5-2. Integrated Break Flow Comparison for Break Orientation Study

28-6 References

Lee, N., et al., 1983, "Phenomenological Uncertainty During Loop Seal Steam Venting in a Small Break Cold Leg LOCA of a PWR," Paper 83-HT-104, National Heat Transfer Conference, Seattle, WA.

WESTINGHOUSE NON-PROPRIETARY CLASS 3

WCAP-14936-NP
Volume 4, Rev. 0
Sections 29-35

Code Qualification Document for Best Estimate Small Break LOCA Analysis

Volume 4: Small Break Uncertainty Methodology

R. M. Kemper
K. Ohkawa
N. Petkov

April 2003

Westinghouse Electric Company LLC
P.O. Box 355
Pittsburgh, PA 15230-0355

© 2003 Westinghouse Electric Company LLC
All Rights Reserved

ABSTRACT

The document "Code Qualification Document for Best Estimate Loss of Coolant Accident Analysis" (WCAP-12945-P-A) discussed the WCOBRA/TRAC computer code and the methodology used to determine the 95th percentile peak cladding temperature (PCT) for a large break loss of coolant accident (LOCA) scenario. Westinghouse has reviewed the large break code and methodology to determine if the same principles could be adapted to reliably predict the processes that occur in a small break LOCA lasting from several hundred to several thousand seconds. This document, "Code Qualification Document for Best Estimate Small Break LOCA Analysis," (WCAP-14936), describes the WCOBRA/TRAC small break LOCA code version, the code validation performed, and a methodology to determine the 95th percentile PCT for small break LOCA transients.

Volume 1 describes the features, models and correlations contained in the small break LOCA version of the WCOBRA/TRAC computer code. First, the small break processes considered to have the greatest effect during a small LOCA event are identified and ranked in the phenomena identification and ranking table (PIRT). The sufficiency of the large break WCobra/TRAC models and correlations for small LOCA analysis is then evaluated. A comprehensive presentation of the WCOBRA/TRAC-SB models and correlations follows.

Volume 2 documents simulations of a large number of separate and integral effects tests using this small break version of the code. The simulations provide, at different scales, predicted transients in which all of the important processes are compared with experimental data. The information obtained from the simulations is used to assess errors within the code. The test simulations and subsequent comparison to experimental data determine the bias and uncertainty of major model packages as they apply to small break LOCA thermal-hydraulic conditions.

Volume 3 reviews the operator actions pertinent to a small break loss-of-coolant accident (LOCA) event using Indian Point Unit 2, a four-loop pressurized water reactor (PWR), as the reference. Sources of uncertainty in the plant condition and the limiting accident analysis assumptions are identified. The effects of various assumptions on small break LOCA transient behavior are investigated through numerous calculations using WCOBRA/TRAC-SB. The calculations examine the sensitivity of the results to the break size, location, orientation, and offsite power availability.

Volume 4 presents calculations that are performed to determine the sensitivity of results to the plant core power distribution, the initial and boundary conditions, and code modelling assumptions. These studies, in which parameters are varied one at a time, are performed for Indian Point Unit 2 to quantify the sensitivity of plant behavior to changes in plant initial conditions and accident modelling. An uncertainty methodology consistent with the Application of the Code Scaling, Applicability, and Uncertainty (CSAU) methodology is identified to define the overall plant analysis uncertainty and is applied to determine the 95th percentile PCT for the Indian Point Unit 2 small break LOCA analysis. Volume 4 also demonstrates the compliance of the Westinghouse best estimate large break LOCA methodology with U.S. Nuclear Regulatory Commission (NRC) Regulatory Guide 1.157 and with 10CFR50.46.

TABLE OF CONTENTS

Volume 1	Models and Correlations
Volume 2	Small Break Code Validation
Volume 3	PWR Uncertainties and Sensitivities for Small Break LOCA
Volume 4	Small Break Uncertainty Methodology

<u>Section</u>	<u>Title</u>	<u>Page</u>
ABSTRACT	iii
LIST OF TABLES	xi
LIST OF FIGURES	xv
LIST OF ACRONYMS AND ABBREVIATIONS	xxiii
COMMONLY USED EQUATION NOMENCLATURE	xxvii

29 PWR POWER DISTRIBUTION STUDIES

29-1	Introduction	29-1
29-2	Plant Initial Operating Conditions	29-2
29-2-1	Core Power Parameters	29-3
29-2-1-1	Core Power Distributions	29-3
29-2-1-2	Transient Power Distributions	29-6
29-2-1-3	Power Distribution Uncertainties	29-9
29-2-1-4	Effect of Fuel Burnup on Power Distributions	29-12
29-2-1-5	Power Distribution Modelling Approach	29-12
29-2-2	Application to PWR Small Break LOCA Analysis	29-26
29-3	Power Distribution Sensitivity Cases	29-63
29-3-1	Effects of Power Distribution Changes - Bottom-Skewed Shape ..	29-63
29-3-2	Variation in Top-Skewed Power Distribution	29-64
29-4	Conclusions	29-71
29-5	References	29-71

TABLE OF CONTENTS (Cont'd)

<u>Section</u>	<u>Title</u>	<u>Page</u>
30 PWR SCOPING STUDIES FOR INITIAL AND BOUNDARY CONDITIONS		
30-1	Introduction	30-1
30-2	RCS Fluid Conditions	30-1
30-2-1	Overview of Plant Fluid Conditions	30-2
30-2-2	Fluid Conditions Modelling Approach	30-3
30-2-3	RCS Temperature Scoping Study	30-4
30-2-4	Pressurizer (RCS) Pressure	30-5
30-2-5	Loop Flowrate	30-6
30-2-6	Pressurizer Water Level	30-6
30-3	Effect of Pumped SI Parameters	30-11
30-3-1	Associated Phenomena	30-11
30-3-2	SI Performance Curves for Indian Point Unit 2	30-11
30-3-3	3-Inch Break Results for Pumped SI Temperature Variation	30-12
30-4	Accumulator Water Temperature, Volume, and Pressure Sensitivities	30-18
30-4-1	Associated Phenomena	30-18
30-4-2	Temperature Sensitivity Results	30-19
30-4-3	Water Volume Sensitivity Results	30-19
30-4-4	Pressure Sensitivity Results	30-19
30-4-5	Conclusions Regarding Sensitivities to Accumulator Parameters ..	30-20
30-5	Effect of Steam Generator Secondary Side Relief Valve Setpoints	30-23
30-5-1	Associated Phenomena	30-23
30-5-2	Results	30-24
30-5-3	Conclusions Regarding the Effects of MSSV Setpoint	30-25
30-6	References	30-32
31 PWR SCOPING STUDIES FOR GLOBAL MODEL RANGING		
31-1	Introduction	31-1
31-2	Critical Break Flow	31-5
31-2-1	Results at 1.15 Discharge Coefficient	31-5
31-2-2	Results at 0.7 Discharge Coefficient	31-6

TABLE OF CONTENTS (Cont'd)

<u>Section</u>	<u>Title</u>	<u>Page</u>
31-3	Mixture Level Swell	31-11
31-3-1	Introduction	31-11
31-3-2	3-Inch Break, High Core Interfacial Drag	31-12
31-3-3	3-Inch Break, Low Core Interfacial Drag.....	31-13
31-3-4	Core Interfacial Drag Summary	31-13
31-4	Steam Generator Hydraulics	31-18
31-5	Loop Seal Clearance	31-21
31-6	Horizontal Stratified Flow	31-27
31-6-1	Introduction	31-27
31-6-2	Horizontal Stratified Interfacial Drag.....	31-27
31-6-3	Horizontal Stratified Entrainment	31-28
31-7	Condensation	31-33
31-7-1	Introduction	31-33
31-7-2	Loop Condensation	31-33
31-7-3	Steam Generator Tube Condensation	31-34
31-7-4	Summary and Conclusions	31-34
31-8	Fuel Rod Model	31-39
31-8-1	Small Break Fuel Model Uncertainties	31-39
31-8-2	Fuel Rod Uncertainty	31-40
31-8-3	Heat Transfer Uncertainty	31-41
31-8-4	Summary	31-42
31-9	Summary and Conclusions	31-48
31-10	References	31-50

32 UNCERTAINTY CONSIDERATIONS

32-1	Stored Energy/Fuel Rod	32-1
32-1-1	Initial Reactor State Uncertainties	32-1
32-1-2	Fuel Rod Model Uncertainties	32-3
32-1-2-1	Hot Assembly Power Distribution Variables	32-3
32-1-2-2	Hot Rod Uncertainties	32-8
32-1-2-3	Hot Spot-SB Model Description	32-9

TABLE OF CONTENTS (Cont'd)

<u>Section</u>	<u>Title</u>	<u>Page</u>
	32-1-2-4 Hot Spot Model Application and Assessment	32-29
	32-1-3 Summary	32-32
32-2	Code and Experiment Accuracy	32-71
	32-2-1 Code Uncertainty	32-71
	32-2-1-1 Code Assessment Process	32-71
	32-2-1-2 Code Convergence and Timestep Size Sensitivity	32-72
	32-2-1-3 Contributors to Computer Code Uncertainty	32-76
	32-2-1-4 Data Screening for PCT Comparisons	32-77
	32-2-1-5 Code Uncertainty Calculation	32-80
	32-2-1-6 Variability of the Test Data	32-82
	32-2-1-7 Final Code Uncertainty Elements	32-93
	32-2-2 Conclusions	32-94
32-3	Core Mixture Level Swell	32-110
	32-3-1 Simulation of G-1 Core Uncovery Tests	32-110
	32-3-2 Simulation of ORNL-THTF Tests	32-111
	32-3-3 Uncertainty Distribution for Core Mixture Level Swell	32-112
	32-3-4 Conclusions	32-113
32-4	Critical Flow	32-120
	32-4-1 Data Assessment	32-120
	32-4-2 Effect of Break Type	32-122
	32-4-3 Limits of Applicability	32-123
	32-4-4 Conclusions	32-123
32-5	Uncovered Core Heat Transfer	32-126
	32-5-1 Evaluation of Heat Transfer Tests	32-127
	32-5-2 ORNL Steady-State Core Uncovery Test Data	32-128
	32-5-3 INEL Single Tube Test Evaluation	32-128
	32-5-4 Data for Small Break LOCA Heat Transfer Multipliers	32-130
	32-5-5 Conclusions	32-130
32-6	Scaling Assessment (Step 10)	32-136
	32-6-1 Introduction	32-136
	32-6-2 <u>WCOBRA/TRAC</u> Scaling Trends	32-136
32-7	References	32-141

TABLE OF CONTENTS (Cont'd)

<u>Section</u>	<u>Title</u>	<u>Page</u>
33 ELEMENT III: SENSITIVITY AND UNCERTAINTY ANALYSIS		
33-1	Introduction	33-1
33-2	Statistical Framework	33-1
33-2-1	Overview	33-1
33-2-2	Statistical Methodology: Example 1	33-2
33-2-3	Statistical Methodology: Example 2	33-3
33-2-4	Statistical Methodology: Example 3	33-5
33-2-5	Application of Data-Based Code Uncertainty	33-8
33-3	Uncertainty Methodology	33-22
33-3-1	Introduction	33-22
33-3-2	Methodology Overview and Assumptions	33-22
33-4	Effect of Reactor Input Parameters and State	33-28
33-4-1	Introduction	33-28
33-4-2	Reference Case Conditions	33-29
33-5	Performing PWR Sensitivity Calculations	33-40
33-5-1	Introduction	33-40
33-5-2	Plant Initial Conditions: Global Effects	33-41
33-5-2-1	Initial Fluid Conditions	33-41
33-5-2-2	Initial Core Power Distribution	33-45
33-5-3	Plant Initial Conditions: Local Effects	33-49
33-5-4	Physical Models and Processes: Global Effects	33-49
33-5-5	Physical Models and Processes: Local Effects	33-50
33-6	Combining Biases and Uncertainties	33-54
33-6-1	Review and Verification of Assumptions	33-54
33-6-2	Methodology Procedure	33-61
33-6-2-1	Phase I: Response Surface Data Generation Steps	33-61
33-6-2-2	Phase II: Initial Monte Carlo Steps	33-66
33-6-2-3	Phase III: Verification/Correction Step	33-69
33-6-2-4	Phase IV: Final Monte Carlo Steps	33-70
33-6-3	Methodology Procedure: Other 10CFR50.46 Criteria	33-71
33-6-3-1	Local Oxidation Calculation	33-71

TABLE OF CONTENTS (Cont'd)

<u>Section</u>	<u>Title</u>	<u>Page</u>
33-6-3-2	Core-Wide Oxidation Calculation	33-72
33-7	References	33-84

34 EXAMPLE PWR ANALYSIS

34-1	Introduction	34-1
34-2	Plant-Specific Results - Indian Point Unit 2	34-1
34-2-1	Reference Case Conditions	34-1
34-2-1-1	Plant Physical Description	34-1
34-2-1-2	Plant Initial Operating Conditions	34-2
34-2-1-3	Accident Boundary Conditions	34-5
34-2-2	Plant Operating Range	34-6
34-2-3	Confirmation of Reference Case Limiting Assumptions	34-7
34-2-4	Reference Case Results	34-7
34-2-5	Initial Condition Uncertainty	34-8
34-2-6	Global Model Results	34-8
34-2-7	Local Model (Hot Spot) Results	34-9
34-2-8	Global Model Response Surface Results	34-10
34-2-9	Local Model Effects for Plant Variations	34-10
34-3	Assessment of Total Uncertainty - Indian Point Unit 2	34-25

35 METHODOLOGY SUMMARY AND CONCLUSION

35-1	Introduction	35-1
35-2	Compliance with 10CFR50.46	35-1
35-3	Compliance with Regulatory Guide 1.157	35-2
35-4	Plant and Evaluation Model Changes and Their Impact on Analysis	35-33
35-4-1	Plant Changes	35-33
35-4-2	Evaluation Model Changes	35-35
35-5	References	35-36

LIST OF TABLES

<u>Table</u>	<u>Title</u>	<u>Page</u>
29-2-1	Hot Assembly Rod Power Census Summary	29-27
29-2-2	Peaking Factor Uncertainties	29-28
30-2-1	Typical Westinghouse Plant Operation Parameters	30-7
30-3-1	PCT Summary - SI Temperature Sensitivities	30-14
30-4-1	Sensitivity Studies - Accumulator Gas Pressure	30-21
31-7-1	PCT Sensitivity Due to Condensation	31-35
31-8-1	HOTSPOT Model Variation Ranges/Distribution Type from Large Break LOCA	31-43
31-8-2	HOTSPOT Model Variation Ranges/Distribution Type	31-44
31-8-3	Fuel and Cladding Model Only Uncertainty	31-44
31-8-4	HOTSPOT-SB Results, No HTC Bias, 50-Percent Uncertainty	31-45
32-1-1	Summary of Fuel Rod Uncertainties Considered in HOTSPOT-SB	32-33
32-1-2	Burst Strain Summary	32-34
32-1-3	Packing Fraction From Burst Strain	32-35
32-1-4	Packing Fractions Using Various Measurements	32-35
32-1-5a	Zircaloy Rate Constants (Total Oxygen)	32-36
32-1-5b	Regression Output	32-36
32-1-6	Predictions Using Equation 32-1-30 and Cathcart and Pawel	32-37
32-1-7	NRU MT-3.06 Test Conditions (Just Below Burst Location)	32-38
32-1-8	NRU MT-3.06 Test - No Burst	32-39
32-1-9	NRU MT3.06 Test - Burst	32-40
32-1-10	Summary of Statistical Variables in HOTSPOT	32-41
32-1-11	Fuel Rod Model Uncertainty	32-42
32-2-1	<u>WCOBRA/TRAC Assessment</u>	32-95
32-2-2	Test Simulation Timestep Control Input	32-96
32-2-3	<i>DTMAX</i> Sensitivity Results for G-1 Test 57	32-98
32-2-4	<i>DTMAX</i> Sensitivity Results for ORNL Test 3.09.10-J	32-98
32-2-5	ROSA-IV SB-CL-03 <i>DTMAX</i> Input and Average Timestep	32-99
32-2-6	<i>DTMAX</i> Sensitivity Results for ROSA-IV SB-CL-03	32-99

LIST OF TABLES (Cont'd)

<u>Table</u>	<u>Title</u>	<u>Page</u>
32-2-7	<u>WCOBRA/TRAC-SB Comparisons to Mean of Small Break LOCA Experimental Data</u>	32-100
32-2-8	Core Uncovery Test Data Uncertainty Parameters	32-101
32-2-9	Summary of Data From Repeat Rod Bundle Heating Tests	32-102
32-2-10	<u>WCOBRA/TRAC Noding and Modelling Sensitivity Studies on Experiments</u>	32-104
32-2-11	Data-Based Code Uncertainty	32-105
32-2-12	Final Code Uncertainty Values	32-105
32-3-1	Core Uncovery Test Matrix	32-114
32-3-2	YDRAG Values to Match G-1 Level Swell Data	32-115
32-3-3	ORNL-THTF Test Simulation Matrix	32-116
32-3-4	YDRAG Values to Match ORNL-THTF Data	32-117
32-5-1	HOTSPOT-SB Probability Distribution Function Values Based on 60 ORNL Points and 197 INEL Points	32-131
33-2-1a	Events and Outcomes for Example 1	33-10
33-2-1b	PCT Distribution for Example 1	33-10
33-2-2a	Events and Outcomes for Example 2	33-11
33-2-2b	Hot Spot PCT Distribution for Example 2 (Method 1)	33-12
33-2-2c	Hot Spot PCT Distribution for Example 2 (Method 2)	33-12
33-2-3	PWR Uncertainty Contributors	33-13
33-2-4	Events and Outcomes for Example 3	33-15
33-4-1	Key LOCA Parameters and Reference Case Assumptions	33-35
33-4-2	<u>WCOBRA/TRAC-SB Run Matrix for a Plant-Specific Analysis</u>	33-38
33-5-1	Peaking Factor Uncertainties Considered for Hot Rod in Best Estimate Methodology	33-51
33-5-2	Core Interfacial Drag/Break Flow Run Matrix	33-52
33-6-1	Typical Superposition Test Calculations, Indian Point Unit 2	33-76
33-6-2	Sample Output from HOTSPOT-SB	33-76
33-6-3	Rod Power Distribution	33-77

LIST OF TABLES (Cont'd)

<u>Table</u>	<u>Title</u>	<u>Page</u>
33-6-4	Local Oxidation Fraction for Rods Operating at Lower Power, Large Break LOCA	33-77
33-6-5	Rod Average Oxidation Fraction for Rods Operating at Lower Power (Large Break LOCA)	33-78
34-2-1	Reference Values and Plant Operating Range - Indian Point Unit 2	34-11
34-2-2	Reference Case, Nominal, and Range Values for Plant Initial Operating Conditions	34-14
34-2-3	Reference Case Confirmatory Studies	34-15
34-2-4	Initial Condition Sensitivity Data for Indian Point Unit 2	34-16
34-2-5	Initial Condition Bias and Uncertainty Indian Point Unit 2	34-17
34-2-6	Typical HOTSPOT-SB Output for Core Boiloff Uncovery PCT	34-18
34-2-7	Hot Spot Lookup Table	34-19
34-3-1	Effect of Uncertainties on Indian Point Unit 2 PCT	34-27
34-3-2	Monte Carlo Results for Indian Point Unit 2 PCT	34-27

LIST OF FIGURES

<u>Figure</u>	<u>Title</u>	<u>Page</u>
29-2-1	(a) Typical Assembly Power Map (b) Assembly Power Distribution, BOL	29-29
29-2-2	(a) Typical Assembly Power Map (b) Assembly Power Distribution, EOL	29-30
29-2-3	Typical Hot Assembly Fuel Rod Power Distribution	29-31
29-2-4	Hot Assembly Rod Power Census for Typical Westinghouse Fuel Designs	29-32
29-2-5	Relative Axial Power Distribution at BOL and EOL During Full Power Steady-State Conditions	29-33
29-2-6	Typical Transient Axial Power Distributions	29-34
29-2-7	Envelope of Peak Linear Heat Rates as Function of Core Height for Typical Westinghouse Core Design	29-35
29-2-8	Typical Steady-State Peaking Factors Versus Peaking Factor Design Limit ...	29-36
29-2-9	Effect of Load Follow Maneuver Period on Decay Heat Equilibrium Fraction for Various Times After Trip	29-37
29-2-10	Typical Measurement of Enthalpy Rise Hot Channel Factor $F_{\Delta H}$	29-38
29-2-11	Typical Measurement of Total Peaking Factor F_Q	29-39
29-2-12	Effect of Burnup on (a) Baseload Peak Linear Heat Rate, (b) Fuel Average Temperature, and (c) Decay Heat Equilibrium Fraction	29-40
29-2-13	[Range]a,c in Low F_Q 29-41
29-2-14	[Range]a,c in High F_Q 29-42
29-2-15	[] ^{a,c}	29-43
29-2-16	[] ^{a,c}	29-44
29-2-17	[] ^{a,c}	29-45
29-2-18	Power Shape 1	29-46
29-2-19	Power Shape 2	29-47
29-2-20	Power Shape 3	29-48
29-2-21	Power Shape 4	29-49

LIST OF FIGURES (Cont'd)

<u>Figure</u>	<u>Title</u>	<u>Page</u>
29-2-22	Power Shape 5	29-50
29-2-23	Power Shape 6	29-51
29-2-24	Power Shape 7	29-52
29-2-25	Power Shape 8	29-53
29-2-26	Power Shape 9	29-54
29-2-27	Power Shape 10	29-55
29-2-28	Power Shape 11	29-56
29-2-29	Power Shape 12	29-57
29-2-30	Power Shape 13	29-58
29-2-31	Power Shape 14	29-59
29-2-32	Power Shape 15	29-60
29-2-33	<u>WCOBRA/TRAC Axial Power Distribution for Rods 1 to 5,</u> Reference Case	29-61
29-2-34	Relationship of Core Design Peaking Factors to LOCA Peaking Factors	29-62
29-3-1	Bottom-Skewed Power Shape	29-66
29-3-2	Core Collapsed Liquid Level, Bottom-Skewed Shape	29-67
29-3-3	PCT for the Bottom-Skewed Shape	29-67
29-3-4	Hot Assembly Collapsed Liquid Level, Reference Case and Power Shape 4 ...	29-68
29-3-5	PCTs for Reference Case and Power Shape 4	29-68
29-3-6	Loop Seal Steam Flowrate for Power Shape 4 Compared to Reference Case ...	29-69
29-3-7	Reactor Vessel Mass Comparison Between Power Shape 4 and Reference Case	29-69
29-3-8	Power Shape 4 Total Loop Seal Mass Compared to Reference Case	29-70
29-3-9	Integrated Break Flow for Power Shape 4 Compared to Reference Case	29-70
30-2-1	Core Collapsed Liquid Level, 3-Inch Cold Leg Break at Reduced T_{avg}	30-8
30-2-2	PCT, 3-Inch Cold Leg Break at Reduced T_{avg}	30-8
30-2-3	Pressurizer Pressure (psia), 3-Inch Cold Leg Break at Reduced T_{avg} Compared to Reference Case	30-9
30-2-4	Break Flowrate (lbm/s), 3-Inch Cold Leg Break at Reduced T_{avg} Compared to Reference Case	30-9

LIST OF FIGURES (Cont'd)

<u>Figure</u>	<u>Title</u>	<u>Page</u>
30-2-5	Void Fraction at the Break, 3-Inch Cold Leg Break at Reduced T_{avg} Compared to Reference Case	30-10
30-3-1	SI Performance Curves for Indian Point Unit 2	30-15
30-3-2	PCTs - 3-Inch Break SI Temperature Sensitivities	30-16
30-3-3	Core Collapsed Liquid Levels - 3-Inch Break SI Temperature Sensitivities ..	30-16
30-3-4	RCS Pressure Transient Details - 3-Inch Break SI Temperature Sensitivities ..	30-17
30-4-1	3-Inch Break Accumulator Gas Pressure Sensitivity Pressure Transients (psia) .	30-22
30-4-2	3-Inch Break Accumulator Pressure Sensitivity PCT Transients	30-22
30-5-1	3-Inch Break MSSV Setpoint Sensitivity Break Flowrates	30-26
30-5-2a	3-Inch Break MSSV Setpoint Sensitivity, Loop 21 Steam Generator Uphill Tube Collapsed Liquid Levels	30-27
30-5-2b	3-Inch Break MSSV Setpoint Sensitivity, Loop 22 Steam Generator Uphill Tube Collapsed Liquid Levels	30-27
30-5-2c	3-Inch Break MSSV Setpoint Sensitivity, Loop 23 Steam Generator Uphill Tube Collapsed Liquid Levels	30-28
30-5-2d	3-Inch Break MSSV Setpoint Sensitivity, Loop 24 Steam Generator Uphill Tube Collapsed Liquid Levels	30-28
30-5-3	3-Inch Break MSSV Setpoint Sensitivity Pump Suction Vapor Flow for the Cleared Loop Seal	30-29
30-5-4	3-Inch Break MSSV Setpoint Sensitivity for Primary System Pressure	30-29
30-5-5	3-Inch Break MSSV Setpoint Sensitivity for Total SI Rate	30-30
30-5-6	3-Inch Break MSSV Setpoint Sensitivity for Reactor Vessel Mass	30-30
30-5-7	3-Inch Break MSSV Setpoint Sensitivity for Core Collapsed Liquid Levels ..	30-31
30-5-8	3-Inch Break MSSV Setpoint Sensitivity PCT Comparison	30-31
31-2-1	Pressurizer Pressure (psia) Comparison Between Reference Case and CD (Two-Phase) = 1.15 Case	31-7
31-2-2	Break Flowrate (lbm/s) Comparison Between Reference Case and CD (Two-Phase) = 1.15 Case	31-7
31-2-3	Integrated Break Flow (lbm) Comparison Between Reference Case and CD (Two-Phase) = 1.15 Case	31-8

LIST OF FIGURES (Cont'd)

<u>Figure</u>	<u>Title</u>	<u>Page</u>
31-2-4	SI (lbm/s) Comparison Between Reference Case and <i>CD</i> (Two-Phase) = 1.15 Case	31-8
31-2-5	Pressurizer Pressure (psia) Comparison Between Reference Case and <i>CD</i> (Two-Phase) = 0.7 Case	31-9
31-2-6	Break Flowrate (lbm/s) Comparison Between Reference Case and <i>CD</i> (Two-Phase) = 0.7 Case	31-9
31-2-7	Integrated Break Flow (lbm) Comparison Between Reference Case and <i>CD</i> (Two-Phase) = 0.7 Case	31-10
31-2-8	SI (lbm/s) Comparison Between Reference Case and <i>CD</i> (Two-Phase) = 0.7 Case	31-10
31-3-1	Comparison of Core Collapsed Liquid Level: High Interfacial Drag Case and Reference 3-Inch Break	31-15
31-3-2	Comparison of PCTs: High Interfacial Drag Case and Reference 3-Inch Break	31-15
31-3-3	Comparison of Upper Plenum Collapsed Liquid Level: Low Interfacial Drag Case and Reference 3-Inch Break	31-16
31-3-4	Comparison of Core Collapsed Liquid Level: Low Interfacial Drag Case and Reference 3-Inch Break	31-16
31-3-5	Comparison of PCTs: Low Interfacial Drag Case and Reference 3-Inch Break .	31-17
31-4-1	Core Pressure Comparison: 3-Inch Break With Increased Steam Generator Condensation and Reference Case	31-19
31-4-2	Comparison of Upper Plenum Collapsed Liquid Levels: 3-Inch Break With Increased Steam Generator Condensation and Reference Case	31-20
31-4-3	Loop Seal Clearance: 3-Inch Break With Increased Steam Generator Condensation	31-20
31-5-1	Comparison of PCTs: Low Loop Seal Drag Case and Reference 3-Inch Break	31-23
31-5-2	Comparison of Core Collapsed Liquid Levels: Low Loop Seal Drag Case and Reference 3-Inch Break	31-23
31-5-3	Comparison of Loop Seal Vapor Flowrates: Low Loop Seal Drag Case and Reference 3-Inch Break	31-24

LIST OF FIGURES (Cont'd)

<u>Figure</u>	<u>Title</u>	<u>Page</u>
31-5-4	Comparison of Reactor Vessel Mass (lbm): Low Loop Seal Drag Case and Reference 3-Inch Break	31-24
31-5-5	Comparison of PCTs: High Loop Seal Drag Case and Reference 3-Inch Break	31-25
31-5-6	Comparison of Core Collapsed Liquid Levels: High Loop Seal Drag Case and Reference 3-Inch Break	31-25
31-5-7	Loop Seal Vapor Flowrates: High Loop Seal Drag Case	31-26
31-5-8	Comparison of Reactor Vessel Mass (lbm): High Loop Seal Drag Case and Reference 3-Inch Break	31-26
31-6-1	<u>WCOBRA/TRAC Prediction of Flooding and CCFL in Horizontal Stratified Flows</u>	31-30
31-6-2	Comparison of PCTs: Low Horizontal Stratified Drag Case and Reference 3-Inch Break	31-30
31-6-3	Comparison of Reactor Vessel Mass Inventories (lbm): Low Horizontal Stratified Drag Case and Reference 3-Inch Break	31-31
31-6-4	Comparison of Core Collapsed Liquid Level: Low Entrainment Case and Reference 3-Inch Break	31-31
31-6-5	Comparison of PCTs: Low Entrainment Case and Reference 3-Inch Break ...	31-32
31-6-6	Loop Seal Clearance in the 3-Inch Break High Entrainment Case: Steam Flowrates	31-32
31-7-1	RCS Pressure Comparison: Reference Case and Intact Loop Condensation Case	31-36
31-7-2	Break Mass Flowrate (lbm/s) Comparison: Reference Case and Increased Intact Loop Condensation Case	31-36
31-7-3	Integrated Break Flow (lbm) Comparison: Reference Case and Increased Intact Loop Condensation Case	31-37
31-7-4	Break Void Fraction Comparison: Reference Case and Increased Intact Loop Condensation Case	31-37
31-7-5	Core Collapsed Liquid Level Comparison: Reference Case and Increased Intact Loop Condensation Case	31-38
31-7-6	PCT Comparison: Reference Case and Increased Intact Loop Condensation Case	31-38

LIST OF FIGURES (Cont'd)

Figure	Title	Page
31-8-1	PCT and Elevation for HOTSPOT Fuel Rod Model Uncertainty Evaluation	31-46
31-8-2	Linear Heat Generation at the 10.5-Foot Elevation for 3-Inch Break	31-47
31-8-3	HTCVs at the PCT Elevation for 3-Inch Break	31-47
32-1-1	Effect of Load Follow on F_Q	32-45
32-1-2	F_Q Histogram [] ^{a,c}	32-46
32-1-3	[Presented in Section 29	32-47
32-1-4	[Presented in Section 29	32-48
32-1-5	Hot Assembly Rod and Hot Rod Power and Uncertainty Relationships	32-49
32-1-6	<u>WCOBRA/TRAC-SB</u> Fuel Model at Burst	32-50
32-1-7	HOTSPOT-SB Fuel Relocation Model Compared with Preburst Condition	32-50
32-1-8a	Thermal Conductivity of UO ₂	32-51
32-1-8b	Specific Heat of UO ₂	32-51
32-1-9	Thermal Conductivity of UO ₂	32-52
32-1-10	Comparison Between Hot Spot and PAD Fuel Temperatures	32-53
32-1-11	Thermal Conductivity of [] ^{a,c}	32-54
32-1-12	ZIRLO™ Burst Temperature Data and Correlation	32-55
32-1-13	Zircaloy Burst Data at Several Heating Rates	32-56
32-1-14	ZIRLO™ Burst Strain Data at Several Heating Rates	32-57
32-1-15	Zircaloy Burst Strain Data for Burst Temperatures Less Than 1600°F	32-58
32-1-16	Zircaloy Burst Strain Data for Burst Temperatures Between 1600°F and 1800°F	32-59
32-1-17	Zircaloy Burst Strain Data for Burst Temperatures Greater Than 1800°F	32-60
32-1-18	ZIRLO™ Burst Strain Data for Burst Temperatures Less Than 1500°F	32-61
32-1-19	ZIRLO™ Burst Strain Data for Burst Temperatures Between 1500°F and 1700°F	32-62
32-1-20	ZIRLO™ Burst Strain Data for Burst Temperatures Greater Than 1700°F	32-63

LIST OF FIGURES (Cont'd)

<u>Figure</u>	<u>Title</u>	<u>Page</u>
32-1-21	[Bound Lines	32-64
32-1-22	Volumetric Increase in Fuel for Corresponding Cladding Volume Increase Derived from PBF Tests (Broughton, 1981)	32-65
32-1-23a	PBF Packing Fraction Data Versus Burst Strain	32-66
32-1-23b	Distribution of Packing Fraction Data	32-66
32-1-24	Prediction of $\sigma^2/2$ for Zircaloy as Function of T ; Upper Line 95-Percent Limit	32-67
32-1-25	Zircaloy Cladding Oxidation Uncertainty for Mean and Point Estimate	32-68
32-1-26	First Five NRU MT-3 Test Hot Spot Simulations	32-69
32-1-27	Predicted Average Burst Strain Distribution for NRU MT-3 Test	32-70
32-1-28	Measured Burst Strain Distribution for NRU MT-3 Test (Mohr et al., 1983) ...	32-70
32-2-1	ORNL Rod Bundle Cross Section [.....] ^{a,c}	32-106
32-2-2	NRU Rod Bundle and <u>WCOPRA/TRAC</u> Channels	32-107
32-2-3	ROSA-IV Facility <u>WCOPRA/TRAC-SB</u> Model	32-108
32-2-4	Illustration of Code Bias Determination (Draper, 1966)	32-109
32-3-1	Small Break LOCA Core Interfacial Drag Multiplier Distribution From ORNL and G-1 Data	32-118
32-3-2	Best Estimate Small Break LOCA Core Interfacial Drag Combined Distribution Based on ORNL and G-1 Data	32-119
32-4-1	<u>WCOPRA/TRAC-SB</u> Critical Flow Predictions Versus Test Data	32-124
32-4-2	Probability Density Function for Two-Phase Discharge Coefficient Multiplier	32-125
32-5-1	PCT Transient	32-132
32-5-2	Comparison of Predicted and Measured HTCs for Combined ORNL and INEL Data Using <u>WCOPRA/TRAC-SB</u> Model	32-133
32-5-3	Steam Re for 3-Inch Break at PCT Elevation	32-133
32-5-4	Small Break LOCA HTC Multiplier Distribution: Distribution from ORNL and INEL Data	32-134
32-5-5	Best Estimate Small Break LOCA HTC Multiplier: Cumulative Distribution Based on ORNL/INEL Points	32-135
32-6-1	Scaling Trends for <u>WCOPRA/TRAC-SB</u> PCT Prediction	32-140

LIST OF FIGURES (Cont'd)

<u>Figure</u>	<u>Title</u>	<u>Page</u>
33-2-1	Input Probability Distribution for Example 1	33-16
33-2-2	Output Probability Distributions for Example 1	33-17
33-2-3	Conditional Probability Distributions of RX for Example 2	33-18
33-2-4	Output Probability Distributions for Example 2	33-19
33-2-5	Relationship of Local Hot Spot Distribution to Nominal Hot Rod Reduction	33-20
33-2-6	Information Transfer from Global Model (<u>WCOBRA/TRAC-SB</u>) to LOCA Model (HOTSPOT-SB)	33-21
33-3-1	Derivation of Initial Condition Uncertainty Distribution	33-26
33-3-2	Superposition of Global Plant Variables	33-27
33-5-1	Range of Power Shape Parameters	33-53
33-6-1	Superposition Prediction Compared to Calculated Results	33-79
33-6-2	Final Superposition Result after Correction	33-80
33-6-3	Flowchart of Uncertainty Determination Procedure	33-81
33-6-4	Comparison of Rod Power Census Envelope to Typical Core Design Data	33-82
33-6-5	Local Average Oxidation Fraction for Lower Power Rods	33-83
34-2-1	Nominal Hot Rod PCT	34-20
34-2-2	Nominal Hot Rod PCT Elevation	34-20
34-2-3	Core Pressure, 3-Inch Break Reference Case	34-21
34-2-4	Core Collapsed Liquid Level, 3-Inch Break Reference Case	34-21
34-2-5	Downcomer Collapsed Liquid Level, 3-Inch Break Reference Case	34-22
34-2-6	PCT Effect of Varying CYDG with $CD = 1.15$ ($CYDG = 1.0$)	34-22
34-2-7	PCT Effect of Varying CYDG with $CD = 1.15$ ($CYDG = 0.4$)	34-23
34-2-8	PCT Effect of Varying CYDG with $CD = 0.7$ ($CYDG = 1.0$)	34-23
34-2-9	PCT Effect of Varying CYDG with $CD = 0.7$ ($CYDG = 0.4$)	34-24

LIST OF ACRONYMS AND ABBREVIATIONS

A. O.	Axial Offset
ACRS	Advisory Committee on Reactor Safeguards
AFLUX	Core Average Heat Flux
ANS	American Nuclear Society
ANSI	American National Standards Institute
BE-SBLOCA	Best Estimate Small Break LOCA
BLD	Blowdown
BO	Boil-off
BOL	Beginning of Life
CAOC	Constant Axial Offset Control
CCFL	Counter-current Flow Limitation
CD	Discharge Coefficient for Two-phase Break Flow
CE	Combustion Engineering
CHF	Critical Heat Flux
COLR	Core Operating Limits Report
COSI	Condensation On Safety Injection
CP	Conditional Probability
CQD	Code Qualification Document
CSAU	Code Scaling Applicability and Uncertainty
DFFB	Dispersed Flow Film Boiling
DNB	Departure from Nucleate Boiling
ECCS	Emergency Core Cooling System
EOP	Emergency Operating Procedure
FAC	Final Acceptance Criteria
FEM	Entrained Droplet Flowrate
FLM	Continuous Liquid Flowrate
GEDM	Generalized Energy Deposition Model
H	High (Importance Level in Los Alamos PIRT Ranking Scheme)
HAFLUX	Hot Assembly Average Power
HAPHR	Hot Assembly Peak Heat Rate
HHSI	High Head Safety Injection
HRFLUX	Hot Rod Average Power
HTC	Heat Transfer Coefficient
IADF	Inverted Annular Dispersed Flow

LIST OF ACRONYMS AND ABBREVIATIONS (Cont'd)

IAFB	Inverted Annular Film Boiling
INEL	Idaho National Engineering Laboratory
IP2	Indian Point Unit 2
JAERI	Japan Atomic Energy Research Institute
L	Low (Importance Level in Los Alamos PIRT ranking scheme)
LOCA	Loss of Coolant Accident
LOCE	Loss of Coolant Experiment
LOFT	Loss of Fluid Test
LOOP	Loss of Offsite Power
LSC	Loop Seal Clearance
LSTF	Large Scale Test Facility
M	Medium (Importance Level in Los Alamos PIRT ranking scheme)
MSSV	Main Steam Safety Valve
MSIV	Main Steam Isolation Valve
MTC	Moderator Temperature Coefficient
N/A	Not Applicable
NC	Natural Circulation
NPP	Nuclear Power Plant
NRC	Nuclear Regulatory Commission
NRU	National Research Universal
NSSS	Nuclear Steam Supply System
NUCL	Saturated Nucleate Boiling
OPA	Offsite Power Available
ORNL	Oak Ridge National Laboratory
PCT	Peak Cladding Temperature
PIRT	Phenomena Identification and Ranking Table
PLHGR	Peak Linear Heat Generation Rate
PLHR	Peak Linear Heat Rate
PLOW	Low Power Region Relative Power
PORV	Pressure-operated Relief Valve
PWR	Pressurized Water Reactor
RABL	Reflood Assist Bypass System
RAI	Request for Additional Information
RAOC	Relaxed Axial Offset Control

LIST OF ACRONYMS AND ABBREVIATIONS (Cont'd)

RCP	Reactor Coolant Pump
RCS	Reactor Coolant System
REC	Core Recovery
RHR	Residual Heat Removal
ROSA	Rig-of-Safety Assessment
RSIC	Radiation Shielding Information Center
RWST	Refueling Water Storage Tank
SBLOCA	Small Break Loss of Coolant Accident
SCNB	Subcooled Nucleate Boiling
SG	Steam Generator
SGTP	Steam Generator Tube Plugging
SI	Safety Injection
SIS	Safety Injection Systems
SPL	Single-phase Liquid Convection
SPV	Single-phase Vapor Convection
SPV	Single-Phase Vapor
THTF	Thermal Hydraulic Test Facility
TPFL	Two-Phase Flow Loop
TRAN	Transition Boiling
TS	Technical Specifications
TSI	Safety Injection Water Temperature
UHI	Upper Head Injection
UPTF	Upper Plenum Test Facility

COMMONLY USED EQUATION NOMENCLATURE

a	sonic velocity	h	heat transfer coefficient
a_r	grid blockage ratio	h	normalized pump head (Ch. 9)
a_v	vapor absorption coefficient	h_i	interfacial heat transfer coefficient
a_l	liquid absorption coefficient	H	enthalpy
A	area	H_{fg}	enthalpy of vaporization
A_x	axial flow area	H_m	Meyer hardness
A_z	lateral flow area	I	grid rewet index (Ch. 5,6)
A_w	wall heat transfer area	I	pump moment of inertia (Ch. 9)
A_I	intercell friction area	k	thermal conductivity
A_i	interfacial area	K	loss coefficient (Ch. 2,4)
B	mass transfer number	K	conductance (Ch. 7)
C_o	slip distribution parameter	K_{ix}	vertical interfacial drag coefficient
C_D	drag coefficient	K_{iz}	transverse interfacial drag coefficient
C_p	specific heat at constant pressure	K_{wx}	vertical wall drag coefficient
C_v	specific heat at constant volume	K_{wz}	transverse wall drag coefficient
D	diameter	K_x	axial flow form loss coefficient
D_h	hydraulic diameter	K_z	transverse flow form loss coefficient
\underline{D}	deformation tensor	L	length
e	specific energy	L_g	gap width
f_w	wall friction factor	L_g^o	orthogonal gap width
f_i	interfacial friction factor	L_b	mean beam length
f	theoretical density fraction (Ch. 7)	ℓ_m	momentum mixing length
F	ramping function	ℓ_H	energy mixing length
\underline{F}	turbulence anisotropy tensor	\dot{m}	mass flowrate
F	gray body factor (Ch. 6)	M	momentum (Ch. 2)
F_{CHEN}	Chen convective boiling multiplier	M	molecular weight (Ch. 7)
\mathcal{F}	force	n	pump head multiplier (Ch. 9)
g	gravitational acceleration	N	mole fraction
g_c	gravitational conversion constant	N	number density
\underline{g}	gravitational acceleration vector	N_μ	pump torque multiplier (Ch. 9)
G	mass flux	P	viscosity number
G_x	axial mass flux	P	pressure
G_z	transverse mass flux		

COMMONLY USED EQUATION NOMENCLATURE (Cont'd)

P_w	wetted perimeter	V	volume
Pr	Prandtl number	V_c	mesh cell volume
P_{rod}	fuel rod pitch	w	transverse velocity component, Cartesian coordinates
q_{we}	wall-liquid heat transfer rate	W	transverse velocity, subchannel coordinates
q_{vv}	wall-vapor heat transfer rate	W^o	orthogonal transverse velocity, subchannel coordinates
q_{il}	interface-liquid heat transfer rate	We	Weber number
q_{iv}	interface-vapor heat transfer rate	x	quality
Q_{we}	wall-liquid heat transfer	x	vertical direction, Cartesian coordinates (Ch. 2)
Q_{vv}	wall-vapor heat transfer	X	vertical direction, subchannel coordinates
r	bubble/drop radius	X	axial direction, 1D components
r	radial coordinate	y	transverse direction, Cartesian coordinates
R	internode resistance (Ch. 7)	z	transverse direction, Cartesian coordinates
R	radiation resistance (Ch. 6)	Z	transverse direction, subchannel coordinates
R	gas constant (Ch. 10)		
R_o	orifice hole radius		
Re	Reynolds number		
s	specific entropy		
S	net rate of entrainment		
S_{CHEN}	Chen building suppression factor		
S_E	rate of entrainment		
S_{DE}	rate of de-entrainment		
St	Stanton number		
t	time		
T	temperature		
T	pump torque (Ch. 9)	α	void fraction
\underline{T}	stress tensor	α_N	normalized pump speed
$\underline{\underline{T}}$	Reynold stress tensor	β	volumetric coefficient of expansion
u	vertical velocity component, Cartesion coordinates	Γ	net rate of mass transfer
U	vertical velocity component, subchannel coordinates	δ	film thickness
v	transverse velocity component, Cartesian coordinates	δ_{ij}	Kronecker delta
		ϵ	thermal emissivity
		ϵ	strain

Greek

α	void fraction
α_N	normalized pump speed
β	volumetric coefficient of expansion
Γ	net rate of mass transfer
δ	film thickness
δ_{ij}	Kronecker delta
ϵ	thermal emissivity
ϵ	strain

COMMONLY USED EQUATION NOMENCLATURE (Cont'd)

η	fraction of vapor generation coming from entrained liquid	<i>crit</i>	critical
η_{NR}	de-entrainment efficiency	<i>cwv</i>	convection wall-vapor
κ	thermal diffusivity	<i>CHEN</i>	Chen correlation
λ	characteristic wave length	<i>CHF</i>	critical heat flux
μ	viscosity	<i>churn</i>	churn flow regime
μ^T	turbulent viscosity	<i>CT</i>	churn-turbulent flow regime
ρ	density	<i>d</i>	drop
Σ	absorption cross section	<i>dcht</i>	direct contact heat transfer
σ	surface tension	<i>DD</i>	dispersed droplet flow regime
σ	stress (Ch. 2, 7)	<i>DE</i>	de-entrainment
$\underline{\sigma}$	fluid-fluid stress tensor	<i>dffb</i>	dispersed flow film boiling
σ_{SB}	Stephan-Boltzmann constant	<i>DFFB</i>	dispersed flow film boiling
τ	shear stress	<i>e</i>	trained field
$\underline{\tau}$	viscous drag force	<i>E</i>	entrainment
τ_i	interfacial drag force	<i>f</i>	saturated liquid
v	specific volume	<i>fb</i>	film boiling
v	normalized pump volumetric flow	<i>fr</i>	flow regime
χ	Martinelli-Nelson factor	<i>fric</i>	friction loss
Ψ_a	absorption efficiency	<i>form</i>	form loss
Ω	source term	<i>FC</i>	forced convection
ω	specific speed	<i>FD</i>	film/drop flow regime

Subscripts

<i>am</i>	annular-mist flow regime	<i>Henry</i>	Henry correlation
<i>ACC</i>	accumulator	<i>i</i>	interfacial
<i>b</i>	bubble	<i>IVA</i>	inverted annular flow regime
<i>br</i>	bubble rise	<i>IVS</i>	inverted liquid slug flow regime
<i>bubbly</i>	bubbly flow regime	<i>k</i>	phase k
<i>Brom</i>	Bromley correlation	<i>l</i>	liquid field
		<i>liq</i>	liquid

COMMONLY USED EQUATION NOMENCLATURE (Cont'd)

<i>LB</i>	large bubble	<i>TQ</i>	top quench
<i>m</i>	mixture	<i>UO₂</i>	uranium dioxide
<i>MIN</i>	minimum film boiling point	<i>v</i>	vapor field
<i>nc</i>	natural convection	<i>vap</i>	vapor
<i>lnc</i>	laminar natural convection	<i>ve</i>	between vapor and entrained fields
<i>lfc</i>	laminar forced convection	<i>vl</i>	between vapor and liquid fields
<i>N</i>	normalized	<i>w</i>	wall
<i>NB</i>	nucleate boiling	<i>wb</i>	wall to fluid as latent heat
<i>o</i>	orifice	<i>wl</i>	wall to liquid
<i>p</i>	pipe	<i>wv</i>	wall to vapor
<i>QF</i>	quench front	<i>x</i>	vertical direction, Cartesian coordinates
<i>r</i>	relative	<i>X</i>	vertical direction, subchannel coordinates
<i>r</i>	radial (Ch. 7)	<i>X</i>	axial direction, 1D components
<i>rwe</i>	radiation wall-entrained field	<i>y</i>	transverse direction, Cartesian coordinates
<i>rwg</i>	radiation wall to grid	<i>z</i>	transverse direction, Cartesian coordinates
<i>rw_l</i>	radiation wall-liquid field	<i>Z</i>	transverse direction, subchannel coordinates
<i>rw_v</i>	radiation wall-vapor field	<i>Zr</i>	Zirconium
<i>s</i>	drop formation	<i>2φ</i>	two-phase
<i>sat</i>	saturation	<i>Γ</i>	phase change
<i>slug</i>	slug flow regime	<u>Superscripts</u>	
<i>s</i>	slug	<i>i</i>	interfacial surface average
<i>SB</i>	small bubble flow regime	<i>n</i>	old time value
<i>SCL</i>	subcooled liquid	<i>ñ</i>	donor cell old time value
<i>SCNB</i>	subcooled nucleate boiling	<i>T</i>	turbulent
<i>SCV</i>	subcooled vapor	<i>t</i>	transpose
<i>SNL</i>	superheated liquid	<i>"</i>	per unit area
<i>SLV</i>	superheated vapor	<i>""</i>	per unit volume
<i>SLB</i>	small to large bubble flow regime		
<i>SPL</i>	single-phase liquid		
<i>SPV</i>	single-phase vapor		
<i>sup</i>	suppression		
<i>TB</i>	transition boiling		
<i>TD</i>	top deluge flow regime		
<i>tnc</i>	turbulent natural convection		

SECTION 29

PWR POWER DISTRIBUTION STUDIES

29-1 Introduction

The core power distribution at the time of a small break LOCA affects PCT predictions. Uncertainties in core-wide power-related parameters can vary during the operation of the core. The power distribution is separated into radial and axial distributions. The radial component is sensitive to the fuel and absorber loading pattern, and presence of control rods. Radial distributions change slowly with time and fuel depletion, and are relatively insensitive to power level, xenon concentration/ distribution, axial burnup distribution, and axial fuel design features. Axial power distributions are relatively insensitive to the loading pattern, but are quite sensitive to axial burnup distributions, control bank position, xenon concentration/distribution, coolant density distribution, and reactor power.

The radial power distribution is primarily a result of core design; only minor changes, such as rod movements within the insertion limits, occur from conditions under operational control. The axial power distribution changes significantly as a function of operational conditions. The power distribution uncertainty (ΔPCT_{PD}) considers the parameters, [

]^{a,c}

29-2 Plant Initial Operating Conditions

Reactor operating conditions and their variations are described by two groups of parameters:

- **Core Power Parameters**

These parameters, listed as follows, define the core power distribution and fuel stored energy at the time of the LOCA.

- a) Core average linear heat rate
- b) Peak linear heat rate
- c) Hot rod average power
- d) Hot assembly average power
- e) Hot assembly peak heat rate
- f) Axial power distribution
- g) Low power region relative power
- h) Hot assembly burnup
- i) Reactor operating power history
- j) Moderator temperature coefficient (MTC)
- k) Hot full power (HFP) boron concentration

- **Plant Fluid Conditions**

These parameters, listed as follows, describe the reactor primary fluid thermodynamic state at the time of the LOCA.

- a) Core average fluid temperature
- b) Pressurizer pressure
- c) Loop flowrate
- d) Upper head fluid temperature
- e) Pressurizer level
- f) Accumulator water temperature
- g) Accumulator pressure
- h) Accumulator water volume
- i) Accumulator line resistance

The basis for the choice of the core power parameters is discussed in the following sections. Plant fluid conditions are discussed in Section 30.

29-2-1 Core Power Parameters

A summary of the core modeling described in Section 26, Volume 3, is given below. There are four core channels and five fuel rods in the PWR model, where the fuel rods are defined as the following:

Rod 1: The rod in the core with the highest linear heat rate, assumed to also have the highest average power and to reside in the assembly with the highest average power

Rod 2: An average rod in the highest power assembly

Rod 3: An average rod in the assemblies residing under support columns

Rod 4: An average rod in the assemblies residing under guide tubes

Rod 5: An average rod in the assemblies residing on the periphery of the core

There are three distinct regions (the hot assembly, the two average channels, and the low power channel) that serve to resolve the radial power distribution in the core in WCobra/TRAC-SB. Each fuel rod group has parameters describing the peak linear heat rate, the average linear heat rate, and the axial distribution of power. [

]^{a,c} The axial and radial core power distribution is of basic importance to the PCT uncertainty, as well as the absolute value of the PCT.

The parameters that affect this distribution, and their variations, are described in the following section.

29-2-1-1 Core Power Distributions

The nuclear design of the reactor core meets constraints on the local power distribution in the fuel to prevent powers that could result in excessive cladding stress or strain, centerline fuel

melting, departure from nucleate boiling (DNB), or PCT in excess of 2200°F during a postulated LOCA.

Power distributions are typically characterized in terms of hot channel factors. These factors relate peak pellet power and hot rod power to core average quantities. These factors and other terms used are defined below:

- Core average heat flux (*AFLUX*) is the average thermal power produced per unit length of active fuel (kW/ft).
- Peak linear heat rate (*PLHR*) is the maximum linear heat rate produced in the reactor (kW/ft).
- Hot assembly peak heat rate (*HAPHR*) is the peak linear heat rate of an average rod in the hot assembly (kW/ft).
- Hot assembly average power (*HAFLUX*) is the average power per unit length in the hot assembly (kW/ft).
- Hot rod average power (*HRFLUX*) is the average power per unit length in the hot rod (kW/ft).
- Total peaking factor (F_Q) is the ratio of the peak linear heat rate to the core average linear heat rate (*PLHR/AFLUX*).
- Enthalpy rise peaking factor ($F_{\Delta H}$) is the ratio of hot rod average power to core average linear heat rate (*HRFLUX/AFLUX*).

PWR power distributions are often separated into their respective radial and axial components. The radial component is sensitive to the fuel and absorber loading pattern and the presence of control rods. Radial distributions change slowly with time and fuel depletion and are relatively insensitive to power level, xenon concentration/distribution, axial burnup distribution, and axial fuel design feature. By contrast, PWR axial distributions are relatively insensitive to the loading pattern, but are quite sensitive to axial burnup distributions (and hence core burnup), control bank position, xenon concentration/distribution, coolant density distribution, and reactor power.

The existence of this radial/axial power distribution separability is frequently used by the nuclear designer. PWR radial power distributions are slowly varying in time, provided that the presence of control rods are accounted for accurately. Axial power distributions are more dependent upon the plant operating parameters, such as current power level, recent changes in power level/distribution, and control bank position. These characteristics allow the analysis of transient three-dimensional (3-D) power distributions to be performed by superposition of transient axial power distributions on steady-state, appropriately rodded, radial power distributions rather than the rigorous direct solution for the 3-D power distribution. While the methods and calculations used to design reload cores are extremely reliable and have been confirmed by measurements taken in many operating reactors, it is a normal practice to design cores with some margin, so that measured power distributions will always fall below the core power limits, even when measurement uncertainties are added. These core power limits are determined from the body of safety analyses that supports the Final Safety Analysis Report (FSAR) and Technical Specifications and ensure that regulatory limits are not exceeded for any postulated transient.

Assembly power distributions in a typical Westinghouse-designed PWR reload core are shown in Figures 29-2-1 and 29-2-2. The radial power distribution can be divided into three core regions: low power peripheral region, fresh high power assemblies distributed throughout the core, and average power regions also distributed throughout the core. These figures show the predicted power of assemblies in a reload core. This is a typical low leakage core loading pattern, in which high burnup assemblies are situated around the periphery of the core, while fresh and low burnup assemblies are in the interior of the core.

[

]^{a,c}

Within the fuel assembly, individual fuel rods vary in power due to the presence of burnable absorbers and water holes near the thimble tubes. Figure 29-2-3 is a histogram showing the distribution of rod powers within the high power assembly of several different fuel designs. The powers are expressed as a fraction of the maximum power allowed by the Technical Specifications. The maximum calculated rod power is, therefore, more than 4 percent lower than the maximum allowed value to accommodate measurement uncertainties during surveillance. Most of the fuel rods are at powers near the middle of the distribution, and the hot assembly power distribution can be modelled with a single average rod and a single hot rod. The

cumulative distribution is shown in Figure 29-2-4. The expected hot assembly power calculated from these distributions, summarized in Table 29-2-1, is seen to lie approximately []^{a,c} below the expected maximum calculated (hot rod) value.

The steady-state axial power distribution also varies as a function of time. Figure 29-2-5 shows the core average axial power distribution at beginning of life (BOL) and end of life (EOL) for the typical reload core illustrated in Figures 29-2-1 and 29-2-2. During the cycle, the steady-state axial peak moves away from the center of the core as the core is depleted.

While a PWR is designed to easily follow load demand, the most likely state of the reactor is full power and equilibrium conditions. Under these conditions, the axial peaking is relatively low. Measurements taken of the maximum peaking factor at HFP nominal conditions are usually well below the Technical Specification limits. The margin to peaking factor limits is intended to allow for the less frequent occurrence of transient reactor operation, usually consisting of power reductions and increases to follow load.

In summary, the design of a core (its geometry, fuel enrichment, and loading pattern) establishes the maximum radial peaking in the core. The radial distribution is determined almost entirely by the core loading and cannot be easily changed by external controls in normal operation. Hence, in ensuring that the measured hot rod power will always lie below the limit, core designs are set allowing for additional margin beyond the 4 percent required by the Technical Specifications.

29-2-1-2 Transient Power Distributions

Short-term changes in reactor power distributions are typically attributable to changes in reactor power level. Changes in power level may require control rod motion and result in changes in coolant density profiles and xenon distribution. Changes in xenon distribution are a strong function of the magnitude and duration of the power change maneuver as well as the operating strategy used during the maneuver.

Westinghouse methodology used to generate axial power distributions has been reviewed by the NRC. Two distinct methods are used in designs based on the *AI* Technical Specifications used. (*AI*, a measure of the axial power distribution, is the flux difference between the top and bottom halves of the core.)

Constant axial offset control (CAOC) methodology (Morita et al., 1974) requires the core designer to simulate various types of load follow maneuvers throughout the cycle to establish the limiting axial power distributions. The approach taken is conservative in that daily load follow swings to various power levels are assumed throughout the cycle. This method is used with plants that have the ΔI Technical Specification defined as an allowable band (typically +5 to -5 percent) about a target ΔI .

Another approach is used for plants with a fixed ΔI Technical Specification. The relaxed axial offset control (RAOC) methodology (Miller et al., 1983) considers the core parameters (power level, xenon distribution, and control rod position) that can affect power distributions and establishes the maximum variability possible in these parameters throughout a given cycle. These parameters are then treated as independent variables, and all possible combinations are checked. Any axial shapes that are found to be within the ΔI operating space defined by the Technical Specifications are taken to be possible. Although conservative, the RAOC approach is analytically easier to implement than CAOC.

Typical transient distributions generated by the RAOC methodology are shown in Figure 29-2-6. The limiting distributions are used to develop an envelope of peak linear heat rate (or peaking factor, when normalized to the core average) as a function of elevation as shown in Figure 29-2-7. These transient shapes sometimes approach the Technical Specification limit for F_Q , which is also shown in Figure 29-2-7. [

]^{a,c}

The basic characteristic of the axial power distribution (near zero at each end of the core, with one or two maxima) suggests several ways the distribution can be characterized in terms of a small number of parameters. [

]^{a,c}

Despite the sensitivity of the core axial power shape to reactor transient operation, the occurrence of high peak linear heat rate power shapes, even with constant daily load follow, is relatively rare.

An additional characteristic of these transient power shapes is that fission products do not have sufficient time to build up in the high power region of the fuel rod. Consequently, if the reactor shut down for any reason at the time the maximum transient linear shapes occurred, the decay heat generated is substantially lower than if the core had been operating indefinitely at these peak linear heat rates.

The reactor heat source is made up of three major constituents. Prompt fission energy, by far the largest component of the heat, comprises approximately 93 to 100 percent of the total heat source for full power operation. The stored energy contribution to the LOCA transient is, therefore, directly related to the fission rate distribution at the time of the LOCA. The magnitude of the decay and actinide heat sources makes them a small contribution to the stored energy component. The decay and actinide components are, however, the principal contributors to the reflood heatup because the fission rate during this portion of the transient is negligible. The decay and actinide heat sources are independent of the instantaneous fission rate at any given point in time, but dependent upon the fission rate time history. This is because decay and actinides are fission products. Their concentrations determine the decay power available because the decay power for radionuclide decay is determined by the product of the energy release per decay, the decay constant, and the concentration. The concentration of a nonabsorbing fission product is dependent upon the fission rate time history, the fission product yield per fission, and the decay constant. Because the yield and time constant for a given fission product are constant for a specified isotope, the time dependent fission product concentration depends only upon the fission rate time history.

Decay heat is the result of a multitude of radionuclide decays (approximately 350 isotopes). These decay processes have been simplified in the American National Standards Institute/American Nuclear Society (ANSI/ANS)-5.1-1979 (American Nuclear Society, 1979) decay heat standard to a summation of 23 exponentials for each fissile isotope. In the absence of significant absorption or isotope decay chain cross-coupling, the ANSI/ANS 5.1-1979 decay heat standard is a 23-group "pseudo-nuclide" representation of the fission product decay process. The magnitude of the decay heat source at any given point in the reactor, therefore, depends on the time history of the fission rate. The decay heat source for a given point in the reactor will be in effective equilibrium (production rate = decay rate) only if the fission rate has been maintained for the

period of time corresponding to 10 to 20 time constants for that nuclide. Figure 29-2-9 illustrates a point evaluation of decay equilibrium fraction versus sinusoidal fission rate period. [

]^{a,c}

29-2-1-3 Power Distribution Uncertainties

After a core has been designed and loaded, it is monitored to confirm that the core operates as designed and to ensure that the reactor is operating within specified limits. The detailed reactor power distribution is monitored by in-core detectors. (There are several other core monitoring systems as well.) The readings from these detectors (which are fission chambers and convert the local neutron flux to a current signal) are transformed to fission rate distributions using analytical factors, based on the specific core design (Spier et al., 1988).

The core power distribution is measured during steady-state operation at regular intervals. The following quantities may be obtained as the result of measurement and data processing:

- $F_{\Delta H}$ The enthalpy rise hot channel factor is the ratio of the integral of local power along the rod (pin) with the highest integrated power in the core to the average rod power.
- $F_{xy}(z)$ The elevation-dependent radial peaking factor is the maximum local power density in the plane at elevation z divided by the average power density of the plane.
- $F_Q(z)$ The elevation-dependent heat flux hot channel factor is the maximum local linear power density at elevation z divided by core average linear power density.

Because the above peaking factors are derived from a combination of instrument measurements and analytical model calculation, the uncertainty associated with these factors is a combination of the two factors.

The peaking factors $F_{\Delta H}$ and $F_Q(z)$ defined previously are typically measured on a monthly basis. In addition to the peaking factors, the core axial flux difference is measured on a continual basis by the ex-core nuclear detectors. This measurement is equivalent to the axial flux difference discussed previously, and provisions are incorporated in the plant computer to provide alarms if limits are exceeded.

The calculational uncertainty on radial power distribution ($F_{\Delta H}$) has been shown (Spier et al., 1988) to be bounded by a factor of []^{a,c} through benchmarks to critical experiments and other data. There is also an uncertainty associated with measuring the radial power distribution, which is bounded by a factor of 4 percent. The plant should not routinely experience flux map measurements that exceed the ($F_{\Delta H}$) limit after a 4-percent uncertainty is applied due to combined effects of calculational and measurement uncertainties. To accomplish this, standard Westinghouse practice is to design the core so that it is predicted to be at least []^{a,c} below the ($F_{\Delta H}$) limit on a best-estimate basis. With this approach, the most probable condition is for the core to be measured at least []^{a,c} below the Technical Specification limit after measurement uncertainty is applied. Typical measurements as seen in Figure 29-2-10 show this is the case.

The margin inherent in the design as it relates to the total peaking factor $F_Q(z)$ is also reflected in typical measurements. Design calculations are performed to conservatively calculate the possible effects of adverse xenon distributions on the maximum total peaking factor. These penalty factors are generated assuming xenon transients are initiated in the core and shift the axial distribution to the full range allowed by the Technical Specifications. The most probable condition for the core is at an equilibrium xenon condition that will produce F_Q values well below the limits. The total peaking factor measurement for a typical core during a cycle is shown in Figure 29-2-11. The measured values include an uncertainty of 8.15 percent, which bounds measurement uncertainty, manufacturing variability, and rod bow effects.

Nuclear design calculations are performed assuming nominal pellet diameter, density, and the like. These calculations form the basis of the analytic factors used to convert in-core measurements to rod power. A study of the effect of variables such as pellet diameter (Chelemer and Tong, 1962) and rod bow (Argall et al., 1979) showed that these variables introduce an additional uncertainty to point measurements.

Because rod bow occurs only at high burnups, this uncertainty does not have to be applied at the beginning of the cycle. However, both factors are currently applied to the hot rod peaking factor

measurement for the entire cycle. These factors are not applied to measurements of the hot assembly and hot rod power. Local linear heat rate depends on the local mass of UO_2 per unit length, or, more specifically, per pellet, and also on the local channel geometry. The local mass varies as a result of manufacturing variations in pellet dimensions and fuel enrichment. [

]^{a,c}

A similar statement can be made for rod bow. [

]^{a,c}

A detailed study of the in-core flux mapping system and its accuracy was performed by Westinghouse (Spier et al., 1988). Because the measured values of $F_{\Delta H}$ and F_Q are actually inferred values obtained from the raw measurement using core model group constants, error contributions from both measurement and modelling sources were considered. Two uncertainties are defined: a measurement uncertainty, to be applied to the inferred peaking factor during normal core surveillance so that the true values are bounded at a high confidence level, and a calculational uncertainty, to be applied to the calculated peaking factors during the core design so that the true values are bounded at a high confidence level. The two uncertainties contain several common components, and therefore are similar in magnitude. In the best estimate LOCA methodology, the concern is with the calculational uncertainty of the predicted peaking factors.

The calculational uncertainty is composed of several independent subcomponents that are summarized in Table 29-2-2. Some of these components are related to uncertainties that should be applied only to the hot rod. In subsequent application of these uncertainties (Section 33), these components are applied separately when considering the calculational uncertainties associated with groups of fuel rods such as the hot assembly. [

]^{a,c}

A final uncertainty related to the power distribution is that associated with the total core power. Core power is inferred from an energy balance using feedwater flow and temperature, and steam flow and pressure. The maximum error from this measurement is typically ± 2 percent,

[

].^{a,c}

29-2-1-4 Effect of Fuel Burnup on Power Distributions

Core burnup has the following effects on the state of the core that may affect the LOCA transient:

- Burnup tends to reduce the fuel average temperature not only because the linear power is being reduced, but also because such phenomena as pellet cracking and cladding creep tend to increase the gap conductance. The gap conductance offsets any decrease in the gap gas conductivity due to low conductivity fission gases. The effect of burnup on fuel temperature is illustrated in Figure 29-2-12.
- Burnup generates fission gases which collect in the fuel rod, raising its internal pressure. During a LOCA, this higher pressure may result in more cladding swelling, burst, and blockage. From this standpoint, ignoring all other factors, a burned core may be more limiting if local flow blockage is only considered to reduce core cooling.
- Burnup generates fission products and heat generated from decay of these products following core shutdown causes an equilibrium value fairly early in the cycle.

29-2-1-5 Power Distribution Modelling Approach

Summarizing the preceding sections, the core power distribution is seen to exhibit the following characteristics:

- The radial power distribution is primarily controlled by core geometry, fuel enrichment, burnable absorber loading, and core loading patterns. It is relatively insensitive to operational procedures such as load follow.
- The axial power distribution is sensitive to operational procedures (such as load follow), which produce nonequilibrium xenon distributions in the core and core burnup. Large axial power distribution variations have a small effect on the radial power distribution. Axial power distributions that produce the limiting F_Q occur during transient operation.

- The power distribution in the core is well described by the following parameters: the average linear heat rate, the hot assembly linear heat rate, the low power assembly linear heat rate, and the peak linear heat rate.
- The average power of the rods in the assembly that contains the hot rod is typically []^{a,c} or more lower than the hot rod.
- The axial peak power may occur at any location within approximately 2 feet from the ends of the core, during both transient and steady-state conditions.
- Burnup tends to reduce radial and axial peaking, and fuel stored energy and increases fuel rod gap pressure.

As described in Section 26, Volume 3, the PWR core is modelled with sufficient detail to resolve both the radial and axial power distributions present in the core. The radial power distribution is resolved using [

].^{a,c}

There are several parameters that play a role in the calculation of rod power in WCOBRA/TRAC. Each parameter, in turn, contributes some uncertainty. Based on the general discussion of power distributions, the parameters as used in WCOBRA/TRAC are described in more detail in the following paragraphs. A final summary of uncertainty contributors is also presented. The discussion shows how several power distribution and fuel rod model related uncertainties can be conveniently combined to simplify the uncertainty analysis.

As described in Section 29-2-1, there are four core channels and five fuel rods in the PWR model.

Each fuel rod has input parameters describing the average linear heat rate and the axial distribution of power relative to the core average linear heat rate. The important parameters used in WCOBRA/TRAC for these fuel rods are described in the following paragraphs. The "0" designates initial or steady-state values of parameters that will change during the LOCA transient.

The reactor power parameters described as follows are directly related to several quantities also measured in the plant during normal operation. These are the total peaking factor (F_Q), the hot channel factor (F_{ZH}), and the axial flux difference. Other quantities of lesser importance are the MTC and the coolant boron concentration. The Technical Specifications call for specific uncertainties and margins to be applied to the measured values of some of these quantities before they are compared to the Technical Specification limit. In the discussion following, these quantities are normally described in terms of calculated or expected values, without uncertainties, and are designated with subscript *BE*.

a. Core Average Linear Heat Rate

The parameter defining core power in WCOBRA/TRAC is the initial core average linear heat rate, calculated by:

$$AFLUX(0) = P(0) / (NFR * L) \quad (29-1)$$

where:

L = nominal fuel length

$P(0)$ = initial core power

NFR = total number of fuel rods

There is a tendency for the fuel pellet stack (L) to shrink during the cycle, which will increase *AFLUX* based on Equation (29-1). However, [

AFLUX

].^{a,c} The only uncertainty affecting *AFLUX* is the core power measurement uncertainty, which results from calorimetric errors in measuring feedwater flow and temperature. As noted in Section 29-2-1-3, the range of this error is estimated at

[].^{a,c} This uncertainty and distribution has been used in statistical DNB methodologies (Chelemer et al., 1975).

The axial power distributions of the core average rods (rods 3, 4, and 5) are determined from the required attributes of the hot rod and hot assembly rod (rods 1 and 2). These distributions and power distribution modelling are discussed at the end of this section.

b. Peak Linear Heat Rate

The peak linear heat rate (*PLHR*) on the hot rod (rod 1) is defined by:

$$[\dots]^{a,c} \quad (29-2)$$

$$]^{a,c}$$

The peak linear heat rate can also be expressed as:

$$[\dots]^{a,c}$$

$$]^{a,c}$$

The variation due to transient operation is the result of assumed load follow operations and other operational transients, which introduce relatively short-lived, skewed power shapes with relatively high peaking factors compared to equilibrium

conditions, when the plant returns to full power. Limiting transient power distributions are generated during the core design analysis to confirm that maximum values remain below limits established in the Technical Specifications. The calculated maximum peaking factor is obtained from the envelope that is generated by these distributions. Peaking factors encountered during normal steady-state operation are normally far below these calculated values (Figure 29-2-8). [

]^{a,c}

FGAM is a measure of how much of the nuclear energy generated in the hot rod is deposited as thermal energy outside of the rod, and is part of the fuel rod nuclear model in WCOBRA/TRAC described in Volume 1. The actual thermal power produced by WCOBRA/TRAC in the hot rod is slightly lower than the nuclear power due to redistribution of the power to the moderator and surrounding rods. The uncertainty in *FGAM(1,0)* from its best estimate value is due to uncertainty in the assumed surrounding rod powers and fluid conditions. This uncertainty is described in Section 32, which addresses model uncertainties.

c. Hot Rod Average Power

Because the hot rod has a small effect on the hot assembly fluid conditions (it is only one rod among more than 200), its total power is not as important as the power in the hot assembly rod. However, total power will affect hot rod gap pressure and cladding burst times.

[

]^{a,c} (29-4)

[]^{a,c}

(29-5)

$F_{\Delta H, BE}$ is defined as the maximum expected average linear heat rate of the highest power rod in the core, relative to the core average linear heat rate. Typically, the calculated $F_{\Delta H, BE}$ for a core design is augmented by 4 percent to account for calculational and measurement uncertainties and up to an additional []^{a,c} as prudent conservatism. The reason for the application of additional margin in $F_{\Delta H}$ is that, unlike total peaking factor, there are few alternatives short of reducing power if the measured value exceeds the designed value. $F_{\Delta H}$ becomes lower at high burnups although there may be an increase in mid-cycle as poisons are depleted.

d. Hot Assembly Average Power

The hot assembly average linear heat rate is important because it will affect fluid conditions in the hot assembly channel. Hot assembly rod (rod 2) average linear heat rate during steady-state is defined as:

[]^{a,c}

(29-6)

[]
]^{a,c}

$FGAM(2,0)$ = fraction of power in the hot assembly average rod which is redistributed to rods in surrounding assemblies

Therefore:

[]^{a,c}(29-7)

The actual thermal power produced in the hot assembly rod relative to its nuclear power may be slightly different from the hot rod due to different levels of redistribution. []^{a,c}

As discussed in Section 29-2-1-1, a review of a large number of core designs in two-, three-, and four-loop plants indicates that the minimum difference between the hot rod and the hot assembly average rod is []^{a,c} power (Figure 29-2-4). This is a conservative estimate of the relationship that will exist between the hot rod and the hot assembly average rod during normal operation for the entire fuel cycle. The relative nuclear power generated in the hot assembly average rod is, therefore, assumed to be []^{a,c} lower than the best estimate value of the hot rod relative nuclear power, $F_{\Delta H, BE}$.

e. Hot Assembly Peak Heat Rate

The hot assembly rod peak linear heat rate is defined as:

$$[\dots]^{a,c} \quad (29-8)$$

Therefore:

$$[\dots]^{a,c} \quad (29-9)$$

Typically, the relationship in power of the hottest rod in an assembly to the assembly average will depend upon the details in the design of that assembly, such as the location of the hot rod in the assembly. In this analysis, it is conservatively assumed that the hottest rod in the core resides in the hottest assembly and the peak power is offset by a constant factor equal to the difference in average power.

The overall uncertainty for the hot assembly average rod peaking factor should be less than that for the hot rod because the concern is with the average value over a number of rods and because the rod bow uncertainty is zero (bowed rods in an assembly create as many water deficient regions as water holes). This is indicated in Table 29-2-2.

There are two items to consider when developing the relationship between the hot rod, which is a single rod, and the hot assembly rod, which represents the average of all the rods in the hot assembly minus the hot rod. The first item is the actual difference between the hot rod and the hot assembly rod powers. The second is the difference in the uncertainty associated with various quantities for the hot rod and the hot assembly rod.

Examination of rod census data indicates that the minimum difference between the hot rod and the hot assembly average rod is []^{a,c}. Absent all uncertainties, this is a conservative estimate of the relationship that will exist between the hot rod and the hot assembly average rod during normal operation for the entire fuel cycle.

A second consideration is the uncertainty associated with the hot rod and with the hot assembly average rod. For a single rod at a single axial location, the following uncertainties exist:

- Uncertainty in the actual linear heat rate, relative to what is predicted
- Uncertainty in the actual fuel pellet geometry
- Pellet at a particular location may be slightly larger or be slightly more enriched than the value intended during manufacture
- Uncertainty in the hot rod subchannel geometry
- Rod bow may slightly distort the subchannel

For a single axial location on a single rod, all these uncertainties must be considered. Because the local axial linear heat rate specified by F_Q is defined at a single location, all these uncertainties must be considered for the hot rod, hence the full column of numbers in Table 29-2-2 for the hot rod F_Q . For integral quantities, such as the rod total power as specified by F_{4H} , local uncertainties such as pellet dimensions should not contribute significantly to the integral uncertainty. [

]^{a,c}

(29-10)

[

(29-11)

(29-12)

]^{a,c}

[

]^{a,c}

When the hot assembly average rod is considered, additional uncertainties due to assembly radial peaking drop out.

The result of the application of these different uncertainties is that the uncertainty associated with the power on the hot rod is typically larger than the uncertainty associated with the power in the hot assembly average rod.

Finally, as shown in Section 29-4, during discussion of the fuel rod modelling, an additional uncertainty affecting linear heat rates comes into effect when the PWR transient is considered. For example, the peak linear heat rate during the LOCA transient is:

[

]^{a,c}

(29-13)

where $DH(t)$ is the fraction of original core power. Because the determination of this fraction introduces additional uncertainties, the overall uncertainty of the peak linear heat rate is increased during the transient.

f. Axial Power Distribution

Axial power distributions vary widely due to burnup and transient operation. The distributions have been correlated with PCT from prior evaluation models using

[

]^{a,c}. Figures 29-2-13 and 29-2-14 represent the widest range expected for any future core design.

The [

]^{a,c}

This approach bounds the widest expected range for most plants. The boxes drawn around the data in Figures 29-2-13 and 29-2-14 represent the widest range expected for any future core design. The fact that some of the data fall outside these boxes is of no consequence; future core designs will produce data within the range specified by the boxes. (This will be verified for each reload.) The ranges chosen are:

If $F_Q < 2.0$, then:

[]^{a,c}

If $F_Q > 2.0$, then:

[]^{a,c}

or:

[]^{a,c}

[

]^{a,c}

]^{a,c}

g. Low Power Region Relative Power

The power in the average rod (rod 5) of the low power region of assemblies is determined from the core design and usually varies from [

].^{a,c} If this region has a low power, the interior channels (rods 3 and 4) have a higher power, but rods 1 and 2 located in the hot assembly do not vary. A

relative power []^{a,c} of the core average, which is typical of current and future low-leakage loading patterns, is used in the WCOBRA/TRAC-SB analyses.

h. Hot Assembly Burnup

Hot assembly burnup affects fuel average temperature during normal operation. Fuel temperatures and steady-state peaking factors are typically highest early in the fuel cycle. Because this results in higher calculated PCT during large break LOCAs, the hot rod and the hot assembly rod are assumed at BOL conditions in the scoping analysis. The core average rods are assumed to be at an average burnup representative of typical reload cycles.

i. Reactor Operating Power History

The power distributions that generate high peaking factors are relatively short lived. A detailed accounting of the buildup of fission products shows that after shutdown, the axial power distribution reverts back to the original, steady-state distribution.

This effect is [

]^{a,c}.

j. MTC

The MTC affects reactor shutdown due to fuel temperature excursions during the first few seconds of a LOCA event. The larger (less negative) this value, the less responsive the reactor is to the increased fluid temperature that can occur in the first seconds of the LOCA. The maximum value specified in the Technical Specifications is assumed to conservatively estimate core reactivity.

k. HFP Boron Concentration

A low initial primary fluid boron concentration slightly increases the total power generated in the core during the first seconds of blowdown. A typical low value consistent with BOL conditions is assumed.

29-2-2 Application to PWR Small Break LOCA Analysis

Figures 29-2-33 presents the power shape used in the Indian Point Unit 2 small break LOCA sequence of runs; []^{a,c}

Figure 29-2-34 illustrates the relationship of the core design to the best estimate LOCA analysis; []^{a,c}

[]^{a,c} In Figure 29-2-33, the axial power distribution as input into the WCOBRA/TRAC-SB PWR model, the hot rod peak power is offset by []^{a,c} from the hot assembly average rod power and is offset from the average rod power by the total radial peaking ($F_{\Delta H}$). The low power rod is offset from the average rod power, in turn, by the factor $PLOW$.

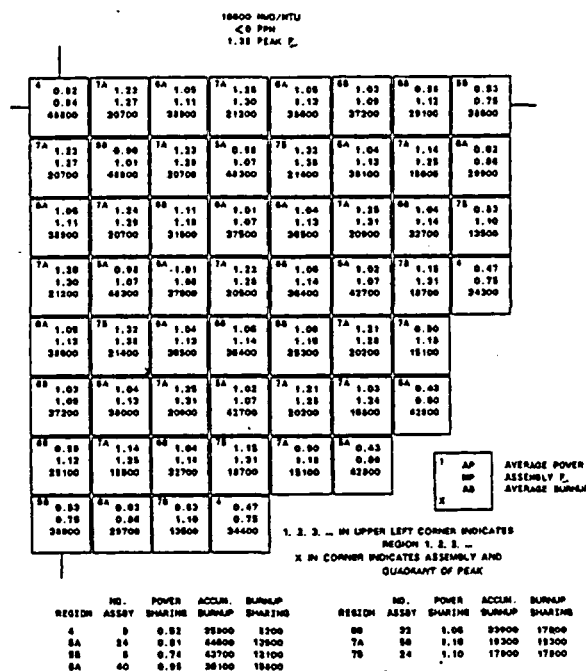
Table 29-2-1
Hot Assembly Rod Power Census Summary

Description	14x14	15x15	16x16	17x17
[

]^{a,c}

Table 29-2-2
Peaking Factor Uncertainties

] a,c



DISTRIBUTION OF ASSEMBLY POWERS

BURNUP = 0 MWD/MTU

NUMBER OF ASSEMBLIES

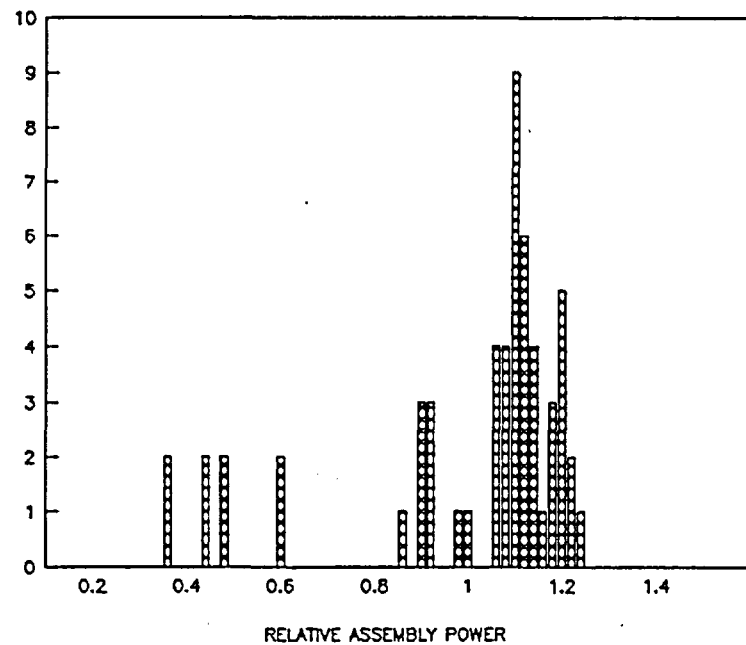
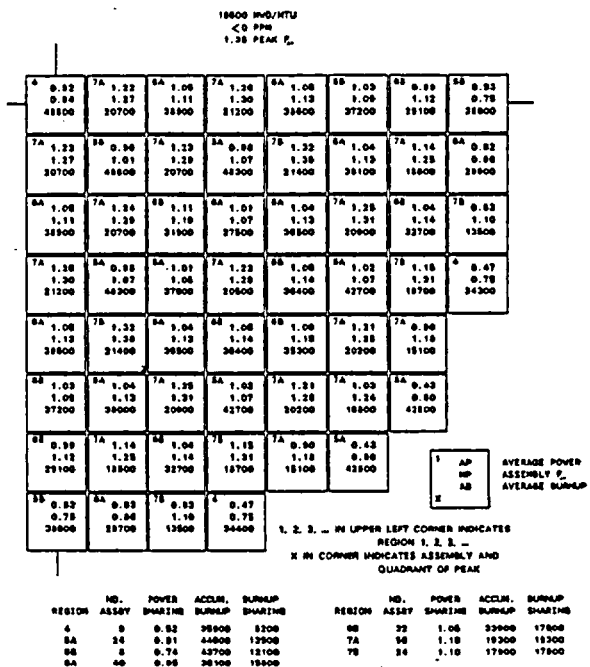


Figure 29-2-1. (a) Typical Assembly Power Map
(b) Assembly Power Distribution, BOL



REGION	NO.	POWER	ACCRUM.	BURNUP	SHARING	REGION	NO.	POWER	ACCRUM.	BURNUP	SHARING
4	9	0.92	98900	9200	00	22	1.06	329000	17800	00	
5A	24	0.81	44800	13900	7A	56	1.10	193000	13200	7B	
5B	5	0.76	42700	12100	7C	34	1.10	179000	17800	7D	
6A	40	0.95	38100	13400							

DISTRIBUTION OF ASSEMBLY POWERS

BURNUP = 16600 MWD/MTU

NUMBER OF ASSEMBLIES

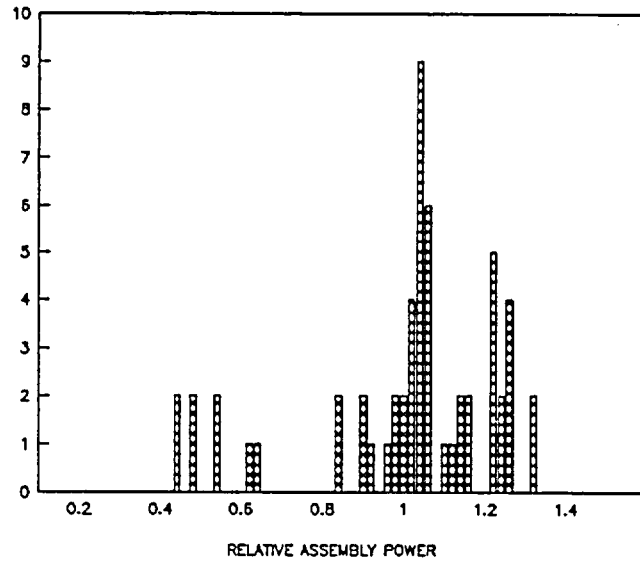


Figure 29-2-2. (a) Typical Assembly Power Map
(b) Assembly Power Distribution, EOL

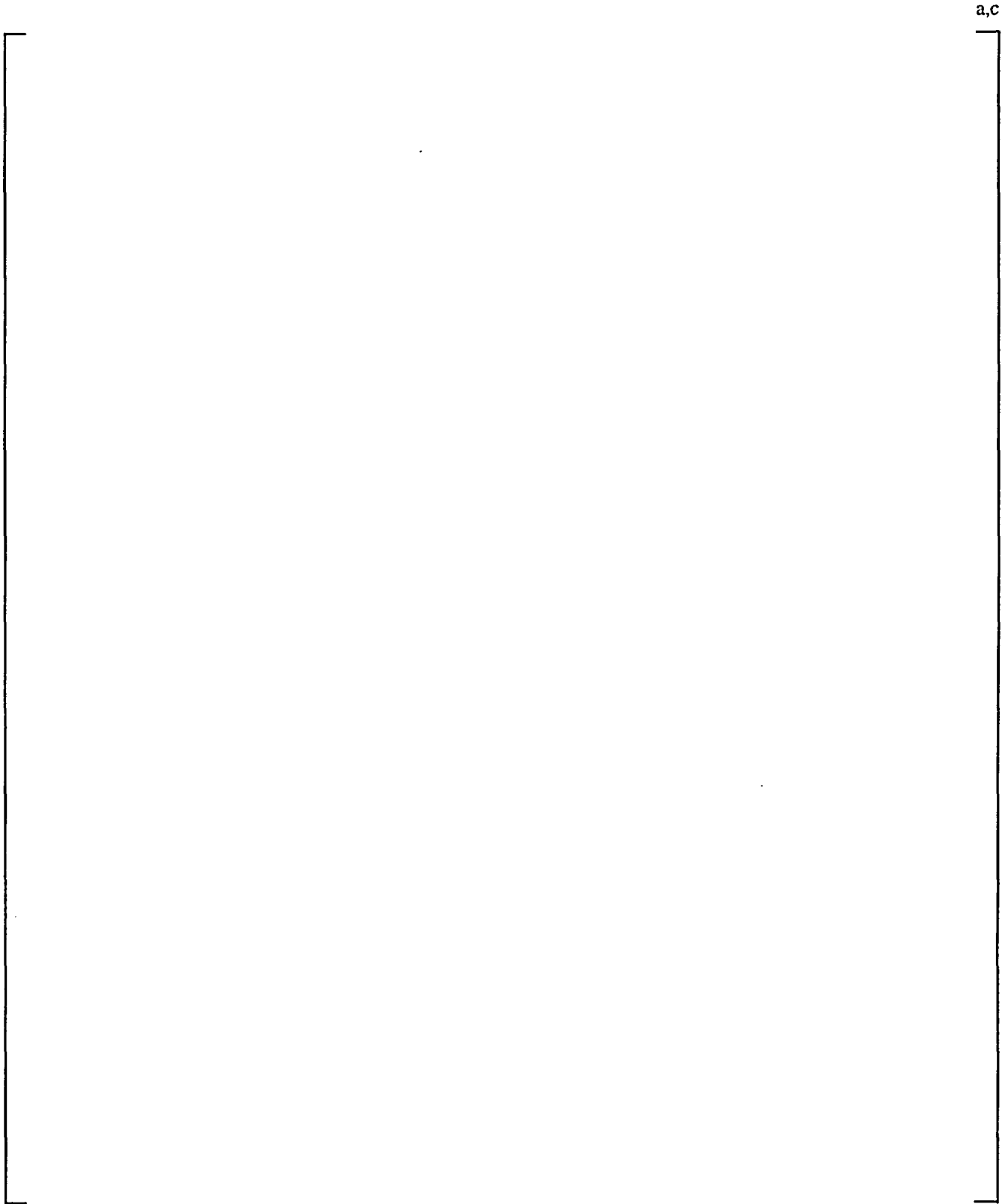


Figure 29-2-3. Typical Hot Assembly Fuel Rod Power Distribution

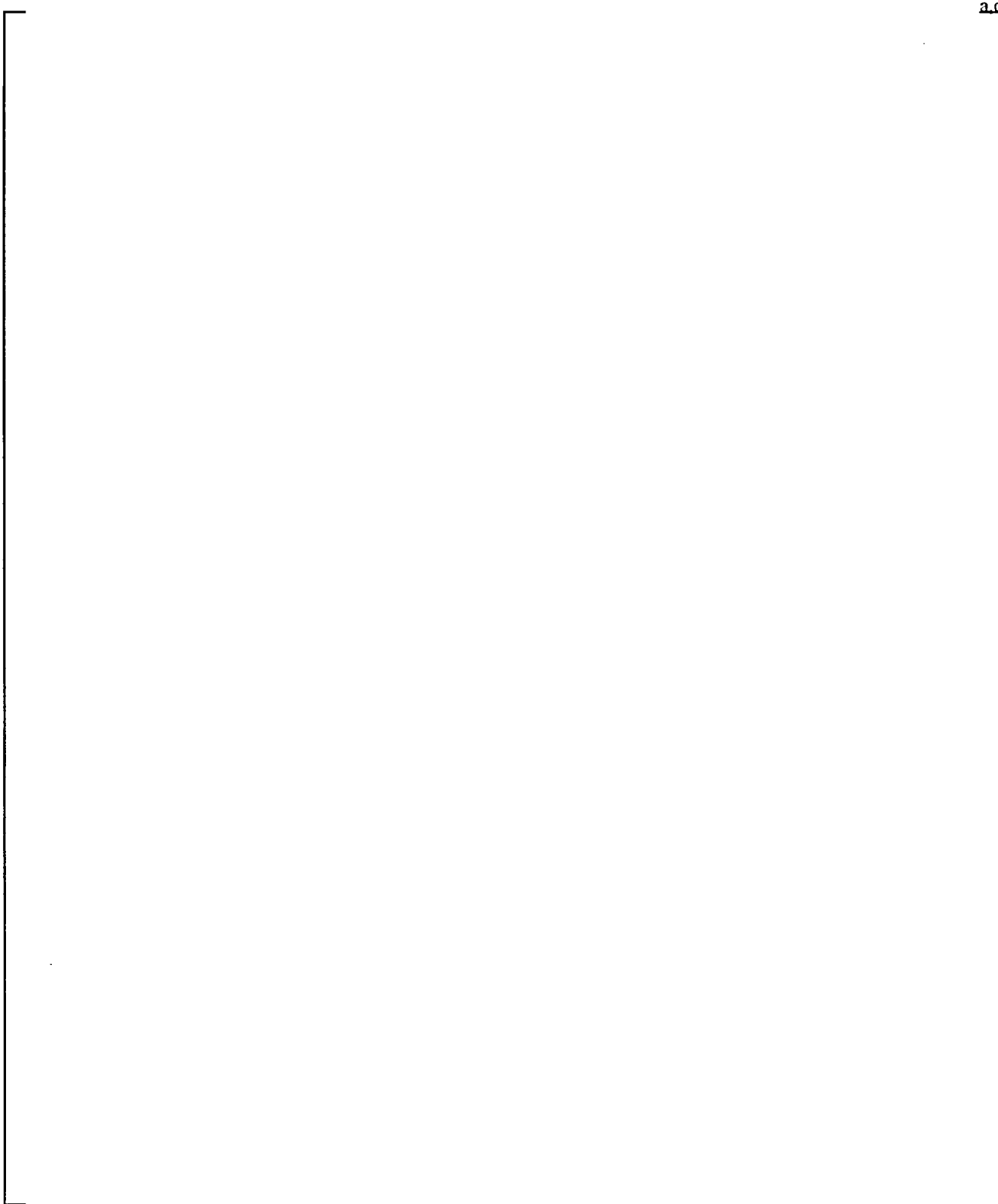


Figure 29-2-4. Hot Assembly Rod Power Census for Typical Westinghouse Fuel Designs

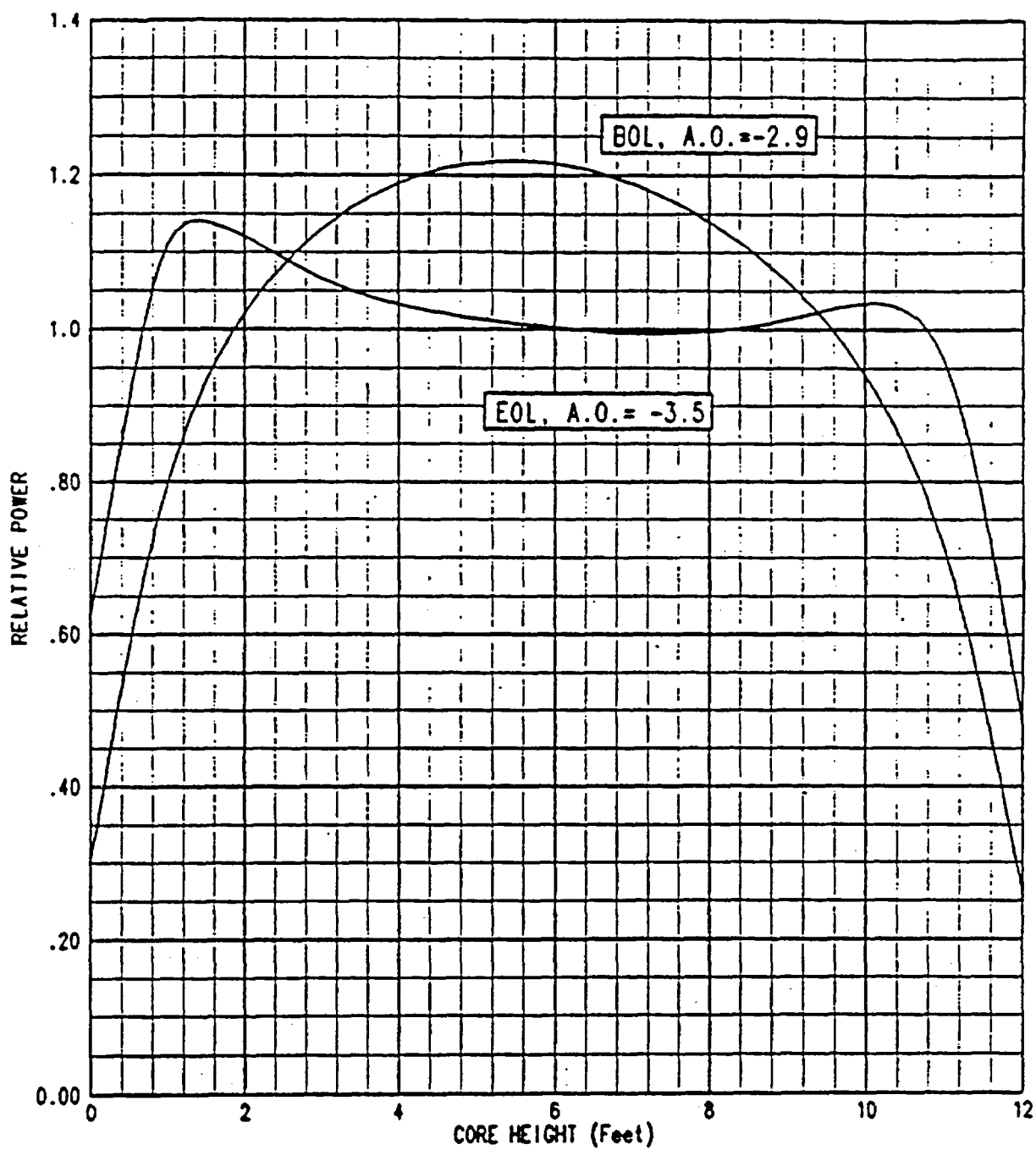
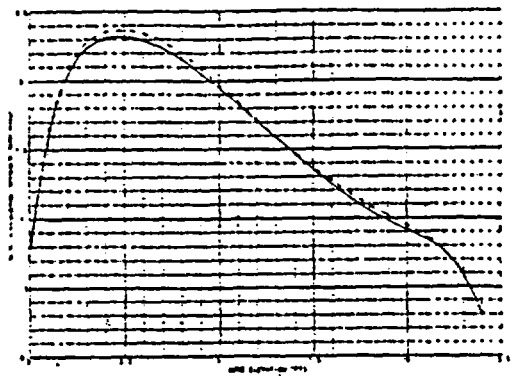
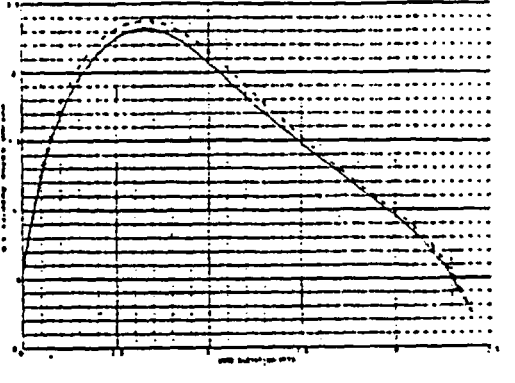


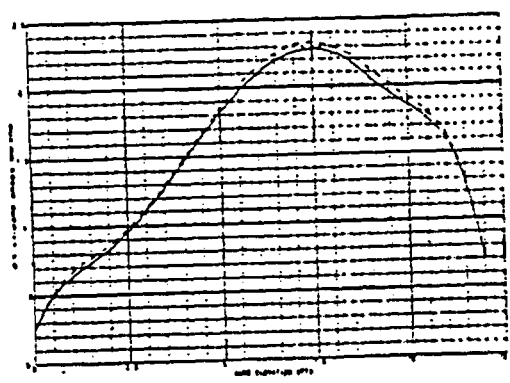
Figure 29-2-5. Relative Axial Power Distribution at BOL and EOL During Full Power Steady-State Conditions



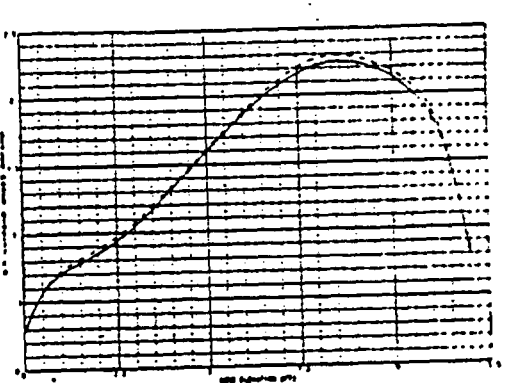
$r_0 = 2.2816 P_{D0} + 1.3500 \text{ DELTA}_r + 23.82 \text{ PIP} + 0.5447 \text{ FLOC} - 7.47$
MAX PIP 2.32 AT 7.37 FT 2883



$r_0 = 2.2453 P_{D0} + 1.3500 \text{ DELTA}_r + 28.87 \text{ PIP} + 0.6492 \text{ FLOC} - 8.62$
MAX PIP 2.32 AT 8.57 FT 2787



$r_0 = 2.2639 P_{D0} + 1.3500 \text{ DELTA}_r + 21.87 \text{ PIP} + 0.6226 \text{ FLOC} - 7.87$
MAX PIP 2.32 AT 7.97 FT 662



$r_0 = 2.2089 P_{D0} + 1.3500 \text{ DELTA}_r + 20.76 \text{ PIP} + 0.7903 \text{ FLOC} - 8.78$
MAX PIP 2.32 AT 9.78 FT 967

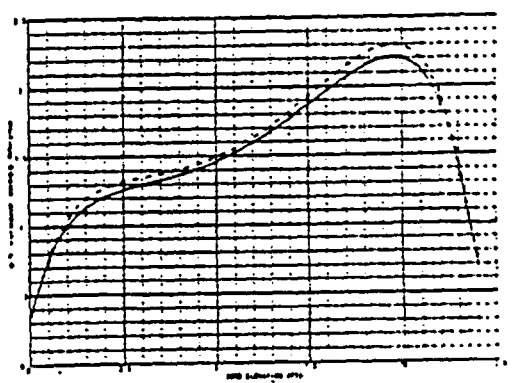
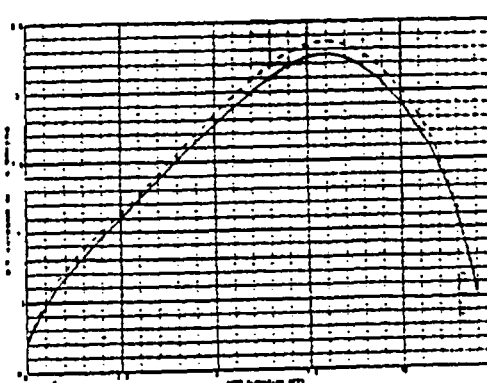


Figure 29-2-6. Typical Transient Axial Power Distributions

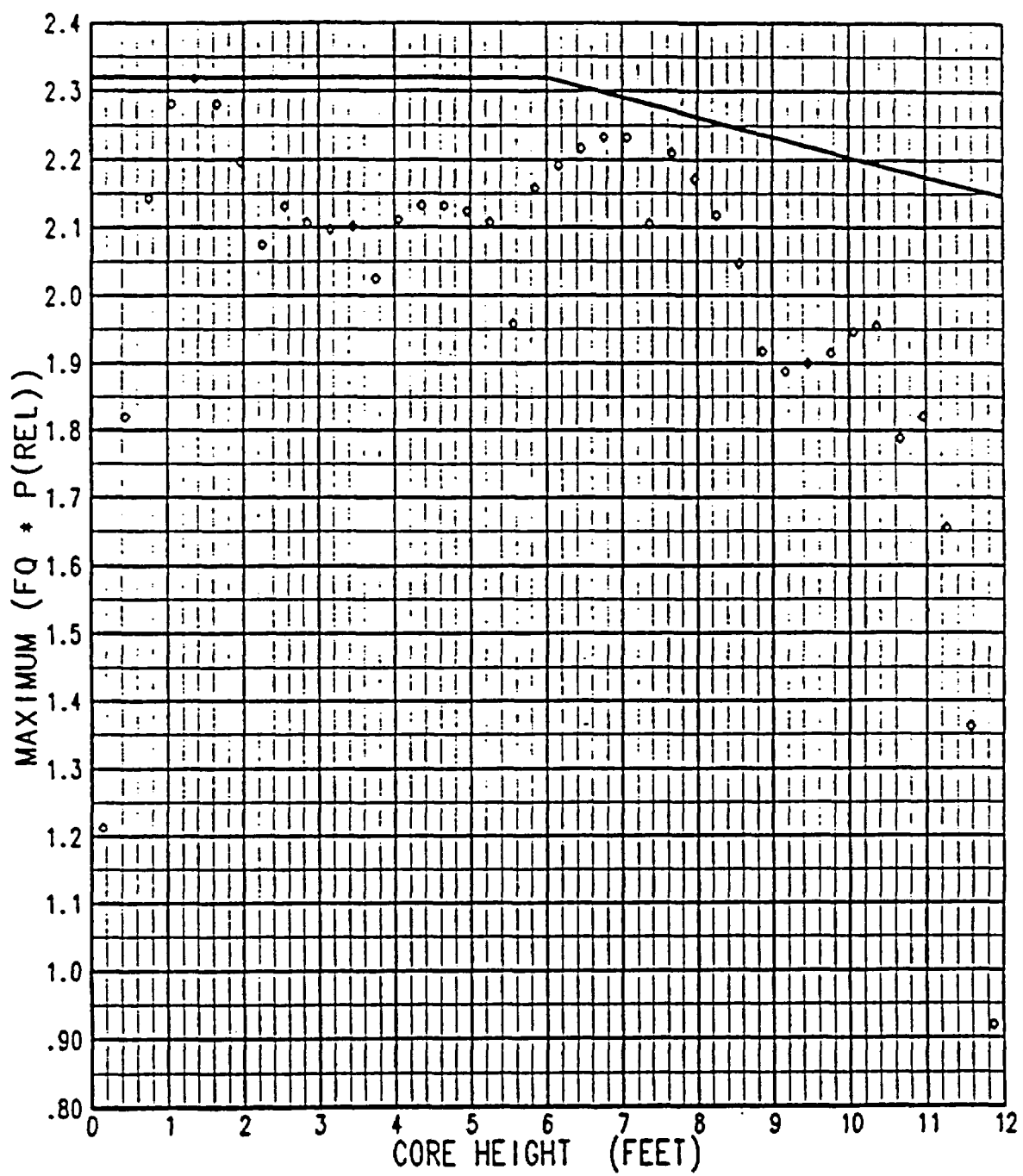


Figure 29-2-7. Envelope of Peak Linear Heat Rates as Function of Core Height for Typical Westinghouse Core Design

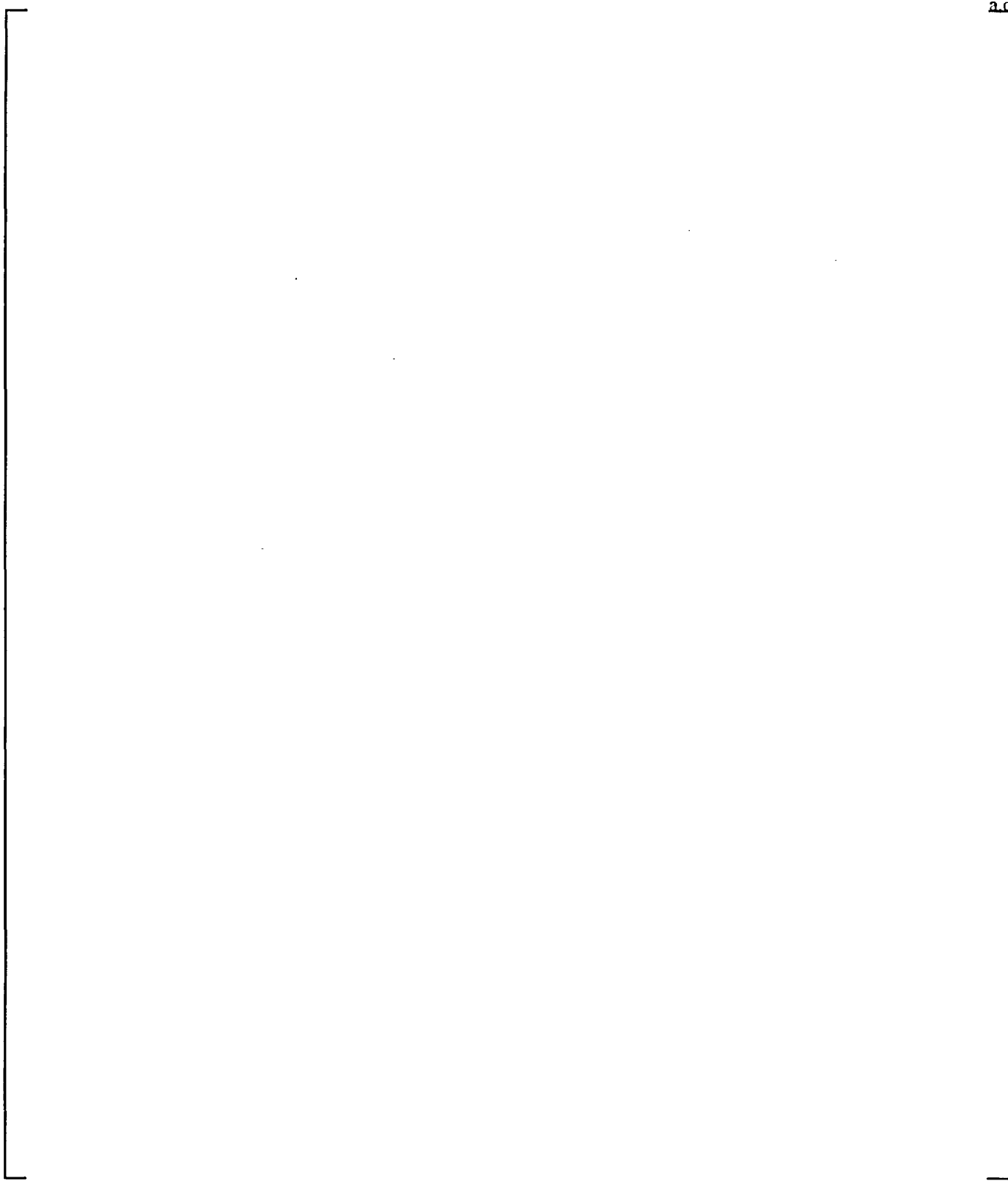


Figure 29-2-8. Typical Steady-State Peaking Factors Versus Peaking Factor Design Limit

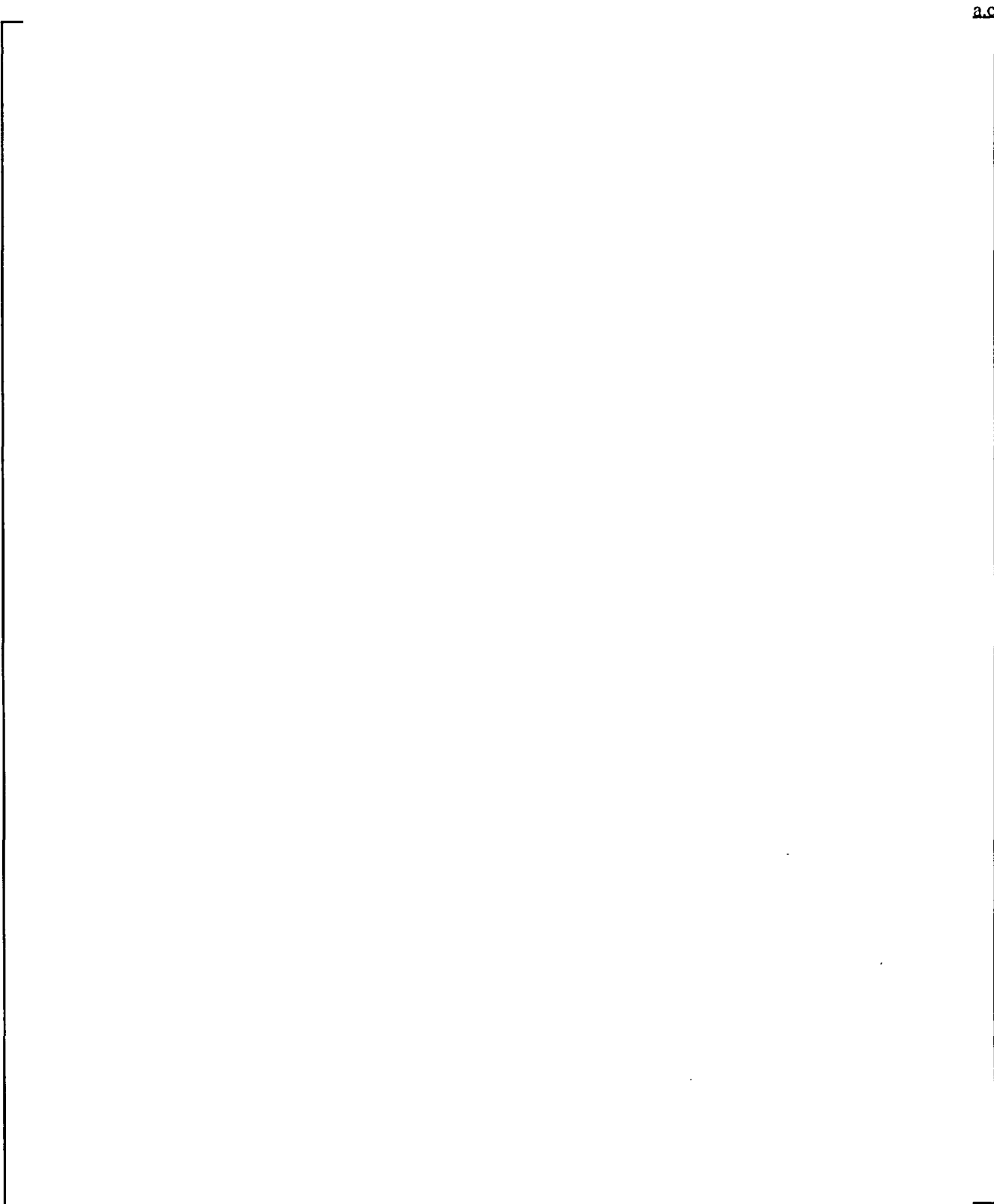


Figure 29-2-9. Effect of Load Follow Maneuver Period on Decay Heat Equilibrium Fraction for Various Times After Trip

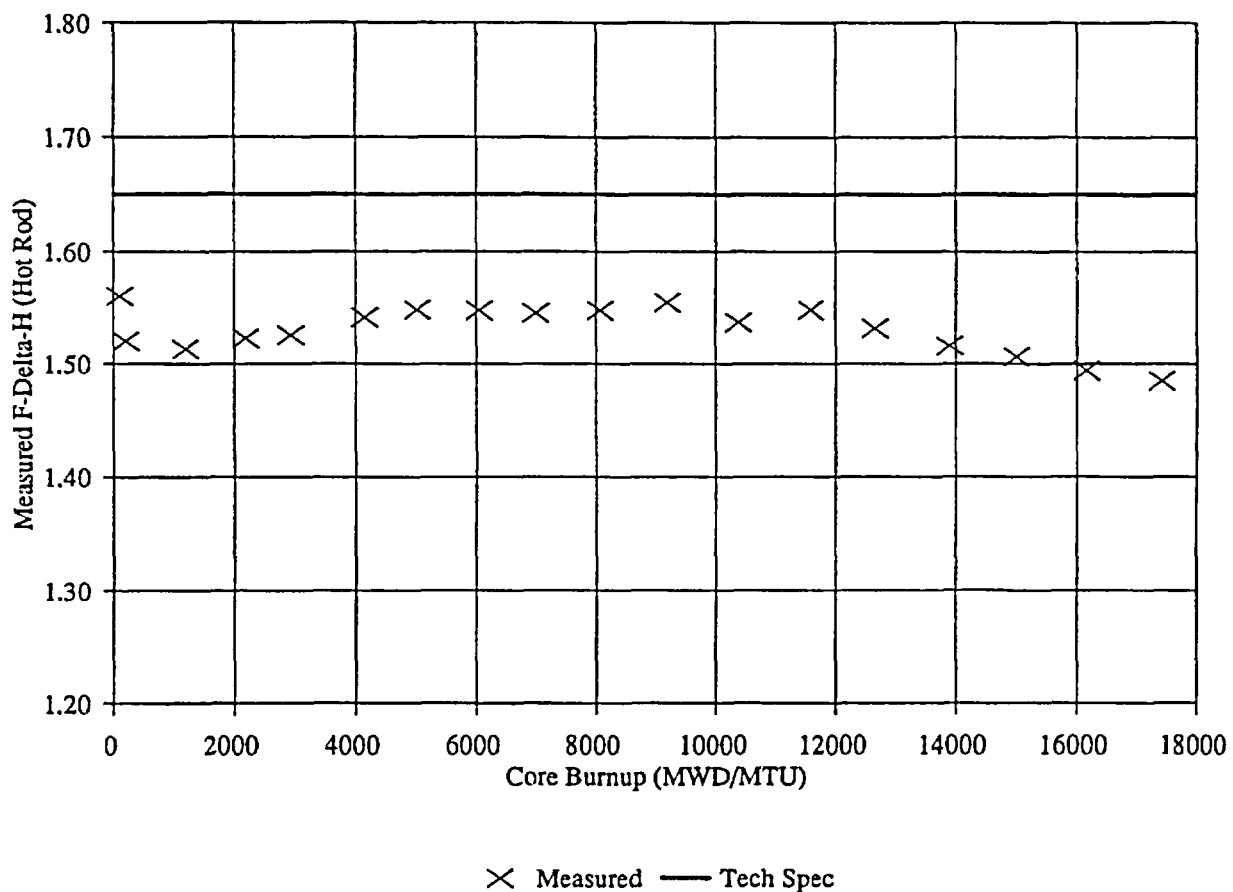


Figure 29-2-10. Typical Measurement of Enthalpy Rise Hot Channel Factor $F_{\Delta H}$

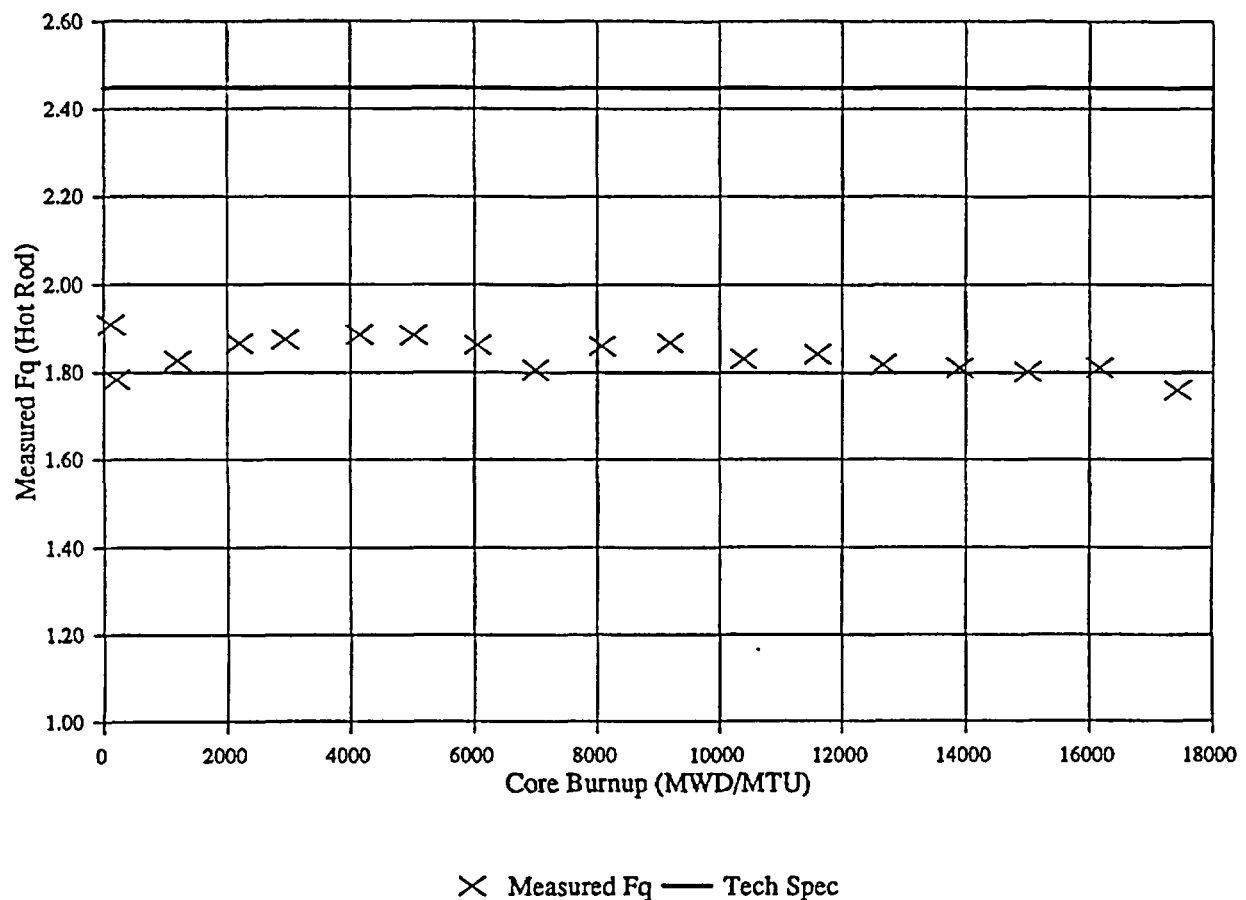


Figure 29-2-11. Typical Measurement of Total Peaking Factor F_q

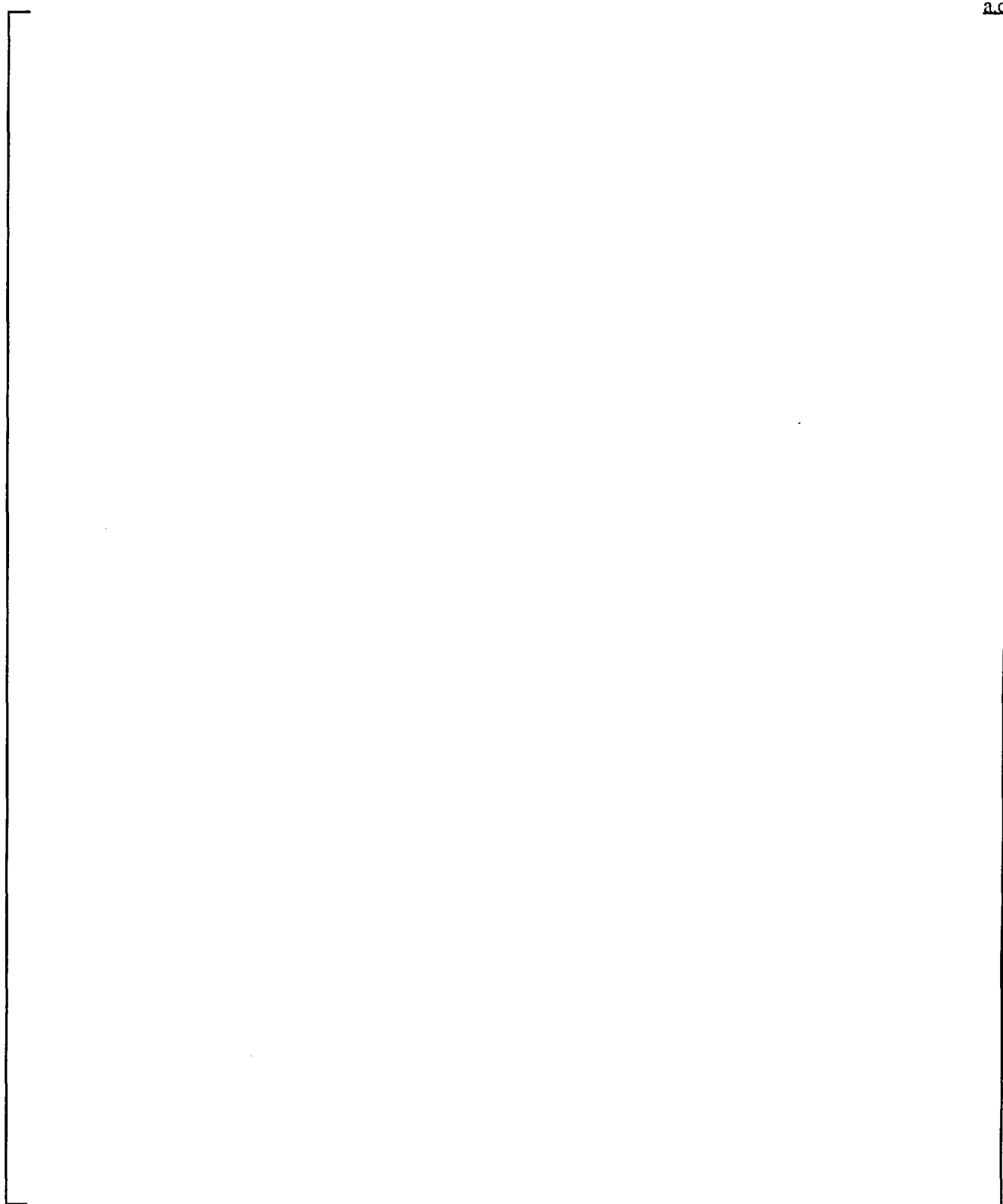


Figure 29-2-12. Effect of Burnup on (a) Baseload Peak Linear Heat Rate, (b) Fuel Average Temperature, and (c) Decay Heat Equilibrium Fraction

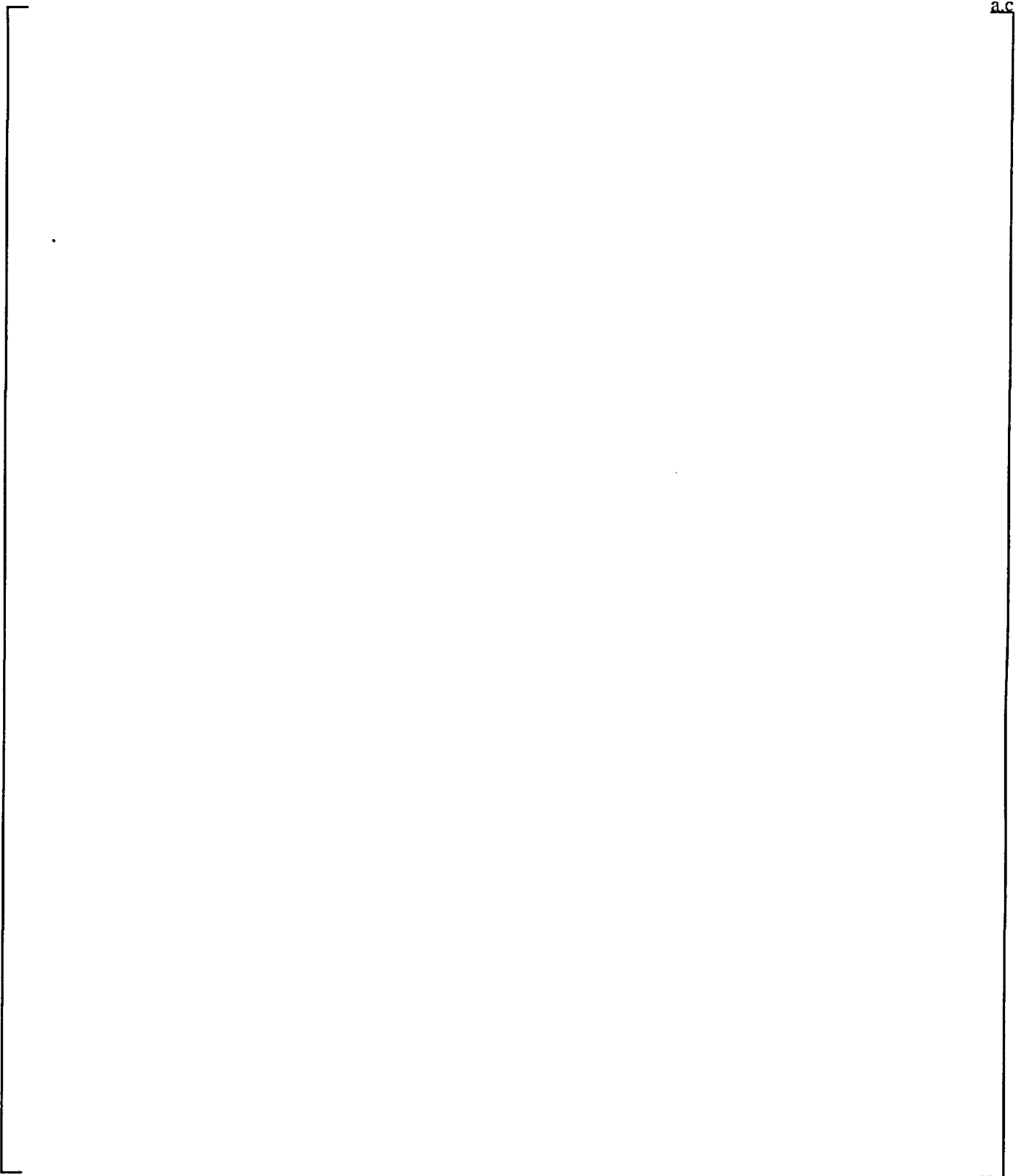


Figure 29-2-13. [
 F_Q Range

]^{a,c} in Low

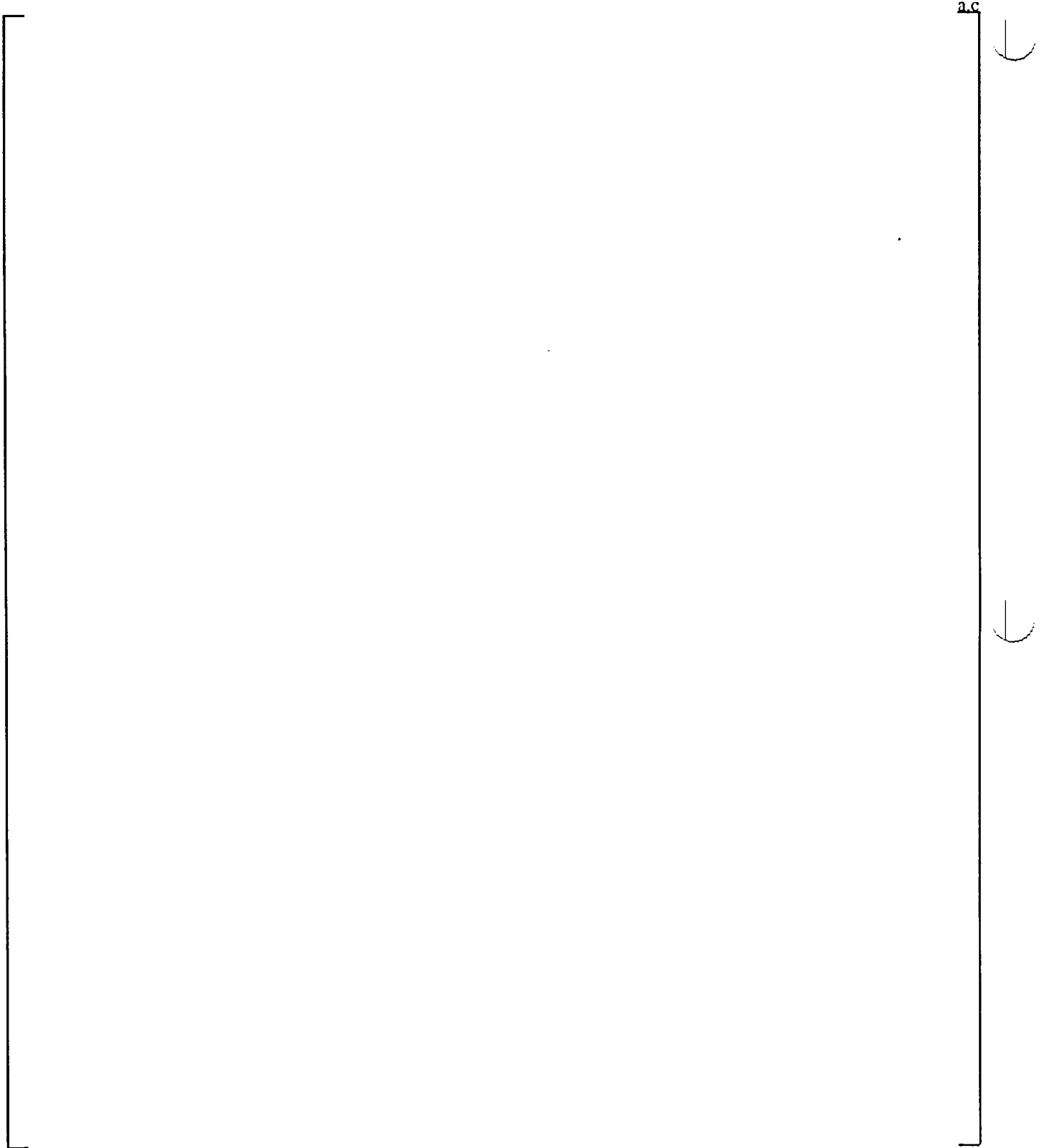
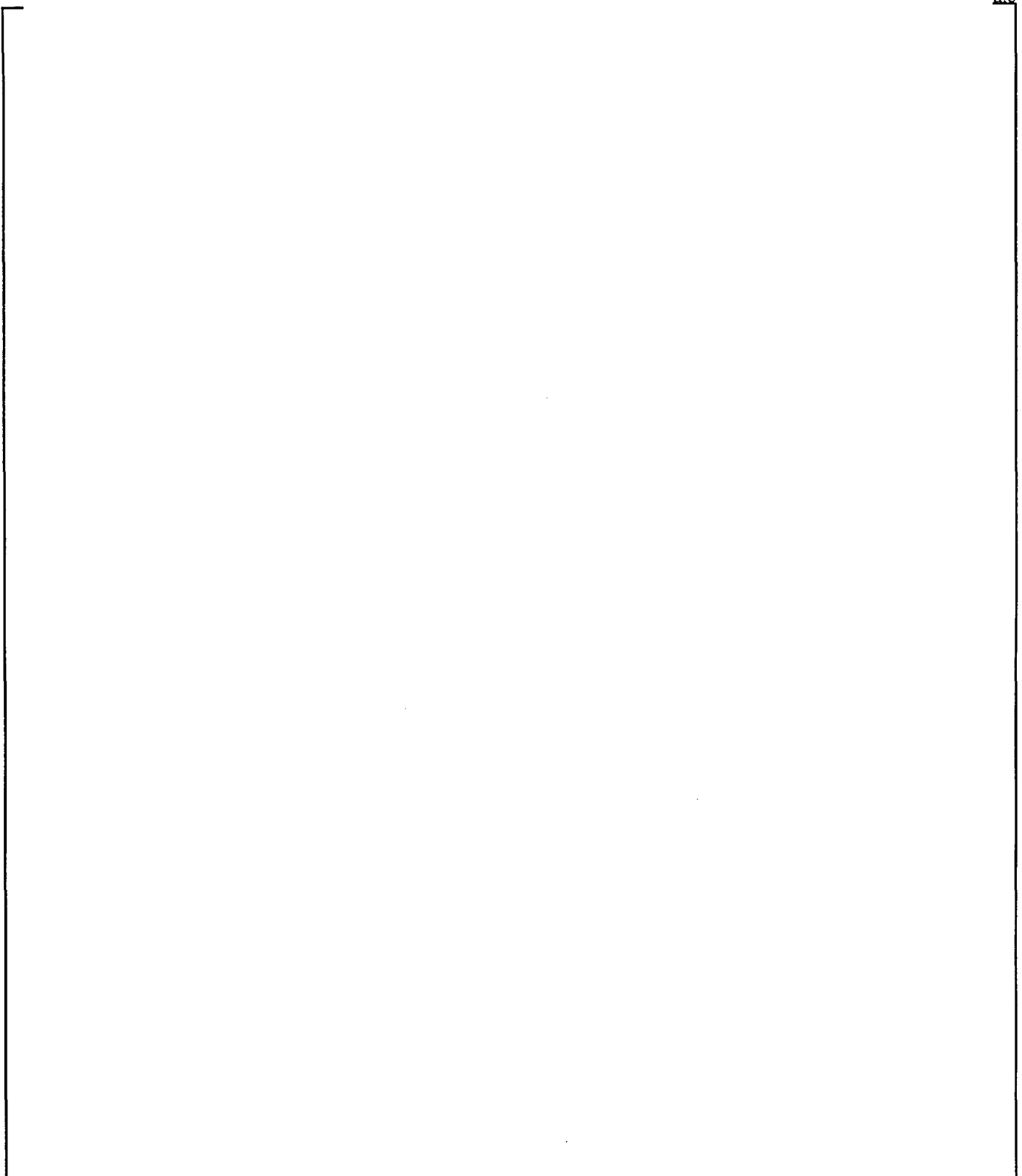


Figure 29-2-14. [
 F_Q Range

]^{a,c} in High



a.c

Figure 29-2-15. [

]^{a,c}

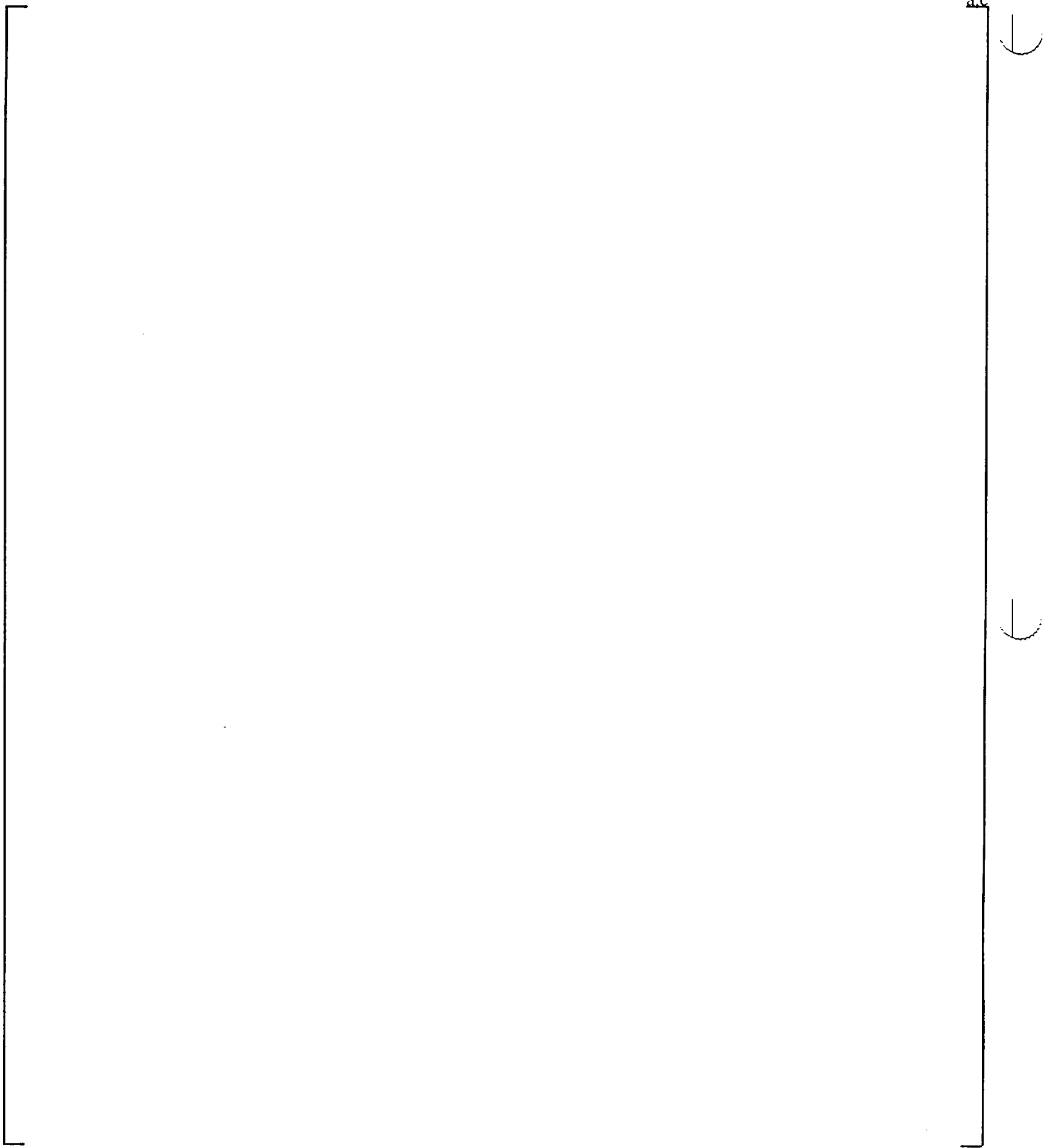
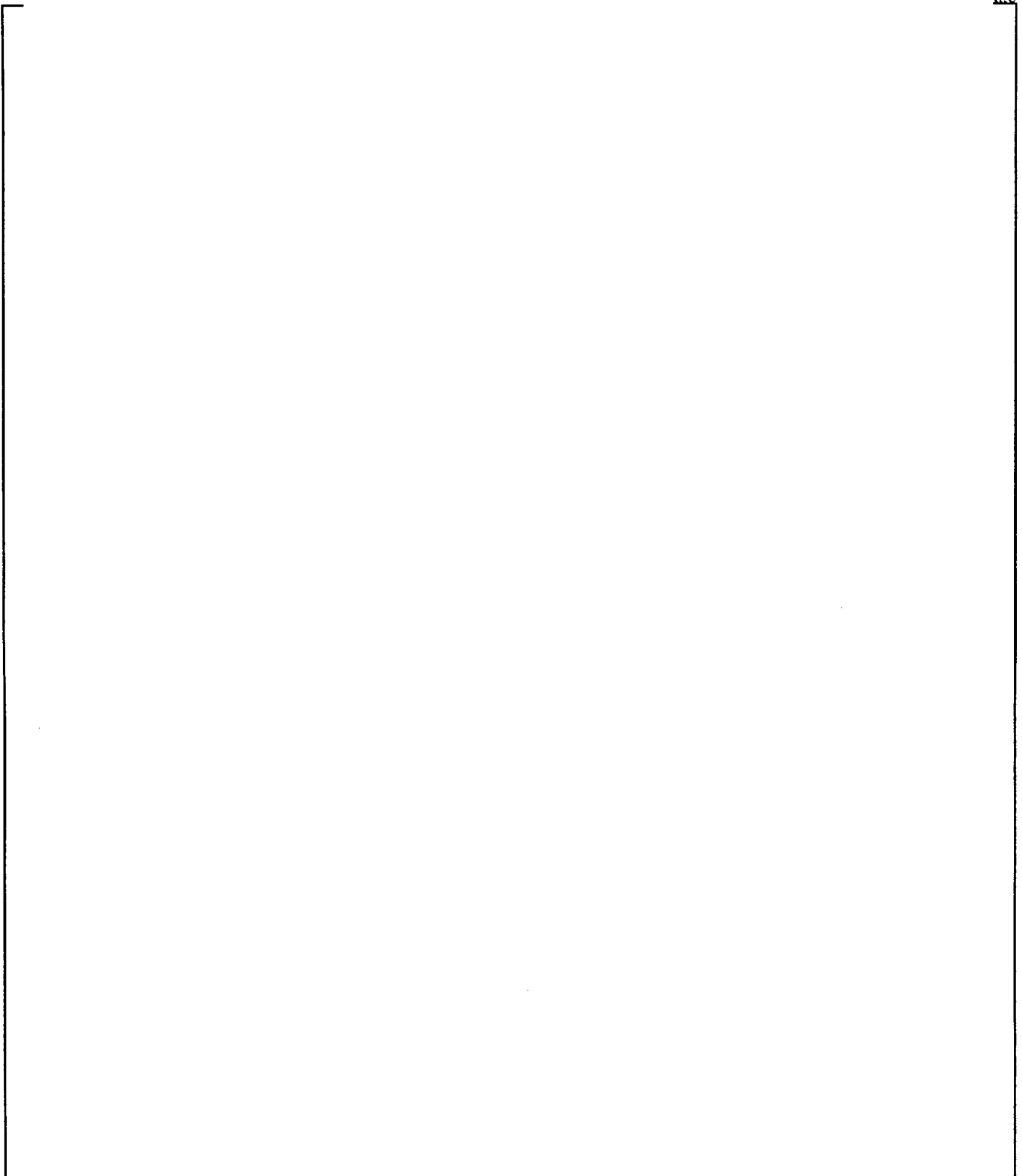


Figure 29-2-16. [

]^{a,c}



a.c

Figure 29-2-17. [
]^{a,c}



Figure 29-2-18. Power Shape 1

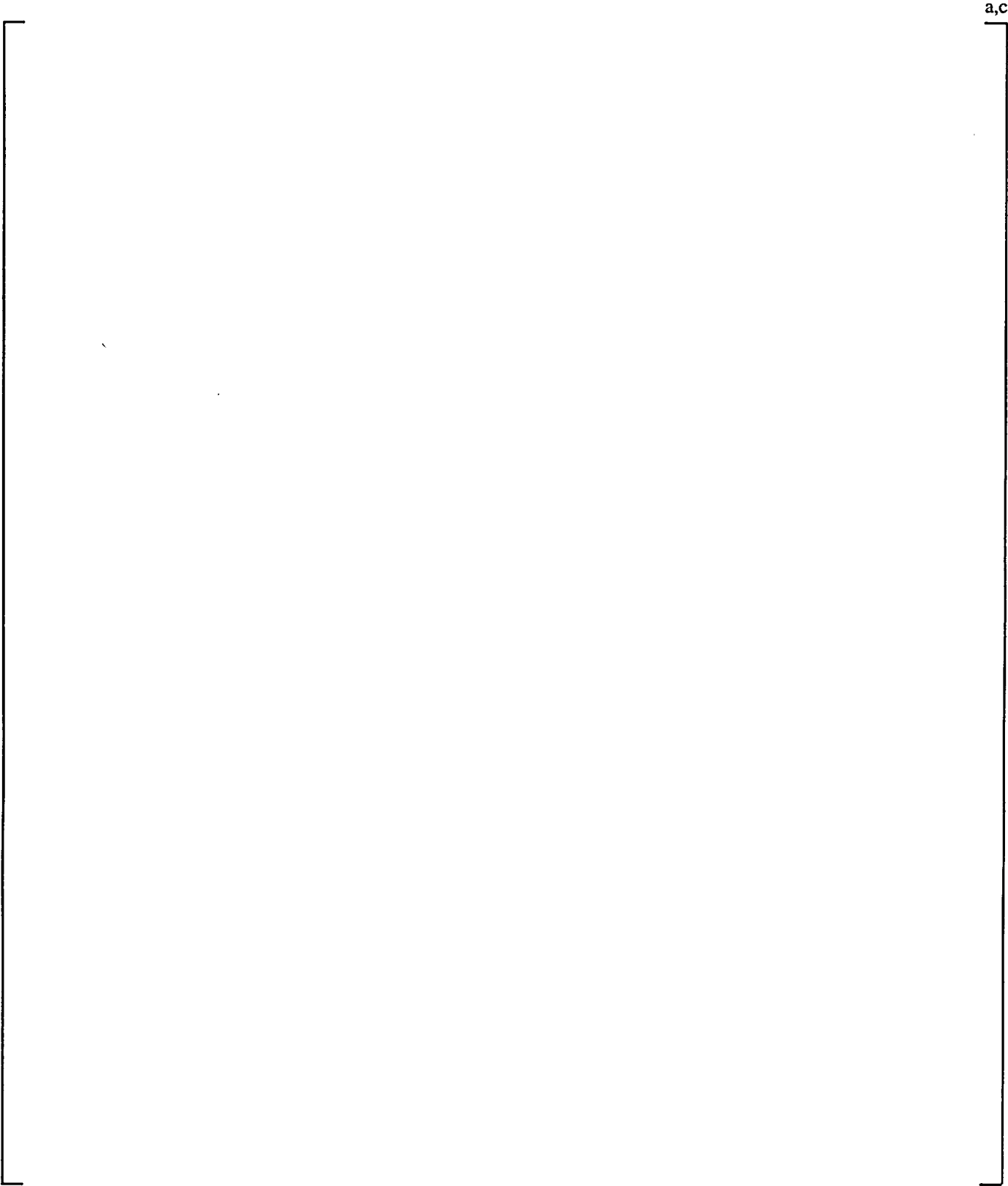


Figure 29-2-19. Power Shape 2

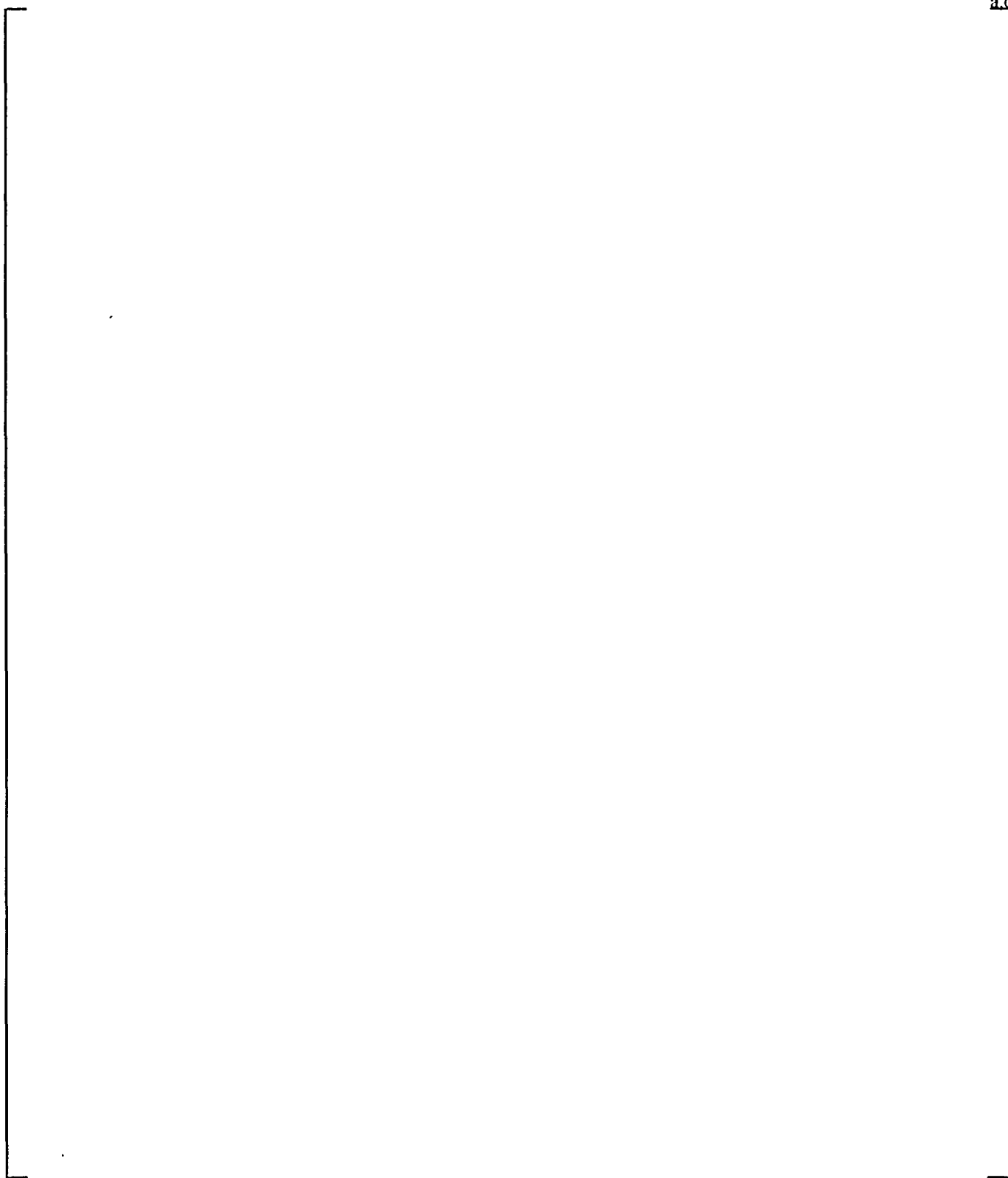


Figure 29-2-20. Power Shape 3

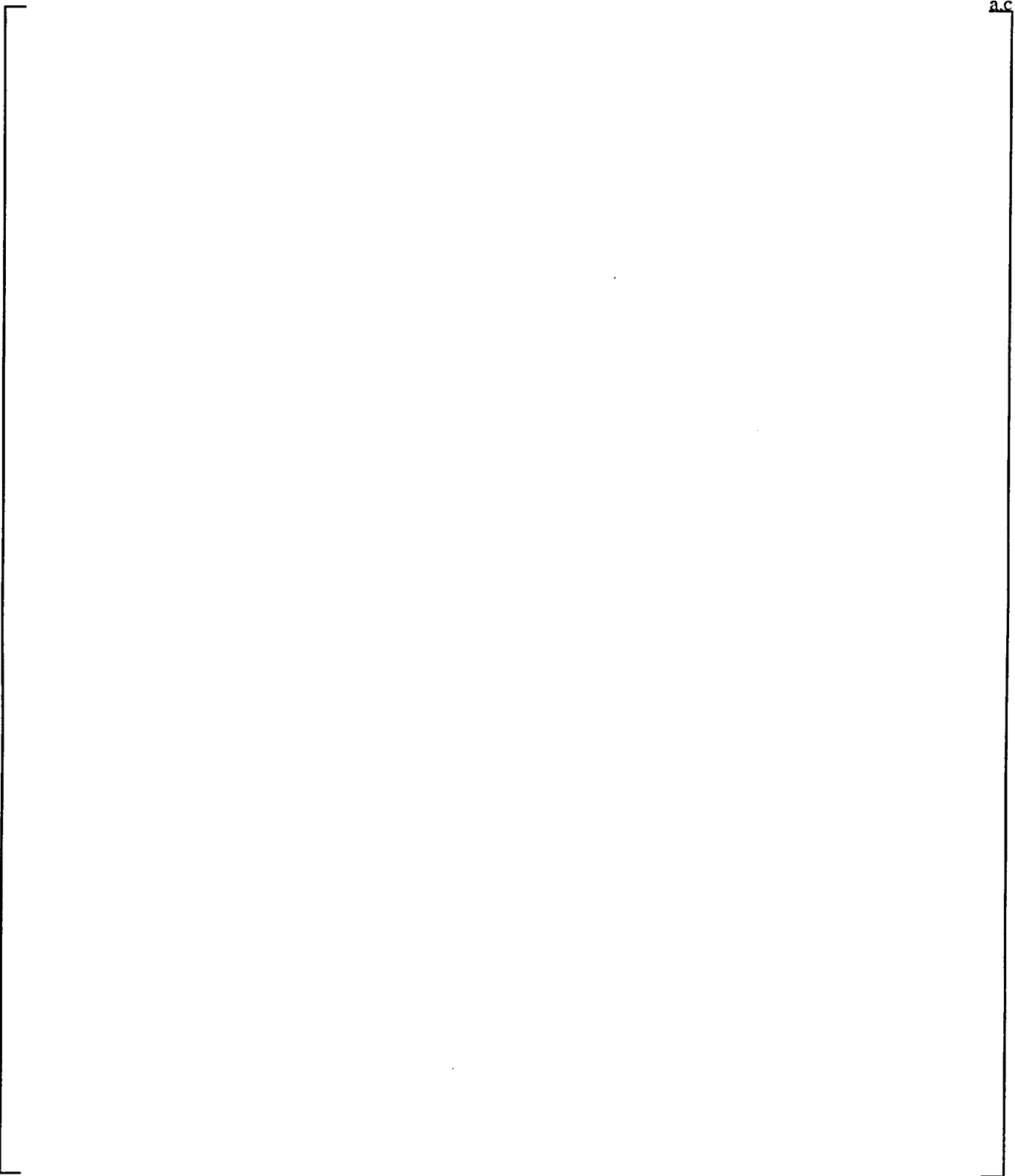


Figure 29-2-21. Power Shape 4

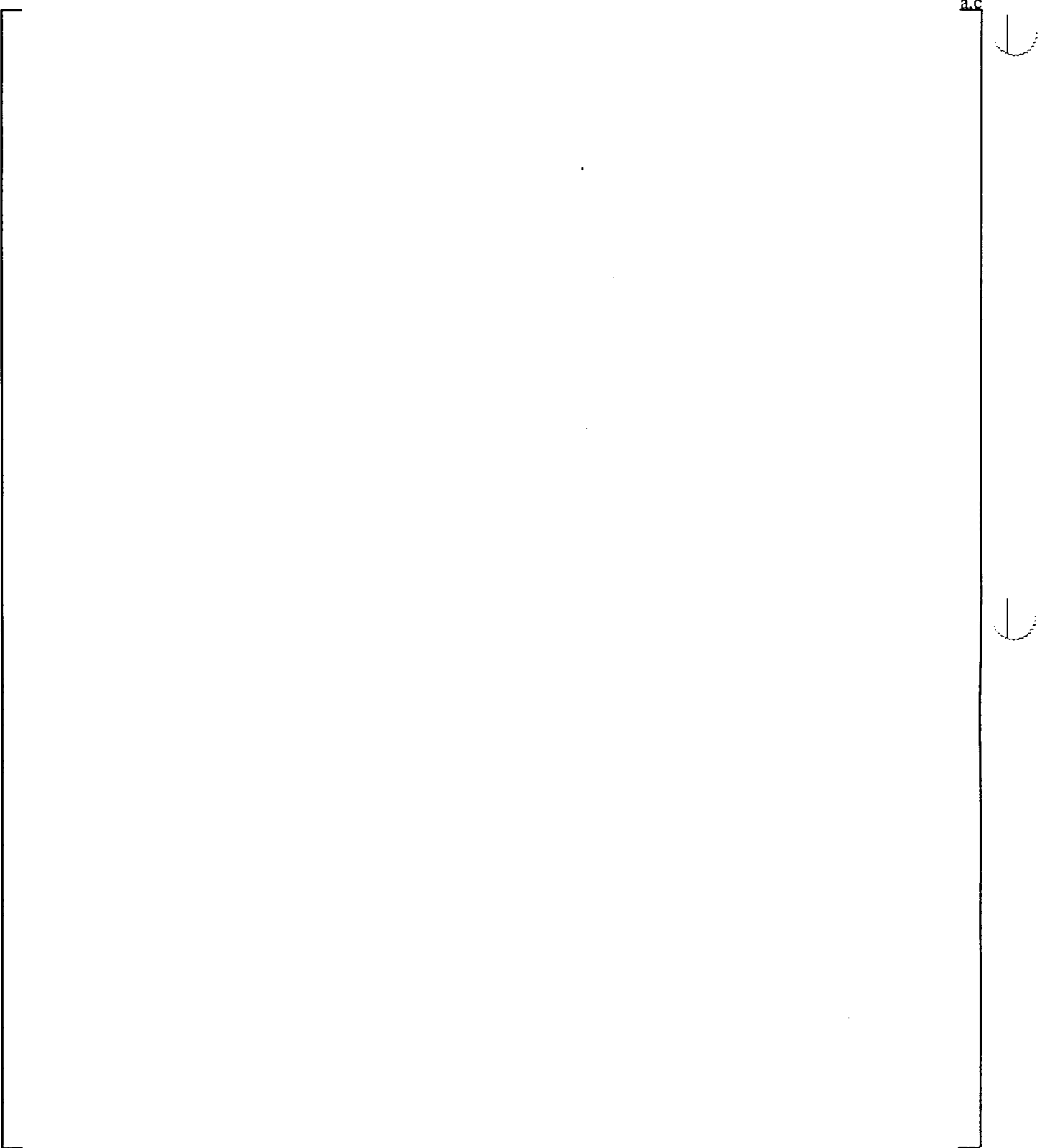


Figure 29-2-22. Power Shape 5

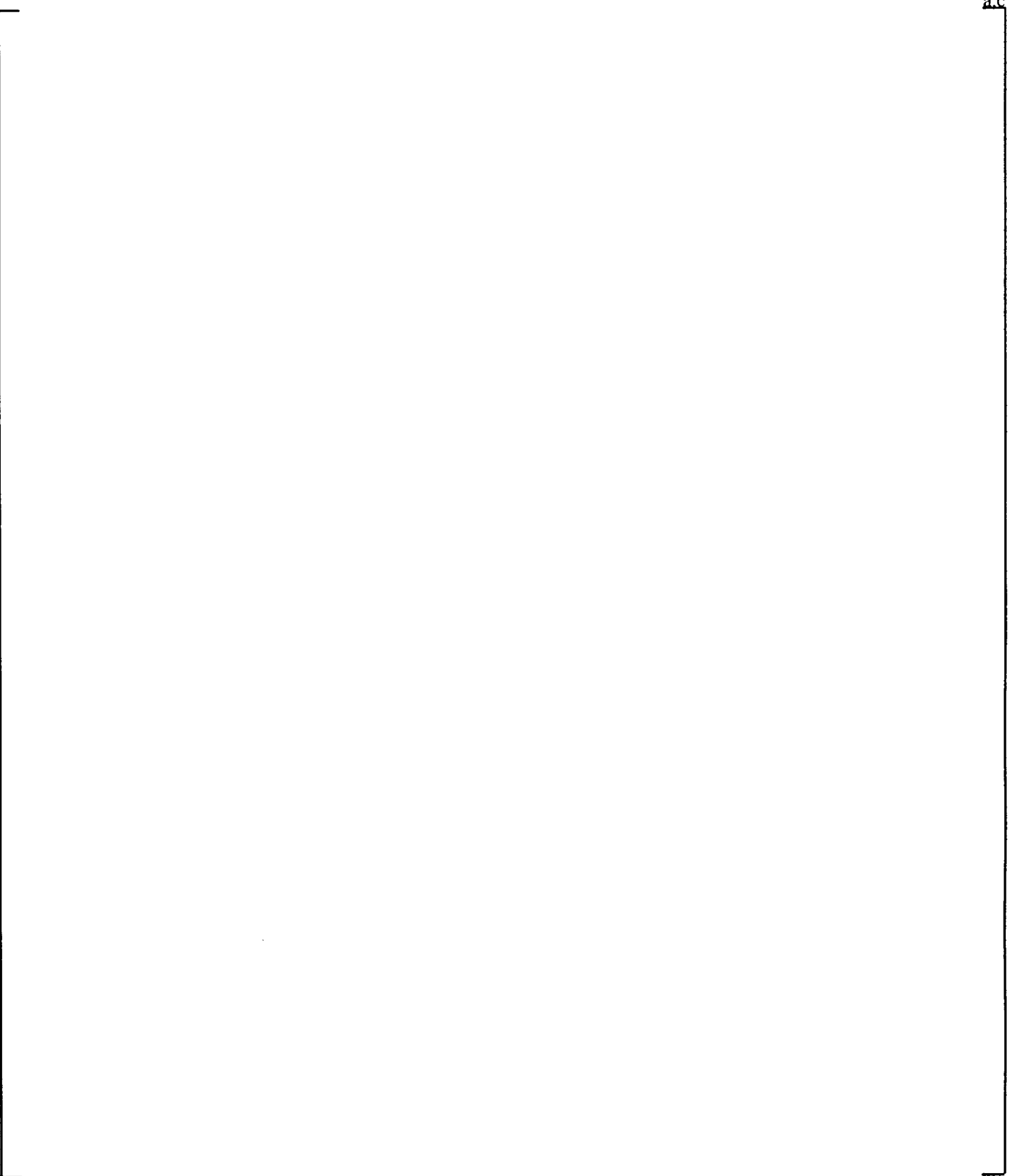


Figure 29-2-23. Power Shape 6

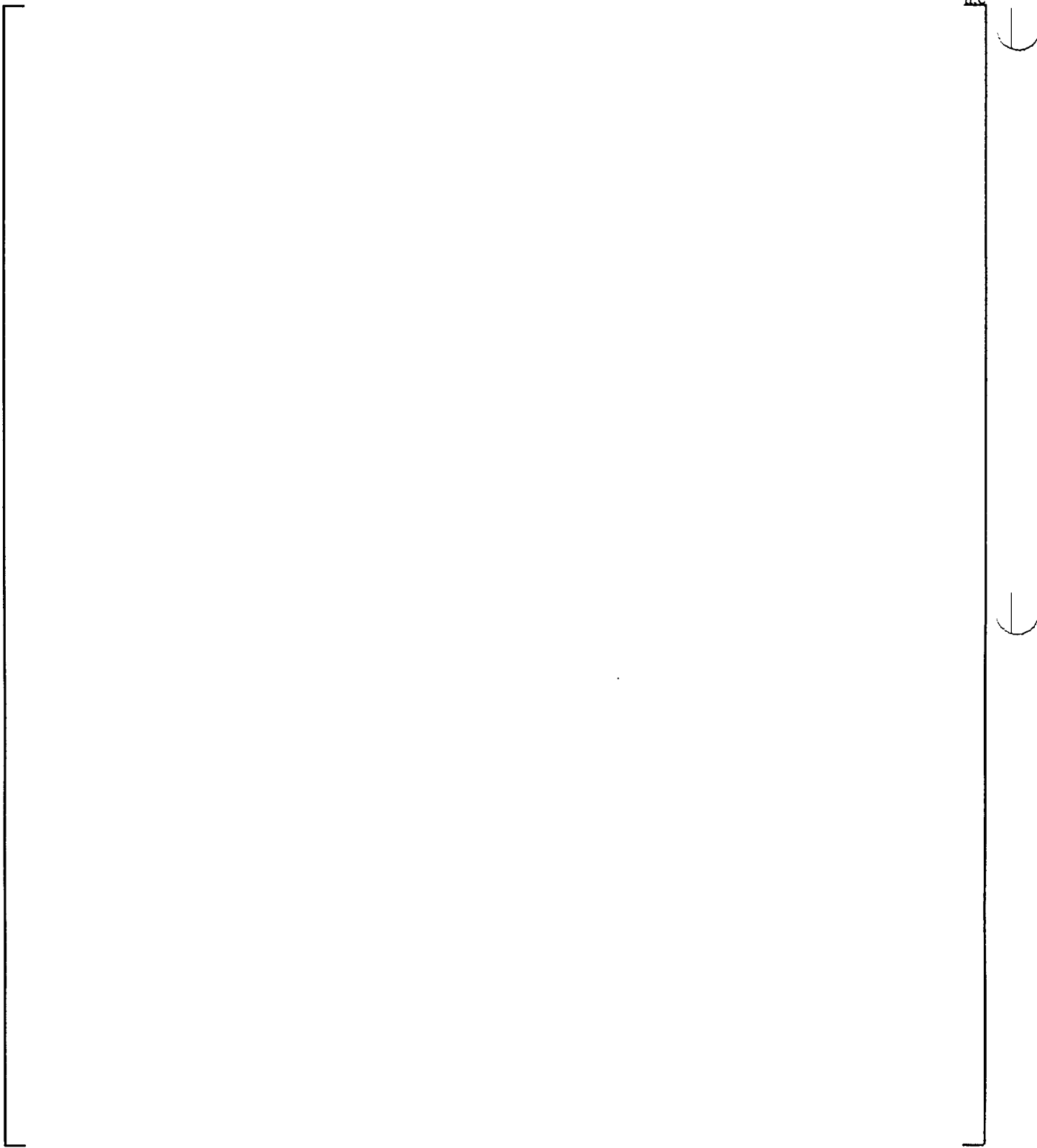
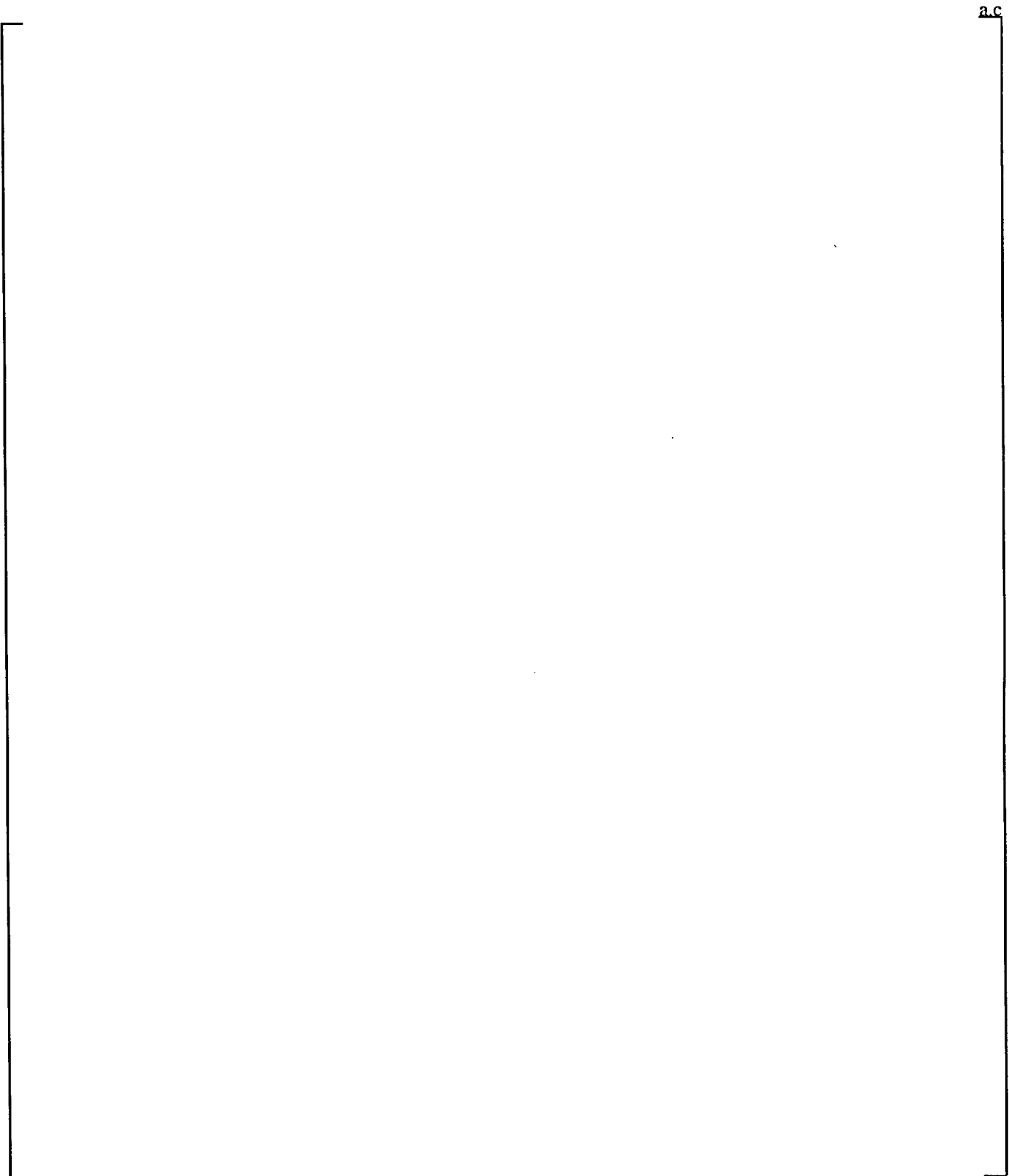


Figure 29-2-24. Power Shape 7



a.c

Figure 29-2-25. Power Shape 8

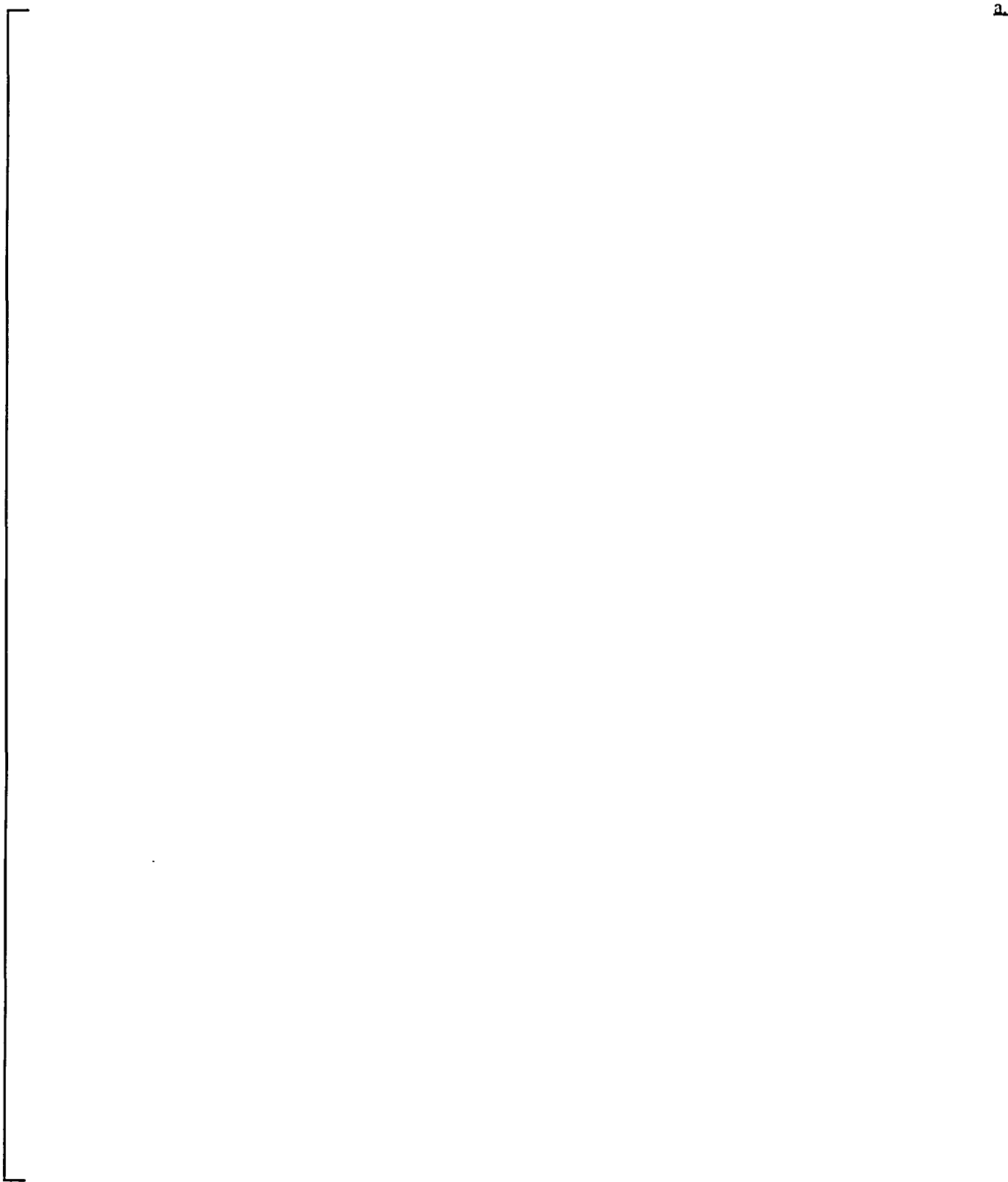


Figure 29-2-26. Power Shape 9

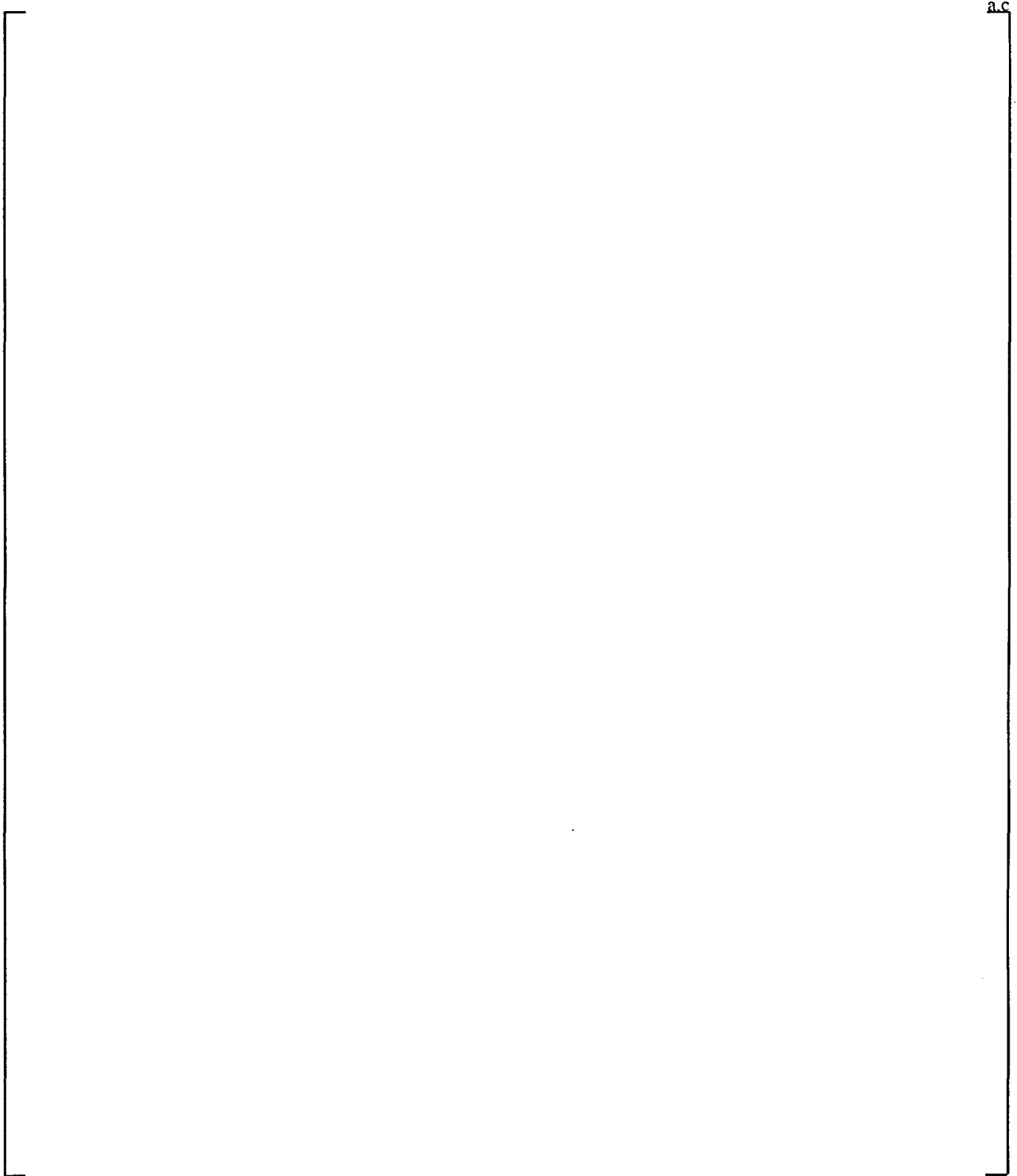


Figure 29-2-27. Power Shape 10

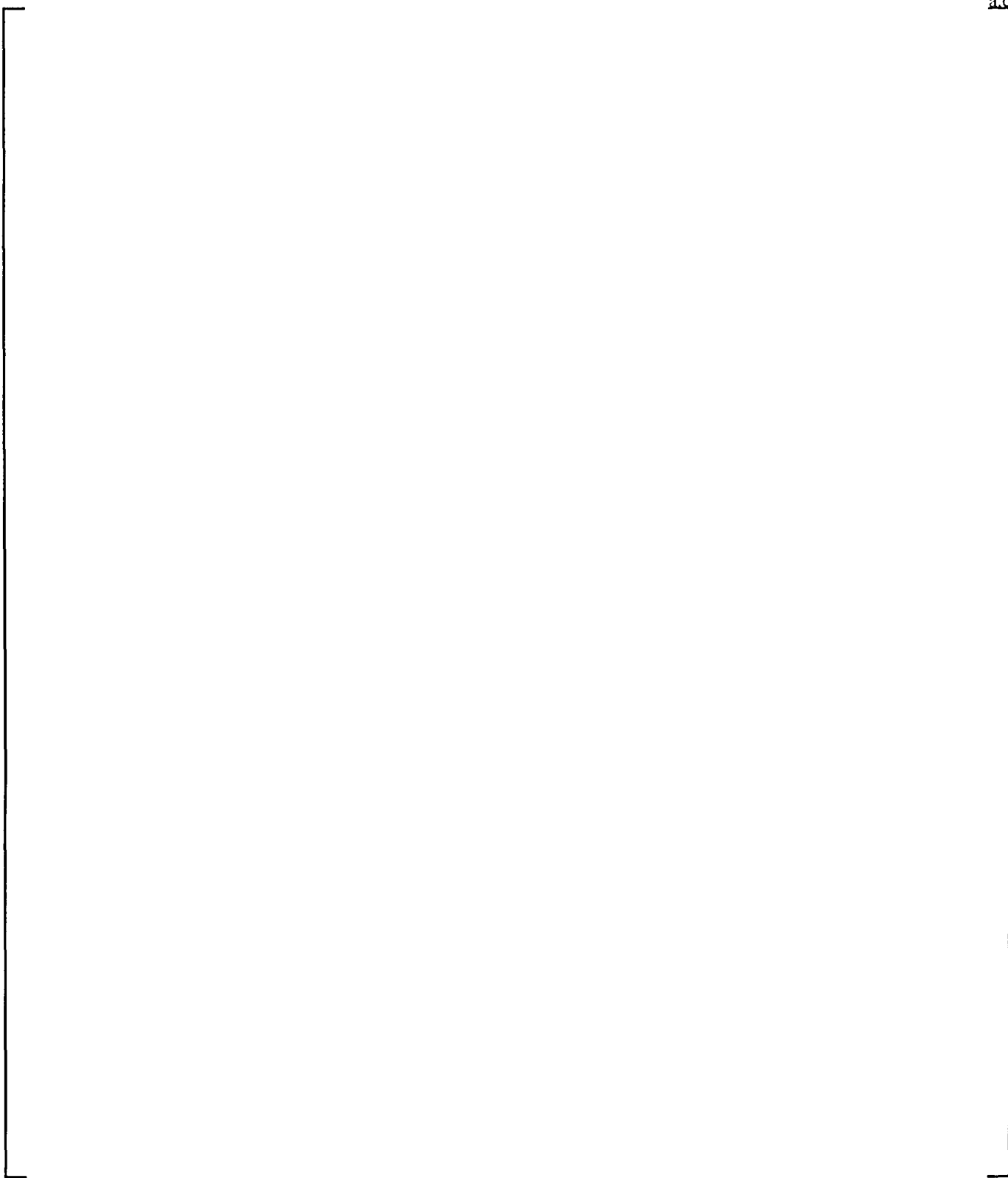


Figure 29-2-28. Power Shape 11

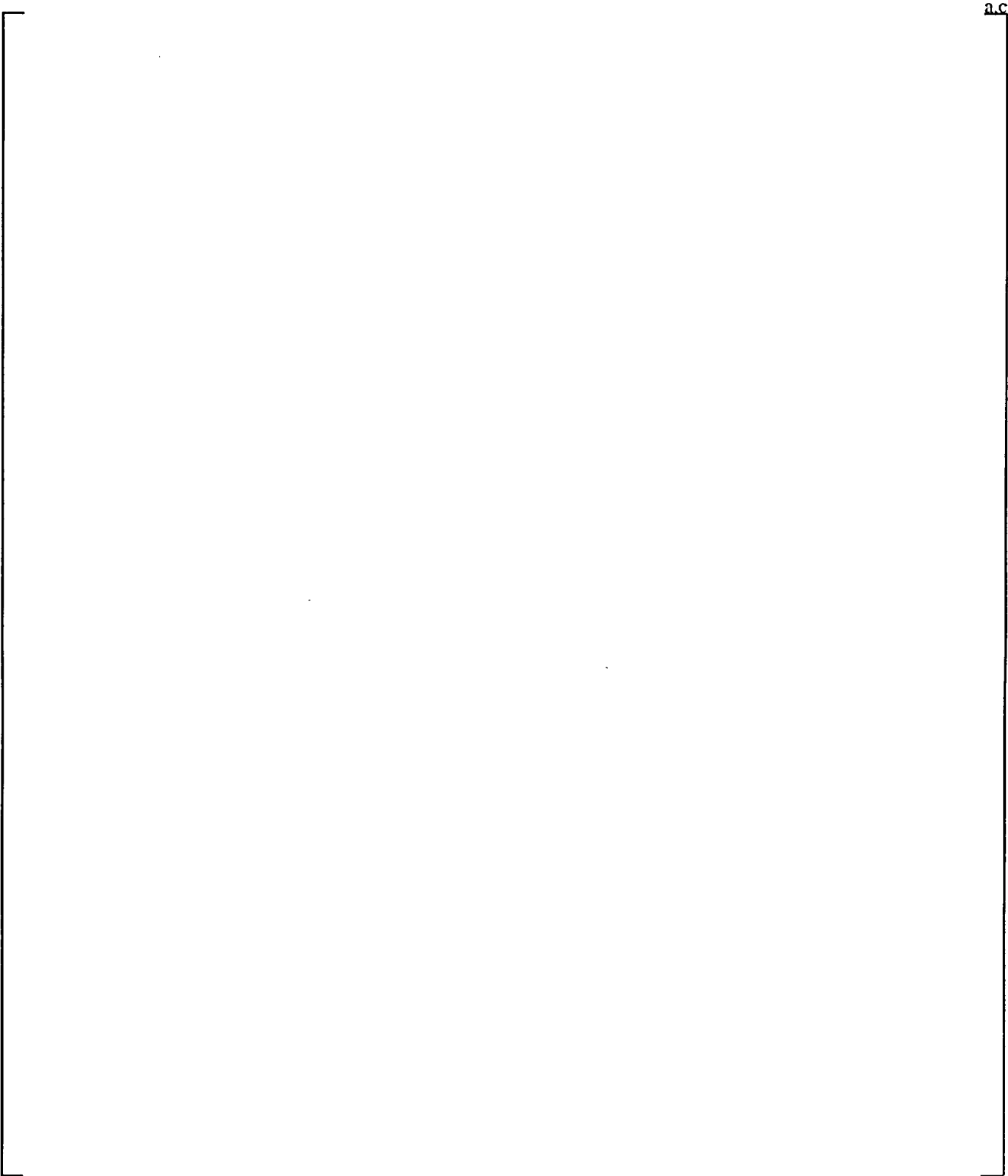


Figure 29-2-29. Power Shape 12



Figure 29-2-30. Power Shape 13

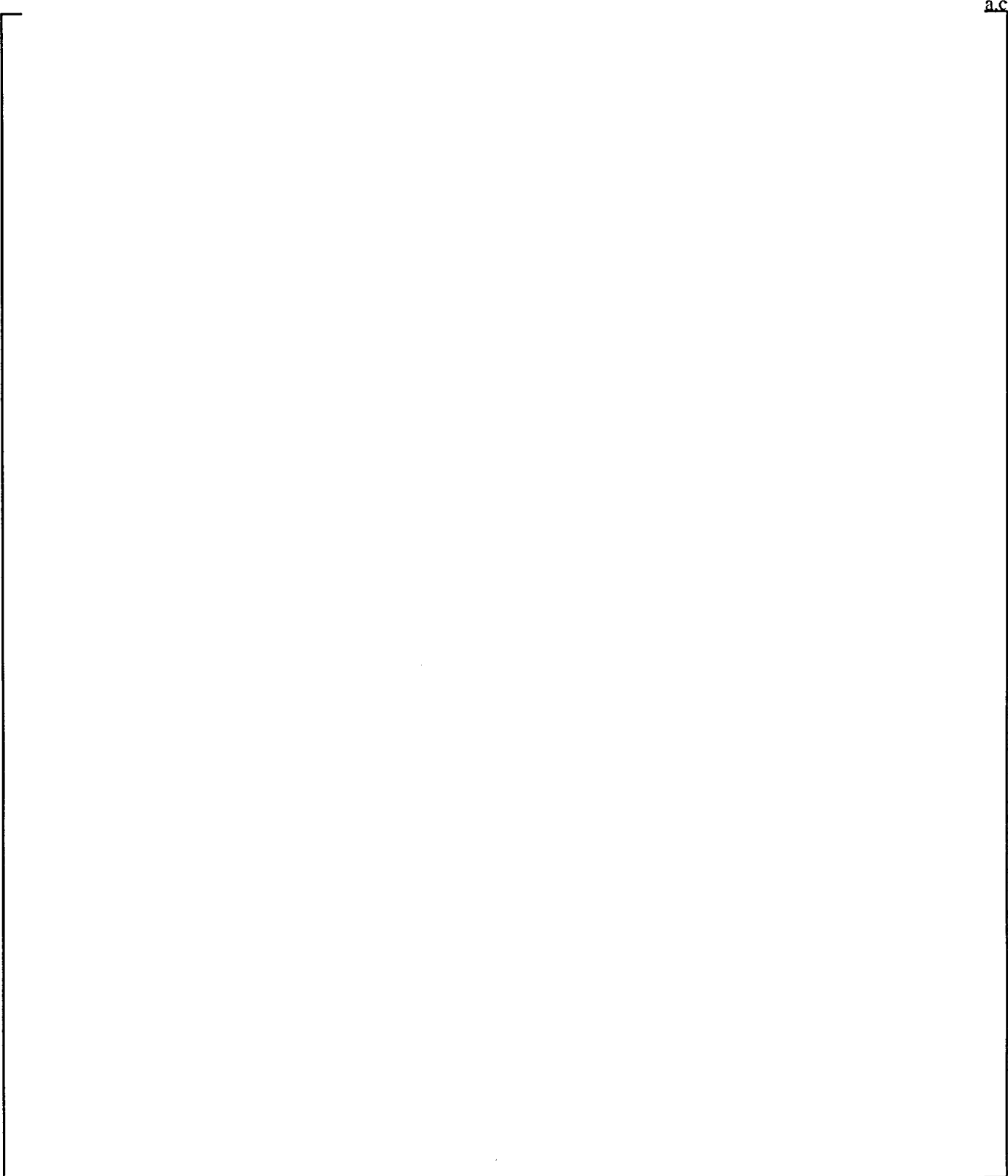


Figure 29-2-31. Power Shape 14

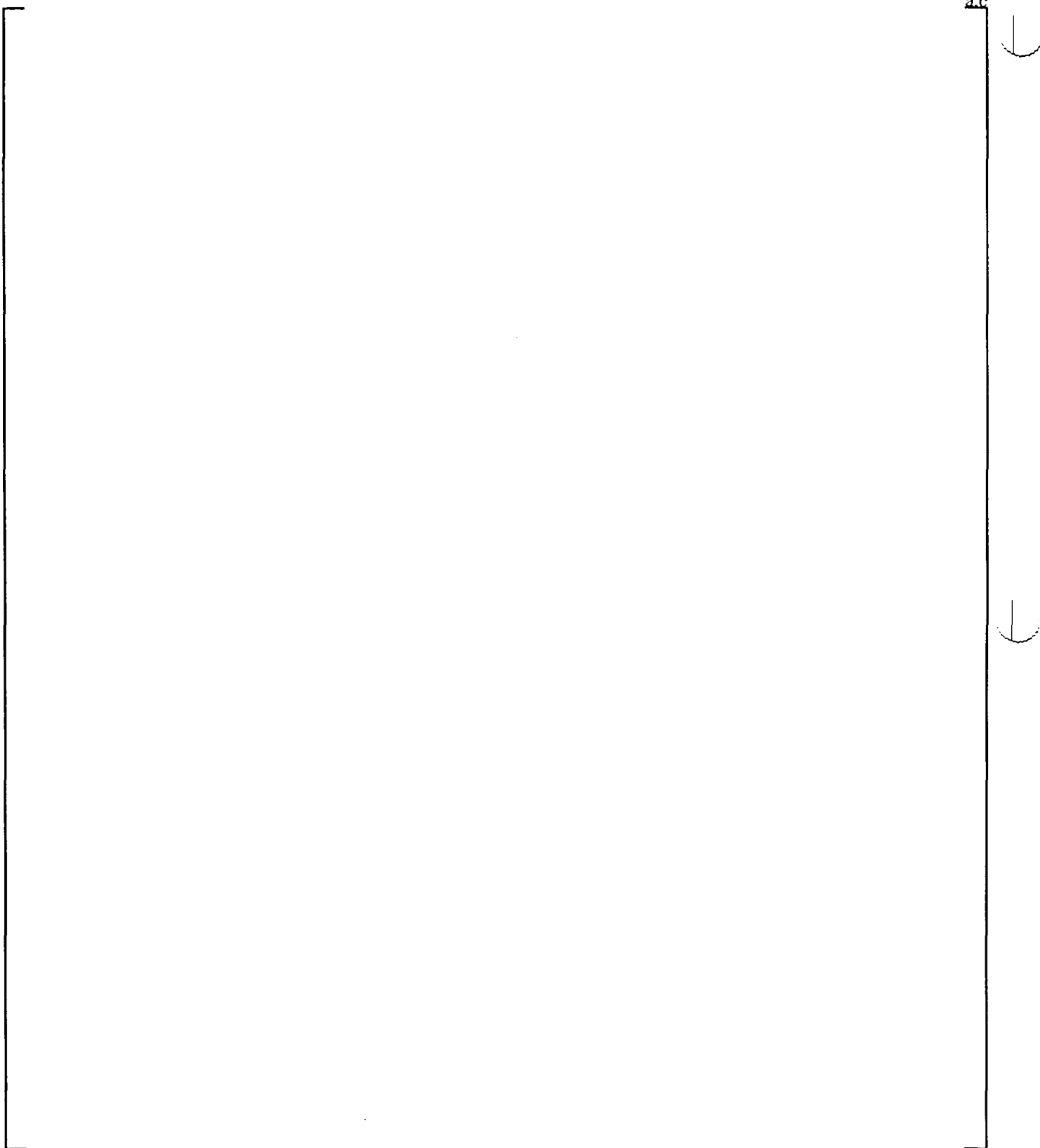
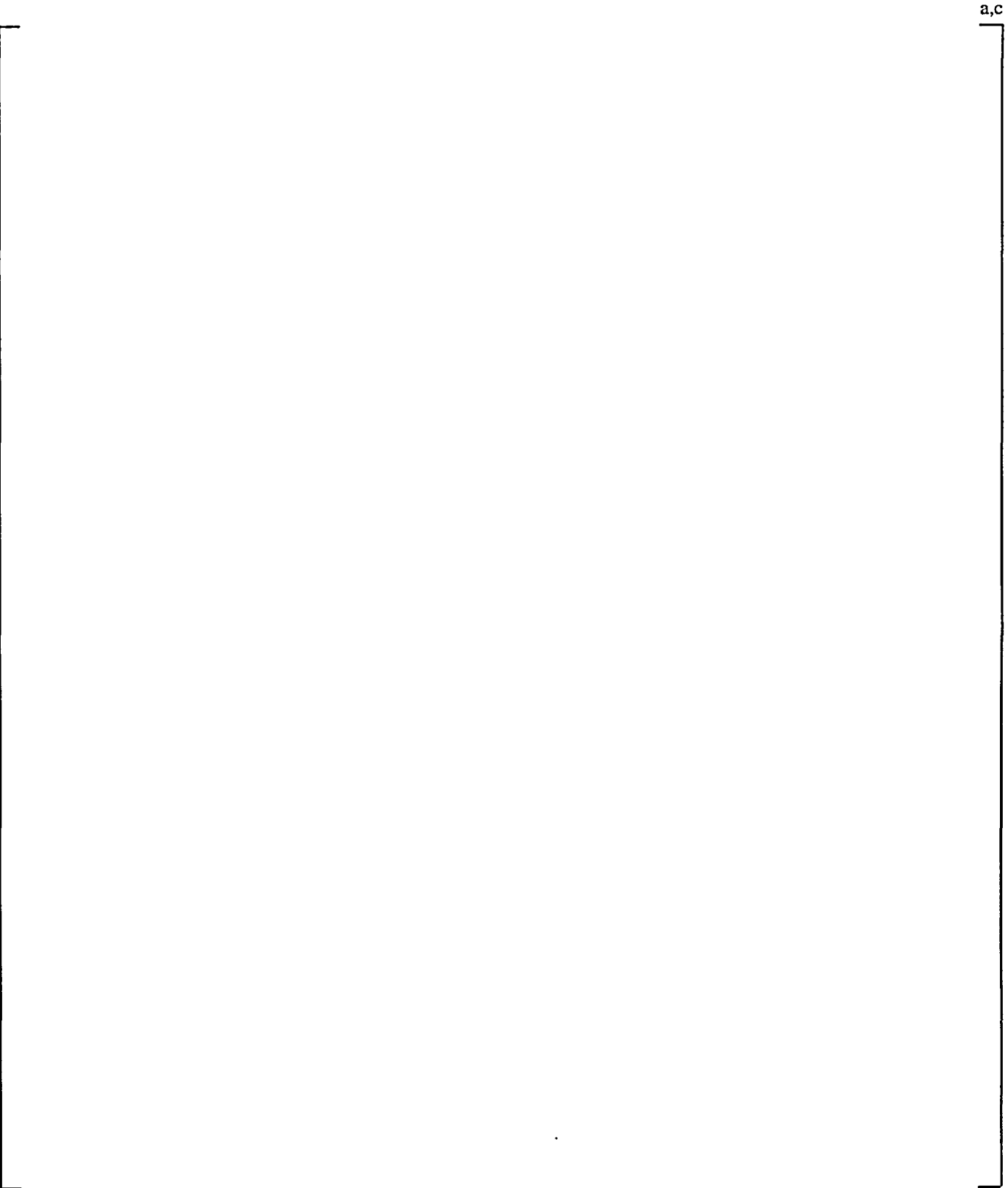


Figure 29-2-32. Power Shape 15



**Figure 29-2-33. WCOBRA/TRAC Axial Power Distribution for Rods 1 to 5,
Reference Case**

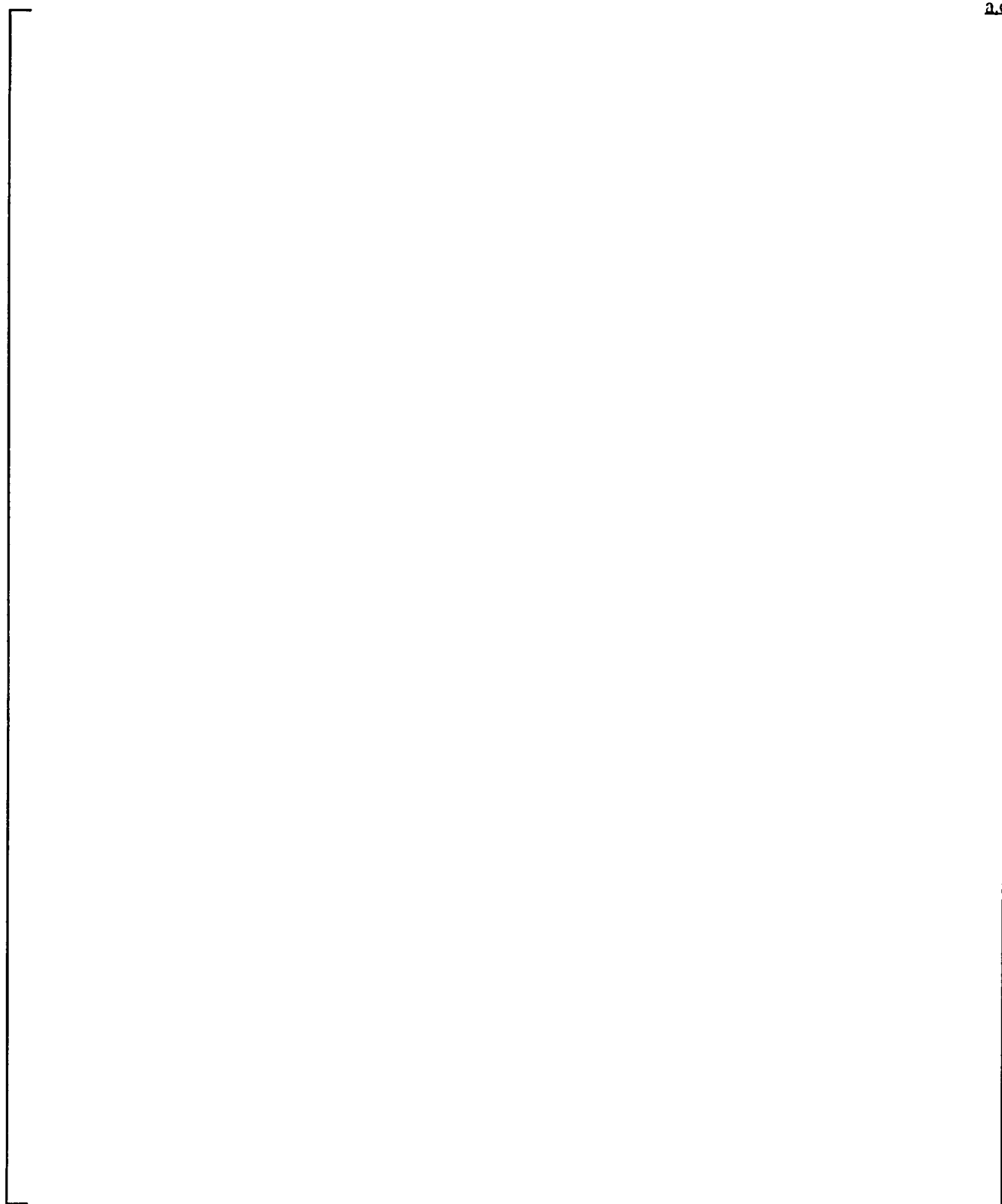


Figure 29-2-34. Relationship of Core Design Peaking Factors to LOCA Peaking Factors

29-3 Power Distribution Sensitivity Cases

This section describes the calculational results for the application of WCOBRA/TRAC-SB to Indian Point Unit 2 for small break LOCA for a bottom-skewed core power distribution and a top-skewed distribution, both of which differ from Figure 29-2-33. Core power distributions may be described in terms of four variables: []^{a,c}. A run matrix based on variations in these four quantities was used in the best estimate large break LOCA analyses (Section 26-3, Volume 5, of WCAP-12945-P-A [Bajorek et al., 1998]). The WCAP-12945-P-A shapes are the power shapes shown as Figures 29-2-18 through 29-2-32.

The power distribution parameters for the reference transient are biased to yield a relatively high PCT. The reference case uses []^{a,c}. This produces the power distribution shown in Figure 29-2-33.

The power shapes for this sensitivity study are the distributions shown in Figures 29-2-21 and 29-2-23 []

[]^{a,c}. Increasing the power generated in the bottom third of the core by skewing the power distribution to the lower third of the core is shown to be nonlimiting for small break LOCA transients. The second run, using power shape 4 (Figure 29-2-21) []

[]^{a,c}. Power shape 4 is similar to the reference case shape, but is slightly more top-skewed. The case examines the sensitivity of PCT to a minor power distribution change. It shows the impact of the WCOBRA/TRAC-SB bounding approach in the reference transient result in the best estimate small break LOCA analysis methodology.

29-3-1 Effects of Power Distribution Changes – Bottom-Skewed Shape

This section examines the effect of power distribution on parameters important to small break LOCA. Among the parameters examined are core collapsed liquid level, hot assembly collapsed liquid level, hot rod PCT, and break flow. The calculations are performed assuming a 3-inch cold leg break with loss of offsite power (LOOP) as in the reference case. The only change from the reference case is the power distribution.

In the case analyzed, [

]^{a,c} These shifts alter the timing at which the core uncovers.

The analysis of the Figure 29-3-1 shape, with high power at the bottom of the core, shows increased boiling and level swell in the lower part of the core. This leads to a lower collapsed level in the time period both before and after loop seal clearance (Figure 29-3-2) than the reference case (Figure 29-3-4, solid curve). Furthermore, the hot assembly collapsed liquid level at which the bottom-skewed case uncovers is 7.6 feet, as opposed to 8.1 feet in the reference case, because the increased power in the core beneath the core mid-plane elevation is swelling the mixture in the Figure 29-3-1 shape case more than the reference case. The core uncovers earlier in the reference case (Figure 29-3-5, solid curve) than in the bottom-skewed case (Figure 29-3-3). When the core starts to refill, the collapsed liquid level increases rapidly in the bottom-skewed case to recover the core. The effect of moving power toward the top of the core is to cause the core to uncover earlier and to delay the recovering of the core.

The earlier uncovering of the core in the reference case occurs at a reactor vessel inventory of 97,000 pounds versus 93,000 pounds in the bottom-skewed case. Beyond the fact that core uncover occurs at a higher mass, increased power in the upper part of the core also leads to a significantly higher PCT in the reference case. The high power at the top of the core represents the limiting case for small break LOCAs.

29-3-2 Variation in Top-Skewed Power Distribution

With the top-skewed power distribution established as limiting, an Indian Point Unit 2 case was executed using power shape 4 [

]^{a,c}. The overall behavior is expected to be similar to that of the reference case. However, as illustrated in Figures 29-3-4 through 29-3-9, a large impact occurs. The effects that predominate are due to variations in clearing loop seals, similar to that observed in the SGTP sensitivity reported in Section 28, Volume 3. Figure 29-3-4 compares the collapsed core liquid level of the power shape 4-based case (dashed line) with the reference case (solid line), and Figure 29-3-5 compares the PCT prediction with the Shape 4-based case (again, the dashed line). No heatup is shown for the power shape 4-based case because no core uncover occurs due to the increase in reactor vessel inventory from the clearing of two loop seals, including the broken loop seal.

The loop seal clearance behaviors of the two cases are presented in Figure 29-3-6. The total steam flow through the two loop seals that clear in the power shape 4-based transient (dashed curves) agrees closely with the steam flow through the one cleared loop seal (solid line) in the reference case. Although the steam venting capability is more than adequate with only one loop seal clearing, the difference is in the water present in the reactor vessel. As shown in Figure 29-3-7, the reactor vessel fluid mass in the reference case (solid line) is well below that of the power shape 4-based case (dashed line). The initial point of departure of the two occurs at the time of loop seal clearance. Figure 29-3-8 shows that almost an additional 4000 pounds of water is swept from the loop seals in the (dashed line) power shape 4-based case at the time of clearance; this liquid is shortly thereafter delivered to the downcomer to increase reactor vessel inventory. The divergence in reactor vessel inventory between the top-skewed shapes widens as time proceeds because the break flow in the power shape 4-based case is reduced. Figure 29-3-9 presents the integrated break flow comparison between the reference case (solid line) and the power shape 4-based case to illustrate this behavior. The difference in break flow between the cases is liquid flowing to the break from the downcomer. After being almost identical for the two cases through loop seal clearance, between 900 and 2000 seconds the break flows diverge; approximately 11,000 pounds more liquid flows out through the break in the reference case than in the power shape 4-based case as a consequence of greater liquid flow to the break from the downcomer.

The impact of varying the nature of the top-skewed power distribution slightly is far greater than is reasonably anticipated. It is attributable to the difference in loop seal clearing predictions for a small perturbation to the boundary conditions. The overall loop seal clearing process – which consists of the level depression, incipient blowout of a seal, short-term partial replugging, subsequent possible oscillations between loops, and longer term sweep out of the piping – is complex, as previously discussed in Section 27. Because the process is so complex, it represents a scatter that can vary greatly in each of four loops and in the aggregate final effect on the post-seal clearing vessel inventory. The behavior observed is comparable to that observed in the SGTP sensitivity case in Section 28, Volume 3. As in Section 28, the prediction of loop seal clearing leads to a major change in PCT for a minor change in conditions.

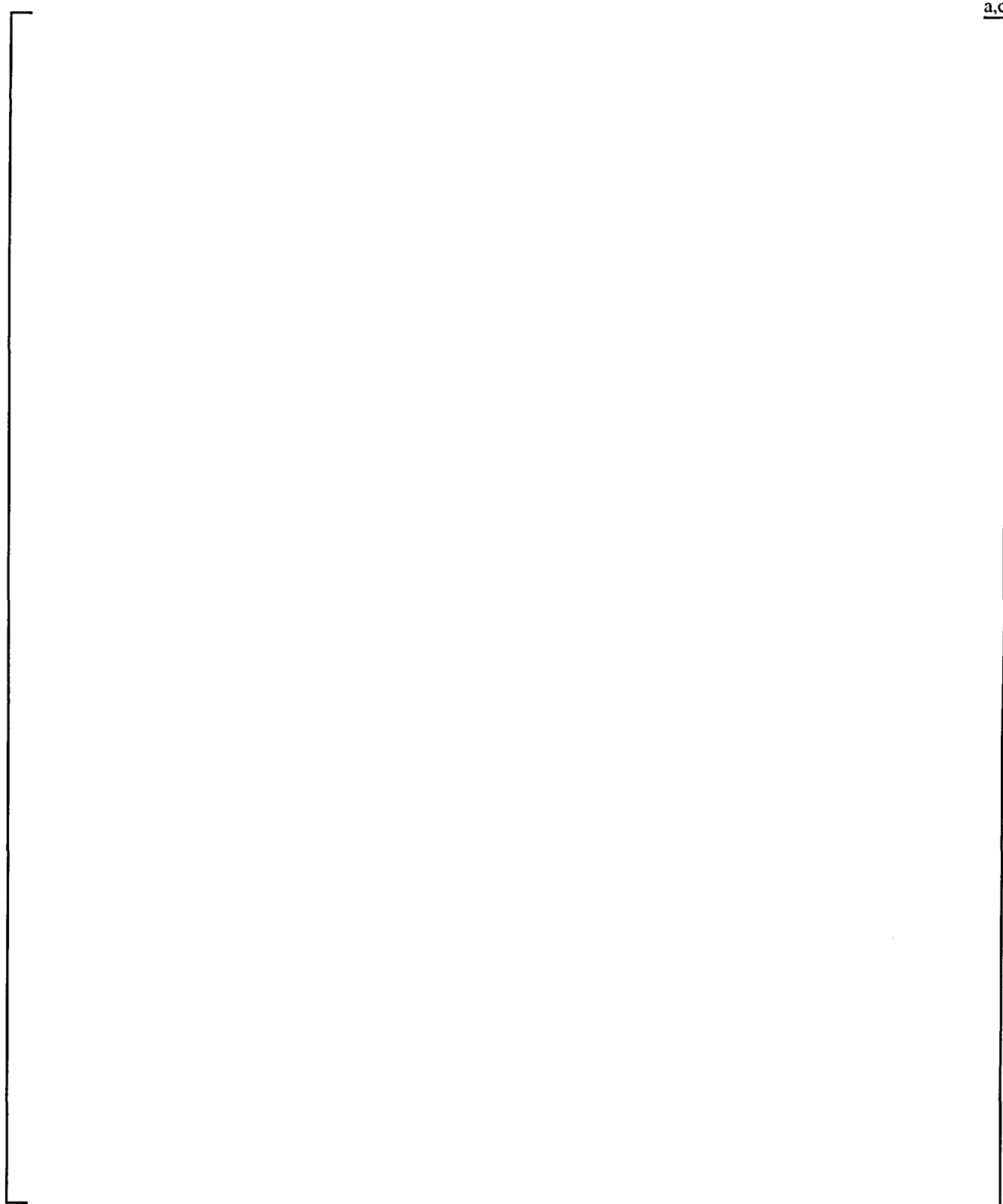


Figure 29-3-1. Bottom-Skewed Power Shape

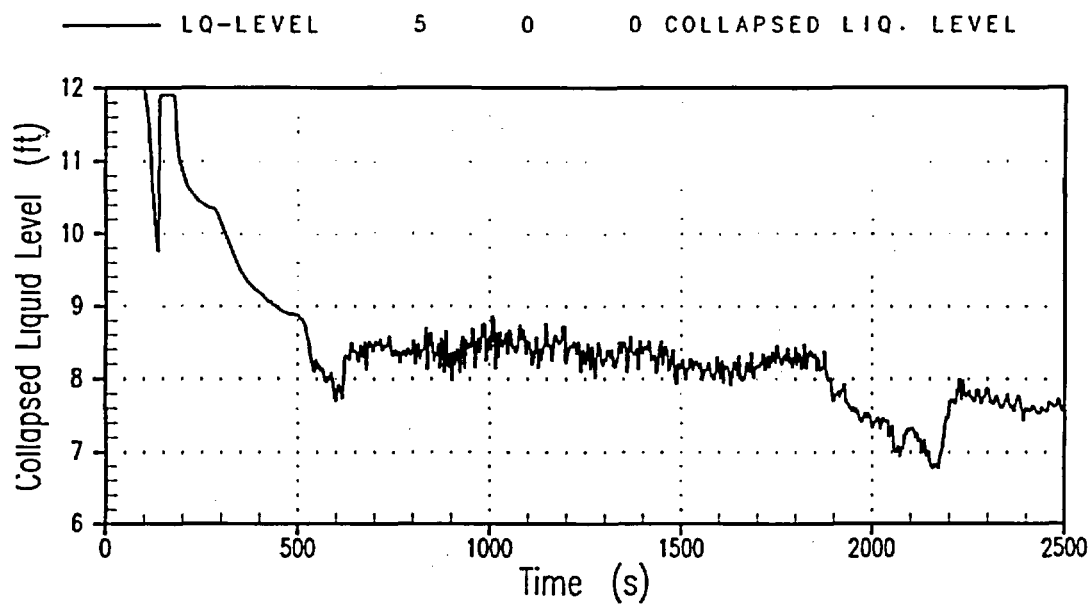


Figure 29-3-2. Core Collapsed Liquid Level, Bottom-Skewed Shape

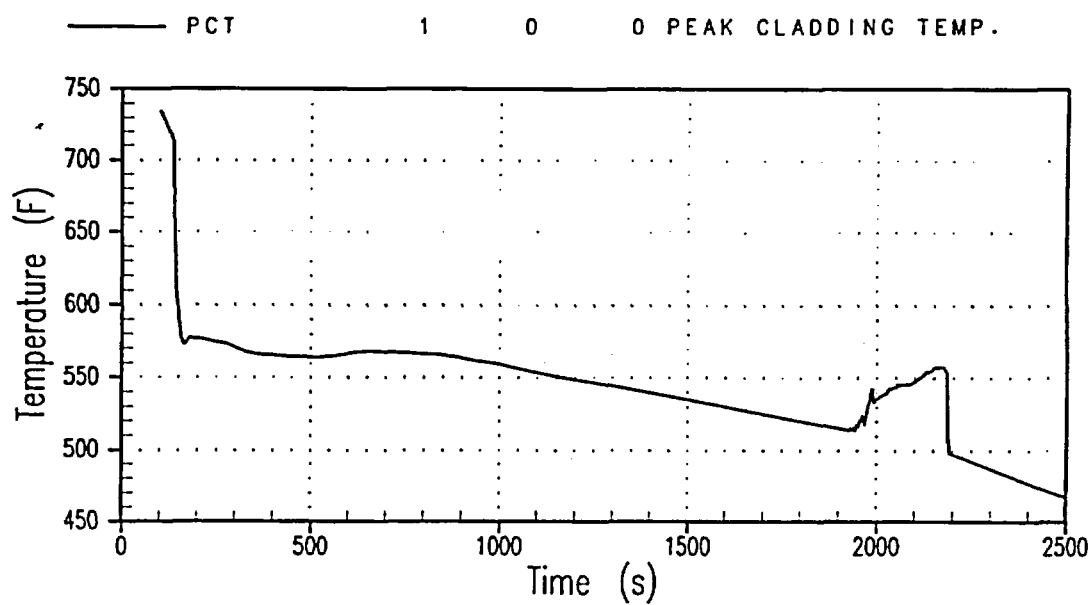


Figure 29-3-3. PCT for the Bottom-Skewed Shape

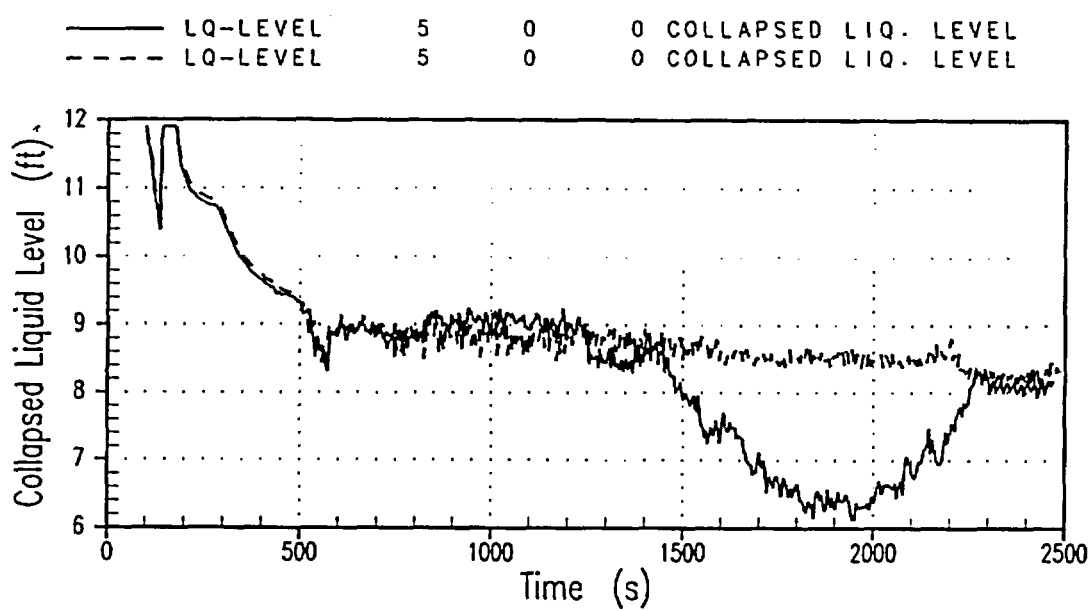


Figure 29-3-4. Hot Assembly Collapsed Liquid Level, Reference Case and Power Shape 4

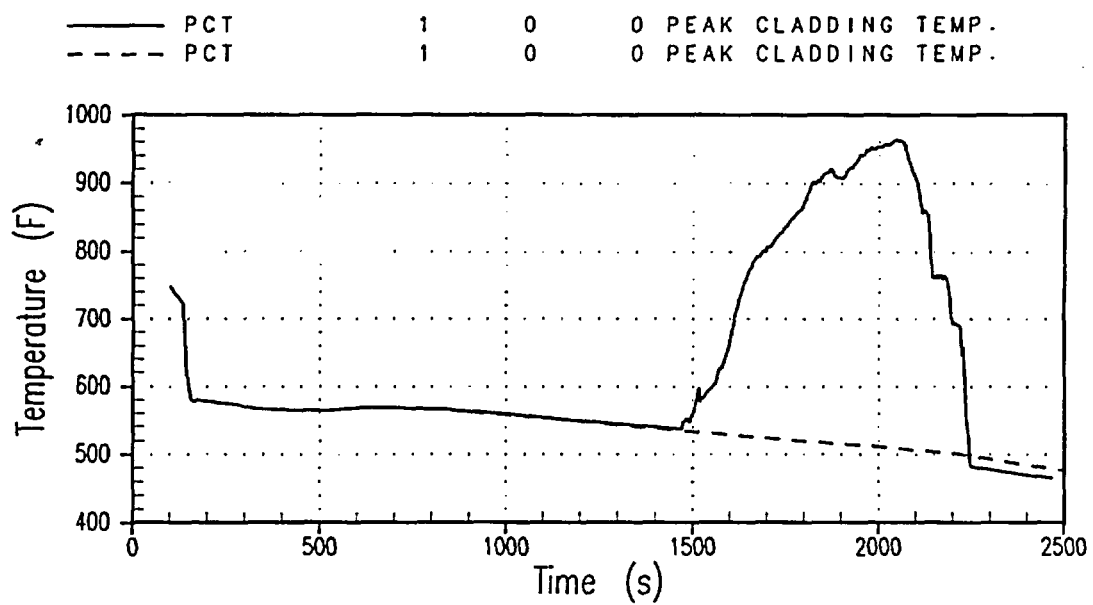


Figure 29-3-5. PCTs for Reference Case and Power Shape 4

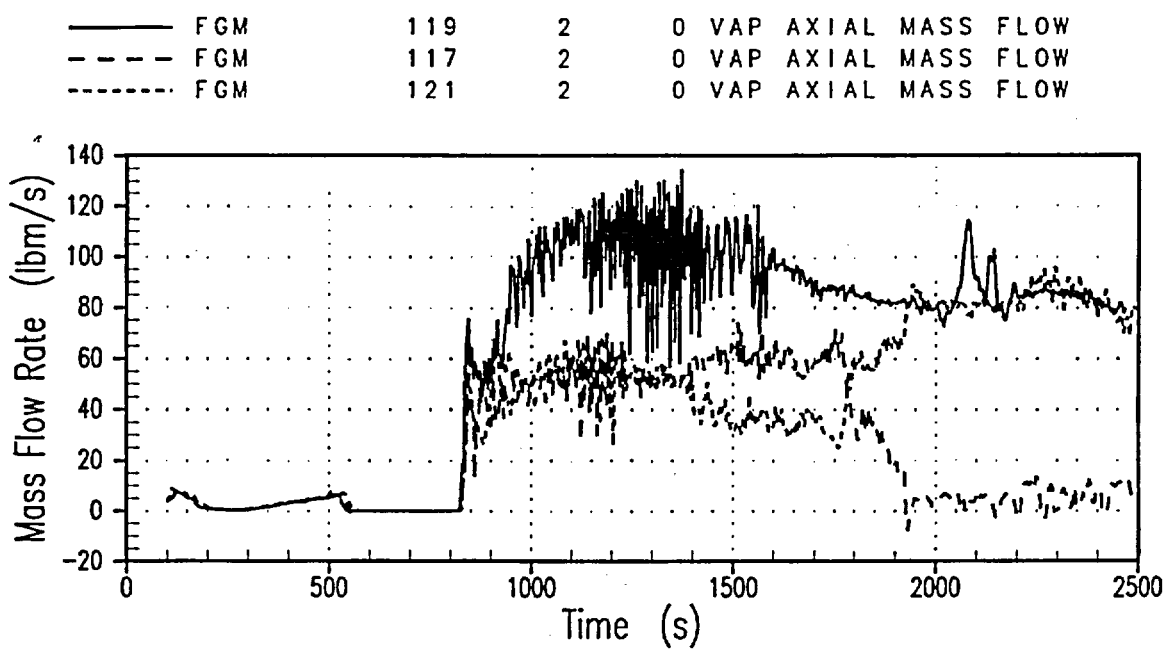


Figure 29-3-6. Loop Seal Steam Flowrate for Power Shape 4 Compared to Reference Case

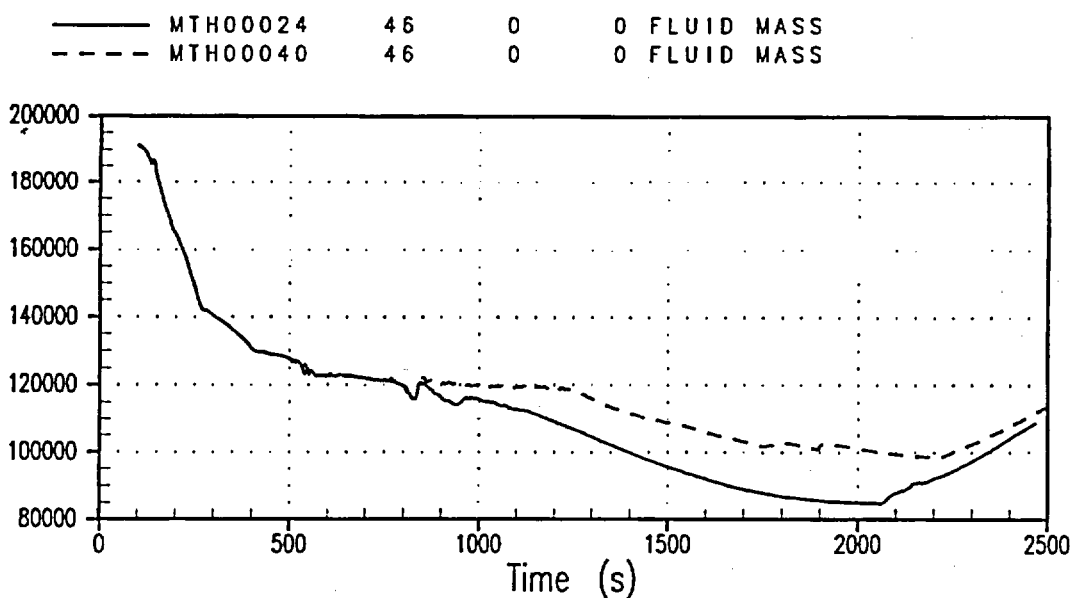


Figure 29-3-7. Reactor Vessel Mass Comparison Between Power Shape 4 and Reference Case

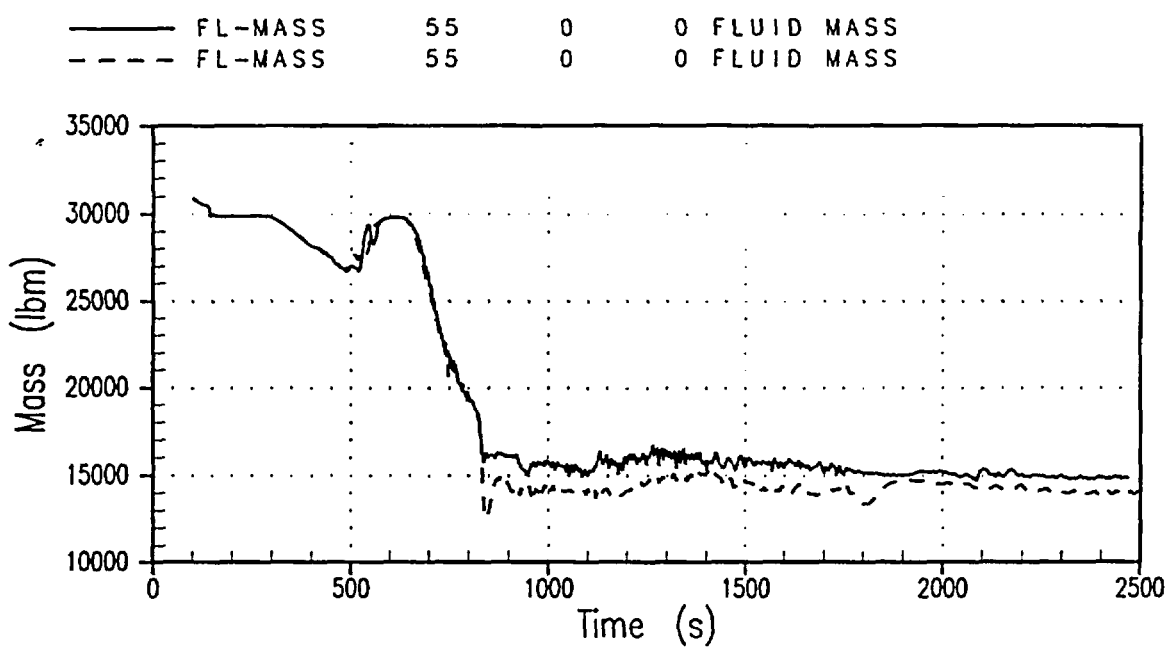


Figure 29-3-8. Power Shape 4 Total Loop Seal Mass Compared to Reference Case

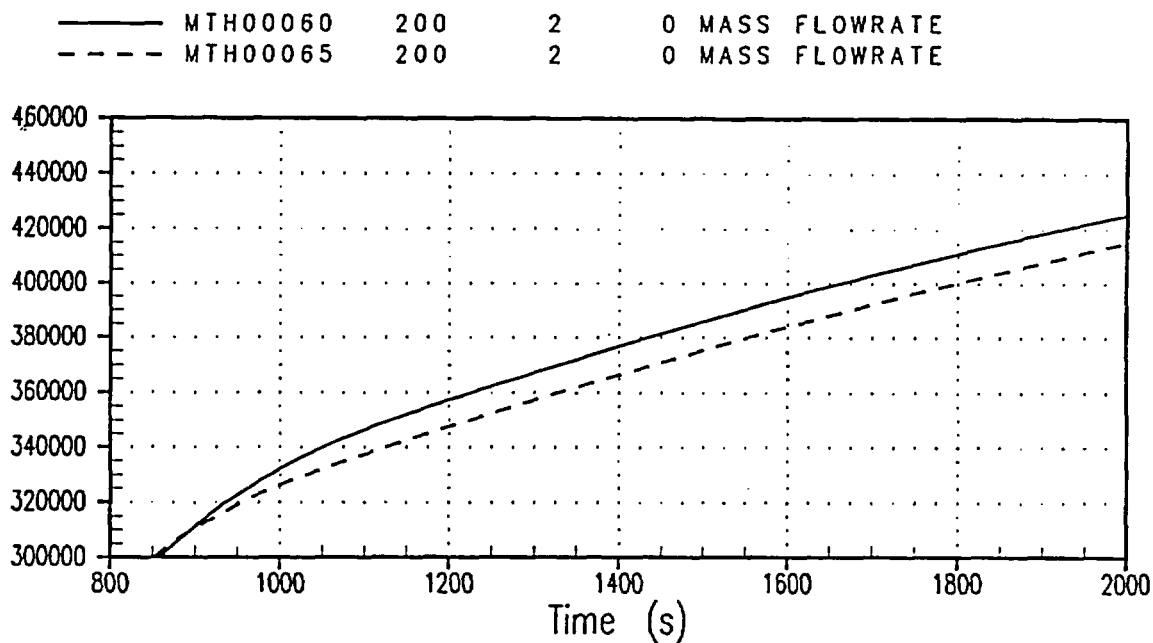


Figure 29-3-9. Integrated Break Flow for Power Shape 4 Compared to Reference Case

29-4 Conclusions

Variations in power distribution on the limiting small break LOCA case have been investigated. Top-skewed power shapes are more limiting than bottom-skewed power shapes. The best estimate small break LOCA methodology will be based on a limiting top-skewed power distribution as discussed in Section 33.

29-5 References

American Nuclear Society, 1979, "American National Standard for Decay Heat Power in Light Water Reactors," ANSI/ANS-5.1-1979.

Argall, B. M., et al., 1979, "Fuel Rod Bow Evaluation," WCAP-8691, Revision 1.

Bajorek, S. M., et al., 1998, "Code Qualification Document for Best Estimate LOCA Analysis Volume V: Quantification of Uncertainty," WCAP-12945-P, Vol. 5.

Chelemer, H. and Tong, L. S., 1962, "Engineering Hot Channel Factors for Open Lattice Cores," Nucleonics, 20, Number 9.

Chelemer, H., et al., 1975, "Improved Thermal Design Procedure," WCAP-8567-P-A.

Miller, R. W., et al., 1983, "Relaxation of Constant Axial Offset Control/ F_q Surveillance Technical Specification," WCAP-10216-P-A.

Morita, T., et al., 1974, "Power Distribution Control and Load Following Procedures," WCAP-8385-P-A.

Spier, E. M., et al., 1988, "Evaluation of Nuclear Hot Channel Factor Uncertainty," WCAP-7308-L-P-A.

Stucker, D. L., et al., 1991, "Westinghouse ECCS Evaluation Model: Revised Large Break LOCA Power Distribution Methodology," WCAP-12909-P.

SECTION 30

PWR SCOPING STUDIES FOR INITIAL AND BOUNDARY CONDITIONS

30-1 Introduction

This section presents the results of scoping studies conducted to examine the effect of variations in the key initial and boundary conditions on small break LOCA transient behavior. The parameters examined in the scoping studies are as follows:

- Initial RCS temperature
- Temperature of pumped safety injection (SI) water; has an allowable Technical Specification range
- Accumulator water temperature, volume, and pressure
 - Temperature of water in the passive loop accumulator tanks; is a function of the containment operating environment
 - Water volume of the passive loop accumulator tanks; has an allowable Technical Specification range
 - Cover gas pressure in the passive loop accumulator tanks; has an allowable Technical Specification range
- Secondary side relief valve (main steam safety valve [MSSV]) setpoint; has an allowable Technical Specification range

30-2 RCS Fluid Conditions

The plant fluid conditions listed in Section 30-2-2 are sufficient to define an overall thermodynamic state of the fluid. Because WCOBRA/TRAC calculates a steady-state condition at the specified power level prior to the LOCA, the thermodynamic state cannot be overspecified. Four basic quantities are defined for the primary fluid: average temperature, pressure, volume, and flowrate. Defined next are the states of significant fluid regions isolated within the RCS during steady-state operation, but which subsequently become an active part of the RCS during

LOCA, such as the upper head. Section 30-2-1 is a brief description of how fluid conditions typically are controlled in a PWR.

30-2-1 Overview of Plant Fluid Conditions

A nuclear power plant is equipped with a variety of control systems. For example, the RCS, with the electric load demand program, controls the neutron generation rate within the core to enable core heat generation rates to be proportional to the demand electric power output. Other control systems are available for control of plant response to rapid disturbances arising from abnormal conditions.

The static and dynamic behavior of the power production process can be determined only by reliable and accurate measurements of process variables. The control and protection systems apply these measurements in a way that ensures proper corrective action and provides protection for the plant and public against extreme accidents. This is normally accomplished by the feedback process, where process variables are controlled to a predetermined value, commonly referred to as a setpoint. When measurements deviate from the setpoint, the deviation is noted as an error by the controller(s) and action is taken to restore the process to its correct state point or condition.

Setpoints generally represent either a desired or target value for a process control variable, or a limit or bounding value of a process control variable. In the case of a target or control setpoint, variation from the desired value results in corrective action to return the plant to the control setpoint. For example, the pressurizer water level control setpoint is approximately 35 percent of the full-scale reading of the measurement span, with either heaters or spray being actuated with a ± 5 -percent variation of full span from the 35-percent span. Violation of limiting or bounding setpoints results in a more radical plant response. Again using the pressurizer as an example, a reactor trip setpoint for high-high pressurizer water level may be 92 percent of full-scale reading of the measurement span.

From this example, it is seen that relatively small variations from control setpoints result in the plant control systems initiating corrective action. These small spans are called control bands. Thus, for a plant maintained at equilibrium conditions, the process control parameters may be taken to vary from their respective setpoints by no more than the bounds of their respective control bands.

In particular, for process parameters subject to automatic control, such as the pressurizer level, the likelihood of the process parameter being significantly different from the target value is extremely small. For those process parameters subject to less frequent surveillance, the potential variation may be larger.

Trip setpoints define the plant operating limits. In reference to the pressurizer example, the plant continues to operate temporarily with a pressurizer water level between 17 and 92 percent of full-scale of the measured span with the plant control systems acting to achieve a level of between 30 to 40 percent of full-scale reading. Owing to operator and/or automatic actions, however, prolonged operation outside the control bands is extremely unlikely. The trip setpoints are established to allow the plant flexibility in responding to changes in operating conditions while providing for the health and safety of the public.

Variations in plant operation parameters significant for LOCA analyses are listed in Table 30-2-1 for a typical PWR. All but primary side loop flow may be considered process control parameters for a nuclear power plant; direct controlling of primary coolant flowrate is not provided. For a typical plant, the variability of the nominal or setpoint values of the parameters is small with a control band of about []^{a,c} on primary loop pressure and fluid temperature, about 1 percent on core power, and about []^{a,c} on pressurizer water volumes.

30-2-2 Fluid Conditions Modelling Approach

In addition to the process parameters identified in Table 30-2-1, additional RCS fluid conditions are important in large break LOCA analyses. The reactor vessel upper head is supplied by a small bypass flow from the upper downcomer. While the incoming fluid is at the cold leg (T_{cold}) temperature, the upper head fluid may be at a different average temperature because of the low bypass flowrate that results in some flow from the upper plenum, which is at a higher temperature (T_{hot}). The initial temperature of the fluid in the upper head (T_{UH}) strongly affects the blowdown PCT in large break LOCA models. Typically, plants can be separated into two categories: those with sufficient bypass flow to maintain (T_{UH}) near T_{cold} and those with low bypass flow, in which T_{UH} remains close to T_{hot} .

The bypass flow is one component of several bypass flows that reduce the core flowrate relative to the loop flowrate by about 4 to 8 percent. This bypass flow has an indirect effect on the LOCA transient by affecting the fluid temperature rise through the core, but is not expected to affect the LOCA transient directly.

Not all the process parameters described in Section 30-2 are independent. Typically, if core power, primary flow, and secondary temperature and pressure are specified, the primary fluid temperature and pressure seek appropriate levels consistent with these boundary conditions. In the modelling of these parameters, the secondary side conditions are adjusted as required to obtain primary side conditions consistent with the Technical Specifications and planned operation. Because the secondary side model is simplified, this may lead to secondary side fluid conditions that may be slightly different from the actual plant values.

The parameters chosen to represent the plant initial RCS fluid conditions are as follows:

- Core average fluid temperature (T_{avg}), °F
- Pressurizer pressure (P_{RCS}), psia
- Loop flowrate (W_{loop}), gpm per loop
- Pressurizer water level (L_p), percentage of full span

The effect that the first of these parameters has on the LOCA transient is evaluated in Section 30-2-3; the others are either bounded or set to nominal values as discussed in Sections 30-2-4, 30-2-5, and 30-2-6. The method for accounting for uncertainties in the T_{avg} parameter, based on these results, is in Section 33.

30-2-3 RCS Temperature Scoping Study

The reference case 3-inch break with LOOP was simulated with an assumed T_{avg} value of 546°F. This T_{avg} value is a lower bound to the expected Indian Point Unit 2 operating window.

The sequence of events and overall behavior for the 3-inch equivalent diameter cold leg break with LOOP at the reduced T_{avg} value differ somewhat from the reference case. Reactor trip occurs 9 seconds earlier in the reduced T_{avg} case because there is less flashing during blowdown and also a more rapid depletion of the initial inventory. SI actuation also occurs earlier in the transient by a similar amount.

The reduction in T_{avg} does not lead to a significant redistribution of mass in the Reactor Coolant System (RCS). Figure 30-2-1 shows the collapsed liquid levels in the core hot assembly and average regions for this case. Time in seconds is the x-axis parameter of each figure in this subsection. Flashing is much reduced at the low T_{avg} value so the initial drop in collapsed core levels is less severe than in the reference case. Figure 30-2-1 also shows that the collapsed level in the core uncover phase from 1500 seconds transient time on is higher in the reduced T_{avg} case.

Despite this fact, the PCT for the low T_{avg} case is 943°F, which is less than 25°F different from the reference case value (Figure 30-2-2).

Figure 30-2-3 compares the pressurizer pressures of the reference case (solid line) and the reduced T_{avg} case (dashed line). Pressure drops almost 200 psi more in the low T_{avg} case during the initial depressurization; the pressures then converge during the natural circulation, when heat transfer to the steam generator secondary dictates the primary side pressure.

Figure 30-2-4 shows the break flow comparison between the cases. The reduced T_{avg} case (dashed line) exhibits the higher peak at the inception of the break due to the low cold leg enthalpy. At 100 seconds transient time, the reference case break flow (solid line) moves higher than the reduced T_{avg} case break flow because its pressure is significantly higher. However, as a consequence of less flashing occurring within the next 200 seconds, the reduced T_{avg} becomes the larger break flow once again (Figure 30-2-5). Loop seal clearance occurs later in Figure 30-2-5 for the reduced T_{avg} case (dashed curve) than in the reference case (solid line) because the RCS contains more initial mass, and therefore more liquid mass must be removed through the break before steam break flow can begin.

[

]^{a,c} the T_{avg} change is included in the initial conditions uncertainty.

30-2-4 Pressurizer (RCS) Pressure

Table 30-2-1 indicates that the percentage variation in pressurizer pressure is small. This parameter is tightly controlled during plant operation by automatic actuation of the pressurizer spray and/or the heater elements. The major impact of the initial RCS pressure on a small break LOCA event [

]^{a,c} is chosen for small break LOCA analysis.

30-2-5 Loop Flowrate

[

]^{a,c} Regarding the RCP performance curves, in Section 27, Volume 3, the effect of the pump was investigated with PWR calculations assuming offsite power available (OPA) so that the RCPs continue to run for an extended time following reactor trip. The effect is significant for breaks near the limiting break size and smaller for breaks greater than the 3-inch size. The small break LOCA transients generally showed the pump to be in one of two conditions: spinning forward while the flow is primarily single-phase liquid, and spinning forward when the flow is nearly single-phase vapor (SPV). Thus, uncertainties in the two-phase degraded pump performance are considered to be small in comparison to the effect of continued pump operation. By adopting the limiting assumption regarding offsite power in PWR analysis, and then varying the operator action time to manually trip the RCPs if the continued availability of offsite power proves to be the limiting assumption, the uncertainties associated with the RCP performance are bounded in the best estimate small break LOCA methodology.

30-2-6 Pressurizer Water Level

The water level in the pressurizer is tightly controlled during plant operation by the plant control systems. Therefore, [

]^{a,c}

Table 30-2-1
Typical Westinghouse Plant Operation Parameters

Parameter⁽¹⁾	Percentage Expected Variation (+)
[
] ^{a,c}

1. Primary side

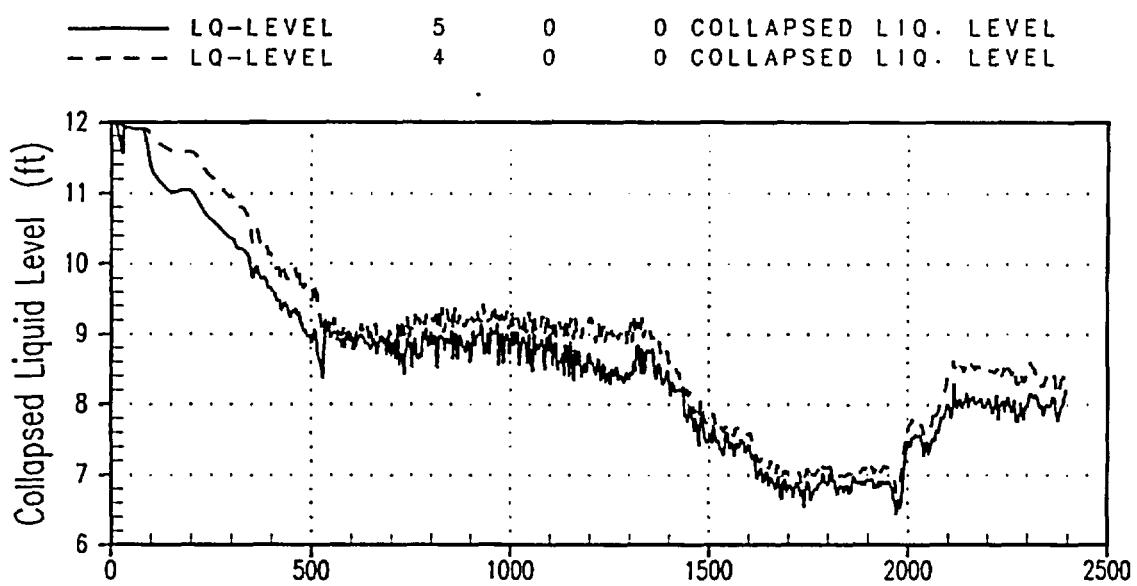


Figure 30-2-1. Core Collapsed Liquid Level, 3-Inch Cold Leg Break at Reduced T_{avg}

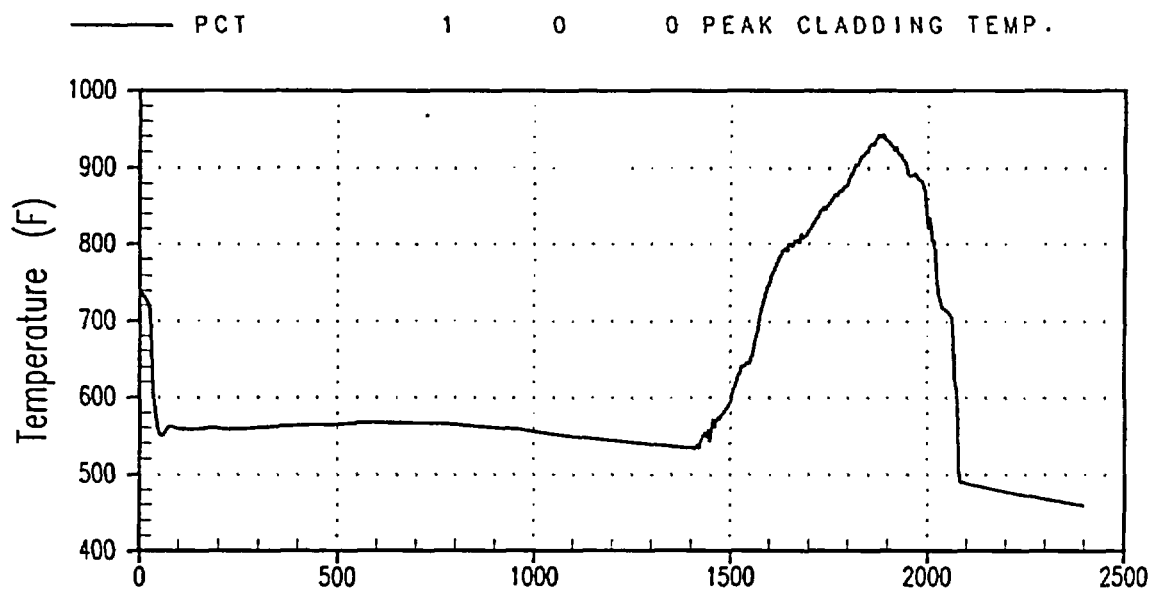


Figure 30-2-2. PCT, 3-Inch Cold Leg Break at Reduced T_{avg}

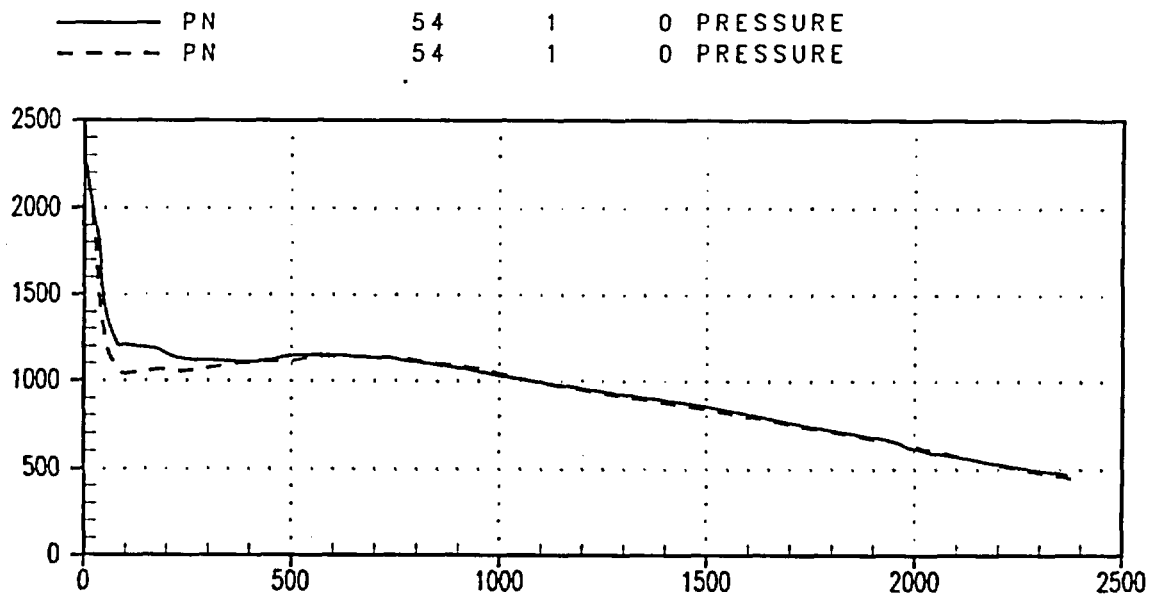


Figure 30-2-3. Pressurizer Pressure (psia), 3-Inch Cold Leg Break at Reduced T_{avg} Compared to Reference Case

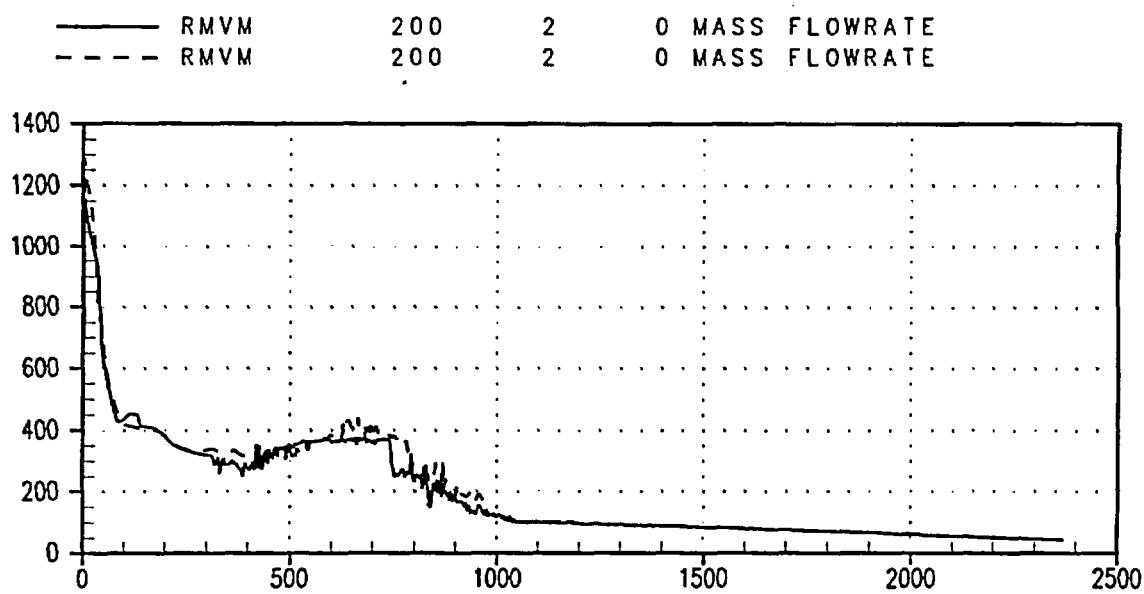


Figure 30-2-4. Break Flowrate (lbm/s), 3-Inch Cold Leg Break at Reduced T_{avg} Compared to Reference Case

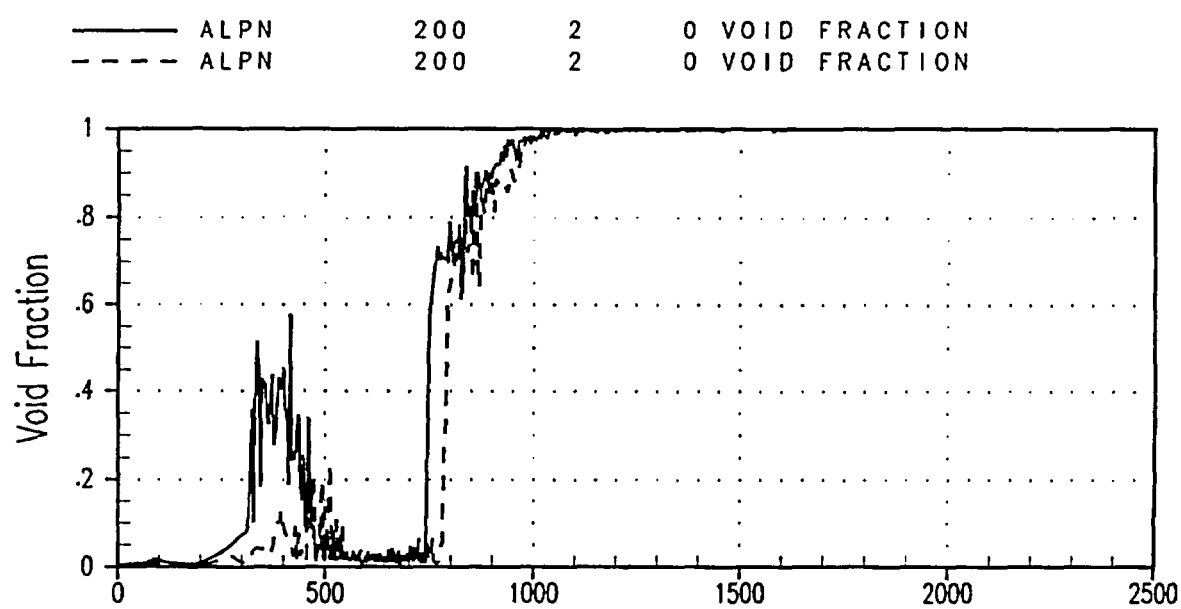


Figure 30-2-5. **Void Fraction at the Break 3-Inch Cold Leg Break at Reduced T_{avg} Compared to Reference Case**

30-3 Effect of Pumped SI Parameters

30-3-1 Associated Phenomena

During the initial (short-term) phase of a LOCA transient, the water that supplies the pumped Emergency Core Cooling Systems (ECCSs) is drawn from the Refueling Water Storage Tank (RWST). This tank is located outside the containment building and is subject to temperature changes. Therefore, the water temperature within this tank is monitored and maintained within an allowable range; at Indian Point Unit 2 plant the range is 40°F to 120°F.

The overall system behavior during a small break LOCA is strongly governed by the balance between the mass and energy removal from the break, and the mass and energy addition by the SI system. These interact to govern the primary depressurization rate, which in turn affects the generation of vapor from bulk flashing, the timing of loop accumulator injection, and the injection rate from the centrifugal SI pumps. The performance of the high pressure injection pumps is crucial to the outcome of small break LOCA events. The SI water temperature also has an influence on this global mass and energy balance and additionally affects condensation in the cold leg, which can have a direct influence on the local fluid conditions upstream of the break.

30-3-2 SI Performance Curves for Indian Point Unit 2

Figure 30-3-1 compares the SI pump delivery characteristics for the cases that presume the limiting single failure. The Indian Point Unit 2 plant has three high pressure injection (high head SI [HHSI]) pumps, which are headered to provide injection to all four cold legs during the small break LOCA transient. The base case curve is typical of those developed for the worst case characteristics as used in Appendix K, 10CFR50, licensing basis analyses. The curves are generated assuming the following conditions:

- One HHSI pump fails, leaving two pumps running.
- For breaks postulated at the top of the cold leg, one injection line severs completely near the cold leg junction, which therefore allows a spill path to containment with negligible backpressure resisting the spill. For breaks oriented at the side or bottom of the cold leg, injection into the broken loop occurs.

- Pump recirculation flow is at its maximum calculated value, which minimizes RCS injection flow; this includes the diversion of approximately []^{a,c} into the accumulator fill lines.
- Maximum line resistances and the most limiting imbalances between branch lines are modelled.
- Pump heads are reduced []^{a,c} below the vendor performance curves.

At approximately 100 psi RCS backpressure, the low pressure injection pumps from the Residual Heat Removal (RHR) system begin to inject. There are similar conservative assumptions made for developing these pump curves, but they are not important for small break LOCA because these low system pressures are not attained in the transients of interest.

The break at the top of the cold leg case injection curve, therefore, represents a significant amount of conservatism in defining the SI capacity because it is based upon one SI delivery line being severed and spilling. Figure 30-3-1 presents this curve (identified as Series 3) and also the calculated cold leg injection rate for the case in which two HHSI pumps operate and all injection lines are fully intact (identified as Series 1); that is, no spill to the containment occurs from any branch line. The assumptions regarding the delivery head of the pumps, injection loss due to pump recirculation flow, and the like, are the same as for the limiting case injection curve. The HHSI injection rate versus RCS pressure curves shown in Figure 30-3-1 illustrate the large reduction in flowrate for a break orientation at the top of the cold leg due to the spill to containment pressure assumption. With all three HHSI pumps injecting, no core uncover is predicted to occur for the 3-inch break size; the transient is largely benign because the pumped SI system is capable of making up the two-phase break flowrate at RCS pressures near the secondary side relief valve setpoint.

For the 3-inch cold leg break orientation at the top of the cold leg, system recovery is dependent upon accumulator injection to terminate RCS mass loss. Therefore, this case will be sensitive to accumulator tank pressure.

30-3-3 3-Inch Break Results for Pumped SI Temperature Variation

In this study, sensitivities to pumped SI temperature are obtained by varying the pumped SI system temperature over the identified range with a selected intermediate temperature case also run for trend information. The 3-inch cold leg break size is examined.

The base case for this study uses a nominal SI temperature of 77.5°F and is the same as used and described in Section 27, Volume 3. The 3-inch cold leg break was previously determined to produce the limiting PCT in the break size spectrum studies. All other boundary conditions are maintained the same with some of the significant parameters being: LOOP at reactor trip, core peaking factors of []^{a,c} 15-percent uniform steam generator tube plugging (SGTP), and 655 psia accumulator tank pressure.

Figure 30-3-2 compares the PCTs for the three cases at different SI temperatures. Table 30-3-1 summarizes the PCTs. In Figure 30-3-2 and all subsequent figures in this section, the solid line is the reference case, the short-dashed curve is the 120°F SI temperature case, the alternate long/short dashed curve is the 40°F SI temperature case, and the x-axis parameter is time in seconds.

Comparing the cladding temperature curves and the core collapsed liquid level curves of Figure 30-3-3 indicates that, overall, the SI temperature is not predicted to have a major influence on this transient. Figure 30-3-4 compares the RCS primary pressures of the three cases during the boiloff phase. The overall behavior of all these parameters indicates that one phenomenon governing the trends is the condensation potential of the SI water. Colder water causes the system to depressurize slightly faster throughout most of the boiloff phase of the transient. This results in the core collapsed liquid level for the warmest (120°F) SI case recovering last and, in that case, the core quench occurring last also. The cold legs in the vicinity of the break void nearly completely in all cases.

The direct influence of SI temperature on the 3-inch break transient PCT is small across a range of allowable RWST temperatures ranging from 40° to 120°F. The 21°F impact of the SI temperature sensitivity is included in the initial conditions uncertainty.

For Indian Point Unit 2, the observed net variation in predicted cladding temperatures is rather small considering the wide range of SI temperatures examined. The direct effect of SI water temperature is manifested in the rate of primary system depressurization resulting from the increased condensation potential of colder injection water.

Table 30-3-1
PCT Summary – SI Temperature Sensitivities

SI Temperature (°F)	PCT (°F)
40	964
77.5	964
120	985

IP2 HHSI Injection Flow

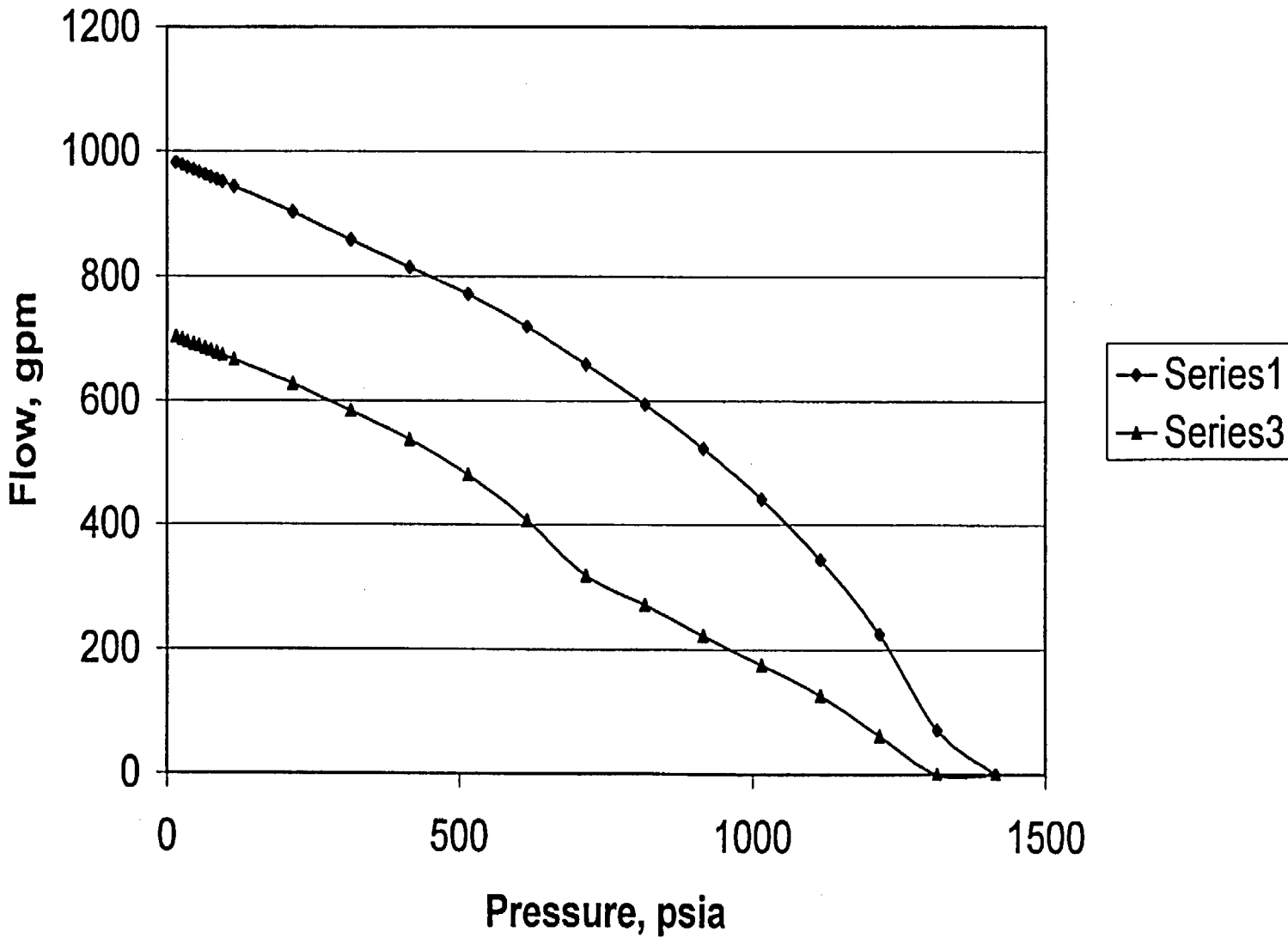


Figure 30-3-1. SI Performance Curves for Indian Point Unit 2

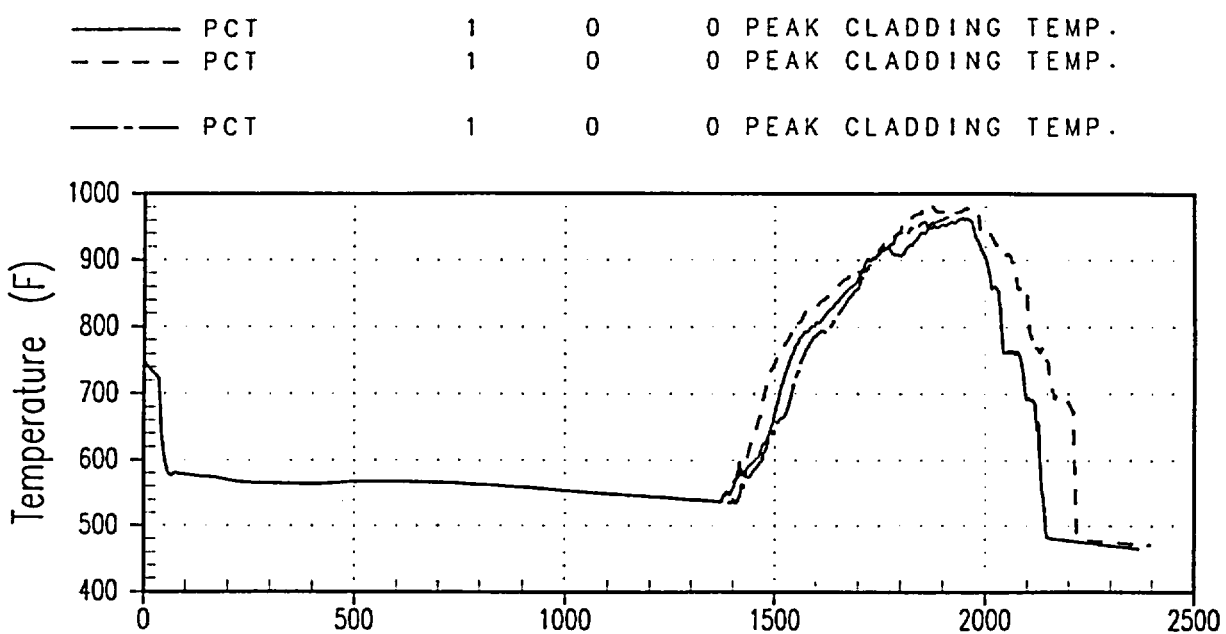


Figure 30-3-2. PCTs - 3-Inch Break SI Temperature Sensitivities

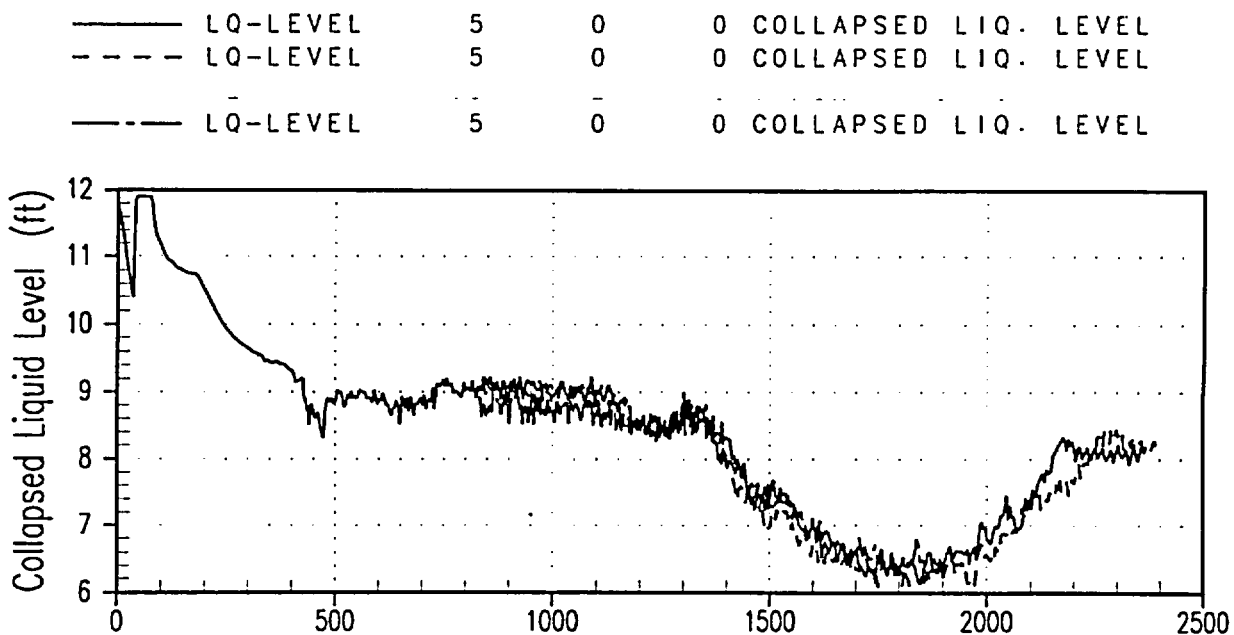


Figure 30-3-3. Core Collapsed Liquid Levels - 3-Inch Break SI Temperature Sensitivities

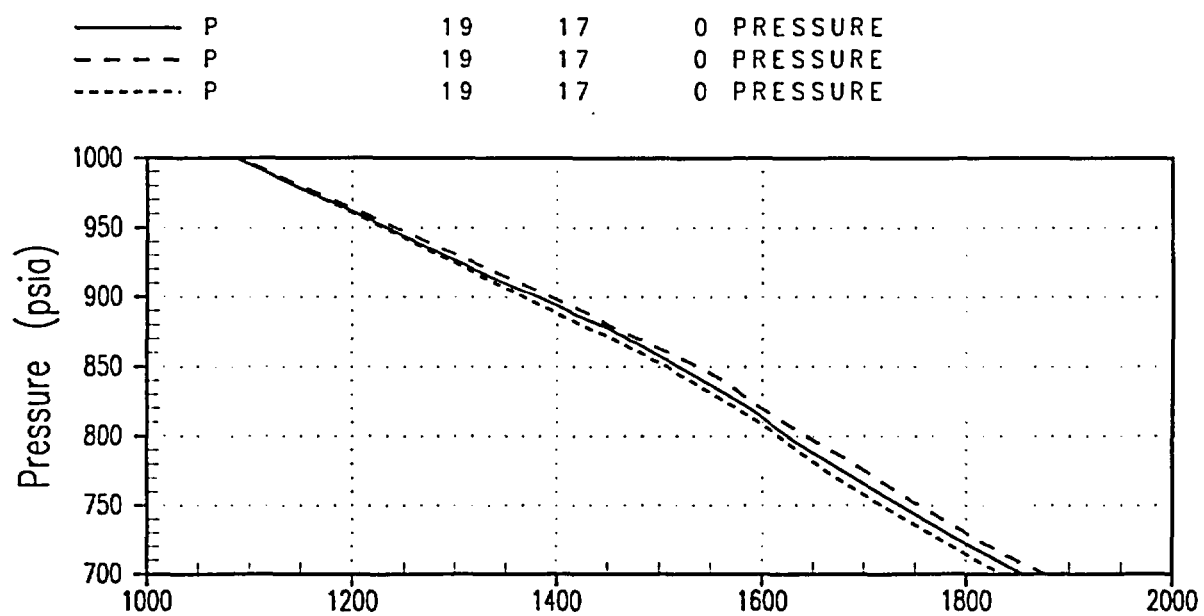


Figure 30-3-4. RCS Pressure Transient Detail - 3 Inch Break SI Temperature Sensitivities

30-4 Accumulator Water Temperature, Volume, and Pressure Sensitivities

During normal operation, the accumulator is isolated from the RCS by a check valve. The performance of the accumulator during the LOCA depends on several factors including the water and cover gas initial pressure, temperature, and volume. These are all subject to some variation. Typically, pressure and volume are controlled to within \pm 10 percent or less. Because the accumulators reside within containment, the long-term temperature of the containment atmosphere affects the accumulator water temperature. The variation in containment temperature is likely to be seasonal to some degree and is limited in most plants to a maximum value to avoid problems with equipment degradation. In general, therefore, the accumulator temperature range is plant-specific. The accumulator line is subject to the same uncertainties as flow resistance; however, plant startup tests reduce this uncertainty to some extent (Section 16-2, Volume 3, of WCAP-12945-P-A [Bajorek et al., 1998]).

While accumulator boron concentration is not likely to have a significant effect on the LOCA PCT, it is an important parameter to consider for long-term cooling after the LOCA.

30-4-1 Associated Phenomena

The temperature of the water stored within the loop accumulator tanks may vary although because these tanks are inside containment, the temperature range is relatively small; for Indian Point Unit 2, the range is 90° to 130°F. In the WCobra/TRAC-SB break spectrum, each case uses a 105°F temperature. The 3-inch break transient is analyzed to establish the effect of accumulator water temperature; cases are executed using accumulator tank temperatures of 90° and 138°F.

The accumulator water temperature is not expected to have a significant effect on either PCT or on the transient itself. This is because although 3-inch break transients rely on accumulator injection to initiate core recovery, in general, the fuel heatup is terminated shortly after the start of accumulator injection by the mass addition. The transient is, therefore, expected to exhibit little sensitivity to the accumulator water temperature. For the same reason, little sensitivity to accumulator water volume is expected.

The nitrogen cover gas pressure in the accumulator tanks is maintained within an allowable Technical Specification band from 598 to 685 psig. For small break LOCAs greater than 2 inches, the termination of core heatup occurs almost immediately after the primary depressurizes to the accumulator pressure and injection begins. There is, therefore, a direct

correlation between accumulator tank pressure and PCT for the limiting 3-inch break size; to investigate the magnitude of the PCT impact for Indian Point Unit 2, the 3-inch break reference transient is restarted prior to accumulator actuation at tank pressures of 600 psia and 700 psia.

30-4-2 Temperature Sensitivity Results

Results of the 90°F accumulator temperature case and the 138°F accumulator temperature case for the 3-inch break exhibit almost no sensitivity to this parameter. The sensitivity study calculations were run by restarting the base case calculations prior to the start of accumulator injection. In the case of the 3-inch break, the accumulator injection begins at 2055 seconds and the calculation is restarted at 2000 seconds. Review of the PCT curves indicate that the transient is not perturbed by the restart. The difference in PCT is a decrease of 3°F in the 138°F temperature case and no change in the 90°F case. These results show that the effect of accumulator water temperature represents a negligible perturbation on the cladding heatup transient.

30-4-3 Water Volume Sensitivity Results

The other sensitivity studies discussed throughout this section use a nominal accumulator water volume of 800 cubic feet. The 3-inch break cases were run at water volumes equal to 723 cubic feet and 875 cubic feet, the extremes of the allowable values in the Indian Point Unit 2 Technical Specifications, to identify the sensitivity to accumulator water volume. The change in PCT from varying the accumulator water volume is 1°F in both cases. There is almost no PCT sensitivity to this parameter because the PCT for the 3-inch break transient turns around immediately after accumulator flow begins. Even though hot rod quench time is delayed by more than 100 seconds for the initial water volume change to 875 cubic feet, initial water volume is unimportant for the 3-inch break PCT result.

30-4-4 Pressure Sensitivity Results

The other sensitivity studies examined throughout this section all use a nominal accumulator pressure of 655 psia, which is the nominal value for the allowed Technical Specification range. A sensitivity case was run at 600 psia, which is less than the Technical Specification minimum value of 598 psig (613 psia) to examine the effect of variations in accumulator pressure. The limiting break size of 3 inches is used, and other boundary conditions are identical to the base case for the accumulator water temperature studies. A second sensitivity case was run at 700 psia, the Technical Specification maximum accumulator pressure.

Figure 30-4-1 compares the depressurization (psia) at accumulator injection for these three transients. Key results are shown in Table 30-4-1. Figure 30-4-1 shows that actuation of the accumulators leads to an increased rate of depressurization for the reference case (solid line) and for the pressure sensitivity cases (dashed lines).

Figure 30-4-2 compares the PCT predicted for the reference case (solid line) with the 700 psia and 600 psia accumulator actuation cases. Review of the figure shows that, as anticipated, the cladding temperature quench is delayed as the accumulator pressure is reduced. The PCT continues to rise until shortly after accumulator injection begins for the 700 psia case. An initial insurge of water into the core follows the initial injection of accumulator water, and there is an earlier turnaround of the cladding heatup due to the accumulator injection at 700 psia; the PCT sensitivity to accumulator pressure is caused by the difference in heatup time resulting from the change in accumulator pressure, or 25°F for the 700 psia case. A lower PCT would be calculated at 735 psia accumulator pressure, the tank pressure relief value, than for the 700 psia case.

Review of the 655 psia and 600 psia figures shows that there is a negligible difference in PCT despite the later time of accumulator injection. This is because the elevation at which the cladding temperature occurs exhibits a quasi-steady-state behavior, as indicated in Figure 30-4-2. This occurs because the minimum hot assembly collapsed liquid level for both the reference case and the 600 psia case occurs prior to depressurization to 655 psia. The level then increases somewhat, and in the 600 psia case remains constant until the accumulator setpoint is reached. Therefore, the additional time of uncover until the accumulator tank pressure is reached results in no additional heatup. While this is the observed behavior for the lower accumulator pressure variation relative to the reference case PCT, when core mixture level parameter *CYDG* is set to 0.4 (instead of the nominal 0.8), a reduction in the accumulator pressure setpoint to 600 psia causes a PCT increase of similar magnitude to the observed decrease at 700 psia in Figure 30-4-2. Therefore, for conservatism, the sensitivity [$d(PCT)/dt$] observed between the 655 and 700 psia setpoint cases will be applied over the entire accumulator setpoint range in the uncertainty methodology.

30-4-5 Conclusions Regarding Sensitivities to Accumulator Parameters

In terms of the PCT obtained for small break LOCAs, both the accumulator water temperature and volume have negligible effects, estimated to be approximately $\pm 3^{\circ}\text{F}$ over the range of accumulator water volumes and temperatures expected to exist during plant operation. The effect of accumulator gas pressure is greater, on the order of $0.5^{\circ}\text{F}/\text{psi}$, and is included in the initial conditions uncertainty.

Table 30-4-1
Sensitivity Studies – Accumulator Gas Pressure

Item	Accumulator Pressure 655 psia	Accumulator Pressure 600 psia	Accumulator Pressure 700 psia
PCT (°F)	964	964	939
Start of accumulator injection(s)	1955	2075	1850
Time of PCT(s)	1948	1972	1859

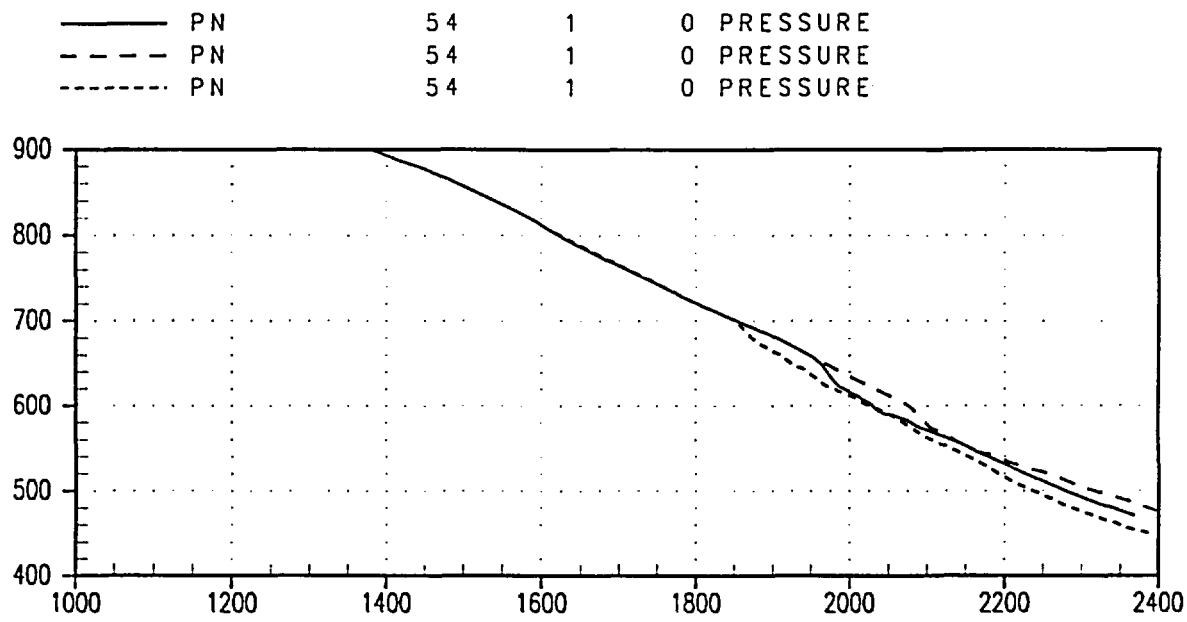


Figure 30-4-1. 3-Inch Break Accumulator Gas Pressure Sensitivity Pressure Transients (psia)

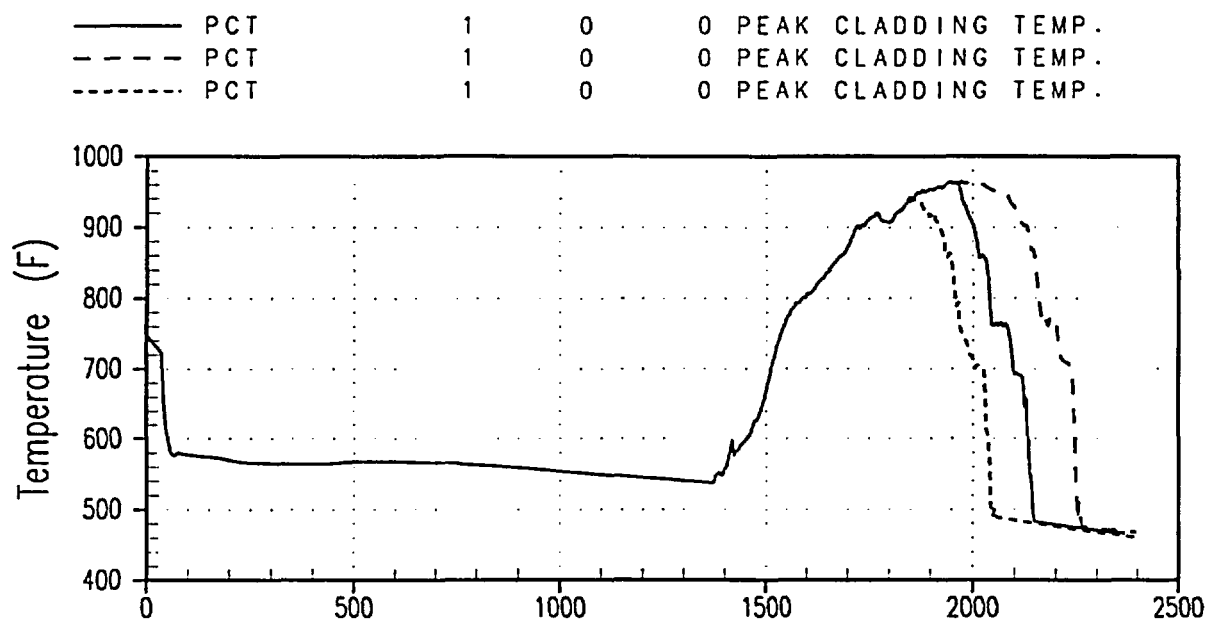


Figure 30-4-2. 3-Inch Break Accumulator Pressure Sensitivity PCT Transients

30-5 Effect of Steam Generator Secondary Side Relief Valve Setpoints

30-5-1 Associated Phenomena

This section analyzes the effect of increasing the setpoint at which the steam generator secondary side vents to the atmosphere during a small break LOCA. In a PWR, reactor trip during a small break LOCA is accompanied by closure of the turbine stop valves which isolates the secondary side. The pressure in the secondaries then rises to the safety relief valve setpoints, and steam relief occurs. (The condenser bypass valves also open upon closure of the turbine stop valves, but another signal caused by the depressurization cooldown of the RCS occurs shortly thereafter and signals these valves to close. Due to the cycle time for the bypass valve, there is negligible steam bypass to the condenser through this event.) The safety relief valve system in the Indian Point Unit 2 plant consists of both atmospheric dump valves and five stages of individual MSSVs, which open progressively beginning at a steam generator secondary pressure of 1065 psia. In general for small break LOCA transients, the first stage MSSV relief valve has sufficient capacity to provide full steam relief and the remaining stages do not open. In the Indian Point Unit 2 plant, the atmospheric dump valve system is a safety grade system, which operates similar to the MSSVs, but opens at a lower setpoint.

The base case calculations, used in the other parametric sensitivity studies in this section, model the safety-grade dump valves, which begin to open at 1065 psia. For examining the sensitivity of the small break LOCA transient to the secondary side relief pressure, an additional calculation was made in which the relief valves begin to open at 1112 psia. The 3-inch cold leg break was selected with the remaining boundary conditions the same as the base cases used in the other sensitivity studies presented in this section. [

]^{a,c}

The expected effect of increasing the safety relief pressure is an overall increase in the primary temperatures and pressures. This in turn is expected to adversely affect the system inventory due to lower SI injection and to suppress level two-phase swell in the core, both of which lead to higher cladding temperatures.

30-5-2 Results

During the first few hundred seconds of the blowdown, there is little difference between the break mass flowrates for the reference and the increased steam generator relief pressure (high MSSV) calculations (Figure 30-5-1). In this figure and in all subsequent figures in this section the x-axis parameter is time in seconds. At about 400 seconds, the transition from low quality two-phase flow to SPV flow begins. During the beginning of this period, liquid held up in the loops 21, 22, 23, and 24 steam generators drains in a manner similar to the reference case (solid lines) (Figure 30-5-2); liquid is predicted to drain slightly more slowly from the loop 24 steam generator in the high MSSV setpoint case (Figure 30-5-2). For both the high MSSV and the nominal setpoint cases, loop 21 is the first to drain; loop 23 drain is completed at about the same time as loop 21 in the reference case, whereas loop 22 is next to drain in the high MSSV setpoint case. The seal of loop 23 is predicted to clear about 10 seconds later in the high MSSV case than the seal of loop 22 in the (solid line) reference case (Figure 30-5-3); loop seal clearance occurs over 100 seconds after each steam generator has drained to a minimal level.

Once the steam generators have drained, and the loop seal has cleared, and the break is in single-phase flow, boildown of the reactor vessel liquid inventory begins. In the high MSSV setpoint case, increased primary system pressure (Figure 30-5-4) causes a decrease in the total SI rate (Figure 30-5-5) through 1400 seconds, where the solid line is the reference case. Because the break flowrates for the two cases (Figure 30-5-1) are not significantly different and the SI rate is less for the (dashed line) high MSSV setpoint case (Figure 30-5-5), the reactor vessel mass inventory is predicted to be less for the (dashed line) high MSSV setpoint case (Figure 30-5-6) after the boildown starts. The uncovering of the core is predicted to be earlier and deeper for the high MSSV setpoint case (Figure 30-5-7). The two calculations of primary system mass converge and then cross over after 1900 seconds (Figure 30-5-6). The fact that the core mixture level has dropped earlier to uncover the core more in the high MSSV case means less steam is being generated in that case. This enables the higher rate of depressurization to occur.

The core is predicted to uncover about 60 seconds earlier for the high MSSV case (dashed line) than the reference case (Figure 30-5-8). The effect is a predicted PCT 53°F higher than the reference case. The predicted difference in PCT due to the variation steam generator safety valve actuation pressure is included in the initial conditions uncertainty.

30-5-3 Conclusions Regarding the Effects of MSSV Setpoint

During a small break LOCA, the MSSV setpoint has a distinct effect on system behavior and on the severity of the predicted PCT. Increasing the secondary relief pressure results in a commensurate rise in the pressure in the primary. This in turn causes higher break flow and lower pumped SI, which adversely affects the primary inventory leading to greater core uncover and higher PCTs.

An increased MSSV setpoint case is performed to examine the PCT sensitivity. The relief pressure is increased over the MSSV setpoint range from a best estimate to a conservative, bounding value to produce a moderate effect on PCT of approximately 50°F. Because a single MSSV stage can adequately relieve pressure for the small break LOCA transient, the range representing the uncertainty in the realistic small break LOCA transient actuation pressure is encompassed in this study. The effect of an MSSV pressure setpoint increase is included in the initial conditions uncertainty.

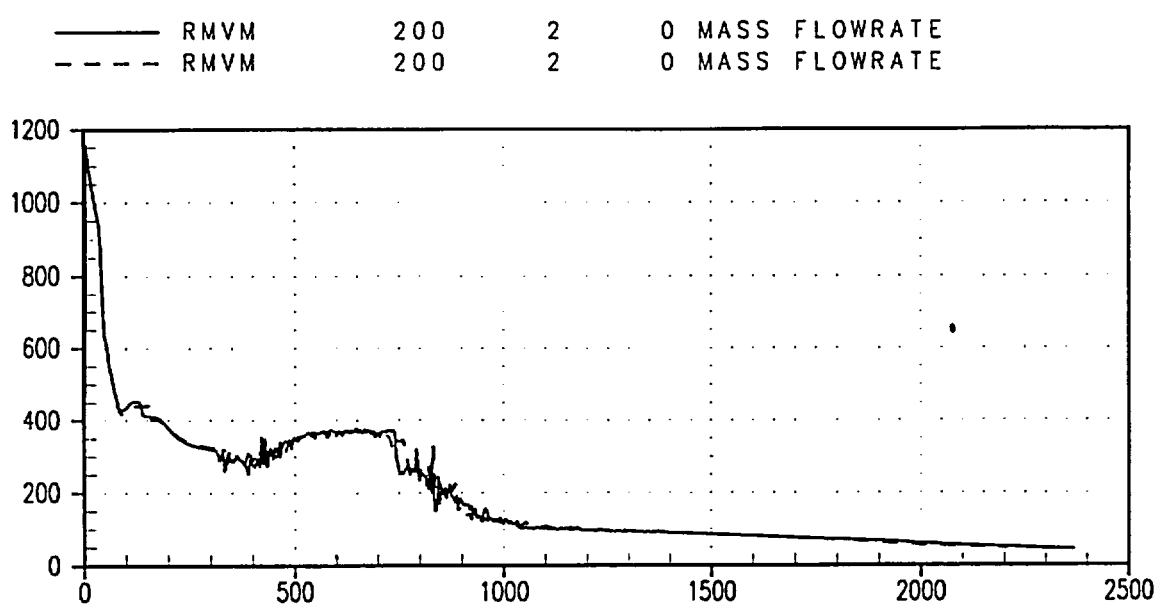


Figure 30-5-1. 3-Inch Break MSSV Setpoint Sensitivity Break Flowrates

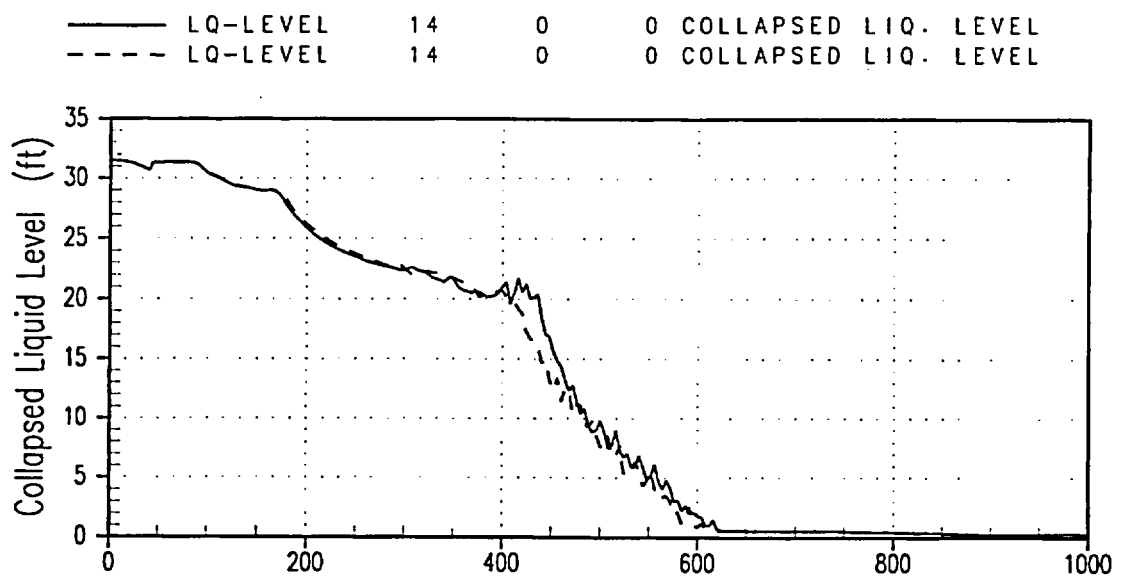


Figure 30-5-2a. 3-Inch Break MSSV Setpoint Sensitivity, Loop 21 Steam Generator Uphill Tube Collapsed Liquid Levels

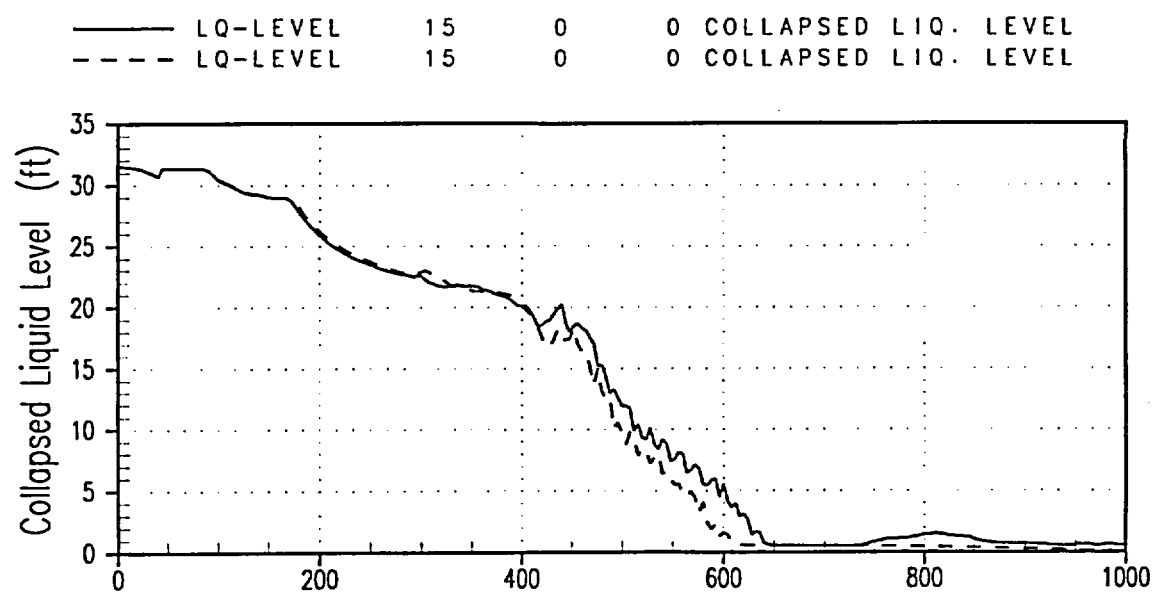


Figure 30-5-2b. 3-Inch Break MSSV Setpoint Sensitivity, Loop 22 Steam Generator Uphill Tube Collapsed Liquid Levels

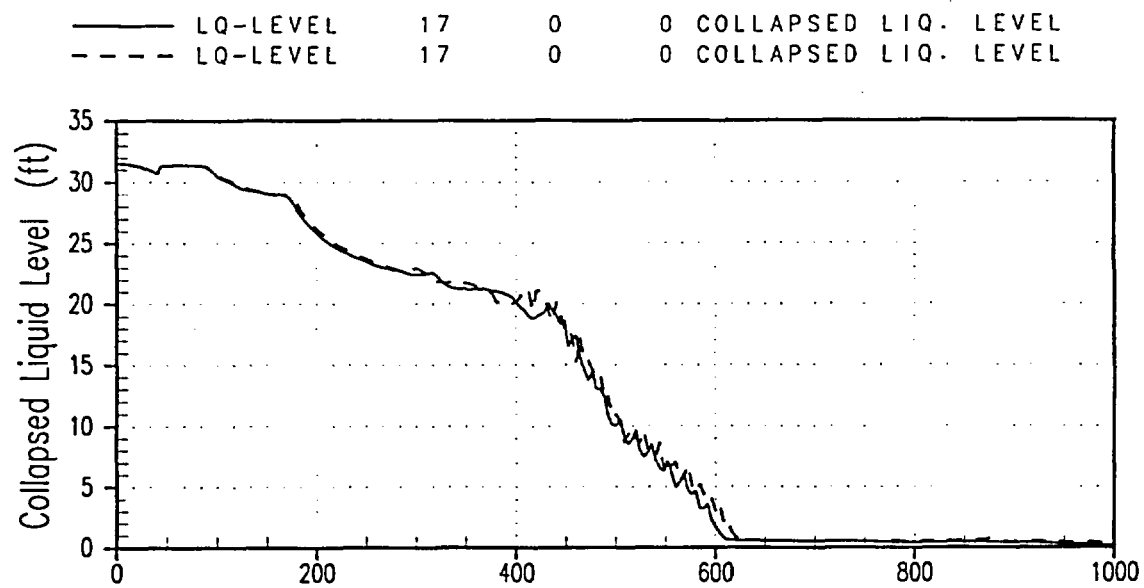


Figure 30-5-2c. 3-Inch Break MSSV Setpoint Sensitivity, Loop 23 Steam Generator Uphill Tube Collapsed Liquid Levels

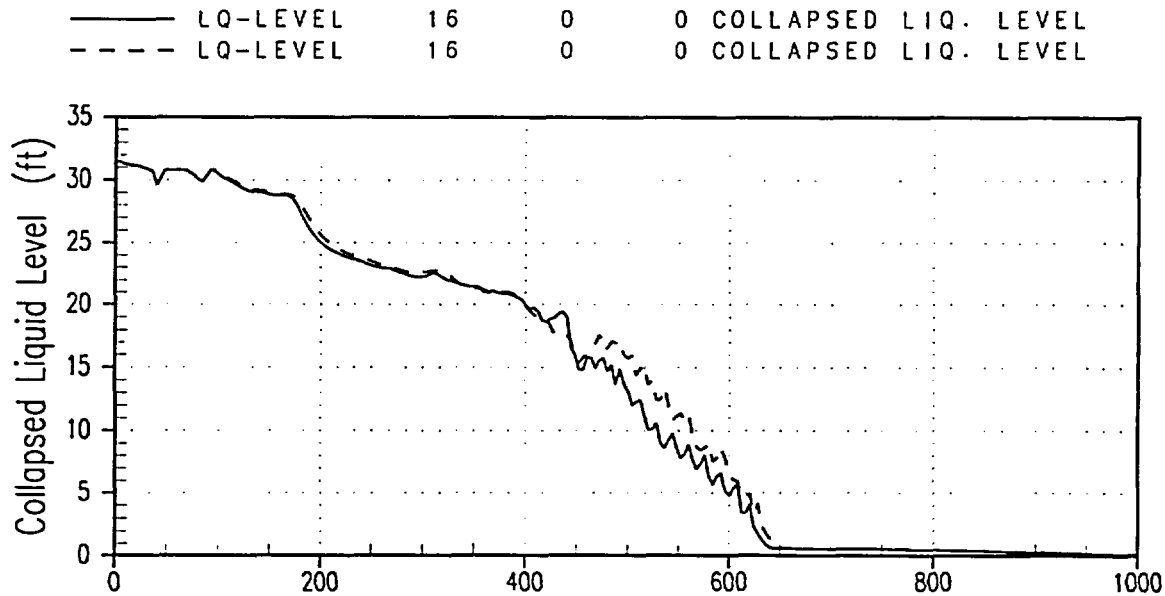


Figure 30-5-2d. 3-Inch Break MSSV Setpoint Sensitivity, Loop 24 Steam Generator Uphill Tube Collapsed Liquid Levels

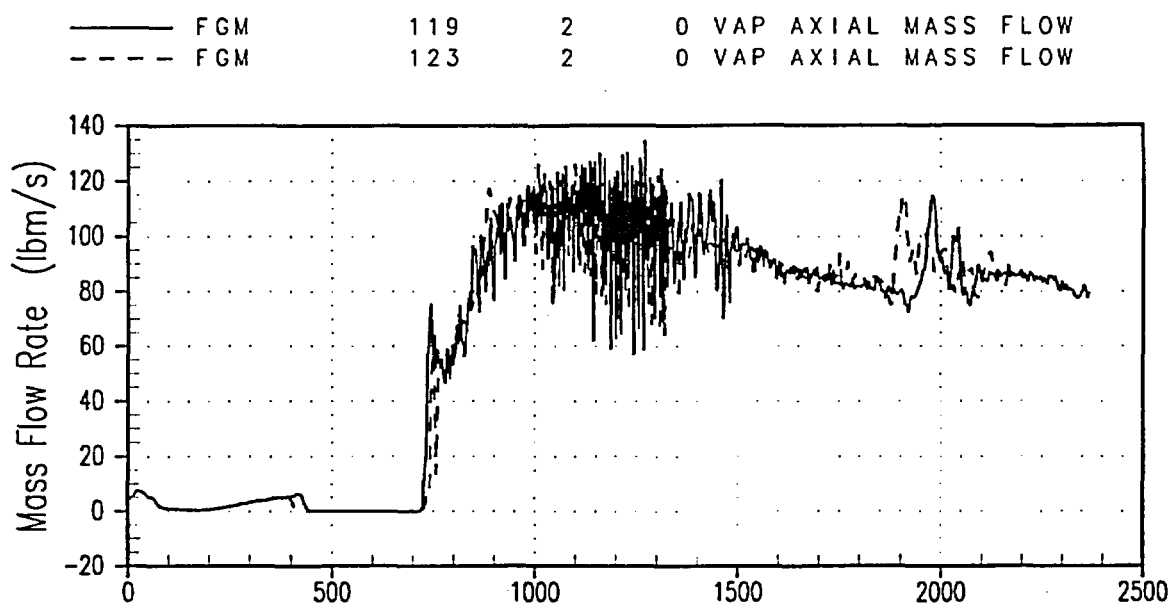


Figure 30-5-3. 3-Inch Break MSSV Setpoint Sensitivity Pump Suction Vapor Flow for the Cleared Loop Seal

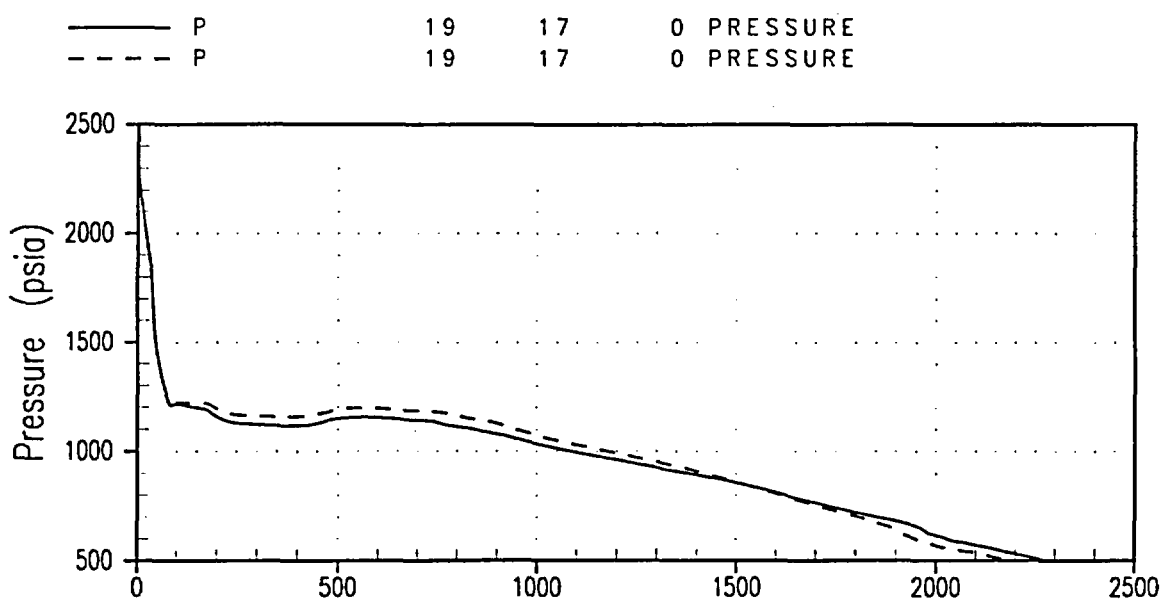


Figure 30-5-4. 3-Inch Break MSSV Setpoint Sensitivity for Primary System Pressure

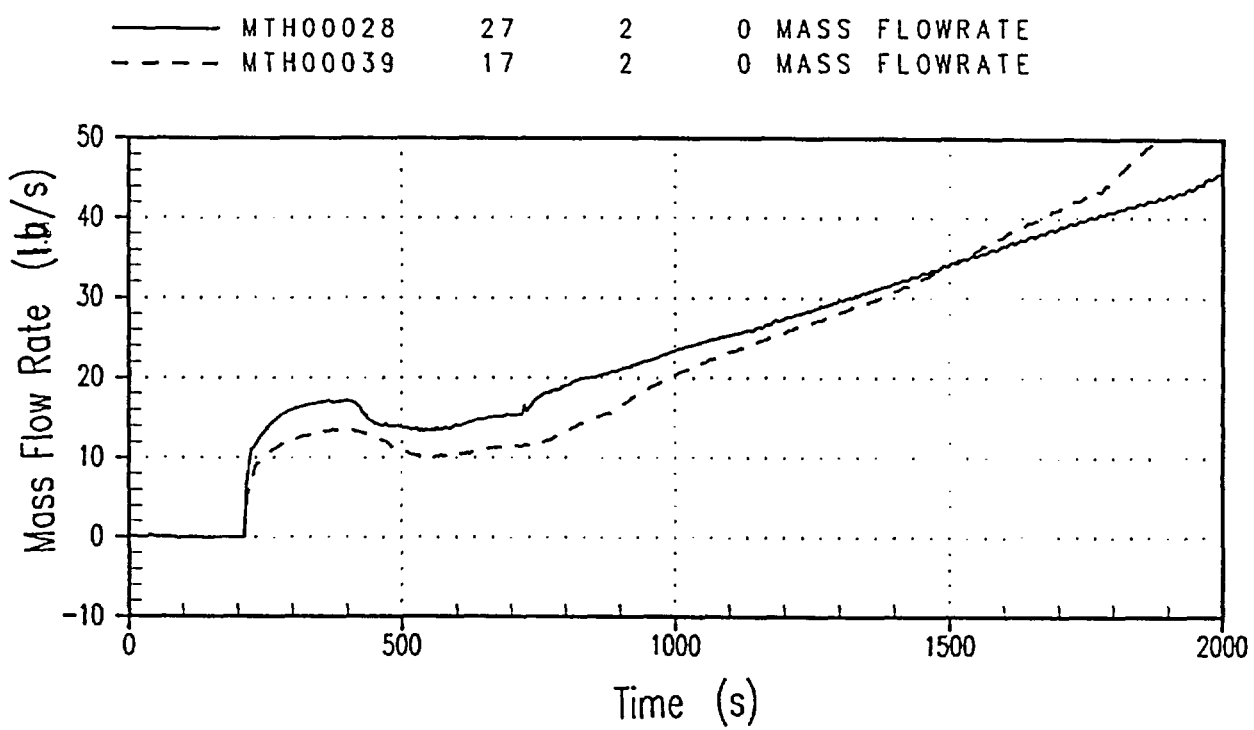


Figure 30-5-5. 3-Inch Break MSSV Setpoint Sensitivity for Total SI Rate

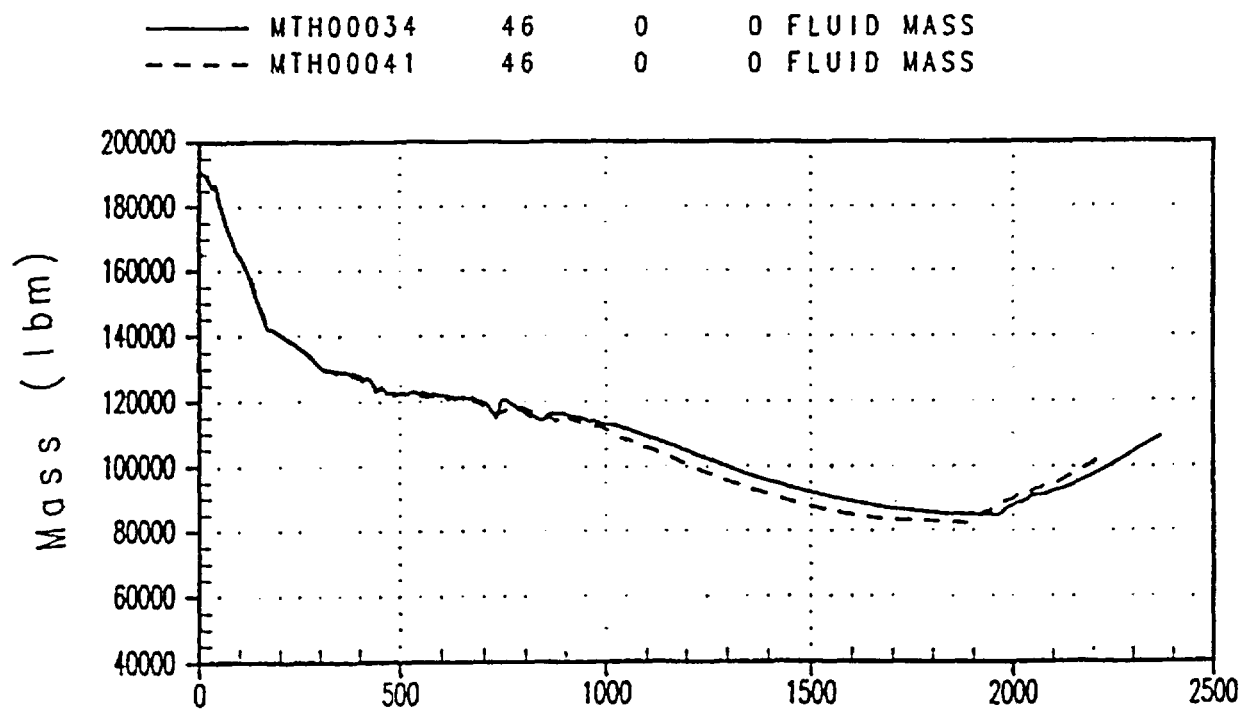


Figure 30-5-6. 3-Inch Break MSSV Setpoint Sensitivity for Reactor Vessel Mass

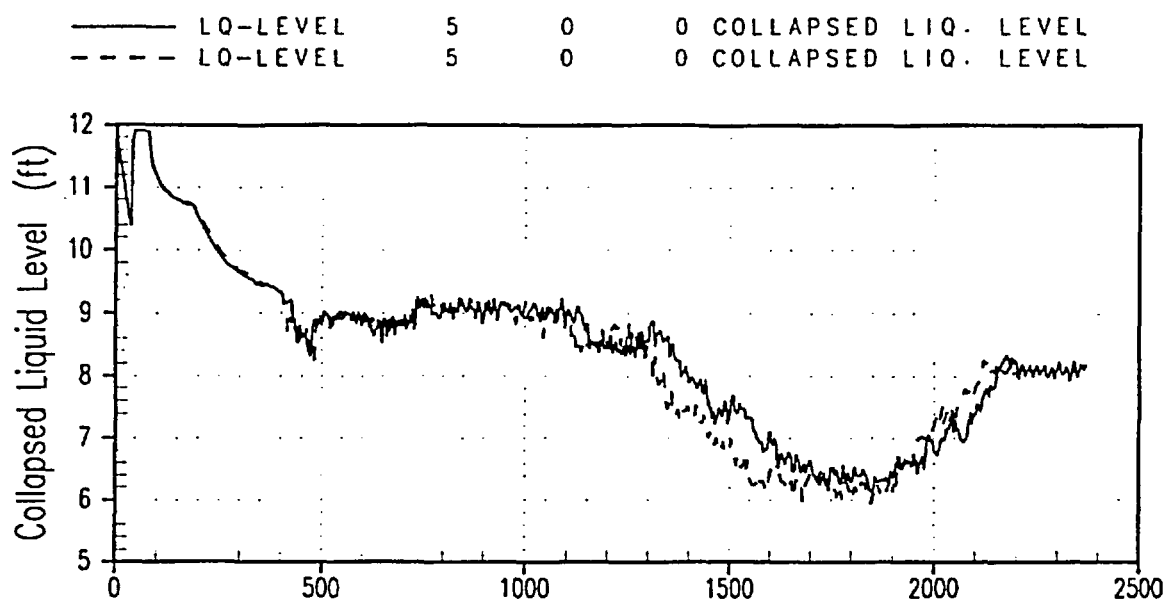


Figure 30-5-7. 3-Inch Break MSSV Setpoint Sensitivity for Core Collapsed Liquid Levels

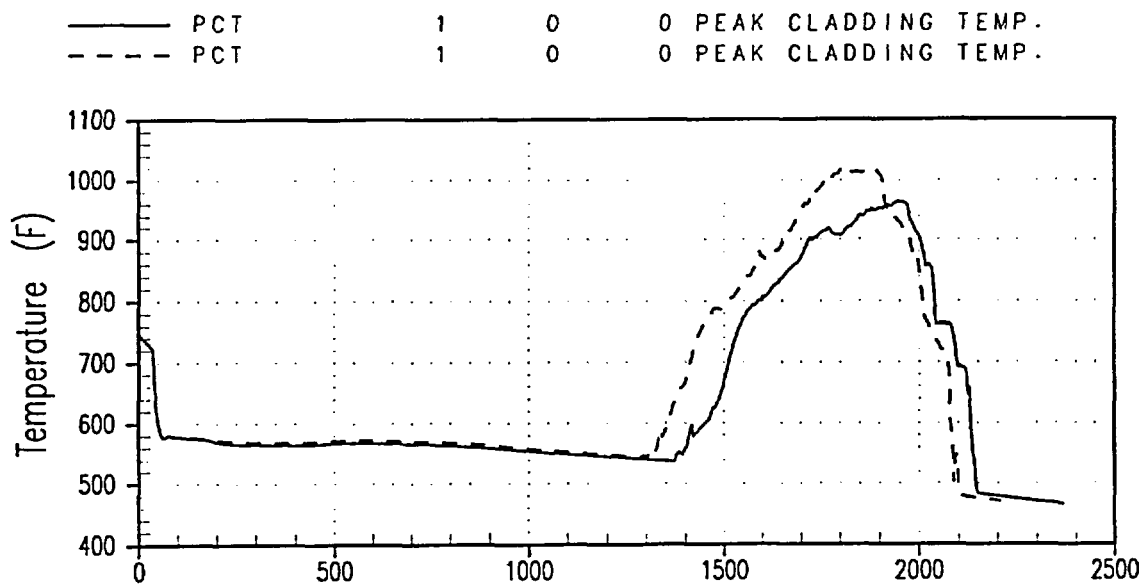


Figure 30-5-8. 3-Inch Break MSSV Setpoint Sensitivity PCT Comparison

30-6 References

Bajorek, S. M., et al., 1998, "Code Qualification Document for Best Estimate LOCA Analysis Volume III: Hydrodynamics, Components and Integral Validation,"
WCAP-12945-P-A, Vol. 3.

SECTION 31

PWR SCOPING STUDIES FOR GLOBAL MODEL RANGING

31-1 Introduction

One of the initial and most important steps in the CSAU process is the development of a Phenomena Identification and Ranking Table (PIRT). For a given accident scenario, the PIRT identifies the physical processes expected to be dominant contributors to uncertainty. These dominant contributors aid in determining the following:

- Computer code to be used for the calculations
- Separate and integral effects tests necessary for validation of the code models and correlations
- Models likely to be ranged at full-scale in PWR simulations

Volume 1 describes the PIRT developed for a conventional Westinghouse PWR assuming a small break LOCA occurs in one of the RCS pipe locations (hot leg, cold leg, or crossover leg). The most dominant small break processes are considered to be the following:

- Break flow
- Mixture level swell
- Loop seal clearance
- Steam generator hydraulics
- Horizontal flow regimes
- Condensation
- Fuel rod model

For each of these processes, uncertainties in the model packages that represent the processes need to be ranged at full PWR scale. Although the calculations in Volume 2 address the uncertainty in some of these model packages, ranging studies are needed to determine the full-scale PWR sensitivity. The following paragraphs describe the Indian Point Unit 2 cases performed relative to ranging:

- Break Flow

The break size is ranged (Section 27, Volume 3) widely—from 2.5-inch to 10-inch equivalent diameter hole size. The studies determine the PCT as a function of break size and identify the limiting size, orientation, and location. Ranging the break size effectively ranges the critical break flow model at PWR scale and captures the sensitivity of PWR results to uncertainty in the subcooled break flow model, which has a small bias. The break flow modeling in the saturated/two-phase flow region, however, exhibits a larger bias and uncertainty; therefore, the break flow in this region will be varied in scoping studies by applying discharge coefficients to the break model.

- Mixture Level Swell

The integral test facility calculations in Sections 19 through 21, Volume 2, bias the vertical interfacial drag in the active core to the 0.8 value obtained in code validation using the Oak Ridge National Laboratory (ORNL) Level Swell Tests (Anklam, 1982) and Westinghouse G-1 Level Swell Tests. Those separate effects test simulations show that the best estimate nominal interfacial drag model overpredicts the level swell; that is, the mixture level is predicted to be at too high a level for a given collapsed liquid level. The bias, applied by reducing the interfacial drag in the small bubble and large bubble regimes by 20 percent, when applied in the analysis of the ORNL and G-1 Level Swell Tests, provides a reasonable prediction of the level swell. The comparison of predicted and measured level swell values suggests that to capture all of the data of these tests, a reduction in the small and large bubble interfacial drag of 60 percent is necessary for some tests, while an increase in the interfacial drag beyond the WCORBA/TRAC-SB best estimate value is needed for others. Because not all of the data is captured by the 20-percent reduction in small and large bubble interfacial

drag, a sensitivity of the PWR results to variation in the core interfacial drag needs to be established.

- Loop Seal Clearance

Loop seal clearance refers not only to those processes that are important in determining the flow through the loop seal, but also those that affect the mass retention and the potential for replugging due to condensate and backflow from the reactor coolant pumps (RCPs). Section 16, Volume 3, shows that countercurrent flow limit (CCFL) in uphill piping to the pump suction is expected to be the most dominant contributor to mass retention and sweep out at PWR scale. Calculations establish the sensitivity of PWR results to interfacial drag in the loop seal exit pipe.

- Steam Generator Hydraulics

Primary to secondary heat transfer is an important means of energy removal from the RCS during the initial phases of a small break LOCA. During the natural circulation phase, condensation in the steam generator tubes removes heat from the primary. However, higher liquid holdup in the uphill steam generator tubes can contribute to the depth during loop seal clearance of mixture in the horizontal pump suction pipe. Flooding in the steam generator tubes also contributes to liquid holdup on the uphill side of the steam generator tubes. The calculations in Section 28, Volume 3, were performed to determine the effect of the total SGTP level. While these simulations alter the primary to secondary heat transfer, they do not address uncertainty in the WCOBRA/TRAC models for wall condensation or natural circulation flow.

Simulations of countercurrent flow in vertical tubes with internal diameters typical of steam generator tubes using WCOBRA/TRAC show that the code predicts flooding at too low a steam superficial velocity. Although this represents a conservative bias in the model, it is not immediately clear if high steam generator tube condensation is necessarily a benefit. Greater steam generator tube condensation retains more liquid inventory that could flow back to the reactor vessel, but may also contribute to more holdup and loss of loop seal mass through the break. Therefore, tube condensation is examined in a sensitivity study.

- Horizontal Flow Regimes

Simulations of countercurrent flow in a large diameter horizontal pipe show that WCOBRA/TRAC tends to predict flooding at too low a value of steam superficial velocity. This may represent a conservative bias in the model because it limits the reflux flow back to the reactor vessel. It is not clear, however, how important are variations in horizontal flow phenomena on PWR results. Therefore, calculations varying the horizontal flow interfacial drag and entrainment determine this sensitivity.

- Condensation

Interfacial heat transfer between subcooled liquid and saturated vapor takes place in several locations in the RCS during a small break LOCA. The most prevalent is condensation in the cold legs. Condensation in the cold legs, a process with considerable uncertainty, could have a significant effect on a small break transient. Condensation of steam flow passing through the cold legs decreases the inventory loss from the RCS. High condensation can also increase the possibility that water could back flow through the pumps to the loop seal and either replug the loop seal or increase the two-phase resistance and increase the core level depression. Therefore, the horizontal stratified condensation needs to be ranged at full PWR scale.

- Fuel Rod Model

The fuel rod models include those that determine heat transfer from the cladding to the fluid and from the fuel pellet to the cladding, and those that account for rod swell and blockage, metal-water reaction, and cladding burst. Most of these models are important only if and when burst occurs. None of the calculations in Section 27, Volume 3, produce PCTs greater than 1000°F for Indian Point Unit 2, which is significantly below the temperature range at which metal-water reaction rates become high. Because heatup rates are relatively slow in a small break LOCA and the cladding temperatures are low, burst is unlikely, even in the most severe realistic small break transient for any Westinghouse PWR. Nevertheless, fuel rod models that determine cladding burst and the like need to be ranged to ensure that for any PWR that may come under consideration in the future, these models do not contribute to the total uncertainty. Because the core becomes uncovered, the wall

to fluid heat transfer coefficient (HTC) uncertainty must be considered; this is accomplished in the HOTSPOT-SB computer code.

The following sections report calculations that estimate the sensitivity of results to variations in the major global models.

31-2 Critical Break Flow

The test facility simulations to assess the WCOBRA-TRAC-SB break flow model in Section 13, Volume 2, identified the individual bias and uncertainty for subcooled break flow and for saturated/two-phase break flow. The bias associated with the code predictions of subcooled break flow is less than 5 percent, and the uncertainty in the subcooled break flow modelling has been addressed by the consideration of a spectrum of break sizes in Section 27, Volume 3. The bias observed in code predictions of saturated and/or two-phase critical break flow is larger at -13.4-percent with a standard deviation of \pm 23.7 percent. Inasmuch as core uncover and the associated PCT transient occur when the break flow has been in the two-phase regime for an extended period, the sensitivity of the code-predicted results to the identified uncertainty in this flow regime should be established. Therefore, the 3-inch reference case transient is simulated with a discharge coefficient applied when two-phase break flow is established after loop seal clearance is predicted to occur. This is accomplished by restarting the reference case after loop seal clearance (at 770 seconds problem time) and applying a discharge coefficient to the break area thereafter. The values chosen for discharge coefficients to range the WCOBRA/TRAC-SB two-phase break flow prediction using this technique are 1.15 and 0.7. [

]^{a,c}

31-2-1 Results at 1.15 Discharge Coefficient

Figure 31-2-1 shows the pressurizer pressure (psia) transient for the reference case (solid line) and the $CD = 1.15$ two-phase break flow case from 500 to 2000 seconds. The x-axis for this and all subsequent figures in subsection 31-2 is time in seconds. Depressurization is delayed in the reference case break because the effective break area is smaller. Figure 31-2-2 shows the break mass flowrate prediction for the $CD = 1.15$ two-phase flow case (dashed line) to be somewhat increased through 1500 seconds transient time. Thereafter, the predicted break flows cross over one another; the pressure in the reference case is high enough that the break flow is larger than

the $CD = 1.15$ two-phase flow case even though the effective break area is smaller. Integral break flows (lbm) following the restart point are compared in Figure 31-2-3. The $CD = 1.15$ two-phase break flow case integrated flow rises above the reference case (solid line) immediately and is about 1.1 times the reference case value at 1000 seconds transient time; from that time forward, the $CD = 1.15$ two-phase break flow case integrated flow is a decreasing multiple of the reference case value.

Figure 31-2-4 compares the total SI flowrates of the reference case (solid line) and the $CD = 1.15$ two-phase flow case. The reference case PCT turns around at the time of accumulator actuation, as does the $CD = 1.15$ two-phase flow case. The $CD = 1.15$ two-phase break flow case PCT turnaround occurs at about 1700 seconds, approximately 250 seconds prior to the reference case. The PCT value of 924°F for the $CD = 1.15$ two-phase break flow case is lower than the reference case value of 964°F.

31-2-2 Results at 0.7 Discharge Coefficient

Figure 31-2-5 shows the pressurizer pressure (psia) transient for the reference case (solid line) and the $CD = 0.7$ two-phase break flow case from 500 to 2500 seconds. Depressurization is delayed in the sensitivity case because the effective break area is smaller. Figure 31-2-6 shows the break mass flowrate prediction for the $CD = 0.7$ two-phase flow case (dashed line) to be significantly reduced through 1500 seconds transient time. Thereafter, the predicted break flows cross over one another; the RCS pressure in the $CD = 0.7$ two-phase break flow case is high enough that the break flow eventually becomes larger than the reference case even though the effective break area is smaller. Integral break flows (lbm) following the restart point are compared in Figure 31-2-7. The $CD = 0.7$ two-phase break flow case integrated flow falls below the reference case (solid line) immediately and is about 0.7 times the reference case value at 1000 seconds transient time; from that time forward, the $CD = 0.7$ two-phase break flow case integrated flow is an increasing fraction of the reference case value.

Figure 31-2-8 compares the total SI flowrates of the reference case (solid line) and the $CD = 0.7$ two-phase flow case. The reference case PCT turns around at the time of accumulator actuation; that time is evident in Figure 31-2-8. The $CD = 0.7$ two-phase break flow case PCT turnaround occurs at 2555 seconds, approximately 300 seconds prior to accumulator actuation. This occurs because the pumped injection approximates the break flow after 2555 seconds in the $CD = 0.7$ two-phase break flow case, and the core collapsed liquid level stops decreasing and exhibits a quasi-steady-state behavior. The PCT value of 954°F for the $CD = 0.7$ two-phase break flow case is close to the reference case value of 964°F.

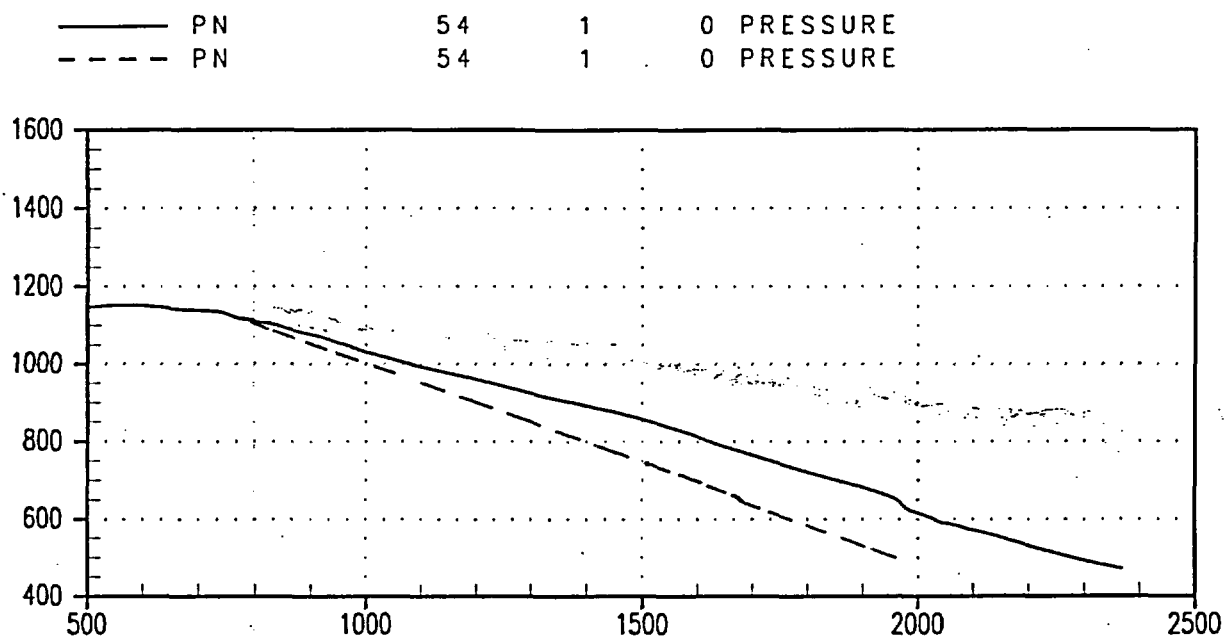


Figure 31-2-1. Pressurizer Pressure (psia) Comparison Between Reference Case and CD (Two-Phase) = 1.15 Case

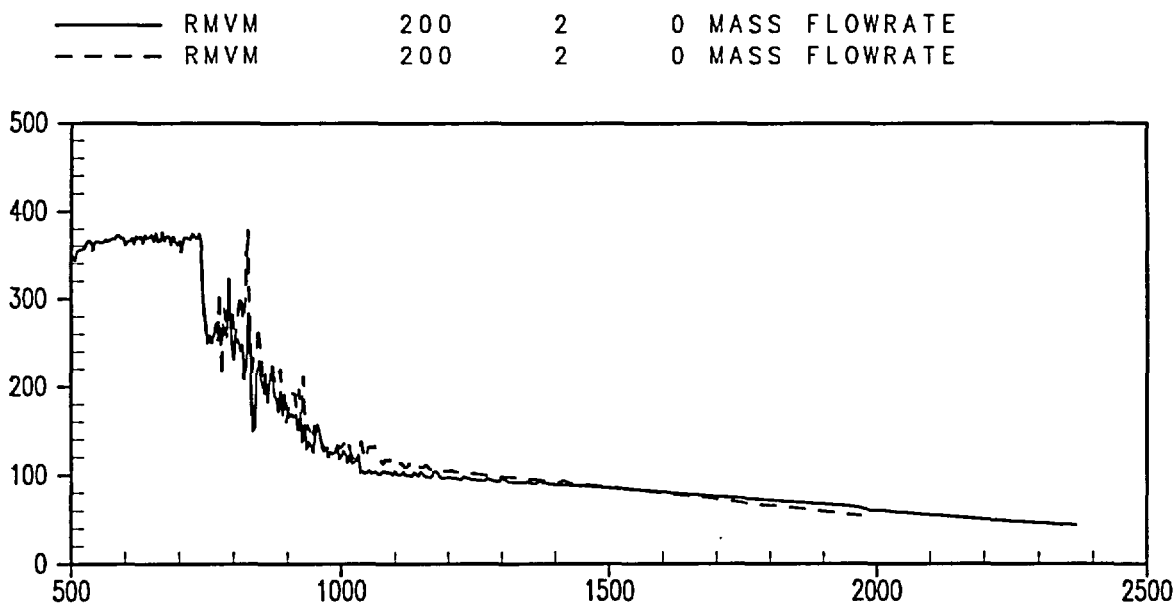


Figure 31-2-2. Break Flowrate (lbm/s) Comparison Between Reference Case and CD (Two-Phase) = 1.15 Case

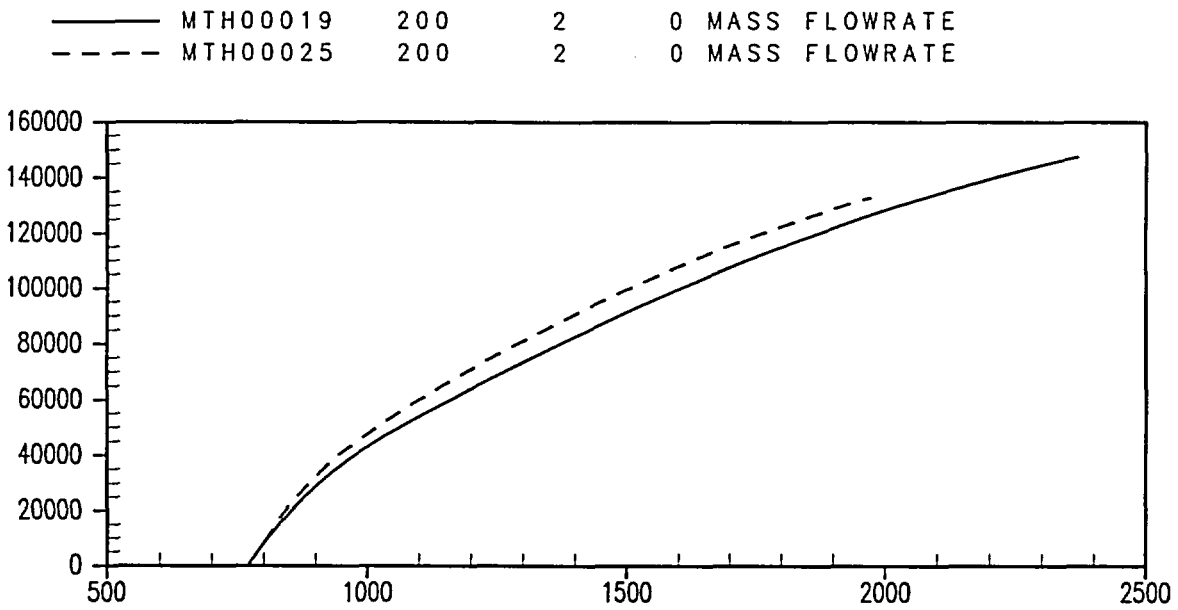


Figure 31-2-3. Integrated Break Flow (lbm) Comparison Between Reference Case and CD (Two-Phase) = 1.15 Case

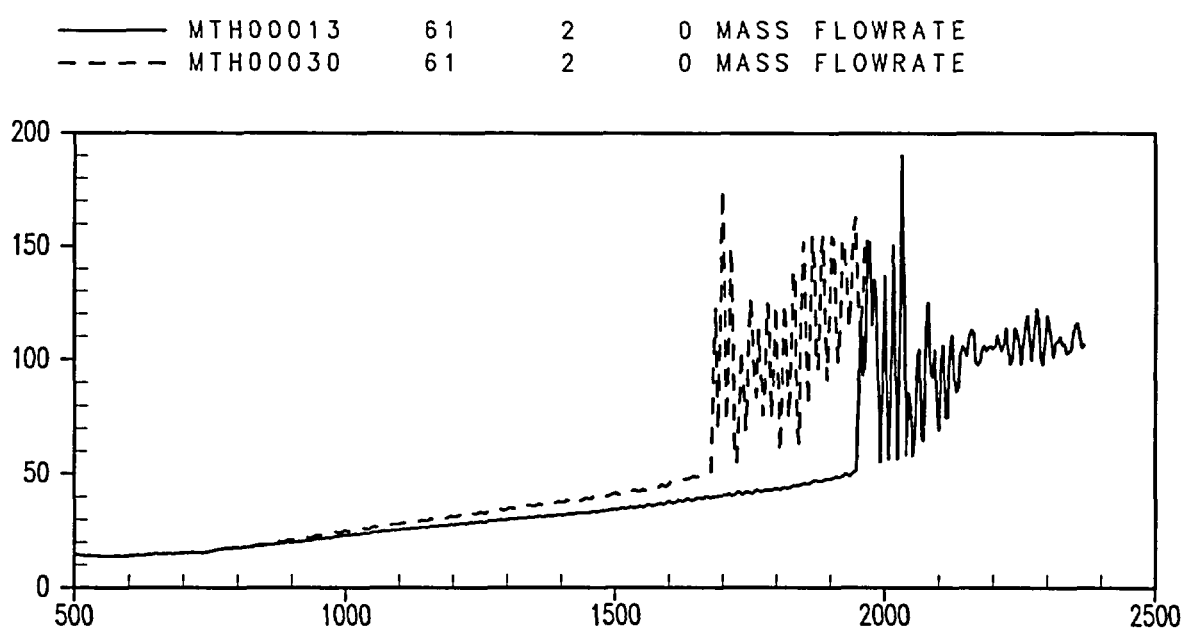


Figure 31-2-4. SI (lbm/s) Comparison Between Reference Case and CD (Two-Phase) = 1.15 Case

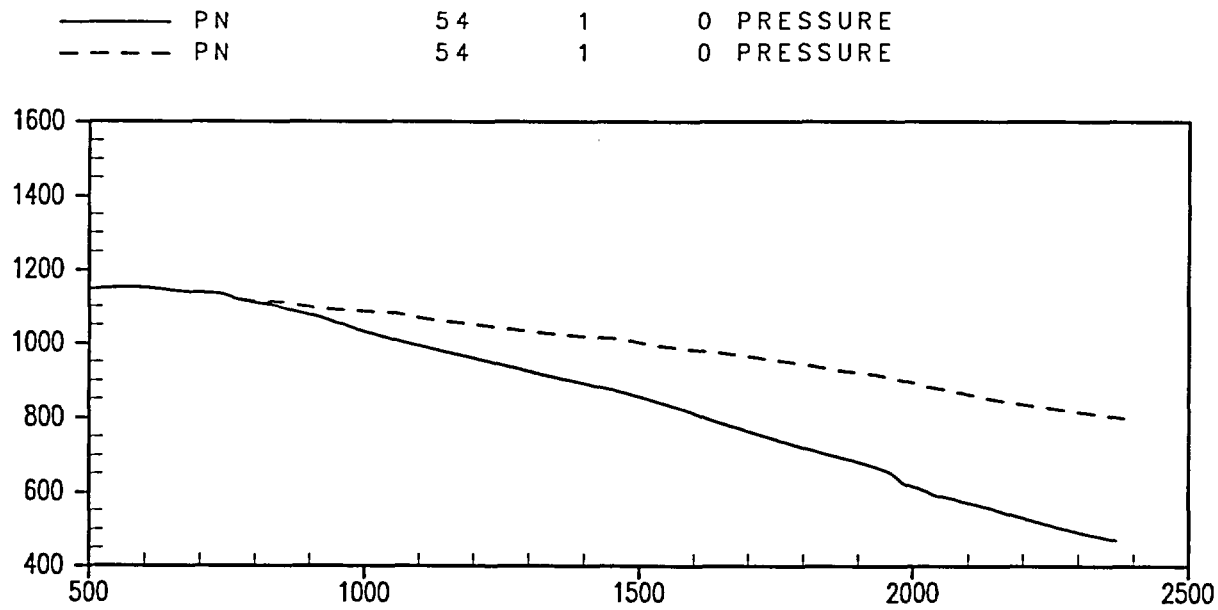


Figure 31-2-5. Pressurizer Pressure (psia) Comparison Between Reference Case and CD (Two-Phase) = 0.7 Case

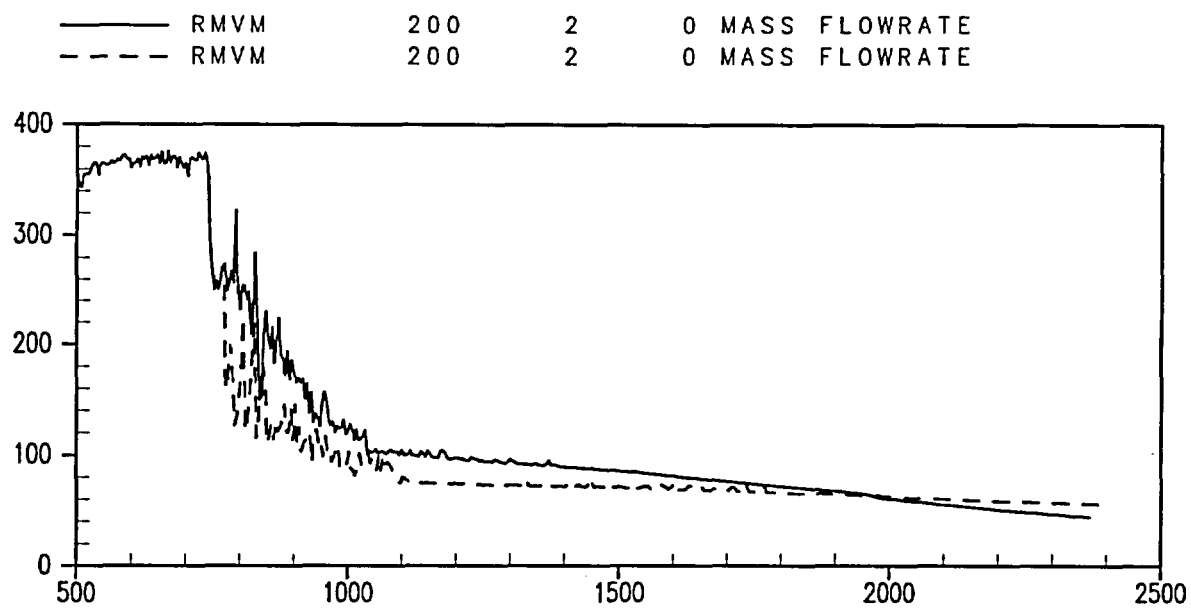


Figure 31-2-6. Break Flowrate (lbm/s) Comparison Between Reference Case and CD (Two-Phase) = 0.7 Case

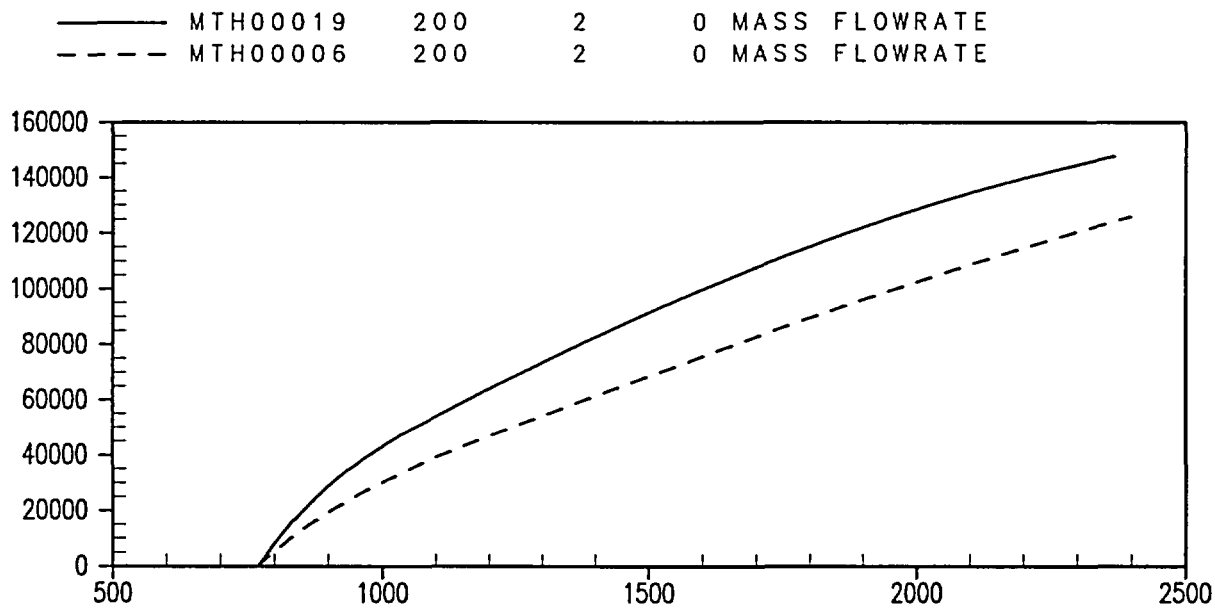


Figure 31-2-7. Integrated Break Flow (lbm) Comparison Between Reference Case and CD (Two-Phase) = 0.7 Case

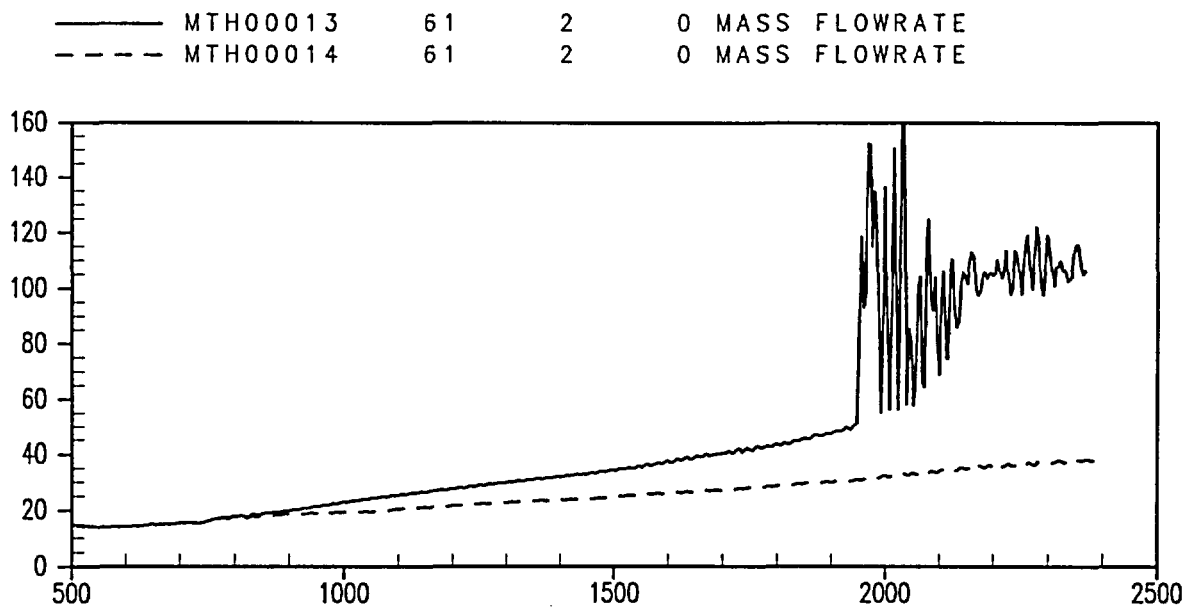


Figure 31-2-8. SI (lbm/s) Comparison Between Reference Case and CD (Two-Phase) = 0.7 Case

31-3 Mixture Level Swell

31-3-1 Introduction

Section 15, Volume 2, examines the prediction of level swell in a heated bundle. The best estimate models in the code underpredict the collapsed level in the ORNL Level Swell and Heat Transfer Tests, while providing a reasonable prediction of the two-phase level. The level swell is defined as:

$$S = \frac{Z_{2\phi} - Z_{CLL}}{Z_{CLL}} \quad (31-1)$$

where Z_{CLL} is the collapsed liquid level and $Z_{2\phi}$ is the two-phase mixture level. If the two-phase level is correct and collapsed level is low, then the level swell is overpredicted.

In the small break analysis of a PWR hot assembly, total bundle mass is calculated. Bundle mass is a function of the break flow and global system hydraulics. The height of the mixture level above the known collapsed liquid level is a function of the interfacial drag in the bundle. The overprediction of level swell in the ORNL simulations suggests that interfacial drag is too high and that application of the models to a PWR will also result in an overprediction of the level swell. This leads to quench at locations above the elevation where quench should take place if the interfacial drag models were exact.

The overprediction in the level swell is attributed to an overestimate of the interfacial drag in the small and large bubble vertical flow regimes. The small bubble regime is assumed in cells with void fraction []^{a,c} and the large bubble regime for []^{a,c}. The results of simulations of the ORNL Level Swell Tests, using the best estimate interfacial drag package in WCORBA/TRAC-SB, indicate the level swell is overpredicted in all but 1 of 12 simulations. With the reduction in interfacial drag, the agreement is much improved. In the Westinghouse G-1 test simulations, the level swell is overpredicted in 8 of 15 cases when the WCORBA/TRAC-SB best estimate package is used.

While the agreement is improved for G-1, there remains scatter about the mean in the predictions. Therefore, the interfacial drag is ranged in several PWR simulations to determine the effect of interfacial drag on uncovery and heatup.

Two simulations were performed for the 3-inch break size. (Each break, as in the reference cases, is at the top of the loop 24 cold leg.) The references for this sensitivity assume LOOP at reactor trip. The interfacial drag is modified by applying a multiplier YDRAG [

]^{a,c} The following sections compare these cases to the appropriate reference cases. A multiplier of 1.0 uses the unmodified, best estimate interfacial drag prediction of WCOBRA/TRAC-SB.

31-3-2 3-Inch Break, High Core Interfacial Drag

A 3-inch break is simulated using an interfacial drag multiplier in the core of YDRAG = 1.0. A multiplier of 1.0 uses the unmodified best estimate interfacial drag and, based on the ORNL and G-1 test simulations, will cause the interfacial drag to be high and overpredict the level swell.

Figures 31-3-1 to 31-3-2 show comparisons between the 3-inch reference case (YDRAG = 0.8) as the solid lines and the high interfacial drag case (YDRAG = 1.0). The x-axis for this and all subsequent figures in subsection 31-3 is time in seconds. As steam is produced in the core, the high interfacial drag between the vapor and continuous liquid fields causes more liquid to be pulled from the core into the upper plenum. The collapsed liquid level in the upper plenum increases at the restart time of 800 seconds and is higher for the YDRAG = 1.0 case than the reference case during most of the rest of the transient. The water in the upper plenum in the YDRAG = 1.0 case drains much later. Simultaneously, the collapsed liquid level in the core for the YDRAG = 1.0 case is less than the reference case over the initial 300-second time period (Figure 31-3-1) following the restart because of voiding. Water is displaced from the core to the upper plenum because the high interfacial drag in the YDRAG = 1.0 case swells liquid out of the core.

Later the collapsed liquid level in the core for the YDRAG = 1.0 case exceeds the level in the reference case during the boiloff period. This is the result of the extra water that was displaced into the upper plenum in the YDRAG = 1.0 case draining back into the core, and also the result of a second loop seal clearing in the YDRAG = 1.0 case. The PCT, shown in Figure 31-3-2, is much lower for the YDRAG = 1.0 case. The PCT for the reference 3-inch break is 964°F, and the PCT in the YDRAG = 1.0 case occurs at the initiation of the transient. Because clearing of the second loop seal is skewing the YDRAG = 1.0 case PCT to a low value, [

]^{a,c}

31-3-3 3-Inch Break, Low Core Interfacial Drag

A second 3-inch break was simulated using an interfacial drag multiplier in the core of YDRAG = 0.4. A multiplier of 0.4 biases the interfacial drag and reduces the value calculated in the code by 60 percent from the best estimate value. The particular value is used because the sensitivity of ORNL and G-1 results to reductions in the small bubble and large bubble interfacial drag indicate that YDRAG = 0.4 would bound nearly all of the data. Therefore, the YDRAG = 0.4 case represents an estimate of the effect of low interfacial drag.

Figures 31-3-3 to 31-3-5 compare the reference 3-inch break (YDRAG = 0.8) as a solid line with the YDRAG = 0.4 case. Now, the collapsed liquid level is higher in the core in the low drag case than in the reference case. Figure 31-3-3 compares the collapsed liquid levels in the upper plenum. The difference begins at the 800-second restart time with a large drop in the YDRAG = 0.4 case collapsed level. The collapsed liquid levels in the core are compared in Figure 31-3-4; the lower interfacial drag YDRAG = 0.4 case exhibits a sudden increase in level at 800 seconds as water moves into the core from the upper plenum. During the core boiloff, the collapsed levels are similar for a period with the YDRAG = 0.4 case minimum level exceeding the reference case minimum level. The core collapsed liquid level at which core uncover begins occurs approximately 90 seconds earlier in the YDRAG = 0.4 case at a value 0.5 feet higher (Figure 31-3-5) with the lower mixture level swell. The PCT for the YDRAG = 0.4 case is 1052°F, well above the YDRAG = 0.8 result.

31-3-4 Core Interfacial Drag Summary

Mixture level swell is a highly ranked process in the small break PIRT, and thus it is important to consider the propagation of uncertainty due to models that determine this process. Code validation simulations for mixture level swell show that the level swell defined by Equation 31-1 is overpredicted for a given collapsed liquid level. The overprediction is due to a bias in the interfacial drag package in the small and large bubble vertical flow regimes in WCobra/TRAC-SB. Reasonable agreement with data could be obtained if the interfacial drag in these two regimes is reduced by 20 percent. This is accomplished by the application of a drag multiplier of YDRAG = 0.8 on the small and large bubble regimes. Because an overprediction of the level swell is nonconservative for PWR calculations, the multiplier of 0.8 is applied in the active core for the reference case break spectrum transients as well as in other scoping calculations. This section considers a variation in the core interfacial drag to confirm that lower

interfacial drag is more conservative and to estimate the effect of a variation of this term on small break PCTs at full PWR scale.

Simulations for the 3-inch break size show that using the WCOBRA/TRAC-SB as-coded interfacial drag model ($YDRAG = 1.0$) results in lower PCTs. The effect of increasing $YDRAG$ from the reference value of 0.8 to 1.0 is dramatic for the 3-inch break reference case. Decreasing $YDRAG$ from the reference case value to 0.4 has the opposite effect on the 3-inch break; it results in a moderate increase in the 3-inch boiloff PCT. In the 3-inch break, steam velocities are low and water cannot be carried to upper elevations unless the interfacial drag is large. Reducing the drag forces more stratification, and as the drag coefficient drops, the vapor velocity is unable to convect as much liquid along with it. Thus, reducing the drag in the 3-inch break case has a major impact on the calculated PCT.

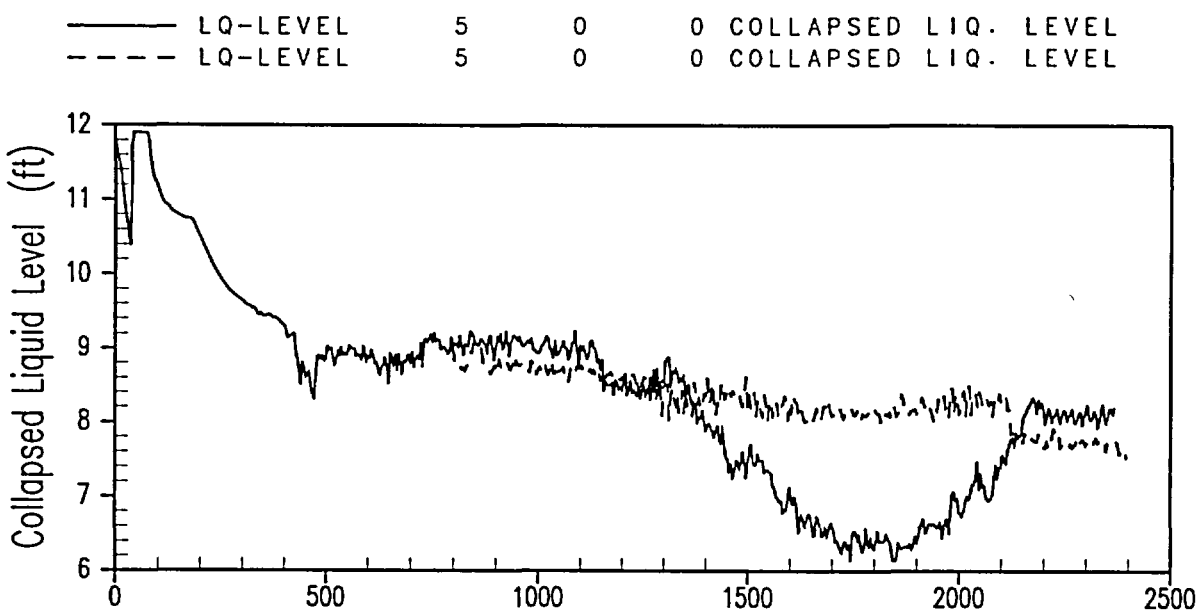


**Figure 31-3-1. Comparison of Core Collapsed Liquid Level:
High Interfacial Drag Case and Reference 3-Inch Break**

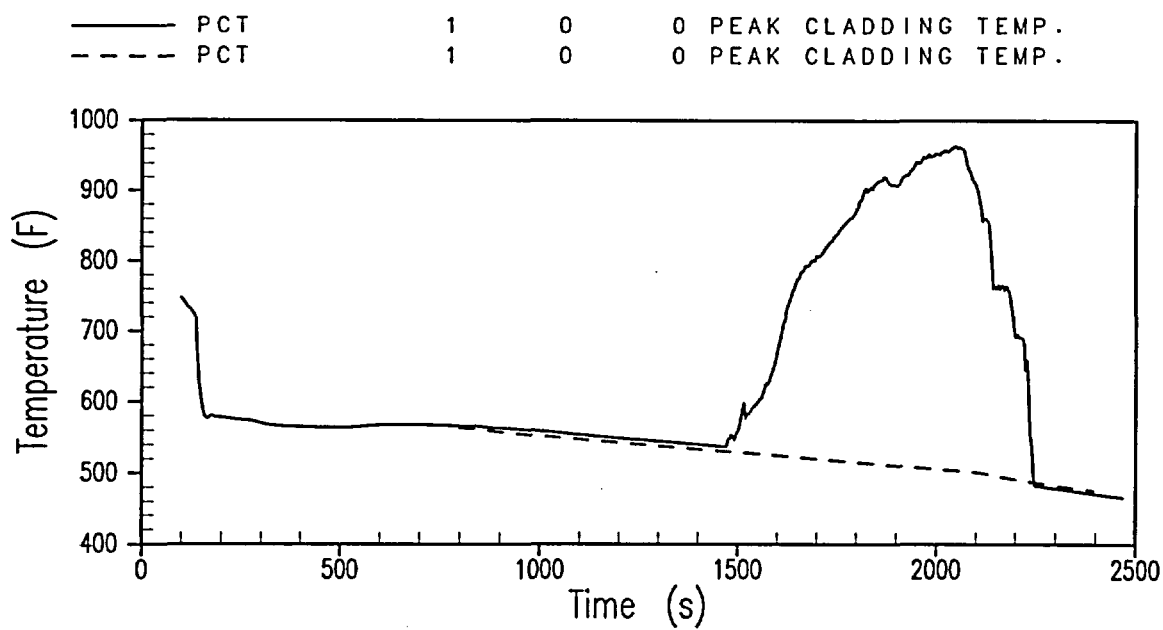


**Figure 31-3-2. Comparison of PCTs: High Interfacial Drag Case and
Reference 3-Inch Break**

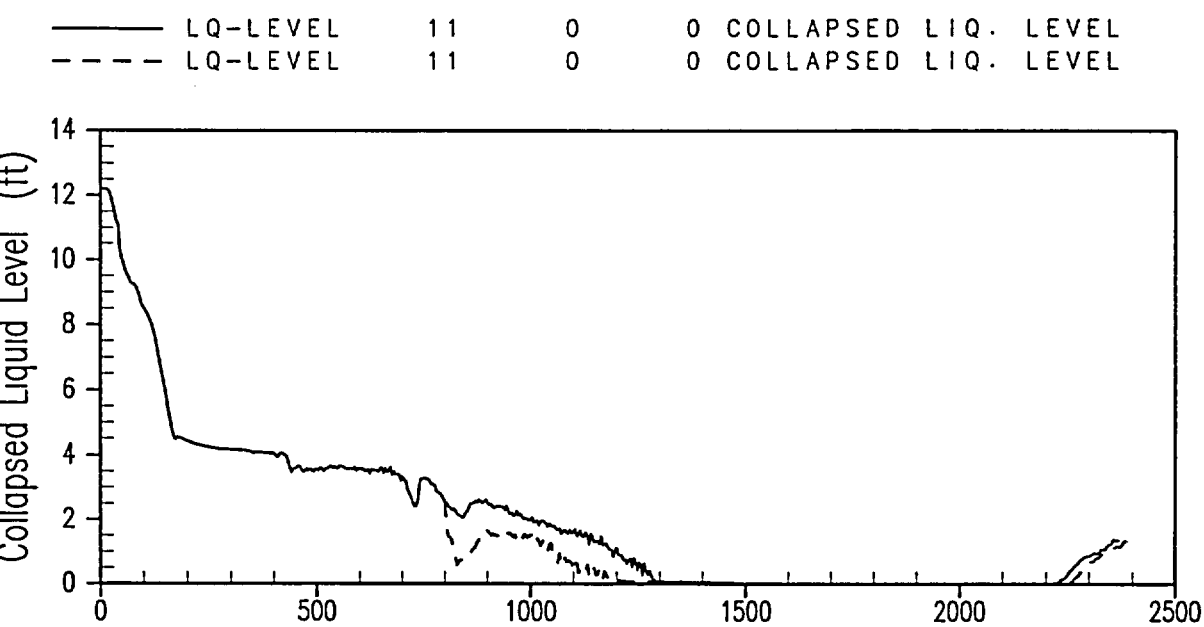


**Figure 31-3-3. Comparison of Upper Plenum Collapsed Liquid Level:
Low Interfacial Drag Case and Reference 3-Inch Break**

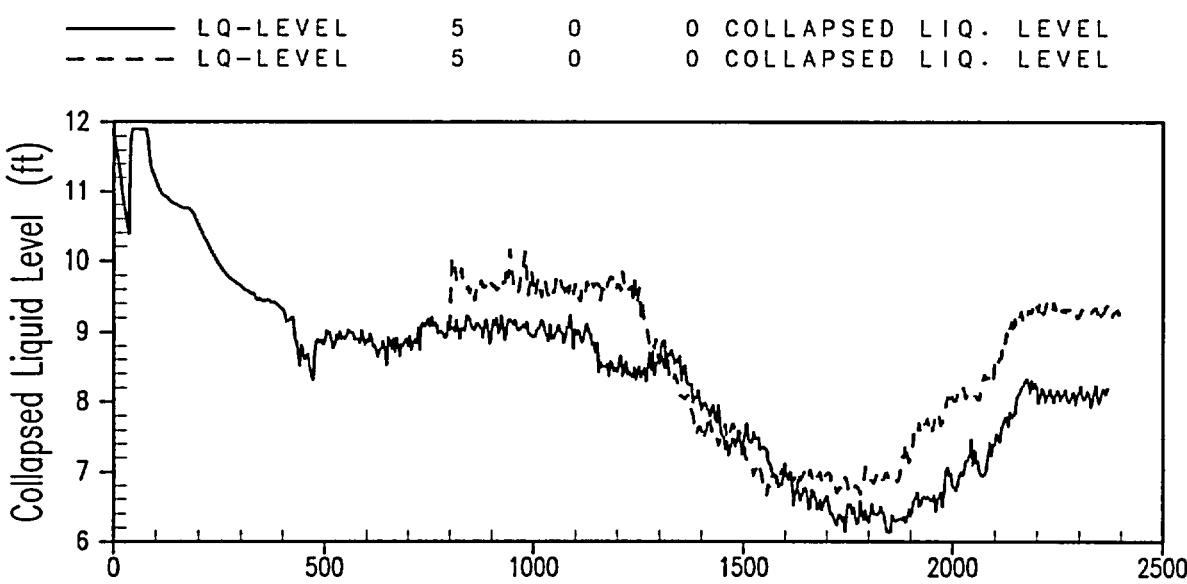


**Figure 31-3-4. Comparison of Core Collapsed Liquid Level:
Low Interfacial Drag Case and Reference 3-Inch Break**

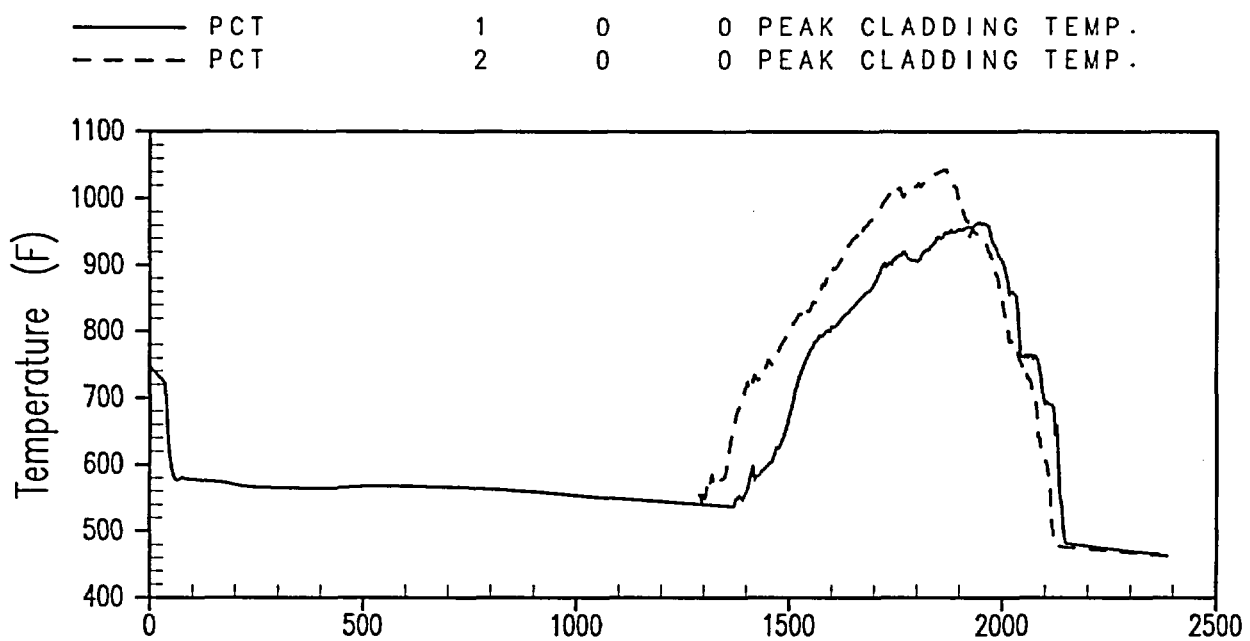


Figure 31-3-5. Comparison of PCTs: Low Interfacial Drag Case and Reference 3-Inch Break

31-4 Steam Generator Hydraulics

The small break PIRT identifies the following steam generator primary side phenomena as High-ranked small break LOCA processes: heat transfer, tube voiding/CCFL, and two-phase flow resistance. Flooding at the steam generator inlet elbow is not of concern at the PWR scale, as discussed in Section 17 of this document.

The effect of the condensation heat transfer magnitude on PWR simulations is not immediately clear. Higher steam condensation allows a more rapid rate of reflux to replenish the hot leg and upper plenum mass inventory. Allowing the steam generator to condense more, however, may increase two-phase resistance to steam flow and mass loss during loop seal clearance in the transient. Therefore, a scoping calculation is done to investigate the potential effect of ranging steam generator wall condensation.

The scoping calculation identifies the result of increasing the steam generator wall condensation in the reference case 3-inch break by [

]^{a,c} Figure 31-4-1 compares the core pressure for the two cases, with the reference case being the solid line. The increased condensation case pressure is lower than the reference case before and after loop seal clearance. Figure 31-4-2 compares the collapsed liquid levels in the upper plenum in the loop seal clearance period. The increased condensation in the high steam generator (dashed line) condensation case requires a greater level depression in the upper plenum to clear loop seal(s). As a result, a second loop seal clears in this case, as shown in Figure 31-4-3, replenishing the downcomer inventory with liquid. Core uncover and heatup do not occur in the high condensation case, and as a result, the PCT is lower than the initial steady-state PCT. The x-axis for the figures in subsection 31-4 is time in seconds.

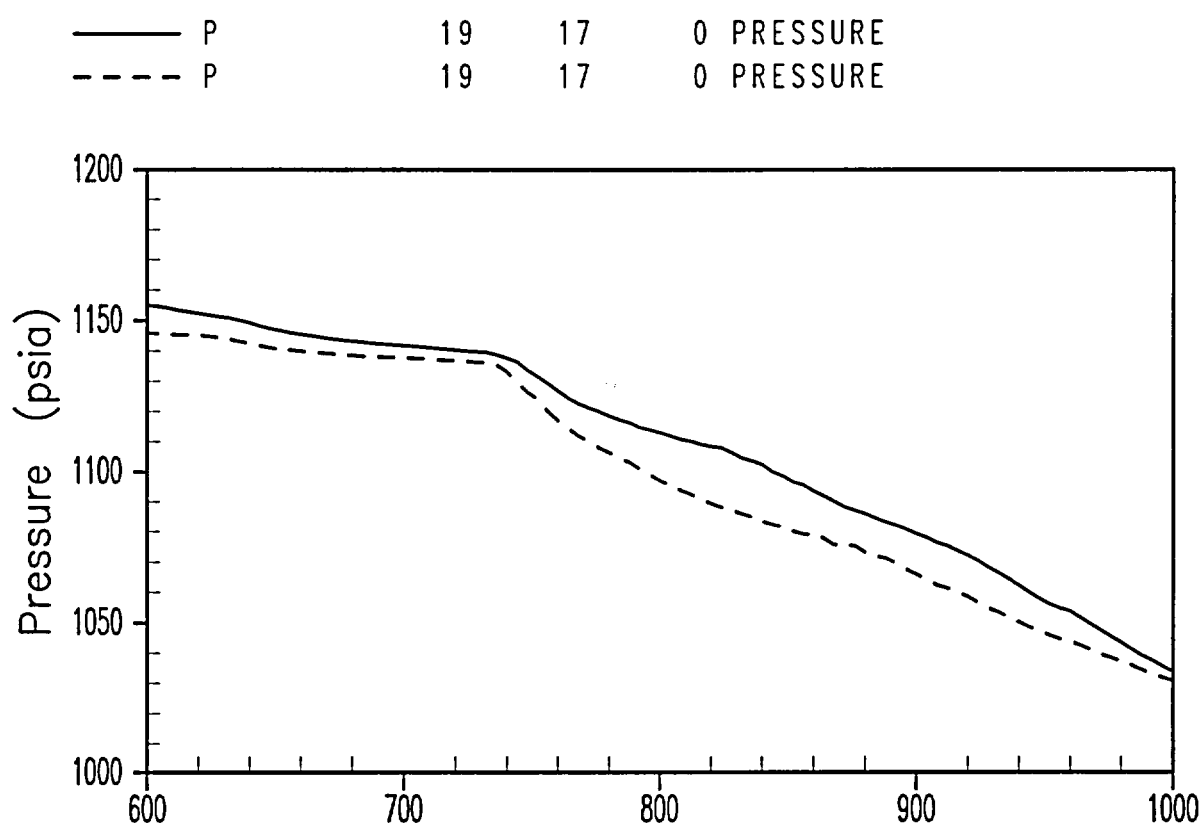


Figure 31-4-1. Core Pressure Comparison: 3-Inch Break With Increased Steam Generator Condensation and Reference Case

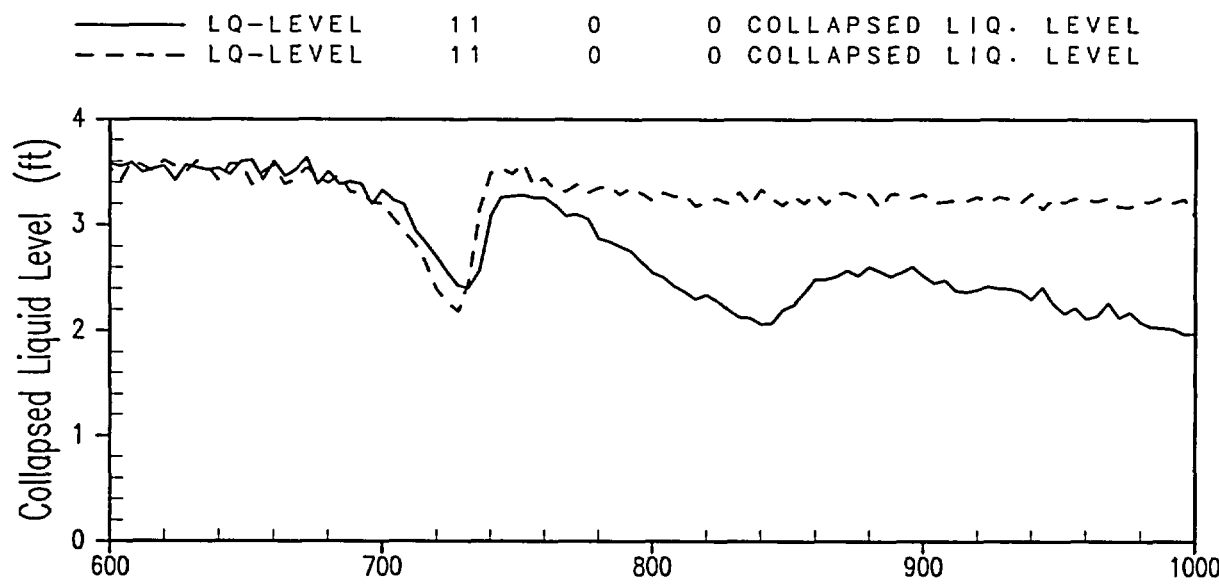


Figure 31-4-2. Comparison of Upper Plenum Collapsed Liquid Levels: 3-Inch Break With Increased Steam Generator Condensation and Reference Case

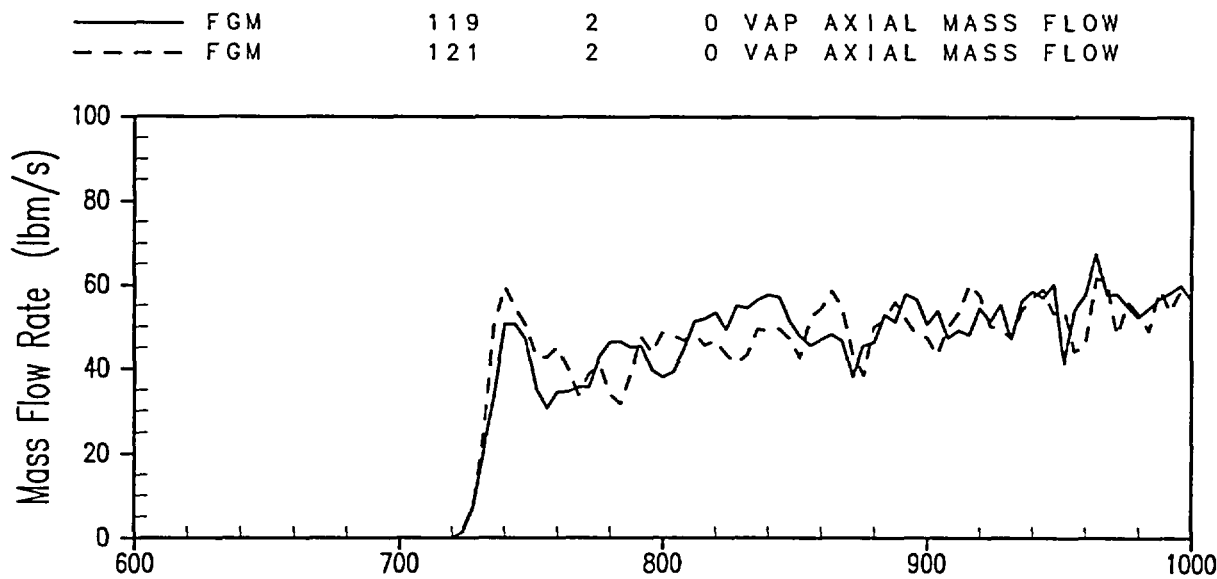


Figure 31-4-3. Loop Seal Clearance: 3-Inch Break With Increased Steam Generator Condensation

31-5 Loop Seal Clearance

The small break PIRT identifies loop seal clearance as one of the dominant small break LOCA processes contributing to the overall uncertainty. When the loop seals clear in a small break LOCA, a large amount of mass initially in the pump suction horizontal piping and in the uphill rise to the RCP is blown out of loop seal where it is redistributed in the RCS. Some mass remains, which can affect the two-phase resistance through the loop seals that clear and have a sustained period of steam flow. As described in Section 16, Volume 2, loop seal clearance at PWR scale is expected to depend on CCFL and flooding in the uphill section of piping to the RCP. The CCFL and flooding behavior in this region is dependent on the interfacial drag, which determines the amount of water that will be carried out of the loop seal for a given steam flow.

In code validation for loop seal clearance, WCOBRA/TRAC tends to overpredict the amount of mass stored in the loop seal for low steam flowrates. The trend reverses at high flowrates as WCOBRA/TRAC overpredicts the amount of mass swept out of the loop seal. The loop seal clearance for the 3-inch break has low steam superficial velocities, which puts the PWR calculation in the range of conditions in which mass is overpredicted. From sensitivity studies, it was found that increasing the interfacial drag approximately []^{a,c} in the uphill section of the piping leading to the pump carries more water out of the loop seal and gives better agreement between predicted and measured mass storage. A scoping study, to examine the effect of the interfacial drag on the loop seal clearance process, was performed for Indian Point Unit 2 in which the vertical interfacial drag in the channels on the uphill side of the pump suction leg is increased by []

[]^{a,c} The break simulated is a 3-inch cold leg break. The x-axis for the figures in subsection 31-5 is time in seconds.

Figures 31-5-1 to 31-5-4 compare the results of the low loop seal drag case to the reference 3-inch break. The PCTs, compared in Figure 31-5-1, show that there is a small effect. The high loop seal drag (dashed curve) case PCT is 972°F, which is less than 10°F higher than the reference case PCT.

The small difference in PCT is due to a slightly smaller vessel inventory in the low loop seal drag case. Figure 31-5-2 compares the core collapsed liquid levels, in which it is seen that the collapsed level in the low loop seal drag case begins decreasing earlier and reaches a value slightly below that of the reference case. The cause of the difference in levels is a result of the

interfacial drag during the brief period in which bubbly flow is convected through the loop seal during natural circulation.

Figure 31-5-3 compares the vapor flow through the cleared loop seal, and Figure 31-5-4 compares the reactor vessel mass for the two cases. Only one loop seal clears in both cases at a different time. Although the same loop clears in both, when the loop seals equilibrate after having cleared the vessel, the collapsed liquid level and fluid mass are reduced slightly in the reduced drag case. The decrease in interfacial drag in the WCOBRA/TRAC-SB channels that represent the pump suction leg makes it more difficult to clear the leg. This has little effect on the overall transient.

Figures 31-5-5 and 31-5-6 compare the results of the high loop seal drag case to the reference (solid line) 3-inch break. The PCTs in Figure 31-5-5 and the collapsed levels in Figure 31-5-6 show the impact of clearing more than one loop seal when increased interfacial drag is assumed. The major difference occurs during the period around 720 seconds, where three loops clear in the high loop seal drag case as opposed to one in the reference case. Figure 31-5-7 shows the vapor through the three loop seals that clear in []^{a,c}

During this time when bubbles are swept from the hot leg through the steam generators and the loop seals, the higher interfacial drag in the sensitivity case enables additional loop seals to clear and more water to be carried (along with the steam) from the loop seals to the downcomer. Figure 31-5-8 compares the reactor vessel mass of the reference case (solid line) and the increased loop seal interfacial drag case. The downcomer inventory of the high loop seal drag case does not diminish at all at loop seal clearance. This results in a larger inner vessel inventory during the boiloff period, and no core uncover is predicted. Thus, although decreasing the loop seal interfacial drag had little effect, increasing it permitted three loops to clear, which significantly affected the transient. In conclusion, decreasing the interfacial drag in the pump suction leg []^{a,c} has an insignificant effect on the Indian Point Unit 2, 3-inch break case results.

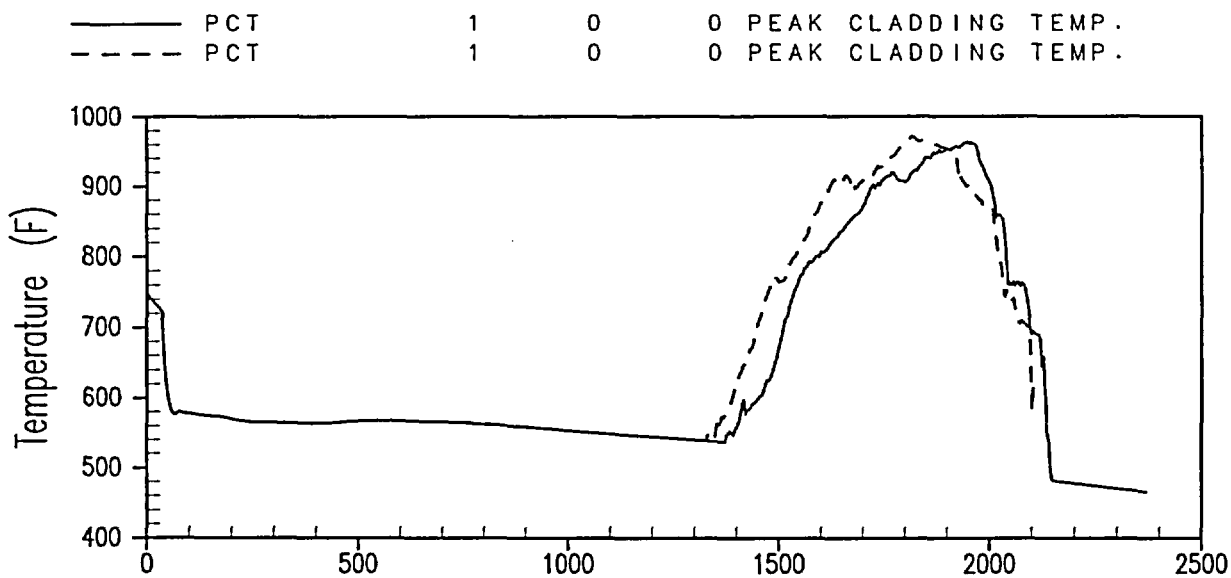


Figure 31-5-1. Comparison of PCTs: Low Loop Seal Drag Case and Reference 3-Inch Break

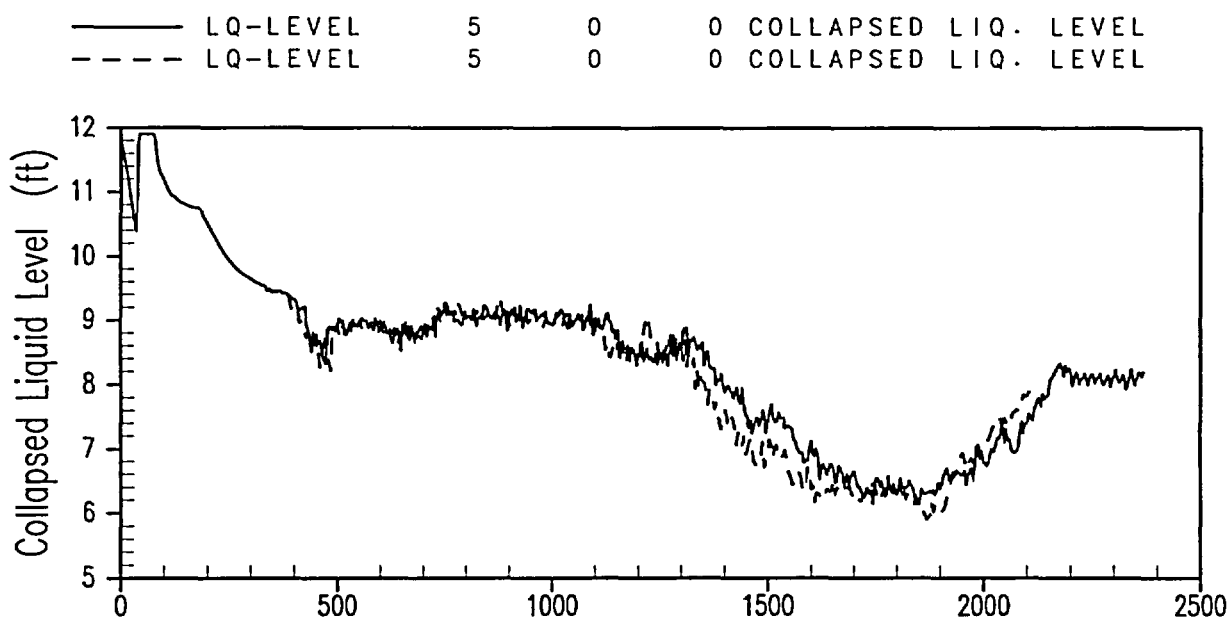


Figure 31-5-2. Comparison of Core Collapsed Liquid Levels: Low Loop Seal Drag Case and Reference 3-Inch Break

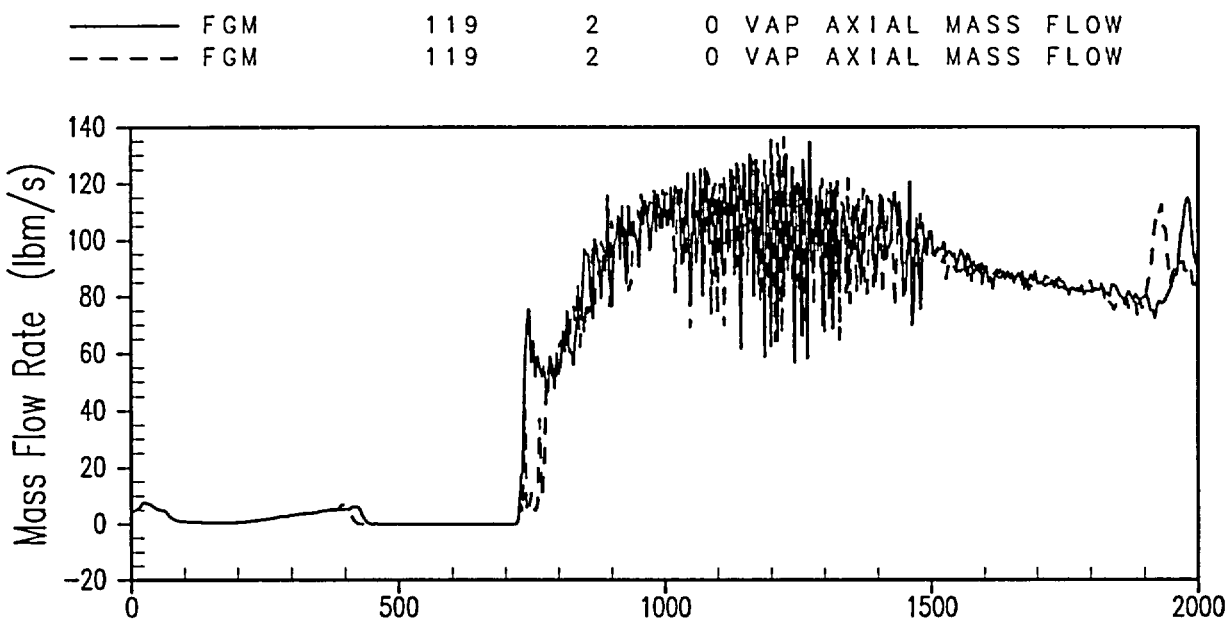


Figure 31-5-3. Comparison of Loop Seal Vapor Flowrates: Low Loop Seal Drag Case and Reference 3-Inch Break

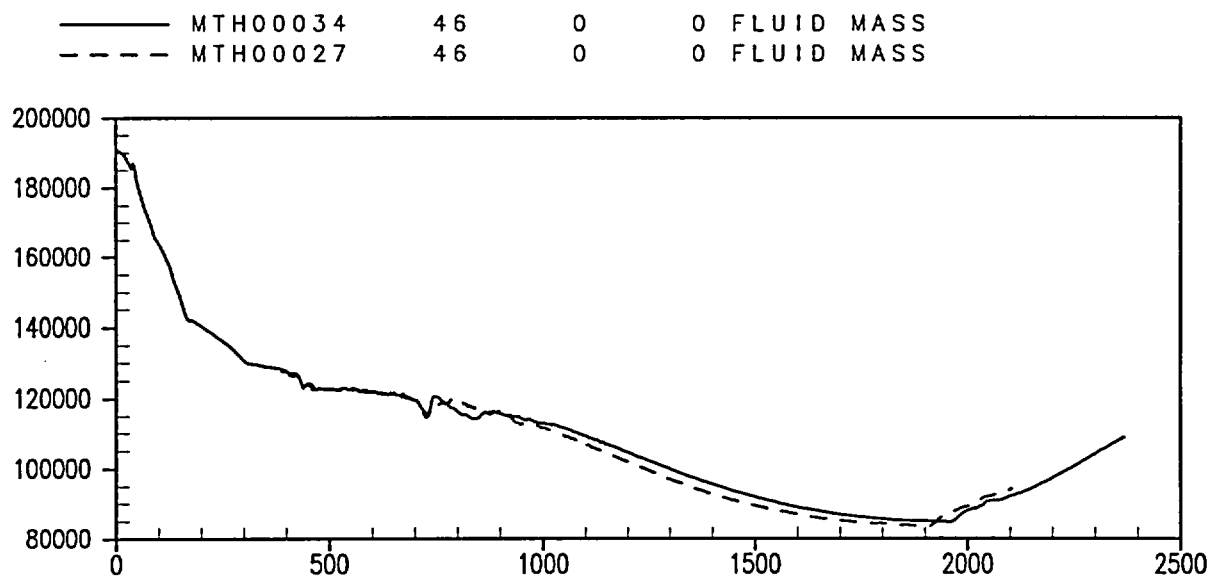


Figure 31-5-4. Comparison of Reactor Vessel Mass (lbm): Low Loop Seal Drag Case and Reference 3-Inch Break

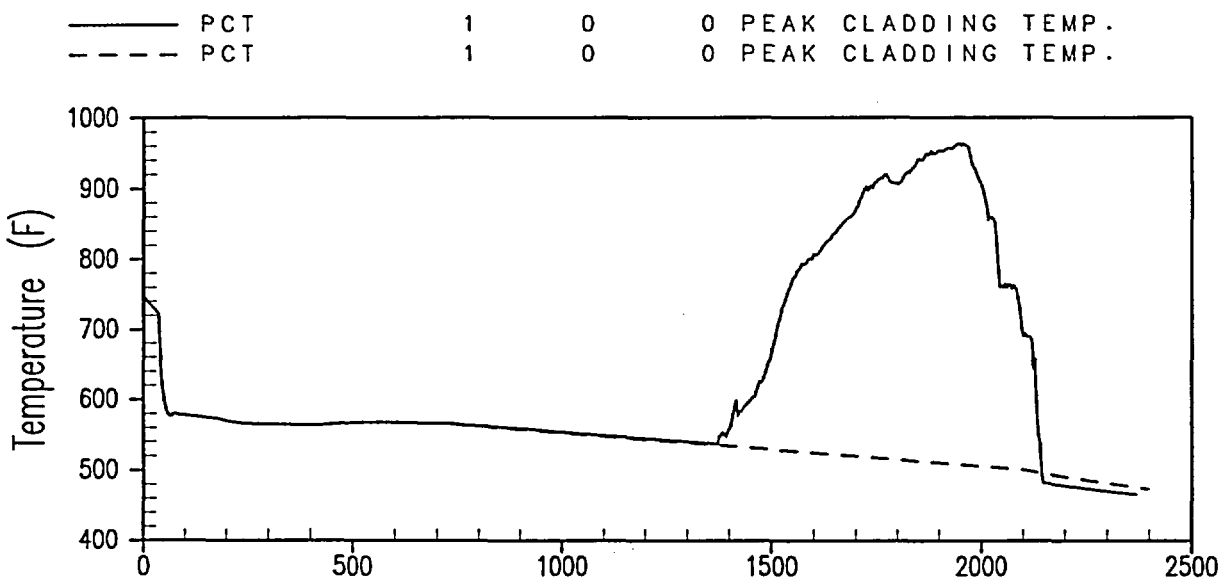


Figure 31-5-5. Comparison of PCTs: High Loop Seal Drag Case and Reference 3-Inch Break

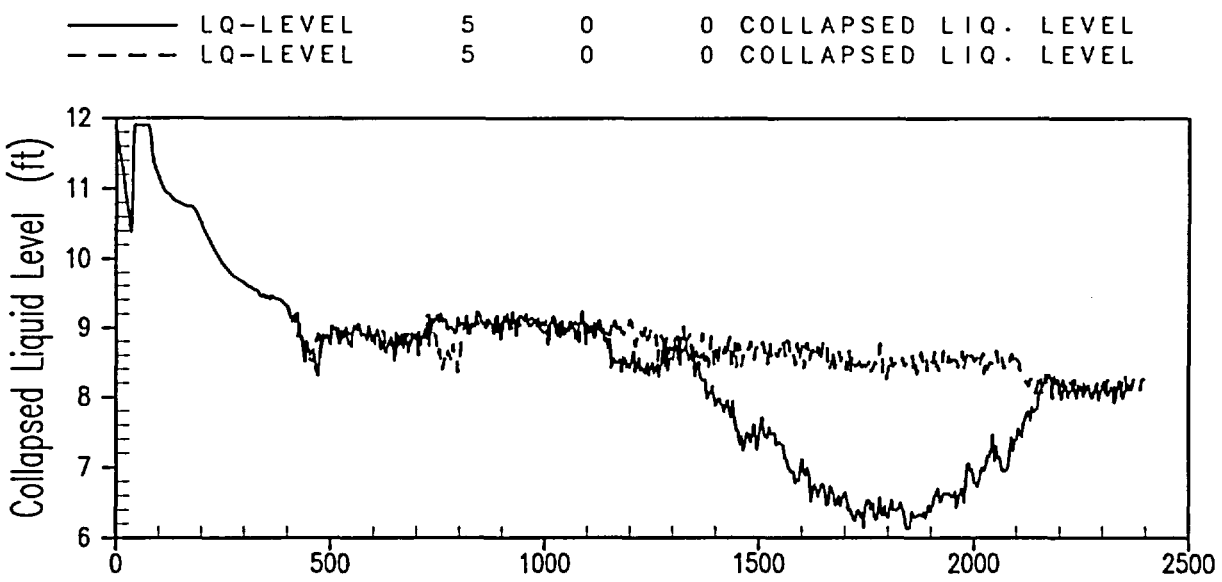


Figure 31-5-6. Comparison of Core Collapsed Liquid Levels: High Loop Seal Drag Case and Reference 3-Inch Break

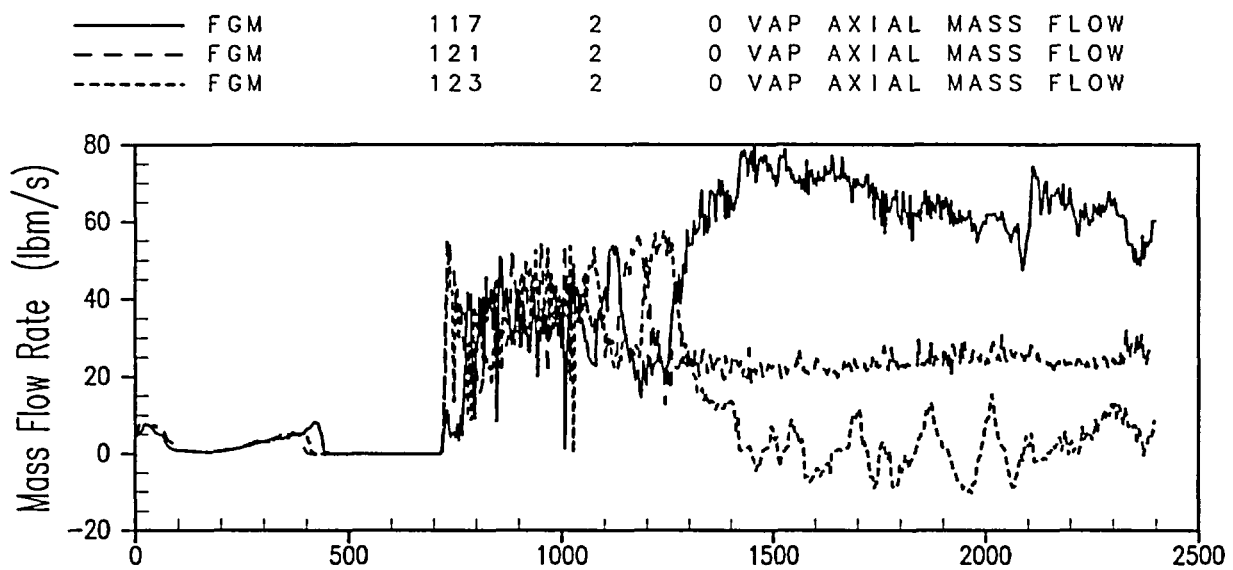


Figure 31-5-7. Loop Seal Vapor Flowrates: High Loop Seal Drag Case

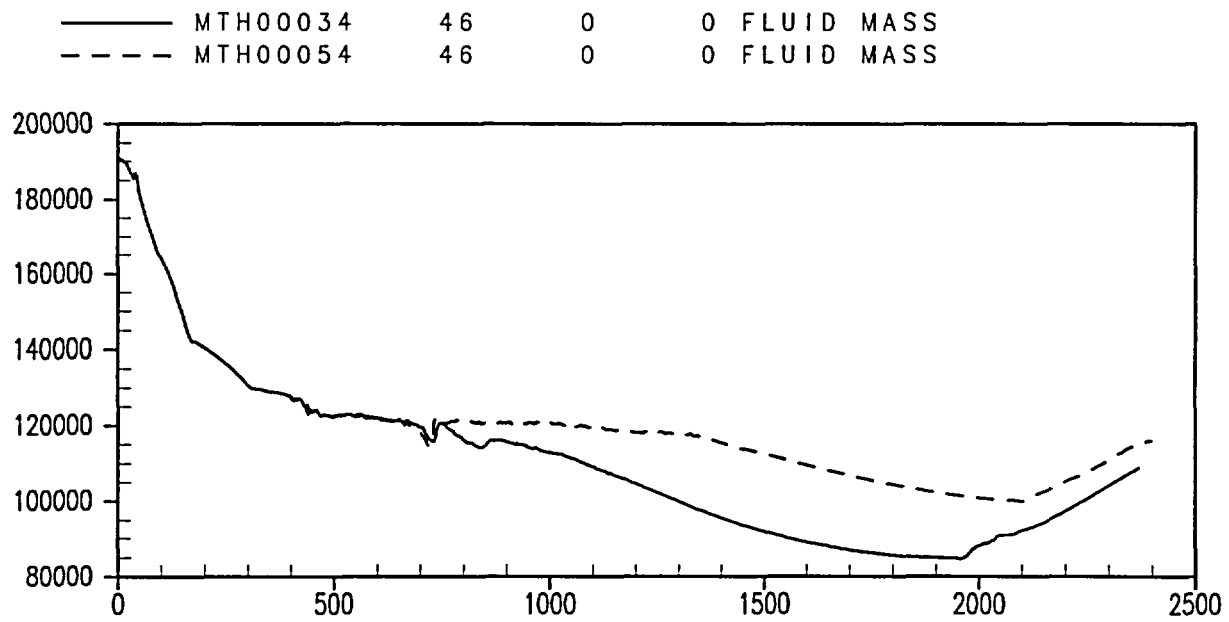


Figure 31-5-8. Comparison of Reactor Vessel Mass (lbm): High Loop Seal Drag Case and Reference 3-Inch Break

31-6 Horizontal Stratified Flow

31-6-1 Introduction

The modifications to WCOBRA/TRAC-MOD7A, Revision 4, to make the code applicable to small break LOAs include the ability to identify conditions of horizontal stratified flow. Models have been added to calculate the interfacial drag and entrainment from a stratified layer when horizontal stratified flow exists. The models for horizontal stratified interfacial drag and entrainment are important in determining CCFL and flooding in horizontal sections of RCS piping. These processes are identified in the PIRT as significant contributors to uncertainty in a small break LOCA. The effect of interfacial drag in the horizontal stratified flow regime is considered in Section 31-6-2. Section 31-6-3 considers entrainment from a horizontal stratified flow.

Included under horizontal flow regimes are CCFL and flooding in the horizontal part of the hot leg where steam velocities in the horizontal stratified flow regime may be sufficient to cause flooding. Another possible location for flooding to occur is at the steam generator inlet elbow. At this location, reflux from the steam generator and water that is forced toward the elbow from the hot leg may cause flooding to occur. As noted in Section 17, Volume 2, PWR scale flooding does not occur in the steam generator inlet elbow.

31-6-2 Horizontal Stratified Interfacial Drag

Figure 31-6-1 shows the results from code validation for CCFL and flooding in horizontal flows with WCOBRA/TRAC. Flooding is predicted at too low a steam flowrate in comparison to experimental information; a possible cause for this discrepancy is that the interfacial drag for the horizontal stratified flow regime is too large. In determining the effect on PWR calculations, a scoping study was made in which the interfacial drag in the horizontal stratified flow regime is reduced. [

]^{a,c} In this way, all horizontal flows in the hot and cold legs are affected. A 3-inch cold leg break with LOOP is simulated; all other input remains as in the reference case.

Figures 31-6-2 and 31-6-3 compare the results of this low horizontal stratified drag case to the reference 3-inch break results; the x-axis for this and all subsequent figures in subsection 31-6 is time in seconds. Figure 31-6-2 compares the PCT transient of the reference case (solid line) with that of the reduced interfacial drag case. Even though Figure 31-6-3 shows that reactor vessel

mass in the low drag case is almost the same as in the reference case (solid line), the core uncover transient is almost the same in the low coolant loop drag case. The low horizontal stratified drag case has a PCT of 966°F, which is virtually the same as the reference case PCT.

The sensitivity shows that variations in the horizontal stratified interfacial drag do not have a significant effect on overall small break LOCA results. The impact of uncertainty in the horizontal interfacial drag is negligible.

31-6-3 Horizontal Stratified Entrainment

Entrainment from a horizontal stratified layer also contributes to the uncertainty in the stratified flow regime. If vapor velocities are sufficiently high, entrainment can occur in the hot and cold legs or in the horizontal section of the loop seals. High entrainment is not expected to play an important role in breaks with relatively small sizes because of the low steam velocities. Thus, variation of the entrainment rate is not expected to impact the 3-inch cold leg break, which produces the limiting PCT. Nevertheless, a scoping study was performed in which the entrainment in horizontal stratified flows everywhere in the RCS is altered both up and down. The 3-inch cold leg break with LOOP is used for the simulation with only that particular input varied from the reference case. The increase is applied in WCOBRA/TRAC by setting the input [

]^{a,c}

Figures 31-6-4 and 31-6-5 compare the results of the low entrainment rate case to the reference 3-inch break. Figure 31-6-4 compares the collapsed liquid levels in the core, showing little overall difference between the reference case (solid line) and the low entrainment rate case. Although there are small differences between the two calculations after the time of core uncover, at about 1750 seconds, the collapsed liquid levels and the PCTs of the cases both equal each other (Figure 31-6-5). The horizontal stratified flow regime occurs in all four of the cold legs. Steam flows are high enough that droplets are entrained in the cold legs where they are carried by the steam to the broken cold leg. However, the flow of entrained drops into the broken cold leg from the vessel side is essentially the same in the reference case and the low entrainment case at a low value []^{a,c} Later on, the reference case PCT reaches and then exceeds the low entrainment rate case value. The decreased entrainment case PCT is almost the same as the reference case (960°F versus 964°F), so the uncertainty effect of decreasing the horizontal stratified flow entrainment rate coefficient is insignificant.

The case in which the input parameter was increased cleared the loop seal in the broken loop shortly after the change was made. Figure 31-6-6 shows that the steam flow through the broken loop rises rapidly (dashed line) when the clearing occurs and that eventually the loop seal that had originally cleared replugs. Because the second loop seal clears, more mass enters the downcomer from the cold leg in the high entrainment case and is available for core inventory replenishment. As a result, core uncovering is delayed and the high entrainment PCT occurs at the start of the transient.

Because increasing the entrainment coefficient facilitates the removal of liquid from a channel in horizontal stratified flow, it is not unexpected that the steam flow proceeding to the break could clear the loop seal of the broken loop at a high entrainment coefficient.

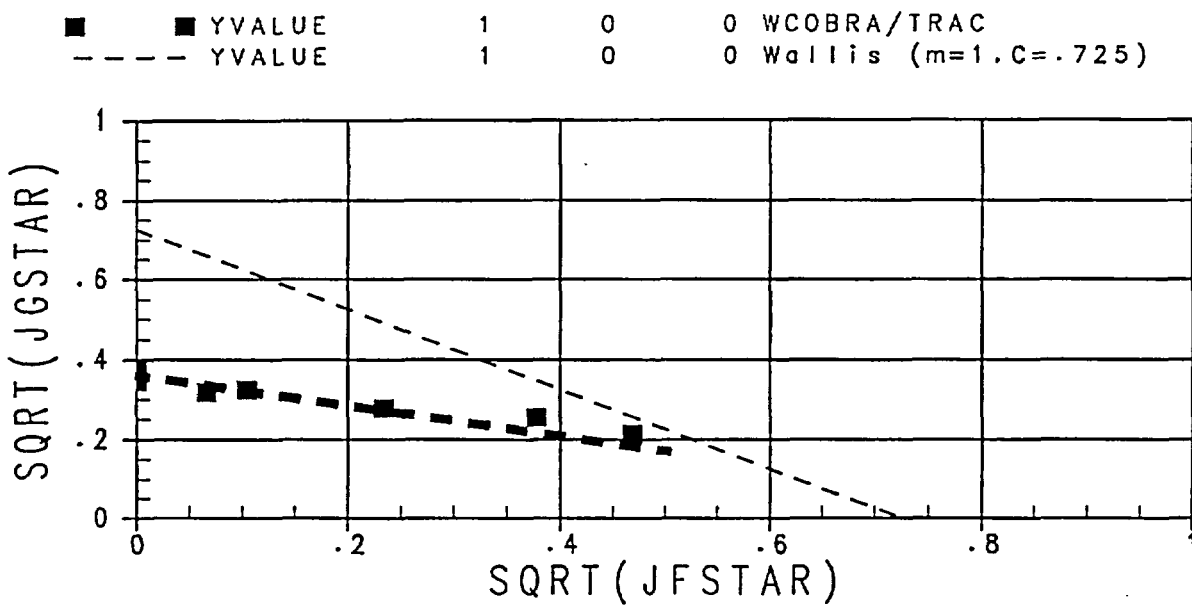


Figure 31-6-1. WCOBRA/TRAC Prediction of Flooding and CCFL in Horizontal Stratified Flows

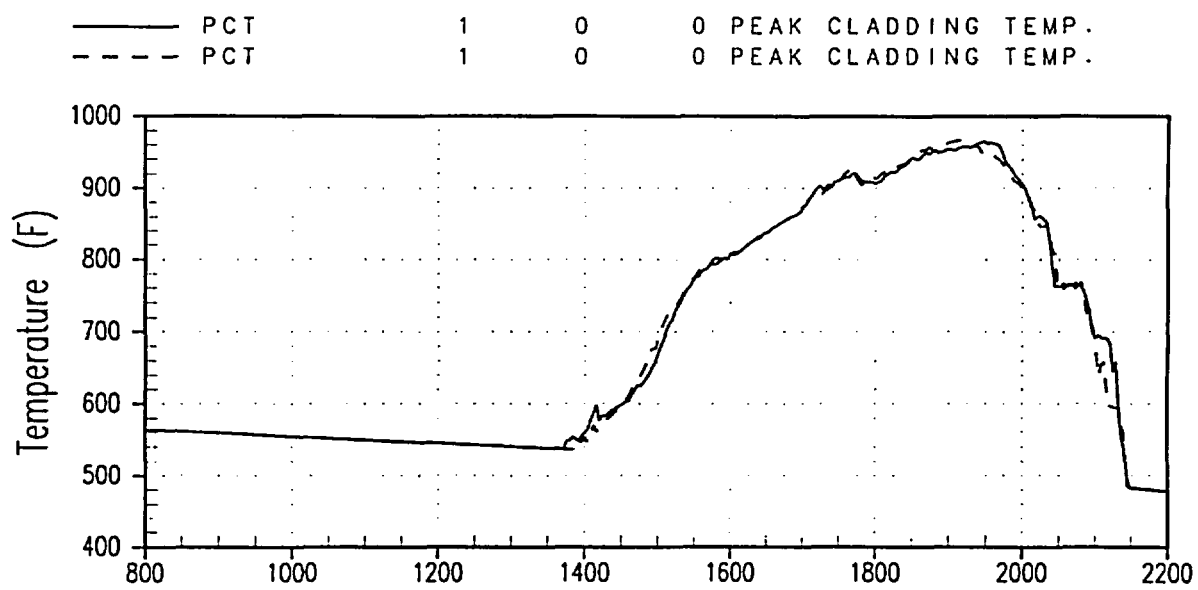


Figure 31-6-2. Comparison of PCTs: Low Horizontal Stratified Drag Case and Reference 3-Inch Break

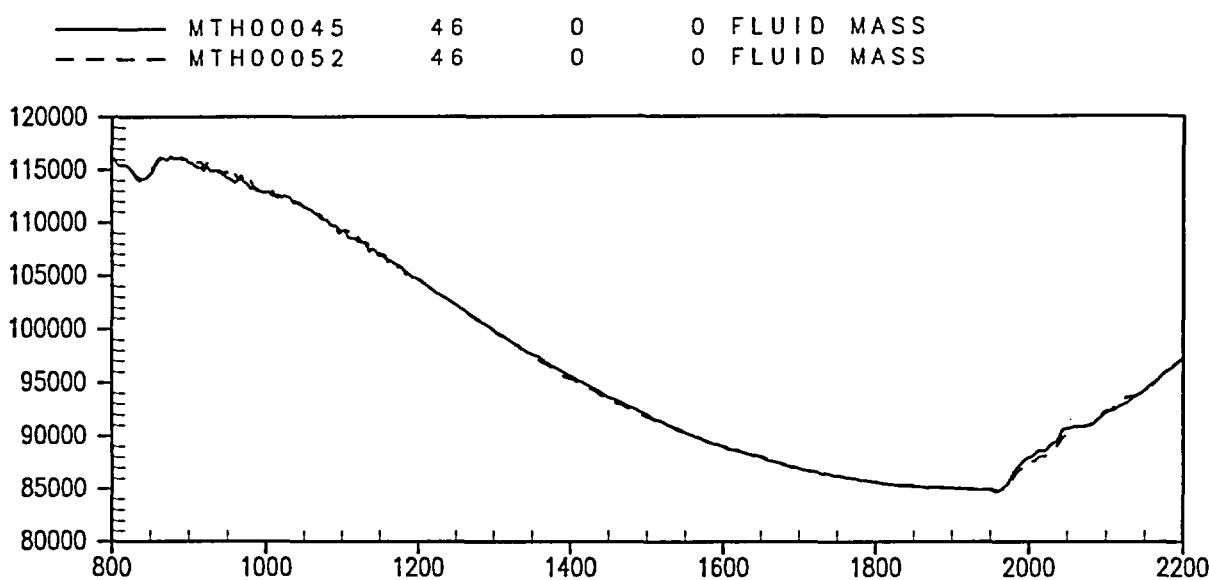


Figure 31-6-3. Comparison of Reactor Vessel Mass Inventories (lbm): Low Horizontal Stratified Drag Case and Reference 3-Inch Break

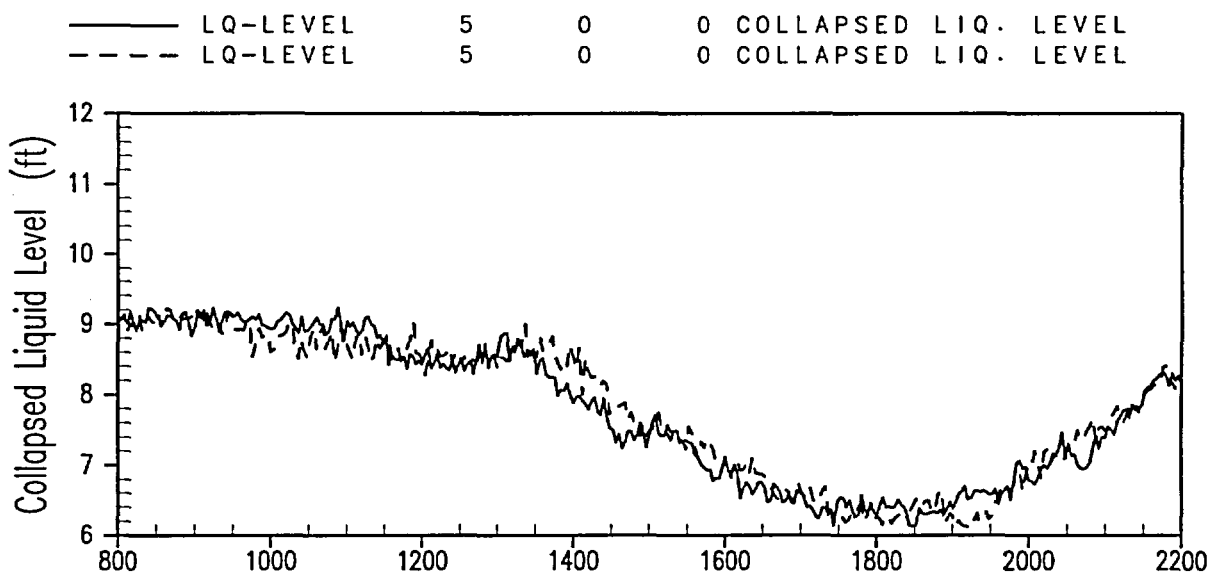


Figure 31-6-4. Comparison of Core Collapsed Liquid Level: Low Entrainment Case and Reference 3-Inch Break

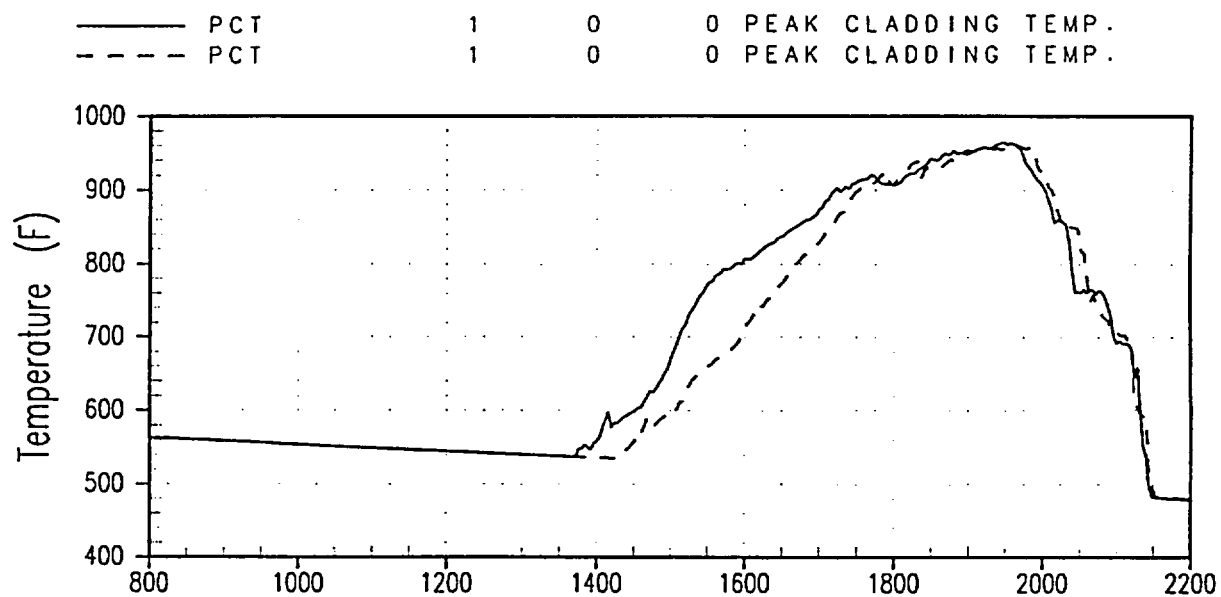


Figure 31-6-5. Comparison of PCTs: Low Entrainment Case and Reference 3-Inch Break

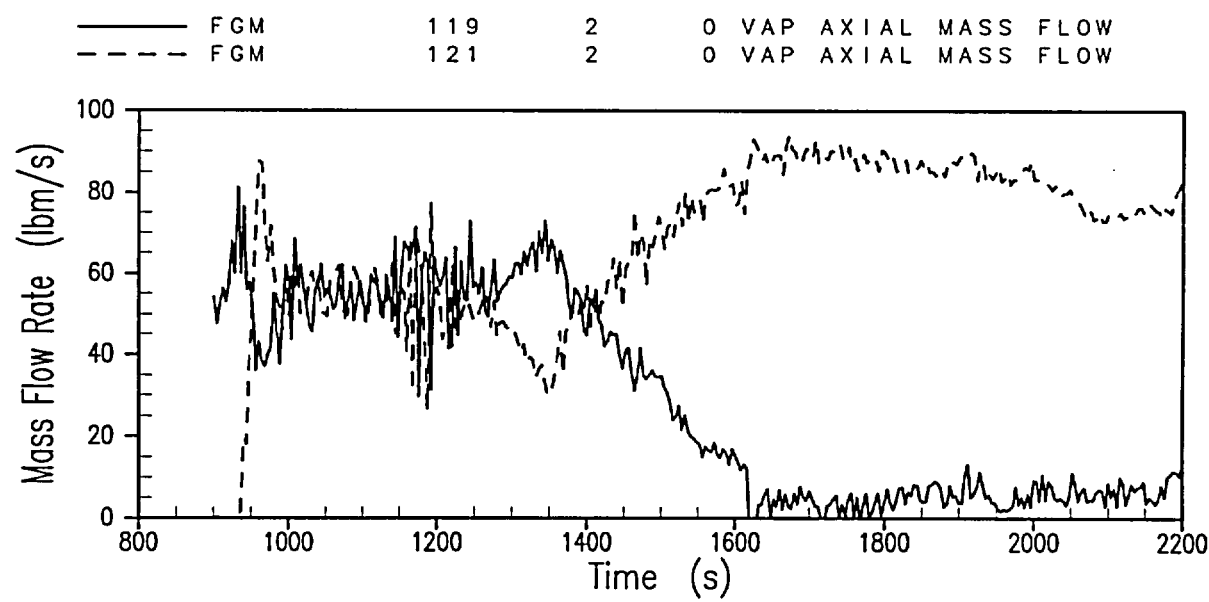


Figure 31-6-6. Loop Seal Clearance in the 3-Inch Break High Entrainment Case: Steam Flowrates

31-7 Condensation

31-7-1 Introduction

Condensation is ranked high in the small break LOCA PIRT (Volume 1) at two locations: at the cold leg steam-water interface after loop seal clearance and in the steam generator tubes during the natural circulation and loop seal clearance periods. Therefore, the sensitivity to increased condensation was investigated at these locations.

31-7-2 Loop Condensation

Condensation in loops is seen when the loop seal clears and the steam generated in the core is able to flow through the crossover leg to the cold leg side of the RCS, where subcooled liquid is present due to SI. Loop condensation should affect the depressurization rate after the loop seal clearance, and possibly the accumulator injection behavior as well. The WCOBRA/TRAC-SB single effects test for horizontal stratified condensation shows that the code underpredicts data (Section 18, Volume 2).

A 3-inch cold leg break case was run with an increased interfacial condensation HTC in the intact cold leg channels (Figures 31-7-1 through 31-7-6). For this run, [

]^{a,c} The x-axis for all figures in subsection 31-7 is time in seconds.

Figure 31-7-1 shows the RCS pressure comparison in which the reference case (solid line) is below the increased condensation case for a period of several hundred seconds. Figure 31-7-2 shows the reason for this is increased break flow before and after 1000 seconds; Figure 31-7-3 shows the integrated break flow comparison with the reference case as the solid line. The reference case shows a higher pressure than the high loop condensation case because of a higher break flow at the increased rate of condensation. This is due to a decreased void fraction at the break with increased condensation (dashed line, Figure 31-7-4) diminishing the steam venting. Subsequently, the increased break flow causes an earlier depletion of the vessel mass inventory to the point of core uncover. The reduced steaming rate, once core uncover occurs together with enhanced condensation, then permits the high condensation case pressure to fall below that of the reference case, and accumulator injection begins earlier. However, the increased break flow also produces a lower collapsed core liquid level in the high loop condensation case (dashed line,

Figure 31-7-5). Consequently, the PCT for the sensitivity case is 985°F, 21°F higher than the reference case (Figure 31-7-6).

31-7-3 Steam Generator Tube Condensation

Condensation in steam generator tubes takes place when the vapor generated in the core reaches the tube region while the steam generators are active heat sinks. The effect should become negligible when the RCS pressure decreases after the loop seal clearance and the steam generator becomes a heat source. The sensitivity to the steam generator tube condensation is presented in Section 31-3.

31-7-4 Summary and Conclusions

Table 31-7-1 summarizes the sensitivity case. As seen in the table, the sensitivity to condensation variation is small compared to the vertical interfacial drag coefficient core model. In the range examined, the pressure transient is somewhat affected. The sensitivity to this condensation variation will be considered in the Indian Point Unit 2 uncertainty methodology in the same way that the plant initial conditions are.

Table 31-7-1
PCT Sensitivity Due to Condensation

Case ID ⁽¹⁾	PCT (°F)	Time of PCT (s)	Remark
Reference case	964	1955	This is the nominal condensation model.
Loop condensation [] ^{a,c}	985	1838	Core mixture level turnaround due to accumulator injection occurs earlier because of higher condensation.

1. Identification

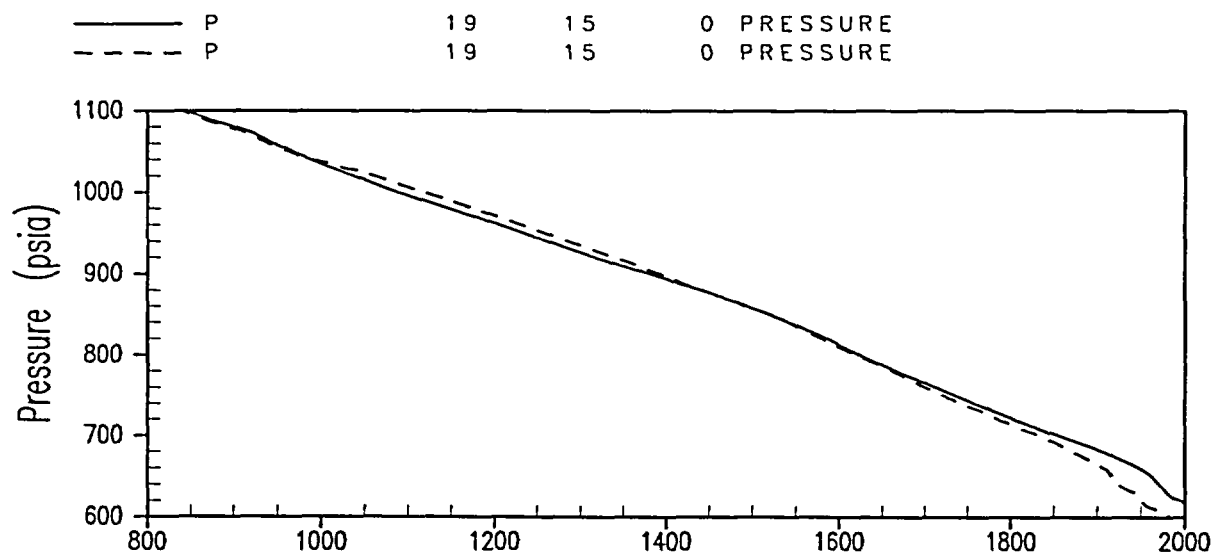


Figure 31-7-1. RCS Pressure Comparison: Reference Case and Increased Intact Loop Condensation Case

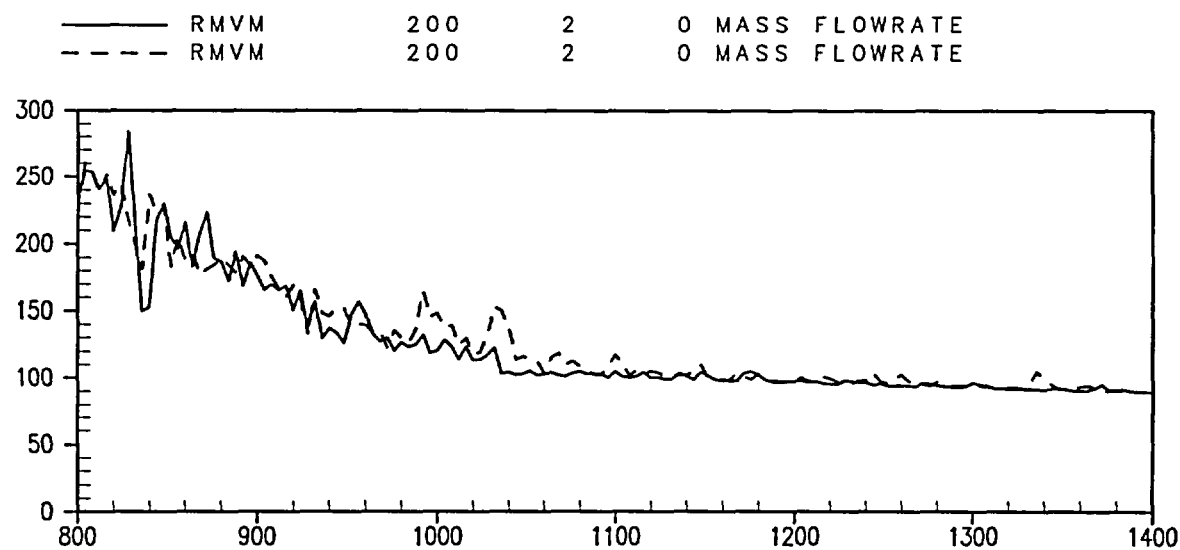


Figure 31-7-2. Break Mass Flowrate (lbm/s) Comparison: Reference Case and Increased Intact Loop Condensation Case

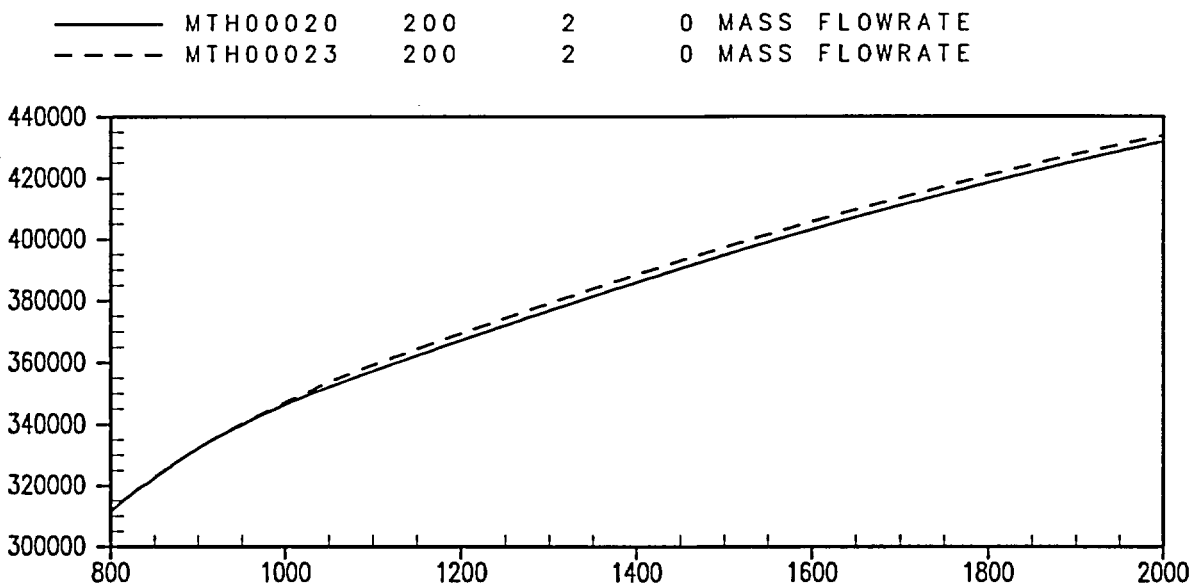


Figure 31-7-3. Integrated Break Flow (lbm) Comparison: Reference Case and Increased Intact Loop Condensation Case

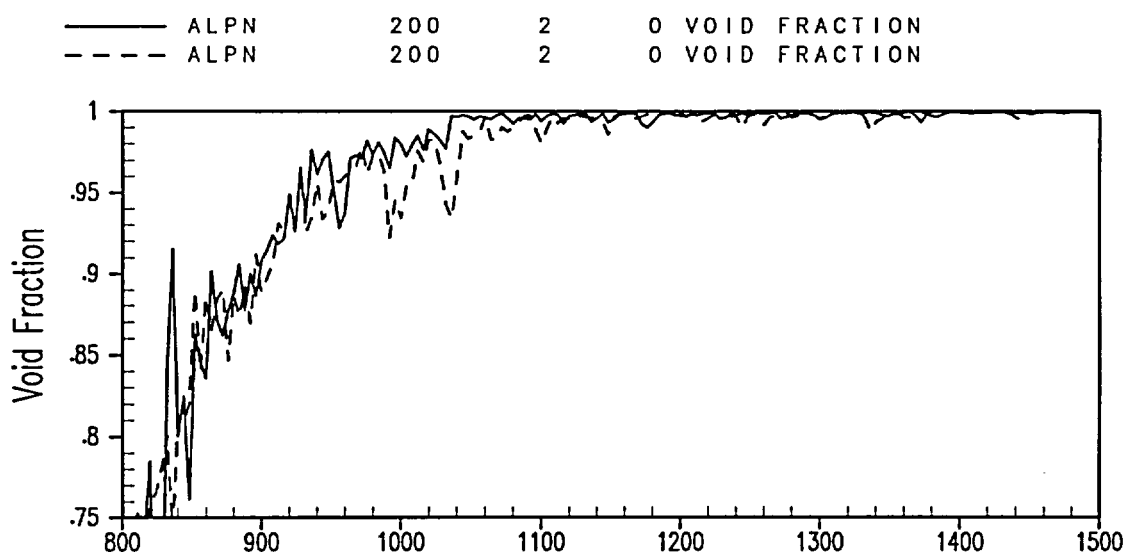


Figure 31-7-4. Break Void Fraction Comparison: Reference Case and Increased Intact Loop Condensation Case

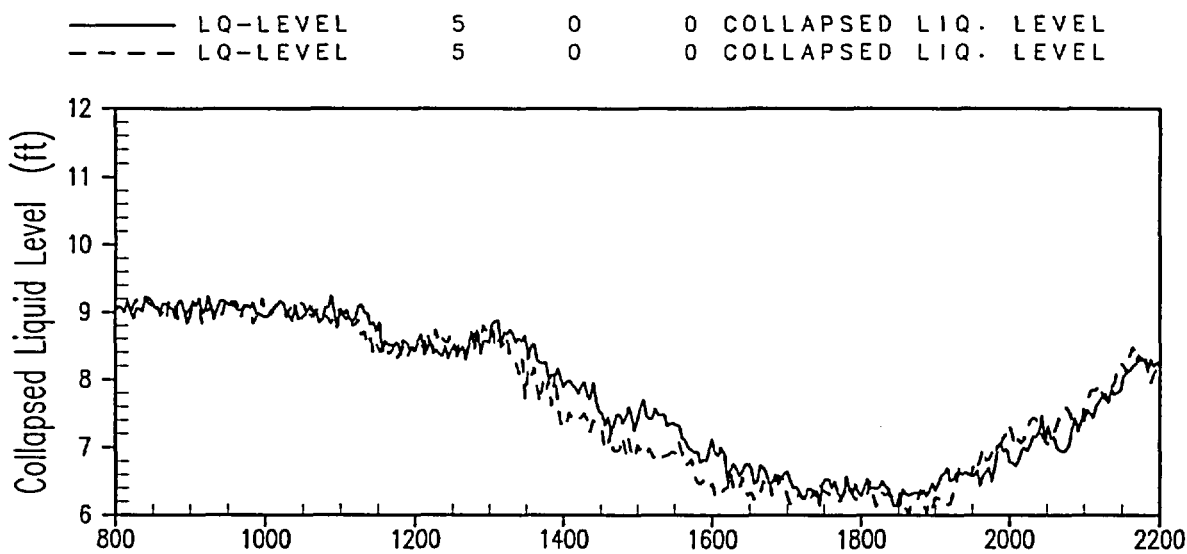


Figure 31-7-5. Core Collapsed Liquid Level Comparison: Reference Case and Increased Intact Loop Condensation Case

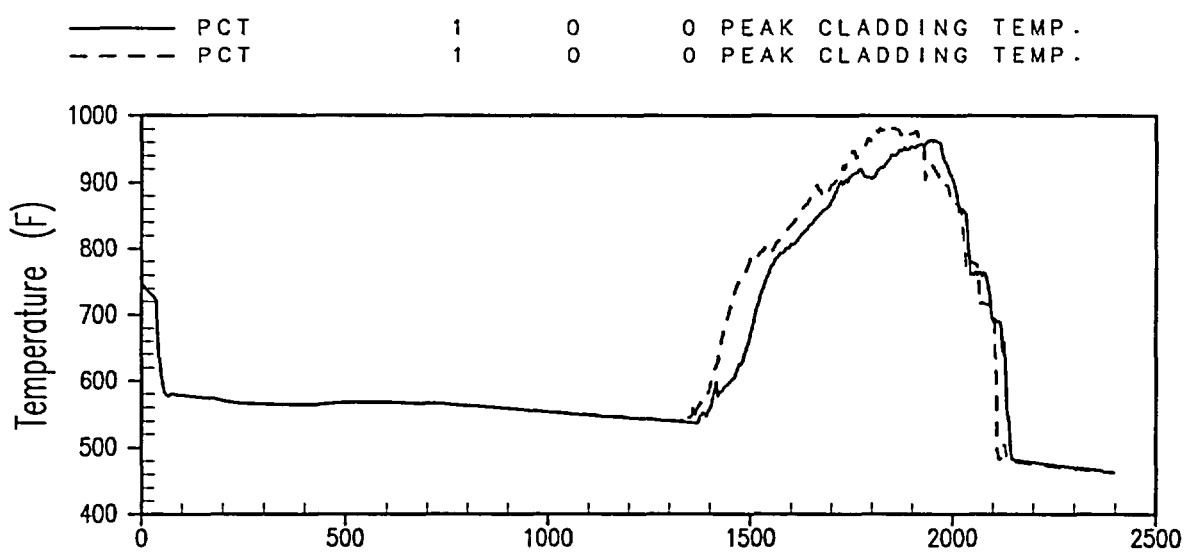


Figure 31-7-6. PCT Comparison: Reference Case and Increased Intact Loop Condensation Case

31-8 Fuel Rod Model

31-8-1 Small Break Fuel Model Uncertainties

The small break LOCA PIRT identifies the fuel rod model as having an important effect on small break LOCA uncertainty. The fuel rod model accounts for several processes that affect the fuel pellet and cladding. Included in fuel rod models are uncertainties due to material properties, metal-water reaction rate, and criteria for cladding swell and burst, as well as uncertainties due to local boundary conditions such as local power and HTCs.

The fuel rod model receives a high ranking in the PIRT for two important reasons. First, it could not be presumed that the small break LOCA transient incurs low cladding temperatures and cladding burst and metal-water reaction could be ignored. Second, some core uncoveries could be deep and prolonged causing the propagation of some uncertainties to become large due to the length of the transient. Therefore, all of the fuel rod model uncertainties identified for large break LOCA uncertainty are included in the small break LOCA uncertainty. This section provides an estimate of the overall effect of the fuel rod model on the small break PCT.

A revised version of the HOTSPOT code was developed to estimate the fuel rod model uncertainty for realistic small break LOCA. [

]^{a,c}

Table 31-8-1 lists the models and processes included in the fuel rod model from the large break LOCA methodology, Volume 4 of WCAP 12495-P-A (Bajorek et al., 1998). The items on the list are clearly applicable for small break LOCA events, [

]^{a,c}

First, the transient information from a WCORBA/TRAC-SB calculation needed by HOTSPOT is considered. For this, the 3-inch cold leg break reference case is used (Section 27, Volume 2). This calculation is run to core recovery, and the calculated PCT is 964°F.

Figure 31-8-1 shows the PCT history for this case and elevation at which the PCT occurred. During the core uncover transient, the PCT is shown to occur at the 10.5-foot elevation most of

the time (Figure 31-8-1). Heatup begins at 1470 seconds, and the core is quenched by 2250 seconds.

Of particular interest are the conditions and combinations of uncertainties that could lead to cladding burst. If burst and any significant metal-water reaction occurs, then the uncertainty associated with the fuel rod models may become large. The rod internal pressure along with the primary system pressure determine the stress on the cladding. In a small break LOCA, heat transfer during the early part of the transient is good and much of the initial stored energy is removed from the rod. As a result, the rod internal pressure does not become large until later.

The pressure decreases initially and remains low until boiloff and core uncover. Even then, the pressure remains below 600 psia and below the initial value.

Figure 31-8-2 shows the linear heat generation rate at the PCT elevation. Following reactor trip and control rod insertion, the internal heat generation decreases rapidly and by the time core boiloff occurs, it is nearly constant. The liquid film at the PCT elevation dries out shortly before 1500 seconds as the liquid phase HTC (HTCL) drops from approximately 2500 Btu/hr-ft²-°F to nearly zero. During heatup at this elevation, the heat transfer is by single-phase forced convection to vapor. The vapor phase HTC (HTCV) is shown in Figure 31-8-3. [

]^{a,c}

The time periods assumed [

]^{a,c}

31-8-2 Fuel Rod Uncertainty

For a 3-inch break case that exhibits a higher PCT than the Indian Point Unit 2 cases, the HOTSPOT-SB code was modified to isolate the fuel models from the heat transfer uncertainty.

[

]^{a,c} The HOTSPOT calculation shows that the uncertainty associated with the fuel rod models is small for this transient. Because this transient is more limiting than any of the Indian Point Unit 2 transients produced, it is not likely that the fuel rod model uncertainty will become larger than this value.

31-8-3 Heat Transfer Uncertainty

A number of the reference case transients, and nearly all of the sensitivity study calculations, predict some period of core uncovering and heatup. The more limiting transients have core uncoveries of over 500 seconds at the PCT elevation. For uncoveries of this length, the propagation of heat transfer uncertainty could become significant. Therefore, HOTSPOT-SB calculations are made in which the heat transfer uncertainty is varied.

A HOTSPOT-SB calculation is made for the same case as in Section 31-8-2 in which the heat transfer multiplier during the boiloff period [

]^{a,c}

Table 31-8-4 summarizes the results of this HOTSPOT calculation [

]^{a,c}

The cladding heatup during an extended uncovering small break LOCA transient occurs when the two-phase mixture level in the reactor vessel falls below the top of the active fuel. Throughout this cladding heatup, single phase steam generated in the core flows through a voided RCS to the break location. A variation in core HTC will affect the enthalpy of steam flowing to the break,

[

]^{a,c}

31-8-4 Summary

Uncertainties in the fuel rod model are investigated by using a version of the HOTSPOT-SB code modified for small break LOCA application. Results show that the uncertainty due to fuel and cladding related models is small for the 3-inch break transient considered. Because the 3-inch break used to supply the boundary conditions to HOTSPOT represented a higher PCT than those predicted in the Indian Point Unit 2 reference and scoping calculations, this is expected to approximate an upper bound on the fuel and cladding model uncertainties. The uncertainty due to these models is small because most of the initial stored energy from the fuel rod is removed well before core uncovering and heatup and because the temperatures are too low to cause cladding burst.

[

]^{a,c}

Table 31-8-1

HOTSPOT Model Variation Ranges/Distribution Type from Large Break LOCA

Table 31-8-2
HOTSPOT Model Variation Ranges/Distribution Type

Table 31-8-3
Fuel and Cladding Model Only Uncertainty

Table 31-8-4
HOTSPOT-SB Results, No HTC Bias, 50-Percent Uncertainty

Parameter	PCT ($^{\circ}$ F)
[
] ^{a,c}

Temperature (F) 1 0 0 PEAK CLADDING TEMP.
 PCT
 Elevation (ft)
 PCT-LOC 1 0 0 PEAK CLAD TEMP LOC.

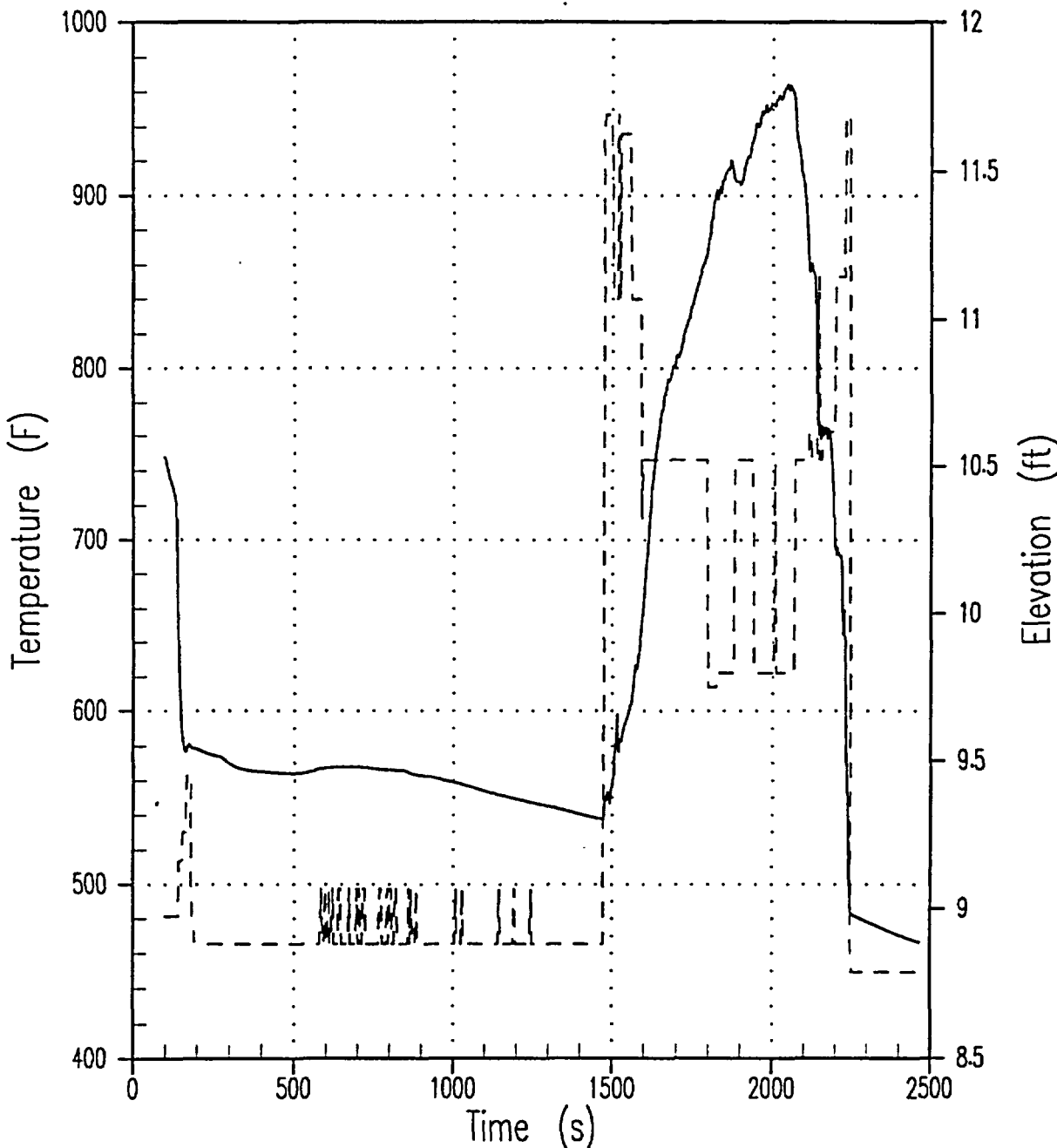


Figure 31-8-1. PCT and Elevation for HOTSPOT Fuel Rod Model Uncertainty Evaluation

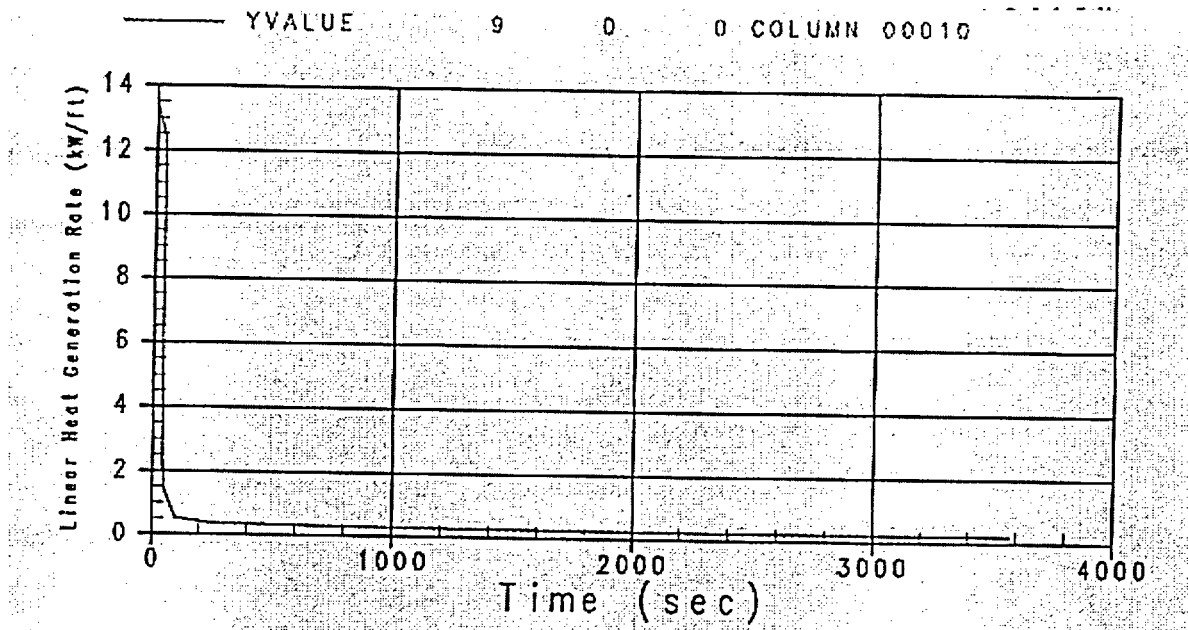


Figure 31-8-2. Linear Heat Generation at the 10.5-Foot elevation for 3-Inch Break

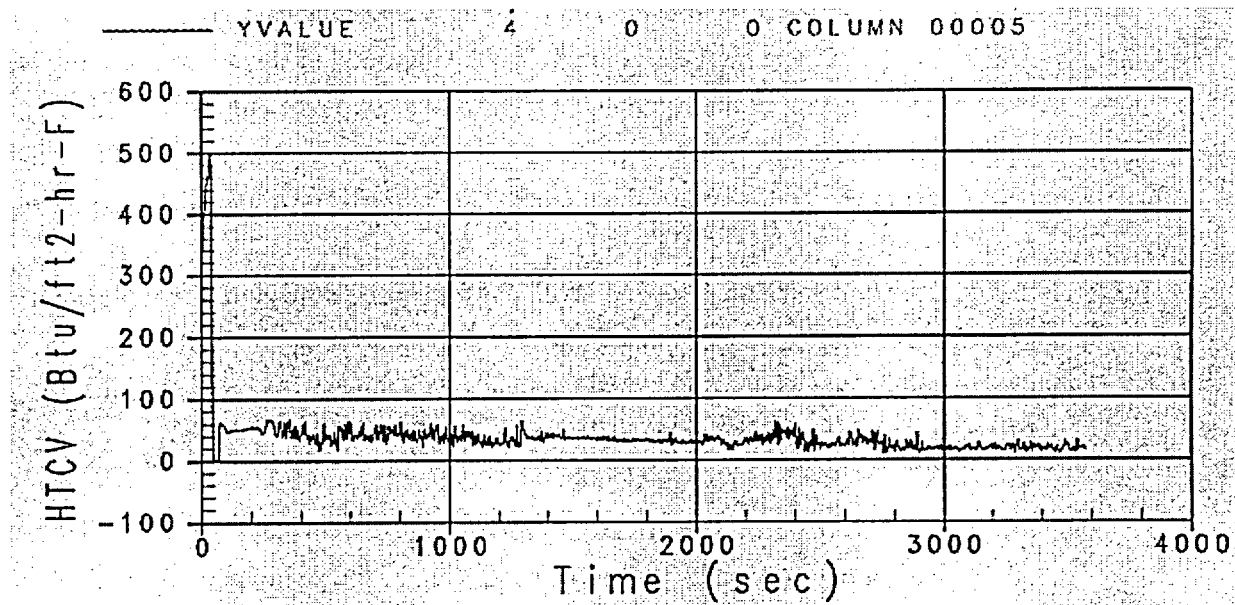


Figure 31-8-3. HTCVs at the PCT Elevation for 3-Inch Break

31-9 Summary and Conclusions

This section summarizes the effect of the models and processes ranked high in the PIRT on PWR small break LOCA transients. After the scoping studies and evaluations, the following conclusions were made on the effect of these dominant processes at full PWR scale:

- Break Flow

Uncertainty in the break flow is accounted for by ranging the equivalent break diameter and determining the limiting size. This is equivalent to specifying a break size and ranging the uncertainty in the break model to determine the particular flow that produces the most conservative results. Furthermore, the uncertainty in two-phase break flow is established by applying a *CD* range in this flow region.

- Mixture Level Swell

Uncertainty in mixture level swell is addressed by ranging the core-wide interfacial (vertical) drag over a range that captures nearly all of the data from a prototypical level swell separate effects test. The ranging is accomplished by applying a multiplier to the core interfacial drag. PWR calculations show that reducing the drag relative to that in the reference cases has a significant penalizing effect on the limiting break size (3-inch). Increasing the interfacial drag to the value nominally calculated in the code produced a benefit for the most limiting break size. The results confirm the importance of level swell in a small LOCA and show that models and correlations affecting level swell must be considered in uncertainty propagation.

- Loop Seal Clearance

Simulations were made specifically to investigate the effects on the PWR transient of decreasing and increasing the interfacial drag in the uphill section of pipe leading to the RCP. This is to modify sweep out of loop seal mass during clearance. The effect on the PCT of a decrease in interfacial drag is small. This suggests that the thermal-hydraulics affecting loop seal sweep out have a small effect on the total transient, given that the same number of loop seals are predicted

to clear. When the interfacial drag is increased, a second loop seal is predicted to clear.

- Steam Generator Hydraulics

Several calculations were performed to determine the effect of uncertainties in condensation in the steam generator tubes; the calculations show that higher condensation results in lower PCTs.

- Horizontal Flow Regimes

Several PWR calculations were made to examine the effects of models and correlations related to representing horizontal flow regimes. The PWR calculations confirm what had been shown in WCOBRA/TRAC-SB simulations of scaled tests: the total effect on the limiting PWR transient is small. The results show that the PCT effect in ranging those models and/or improving on the correlations is small.

- Condensation

Condensation in the cold legs was investigated in scoping studies. Ranging of the interfacial condensation HTCs is based on separate effects test simulations that show WCOBRA/TRAC-SB underpredicted the overall condensation in the cold leg. The study shows that increasing the loop condensation increases the PCT by an amount on the order of 20°F.

- Fuel Rod Model

A bounding small break LOCA transient (3-inch break) is used to supply thermal-hydraulic conditions for HOTSPOT-SB calculations at the PCT location. The HOTSPOT-SB calculations show that for this limiting transient, the fuel and cladding models do not significantly contribute to the uncertainty. The propagation of uncertainty for these models is almost negligible. The reason is that due to the low temperatures predicted for a realistic small break LOCA, burst and the subsequent metal-water reaction do not occur. The heat transfer, however, is an important contributor to the uncertainty. An uncertainty typical of the

[

]^{a,c}

In summary, the PWR calculations show that of the dominant small break LOCA processes identified in the PIRT, break flow, interfacial drag in the core, and convective heat transfer to steam during uncovering have an important effect on a realistic small break transient.

31-10 References

Anklam, T. M., et al., 1982, "Experimental Investigations of Uncovered Bundle Heat Transfer and Two-Phase Mixture Level Swell Under High Pressure Low Heat Flux Conditions," NUREG/CR-2456.

Bajorek, S. M., et al., 1998, "Code Qualification Document for Best Estimate LOCA Analysis Volume IV: Assessment of Uncertainty," WCAP-12945-P-A, Vol. 4.

Bajorek, S. M., et al., 1998a, "Code Qualification Document for Best Estimate LOCA Analysis Volume V: Quantification of Uncertainty," WCAP-12945-P-A, Vol. 5.

SECTION 32

UNCERTAINTY CONSIDERATIONS

32-1 Stored Energy/Fuel Rod

This component of uncertainty requires consideration of the initial reactor state in combination with the models involved in calculating fuel and cladding temperature; each component is discussed in the following sections.

32-1-1 Initial Reactor State Uncertainties

Reactor core power distributions are characterized by radial and axial power distributions as discussed in Section 29. The steady-state radial distribution is established by core loading pattern, fuel enrichment, fixed burnable absorbers, and the like, and is not subject to wide variation during normal operation. The maximum of the radial distribution is defined by $F_{\Delta H}$ (the hot rod average power divided by the core average rod average power). Predictions of $F_{\Delta H}$ are accurate to within []^{a,c} probability (Section 29).

In core design, the calculated $F_{\Delta H}$ is augmented by 4 percent to account for prediction and measurement uncertainty, and by an additional []^{a,c} to provide design margin.

Steady-state axial distributions are established by core loading pattern and burnup. The axial distribution tends to vary widely as a result of changes in external controls, such as boron or control rods. The maximum of the radial distribution multiplied by the maximum of the axial distribution is F_Q (maximum linear heat rate divided by the core average linear heat rate).

Predictions of F_Q are accurate to within []^{a,c} probability (Section 29).

Local variations in pellet and subchannel geometry are also considered for the hot rod (additional []^{a,c} F_Q uncertainty). Transients are simulated in the core design process and yield a wide range of possible power distributions and F_Q 's. As described in Section 29, the axial distribution is further specified by []^{a,c}.

In core design, the calculated F_Q for each power distribution is augmented by []^{a,c} prior to comparing to the Technical Specification to bound calculational, measurement, and local uncertainties.

Plants operate in baseload (that is, full power, all control rods out) nearly all the time. In baseload operation, F_Q varies slowly with time. However, the Technical Specifications allow for transient operation. Figure 32-1-1 shows the effect of a typical load follow maneuver on peaking factor ($F_Q \times$ power) for a plant with a Technical Specification F_Q limit of 2.40. Figure 32-1-2 shows the F_Q probability distribution for the load follow maneuver in Figure 32-1-1 for the portions of the figure where the reactor is at full power. In the Westinghouse best estimate small break LOCA methodology, the plant is assumed to be [

]^{a,c}.

Figures 29-2-13 through 29-2-15, Section 29, show the values of []^{a,c} for many samples of power distributions that have F_Q in the range shown below the figure. These samples are for power distributions without the normal core controls, such as rod insertion limits, so they represent bounding variations. It can be seen that the [

]^{a,c}.

The best estimate small break LOCA methodology has two approaches that may be used to establish the reactor core power distribution:

- Generic Methodology

The boxes drawn around the data in Figures 32-1-3 and 32-1-4 represent the widest range expected for any future core design. The fact that some of the data fall outside these boxes is of no consequence; future core designs will produce data within the range specified by the boxes. (This will be verified for each reload.) For a small break LOCA event, top-skewed power distributions are limiting as discussed in Section 29. The range of interest in Figure 32-1-4 for the small break LOCA power distribution is:

[

]^{a,c}

[
]
• Plant-Specific Methodology

A shape defined by the plant-specific core design is used for all F_Q values.

For Indian Point Unit 2, the core axial power shape for best estimate small break LOCA analysis is discussed in Section 29.

32-1-2 Fuel Rod Model Uncertainties

Contributions from two sources are considered for uncertainties. The first source of uncertainty involves the accuracy with which the power distribution in the hot assembly and remainder of the core can be defined. The second source of uncertainty involves the accuracy with which the power at the hot spot can be defined and also includes the accuracy of various physical models applied to single rods.

32-1-2-1 Hot Assembly Power Distribution Variables

Uncertainty and variability in hot assembly power distribution contribute to the thermal-hydraulic uncertainty. The following contributors are considered:

[

]^{a,c}

Each of these contributors affects the power generation in the hot assembly and hot rod, and therefore, their uncertainties must be accounted for. The method used is as follows.

The hot assembly and core radial power distributions are modelled by defining the following variables:

- [

]^{a,c}

The axial power distribution is modelled by defining the following variables:

[

]^{a,c}

[

]^{a,c}

The remaining variables – core average power, gamma redistribution, and decay heat – contribute additional uncertainty to the peak linear heat rate. In WCOBRA/TRAC-SB, the peak linear heat rate (*PLHR*) during the transient is as follows:

[

]^{a,c} (32-1-1)

[
]^{a,c}

The average linear heat rate on the hot rod is as follows:

[
]^{a,c} (32-1-2)

The peak linear heat rate of the hot assembly rod is as follows:

[
]^{a,c} (32-1-3)

The gamma redistribution factors are slightly different for the hot rod and hot assembly, but the ratio is close to unity.

The average linear heat rate of the hot assembly rod is as follows:

[
]^{a,c} (32-1-4)

The following uncertainties are, therefore, relevant to the hot rod and hot assembly power distributions:

[
]^{a,c}

[

L

(32-1-5)

]^{a,c}

or:

[

(32-1-6)

L

]^{a,c}

The initial power generation rate at the hot spot is specified by the [

]^{ac}

L

[

]^{a,c} their effects are obtained in the WCOBRA/TRAC-SB calculations.

The uncertainty in core power ($AFLUX_0$) at a \pm 2-percent range, uniformly distributed, was quantified in Section 29. The uncertainties in gamma redistribution ($FGAM$) and decay heat (DH , []^{a,c}) are quantified in the following paragraphs. The primary parameters affecting decay heat are the time in the fuel cycle and the time after shutdown. The uncertainty in decay heat is a result of data uncertainty in the ANS Standard (American Nuclear Society, 1979).

The decay heat uncertainty is derived from the approach recommended in the ANS Standard using Equation 9 in the Standard. The uncertainty in the total recoverable energy Q is estimated at 0.5 percent (Ford et al., 1982). The second term is calculated by first calculating the fission fractions of U-238, U-235, and Pu-239 as a function of burnup, using the graphs in Figures 8-1 to 8-3 in Volume 1. These fission fractions can also be obtained by examining steady-state WCOBRA/TRAC-SB output. Because the hot assembly is assumed to be at the beginning of its cycle, the burnup is relatively low (about [

].^{a,c}

The nuclear model includes a gamma redistribution model, which redistributes a portion of the energy generated in the hot rod and hot assembly to the coolant and the surrounding, lower power fuel rods (Section 8-6, Volume 1). Uncertainties in this model are related primarily to the uncertainty in the power of the surrounding fuel rods.

The gamma redistribution uncertainty is estimated by [

].^{a,c}

As described in Section 8-6 (Volume 1), [

]^{a,c}

32-1-2-2 Hot Rod Uncertainties

Additional uncertainty in hot rod local power and in fuel rod models contributes to local hot spot uncertainty. The following contributors based on the PIRT analysis are considered:

- Hot rod peaking factor additional calculational uncertainty
- Hot rod pellet diameter, enrichment, and rod bow uncertainties
- Fuel density (specific heat) and conductivity
- Gap HTC
- Rod internal pressure
- Cladding burst temperature
- Cladding burst strain
- Zirconium-water reaction
- Fuel relocation

Fuel relocation occurs because the pellets are cracked and pieces may accumulate within the burst region. This increases the total power within that region. This phenomenon is on the NRC list of "unresolved safety issues" reported in NUREG-0933 (USNRC, 1984). While the NRC categorized the issue as "LOW" in priority and concluded that current Appendix K, 10CFR50, evaluation models contain sufficient conservatism, the NRC stated that this effect has to be considered in best estimate LOCA models.

The phenomenon of fuel relocation also affects fuel-to-cladding gap heat transfer. The idealized gap heat transfer model in WCOBRA/TRAC is unrealistic in that it assumes that the fuel pellet stack remains centered within the cladding as the cladding swells and bursts. When this happens, the fuel/cladding gap increases and the gap HTC decreases. The fuel is insulated from the coolant as a result. In some cases, this model results in a reduced PCT. In other cases, a PCT increase could result if after cladding swelling and burst and a period of fuel pellet insulation, heat transfer is reduced. The cladding then heats up rapidly from the hotter pellet. In reality, the fuel pellet stack is unstable and during normal operation rests against the cladding in a random

pattern (Burman, 1980). During the LOCA, individual pellets continue to rest against the cladding as the cladding moves away. If the pellets are cracked, as is likely under most operating conditions, the pellet is even less likely to remain centered. As a result, the gap HTC remains high throughout the transient.

The uncertainties in the models discussed are expected to be particularly important for cases where the PCT is relatively high and where the PCT occurs at the burst location.

A stochastic hot spot model was developed (the computer program, HOTSPOT-SB) to account more fully for uncertainties associated with the hot spot and to take into account fuel relocation following burst. This is a model of a single axial location in which the following phenomena are simulated:

- Transient conduction within the fuel and cladding

A model identical to WCOBRA/TRAC is used, with identical or slightly simplified fuel and cladding properties.

- Cladding burst and strain

[

]^{a,c}

- Inside and outside cladding reaction
- Fuel relocation following cladding burst

Figures 32-1-6 and 32-1-7 contrast the fuel rod pellet behaviors assumed at burst for WCOBRA/TRAC-SB and HOTSPOT-SB, respectively.

32-1-2-3 HOTSPOT-SB Model Description

The HOTSPOT-SB model reads HTCV and HTCL, vapor temperature, liquid temperature, and fluid pressure from WCOBRA/TRAC-SB output at a specified location in the hot assembly. This approach assumes that the HTCs are independent of the wall temperature, which is not strictly true. However, it is expected that for convection to SPV, which is the most important

heat transfer mode for this application, the dependence will be weak. Other input values are the pellet and cladding geometry, the linear heat rate, the steady-state gap pressure, and the steady-state gap HTC.

The model is run through a transient at constant power and heat transfer conditions so that a steady-state is reached. Once the steady-state has been achieved, the transient is calculated. The burst temperature is calculated, and if the burst temperature is exceeded, a burst strain is calculated. [

]^{a,c} At burst, inside zirconium-water reaction is assumed to commence.

The application of this model to calculate the effect of various uncertainties in these models resembles the Monte Carlo simulations in other areas of the best estimate LOCA methodology, except that instead of using response surface equations approximating a complex model, a relatively simple physical model is used directly. Uncertainty is assumed in several key parameters and models affecting the hot spot temperature. The transient calculation is repeated many times with parameter values that randomly vary according to specified assumed distributions. The result is a PCT distribution, as well as a distribution of the amount of cladding reacted, from which 95-percent probability estimates can be derived.

The hot spot model is used to calculate the probability distribution of PCT at the hot spot for specific WCOBRA/TRAC thermal-hydraulic transients listed as follows:

- a) Fuel Rod Conduction Model
- b) Fuel Rod Thermal Properties
- c) Fuel Internal Heat Generation
- d) Gap HTC
- e) Cladding Burst
- f) Fuel Relocation Following Burst
- g) Zirconium-Water Reaction

In addition to the consideration of fuel rod model uncertainties, uncertainty in the HTC is also considered (Section 32-5). Table 32-1-1 summarizes the model uncertainties considered. Additional details are provided in the following paragraphs.

a) Fuel Rod Conduction Model

The model used to calculate transient conduction within the fuel and cladding is taken from WCOBRA/TRAC (Section 7-2-1, Volume 1). The conduction equation is as follows:

$$\frac{(\rho C_p A_i)}{\Delta t} (T_i - T_i^n) = K_{i,i-1}(T_{i-1} - T_i) + K_{i,i+1}(T_{i+1} - T_i) + Q_i''' A_i \quad (32-1-9)$$

where the various quantities are as defined in Section 7. Internal heat generation is expressed in terms of linear heat rate:

$$Q_i' \frac{Btu}{s \cdot ft} = Q_i''' \frac{Btu}{s \cdot ft^3} A_i \frac{ft^3}{ft} \quad (32-1-10)$$

Heat generation is assumed in both the fuel and the cladding elements. The fuel and cladding element masses are [

]^{a,c}.

b) Fuel Rod Thermal Properties

Fuel thermal properties are taken from the WCOBRA/TRAC models. Fuel density is 684.86 (F_d) lb/ft³ (Equation 10-140, Volume 1) where F_d is the fraction of theoretical density. Fuel specific heat is from Equation 10-144, and fuel conductivity is from Equation 10-141. Plots of these properties are shown in Figure 32-1-8.

Data from several references for the thermal conductivity of UO₂ are shown in Figure 32-1-9 and are compared with the correlation. This figure indicates that [

]^{a,c}

[]
]^{a,c}.

Figure 32-1-9 shows a relatively large variation in conductivity as a function of temperature. It is important to consider the [

]^{a,c}, gives average and 95-percent fuel average temperatures, which are in good agreement with the values calculated by the NRC-approved PAD fuel rod design code (Weiner et al., 1988), as seen in Figure 32-1-10.

As described in item f, the fuel [

]^{a,c}

Comparisons of this model to data indicate that a constant needs to be added to the relation. This constant is probably dependent on the materials being studied.

Assume the following conditions:

- UO_2 temperature = 2000°F (1100°C). The corresponding fuel conductivity ranges from 1.2 to 1.7 Btu/hr/ft/ $^{\circ}\text{F}$ (Figure 32-1-9).
- Steam temperature = 1500° to 1800°F . The corresponding steam conductivity ranges from 0.064 to 0.078 Btu/hr/ft/ $^{\circ}\text{F}$ (Figure 10-15, Volume 1).

[

]^{a,c}

The theoretical model was compared with [

]^{a,c}

[

]^{a,c}

Kerrisk and Clifton (Kerrisk and Clifton, 1972) provide confidence limits at 2σ for the specific heat of UO₂ of \pm 2 percent for temperatures less than 2500°F. [

]^{a,c}

Cladding thermal properties are approximations of the curves used in WCOBRA/TRAC. Uncertainty in cladding specific heat and conductivity is negligible relative to fuel uncertainties and is ignored.

c) Fuel Internal Heat Generation

The local power calculated by WCOBRA/TRAC for the hot rod at the elevation being analyzed is read in and interpolated in the same way as the heat transfer coefficients.

The uncertainty related to the hot spot needs to be considered within the context of the overall methodology. As indicated in item b, the uncertainties on the hot rod are considered to be composed of a hot assembly component and a local component.

[

(32-1-12)

(32-1-13)

]^{a,c}

d) Gap HTC

The gap HTC is assumed to consist of [

]^{a,c} (32-1-14)

]^{a,c}

The gap heat transfer uncertainty is assumed to be []^{a,c}. The basis for this uncertainty is indirect; it results in an uncertainty in initial fuel temperature that closely approximates that calculated by the PAD code (Weiner et al., 1988), as shown in Section 32-1-2-4.

e) Cladding Burst

Cladding burst is calculated by monitoring the pressure difference between the gap and the fluid, and using cladding rupture correlations such as from Equation 7-66, Volume 1.

There are two models available to calculate the rod internal pressure. The first model uses a simple perfect gas model. [

]^{a,c} (32-1-16)

(32-1-17)

]^{a,c}

The cladding burst temperature can be correlated well as a function of hoop stress as shown in Figure 32-1-12. This figure for ZIRLO™ indicates that a band of []^{a,c} of the calculated burst temperature captures all of the data.

The []^{a,c} uncertainty range on cladding burst temperature is used for both zircaloy and ZIRLO™ cladding. The ZIRLO™ data shown in Figure 32-1-12 actually indicate a smaller uncertainty than the assumed []^{a,c}. These data were obtained by Westinghouse using a consistent testing method. The zircaloy data from NUREG/CR-0630 (Powers and Meyer, 1980), which were used to develop the zircaloy burst temperature and burst strain models in WCOBRA/TRAC and the hot spot model, show scatter more consistent with the []^{a,c} range (Figure 1, NUREG/CR-0630). This is believed to be at least partly attributable to the variety of testing methods used to obtain the zircaloy data. Although it is believed that the ZIRLO™ testing methods are as valid as those in Powers and Meyer, there may be some uncertainty due to the testing method. Westinghouse elected to use the larger uncertainty for both cladding materials.

In contrast to the cladding burst temperature, the cladding burst strain shows wide scatter. Figures 32-1-13 and 32-1-14 show the maximum burst strain as a function of burst temperature for zircaloy and ZIRLO™. In both cases, the scatter is large except within the alpha/beta transition region. The data simply reflect that the burst process is subject to several stochastic or random influences. Burman (Burman, 1980) discusses how burst occurs randomly at hot spots, which are the results of small azimuthal temperature gradients around the cladding. Burman also argues that in fuel rods, these gradients are larger due to random contact of the pellet against the cladding, which then causes smaller burst strains to occur. This, therefore, precludes the occurrence of sausage ballooning, which was postulated by some authors. (The term is used to describe a slow, plastic deformation over significant lengths of cladding. This was observed in some experiments where the cladding temperature was carefully controlled to prevent burst.)

Figures 32-1-15 to 32-1-17 show the zircaloy burst data in the form of histograms, indicating the frequency of occurrence of a particular burst strain within a range of burst temperatures. []^{a,c}

[

]^{a,c} In all cases,

there is a wide range of burst strains except near the alpha phase transition (for zircaloy, between about 1600 and 1800°F).

The ZIRLO™ data, shown in Figures 32-1-18 to 32-1-20, exhibit a similar behavior except for the difference in the transition temperature. [

]^{a,c}

[

]^{a,c}

f) Fuel Relocation Following Burst

The phenomenon of fuel relocation following cladding burst was recognized in the early 1980s during various experimental studies, including those performed at the Power Burst Facility (PBF) in Idaho. A review and analysis of these tests was performed by Westinghouse and National Nuclear Corporation (NNC) during preparation of the safety case for Sizewell B in the United Kingdom; results of that analysis and application to the present situation are summarized in the following.

A number of short (approximately 3-foot) pre-irradiated and unirradiated test specimens were taken through depressurization and heatup transients at the PBF. Three tests are reported: LOC-3 and LOC-5 from NUREG/CR-2073 (Broughton, 1981), and LOC-6 from NUREG/CR-3184 (Broughton, 1983). The different tests were designed to cause rupture at different temperatures: LOC-3 in the alpha plus beta region (approximately 1680°F), LOC-5 in the beta region (approximately 2000°F), and LOC-6 in the alpha region (approximately 1470°F). The rods, which were highly enriched (12.5 percent), experienced variable ratings during pre-irradiation, on average about 12kW/ft, with as high as 18 kW/ft peak

ratings, which are expected to promote more extensive fuel cracking than normal reactor conditions. Data about fuel relocation were available in the following forms from these tests:

- Post-test neutron radiographs were available for most rods.
- Niobium-95 gamma ray count rates were monitored after the tests to determine the axial location of the fuel.
- Information from photo micrographs was presented in NUREG/CR-3184 (Broughton, 1981) for tests LOC-3 and -5.
- Photographs of the cross sections of some of the rod specimens were available from the literature.

The relocation evidence from these tests was summarized by Idaho National Engineering Laboratory (INEL) in NUREG/CR-2073 (Broughton, 1981) and as shown in Figure 32-1-22. This figure shows the increase in fuel volume as a function of the increase in cladding volume after burst. A review of the data indicates some discrepancies with this figure [

]^{a,c}. The data indicate that because the fuel volume increases less than the cladding volume, the fuel does not completely fill the available cladding volume; there is a decrease in the fuel density along with an increase in the fuel volume. This change in fuel density can be described in terms of a [

]^{a,c} (32-1-18)

[

1

(32-1-19)

1

(32-1-20)

]^{a,c}

1

[]
]^{a,c} (32-1-21)

where R_f and R_c are the preburst fuel radius and cladding inner radius respectively (for 17x17 Westinghouse-designed fuel, the values for R_f and R_c are typically 0.16125 and 0.1645 inches, respectively).

[]
]^{a,c}

]

The INEL study includes data from several sources and uses several measurement methods. In addition, NNC performed additional analyses using photographs of the fuel cross sections. These data are summarized in Table 32-1-4. A plot of this data versus burst strain (Figure 32-1-23a) appears to []^{a,c}

]^{a,c}.

When the fuel relocates into the burst region, its mass increases. As a result, the heat generation rate within the burst zone is affected. The linear heat rate resulting from the fuel relocation is calculated in Equations 32-1-23 through 32-1-26.

The heat generation rate per unit mass of fuel (q_m) is related to the linear heat rate under normal conditions by:

$$q_m \frac{Btu}{s \cdot lb} = q' \frac{Btu}{s \cdot ft} \frac{1}{A_f} \frac{ft}{ft^3} \frac{1}{\rho_{UO2}} \frac{ft^3}{lb} \quad (32-1-23)$$

When burst occurs, the fuel mass in the burst region [

(32-1-24)

(32-1-25)

(32-1-26)

]^{a,c}

The result obtained if there was no fuel relocation can be derived to confirm that the preceding equation is a correct representation of the linear power. In this case, [

(32-1-27)

(32-1-28)

]^{a,c}

g) Zirconium-Water Reaction

The zirconium-water reaction rate calculations are performed using methods similar to those in WCOBRA/TRAC (Section 7-5, Volume 1). When burst occurs, the [

^{a,c} using the same approach as in WCOBRA/TRAC
(Equations 7-85 and 7-87, Volume 1).

The data upon which the ZIRLO™ and zircaloy reaction rate equations are based are from Burman (Burman, 1990) and Cathcart and Pawel (Cathcart and Pawel, 1977), respectively. The prediction interval at 95-percent probability for these equations was calculated from the data using the following equation (Draper and Smith, 1981):

$$Y + t(95\%, n-2) \left[1 + \frac{1}{n} + \frac{(X - \bar{X})^2}{\sum (X_i - \bar{X})^2} \right]^{1/2} s \quad (32-1-29)$$

where $t(95\%, n-2)$ is the 95th percentage point of a t-distribution with $n-2$ degrees of freedom to account for sample size, \bar{X} is the average of the X values, and s^2 is the residual mean square of the data around the reaction equation line.

Equation 32-1-29 is the prediction interval for the next point estimate of the reaction rate; the uncertainty interval for the prediction of the mean of the data is smaller (the equation is similar to that above except that the 1 is missing).

- Zircaloy

The uncertainty cited in [

]^{a,c}. A model is

assumed of the form:

$$\ln(\delta^2/2) = A + B(1/T(K)) \quad (32-1-30)$$

The regression output is shown in Table 32-1-5b. The output shows that the constants A and B are as follows:

$$A = -1.709863$$

$$B = -20098$$

These numbers compare to those in Table A2 of Cathcart and Pawel (Cathcart and Pawel, 1977):

$$A = -1.70986$$

$$B = -20100$$

[

]^{a,c}

[
]^{a,c}

- ZIRLOTM

The reaction rate uncertainty for ZIRLOTM was derived using the same approach as described for zircaloy. Using the data for $T \geq 1000^{\circ}\text{C}$ in Table E-1 of Burman (Burman, 1990), the equivalent prediction uncertainty for ZIRLOTM is estimated as [

]^{a,c}.

32-1-2-4 HOTSPOT Model Application and Assessment

The uncertainties for the input variables are introduced into the calculation of PCT in a manner similar to that used in the Monte Carlo simulations described in Section 33. For example, the linear power is first calculated as described. Then, a [

]^{a,c} is sampled. Because this uncertainty is expressed as a percentage, the resulting value, say 1.008, multiplies the calculated value. In some cases, the uncertainty is expressed in dimensional form. In this case, the sampled value (for example, [
]^{a,c}) is added to the calculated value.

NRU Reflood Tests

The NRU MT-3 tests (Mohr et al., 1983) used full-length pressurized fuel rods under reflood conditions. The reflood rate was not designed to simulate actual PWR conditions; instead, the flooding rate was controlled to keep the cladding temperature within a narrow temperature band between 1400 and 1500°F for a prolonged time period. In this temperature range, the cladding was expected to experience significant burst strains. The test was designed to provide information on the extent of cladding strain and burst, and its effect on heat transfer. Consistent with other flow blockage tests, the NRU tests indicated no degradation of heat transfer due to flow blockage even though all interior rods burst, some with high burst strains.

This test can be used to provide a benchmark for the hot spot methodology being developed here. First, the cladding temperature at a location where measurements are available (there were no measurements at the burst location) can be predicted, taking into account uncertainties likely to exist in the fuel rod local heat generation rate and fuel properties, to determine how much of the variation in measured PCT can be explained by these uncertainties. Then, the likely cladding PCT, burst times, and burst strains at the burst elevation can be predicted to determine how much larger the range of PCTs will be when these other variables are included.

The only aspect of the model that cannot be verified is the internal gas pressure model. The MT-3.06 test was controlled to cause burst to occur as late as possible in the test. This was done by filling the bundle rapidly with water until the bundle quenched to about 4 feet and then reducing the flooding rate to slow the quench front advance and allow the upper elevations to remain at temperatures near 1600°F. Under these conditions, the simple model described in Section 32-1-2-3(d) is not appropriate. Consequently, the measured internal pressure was used in the calculation. The key input variables and uncertainties for MT-3 are listed in Table 32-1-7.

The uncertainty in linear heat rate was estimated by assuming the same uncertainty as in the PWR resulting from variations in fuel pellet geometry and enrichment (see item 5 in Table 29-2-2). Other variations such as rod bow were considered negligible. In addition, variations such as uncertainties in bundle power were considered to affect all rods equally and so were not considered. The nominal value of the gap HTC was taken from the value calculated by WCOPRA/TRAC.

From the data for test MT-3, the distribution of cladding temperatures at the end of the test at level 15 (the peak temperature location, just below the elevation where the rods burst) is about 50°F (Figure 51 of NUREG/CR-2528 [Mohr et al., 1983]). The measured average PCT is 1508°F, while the measured maximum PCT is 1567°F. Tables 32-1-8 and 32-1-9 provide summaries of 100 transient calculations performed with the hot spot model. Table 32-1-8 shows results when burst was prevented from occurring. The nominal conditions summary shows results when all models are used at their best estimate settings. The predicted average PCT is 1503°F, while the calculated maximum is [

]^{a,c}.

Table 32-1-9 shows calculated results when the rod is allowed to burst. The model predicts a wide range of burst times, including instances where no burst was predicted.

The first five transients from the results of Table 32-1-9 are plotted in Figure 32-1-26. When the cladding bursts, the increased heat transfer surface cools the cladding momentarily.

Subsequently, the cladding heats up as the relocated fuel heats up. The average PCT is 1475°F, substantially lower than the case with no burst. However, the maximum PCT is higher, as is the PCT spread. Figures 32-1-27 and 32-1-28 show the predicted and measured distribution of burst times and average burst strains. While the burst times are predicted earlier, the distribution of burst strains agrees well with the data.

The list of model parameter settings, when the maximum PCT is calculated in Tables 32-1-8 and 32-1-9, also provides an indication of what combinations result in the highest PCT.

Table 32-1-10 provides a description of what each parameter variation (*PV*) value means and also a summary of the statistical variables.

When the statistical fluctuation is expressed as a percentage of the best estimate value and the population is normal, *PV* is defined as $I + V_n$, where V_n is a random sample from a normal distribution with mean 0 and standard deviation σ . When the statistical fluctuation is expressed as a percentage of the best estimate value and the population is uniform, *PV* is defined as $1 + RNG * V_u$, where V_u is a random number between -1 and 1 and *RNG* is the range of the distribution. When the statistical fluctuation is a dimensional number and the population is normal, *PV* is defined as $0 + V_n$, where V_n is a random sample from a normal distribution with mean 0 and standard deviation σ . Finally, when the statistical fluctuation is a dimensional number and the population is uniform, *PV* is defined as shown previously where V_u is a random variable between -1 and 1.

Values close to $PN(I) \pm SP(I)$ in Tables 32-1-8 and 32-1-9 denote extreme values likely affecting the PCT. When no burst is calculated, heat sources dominate as seen from the linear heat rate and cladding reaction rate. When burst is calculated, burst strain and fuel relocation (fuel density after burst) dominate. The fuel density after burst and the burst strain are both high, suggesting higher fuel relocation and linear heat rates for this case.

Initial Fuel Temperature

The hot spot model was used to estimate the uncertainty in the fuel average temperature during steady-state. [

]^{ac}

[]
J^{a,c}

Figure 32-1-10 compares the calculated average and 95-percent probability fuel temperature with values obtained from the PAD fuel design code (the PAD uncertainty is derived from comparisons of the code to in-pile test data). The comparison is conservative and is indicative that the assumed uncertainties for gap HTC and fuel conductivity are conservative.

32-1-3 Summary

The reactor initial condition and fuel rod model uncertainties considered in the Westinghouse methodology are summarized in Table 32-1-11. These uncertainties are coupled with the HTC uncertainties as described in Section 32-5.

Table 32-1-1
Summary of Fuel Rod Uncertainties Considered in HOTSPOT-SB

Variable	How Treated
Fuel rod conduction model	Best estimate with uncertainties
Fuel rod thermal properties	Best estimate with uncertainties in fuel conductivity, fuel density after burst
Fuel internal heat generation	[] ^{a,c} above hot assembly, with uncertainties
Gap HTC	Best estimate accounting for fuel relocation and uncertainties
Cladding burst	
Temperature	Best estimate with uncertainties
Strain	Best estimate with uncertainties
Fuel relocation following burst	Best estimate with uncertainties
Zirconium-water reaction	Best estimate with uncertainties

Table 32-1-2
Burst Strain Summary

] ^{a,c}

Table 32-1-3
Packing Fraction From Burst Strain

[
] ^{a,c}

Table 32-1-4
Packing Fractions Using Various Measurements

Table 32-1-5a
Zircaloy Rate Constants (Total Oxygen)

Table 32-1-5b
Regression Output

Table 32-1-6
Predictions Using Equation 32-1-30 and Cathcart and Pawel

]^{a,c}

Table 32-1-7
NRU MT-3.06 Test Conditions (Just Below Burst Location)

[

]^{a,c}

Table 32-1-8
NRU MT-3.06 Test – No Burst

]^{a,c}

Table 32-1-9
NRU MT3.06 Test – Burst

] a.c

Table 32-1-10
Summary of Statistical Variables in HOTSPOT

Table 32-1-11
Fuel Rod Model Uncertainty^(a)

(a) Footnotes for Table 32-1-11

[

]^{a,c}

[

L

]^{a,c}

L

L

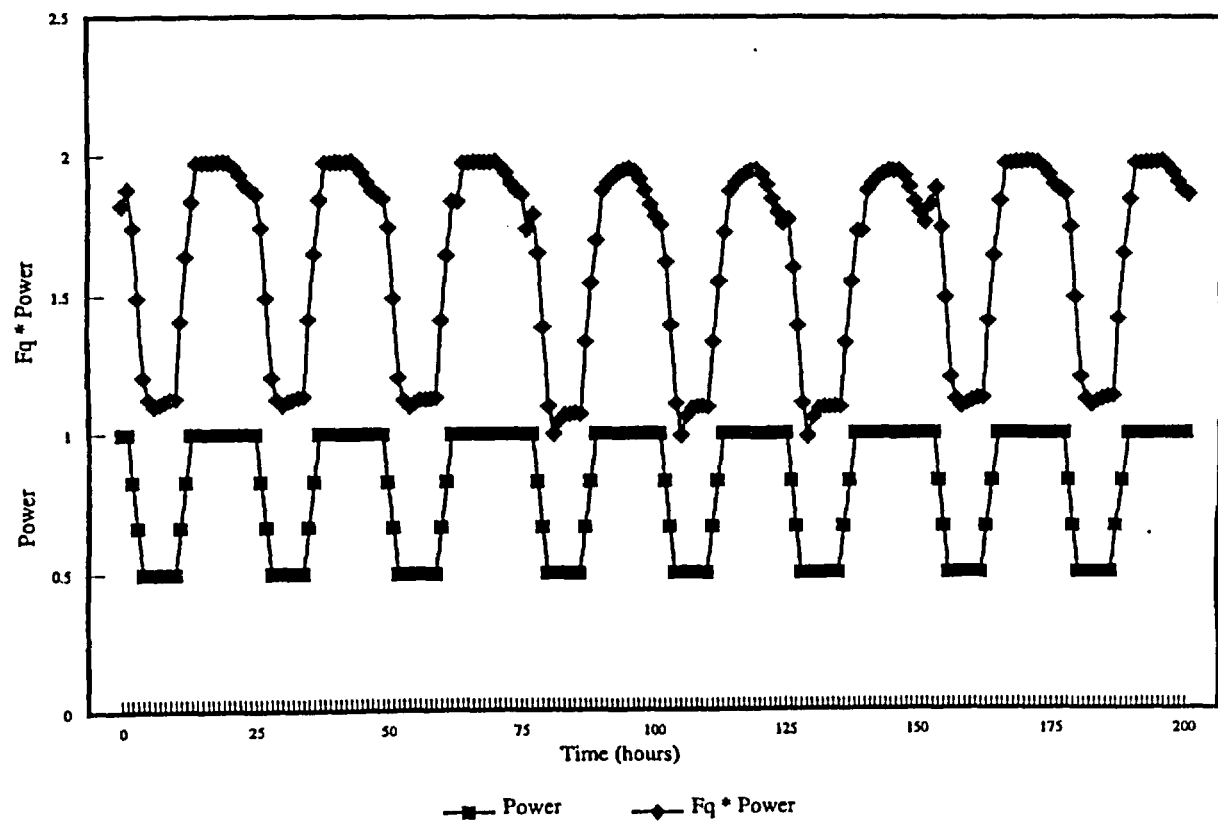


Figure 32-1-1. Effect of Load Follow on F_Q



Figure 32-1-2. F_Q Histogram [

]^{a,c}

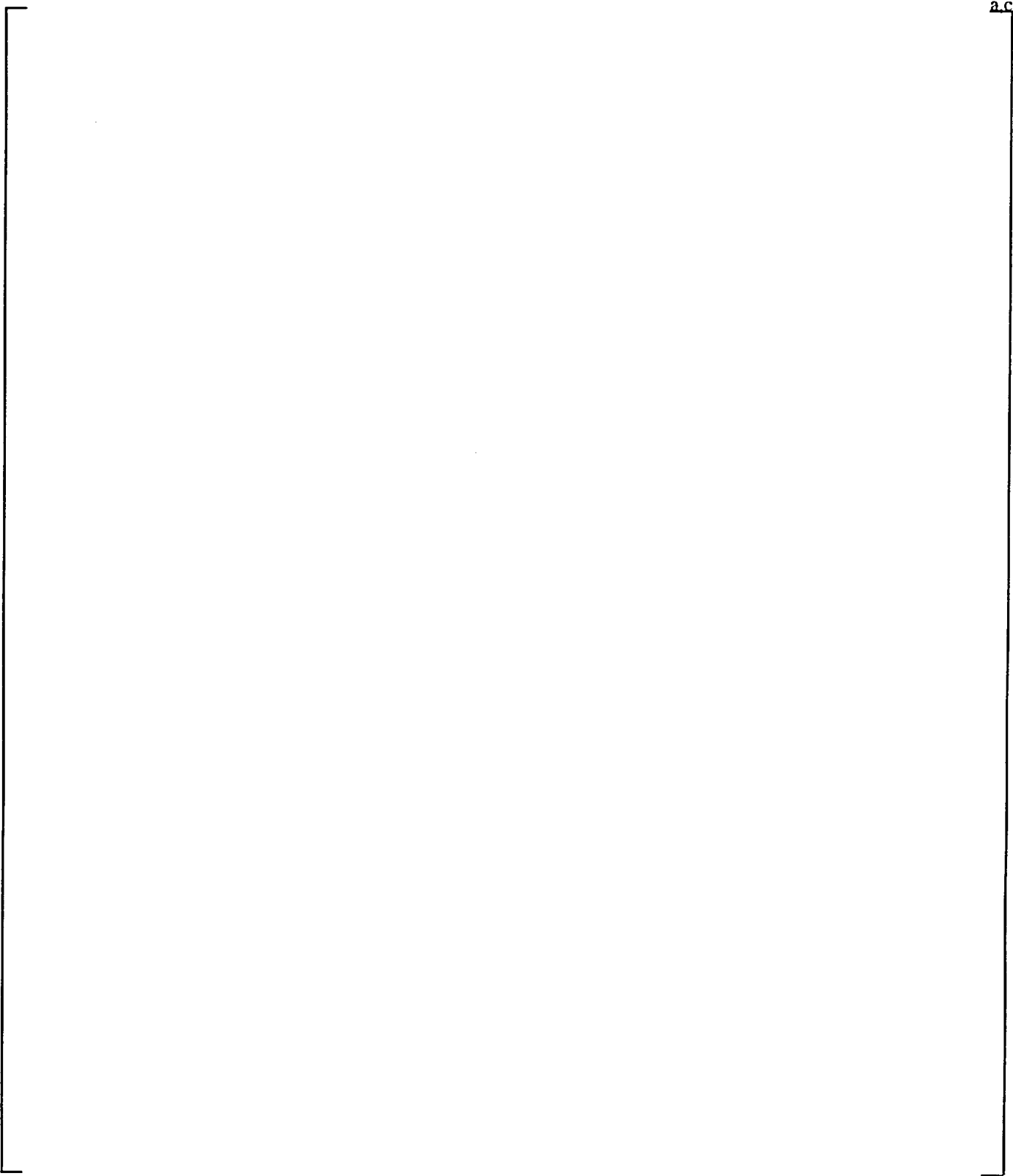


Figure 32-1-3. [
Presented in Section 29

]^{a,c} Shapes

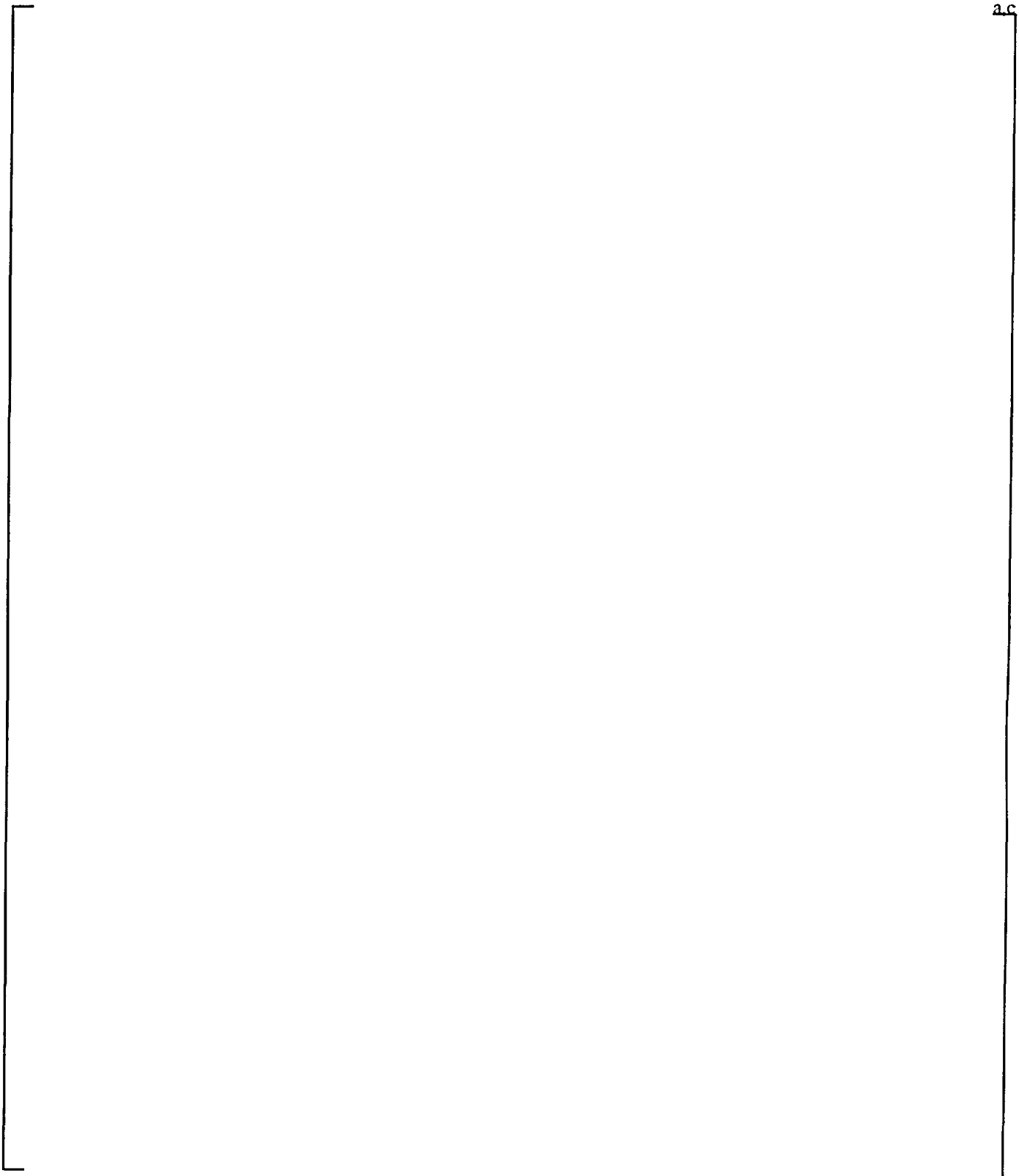


Figure 32-1-4. [
Presented in Section 29

]^{a,c} Shapes

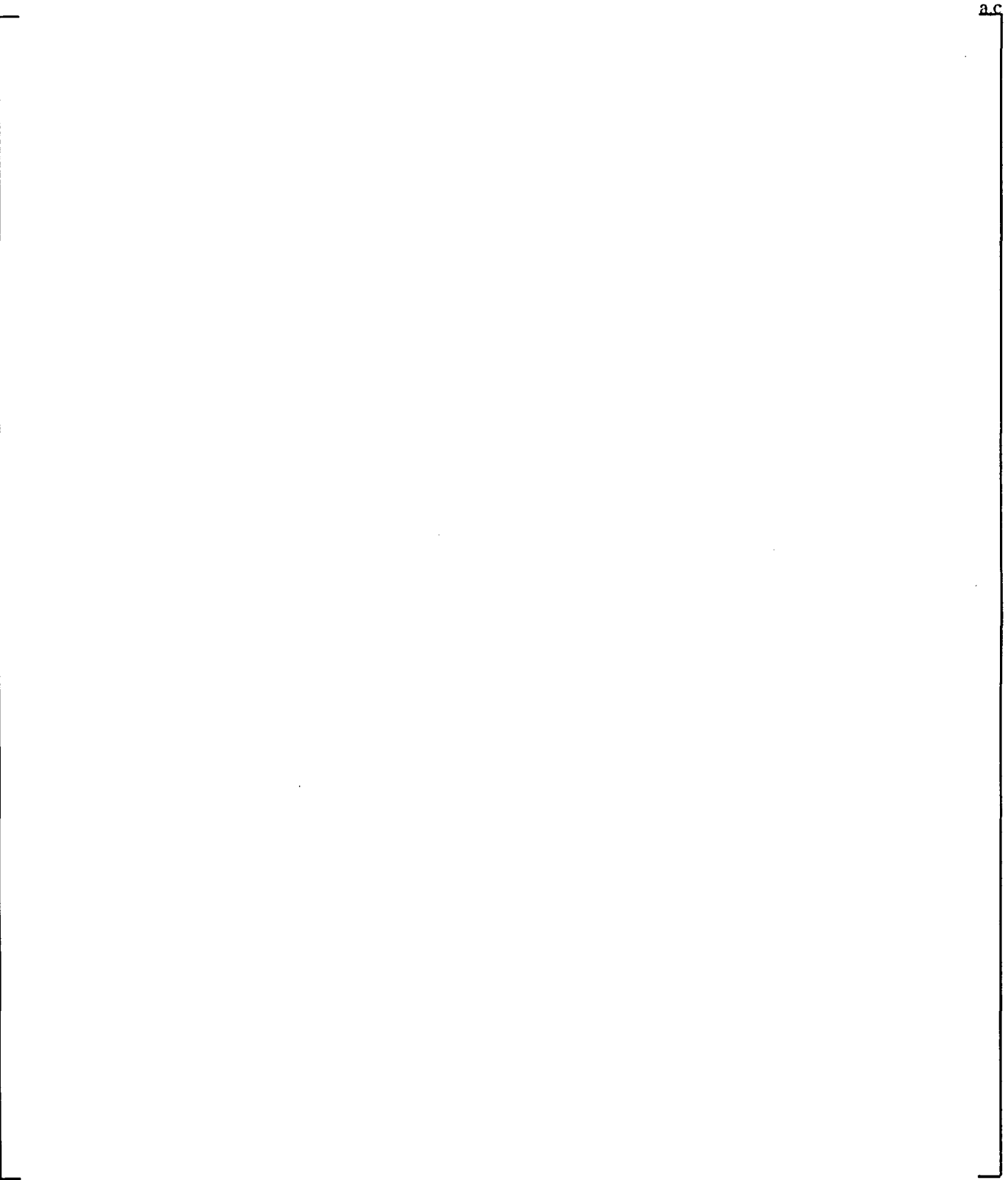


Figure 32-1-5. Hot Assembly Rod and Hot Rod Power and Uncertainty Relationships



Figure 32-1-6. WCOBRA/TRAC-SB Fuel Model at Burst



Figure 32-1-7. HOTSPOT-SB Fuel Relocation Model Compared with Preburst Condition

Figure 32-1-8a. Thermal Conductivity of UO_2

Figure 32-1-8b. Specific Heat of UO_2

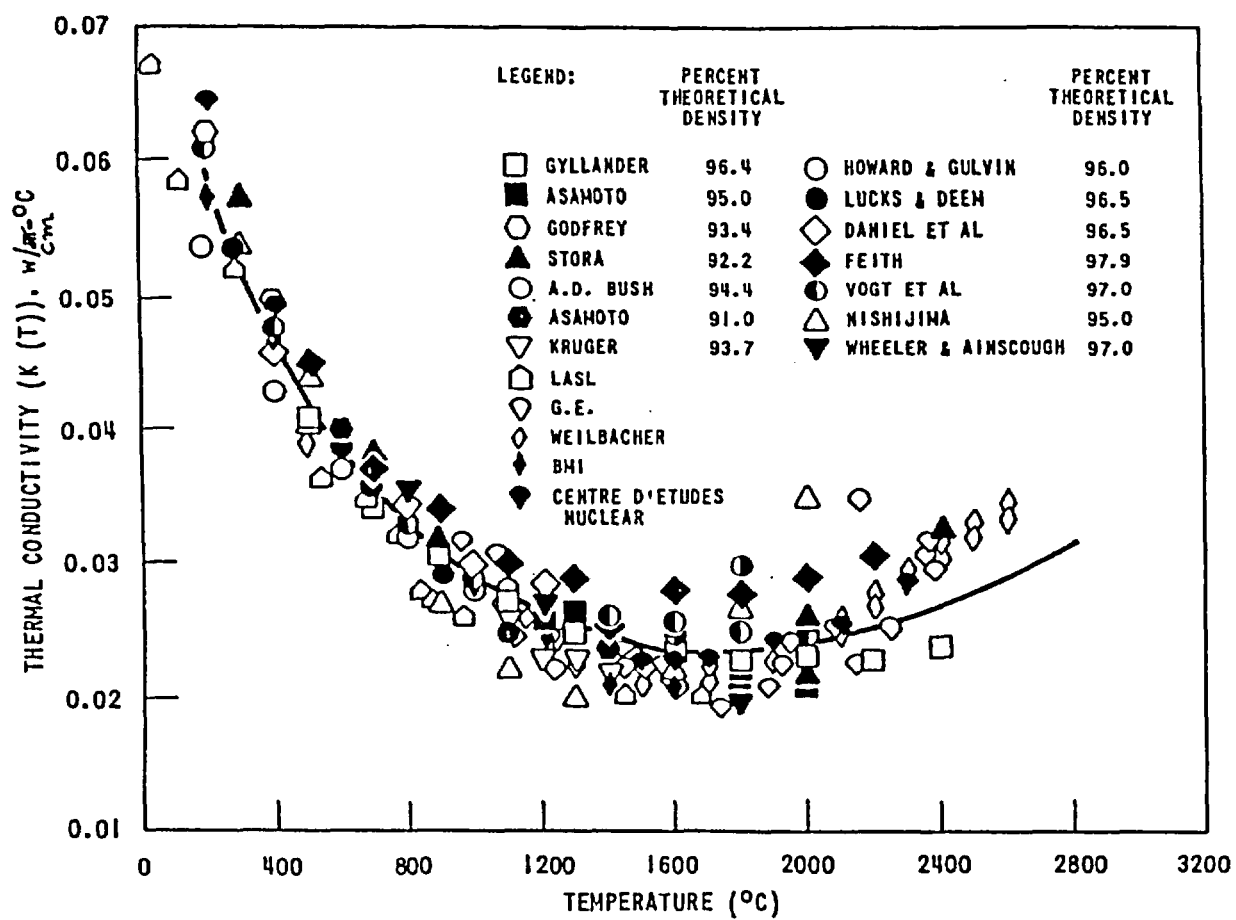


Figure 32-1-9. Thermal Conductivity of UO_2

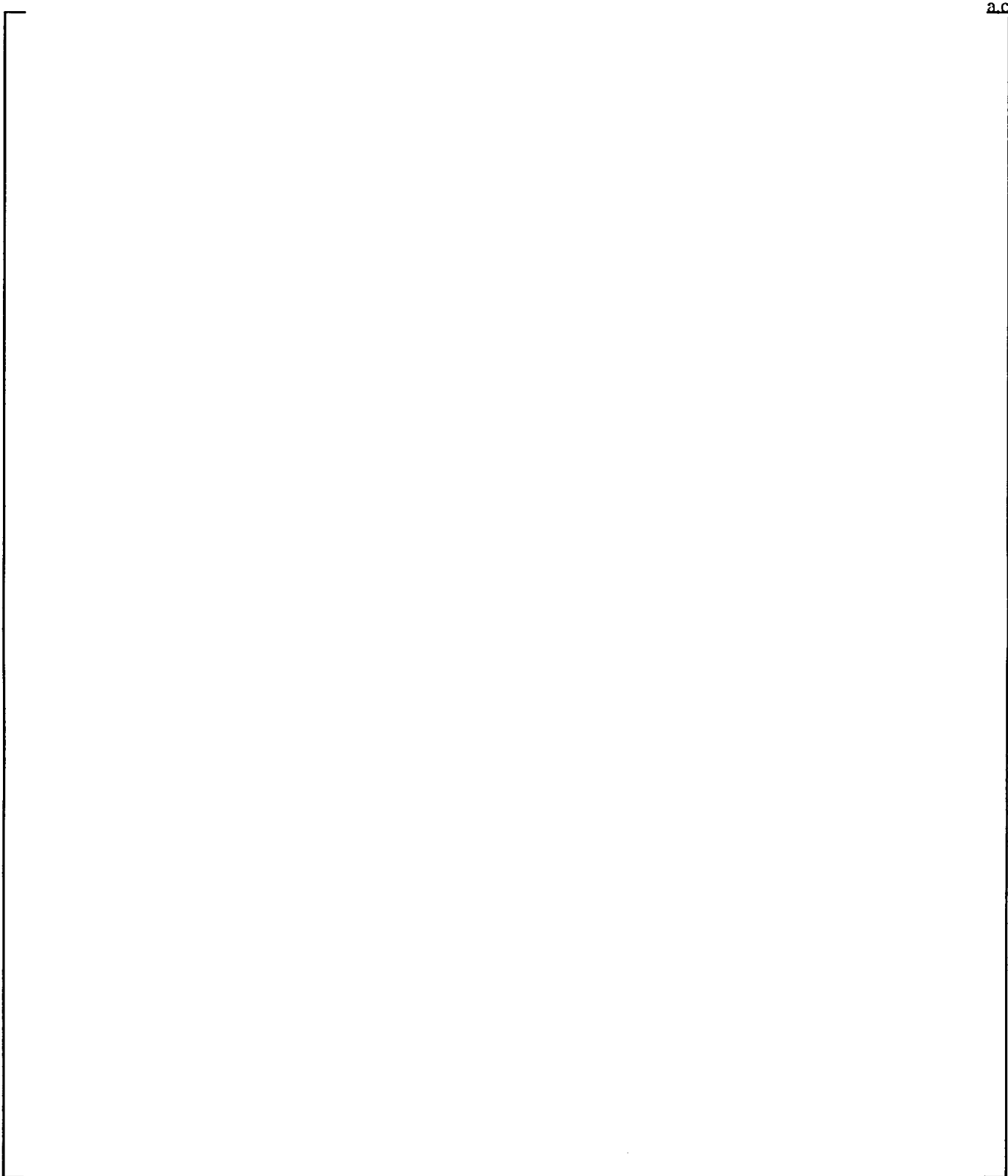
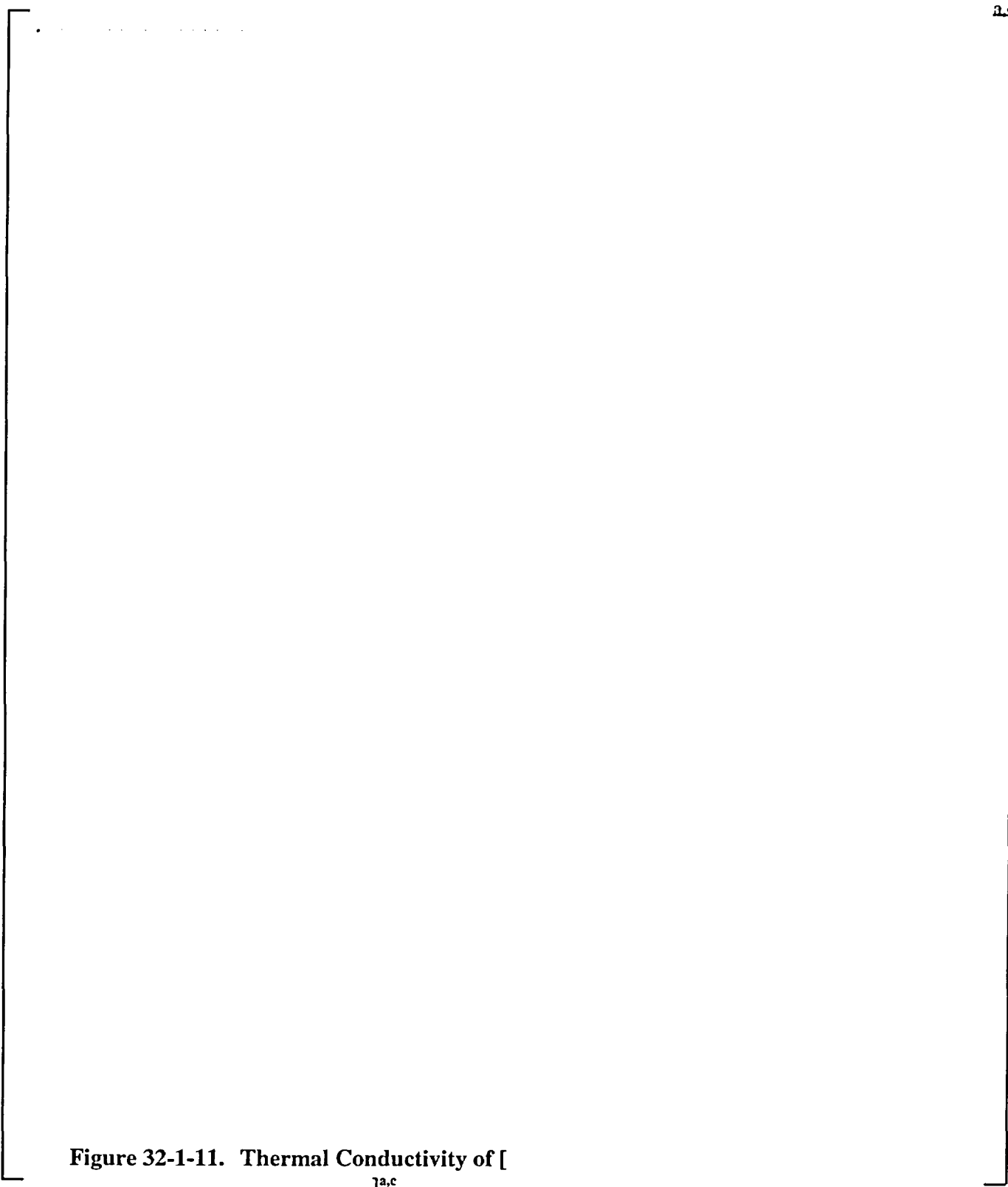


Figure 32-1-10. Comparison Between Hot Spot and PAD Fuel Temperatures



**Figure 32-1-11. Thermal Conductivity of [
]^{a,c}**

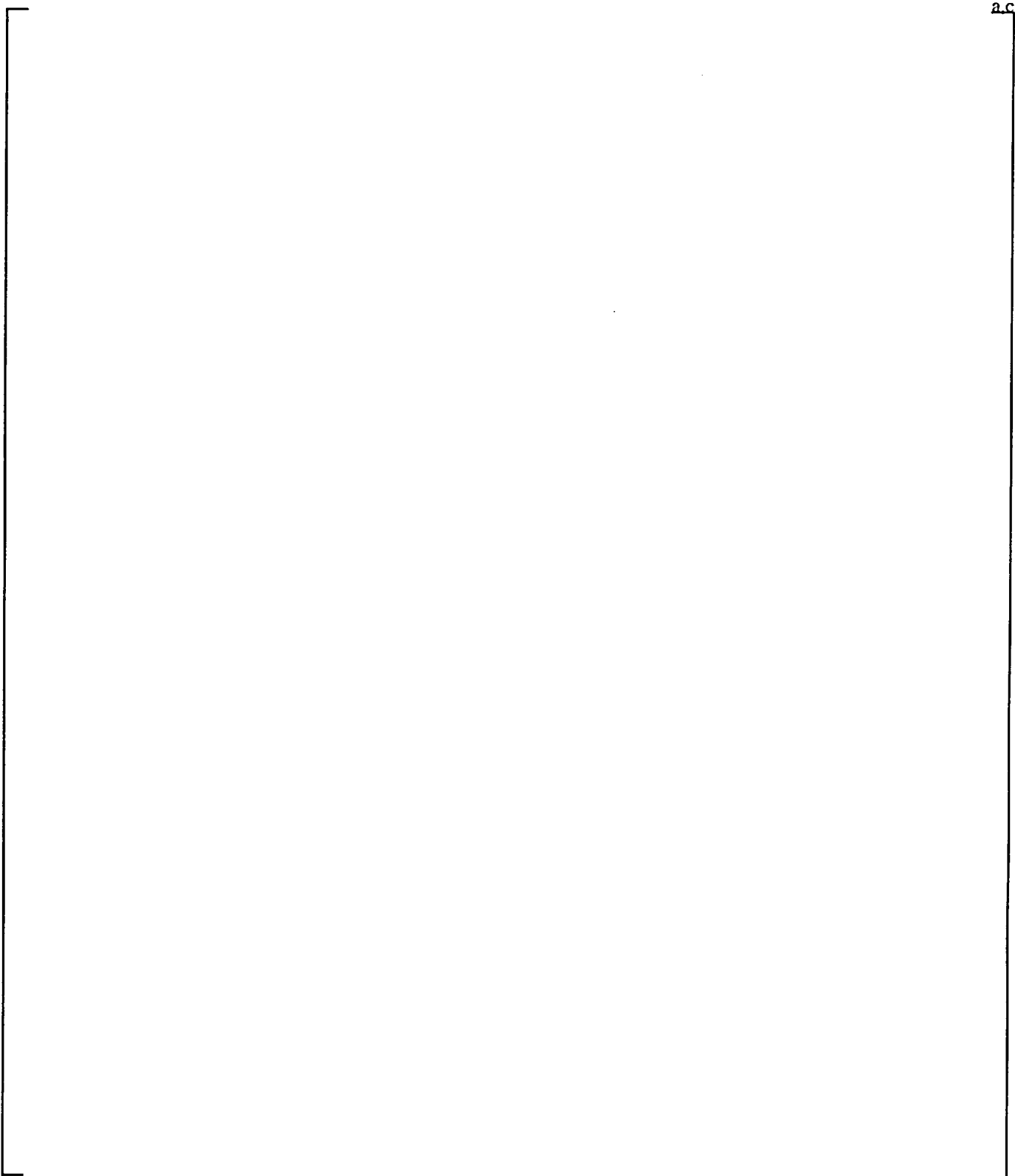


Figure 32-1-12. ZIRLO™ Burst Temperature Data and Correlation

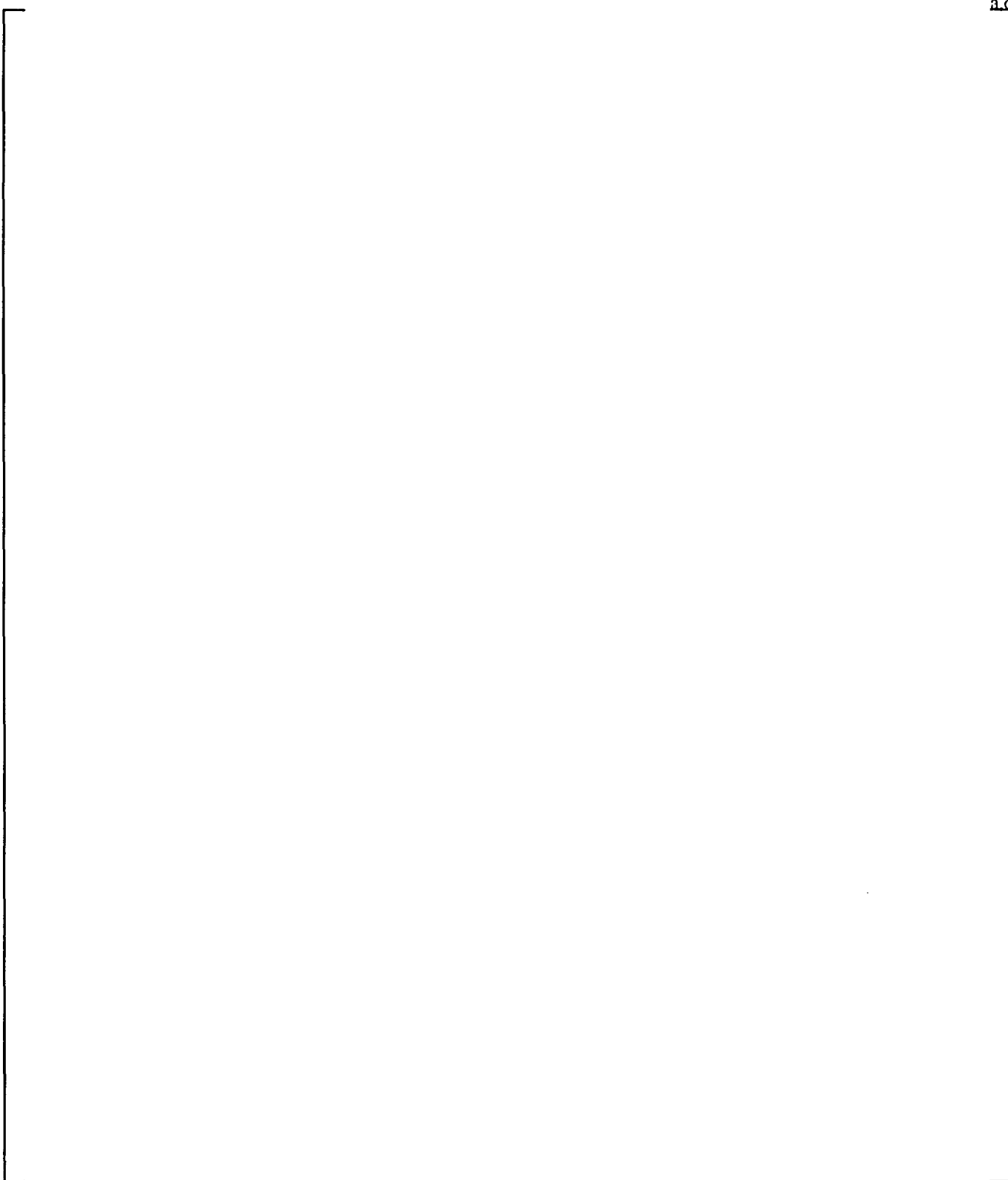


Figure 32-1-13. Zircaloy Burst Data at Several Heating Rates

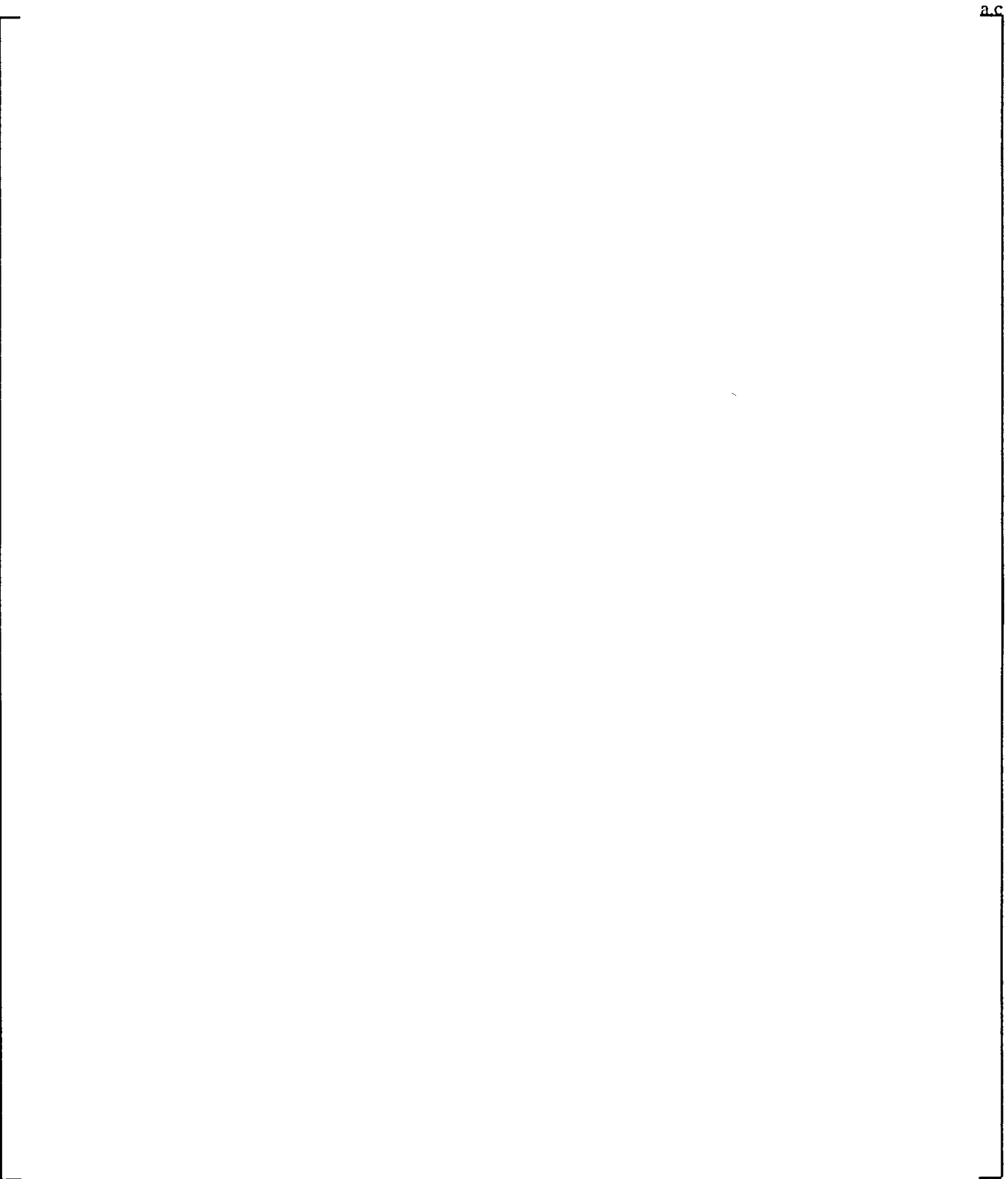


Figure 32-1-14. ZIRLO™ Burst Strain Data at Several Heating Rates



Figure 32-1-15 Zircaloy Burst Strain Data for Burst Temperatures Less than 1600°F

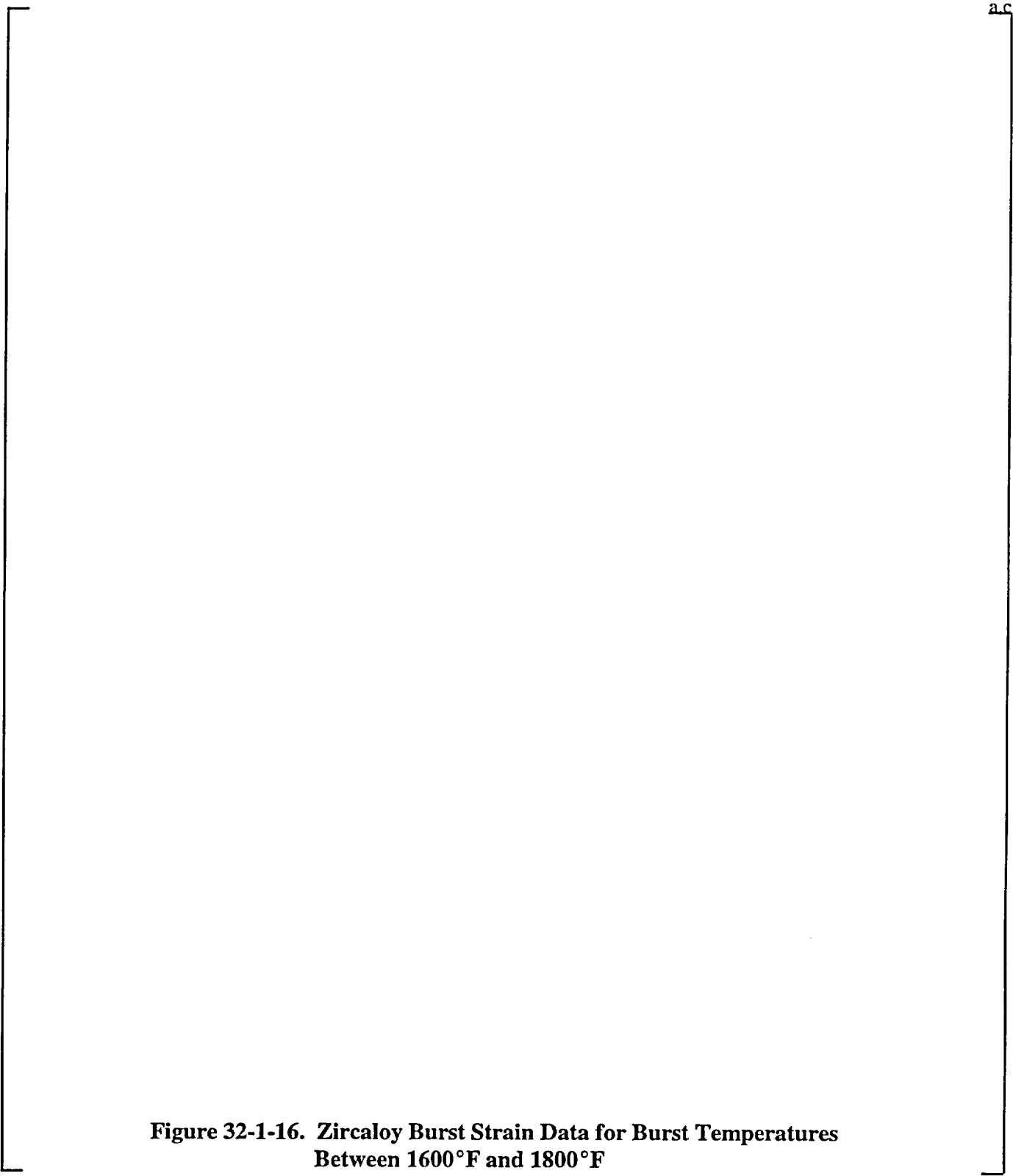


Figure 32-1-16. Zircaloy Burst Strain Data for Burst Temperatures Between 1600°F and 1800°F

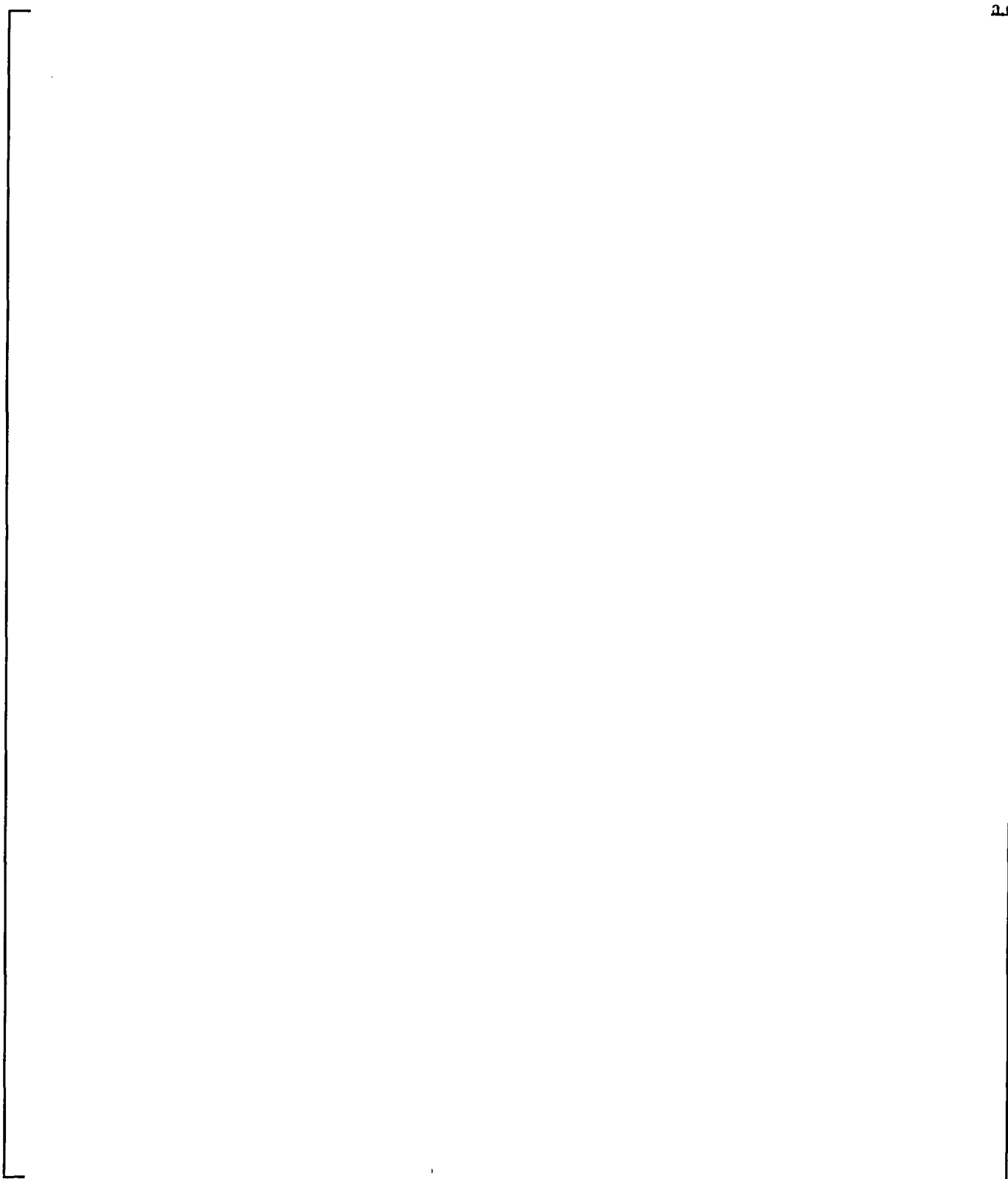


Figure 32-1-17. Zircaloy Burst Strain Data for Burst Temperatures Greater Than 1800°F

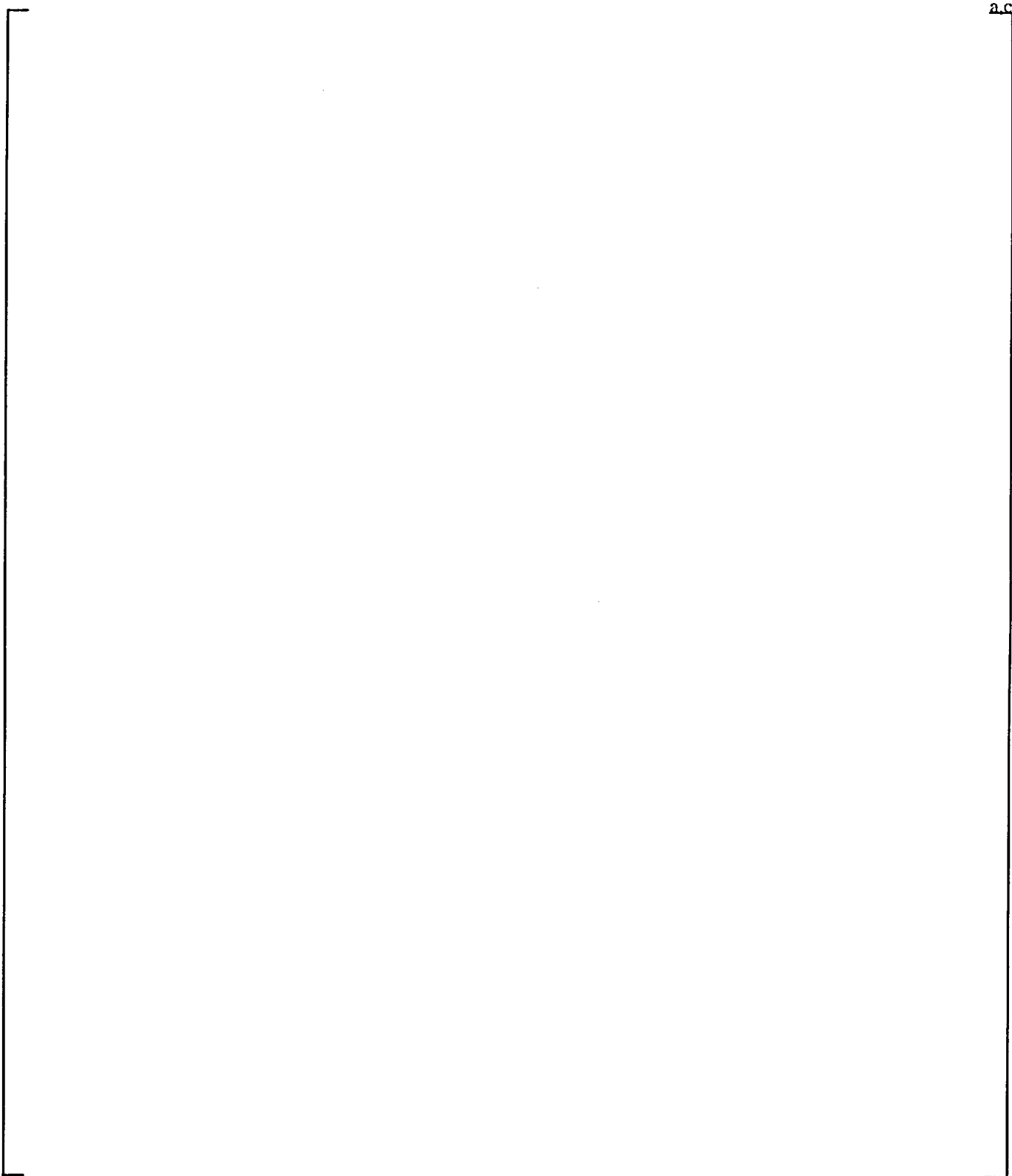


Figure 32-1-18.ZIRLO™ Burst Strain Data for Burst Temperatures Less Than 1500°F

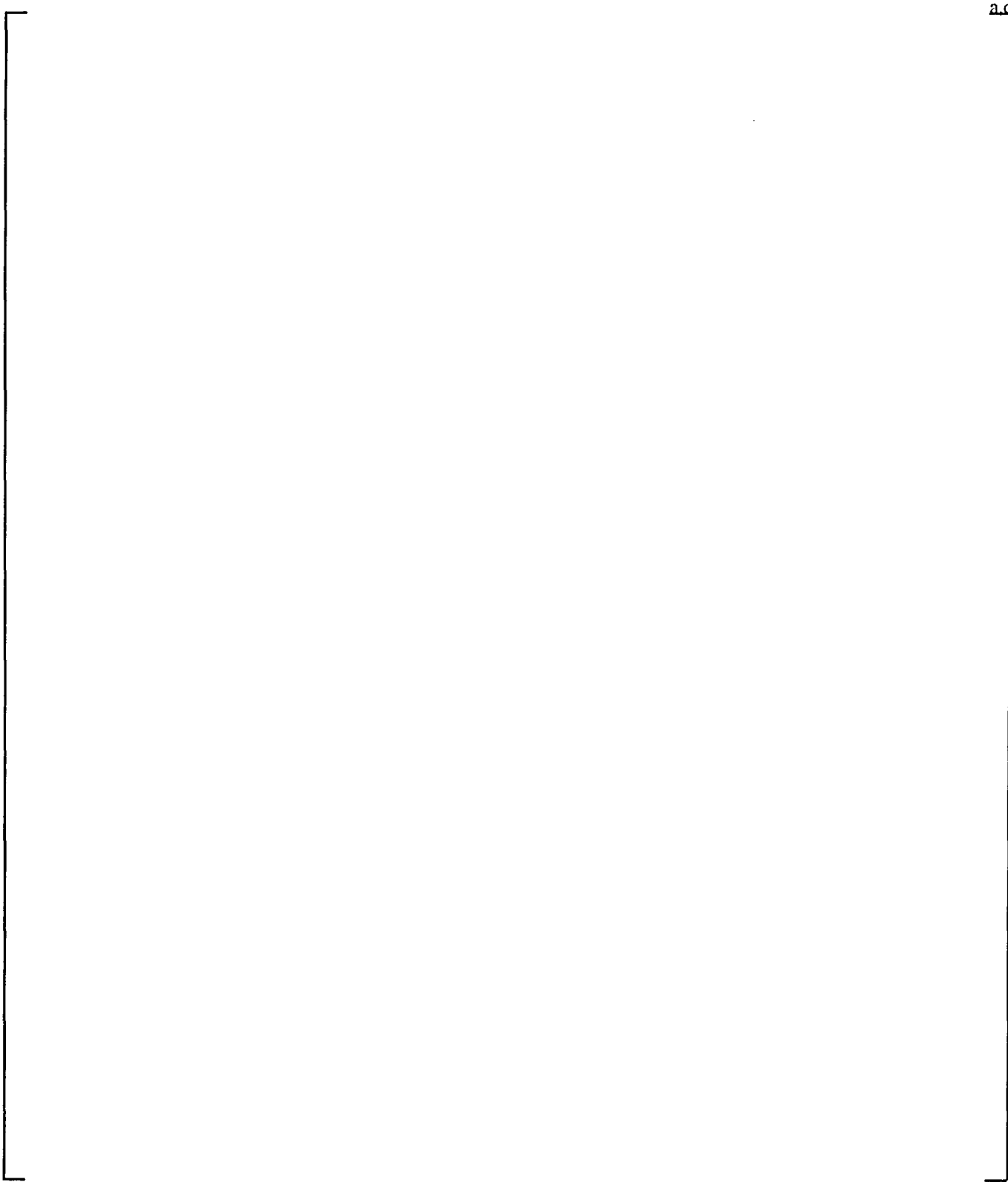


Figure 32-1-19. ZIRLO™ Burst Strain Data for Burst Temperatures Between 1500°F and 1700°F

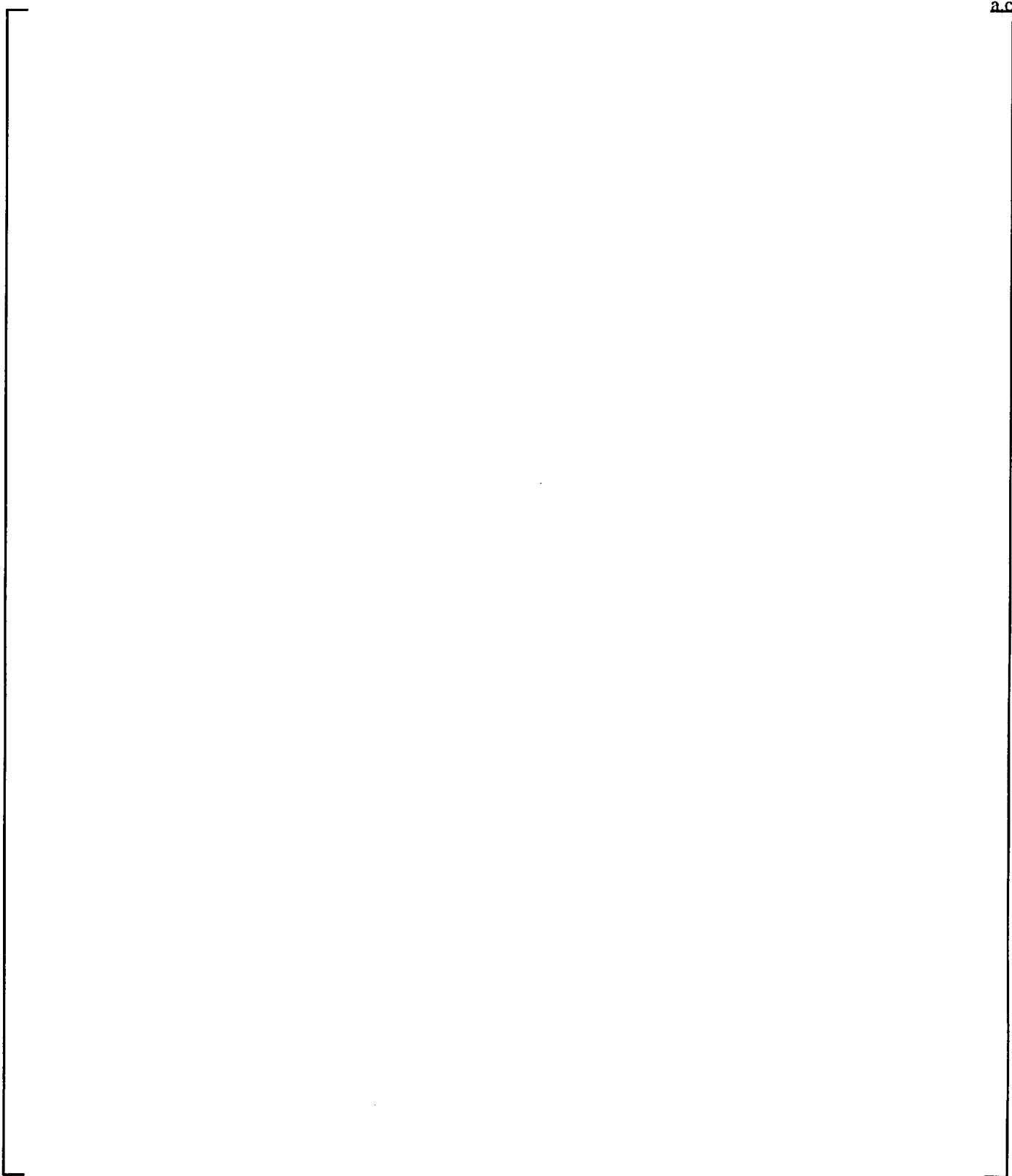


Figure 32-1-20. ZIRLO™ Burst Strain Data for Burst Temperatures Greater Than 1700 °F

Figure 32-1-21. [Ratio of 1-Inch Average Strain to Maximum Strain]^{a,c}; Best Fit and Upper Bound Lines

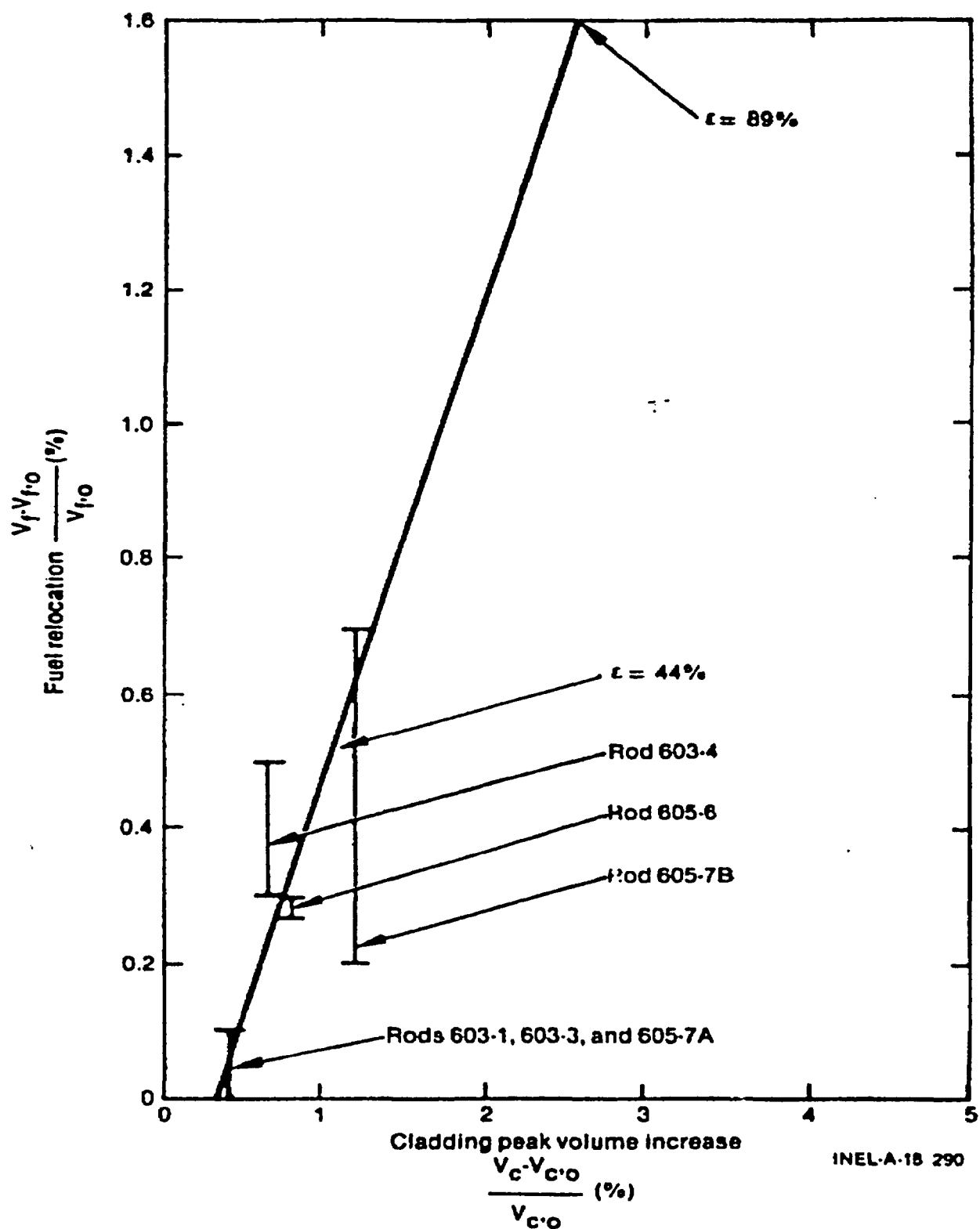


Figure 32-1-22. Volumetric Increase in Fuel for Corresponding Cladding Volume Increase Derived from PBF Tests (Broughton, 1981)

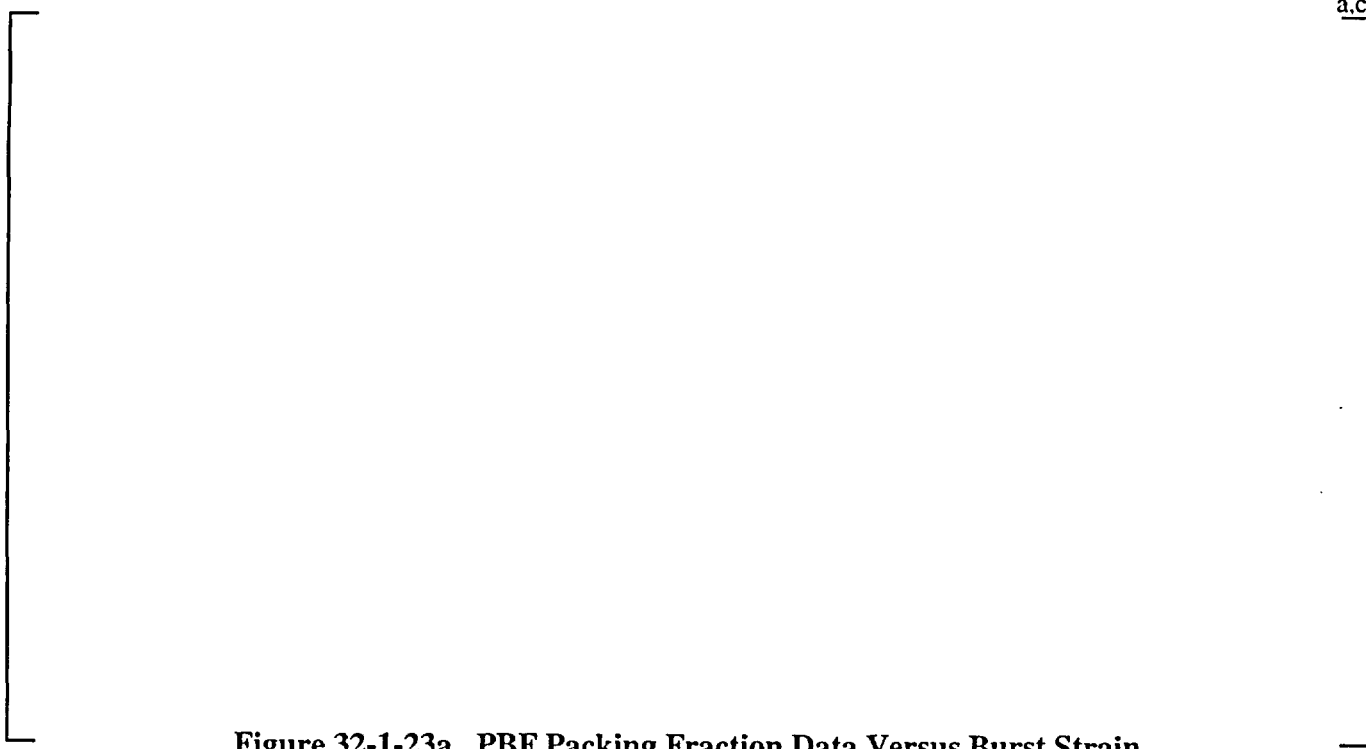
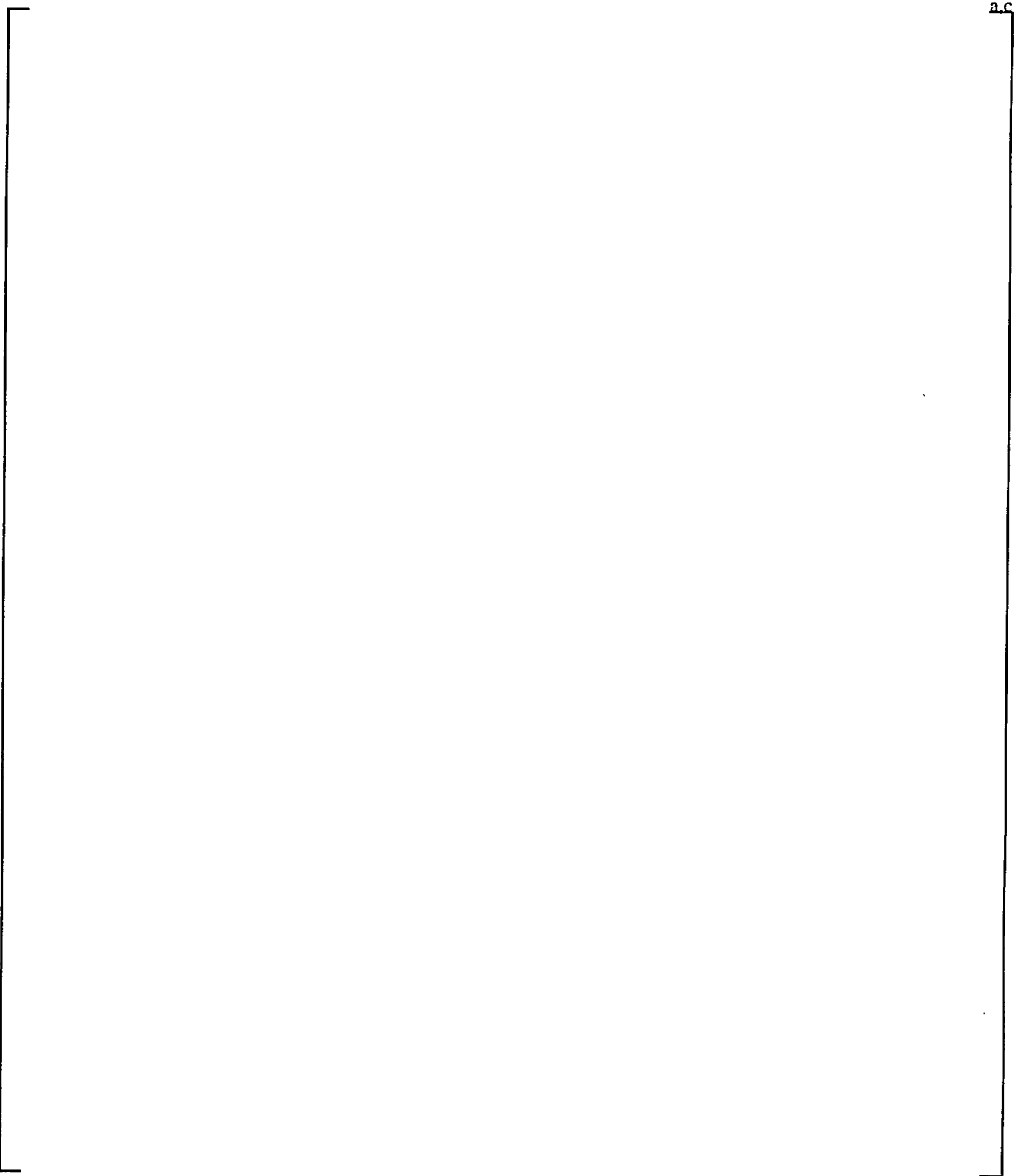


Figure 32-1-23a. PBF Packing Fraction Data Versus Burst Strain



Figure 32-1-23b. Distribution of Packing Fraction Data



**Figure 32-1-24. Prediction of $\sigma^2/2$ for Zircaloy as Function of T ; Upper Line
95-Percent Limit**

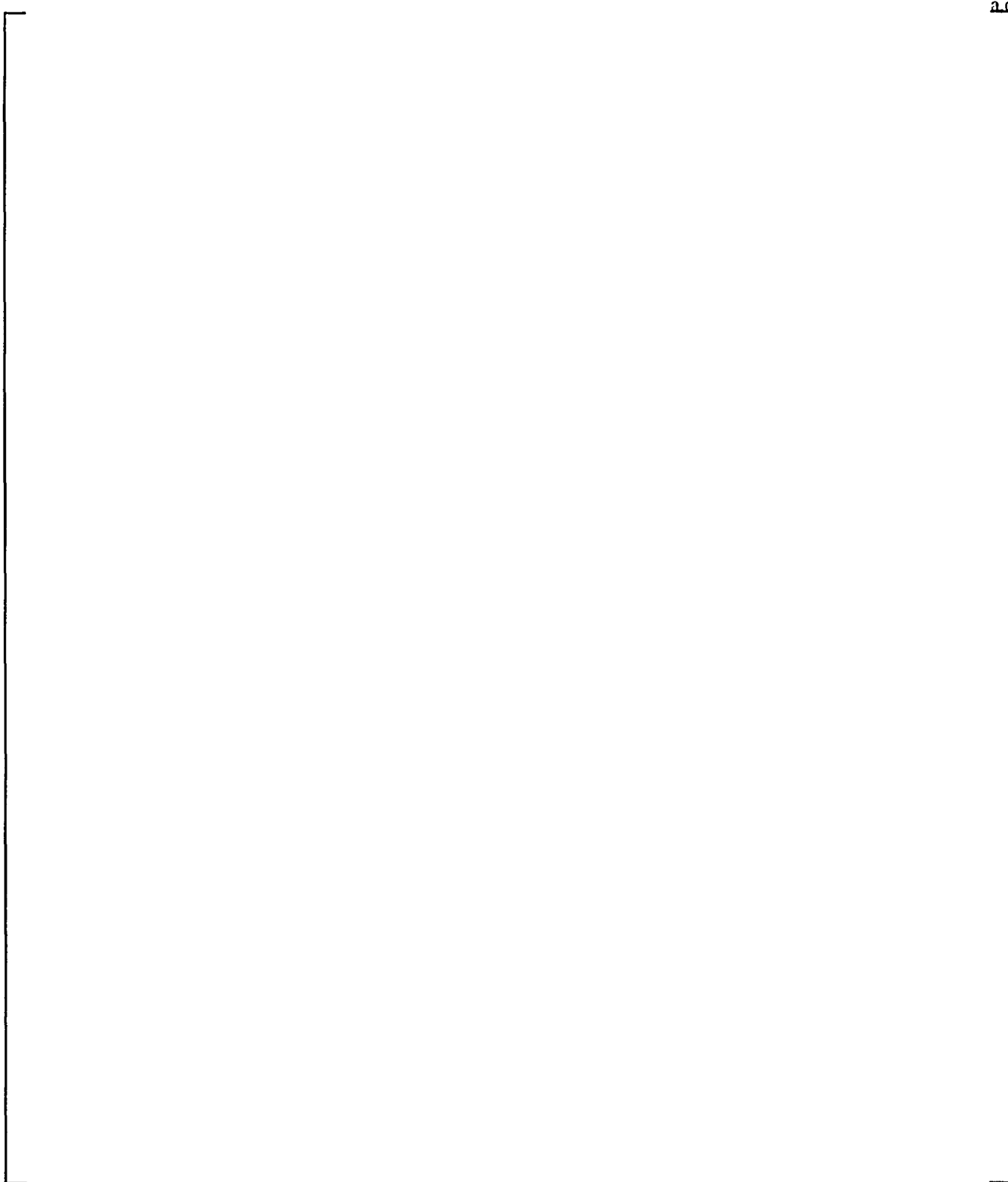


Figure 32-1-25. Zircaloy Cladding Oxidation Uncertainty for Mean and Point Estimate

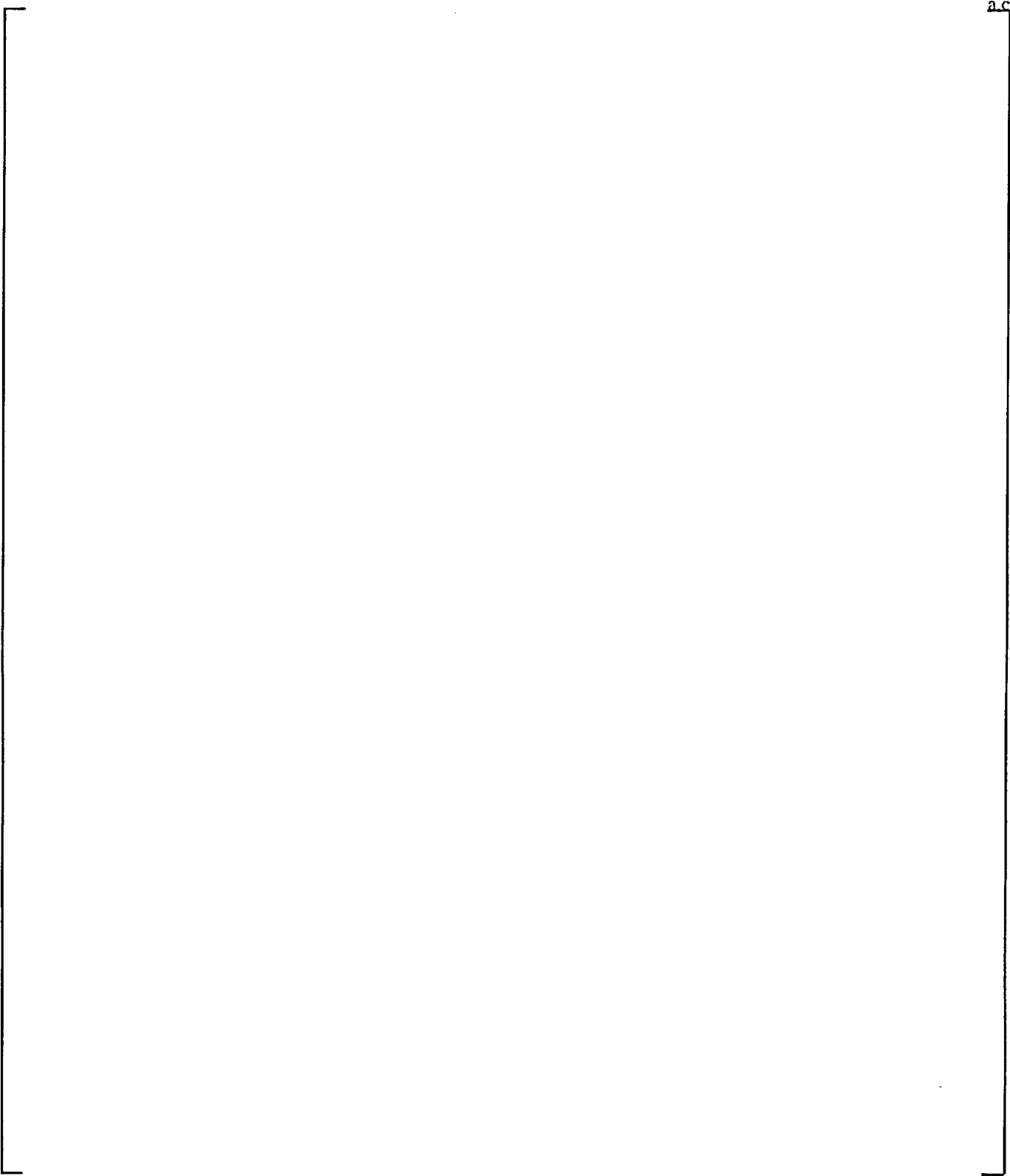
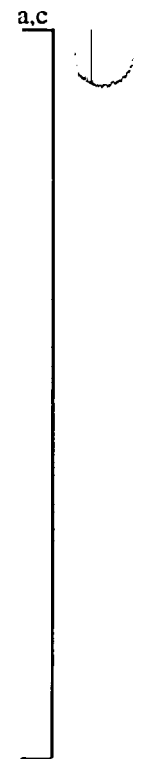
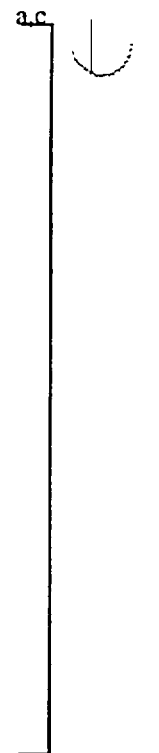


Figure 32-1-26. First Five NRU MT-3 Test Hot Spot Simulations

Figure 32-1-27. Predicted Average Burst Strain Distribution for NRU MT-3 Test



**Figure 32-1-28. Measured Burst Strain Distribution for NRU MT-3 Test
(Mohr et al., 1983)**



32-2 Code and Experiment Accuracy

This section describes the second part of CSAU step 9: "Code and Experimental Accuracy." In this step, the code is compared directly to heat transfer experiments that produce a PCT.

32-2-1 Code Uncertainty

WCOBRA/TRAC-SB was assessed by comparing predictions with a large number of tests in which aspects of each of the important small break LOCA phenomena could be evaluated (Volume 2). Table 32-2-1 identifies the tests used to assess the modeling capabilities of WCOBRA/TRAC-SB.

The code uncertainty relative to test predictions is determined by comparing the code-predicted PCT to the PCT measured in tests that exhibit heater rod uncover. Because the prediction of heat transfer in many of these tests required a correct prediction of such phenomena as entrainment and mixture level swell, it was assumed that the average difference between the PCT prediction and the data also reflected specific uncertainties or deficiencies in these fluid models.

This approach allows the explicit treatment of the uncertainty in the data, which was included as an additional component in the uncertainty. The resulting code bias and uncertainty for WCOBRA/TRAC-SB are developed in this section.

Computer programs used to realistically simulate the thermal-hydraulic response of a PWR to a postulated large-break LOCA must be evaluated to demonstrate the adequacy of the thermal-hydraulic models and to quantify the degree of uncertainty for the computational techniques. An important part of this evaluation is the computer code assessment that compares the results of simulations of relevant experiments to the measured data from the experiments. These comparisons provide the basis for establishing an overall code uncertainty, which must be accounted for in the total uncertainty of the PWR calculation.

32-2-1-1 Code Assessment Process

The process of verifying a computer code for use in PWR large-break LOCA calculations contains steps that ensure that the comparisons are applicable and that the range of the number and type of experiments is sufficient to provide a strong foundation for justifying the use of the computer code for the simulation of PWRs.

During the development of a computer code, some of the thermal-hydraulic models may be improved because deficiencies were identified while trying to simulate various experiments. Depending on what stage of development the code is in, the comparison with the data may vary and has no bearing on the uncertainty of the final version of the code. Although the process of code refinement is an integral part of the code development, code comparison results obtained during the evolutionary stages of a code should not be used when trying to evaluate the overall uncertainty of a mature code. Thus, only the final “frozen” version of the code and its models should be used for the verification studies and code uncertainty determination. Volumes 2 and 3 present the verification results using versions of WCOBRA/TRAC-SB that are final in regard to the models relevant to the simulation being performed.

The code predictions depend to some degree on the type and detail of noding used to represent the different experiments; use of relatively coarse noding for the PWR is usually desired to reduce computing costs. Calculations that model experiments should use a similar noding detail such that the uncertainty derived from the data comparisons can be applied to the PWR.

The experiments selected to be simulated should also span the entire range of conditions and phenomena expected to occur in PWR calculations to be confident that the PWR calculations are being performed within a range that the code has already been verified.

The approach used to assess WCOBRA/TRAC-SB is consistent with the methodology recommended by the NRC (Wilson et al., 1989). The version of the code used in each simulation was valid for the predictions and their uncertainty to be applicable to the final frozen version of the code. The noding used for the experimental simulations was consistent with the noding schemes used for the PWR analysis such that uncertainty derived from the experiments was applicable to the PWR.

32-2-1-2 Code Convergence and Timestep Size Sensitivity

The timestep size in WCOBRA/TRAC calculations is controlled by several parameters that are supplied as input. These input parameters are described in Section 2-7, Volume 1. Tables 2-1 and 2-2, Volume 1, list two sets of input parameters that control timestep size based on changes in various thermal-hydraulic quantities. The inputs listed in Table 2-1 reduce the timestep size for the next timestep, while those in Table 2-2 determine when the code should stop, back up to conditions existing at the start of the previous timestep, and repeat the solution with a timestep size one-half that of the first solution. In addition, the range of permissible timestep sizes is prescribed by input. The maximum allowable value of timestep is given by *DTMAX*, and the

minimum timestep size is given by *DTMIN*. If the code attempts to reduce the timestep size below *DTMIN*, execution is terminated.

Table 32-2-2 lists the values of the timestep control parameters used in the test simulations in Volume 2. They are the same as Volumes 2 and 3 in WCAP-12945-P-A (Bajorek et al., 1998 and 1998a). Several of the validation test simulations reported in WCAP-12945-P-A (Volumes 2 and 3) were repeated with different timestep control input values to determine the sensitivity of the results on those parameters; Section 19, Volume 4, of WCAP-12945-P-A (Bajorek et al., 1998) discusses these timestep studies for the validation test simulations using WCOPRA/TRAC MOD7. This section describes similar studies for small break LOCA test simulations performed with WCOPRA/TRAC-SB.

[

]^{a,c}. Several simulation tests were repeated with different values of *DTMAX* to evaluate the sensitivity of results on the choice of convergence input. G-1 Test 57, a test representative of the core uncover power and pressure in PWRs among the separate effects tests, was used to examine the sensitivity of level swell and fuel cooling to timestep size. From the ORNL Core Uncovery Tests, Test 3.09.10-J was chosen for the convergence studies because it was conducted at the pressure of most interest for core uncovery in the Reynolds number (Re) range of most interest. Because the Rig of Safety Assessment (ROSA)-IV facility was the test facility with characteristics most similar to a PWR, it was also used for a series of convergence studies. The following paragraphs summarize the results of these studies.

G-1 Test 57

Level swell separate effects tests are reported in Section 15, Volume 2. G-1 Test 57 is representative of these tests and was used for a timestep size sensitivity study. The value of *DTMAX* was varied from []^{a,c} to examine the effect of allowable timestep size on the results. Table 32-2-3 lists the results of this study.

[

]^{a,c}

Table 32-2-3 indicates a weak sensitivity of results on *DTMAX*. From the average timestep size, it can be seen that [

]^{a,c}.

ORNL Core Uncovery Tests

ORNL Core Uncovery Test 3.09.10-J was selected for timestep size sensitivity studies. Test J, described in Section 15, Volume 2, is the intermediate power case at the lower pressure condition. Table 32-2-4 summarizes the results for six different values of *DTMAX* ranging from [

]^{a,c}.

Table 32-2-4 also lists the average timestep size for each case, which indicates [

]^{a,c}.

ROSA-IV Test SB-CL-03

Simulations of ROSA-IV Test SB-CL-03 were made using two sets of timestep control input. These input values are listed in Tables 32-2-5 and 32-2-6. Table 32-2-5 shows the code timestep in separate runs performed in which the maximum allowable timestep calculated by the code was reduced and increased. The calculated results for the transient portion of the calculation are shown in Table 32-2-6, and [

]^{a,c}

[

]^{a,c}

Conclusions

The test simulations were examined, and the results were insensitive to the changes in timestep control input. Sensitivity studies were run for three different tests: G-1 Test 57, a core uncover transient; ORNL Test 3.09.10-J, a steady-state uncovered core simulation; and ROSA-IV Test SB-CL-03, a complete LOCA transient in an integral system. [

]^{a,c}

32-2-1-3 Contributors to Computer Code Uncertainty

The main purpose for performing computer code verification is to verify that the code will predict the correct thermal-hydraulic phenomena, as well as to quantify the uncertainty that should be assessed to the computed results for PWR analysis. Comparisons between the calculated results and the experimental test data indicate the accuracy of the models and correlations in the computer code being assessed and how these models and correlations, as programmed into the code, perform as a total package. The comparison validates the assumption used in the code on the choice or selection of the correlations. The resulting calculated uncertainty gives a numerical value that is a measure of the "goodness" of the code relative to the test data and phenomena observed in the experiments.

The quality of these comparisons also strongly depends on the experimental design, the type and amount of experimental instrumentation, the control of the experimental boundary conditions, and the modeling sophistication used to represent the experiment.

Uncertainties that occur when a computer model is used to predict experimental data arise from the following sources:

- Noding detail and assumptions made in simulating the experimental test geometries within the computational cell
- Accuracy of the measured initial and boundary conditions used as input
- Accuracy of the models developed to account for unique facility characteristics
- Ability of the computer code model to represent systems at different scale, as discussed in Section 32-6

These uncertainties can be addressed using several techniques. The methods are similar in that they each try to isolate a particular contributor of the code uncertainty and evaluate the uncertainty of that contributor.

Prior to the evaluation of the computer code uncertainty, a set of appropriate separate and integral effect experiments must be selected so the code can be exercised over the range of phenomena

expected to occur in a postulated large break LOCA. This set of experiments is called the test matrix for code verification. The experiments chosen are described in Sections 12 to 21, Volume 2.

The process of determining code uncertainty during code verification would be relatively simple if the same noding was used for every experiment, if the measured data had no uncertainty, and if the experiments were conducted in full-scale facilities. Although the noding philosophy used for the code verification is the same as that used for the PWR application, unique characteristics in the geometry of certain components in an experimental facility often make it impossible to completely duplicate the noding used in a PWR. Thus, it is necessary to try to evaluate the effect of such variations and modeling in the code verification process. This evaluation consists of performing sensitivity studies that vary the noding in the computer model to provide a basis used to calculate the modeling uncertainty for the experiments (Hochreiter et al., 1988). The effect of variations in timestep size on PWR results could also be captured here (Section 33).

The uncertainty of the measured data is affected by the accuracy of the instruments used for the measurements, the ability of the experiment operator to achieve the desired initial conditions, and the ability of the experiment operator to maintain the proper boundary conditions for the duration of the test. Later in this section, possible contributors to the measurement uncertainty are addressed.

Section 32-6 addresses the effects of additional uncertainty due to scaling and indicates that no additional uncertainty should be added to WCOBRA/TRAC-SB uncertainty because of scaling.

Once all of the components of uncertainty have been identified and quantified, the overall code verification uncertainty can be calculated.

32-2-1-4 Data Screening for PCT Comparisons

Introduction

The data from several different experiments were used to estimate the overall code uncertainty. Each set of data, for a given experiment, was screened to eliminate experimental bias resulting from nontypical parameters that could affect the measured heater or nuclear rod transient. For example, heater or nuclear rods adjacent to cold test housings or to failed rods were eliminated because these rods experience higher than expected radiation heat transfer. In addition, the thermocouple data were screened to eliminate erroneous thermocouple readings. This was done

by examining thermocouple behavior during the transient, checking the initial thermocouple readings at the beginning of the transients, and examining the response of the thermocouples test-to-test to see how individual thermocouples performed.

Finally, the data were grouped to be consistent with the nodalization scheme used in the computer code. For example, measurements at a given elevation within specific cells were grouped to obtain the correct code-to-data comparisons.

Most of the experiments that WCOBRA/TRAC-SB simulations were compared to used electrically heated rods, which were all at the same power and were manufactured in the same fashion. A two-channel WCOBRA/TRAC-SB nodalization was used to model the rod bundle in the ROSA-IV experiments. The outer channel included the lower power rods and considered the hydraulic effects of the test facility housing, as well as the convective heat transfer effects to the colder structure; because the test section housing is not present in a PWR, the data from these heater rods were not used in the code comparisons or uncertainty calculation. The inner WCOBRA/TRAC channel contained the hotter heater rods that did not have a significant surface radiation heat transfer component to the test section housing. The comparison of the WCOBRA/TRAC inner channel calculations to the heater rods in this channel was used to assess the code uncertainty. The influence of the test section housing was accounted for, and the heater rods and thermocouple readings that could have a nontypical bias were eliminated from the code data sample, which is compared to the code calculation, as indicated. Unless the test had a built-in radial power distribution, the remaining rods should have an equal probability of being the hottest rod in the experiment because they were all manufactured to the same specifications and were operated at the same power. Therefore, there is no single rod with the true PCT for most electrically heated tests, but rather a distribution of those rods, any of which could be the true PCT for the experiment. The distribution of the heater rod PCT values is caused by variations in the manufacturing, local power differences caused by electrical resistance variations, and physical property variations of the cladding, coil and boron nitride insulator, and individual subchannel flow differences. Due to the bias effects in the test having been removed, uniform weighing is the best choice because the remaining rods should have the same probability of being the hot rod in the test bundle.

In a nuclear reactor fuel assembly, the fuel rod power depends on where the rods are within an assembly. Fuel rods adjacent to guide tube thimbles experience a larger thermal neutron flux. These neutronic properties of the fuel assembly can lead to higher power rods within the assembly, whereas with an electrically heated fuel bundle, there is no comparable effect. In conclusion, there may be nuclear rods that represent the true PCT within a fuel assembly, but not

true PCT rods within an electrically heated assembly unless higher power rods are specifically simulated.

In the following sections, data from each test provide the average measured PCTs (\overline{PCT}_{mi}), which represent the average of the valid thermocouple readings at a given elevation for Test I. This can be compared to a specific WCOBRA/TRAC predicted value (\overline{PCT}_{pi}), which is the calculated rod temperature for the same location as the data.

G-1 High Pressure Core Uncovery Experiments

These G-1 high pressure small break heat transfer experiments [

]^{a,c}

ORNL Uncovered Bundle Experiments

These ORNL high pressure level swell experiments were analyzed using the WCOBRA/TRAC-SB model as shown in Volume 2, Section 15. In the bundle were four unpowered rods which simulated the unheated guide tubes. This way a more typical PWR power-to-flow ratio was used in the experiments. For these tests, the experimenters reported heater rod surface temperatures, which were used in the code uncertainty calculation directly. The ORNL rod bundle cross section is shown in Figure 32-2-1; one WCOBRA/TRAC-SB channel is used to model the rod bundle. The WCOBRA/TRAC-SB calculation was compared to the heater rod thermocouple data at two different elevations along the rod bundle.

NRU Nuclear Rod Reflood and Cladding Swelling Experiments

A series of nuclear rod reflood and cladding swelling experiments were conducted, inpile, in the NRU reactor for the NRC. These experiments, along with the LOFT tests, account for some of the fuel rod uncertainties in the WCOBRA/TRAC fuel rod model. The NRU experiments were modeled using the WCOBRA/TRAC code as described in Volume 2. There are a total of 32 nuclear fuel rods in the NRU test bundle (Figure 32-2-2). A two-channel WCOBRA/TRAC

model was used to model the center region of the bundle, where the fuel rods were pressurized for the cladding swelling test, and the outer channel was used to model the guard fuel rods, which were unpressurized. The measured inlet flow and pressure conditions were used as the boundary conditions for the model calculations as well as the measured nuclear power for the test assembly. Because there were only a few data points at a given elevation, the data were used to compare the code to the test results as shown in Volume 2, but this test was not used in the statistical calculations for code uncertainty.

ROSA-IV Tests

The ROSA test facility is shown in Figure 32-2-3. For the ROSA tests, the data from the central fuel assembly were used to calculate \overline{PCT}_{mi} . In this case, all valid thermocouples in the hot assembly were used because there were no cold artificial boundaries such as test section housings. [

J^{a,c} Because most of the ROSA center fuel assembly thermocouples are toward the assembly interior, the effect of the radial power distribution on the data average will be small.

32-2-1-5 Code Uncertainty Calculation

Introduction

When the best estimate LOCA methodology is applied to a PWR, the calculated PCT occurs in the core uncoverage phase of the postulated small break accident. Therefore, a numerical value for the WCOBRA/TRAC-SB code uncertainty has been calculated for the peak PCT values.

Among the experiments that WCOBRA/TRAC-SB has been compared to, three separate test facilities, each with different characteristics, are used to compare predicted temperatures with data.

There are several components to the total code uncertainty calculation as described in the following. The components include the code bias, which is the code comparison to the average of the data at a given elevation. The code uncertainty calculation accounts for the scatter of the test data relative to the average used to compare to the code predictions, the modeling uncertainty for the experiments, and the scatter of the data average-to-code predictions.

Code Bias Determination

The code bias indicates, on an average, if the code overpredicts or underpredicts the average of the test data at a particular node. A negative value for the bias indicates that the code yields higher calculated PCT values than seen in the experiment. The code bias is determined by examining the mean of the difference between the predicted PCT and the average of the measured PCT for the peak temperature node for each PCT at different elevations and different times, that is:

$$\Delta PCT_{I, j, k} = \frac{1}{N} \sum_{i=1}^N \left(\overline{PCT}_{m_{i, j, k}} - PCT_{p_{i, j, k}} \right) \quad (32-2-1)$$

where:

$\Delta PCT_{I, j, k}$ = Code bias, for Test I, at elevation j , time period k

N = Number of experiments analyzed

$PCT_{p_{i, j, k}}$ = PCT predicted for Test I at elevation j , time period k

$\overline{PCT}_{m_{i, j, k}}$ = Average of measured PCTs for Test I for elevation j , time period k

For convenience, the k subscript is dropped because all of the test data is for the core boiloff uncov ery time period. The calculated code bias and uncertainty in the bias were calculated as shown in Table 32-2-7 at the elevations specified.

The interpretation of the bias results contained in Table 32-2-7 is that, on average, WCORBA/TRAC-SB underpredicts the mean of the data.

Uncertainty in the Code Bias

In addition to a bias in predicting the average PCTs, there is also test-to-test variability on how well the computer code predicts one or another set of data.

The uncertainty in the code bias at each elevation (j) is defined as the standard deviation of the calculated PCT relative to the average measured PCT for the same node, that is:

$$\sigma_{WCIT_j}^2 = \frac{1}{N-1} \sum_{i=1}^N \left\{ \left(\overline{PCT}_{m_{i, j}} - PCT_{p_{i, j}} \right) - \Delta PCT_{I, j} \right\}^2 \quad (32-2-2)$$

which is a measure of the uncertainty or variability of the code bias relative to the averaged PCT data over a range of different experiments, at different elevations (j), for each PCT.

The variances of each experimental result and the WCOBRA/TRAC-SB calculation $(\overline{PCT}_{mi} - PCT_{pi})$ are calculated; Table 32-2-7 presents the calculated values for $\Delta PCT_{i,j}$ and σ_{WCT_j} for WCOBRA-TRAC-SB. [

]^{a,c}

32-2-1-6 Variability of the Test Data

The data derived from a particular experiment have an associated uncertainty that reflects the combination of several sources of uncertainty in design and construction, test operating procedures, instrumentation, and data collection methods. Each of these areas is discussed, and the sources of uncertainty are identified. For this discussion, the Westinghouse-performed FLECHT and FLECHT-SEASET experiments are used. It is expected that the experiments used herein will have similar sources of uncertainty because they are similar heater rod heatup experiments.

The sources of uncertainty in the design and construction of the experiment are as follows:

- Uncertainty in the as-built dimensions of the test section as compared to that which was specified, for example, the test section inside diameter, variation along the length of the test section, degree of ovality, degree of straightness, wall thickness, and length
- Placement of the test rod bundle in the test article housing, the straightness of the rod bundle, the uniformity of the clearances around the test bundle, and the position of the spacer grids on the rod bundle relative to the design placement
- Uncertainties in the heater rod construction and fabrication, such as:
 - Heater rod diameter
 - Cladding thickness
 - Rod ovality
 - Thermocouple location

- Insulator density at thermocouple point
 - Heater coil spacing relative to the cladding (degree of ovality)
 - Heater coil pitch variations (power step variation)
 - Insulator thermal conductivity variabilities
 - Insulator specific heat variabilities
 - Heater coil resistivity variabilities
 - Cladding thermal properties variations
 - Heater rod thermocouple calibration variations
 - Aging effects on heater rod thermocouple response
 - Uncertainties in gap between the cladding and electrical insulation
 - Uncertainties in gaps between adjacent coils of the electrical heating element
- Uncertainties in the piping diameters where flow measurements are made: ovality of the pipe and roughness of the pipe wall
- Uncertainties in the heat losses from the system
- Uncertainties in the specific heat, conductivities, densities, thermal expansion of the material used for the piping, and flow measurement locations
- Electrical wiring of the instrumentation and power to ensure no common electrical grounds or interference

The operation of the test facility also introduces several sources of uncertainty as listed below:

- Measured power, flows, pressures, and temperatures
- Variation of the steadiness of the test boundary conditions
- Variance in when an acceptable heatup criteria is achieved before the initiation of the experiment
- Variation from operator-to-operator in performing a test

Other sources of uncertainty in the instrumentation used to obtain the data are as follows:

- Stated range, linearity, and accuracy of the instruments chosen
- Environment in which the instrument operates
- Uncertainty in the power to the instrument, electrical noise, and grounds
- Uncertainty in the instrument calibration and drift
- Uncertainty in instrument aging
- Uncertainty in instrument installation and references
- Uncertainty of the wiring of the instrument to the data processing computer

How the data are electronically collected can also introduce uncertainties to the final data used in analysis. These sources of uncertainty are as follows:

- Round-off error of the computer A/D converter at the front end
- Variability of electrical power spikes to the computer
- Signal processing uncertainty
- Variability caused by temperature or environmental changes on the computer

Experimental programs are costly in the nuclear area because of the needs for high pressure, high temperature, complex heated surfaces (rod bundles), and large-scale as compared to exploratory bench experiments. Because the cost for the data is large, great care is used to reduce the sources of uncertainty to a minimum. The methods used to reduce the uncertainty for the FLECHT and FLECHT-SEASET experiments are described in the following paragraphs. Similar methods are used in other experiments to reduce their uncertainties.

For the FLECHT-SEASET experiments, in the test design and construction phase, the hardware was inspected and measured after fabrication to ensure manufacturing within the allowable tolerances. Deviations were so noted and drawings or input to data reduction codes were changed to reflect the new area, volume, and length (this removes the uncertainty from the data). For example, all test bundles were filled and drained to get an accurate cross-sectional area to be used with the differential pressure cells. The heater rods were inspected by both the vendor and Westinghouse to reduce and minimize any uncertainties in manufacturing. The heater rods were X-rayed to find and locate the thermocouples, leak checked, measured (diameter and ovality), and infrared scanned to obtain the as-built power shape and to find voids in the electrical insulator.

The heater rod X-rays were read to obtain the local power distribution, and the coil resistance was measured by the vendor and by Westinghouse. Heater rods that did not meet the acceptance criteria were rejected and not included in a test bundle (approximately 10 percent of the rods are in this category). Calibrated premium grade thermocouple wire was used for all heater rod thermocouples.

The wiring of all thermocouples was double-checked and logged in during construction. There were also shakedown tests, where each rod was individually tested to ensure that it was wired correctly, and the proper thermocouple channels were identified. Complete bundle shakedown tests were also done to verify the heater rod thermocouple channel sequence on the computer.

The entire electrical system was checked to ensure there were no spurious electrical signals that could be interpreted as data.

Each test had written procedures for the operator to follow. Deviation outside these criteria, which are set by the measurement accuracies, resulted in a repeat of the test. The operators were trained in the test procedure and practiced test operations on room temperature tests. The same team of operators was assigned to a given facility. The test sponsor wrote a test validation criteria that the operator was to meet.

The data processing computer used to record and store the data obtained from a test was also calibrated such that no spurious signals were regarded as data. The computer was also in a controlled environment to prevent any drift or erroneous operating characteristics.

The instrumentation chosen for the experiments had tight tolerances on linearity, drift, aging, and response, so its uncertainty is small. The instrumentation was calibrated against standards, and for example, flow meters were calibrated in place to account for variabilities in the piping, instruments, and flow orifice. The instrumentation was recalibrated on a regular basis to reduce uncertainties.

The careful experimental preparation reduced the uncertainties to items such as the calibration variations, the heater rod manufacturing tolerances, and the measurement uncertainties from the instrumentation on power, flow, pressure, and temperature. Parameters such as flow areas were obtained in place such that these independent uncertainties are reduced to measurement or weight uncertainty of the mass of water to fill the test section.

The data uncertainties that reflect all the above uncertainties are considered in two ways in the WCORBA/TRAC uncertainty analysis. The combination of all uncertainties and how they affect the measured temperature response are included in the variability of the mean of the data relative to the code prediction, which determines the code bias as well as the variance of the code bias. The combination of the uncertainties is also accounted for in the variance of the mean of the data, that is, the scatter of individual thermocouples relative to their mean.

There are several possible sources of data uncertainty, one of which is measurement uncertainty. When the individual heater rod thermocouples are used to calculate the uncertainty, the measurement uncertainty is included along with all the other uncertainties described previously. The measurement uncertainty can be positive or negative for a given heater rod thermocouple and should not be regarded as a bias. The measurement uncertainties have been quantified for the G-1 and ORNL tests, as well as some uncertainty analysis for the ROSA tests. The thermocouple measurement uncertainty for heater rods is usually quite small, as shown in the FLECHT-SEASET experiments, because calibrated thermocouple wire of premium grade is used.

A computer code can, at best, represent the average behavior inside a thermal-hydraulic node or volume for a given experiment. The computer code calculates an average hydraulic condition and applies that condition to an average representation of a heater or fuel simulator to calculate its temperature response. The individual thermocouple readings provide an estimate of what the true value might be at that point in the control volume. The uncertainties listed previously cause variability relative to the WCORBA/TRAC-SB calculated temperature for that hydraulic node. The variability of individual data points relative to their average can be treated as an independent uncertainty that can be statistically combined with σ_{WC/T_j} , that is:

$$\sigma_{2i}^2 = \frac{1}{K_i - 1} \sum_{k=1}^{K_i} (PCT_{m_k} - \overline{PCT}_{m_i})^2 \quad (32-2-3)$$

where:

σ_{2i} = standard deviation of individual data points from their mean for experiment or test series *i*

\overline{PCT}_{m_i} = average of the individual data points for a given test or test series

PCT_{m_k} = an individual data point k within the node modeled by WCOBRA/TRAC

K_i = total number of data points in the sample for each test series

σ_{2i} represents the variability in the average measured PCT due to heater rod manufacturing differences, subchannel flow differences, radial position in the bundle, and local heater rod differences.

The method of characterizing the spread of the individual data points relative to the mean of data and the WCOBRA/TRAC-SB calculation is to use the uncertainty specified by the ORNL experimenters for the 3.09.10 test series, Tests I through N. Table 32-2-8 presents the uncertainty data given by Anklam (Anklam et al., 1982) for the elevations at which data and the WCOBRA/TRAC-SB predictions are compared (9.91-foot and 11.88-foot).

Because each experiment or data set is different, each has a separate independent variance or σ_{2i} value. These standard deviations for each separate experiment can be pooled together to obtain the total variance of all the data points given in Table 32-2-8 for the PCT peak, that is:

$$\sigma_{2p}^2 = \frac{(K_1 - 1) \sigma_{21}^2 + (K_2 - 1) \sigma_{22}^2 + \dots + (K_N - 1) \sigma_{2N}^2}{K_1 + K_2 + \dots + K_i - N} \quad (32-2-4)$$

where:

σ_{2p} = pooled data uncertainty

K_1, K_2, \dots, K_i = number of data points for each experiment $i = 1, 2, \dots, N$

N = number of experiments or data sets

σ_{2i} = individual standard deviation of the data from each experiment or data set

Experiments conducted at a given nominal pressure and power condition are considered to comprise a specific data set. Each experiment has a relatively small sample size, less than 40 individual thermocouples per test, from which the mean and variance were calculated. Taken as an entire population, however, the sample size is large, approximately 234 points in the uncovered core. In addressing the effects of small sample size, the values of the individual test

uncertainties were increased using the ratio of the student t table value at the 95th percentile to the normal distribution at the 95th percentile (the 1.645 value). For example, the new uncertainty for experiment i becomes:

$$\frac{t(K_i), 95}{1.645} \sigma_{2_i} \quad (32-2-5)$$

where $t(K_i), 95$ is the student t value at the 95th percentile for experiment i of size K , while 1.645 is the normal distribution value for the 95th percentile assuming an infinite sample size. Using the t table in this fashion increases the overall uncertainty for those experiments with small sample sizes.

The approach used to collectively estimate the total uncertainty of all the different experiments was to pool the uncertainties from the ORNL uncovered bundle experiments to obtain the best estimate of the experimental data uncertainty. The pooled variance equation, using the student t values to increase the individual experiment sample uncertainty, becomes:

$$\sigma_{2p}^2 = \frac{(K_1 - 1) \left(\frac{t(K_1) 95}{1.645} \right)^2 \sigma_{2_1}^2 + (K_2 - 1) \left(\frac{t(K_2) 95}{1.645} \right)^2 \sigma_{2_2}^2 + \dots + (K_N - 1) \left(\frac{t(K_N) 95}{1.645} \right)^2 \sigma_{2_N}^2}{K_1 + K_2 + K_3 \dots K_N - N} \quad (32-2-6)$$

Because the individual σ_{2_i} values are estimates of the data variability, the pooled uncertainty is simply a better estimate across a range of experiments of the uncertainty of all the experimental data. Pooling of uncertainties is used in statistical testing of distributions along with the t distribution (Volk, 1958). Therefore, the use of the pooled uncertainty is appropriate and is probably the best measure of composite uncertainty for the different experiments.

The approach used to consider the individual test data uncertainties was to use the data from the elevations within the test with the most instrumentation. The value of σ_{2_i} was then obtained for these elevations for all the tests from NUREG/CR-2456 (Anklam et al., 1982) that were bundle heatup tests. The individual values of σ_{2_i} from the two elevations for the same test data set were then averaged, as well as the number of points (k_i) used for each value of σ_{2_i} , as shown in Table 32-2-8. Each averaged value of σ_{2_i} was then increased using the student t distribution as shown in Equation 32-2-5. The pooled data uncertainty was then calculated for the ORNL tests as shown in Table 32-2-8. The pooled data uncertainty was then combined with the standard

deviation of the data-to-code bias (σ_{WCT_j}) as two elements of the total WCOPRA/TRAC-SB code uncertainty.

The value for the standard deviation for each experiment is given in Table 32-2-8 along with the individual number of data points and the value of the pooled standard deviation given by Equation 32-2-6. This value represents the pooled deviations in individual data points in a WCOPRA/TRAC hydraulic cell, relative to the mean of the data in that cell.

The experimental measurement uncertainty is not explicitly separated in this analysis approach. However, this uncertainty has already been accounted for when comparing the test data to the code predictions and in the calculation of the σ_{WCT_j} and σ_{2_i} values for each test. Some fraction of the variability in the individual data points relative to their mean is due to the uncertainty of the measurement itself. If a separate uncertainty of the measurement was calculated and added to the uncertainties calculated from σ_{WCT_j} and σ_{2_i} , there would be a double accounting of the measurement uncertainty because the measurement uncertainties are inherently included in σ_{WCT_j} and σ_{2_p} .

32-2-1-5 Variability in Test Initial and Boundary Conditions

When a computer code is compared to a particular experiment, the as-measured boundary and initial conditions are used in the code calculation. As with all experiments, there is uncertainty in the test initial and boundary conditions due to operating procedures, instrumentation drift, instrumentation uncertainty, and operating personnel. These uncertainties can result in variability of the real boundary and initial conditions simulated in WCOPRA/TRAC.

The best method of verifying that the composite effect of all the test uncertainties is small is to run repeat experiments. Good test repeatability indicates that the care and precision used in the design, construction, operation, and analysis of the data have reduced the total uncertainty on the data to an acceptably small value. Because repeat tests were not performed for the tests used to identify the WCOPRA/TRAC-SB code uncertainty, data for reflood-phase large break LOCA experiments are used to investigate test repeatability; the predominant phenomena in the reflood tests are the same as during core uncover in a small LOCA. Repeat tests performed in the FLECHT, FLECHT-SEASET, and Cylindrical Core Test Facility (CCTF) programs showed the repeatability was excellent.

Table 32-2-9 summarizes the results from the available repeat tests. Although they are large break LOCA reflood tests, the important phenomena of core reflood and small break LOCA core

uncovery transients are similar. Taking the FLECHT tests as one population, the average difference between repeat tests is 17.5°F with a standard deviation of 22.5°F. Taking the CCTF tests as one population, the average difference is 15°F with a standard deviation of 26°F.

In Section 32-2-1-3, the evaluation of the code uncertainty was separated into two components: 1) the average bias of the code prediction of a bundle average PCT (ΔPCT_i) and the scatter of the bundle average data around that bias (σ_{WCT_i}) resulting from inaccuracies in the computer model, and 2) given the prediction or measurement of a bundle average PCT, the scatter about that average (σ_{2p}) of individual PCTs resulting from measurement inaccuracies, subchannel variations, and the like. The uncertainty or variation in the bundle average PCT was not explicitly treated. The following discussion includes the effect of bundle average variations.

[

(32-2-7)

]^{a,c}

The situation is illustrated in Figure 32-2-4. [

]^{a,c} (32-2-8)

[
]

(32-2-9)

[
]

(32-2-10)

]^{a,c} (32-2-11)

and:

[
]

]^{a,c}

[

]^{a,c}

In effect, the estimate of the uncertainty of the bias (Equation 32-2-10) must include the variance associated with the “all data” mean. Table 32-2-9 indicates that [

]^{a,c}

In conclusion, the effect of variability in the average of bundle average PCTs on the code uncertainty is small, but should be added to the code uncertainty estimate to account for test-to-test variation. This is done later in this section.

32-2-1-6 Test Facility Modelling

When modelling an experiment with a complex code such as WCOBRA/TRAC, the quality of the comparisons between the code and the experiment can be affected by how the engineer chooses to model the experimental facility. The nodalization can influence code-to-data comparisons such that an estimate of the expected variance in the code-to-data comparisons caused by the noding should be addressed. Specific noding guidelines and requirements have been specified (Volume 2) such that the test noding is consistent with the PWR noding.

There were noding sensitivity studies performed on earlier versions of WCOBRA/TRAC (Hochreiter et al., 1988) to assess possible variability caused by the noding. Noding and modelling sensitivity studies were performed on several of the small break LOCA simulations

analyzed with WCOBRA/TRAC-SB to estimate this possible variance. Table 32-2-10 lists the noding and modelling changes examined and their effect on the calculated PCT.

[

(32-2-12)

]^{a,c}

32-2-1-7 Final Code Uncertainty Elements

The code uncertainty elements were as follows: First, the code bias ($\Delta PCT_{I,j}$) was recalculated. The code bias is defined as the average difference between the measured average bundle PCT and the predicted average bundle PCT ($PCT_m - PCT_{WC\!T}$). [

]^{a,c}

[

]^{a,c}. The overall results are summarized in Table 32-2-12.

The data-based code uncertainty consists of [

]^{a,c} (32-2-14)

The code bias and uncertainty with the highest potential positive (conservative) value, to ensure that the data-based code uncertainty is not underestimated, was chosen by evaluating the value of the bias at 95-percent probability. The most conservative value for the data-based bias identified for small break LOCA PCT prediction is then []^{a,c}.

32-2-2 Conclusions

An assessment of the WCOBRA/TRAC-SB code has been made by comparing code predictions to experimental data at different scales to capture the thermal-hydraulic phenomena expected to occur for a postulated LOCA. It has been shown that WCOBRA/TRAC-SB can predict the different thermal-hydraulic parameters measured in the experiments such that statistics used to characterize adequate code prediction, the PCT, agree well with the data. The different uncertainties associated with conducting experiments (which causes data scatter) and modeling assumptions (which cause analytical prediction differences) have been quantified for the experiments that were compared to WCOBRA/TRAC-SB. The total code uncertainty was calculated as well as the code bias.

The methods outlined in this document can be readily applied to other thermal-hydraulic codes. The uncertainty values as calculated are code-dependent, and a similar judgment can be made on the accuracy of any other code using this approach.

Table 32-2-1
WCOBRA/TRAC Assessment

Model	Assessment (Facility and Number of Tests) ⁽¹⁾
Critical flow	Marviken (4) Sozzi and Sutherland (21) Amos and Schrock (2) Boivin (3) Seven other facilities with (1) or (2)
Fuel rod	NRU (2)
Core heat transfer	ORNL-THTF Uncovered Bundle (6) INEL (197)
Condensation	Lim/Bankoff steam/water mixing (11) COSI steam/water mixing (7)
Vertical interfacial drag (core mixture level)	ORNL-THTF Uncovered Bundle Westinghouse G-1 Core Uncovery GE Vessel Blowdown
Lateral interfacial drag and vertical interfacial drag (loop seal clearance)	UPTF Loop Seal ROSA-IV
Lateral interfacial drag (horizontal flow)	Horizontal Flow Regime (Lim/Bankoff)
Vertical interfacial drag (steam generator hydraulics)	Semiscale NC

1. TPFL = Two-Phase Flow Loop
- THTF = Thermal Hydraulic Test Facility
- COSI = Condensation on Safety Injection
- GE = General Electric
- UPTF = Upper Plenum Test Facility

Table 32-2-2
Test Simulation Timestep Control Input

[
] ^{a,c}

Table 32-2-2 (Con't)
Test Simulation Timestep Control Input

[]		
] ^{a,c}

Table 32-2-3

Table 32-2-4

Table 32-2-5
ROSA-IV SB-CL-03 DTMAX Input and Average Timestep

[
] ^{a,c}

Table 32-2-6
DTMAX Sensitivity Results for ROSA-IV SB-CL-03

[
] ^{a,c}

Table 32-2-7
WCOBRA/TRAC-SB Comparisons to Mean of Small Break LOCA Experimental Data⁽¹⁾

[

]^{a,c}

Table 32-2-8
Core Uncovery Test Data Uncertainty Parameters⁽¹⁾

]^{a,c}

Table 32-2-9
Summary of Data From Repeat Rod Bundle Heating Tests

Table 32-2-9 (Cont'd)
Summary of Data From Repeat Rod Bundle Heating Tests

[

]^{a,c}

Table 32-2-10

] a,c

Table 32-2-11
Data-Based Code Uncertainty

<i>I</i>							

]^{a,c}

Table 32-2-12
Final Code Uncertainty Values

[
] ^{a,c}

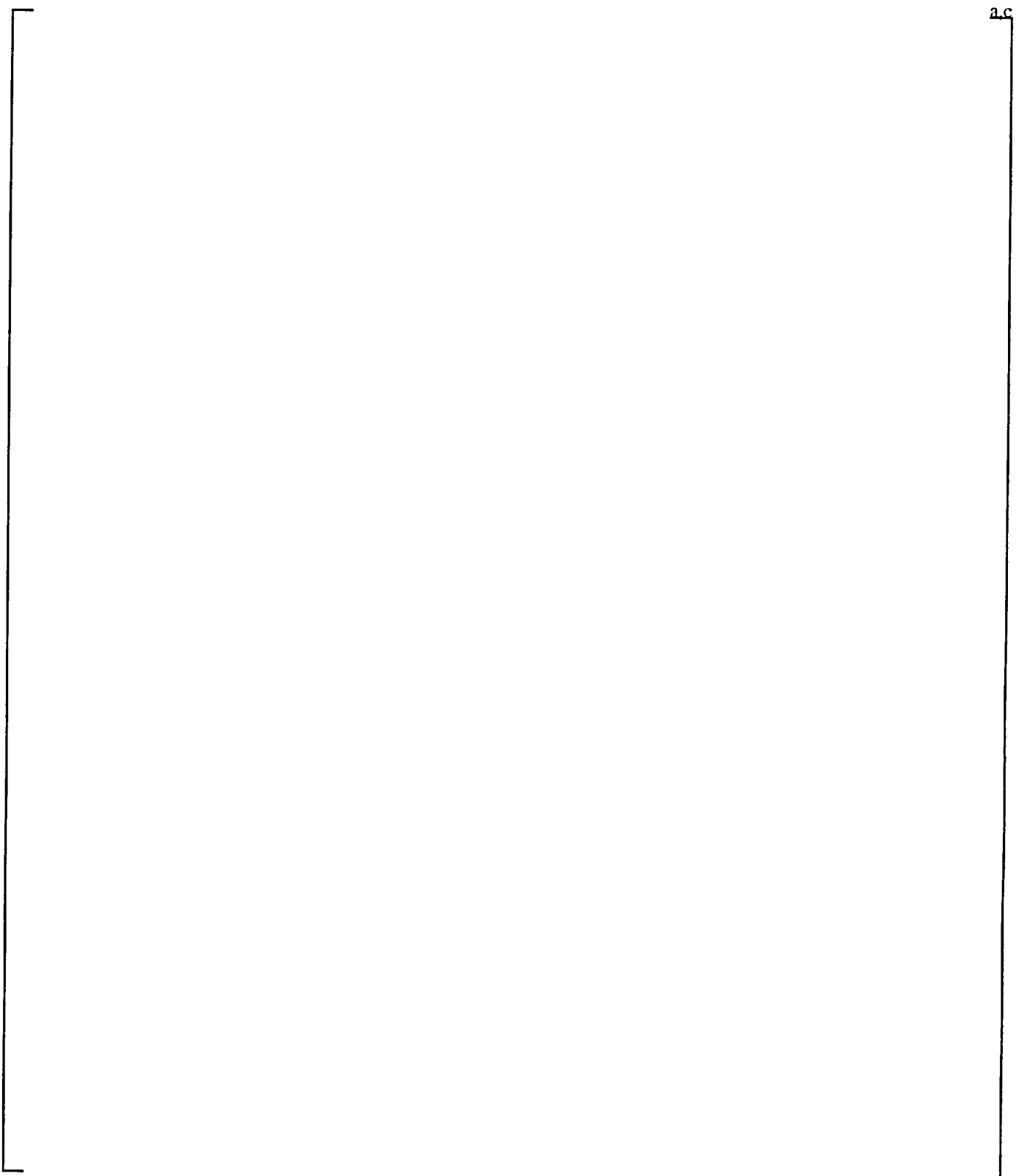


Figure 32-2-1. ORNL Rod Bundle Cross Section [

]^{a,c}

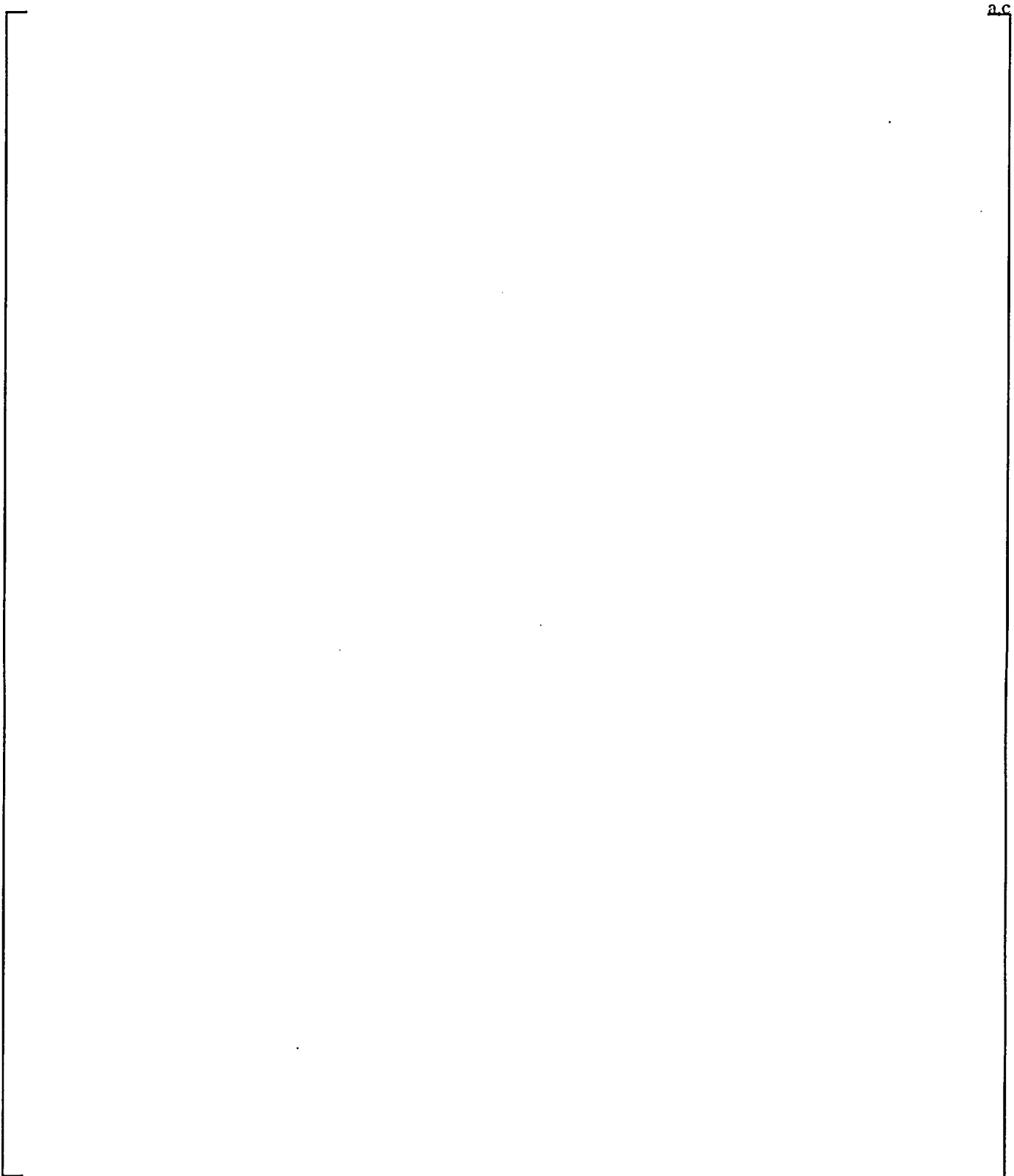


Figure 32-2-2. NRU Rod Bundle and WCOBRA/TRAC Channels

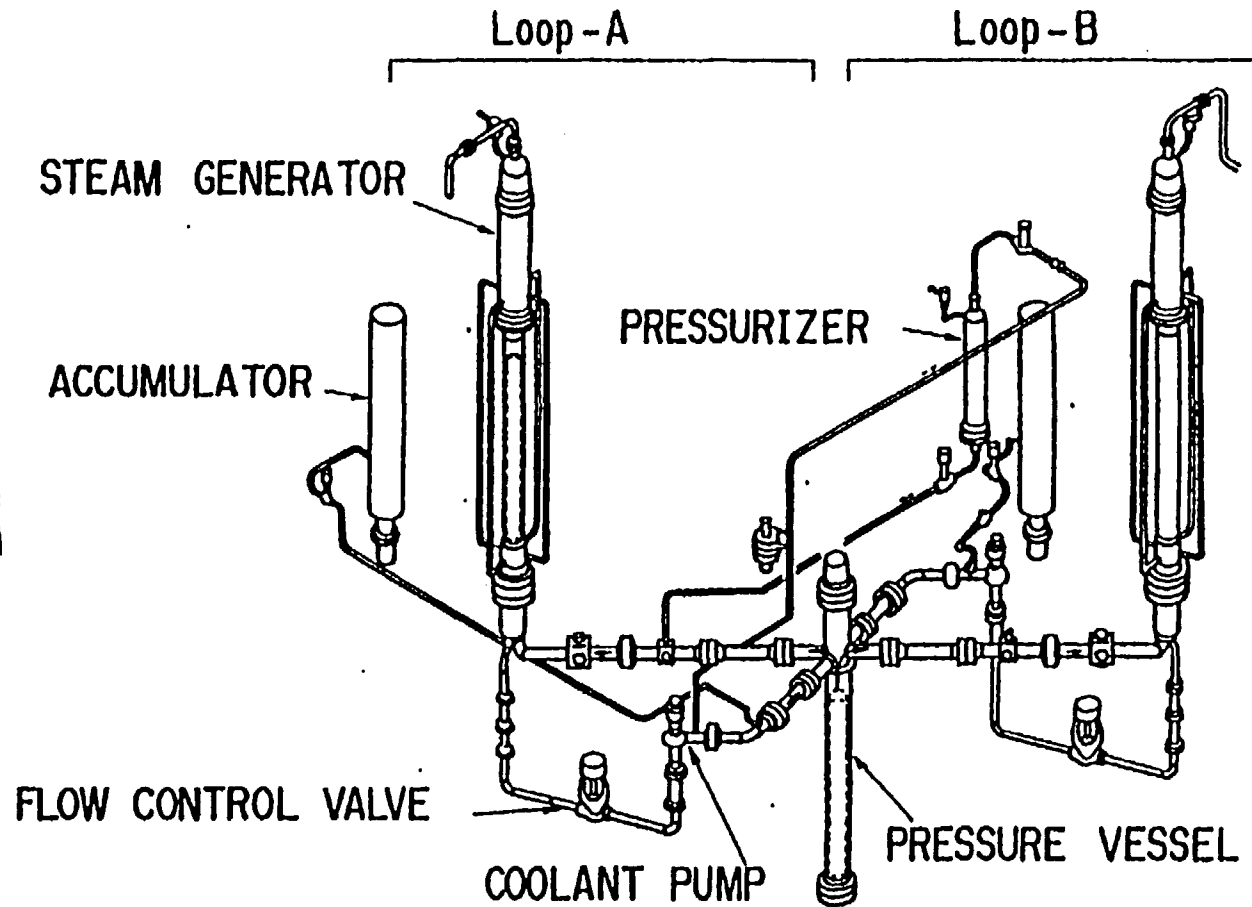


Figure 32-2-3. ROSA-IV Facility WCOBRA/TRAC-SB Model

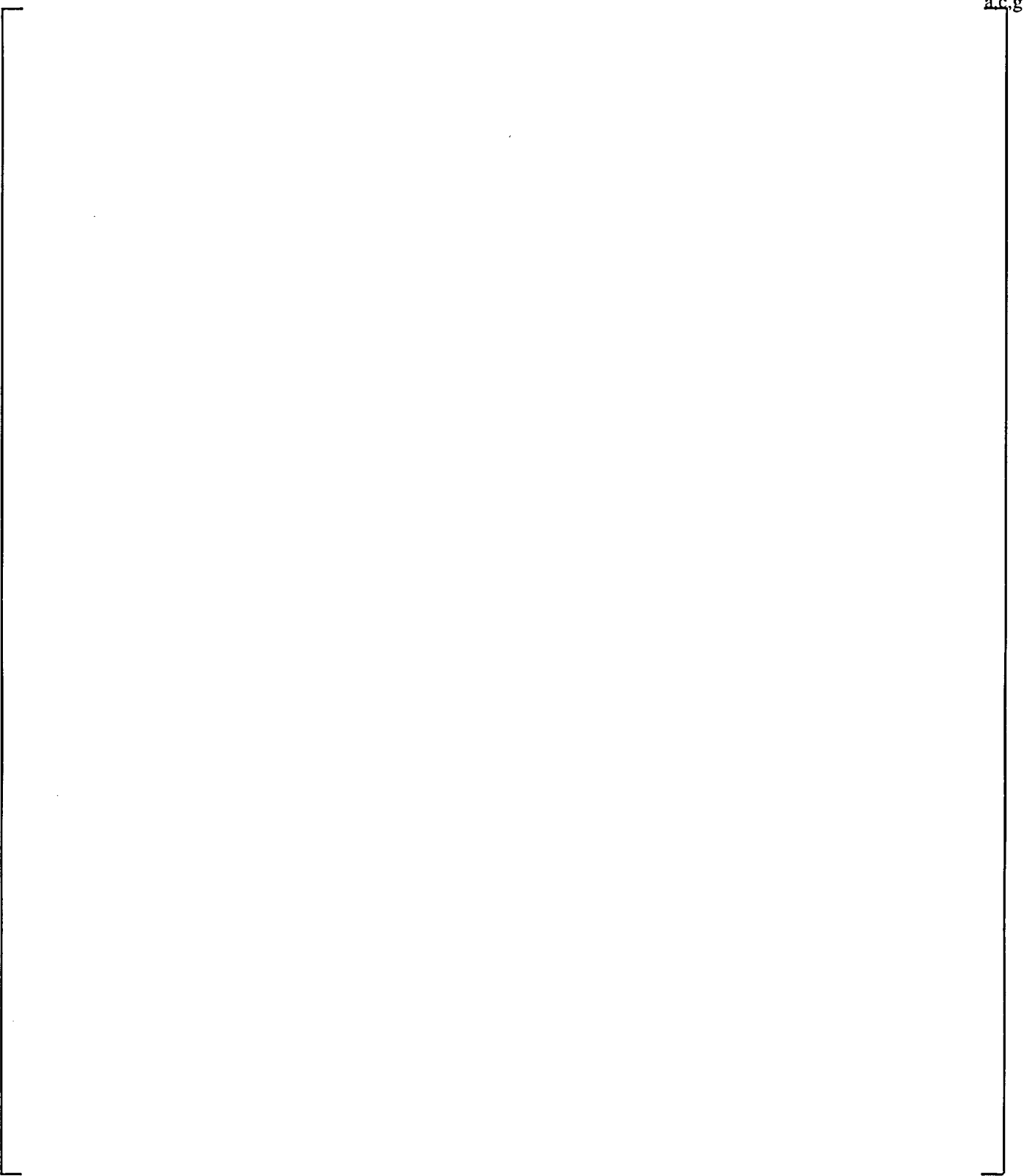


Figure 32-2-4. Illustration of Code Bias Determination (Draper, 1966)

32-3 Core Mixture Level Swell

The swell of the liquid present in the core to establish a two-phase mixture level is an important phenomenon in small break LOCA performance. The uncertainty in the WCOBRA/TRAC-SB prediction of level swell in a heated rod bundle is determined by simulating the G-1 Core Uncovery Tests and the ORNL-THTF Uncovered Bundle Tests.

32-3-1 Simulation of G-1 Core Uncovery Tests

A series of core uncovery experiments was conducted in the Westinghouse ECCS High Pressure Test Facility. A detailed discussion of the G-1 facility and the WCOBRA/TRAC-SB model used to analyze tests performed there is presented in Section 15-4-3, Volume 2. The tests in the range of conditions expected during a PWR small break LOCA are listed in Table 32-3-1.

Each test in Table 32-3-1 was simulated [

]^{a,c}

Section 15-4-3, Volume 2, presents the results obtained using the WCOBRA/TRAC-SB computer code as programmed, that is, with the interfacial drag multiplier YDRAG set to 1.0. The use of YDRAG is a convenient way of modifying the code-predicted interfacial shear in a heated bundle to produce different values of mixture level swell for a given set of boundary conditions. The results of the simulations were compared to the experimental data, and the YDRAG = 1.0 results show that WCOBRA/TRAC-SB predicted level swell is greater than the data average for some tests and elevations and less than the average for others. This implies that the WCOBRA/TRAC-SB core interfacial drag prediction has uncertainty associated with it.

In establishing the uncertainty distribution for the WCOBRA/TRAC-SB prediction of core interfacial drag, calculations were performed to identify the YDRAG that would cause the predicted and measured level swells to agree. Results were interpolated when the YDRAG simulations generated a level swell that bounded the data average swell. Table 32-3-2 shows these results.

No significant trend in the comparison of predicted values with data was present relative to the test variations in power or elevation. The YDRAG values at which predicted level swell matches the measured value tend to be higher at the high pressure (1165 to 1170 psia) tests than for the low pressure tests. This is consistent with the trend of level swell in the test data itself.

The YDRAG range to match test level swell for these G-1 simulations can be summarized as:

$$YDRAG_{min} = 0.353$$

$$YDRAG_{max} = 1.121$$

These results are combined with those obtained from the ORNL uncovered bundle test simulations to define the uncertainty distribution for core interfacial drag in the PWR calculation.

32-3-2 Simulation of ORNL-THTF Tests

The ORNL-THTF uncovered bundle series of experiments were performed at small break LOCA conditions of power and pressure. The ORNL-THTF contained a full height rod bundle of 64 electrically heated rods.

Two types of experiments were conducted in the THTF. One series consisted of several uncovered bundle heat transfer tests. These tests were continued until a steady-state condition was reached. At steady state, part of the bundle was uncovered and the rods were heated to a

high temperature. The second series of tests did not have bundle uncover. The bundle remained covered, and a void profile over the entire axial length was measured.

Table 32-3-3 lists tests selected for simulation by WCOBRA/TRAC-SB. Six of the tests are bundle uncover tests. Three are at relatively low pressure (580 to 650 psia), and three are at high pressure (1010 to 1090 psia). All six had roughly one-half the bundle uncovered. Six other tests are from the level swell test series. Again, three were at low pressure (520 to 590 psia), and three were at high pressure (1090 to 1170 psia). These tests span the expected range of conditions for uncover in PWR calculations leading to the most limiting PCTs.

Section 15-4-2, Volume 2, presents the results obtained in WCOBRA/TRAC-SB simulations with YDRAG values of 1.0 and 0.8. In general, the WCOBRA/TRAC-SB predicted level swell is greater than the data average for the ORNL-THTF tests. Section 15-4-2 presents the results obtained in detail.

The results do not indicate a trend with power or pressure.

Simulations of the ORNL-THTF tests were conducted for a range of core interfacial drag multipliers to establish the uncertainty distribution for the WCOBRA/TRAC-SB prediction of core interfacial drag. The multipliers were ranged from 1.2 to as low as 0.5 in calculations to identify the YDRAG values at which WCOBRA/TRAC-SB predicts the level swell in these tests.

Interpolating the WCOBRA/TRAC-SB results that bound the data, the values of YDRAG to force the predicted level swell to match the data are estimated to be:

$$YDRAG_{min} = 0.503$$

$$YDRAG_{max} = 1.169$$

Table 32-3-4 presents the YDRAG values at which WCOBRA/TRAC-SB-predicted level swells match the ORNL-THTF individual test values.

32-3-3 Uncertainty Distribution for Core Mixture Level Swell

The core interfacial drag coefficients (YDRAG values) at which WCOBRA/TRAC-SB matches the experimental level swells of G-1 and ORNL-THTF were [

]^{a,c}

]^{a,c} the core channels in the PWR reference case use an 0.8 YDRAG multiplier.

The uncertainty distribution [

]^{a,c}

32-3-4 Conclusions

WCOBRA/TRAC-SB simulations of the Westinghouse G-1 and ORNL-THTF tests at different values of YDRAG were conducted to produce a set of results that identify the heated core interfacial drag multipliers for a small LOCA calculation in a PWR.

A set of multipliers that would force the code to match the data level swell in these tests was produced. The minimum value for this set is $YDRAG_{min} = 0.353$, and the maximum is $YDRAG_{max} = 1.169$.

The multipliers obtained in these simulations of two separate level swell tests provide a basis for establishing a distribution for application to small break LOCA uncertainty analysis in a PWR.

Table 32-3-1
Core Uncovery Test Matrix

[
] ^{a,c}

Table 32-3-2
YDRAG Values to Match G-1 Level Swell Data

Test Number	Elevation (ft)	Pressure (psia)	Bundle Power (MW)	YDRAG
54	10	785	1	0.926
54	8	785	1	0.414
55	10	800	1.5	0.686
55	8	800	1.5	0.577
56	10	795	2	0.353
56	8	795	2	0.354
57	10	795	0.5	0.644
57	8	795	0.5	0.775
62	10	1170	1	0.9
62	8	1170	1	0.5
63	10	1165	1.5	1.121
63	8	1165	1.5	0.8
64	10	1170	0.5	0.55
65	10	1170	2	0.89
65	8	1170	2	0.897

Table 32-3-3
ORNL-THTF Test Simulation Matrix

Test No.	Pressure (psia)	Rod Power (kW/ft)	Data Mixture Level (ft)	Data Collapsed Liquid Level (ft)
Bundle Uncovery Tests				
3.09.10I	650	0.68	8.60	4.39
3.09.10J	610	0.33	8.10	5.31
3.09.10K	580	0.10	6.98	5.31
3.09.10L	1090	0.66	9.02	5.77
3.09.10M	1010	0.31	8.60	6.20
3.09.10N	1030	0.14	6.98	6.10
Level Swell Tests				
3.09.10AA	590	0.39	11.23	6.56
3.09.10BB	560	0.20	10.85	7.61
3.09.10CC	520	0.10	11.80	9.45
3.09.10DD	1170	0.39	10.61	7.84
3.09.10EE	1120	0.19	11.40	9.35
3.09.10FF	1090	0.098	10.61	9.51

Table 32-3-4
YDRAG Values to Match ORNL-THTF Data

Test Number	Pressure (psia)	Rod Power (kW/ft)	YDRAG
3.09.10AA	590	0.390	0.827
3.09.10BB	560	0.200	0.908
3.09.10CC	520	0.100	0.698
3.09.10DD	1170	0.390	0.881
3.09.10EE	1120	0.190	0.752
3.09.10FF	1090	0.098	0.635
3.09.10I	650	0.680	0.779
3.09.10J	610	0.330	0.840
3.09.10K	580	0.100	0.871
3.09.10L	1090	0.660	0.503
3.09.10M	1010	0.310	1.169
3.09.10N	1030	0.140	0.61



Figure 32-3-1. Small Break LOCA Core Interfacial Drag Multiplier Distribution From ORNL and G-1 Data



**Figure 32-3-2. Best Estimate Small Break LOCA Core Interfacial Drag
Combined Distribution Based on ORNL and G-1 Data**

32-4 Critical Flow

In a small break LOCA event, especially with the break in the limiting location of a cold leg, the break flow is critical and subcooled (or low quality) for a significant portion of the transient until loop seal clearing occurs. Critical break flow is ranked high in the small break LOCA PIRT and accurate predictions of subcooled critical flow and two-phase critical flow are necessary.

The critical flowrate through the break is a dominant parameter, and a separate consideration is made [

]^{a,c} Critical flow test data and the WCOBRA/TRAC-SB predictions were assessed in Section 13; in this section the overall bias and uncertainty are discussed.

32-4-1 Data Assessment

The WCOBRA/TRAC-SB critical flow model was assessed against four Marviken tests, the Sozzi and Sutherland tests, the TPFL tests, the Amos and Schrock tests, and seven other tests (Section 13, Volume 2). In addition, for the integral effects tests, direct comparisons were made with measured break flow. Table 13-4-1, Volume 2, summarizes the test range; compared with the PWR range of interest for small break LOCA, the data are sufficient to provide a basis for considering the break flow model in the uncertainty analysis.

Some of these tests had distinct periods of subcooled and saturated critical flow. The transient flow data from each Marviken test were initially divided into 30 to 40 time increments, and comparisons were made to the corresponding predicted flow. In PWR simulations, the discharge coefficient (CD) which equals measured flow divided by predicted flow is used to describe the modeling bias. Comparisons of predictions to data did not reveal significant differences in predictive performance for variations in length to diameter (L/D_H) ratios or to pressure. The inlet condition quality did show a trend in predicted results versus data.

Figure 32-4-1 is a scatter plot of the code-predicted mass flux (G_{calc}) versus measured mass flux (G_{meas}) values for all WCOBRA/TRAC-SB simulations.

A total of 1427 (N) data points from 40 nozzle geometries were used for the determination of bias and uncertainty associated with the critical flow model predictions of WCOBRA/TRAC-SB.

$$\sum_i^N \left(\frac{G_{calc} - G_{meas}}{G_{meas}} \right)$$

The mean error ($\bar{\varepsilon} = \frac{\sum_i^N (G_{calc} - G_{meas})}{N}$) defines the code bias, and the standard deviation is

$$\sqrt{\frac{\sum_i^N (\varepsilon_i - \bar{\varepsilon})^2}{N}}$$

given by $\sigma(\varepsilon) = \sqrt{\frac{\sum_i^N (\varepsilon_i - \bar{\varepsilon})^2}{N-1}}$. A valid range of the bias and uncertainty estimate given here is

based on selected experimental data. A comparison was made for $0 < L < 2335$ mm, and $0.418 < D_H < 500$ mm. As indicated on Figure 32-4-1, for all fluid conditions in this range, ($-0.039 < \text{Quality} < 1.0$), the WCOBRA/TRAC-SB critical flow predictions exhibit the following:

- Bias = 8.2 percent
- Standard deviation = 19.8 percent

Underprediction near the mass flux of 40,000 kg/m²-s is observed from the comparison to the Sozzi and Sutherland data. This caused the overall bias to be negative. The apparent trend with respect to the upstream quality is that WCOBRA/TRAC-SB tends to underpredict the break mass flux in the two-phase regime at or near the liquid saturation point (Quality ~ 0) and overpredicts in two-phase flow with higher void fractions. The overprediction becomes significantly smaller as the upstream condition approaches SPV (Quality = 1). The uncertainties associated with subcooled and saturated flow conditions were determined separately due to this observation.

In the subcooled liquid region ($-0.039 < \text{Quality} < 0$), the WCOBRA/TRAC-SB critical flow predictions compared to data exhibit the following:

- Bias = -4.3 percent
- Standard deviation = 14.9 percent

Figure 32-4-2 presents the probability density function of the discharge coefficients which enable WCOBRA/TRAC-SB predicted break flows to match two-phase critical flow experimental data;

it is generated for 620 data points. The mean multiplier is greater than one, indicating underprediction by the code of the overall data set.

In the saturated two-phase flow region ($0 < \text{Quality} < 1.0$), the WCORBA/TRAC-SB critical flow predictions compared to data exhibit the following:

- Bias = -13.40 percent
- Standard deviation = 23.7 percent

The small bias identified for subcooled liquid critical flow justifies the application of WCORBA/TRAC-SB to PWR calculations with no adjustment; the standard deviation is also small, and this uncertainty is covered by performing a spectrum of break sizes. The saturated/two-phase region, on the other hand, shows a higher standard deviation with an average bias of about 1.15. Therefore, the critical break flow uncertainty in this region is investigated in PWR calculations, [

]^{a,c}

using the methods described in Section 33.

[

]^{a,c}

32-4-2 Effect of Break Type

There are two break types that must be considered for large break LOCA: the guillotine break and the split break of a primary coolant pipe. The guillotine break does not apply to small break LOCA events. For small break LOCA split breaks, both geometrical and modeling uncertainties exist. The break flowrate is a function of the product of break area and break flow CD . Since a probability distribution for the break area will be difficult to establish, the small break LOCA analysis is simplified by performing a spectrum of sizes to determine the one that produces the highest PCT (all other factors at nominal conditions). When the limiting size and loop location is established, the orientation of the break around the perimeter of the pipe at the limiting location is identified. The uncertainty in the break flow is then investigated for the saturated two-phase flow region.

32-4-3 Limits of Applicability

The critical flow model bias and uncertainty determined in this section are valid for a range of pressure and temperature conditions of the experimental measurement database, which covers the break upstream range typically found in postulated small break LOCA events. The methodology considers separately the small break LOCA saturated/two-phase and subcooled liquid regions.

[

]^{a,c}

32-4-4 Conclusions

Critical break flow is a dominant parameter in small break LOCA. [

]^{a,c}

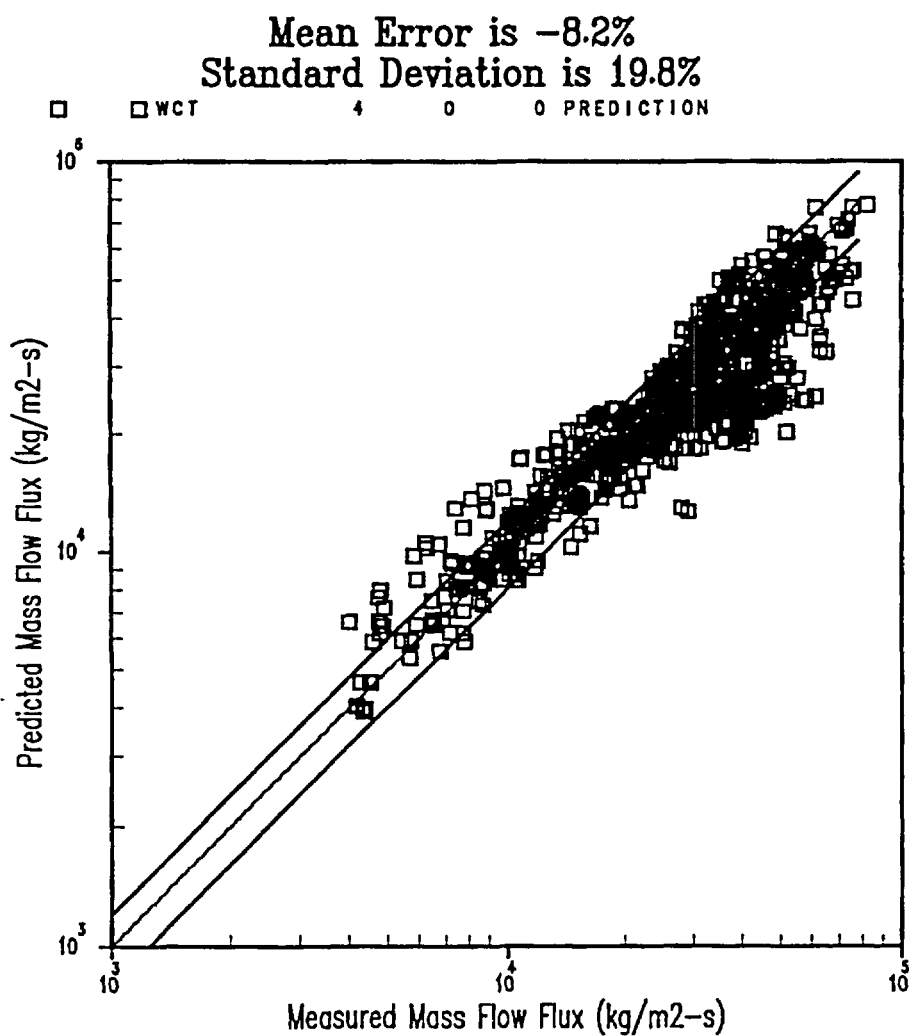


Figure 32-4-1. WCOBRA/TRAC-SB Critical Flow Predictions Versus Test Data

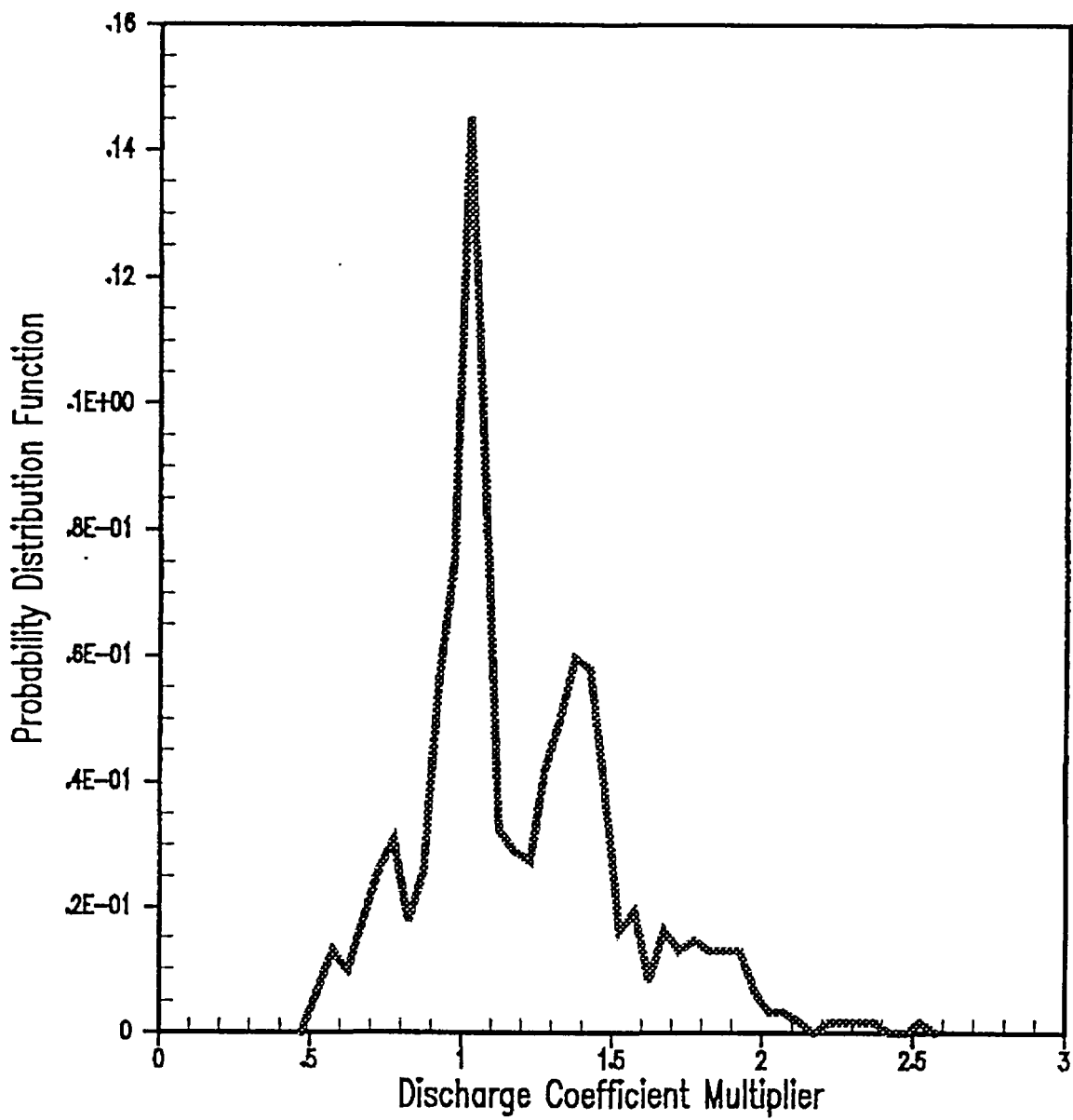


Figure 32-4-2. Probability Density Function for Two-Phase Discharge Coefficient Multiplier

32-5 Uncovered Core Heat Transfer

The methodology for uncertainty propagation considers, in addition to fuel rod model uncertainties, the local variation in heat transfer. The minimum stable film boiling temperature []^{a,c}

The predicted HTC for a PWR transient is corrected using a multiplier that is derived from a comparison between predicted and measured HTCs in separate effects tests. This section provides information on the HTC multipliers.

Figure 32-5-1 shows a possible cladding temperature transient for a PWR small break LOCA. The transient can be characterized by the cladding temperature and thermal-hydraulic behavior during time periods of core uncovering. The first heatup shown following the break occurs due to a core level depression while loop seal clearance occurs. After the cladding heats to a peak value, a second period occurs during which the cladding cools back to saturation temperature when the core recovers with liquid. During the third period, the cladding temperature increases after the liquid inventory has boiled off enough to uncover the core. Eventually, when injection flow exceeds break flow (usually after the accumulator water injection begins), the liquid is replenished until the PCT location quenches.

The following paragraphs discuss various issues related to heat transfer multipliers. The heat transfer []^{a,c}

]^{a,c} (32-5-1)

HTCs from the experiments are defined as: []^{a,c}

]^{a,c} (32-5-2)

Therefore, the code phasic HTCs are used to define an HTC using $(T_w - T_{sat})$. That is: [

(32-5-4)

]^{a,c}

The two heatup periods shown in Figure 32-5-1 are similar in regard to the heat transfer mechanisms. It is anticipated that the loop seal clearance uncovering depicted will typically not occur during a PWR small break LOCA transient. In the event that it did, such an uncovering would be basically the same phenomenologically as the core boiloff uncovering; the same experimental data apply to both.

32-5-1 Evaluation of Heat Transfer Tests

Section 12, Volume 2, shows a comparison of predicted versus measured HTCs based on simulations of the ORNL-THTF DFFB Tests, the ORNL-THTF Uncovered Bundle Tests, and the INEL Single Tube Tests. The measured HTCs from the ORNL-THTF DFFB tests are typically an order of magnitude greater than those from the INEL tests.

Figure 32-5-2 shows a comparison of predicted and measured HTCs for the ORNL-THTF DFFF tests and the INEL tests. This is [

]^{a,c}

32-5-2 ORNL Steady-State Core Uncovery Test Data

An analysis of the ORNL-THTF Uncovered Bundle Tests was made to provide an assessment of the WCORBA/TRAC-SB film boiling and SPV heat transfer correlations. The ORNL-THTF test facility test section was composed of an 8x8 rod bundle. The 3.09.10I through N experiments provided heat transfer data for small break LOCA conditions over a range of applicable Re. Anklam (Anklam, 1982) provides a summary of the tests and a tabulation of data, and Section 12-4-3, Volume 2, presents a detailed discussion of the WCORBA/TRAC-SB simulations.

The uncovered bundle tests were steady-state experiments (with inlet liquid mass flow approximately equal to exiting steam mass flow), providing rod temperatures and HTCs in the steam-cooling region of the rod bundle. Overall, rod temperatures were underpredicted by WCORBA/TRAC-SB for the uncovered bundle tests, while the vapor temperatures were slightly overpredicted. The predicted vapor HTCs were generally greater than the experimental values. With all 10 ORNL experimental levels included (top 2 feet of the bundle), the average ratio of experimental to predicted HTCs (E_i) was 0.777 with a 95-percent confidence interval of 0.777 ± 0.36 . As indicated in Section 12, Volume 2, no apparent correlation exists between E_i and the pressure or linear heat rate, or vapor Re, other than scatter appears to be greater in the WCORBA/TRAC-SB prediction at lower vapor Re.

32-5-3 INEL Single Tube Test Evaluation

A driver-plotter program (COBRAHT), similar to that used in large break LOCA heat transfer assessment, was used to examine the performance of WCORBA/TRAC-SB in the SPV and DFFF regimes, important to small break LOCA PCT for the INEL single-tube tests (Gottula, 1985), and to determine the bias and uncertainty of these models. In testing

performance, HTCs predicted from the WCOBRA/TRAC heat transfer package were compared to experimental test data. The test data for comparison contained a complete set of local measurements so that the HTC could be assessed without uncertainty due to compensating error. Section 12-4, Volume 2, provides additional information about COBRAHT and the INEL test simulation.

The local conditions for each (steady-state) test-wall temperature, vapor temperature, quality, pressure, and total mass flux were used as input to the driver-plotter routine. This driver-plotter routine consisted of the WCOBRA/TRAC heat transfer package, property routines, and drop size correlations. The input hydraulic conditions were used to estimate the DFFB and/or SPV HTCs (based on $\Delta T = T_w - T_{sat}$), which were then compared to the measured HTCs for each test.

The driver-plotter routine calculates an overall HTC in terms of the local heat flux and wall superheat, defined as:

$$h = \frac{q''}{(T_w - T_{sat})}$$

The SPV and/or DFFB HTCs are then compared with the HTC values reported by the experimenters to validate the performance of WCOBRA/TRAC-SB.

Driver-plotter calculations were performed for the 198 INEL data points. The comparison of predicted and measured HTCs is shown in Figure 32-5-2. In this figure, two features are clearly apparent. At low HTCs, the HTCs are well predicted. However, at higher HTCs in the middle range of $HTC = 20$ to 60 Btu/hr-F-ft 2 , the trend is toward underprediction by WCOBRA/TRAC-SB.

As previously indicated, [

]^{a,c}

32-5-4 Data for Small Break LOCA Heat Transfer Multipliers

[

]^{a,c} Table 32-5-1 lists the values in the probability distribution function as placed into the HOTSPOT-SB computer code; [

]^{a,c}

32-5-5 Conclusions

A heat transfer multiplier distribution based on the WCOBRA/TRAC-SB model is developed, and the cumulative distribution function is calculated. The multiplier function is appropriate for small break LOCA, [

]^{a,c}

a.c

Table 32-5-1
HOTSPOT-SB Probability Distribution Function Values

3-INCH CL BREAK WITH LOOP
Peak Cladding Temperature

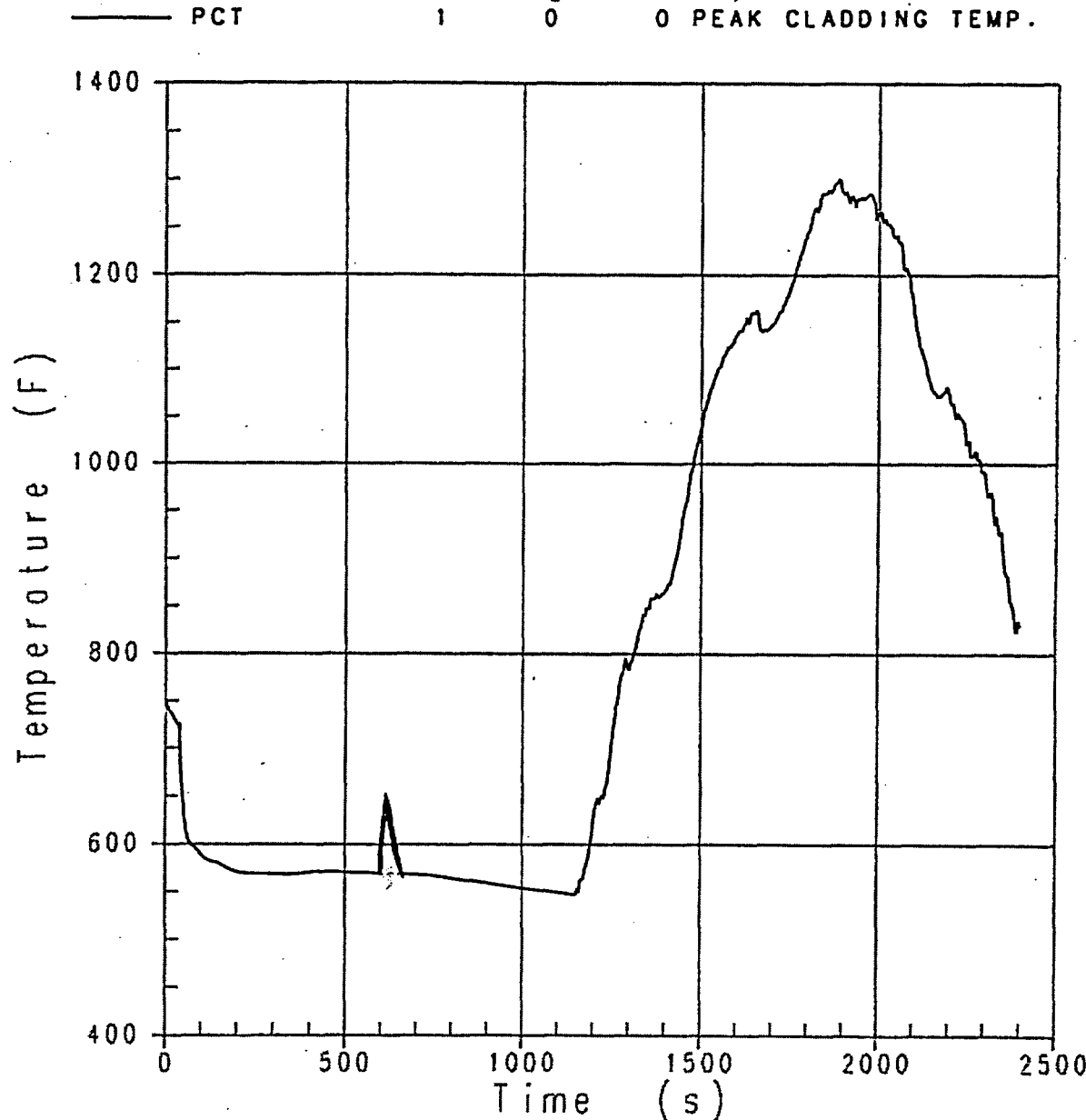


Figure 32-5-1. PCT Transient

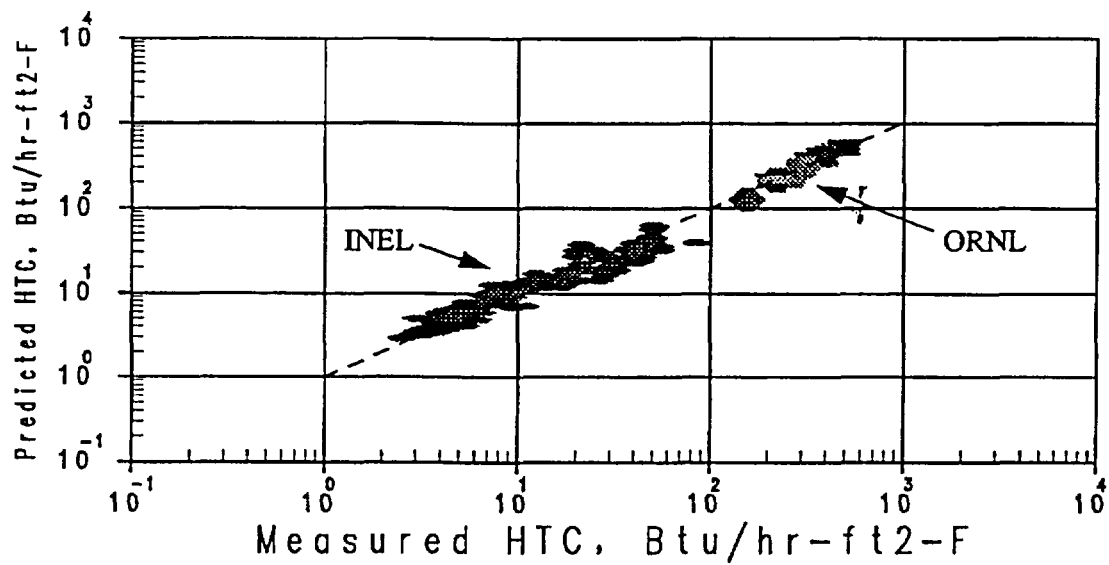


Figure 32-5-2. Comparison of Predicted and Measured HTCs for Combined ORNL and INEL Data Using WCOPRA/TRAC-SB Models



Figure 32-5-3. Steam Re for 3-Inch Break at PCT Elevation

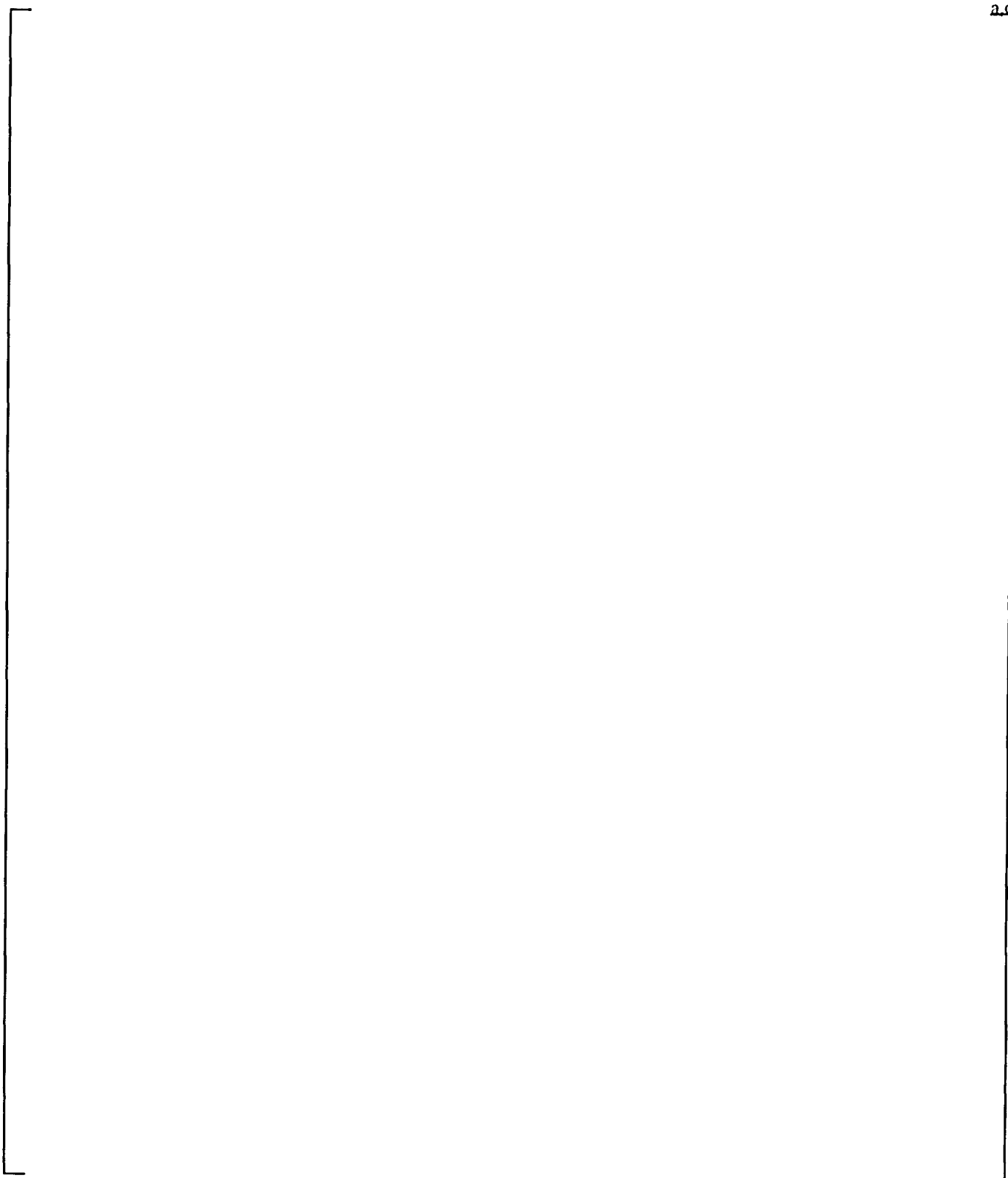


Figure 32-5-4. Small Break LOCA HTC Multiplier Distribution

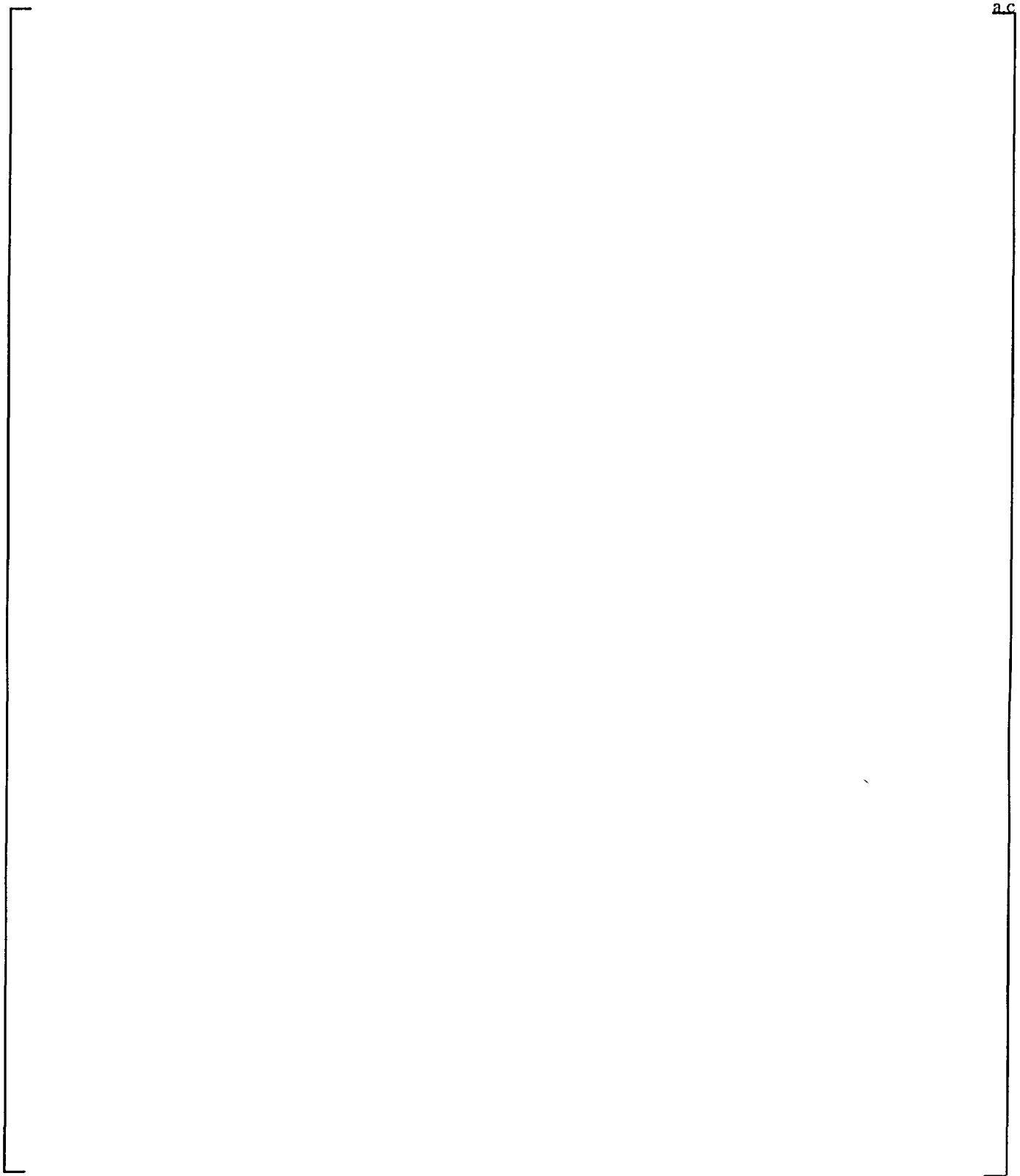


Figure 32-5-5. Best Estimate Small Break LOCA HTC Multiplier

32-6 Scaling Assessment (Step 10)

32-6-1 Introduction

The CSAU report (Boyack et al., 1989) analyzes the effects of scale for the large-break LOCA. The report concludes that the full-length, power-to-volume scaling basis was appropriate for most of the LOCA experiments and that this scaling rationale will capture the majority of the large-break LOCA phenomena. Blowdown and reflood cladding temperature data were examined, and the report concludes that any scale effect, if present, was within the uncertainty of the data. The majority of the experiments examined were full-length rod bundle tests as well as part-length experiments with electrical heater rods as well as nuclear rods.

The small break LOCA consists of two distinct phases: an initial rapid depressurization and continued circulation, and a slow depressurization and phase separation. Each phase is subject to different rules regarding scaling.

The objectives of this step are to do the following:

- Identify those components and phenomena for which supporting tests and facilities are subject to significant scale distortion.
- For the identified components and phenomena from Objective 1, perform verification against full-scale experiments if available, or perform specific analyses to confirm that the code correctly predicts the effect of scale.

32-6-2 WCOBRA/TRAC Scaling Trends

Westinghouse concurred with the CSAU findings that full-height, power-to-volume scaling captures the majority of the thermal-hydraulic phenomena of interest for the large-break LOCA (Volume 4 of WCAP-12945-P-A [Bajorek et al., 1998]). Westinghouse also investigated the effects of scale for different scaled test facilities to determine if a scale bias was apparent.

Power-to-volume scaled test facilities correctly preserve key features of rapid transients, such as a large break LOCA. In such transients driven by large pressure gradients and thermal processes, scaling distortions that arise from excess surface area per unit volume, and small lateral dimensions, are not important relative to volumetric heat generation.

For the smaller small break LOCA events, much of the transient occurs at nearly constant pressure and the extent of mass depletion is controlled not so much by core power, but by flow regimes upstream of the break. Flow regimes are known to depend primarily on lateral scale (for example, vertical height of a horizontal duct). Lateral scale is greatly distorted in power-to-volume scaled facilities. The frictional losses in the components become important in a natural circulation condition, and power-to-volume scaled facilities exaggerate this effect due to distortions in surface area.

Some facilities specifically designed for small break LOCA transients preserve the overall power-to-volume scaling approach, but then scale specific components, such as the hot leg, according to different laws dictated by the expected processes occurring in the component.

In the CSAU methodology, propagation of uncertainty is calculated by ranging input and model variables directly in the PWR calculation. This allows the effect of scale to be directly accounted for. However, for this approach to work, the computer code must be demonstrated to scale up key physical processes, particularly those for which there is no full-scale data.

Many of the dominant phenomena identified through the PIRT process have been investigated in full-scale tests. Mixture level swell data are obtained in the G-1 Core Uncovery and ORNL-THTF Uncovered Bundle Tests. Both of these facilities used full-height heater rod bundles, so there is no height distortion. Figure 32-6-1 compares the WCOBRA/TRAC-SB-predicted PCT minus the average measured PCT for these facilities and the ROSA-IV facility as well; [

]^{a,c}

Loop seal clearance is another dominant phenomenon in the small break LOCA event.

The completion of the full-scale UPTF experiments (Section 16, Volume 2) has provided the necessary data to determine the important thermal-hydraulic phenomena for loop seal clearance. Computer code assessment for small break LOCA can be performed using the UPTF data.

[

]^{a,c}

Critical break flow is ranked high in the small break LOCA PIRT for all phases of a small break LOCA event. Therefore, the prediction of subcooled and two-phase critical break flow is important, and a computer code should be assessed against a range of pertinent data.

A number of test data sources exist for validation of the break flow model for small break LOCA events, including:

- Amos and Schrock
- Sozzi and Sutherland
- Marviken
- TPFL

Test diameters associated with these tests vary in size from 0.03 to 20 inches. Upstream pressure varies from 400 to 2250 psia. Quality variation varies from 0 to 1.0 at three pressures. Liquid subcooling varies from 0 to 108°F. The break is often simulated with an orifice of varying length and diameter as L/D ranges from 0.3 to about 85. As a wide range of break geometry, subcooling, L/D, and area is represented, there are sufficient data available to validate a break flow model applied to the subcooled liquid regime.

During a small break LOCA event, flow in horizontal sections of main reactor coolant loop piping will eventually become two-phase and stratify. Stratified flow regime near or upstream of the break may lead to liquid entrainment into the break flow depending upon characteristics such as the velocity of the gas phase near the break and height of liquid in the pipe relative to the break elevation. The integral test simulations (ROSA-IV, LOFT, and Semiscale) provide validation of the code's predictive capability in this regime over a range of scales.

WCOBRA/TRAC-SB uses flow regime maps to determine the interfacial heat transfer and shear for the two-phase mixture flowing in the reactor system. [

]^{a,c}

For horizontal flow regimes, the Taitel-Dukler flow regime map and transition criteria include a dependence on pipe diameter. Therefore, the scale diameter dependence is included in WCOBRA/TRAC-SB modeling of horizontal flow.

In conclusion, the WCOBRA/TRAC-SB code has been compared to experimental data to determine if an observable scale effect exists. [

]^{a,c}

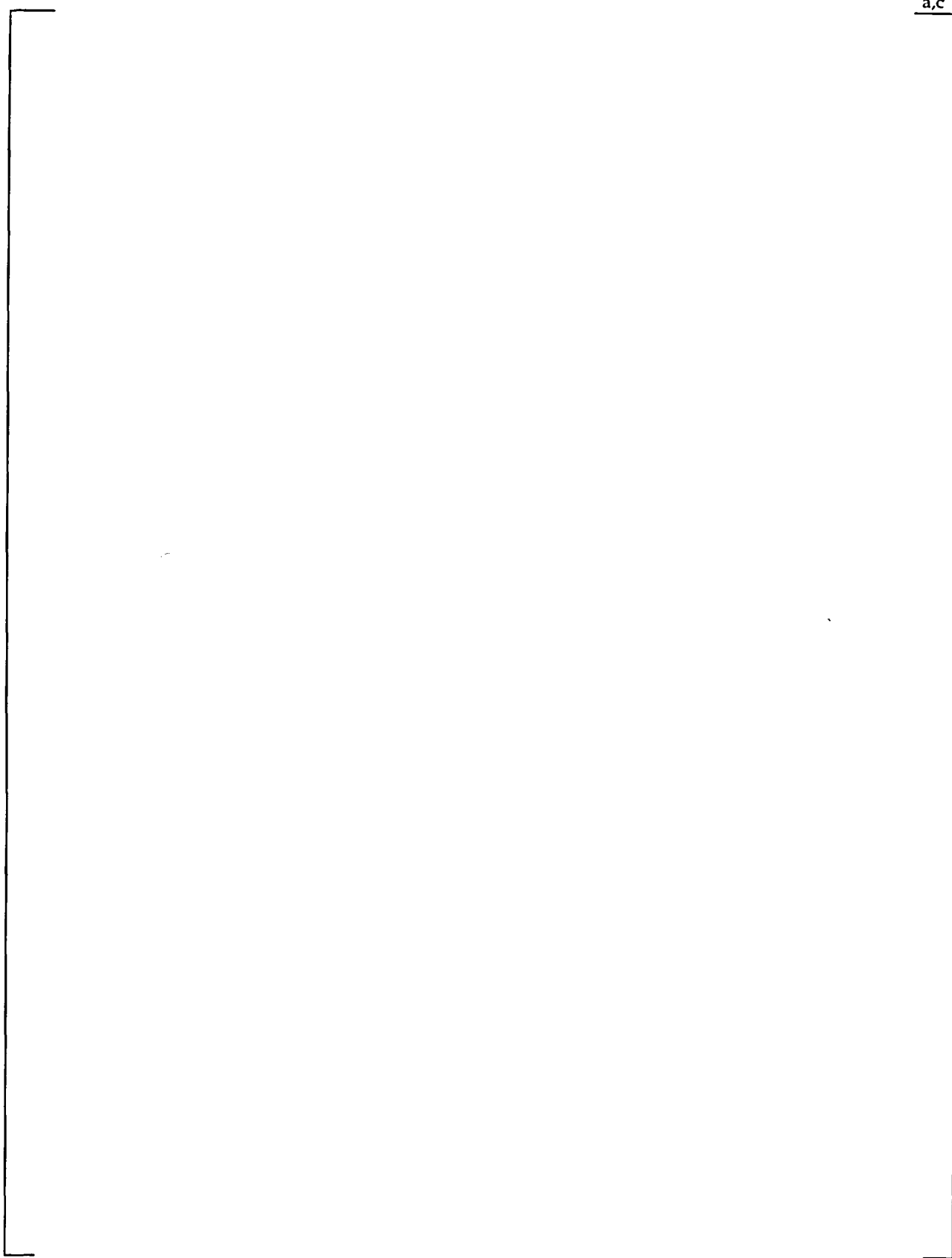


Figure 32-6-1. Scaling Trends for WCOBRA/TRAC-SB PCT Prediction

32-7 References

American Nuclear Society, 1979, "Decay Heat in Light Water Reactors," ANSI/ANS-5.1-1979.

Anklam, T. M., et al., 1982, "Experimental Investigations of Uncovered Bundle Heat Transfer and Two-Phase Mixture Level Swell Under High Pressure Low Heat Flux Conditions," NUREG/CR-2456.

Bajorek, S. M., et al., 1998, "Code Qualification Document for Best Estimate LOCA Analysis, Volume IV: Assessment of Uncertainty," WCAP-12945-P-A, Vol. 4.

[

]^{a,c}

Boyack, B., et al., 1989, "Quantifying Reactor Safety Margins: Application of Code Scaling, Applicability, and Uncertainty Evaluation Methodology to a Large-Break, Loss-of-Coolant Accident," NUREG/CR-5249.

Broughton, J. M., 1981, "PBF LOCA Test Series, Test LOC-3 and LOC-5 Fuel Behavior Report," NUREG/CR-2073.

Broughton, J. M., 1983, "PBF LOCA Test LOC-6 Fuel Behavior Report," NUREG/CR-3184.

Burman, D. L., 1980, "Comparison of Westinghouse LOCA Burst Tests Results with ORNL and Other Program Results," Specialist Meeting on Fuel Behavior Under Accident Conditions, September 1-4, Helsinki, Finland.

Burman, D. L., 1990, "ZIRLO™ High Temperature Oxidation Tests," Appendix E to WCAP-12610-P-A, Westinghouse Electric Corporation, Pittsburgh, PA. (PROPRIETARY)

Cathcart, J. V., and Pawel, 1977, "Zirconium Metal-Water Oxidation Kinetics IV - Reaction Rate Studies," ORNL/NUREG-17, Oak Ridge National laboratory, Oak Ridge, TN.

Chelemer, H., et al., 1975, "Improved Thermal Design Procedure," WCAP-8567-P-A (PROPRIETARY).

[

]^{a,c}

Draper N. and Smith, H., 1981, Applied Regression Analysis, Second Edition, John Wiley and Sons.

Draper, N. R., 1966, Applied Regression Analysis, John Wiley and Sons.

Ford, W. E., et al., 1982, "CSRL-V: Processed ENDFB-V 227-Neutron-Group and Pointwise Cross Section Libraries for Criticality Safety, Reactor and Shielding Studies," NUREG/CR-2306, ORNL/CSD/TM-160.

Gottula, et al., 1985, "Forced Convective, Non-Equilibrium Post-CHF Heat Transfer Experiment Data and Correlation Comparison Report," NUREG/CR-3193.

Hochreiter, L. E., et al., 1988, "Westinghouse Large Break LOCA Best Estimate Methodology - Applications to Plants Equipped with UP," Volume 1, WCAP-10924-P-A.

Kerrisk, J. F. and Clifton, D. G., 1972, "Smoothed Values of the Enthalpy and Heat Capacity of UO₂," Nuclear Technology, Vol. 16.

Mohr, C. L., et al., 1983, "LOCA Simulation in the National Research Universal Reactor Program" NUREG/CR-2528.

Powers, D. A. and Meyer, R. O., 1980, "Cladding Swelling and Rupture Models for LOCA Analysis," NUREG/CR-0630.

USNRC, 1984, "Prioritization of Generic Safety Issues," NUREG-0933.

Volk, W., 1958, Applied Statistics for Engineers, McGraw-Hill Second Edition, pp. 128-130.

Weiner, R. A., et al., 1988, "Improved Fuel Performance Models for Westinghouse Fuel Rod Design and Safety Evaluations," WCAP-10851-P-A (PROPRIETARY).

Westinghouse Electric Corporation, 1998, "AP600 Standard Safety Analysis Report," Revision 21, Subsection 15.6.5.4A.

Wilson, G., et al., 1989, "Quantifying Reactor Safety Margins," NUREG/CR-5249.

SECTION 33

ELEMENT III: SENSITIVITY AND UNCERTAINTY ANALYSIS

33-1 Introduction

In Sections 29 through 31, the effects of the most important contributors affecting the PCT are quantified. These contributors were divided into three classes: models (that is, variables describing the variations in key physical processes), plant initial conditions (variables describing the initial plant operating state), and power distribution (variables describing the initial reactor core conditions). In this section, the methodology for combining and propagating the uncertainties from the first two of these sources into the PCT is described. First, the statistical framework for the methodology is described and clarified with some simple examples (Section 33-2). Next, an overview is given of the methodology used, and simplifying assumptions, made as part of the methodology, are identified (Section 33-3). Next, the steps taken to generate the necessary data (that is, PCT change for given model or plant condition) to relate input variables to variations in PCT are described (Sections 33-4 and 33-5). Finally, a detailed step-by-step description of the methodology, from the tabulation of WCOBRA/TRAC-SB results to the generation of the PCT distribution and the verification of assumptions, is given (Section 33-6).

33-2 Statistical Framework

The statistical framework used to perform the uncertainty analysis is described first because it determines the overall structure of the methodology. The objective of this analysis is to quantify the contributions to PCT uncertainty from various sources, including the following:

- Plant variables, such as RCS and accumulator temperatures
- Physical process predictions such as break flow and HTC

33-2-1 Overview

In the Westinghouse methodology, the problem is divided into two parts:

- Prediction of the nominal behavior of fuel rods in the high power fuel assembly, as a result of variations in global variables

Global variables, such as break flow, and local variables, such as fuel conductivity, are at their as-coded or best estimate values.

- For a given RCS response and nominal hot assembly behavior, prediction of the behavior of individual fuel rods as a result of variations in local variables

Local variables, such as cladding reaction and fuel conductivity, affect hot rod response, but have a small effect on system thermal-hydraulics.

The approach is first illustrated by the simple examples in the following sections.

33-2-2 Statistical Methodology: Example 1

Simple examples are provided first for both the global variables and the local variables. The following is an example of statistical methodology for those variables that affect the overall system thermal and hydraulic transient as a whole, the global variables:

- Assume the only variables affecting the PCT are the SI water temperature (*TSI*) and the discharge coefficient (*CD*) for two-phase break flow.
- Assume *TSI* and *CD* exhibit the discrete probabilities shown in Figure 33-2-1. This figure means that, for example, there is an equal chance that *TSI* will take on the value 40, 77.5, or 120°F. Next, assume that WCOBRA/TRAC-SB calculations have been performed for all nine combinations of *TSI* and *CD*, and PCT results have been obtained. Develop an events and outcomes table as shown in Table 33-2-1a.

In this table, the event *IJ* is identified by the integer *ID(IJ)*, where each digit represents a particular state of *TSI* or *CD*. The outcome is the PCT resulting from that state as follows:

- 0: *TSI* = 77.5°F or *CD* = 1.0 results in: $\Delta PCT = 0$
- 1: *TSI* = 120°F or *CD* = 0.8 results in: $\Delta PCT = 100$
- 2: *TSI* = 40°F or *CD* = 1.2 results in: $\Delta PCT = -100$

where $NPCT_{00} = 1900$ has been assumed.

The identification is arbitrary. In this section and in Section 34, the identifier 0 means the reference value; that is, the value against which other values are compared to identify that the “..change from the reference value is..”. $NPCT_H$ is the PCT of the nominal (as-coded) hot rod in the hot assembly.

The probability $P(IJ)$ that a particular combination of TSI and CD occurs is the product of the individual probabilities:

$$0.333 * 0.333 = 0.1111$$

The resulting PCT distribution is obtained by arranging the calculated $NPCT$ into bins and developing a histogram as shown in Table 33-2-1b.

The probability $P(NPCT)$ for each bin is the sum of the probabilities of all events whose outcomes reside in the bin. An alternative method of obtaining the probability is by counting the number of occurrences; there are nine total events, one of which leads to a PCT of 2100. Therefore, the probability that the PCT will be 2100 is $1/9 = 0.1111$, and so on.

The overall approach and resulting PCT distribution is illustrated in Figure 33-2-2.

33-2-3 Statistical Methodology: Example 2

The following is an example of statistical methodology for local variables:

- Suppose that uncertainty in cladding reaction rate (RX) affects the response of the cladding at a point (the hot spot) to a given transient. Assume that when the nominal hot rod PCT is relatively high, the probability that the hot spot will actually be 100 degrees higher than the nominal value is also high, and when the nominal PCT is low, the probability of exceeding the nominal PCT is low. This probability, therefore, depends on a previous outcome and is usually termed a conditional probability (CP).
- Assume for CP that the cladding is hotter than the nominal value by 100 degrees as given by the discrete probabilities shown in Figure 33-2-3.

As in the first example, for each global event (IJ), there is a resulting nominal PCT ($NPCT_{IJ}$). In addition, for each global event, there is a new local event (K), as shown in Table 33-2-2a. This event leads to two possible outcomes: either the hot spot PCT ($HPCT_{IJK}$) is higher than the nominal value by 100 degrees due to cladding reaction ($K = 1$), or it is the same as the nominal value ($K = 0$). The probability of each outcome depends on (is conditional on) the global outcome of the nominal hot rod PCT.

A hot spot average PCT (call it $HPCT_{IJ\bullet}$) can be calculated for each global event (IJ). This average can be calculated by weighing the local outcome by its conditional probability. The dot in the subscript (rather than K) indicates that the detailed local outcomes information has been collapsed to a single average value. That is:

$$HPCT_{IJ\bullet} = \sum_K HPCT_{IJK} CP_K(NPCT_{IJ}) \quad (33-2-1)$$

An overall hot spot PCT distribution is calculated by summing over all events (IJ). This produces the results in Table 33-2-2b.

In this case, the probability of each local outcome is the probability of the global event (0.1111) times the conditional probability of the local event. The probability $P(HPCT)$ for each bin is then the sum of the probabilities of all outcomes in that bin.

In this case, the probabilities obtained by counting the number of occurrences are different from the probabilities calculated directly. This discrepancy occurs only because not enough samples have been taken to resolve the detailed behavior imparted by the local event.

The following approach should be taken: Each event should be replicated 10 times. This can be done by marking 10 pieces of paper with "11," 10 with "10," and so on. Now, by tossing all 90 slips into a hat, the population of global events is sampled by drawing a paper at random. Because each event has the same chance of occurring, event 11 will be pulled 10 times, and so on. Of the type 11 events, 2 will result in a local PCT of 2100, and 8 will result in a local PCT of 2200 according to Table 33-2-2a. Repeating the process with all events and counting local outcomes result in the number of occurrences shown in Table 33-2-2c.

The probability calculated by dividing the number of occurrences by 90 is now identical to those in Table 33-2-2b. The resulting distributions for this example are illustrated in Figure 33-2-4.

The following key differences between these simple examples and the actual problem must be solved. In the PWR problem, there are many more contributors to uncertainty and more possible events. Rather than three discrete occurrences of *TSI*, for example, there could be a large number of possible values.

The larger number of events results in a potentially much larger set of possible combinations of events.

Next is a description of an exact application using the complete list of contributors identified for the PWR from the Westinghouse best estimate small break LOCA methodology. Exact here means that the number of computer runs that can be made has no practical limit. The advantage of this example is that the method is conceptually relatively simple.

As the final statistical methodology is described, key assumptions made during its development are identified. These are indicated in underlined type. How these assumptions are dealt with is described in later sections.

33-2-4 Statistical Methodology: Example 3

Here all the variables that contribute uncertainty to the PCT are introduced. These variables were identified previously by constructing a PIRT, as described in Section 1, Volume 1. There are a number of other contributors, but these are assumed second order in significance, or are set to bounded (high PCT) values and are not included in the uncertainty analysis.

First the identification and division of all the contributors into groups are as shown in Table 33-2-3. (The nomenclature used to refer to these variables in this and later sections is also given.)

Assumption 1: [

]^{a,c}

Instead of just 2 global variables and 9 different possibilities, as in the simple example, there are now a number of global variables, and many more possible events (combinations of variables). Each of the defined variables has a corresponding probability distribution, which expresses the uncertainty about the actual value of that variable, either due to data uncertainty, modelling

uncertainty, or plant operating uncertainty. Distributions of the most important variables are derived and justified in Section 32.

The effect on the nominal cladding temperature and system thermal-hydraulics due to a change in a global variable or combination of variables is determined using WCOBRA/TRAC-SB. The result can be viewed as one global outcome (the transient PCT curves shown in Figure 33-2-5). The effect of local uncertainties on the local outcome for a specific global outcome is determined by using a stand alone model of the fuel rod to investigate the local variables with boundary conditions from WCOBRA/TRAC-SB. This is the purpose of the program HOTSPOT-SB (Section 32-4). The flow of information from WCOBRA/TRAC-SB to HOTSPOT-SB is illustrated in Figure 33-2-6. For any WCOBRA/TRAC-SB run, the effect of the 11 local uncertainties can be collapsed to a probability distribution by performing a large number (1000) of repeated cladding temperature calculations (trials) in which the different values of the local (subscript “ γ ”) variables are randomly sampled from their distributions. This type of operation is usually called a Monte Carlo simulation and is essentially the same as the sampling procedure described in Section 33-2-3, except that in the simple example, all possible events could be drawn from the population. In this case, only a sample of the total population is pulled and estimates are made of the actual probability distribution from the sample. Sufficient trials are taken (about 1000) such that reliable estimates can be made. The possible outcomes are, therefore, described by a histogram which looks nearly continuous as illustrated in Figure 33-2-5; for simplicity, the subscript “ γ ” variables are represented with a “•” in this figure, and in the text that follows.

After the histogram has been generated, standard quantities – such as average, standard deviation, 50th percentile, and 95th percentile – can be obtained. The average value may be different from the as-coded or nominal value by a bias X (or x , depending on the reference used), as illustrated in Figure 33-2-5.

The use of $ia\beta$ describes an event of a particular set of plant initial conditions, power distributions, and model conditions.

For example:

$$NPCT_{ia\beta} = \text{nominal hot rod PCT}$$

where:

ι is the plant condition:

$T_{avg} = 560$, and the like

α is the power distribution:

in the best estimate small break LOCA methodology, [

]^{a,c} The

subscript α is deleted from this point forward.

and β is the model condition:

$CD = 1.15$, $CYDG = 0.8$, and the like

The exact uncertainty analysis proceeds as follows:

1. Sample the global variable distributions to obtain a specific set of ι and β variables.
2. Perform a WCOBRA/TRAC-SB calculation for this combination of the global variables $\iota\beta$ (upper transient PCT curve in Figure 33-2-5).
3. Run HOTSPOT-SB for this WCOBRA/TRAC-SB run at several axial locations to obtain a probability distribution for the local hot spot PCT $P(HPCT_{\iota\beta})$ (distribution in Figure 33-2-5).
4. Sample the distribution $P(HPCT_{\iota\beta})$ to obtain a point value for the local hot spot PCT.
5. Repeat steps 1 to 4 many times (up to 500 to 1000 WCOBRA/TRAC-SB and/or HOTSPOT-SB runs) to develop an events and outcomes table like Table 33-2-4.
6. Develop a histogram, sorting the resulting hot spot PCTs into bins. Beginning with the highest PCT bin and working downward, count the number of occurrences in each bin until 5 percent of all occurrences (50 out of 1000, for example) has been

counted. The PCT bin where this occurs is the PCT at 95-percent probability (that is, 5 percent of all PCTs will be higher than this value).

33-2-5 Application of Data-Based Code Uncertainty

The procedure described in example 3 of Section 33-2-4 essentially propagates, in the statistical sense, the effect of uncertainty from the global and local variables, listed at the beginning of the example, to the final estimate of the PCT. An alternative approach to estimating uncertainty in the PCT prediction is to compare the computer code to many tests that simulate conditions in a PWR and result in a measured PCT. The code bias and uncertainty is then determined from a scatter plot. The advantage of this approach is that it effectively encompasses all potential contributors to uncertainty because all the code models are used to predict the tests. The disadvantages are that the individual contributors cannot be separated and the propagation of the dominant contributors at full-scale may not be adequately represented in the data base (for example, most tests producing a PCT are single effects tests and are small scale).

While the plant-specific uncertainty propagation methodology illustrated in Section 33-2-4 is the superior approach, it has one disadvantage in that the list of dominant contributors does not identify all contributors. If the PCT uncertainty of a test was predicted in which all the global variables listed as dominant were precisely controlled with no uncertainty, the procedure outlined in Section 33-2-4 would result in a hot spot average PCT (*HPCT*), which would have almost no uncertainty. In actuality, there would still be a residual uncertainty in the prediction of this value resulting from the uncertainty of second order effects excluded from the list of dominant contributors during the PIRT process. A similar statement could be made regarding the local variables. A minimum uncertainty (s_1) is established, to account for this, for the prediction of the hot spot average PCT for any given global transient (that is, a transient where the global variables are known exactly). The minimum uncertainty is calculated by comparing the uncertainty associated with the prediction of *HPCT* from WCOBRA/TRAC-SB and HOTSPOT-SB, to the uncertainty associated with the prediction of *HPCT* for various single and integral effects tests:

[

]^{a,c} (33-2-2)

]^{a,c}

Similarly, a minimum uncertainty (s_2) can be established for the prediction of the local hot spot uncertainty (σ_{β_s}). It is calculated as: [

(33-2-3)

]^{a,c}

Table 33-2-1a
Events and Outcomes for Example 1

Event ID(IJ)	$TSI(I)$, °F	$CD(J)$	$P(IJ)$	Outcome $NPCT_H$
11	120	0.8	0.1111	2100
10	120	1.0	0.1111	2000
12	120	1.2	0.1111	1900
01	77.5	0.8	0.1111	2000
00	77.5	1.0	0.1111	1900
02	77.5	1.2	0.1111	1800
21	40	0.8	0.1111	1900
20	40	1.0	0.1111	1800
22	40	1.2	0.1111	1700

Table 33-2-1b
PCT Distribution for Example 1

Bin	$NPCT$	No.	$P(NPCT)$
1	2100	1	0.1111
2	2000	2	0.2222
3	1900	3	0.3333
4	1800	2	0.2222
5	1700	1	0.1111

Table 33-2-2a
Events and Outcomes for Example 2

Event ID(IJ)	TSI (I)	CD(J)	Local Event K ID	Global Outcome $NPCT_{IJ}$	Local Outcome $HPCT_{IJK}$	CP	Average Outcome $HPCT_{IJ}$.
11	120	0.8	0	2100	2100	0.2	2180
11	120	0.8	1	2100	2200	0.8	
10	120	1.0	0	2000	2000	0.3	2070
10	120	1.0	1	2000	2100	0.7	
12	120	1.2	0	1900	1900	0.4	1960
12	120	1.2	1	1900	2000	0.6	
01	77.5	0.8	0	2000	2000	0.3	2070
01	77.5	0.8	1	2000	2100	0.7	
00	77.5	1.0	0	1900	1900	0.4	1960
00	77.5	1.0	1	1900	2000	0.6	
02	77.5	1.2	0	1800	1800	0.5	1850
02	77.5	1.2	1	1800	1900	0.5	
21	40	0.8	0	1900	1900	0.4	1960
21	40	0.8	1	1900	2000	0.6	
20	40	1.0	0	1800	1800	0.5	1850
20	40	1.0	1	1800	1900	0.5	
22	40	1.2	0	1700	1700	0.6	1740
22	40	1.2	1	1700	1800	0.4	

Table 33-2-2b
Hot Spot PCT Distribution for Example 2 (Method 1)

Bin	HPCT	No.	P(HPCT)
1	2200	1	0.0889 [= (1/9) 0.8]
2	2100	3	0.1778 [= (1/9) (0.2 + 0.7 + 0.7)]
3	2000	5	0.2667
4	1900	5	0.2444
5	1800	3	0.1555
6	1700	1	0.0667 [= (1/9) 0.6]

Table 33-2-2c
Hot Spot PCT Distribution for Example 2 (Method 2)

Bin	HPCT	No.	P(HPCT)
1	2200	8	0.0889
2	2100	16	0.1778
3	2000	24	0.2667
4	1900	22	0.2444
5	1800	14	0.1555
6	1700	6	0.0667

Table 33-2-3
PWR Uncertainty Contributors

Item	Definition
1. Contributors Classed as Global	
Plant Initial Operating Conditions (Group τ)	
T_{avg}	RCS average fluid temperature
TSI	SI temperature
$MSSV$	Pressure setpoint of the steam generator secondary relief valves
$TACC$	Accumulator fluid temperature
$PACC$	Accumulator pressure
$VACC$	Accumulator volume
$KACC$	Accumulator line resistance
Plant Initial Core Power Distribution (Group α)	
F_O	Nominal hot rod peaking factor
$F_{\Delta H}$	Nominal hot rod average relative power
$PBOT$	Average relative power, lower third of core
$PMID$	Average relative power, middle third of core
Global Models (Group β)	
CD	Critical flow modelling bias, two-phase break flow
$CYDG$	Core mixture interfacial drag multiplier
$LSDG$	Loop seal interfacial drag multiplier
$XCLL$	Condensation modelling bias in cold legs
$HSNT$	Horizontal flow-entrainment bias
$HSDG$	Interfacial drag bias horizontal stratified flow
$XSHASB$	Steam generator condensation heat transfer multiplier

Table 33-2-3
PWR Uncertainty Contributors (Cont'd)

Item	Definition
2. Contributors Classed as Local (Group γ)	
$F_G H$	Local hot spot peaking factor
K_F	Fuel conductivity
H_G	Gap HTC
E_H	Local HTC
T_M	T_{min}
K_B	Fuel conductivity after burst
R_F	Fuel density after burst
R_X	Cladding reaction rate
P_G	Rod internal pressure
T_B	Burst temperature
B_S	Burst strain

Table 33-2-4
Events and Outcomes for Example 3

Global Events				Local Outcomes PCT
$\alpha\beta$	α Sample	β Sample		
0 0	587, 77.5 ..	1.0, 1.0 . . .		1800
1 1	560, 120 ..	1.1, 0.8 . . .		1905
.				.
20 50	550, 66 ..	0.8, 0.82 ..		2000
.				.
20 500	550, 66 ..	0.9, 0.4 ..		1600
.				.
.				.
.				.

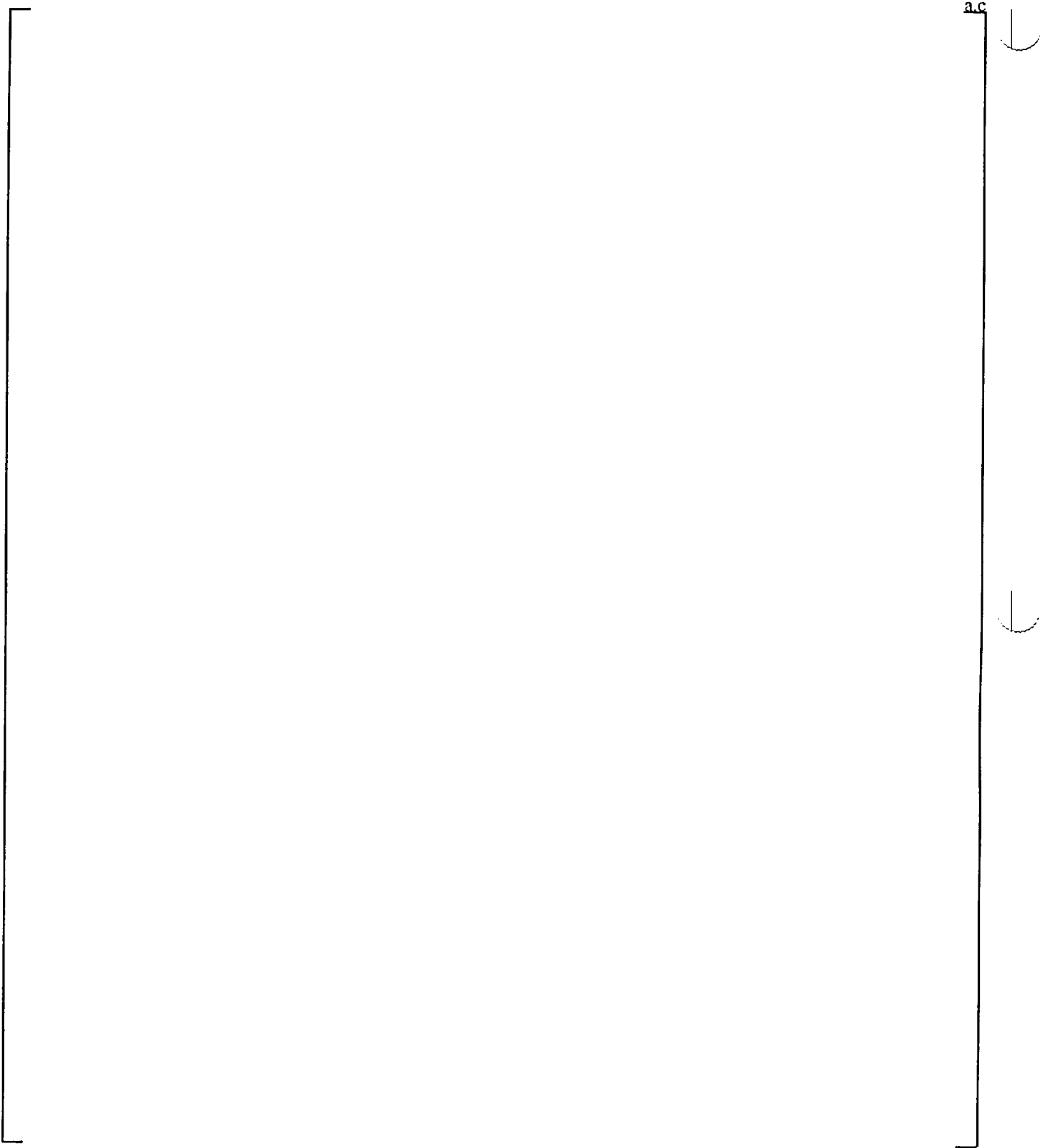


Figure 33-2-1. Input Probability Distribution for Example 1

a.c

Figure 33-2-2. Output Probability Distributions for Example 1

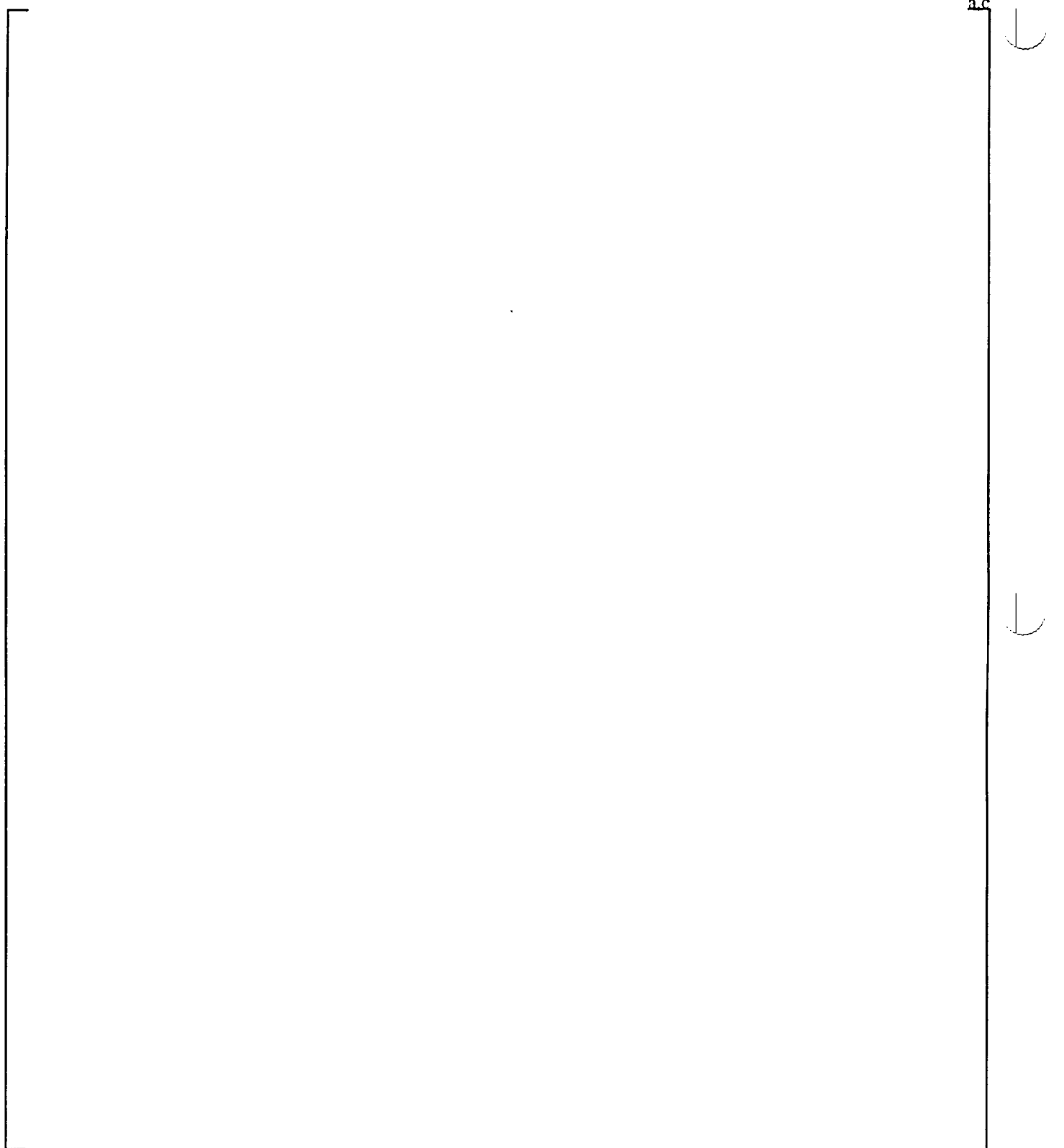


Figure 33-2-3. Conditional Probability Distributions of RX for Example 2

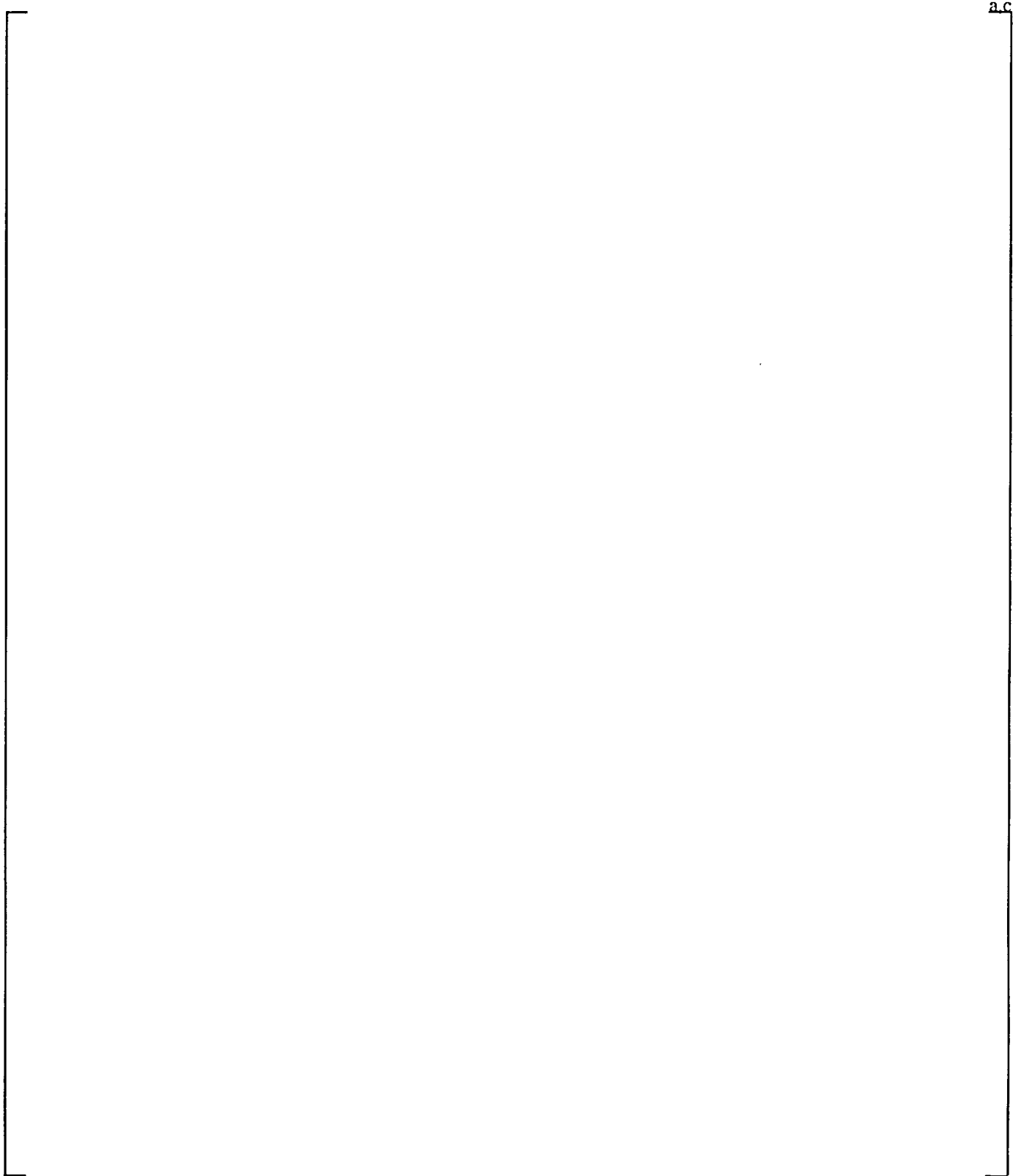


Figure 33-2-4. Output Probability Distributions for Example 2

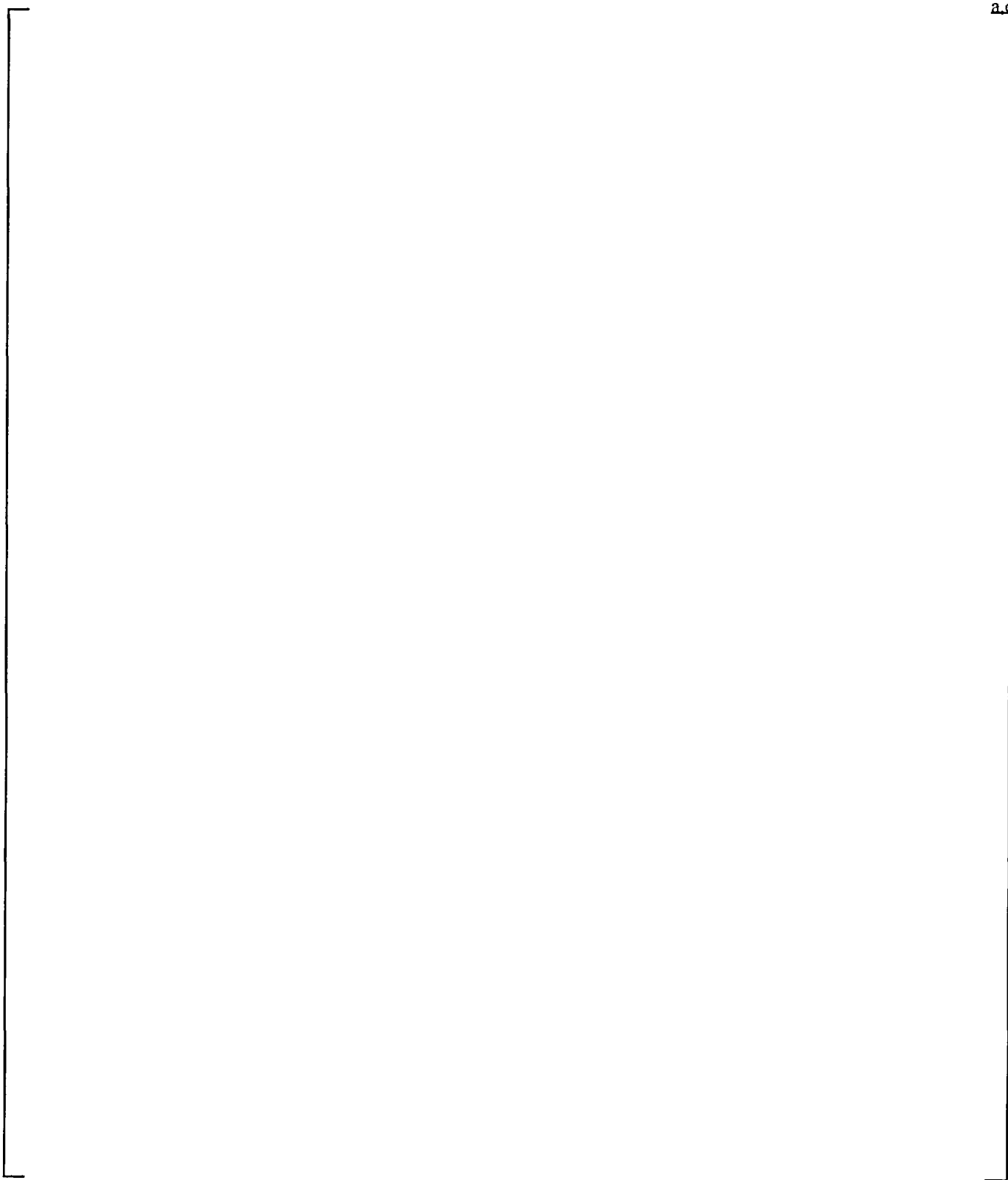


Figure 33-2-5. Relationship of Local Hot Spot Distribution to Nominal Hot Rod Reduction

Figure 33-2-6. Information Transfer from Global Model (WCOBRA/TRAC-SB) to Local Model (HOTSPOT-SB)

33-3 Uncertainty Methodology

33-3-1 Introduction

The exact approach, while simple in principle, is impractical due to the large number of required global (WCOBRA/TRAC-SB) calculations. The basic simplification that must be made is to find some way to obtain the global outcome for any set of global variables without resorting to a multitude of WCOBRA/TRAC-SB calculations. The method developed relies on response surfaces and simplifying assumptions to solve this problem. However, the assumptions and approximations that must be made to arrive at a practical method add more steps and more complexity to the process.

The methodology is divided into four phases as follows:

- Response surface generation steps
- Preliminary Monte Carlo steps
- Verification/correction steps
- Final Monte Carlo steps

33-3-2 Methodology Overview and Assumptions

An overview is first given of the procedure to be used. One assumption has already been made related to []^{a,c} (Section 33-2-4). Additional assumptions are introduced as follows and addressed in the next section.

First, the following quantities are defined (Figure 33-2-5):

Subscript 0 = nominal (as-coded) conditions

Subscript 000 = reference nominal condition (all variables as-coded or at reference values, $NPCT_{000}$)

$HPCT_{i\beta}$ = hot spot average PCT for event $i\beta$, including uncertainties from group γ

$\sigma_{i\beta}$. = hot spot uncertainty, defined as the standard deviation of the hot spot PCT distribution

$X_{i\beta}$. = $HPCT_{i\beta} - NPCT_{000}$

$x_{i\beta}$. = $HPCT_{i\beta} - NPCT_{i\beta 0}$
= hot spot bias

As previously described, the various contributors to uncertainty are divided into several groups called iota (initial conditions), beta (global models), and gamma (local models). The overall PCT resulting from a combination of variables is then calculated as the sum of the contributions from each group. [

]^{a,c}

First, a sample of the global variables is obtained by randomly drawing from the respective distributions as described in example 3 of Section 33-2-4. The PCT resulting from these values is then estimated. The basic assumption made is that [

]^{a,c}

Assumption 2: [

]^{a,c}

The change in average PCT from the reference value, as each initial condition varies within its operating range, is considered first. [

]^{a,c}

[
]^{a,c}

Assumption 3: [
]^{a,c}

Response surfaces are used to predict the contribution from group β variables [
]^{a,c}

Assumption 4: [
]^{a,c}

]^{a,c} (33-3-1)

If there is no hot spot bias to be added to the hot spot average PCT, then:

$$\text{"HPCT}_{i\beta} \text{"} = \text{"NPCT}_{i\beta} \text{"} \quad (33-3-2)$$

[
]^{a,c}

Assumption 5: [

(33-3-3)

]^{a,c}

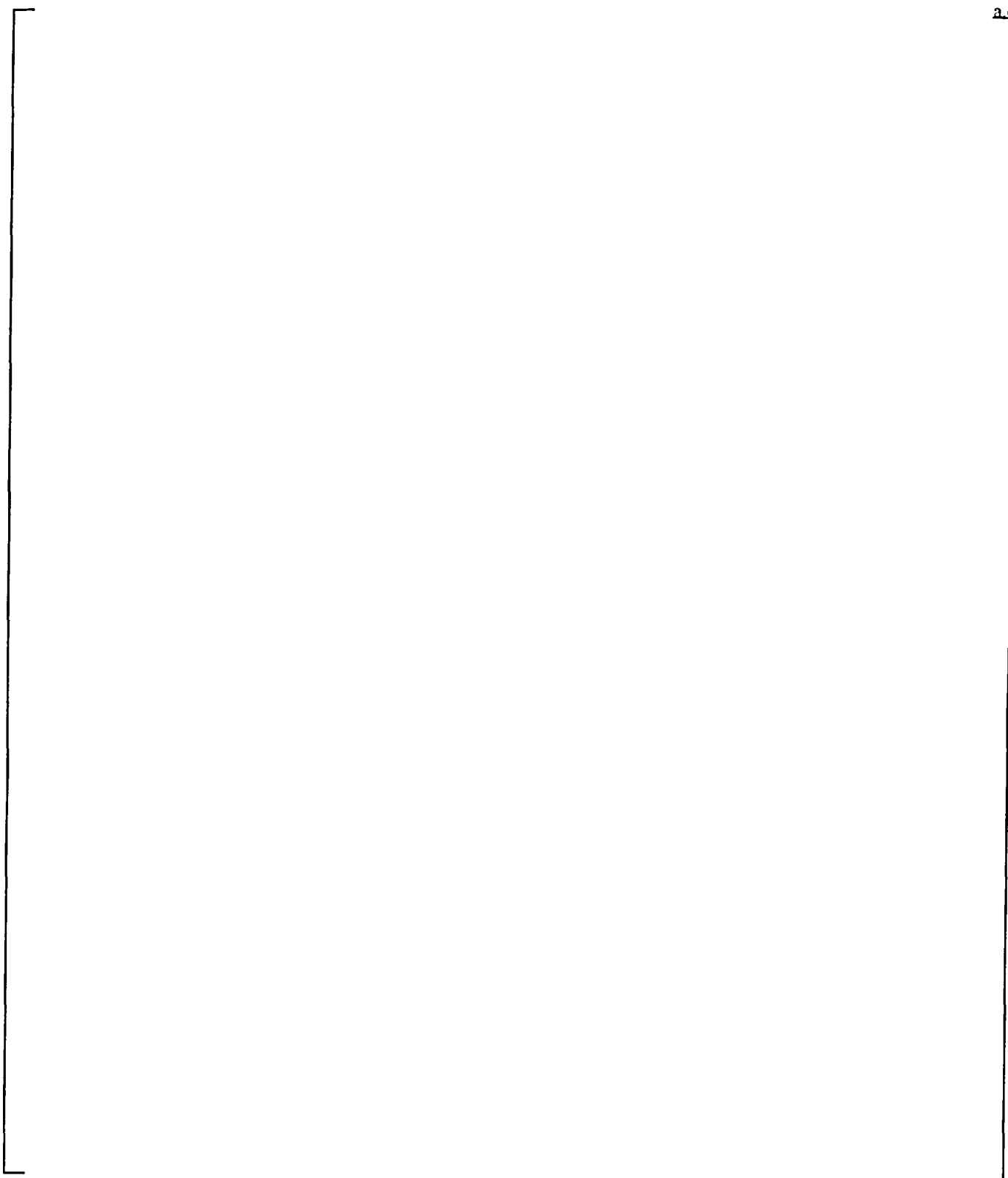
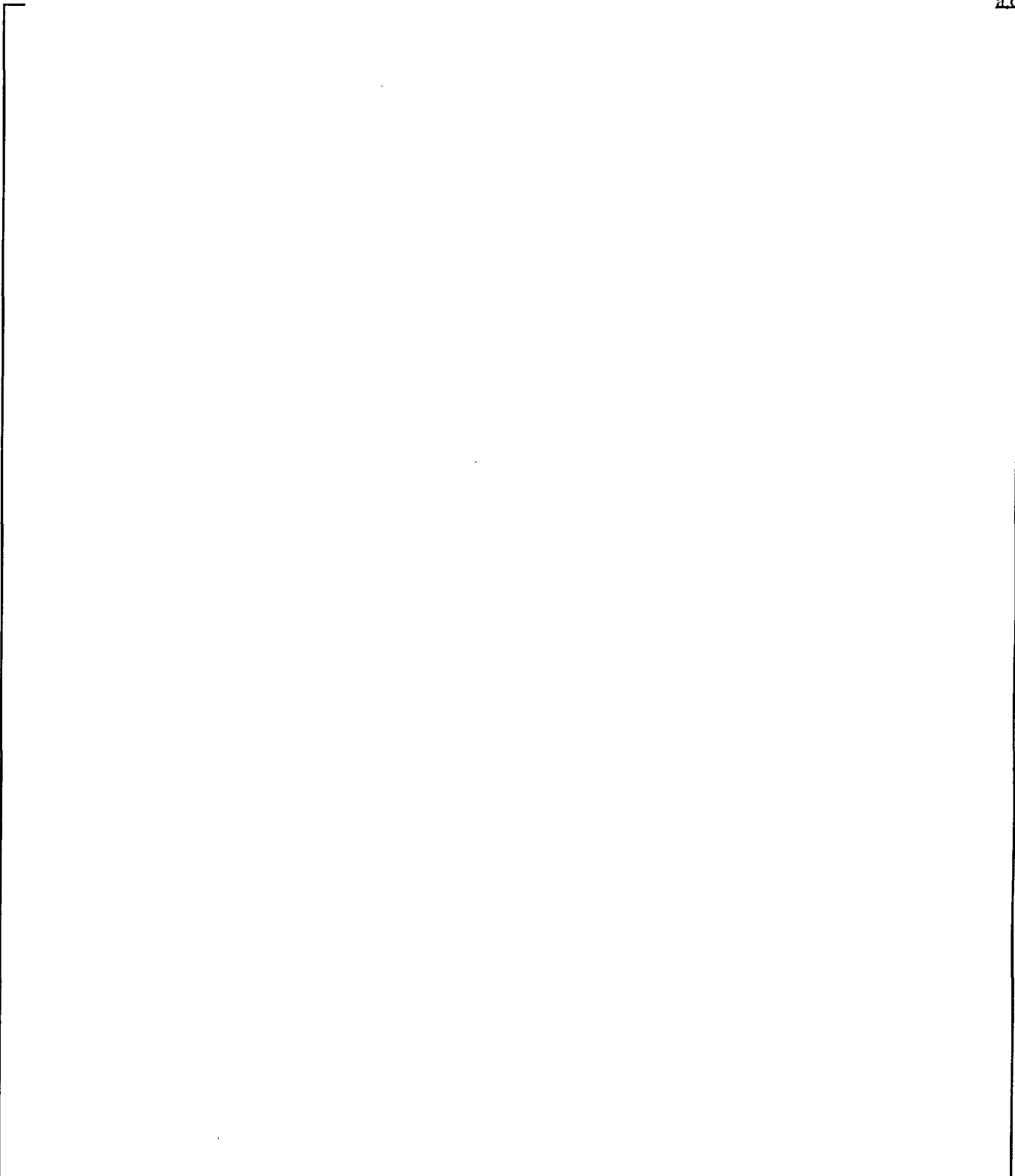


Figure 33-3-1. Derivation of Initial Condition Uncertainty Distribution



a.c

Figure 33-3-2. Superposition of Global Plant Variables

33-4 Effect of Reactor Input Parameters and State

33-4-1 Introduction

In addition to the peaking factor and fuel stored energy discussed in Section 29, there are a number of other plant input variables that affect the PCT. These additional variables are described in Section 24, Volume 3, and a number of sensitivity studies were performed and are presented in Section 30 to understand the effect of these parameters on the calculated small break LOCA transient. The results were used to determine how to treat each of these parameters in the overall uncertainty assessment. This treatment falls into three general categories as follows:

- Nominal Without Uncertainty

The nominal (expected or midpoint) value of the parameter is used [

]^{a,c.}

- Bounded

A conservative value of the parameter is used when the parameter varies gradually as a function of operating history, such as the burnup level, or when the value of the parameter at the time of the accident is indeterminate, such as location of the pressurizer relative to the break. A parameter may also be bounded when the sensitivity of the transient results to variations in the parameter is small, such as MTC, or when the effort to develop and justify a detailed uncertainty treatment was judged to exceed the benefits of doing so, such as core power distribution.

- Nominal With Uncertainty

The Westinghouse methodology includes two components of uncertainty in the overall uncertainty assessment. As indicated in Section 33-2-4, these are the code and model uncertainty, and the initial and boundary conditions uncertainty.

33-4-2 Reference Case Conditions

As described in Section 33-3, the Westinghouse uncertainty methodology makes use of a reference case, from which $NPCT_{0000}$ will be determined. The input values to be used in this case can now be more precisely defined relative to the key LOCA parameters. As noted, the general rule applied is to use limiting assumptions in cases where the parameter effect is relatively small or where the parameter is difficult to quantify statistically. The summary that follows describes the assumptions for each parameter, how it is treated in the analysis, and its basis.

1.0 Plant Physical Description

- a. Dimensions: []^{a,c}
- b. Flow Resistance (KN): Best estimate values of loop flow resistance are assumed. Variations in this parameter important to small break LOCA are accounted for in []^{a,c}
- c. Pressurizer Location: []^{a,c}
- d. Hot Assembly Location: An established location for the hot assembly is assumed, as described in Section 28, Volume 3.
- e. Hot Assembly Type: The hot assembly is a fresh reload assembly, which exhibits the highest linear heat rates and stored energy.
- f. SGTP Level: The SGTP level that results in the highest PCT based on sensitivity studies is used. The limiting tube plugging level is identified for each plant analyzed.

2.0 Plant Initial Operating Conditions

2.1 Reactor Power Distribution

a. Initial Core Average Linear Heat Rate: [

]^{a,c}

b. Hot Rod Peak Linear Heat Rate (F_Q): Power shape 10 (Figure 29-2-33, Section 29) is used to define the power distribution for the reference case. The peaking factor (F_Q) or normalized peak linear heat rate for this power distribution [

]^{a,c}

c. Hot Rod Average Linear Heat Rate: The value used in power shape 10 [

]^{a,c}

d. Hot Assembly Average Linear Heat Rate: As described in Section 29, the power generated in the hot assembly average rod is conservatively estimated to be []^{a,c} lower than that generated in the hot rod.

e. Hot Assembly Peak Linear Heat Rate: The peak linear heat rate in the average rod is also []^{a,c} lower than the peak linear heat rate in the hot rod.

f. Axial Power Distribution (*PBOT*, *PMID*): Power shape 10, a spline shape with a [

]^{a,c}

g. Low Power Region Relative Power (*PLow*): A typical relative power in the low power region is assumed. This typical value is determined on a plant-specific basis.

h. Hot Assembly Burnup: BOL conditions in the hot assembly exhibit the greatest stored energy and are assumed in the reference case. The core average rods are assumed to be at an average burnup representative of typical reload cycles.

- i. Prior Operating History: The power distribution assumed to exist at the time of the LOCA is conservatively assumed to have existed since plant startup when determining fission product inventories.
- j. MTC: The maximum value specified in the Technical Specifications is assumed to conservatively estimate core reactivity and fission power.
- k. HFP Boron Concentration: A value typical of those used in current cores at BOL conditions is assumed. [
]^{a,c}

2.2 RCS Fluid Conditions

- a. Average Fluid Temperature (T_{avg}): As indicated in Section 30, plants may operate at different steady-state values of T_{avg} . [
]^{a,c} The effect of uncertainties is accounted for in the initial condition uncertainty as discussed in Section 33-5.
- b. Pressurizer Pressure (P_{RCS}): As indicated in Section 30, plants operate at a specific normal pressure, usually 2250 psia. [
]^{a,c}
- c. Loop Flowrate: [
]^{a,c}
- d. Upper Head Fluid Temperature: The fluid in the reactor vessel upper head may vary from plant to plant depending on the bypass flow into the upper head. The variation during normal operation in a single plant is small, so the appropriate best estimate value of the fluid temperature in the upper head consistent with the

assumed T_{avg} value is used. Because variation in this parameter is small, uncertainties are not included.

- e. Pressurizer Level: The nominal value of pressurizer level is assumed. [
]^{a,c}
- f. Accumulator Water Temperature ($TACC$): A nominal (midpoint) value is assumed with variations treated in the initial condition uncertainty as described in Section 33-5.
- g. Accumulator Pressure ($PACC$): A nominal (midpoint) value of accumulator pressure is assumed. Variations in pressure are included in the initial condition uncertainty as described in Section 33-5.
- h. Accumulator Water Volume ($VACC$): A nominal (midpoint) value of accumulator water volume is assumed. Variations in volume are included in the initial condition uncertainty as described in Section 33-5.
- i. Accumulator Line Resistance ($KACC$): A best estimate value of accumulator line resistance is assumed. Variations in line resistance are not included in the small break LOCA initial condition uncertainty because the accumulators empty only partially during the small LOCA PCT excursion and KACC is unimportant.
- j. Accumulator Boron Concentration: The Technical Specification minimum value is assumed. This is a conservative value because it reduces the reduction in the residual core power during reflood.

3.0 Accident Boundary Conditions

- a. Break Location: Scoping studies are performed on a plant-specific basis to confirm that the cold leg remains the limiting location for small break LOCA (Sections 27 and 28, Volume 3).

- b. Break Type: Breaks are modelled using a 1-D PIPE component in the reference case and the scoping and sensitivity studies. Uncertainties in the orientation of the break around the pipe perimeter are accounted for in a further scoping analysis as described in Section 28.
- c. Break Size: Variations in break size are considered with the limiting value chosen as the reference case as described in Section 27, Volume 3.
- d. Offsite Power: Continued availability of offsite power during the LOCA determines whether the RCS pumps may continue to operate during the transient until manually tripped by the operator and affects the delay in actuation of SI and auxiliary feedwater pumped flows. The limiting condition (LOOP or OPA) is assumed based on plant-specific sensitivity studies.
- e. SI Flow: Minimum SI flow is assumed and is calculated using methods consistent with those currently used for Appendix K analysis. Section 30 indicates that SI flow differences may result depending on the presumed cold leg break orientation and the SI system design.
- f. TSI: Nominal (midpoint) values are assumed. Variations are accounted for in the initial conditions uncertainty as described in Section 33-5.
- g. SI Delay: Maximum values consistent with the limiting offsite power assumption are used.
- h. Containment Pressure: Inasmuch as the small break LOCA transient exhibits critical break flow throughout the WCOBRA/TRAC-SB calculation beyond the PCT time and core quench, containment pressure is unimportant; a value of 14.7 psia is assumed.
- i. Single Failure Assumption: Typically, the loss of an entire train of SI high pressure and auxiliary feedwater pumps is assumed for the WCOBRA/TRAC-SB LOOP calculations. If desired, a more detailed analysis may be used which explicitly examines several different single failure scenarios on a consistent basis to justify additional SI injection in WCOBRA/TRAC-SB with continued OPA, with the limiting scenario being chosen.

- j. Control Rod Drop Time: Consistent with the current design basis for PWRs, control rods are assumed to drop through the core over a 2.4-second interval during a small break LOCA following reactor trip.
- k. Steam Generator Secondary Safety Valve Setpoint: Nominal values are assumed in the reference case. Variations are accounted for in the initial condition uncertainty.

4.0 Model Parameters

All model parameters are used at their best estimate or as-coded values in the reference case. Uncertainties in some models are accounted for in the global and local contributors uncertainty, while other models have been shown to be conservative as-coded. In addition, a lower limit is placed on the estimated uncertainty as described in Section 33-2-5.

Table 33-4-1 summarizes the described reference case assumptions.

While the reference case includes several best estimate assumptions, it still represents a conservative set of conditions. The power distribution assumptions alone provide a level of conservatism.

Many WCOBRA/TRAC-SB calculations are performed (Table 33-4-2) to confirm the limiting direction of several variables and to establish the necessary data base for the uncertainty evaluation. Additional details on the types of calculations performed are provided in subsequent sections.

Table 33-4-1
Key LOCA Parameters and Reference Case Assumptions

[

]^{a,c}

Table 33-4-1 (Cont'd)
Key LOCA Parameters and Reference Case Assumptions

[

Table 33-4-1 (Cont'd)
Key LOCA Parameters and Reference Case Assumptions

[

]^{a,c}

Table 33-4-2
WCOBRA/TRAC-SB Run Matrix for a Plant-Specific Analysis

[

] a,c

Table 33-4-2 (Cont'd)
WCOBRA/TRAC-SB Run Matrix for a Plant-Specific Analysis

[

]^{a,c}

33-5 Performing PWR Sensitivity Calculations

33-5-1 Introduction

In addition to the plant initial conditions described in the previous section, global models describing the following physical processes have been identified as contributors to the overall uncertainty:

- a) Critical flow
- b) Core mixture interfacial drag
- c) Fuel rod (stored energy, gap HTC, and cladding burst)
- d) Heat transfer to uncovered fuel
- e) Loop seal pipe interfacial drag
- f) Horizontal stratified flow entrainment
- g) Horizontal stratified flow interfacial drag
- h) Condensation in the cold legs
- i) CCFL in the RCS piping
- j) Steam generator heat transfer (primary to secondary)

Model i has been shown (Section 17, Volume 2) to exhibit conservative modelling bias relative to data and is not ranged. The following models are anticipated to have a minor impact on PCT and, therefore, are [

]^{a,c}

- e) Loop seal pipe interfacial drag
- f) Horizontal stratified flow entrainment
- g) Horizontal stratified flow interfacial drag
- h) Condensation in the cold legs
- j) Steam generator heat transfer (primary to secondary)

The following models are important as local effects (Section 32-3), but do not affect the system thermal-hydraulics:

- c) Fuel rod (stored energy, fuel rod models such as cladding burst and gap HTC)
- d) Heat transfer to uncovered fuel

The impact of uncertainty in critical flow in the subcooled break flow regime is dealt with by identifying and then using the limiting break size as the reference case (Section 27, Volume 3).

This leaves the following models, which lead to global effects, to be ranged in thermal-hydraulic calculations:

- a) Critical flow (in the two-phase regime)
- b) Core mixture interfacial drag

In the event that a particular plant exhibits a large PCT sensitivity to items e, f, g, h, or j, that particular parameter will be included with items a and b in the ranging to obtain a response surface.

As described previously, uncertainties are considered to propagate globally, where the entire system response is affected, and locally, where only conditions at the PCT location are affected. The global effect is determined using the WCOBRA/TRAC-SB code. Because WCOBRA/TRAC-SB runs require substantial computer time, a limited number of calculations are used from which response surfaces are derived. These response surfaces are then used to calculate the effect on PCT for intermediate values of the global parameters.

The local effect is determined using the HOTSPOT-SB code. This program (Section 32-2) models the heat conduction, cladding deformation fuel relocation, cladding reaction, and heat transfer occurring at a single location on the hot rod, using fluid conditions obtained from a WCOBRA/TRAC-SB calculation. Because this computer program does not require much computer time, it is used in a direct Monte Carlo simulation as described in Section 33-2-4.

33-5-2 Plant Initial Conditions: Global Effects

This section discusses plant initial conditions that have a global effect on the thermal-hydraulic transient; that is, changes in these conditions result in changes in transient response that affect the fluid conditions near the hot rod.

33-5-2-1 Initial Fluid Conditions

The initial condition uncertainty accounts for variations in the plant initial conditions such as T_{avg} , MSSV, and the like (Table 33-2-3, group i).

During plant operation, the variables identified vary within a specified range due to normal operating fluctuations. In addition, measurement uncertainties limit the accuracy to which these conditions can be monitored. At any point in time, therefore, the fluid conditions are slightly different from those assumed in the reference calculation. If a LOCA occurred, the predicted PCT would be different from the reference prediction as a result of these differences.

As noted in Section 33-5-1, it is assumed that [

(33-5-1)

]^{a,c}

[
]

(33-5-3)

(33-5-4)

(33-5-5)

]^{a,c} (33-5-6)

[

L

(33-5-7)

L

(33-5-8)

]^{a,c}

L

(33-5-9)

]^{a,c}

33-5-2-2 Initial Core Power Distribution

As discussed in Section 21, Volume 2, the axial power distribution on the nominal hot rod and the hot assembly can be described in terms of [

]^{a,c}

As discussed in Section 29, variations in these quantities come from two sources:

- Variations in core and hot assembly conditions

These variations affect the thermal-hydraulic conditions in the hot assembly during the transient.

- Variations in hot rod local power

These variations consist of two independent components. The first is due to variations in hot assembly power. Because the hot rod is assumed to reside in the hot assembly, its power varies by the same amount. The second is due to variations, independent of the hot assembly variation, caused by uncertainties in the local, or hot spot, conditions such as pellet geometry. This second element is considered among the local uncertainties.

The approach to power-related parameters is simplified compared to the large break LOCA methodology (Bajorek et al., 1998). [

]^{a,c} A description of the best estimate small break LOCA methodology follows.

The following steps are taken to establish the WCOBRA/TRAC-SB input for core power distribution:

1. The design or Technical Specification values are established for F_Q and $F_{\Delta H}$, which are to be used. Assume, for example, that the Technical Specification (*TS*) operating limits are $F_{Q,TS} = 2.7$, and $F_{\Delta H,TS} = 1.8$.
2. The maximum nominal linear heat rate during a transient is the [

].^{a,c} Defining the core average linear heat rate as *AFLUX* gives:

$$[]^{a,c}$$

As in the large break LOCA best estimate methodology, [

$$]^{a,c}$$

When the pertinent core design uncertainties are applied, the 95th percentile maximum local linear heat rate is [

$$]^{a,c}$$

3. The maximum $F_{\Delta H}$ allowed in the core design is [

]^{a,c}

For the small break LOCA methodology, the maximum rod average linear heat rate is [

].^{a,c}

Based on core design methodology, the maximum rod average linear heat rate [

]^{a,c} The corresponding F_Q and $F_{\Delta H}$ for the hot assembly average rod are []^{a,c} lower. This maximizes the hot assembly power relative to the hot rod.

[

]^{a,c}

]^{a,c}

33-5-3 Plant Initial Conditions: Local Effects

A given thermal-hydraulic transient resulting from a given initial plant condition gives rise to a set of conditions at the hot spot which then results in a number of possible hot spot paths, depending on local conditions. [

]^{a,c}

33-5-4 Physical Models and Processes: Global Effects

As indicated in Section 33-5-1, the physical models affecting the global response of the system, and which must be accounted for in the uncertainty evaluation, are as follows:

- Critical flow in the two-phase flow regime: *CD*
- Core mixture level swell: *CYDG*

The method for estimating the *PCT* uncertainty contributed by these variables is described next.

[

L

]^{a,c}

L

Run 09 is the reference case from Section 27.

33-5-5 Physical Models and Processes: Local Effects

[

]^{a,c}

L

Table 33-5-1
Peaking Factor Uncertainties Considered for Hot Rod
in Best Estimate Methodology

[

]^{a,c}

Table 33-5-2
Core Interfacial Drag / Break Flow Run Matrix

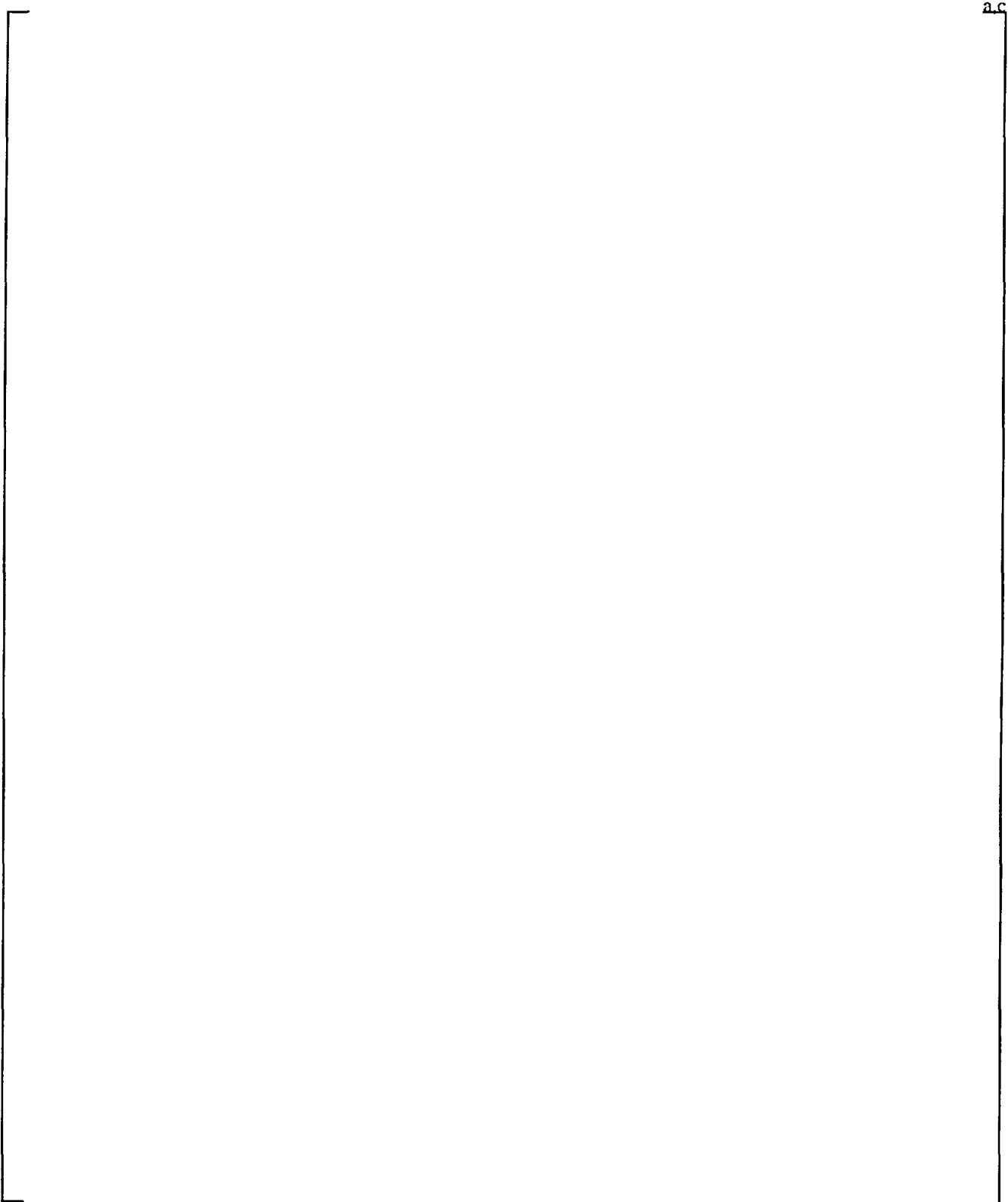


Figure 33-5-1. Range of Power Shape Parameters

33-6 Combining Biases and Uncertainties

The final step in the uncertainty methodology is to combine biases and uncertainties. In this methodology, biased predictions are accounted for directly in the statistical analysis or are ignored if to do so is conservative. If, for example, the predicted HTC is underpredicted for some time period when compared with tests, then the mean of the modelling bias distribution for the HTC is less than 1.0 (Section 32-5). Some biases that may reduce or increase the PCT, such as the tendency of WCOBRA/TRAC-SB to underpredict the amount of critical break flow in the two-phase region, are considered. First, the assumptions in the methodology are reviewed in light of Sections 33-4 and 33-5.

33-6-1 Review and Verification of Assumptions

In this section, the assumptions made in the development of the methodology are reviewed and discussed. The steps taken to verify each assumption are also described.

- Assumption 1: [

]^{a,c}

- Assumption 2: [
]^{a,c}

This assumption is verified on a plant-specific basis by performing additional calculations as described in the following paragraphs [

]^{a,c}

[

]^{a,c}

[

L

(33-6-1)

L

]^{a,c}

L

[

(33-6-2)

(33-6-3)]^{a,c}

- Assumption 3: [

]^{a,c}

- Assumption 4: [

]^{a,c}

- Assumption 5: [

]^{a,c}

This assumption is checked in each case as follows.

Table 33-6-2 shows typical output from a HOTSPOT-SB run.

[

(33-6-4)

]^{a,c}

[(33-6-5)

(33-6-6)

]^{a,c}

- Assumption 6: [

]^{a,c}

The assumption of normality used to establish the prediction uncertainty above is tested using standard statistical tests (Shapiro and Wilk, 1965). In the event that the assumption does not hold, alternate steps as described in the following paragraphs are taken.

[

(33-6-7)

]^{a,c}

(33-6-8)

(33-6-9)

]^{a,c}

]^{a,c}

33-6-2 Methodology Procedure

The following steps take place after the plant operating data have been gathered and input variable distributions have been established. The flowchart shown in Figure 33-6-3 illustrates the relationships among the steps.

33-6-2-1 Phase I: Response Surface Data Generation Steps

The Phase I steps are as follows:

1. Perform WCOBRA/TRAC-SB calculations.

For the global contributors, run WCOBRA/TRAC-SB for specified combinations of variables as described in Section 33-5 to obtain relationships between global variables and *NPCT* (flowchart boxes 1 and 6). The following calculations are performed after the reference is established:

- a) [

]^{a,c} All other

variables are at reference case conditions in a given case.

- b) [

]^{a,c} All other

variables are at reference case conditions.

2. Obtain WCOBRA/TRAC-SB information for HOTSPOT-SB.

Information obtained from the WCOBRA/TRAC-SB calculations is used to generate response surfaces. For some calculations, additional information is needed for input into the HOTSPOT-SB calculation.

Perform steps a through c for WCOBRA/TRAC-SB calculations (referred to later as the hot spot cases: []^{a,c} that exhibit a loop seal uncovery:

a) Loop seal uncovery *NPCT (BLD)*, location, and value

It is anticipated, based on experience, that PCT during loop seal clearance does not exceed the initial cladding temperature prior to the transient, while the RCS is still at steady-state operation. Nevertheless, the methodology is constructed to take account of a PCT occurring in this time interval in the event core uncovery does occur.

b) End of loop seal uncovery heatup/beginning of initial recovery cooldown (*TE1*)

This is when the loop seal uncovery *PCT* is reached.

c) End of loop seal recovery (*TE2*)

This is when the *PCT* excursion due to loop seal clearance reaches its minimum *PCT* or core quench is achieved.

Perform steps d through h for all WCOBRA/TRAC-SB calculations among the hot spot cases that exhibit a boiloff core uncovery:

d) Beginning of boiloff uncovery period *NPCT* location (*RFL1*) and value (*TE3*)

This is when the upper plenum collapsed liquid level has reached the top of the active fuel. Core uncovery due to boiloff begins immediately thereafter.

The heatup process is rapid, so that this criterion fixes the beginning of core uncovery within a fraction of a second.

- e) End of first core boiloff uncovery heatup period (*TE4*)

This is normally when the PCT bottoms out after it reaches its maximum value. A second core heatup period may occur because, in some cases, boiling of the water in the core after accumulator injection begins in the small LOCA transient causes a depletion of the vessel inventory when RCS repressurization terminates accumulator flow temporarily.

In general, it is expected that such a second PCT during core boiloff will not occur; that is, the cladding temperature continually decreases after the first peak during core boiloff. In these cases, *TE4* is the time at which core quench occurs.

- f) Second boiloff uncovery (*RFL2*) *NPCT*, location, and value

The second boiloff PCT is the maximum reached after *TE4*. In most cases, however, a second boiloff PCT will not occur; [

]^{a,c}

- g) End of second boiloff heatup/cooldown period (*TE5*)

This is the end of the WCOBRA/TRAC-SB core uncovery transient. The cladding is clearly completely quenched, and all elevations have turned around. In the event that no second boiloff heatup occurs, this *TE5* time is meaningless.

- h) Identify hot rod burst location, if applicable:

[

]^{a,c}

[

L

]^{a,c}

Perform step i for the HOTSPOT-SB hot spot cases that exhibit core uncoverage:

- i) Extract the following information from the WCOBRA/TRAC-SB calculation for each location *BLD*, *RFL1*, *RFL2*, as appropriate, and [

]^{a,c} for input into HOTSPOT-SB:

• [

L

]^{a,c}

As a function of time:

• [

]^{a,c}

At the end of this step, the following information exists:

[

]^{a,c}

3. Perform HOTSPOT-SB calculations.

[

]^{a,c}

4. Develop response surfaces (Figure 33-6-3, box 8):

[

(33-6-11)

]^{a,c}

5. Develop initial condition probability distribution (Figure 33-6-3, box 2).

Calculate the initial condition normal distribution according to the steps described in Section 33-5-2. [

]^{a,c}

33-6-2-2 Phase II: Initial Monte Carlo Steps

The Phase II steps are as follows:

6. Sample from the input distributions.

The distributions of the global model variables (group β) are sampled (box 5).

7. Find $\Delta NPCT_{00}$ (Figure 33-6-3, box 3), and x_{i00} :

a) In step 5, a PCT distribution was developed which represented the expected variations in PCT resulting from variations in all the initial condition

parameters. Sampling from the initial condition distribution gives the variation in PCT due to a random sample i of initial conditions for this trial.

b) [

]^{a,c}

c) [

]^{a,c}

8. a) Find $X_{0\beta*}$ and $\sigma_{0\beta*}$, using response surfaces A and B (Figure 33-6-3, box 9).

When a parameter value outside the range of the response surface is calculated, [

(33-6-13)

]^{a,c}

[

]^{a,c}

b) [

(33-6-14)

]^{a,c} (33-6-15)

where:

[

(33-6-16)

]^{a,c}

9. Repeat the steps in Phase I many times and generate a *PCT* histogram; then calculate the averages, standard deviations, and *PCT* value at 95-percent probability.

33-6-2-3 Phase III: Verification/Correction Step

At the end of Phase II, there exists a best estimate prediction of *HPCT*, which does not include uncertainty introduced by the []^{a,c}.

In these steps, the estimate of the code uncertainty based on direct comparisons with data is compared with the response surface uncertainty, and the larger is applied. []^{a,c}.

10. []^{a,c}

11. Tabulate the dependent variable []^{a,c}

12. Develop a correction of the form:

$$[]^{a,c} \quad (33-6-17)$$

13. []^{a,c} (33-6-18)

14. []
]a,c

15. Tabulate the dependent variable []
]a,c

16. Develop a correction of the form:

[]
]a,c (33-6-19)

17. []
]a,c

]a,c (33-6-20)

33-6-2-4 Phase IV: Final Monte Carlo Steps

Phase IV steps are as follows:

18. Repeat Phase II steps 3 through 8 for the limiting break type to calculate the best estimate values of " $HPCT_{\beta*}$ " and " $\sigma_{\beta*..}$ "

19. []
]a,c

20. []
]a,c

21. []
]a,c

22. []
]a,c

23. []
]^{a,c}
24. Repeat steps 18 to 23 many times and generate a PCT histogram; then calculate averages, standard deviations, and the PCT value at 95-percent probability.

33-6-3 Methodology Procedure: Other 10CFR50.46 Criteria

In addition to PCT, 10CFR50.46 requires the evaluation against specific criteria of maximum local cladding oxidation and the total amount of hydrogen generation. The maximum thickness of cladding allowed to become oxidized during the LOCA transient is 17 percent of the local cladding thickness. The maximum amount of hydrogen allowed to be generated is 1 percent of the hypothetical amount that would be generated if all the cladding in the core surrounding the fuel were to be oxidized.

The following sections describe the methodology used to determine maximum local and core-wide oxidation.

33-6-3-1 Local Oxidation Calculation

For best estimate small break LOCA calculations, compliance with the maximum local oxidation fraction is examined by performing the following steps. Inasmuch as oxidation is insignificant at cladding temperatures below 1800°F, this is performed solely when the HOTSPOT-SB PCT value exceeds 1800°F.

1. Select a WCOBRA/TRAC-SB transient run using the method described below:

- []
]^{a,c}
2. []
]^{a,c}

[

]^{a,c}

It is concluded that, if a thermal-hydraulic transient results in a nominal hot rod PCT higher than 95th percentile PCT and this transient is used in conjunction with a HOTSPOT-SB analysis, then this represents a conservative approach to estimating percentage local cladding reacted.

33-6-3-2 Core-Wide Oxidation Calculation

Rod Power Census

[

]^{a,c}

Extension of Hot Rod Oxidation Calculation to Other Rods (From Large Break LOCA)

[

]^{a,c}

]^{a,c} (33-6-21)

Calculation of Core-Wide Oxidation Fraction

Table 33-6-5 presents a typical core-wide rod average oxidation fraction for large break LOCA (Bajorek et al., 1998). [

(33-6-22)

(33-6-23)

]^{a,c}

Rod Burst Consideration

[

]^{a,c}

[

(33-6-24)

(33-6-25)

]^{a,c} (33-6-26)

Conclusions

For best estimate small break LOCA analyses, compliance with the maximum core-wide oxidation fraction will be examined by the following procedure when the HOTSPOT-SB result exceeds 1800°F:

1. Using the same WCOBRA/TRAC-SB transient run selected for the maximum local oxidation

2. [

]^{a,c}

3. [

]^{a,c}

4. Comparing the result to the maximum core-wide oxidation limit of 1 percent in accordance with 10CFR50.46 acceptance criteria

If the result exceeds the limit, the following options are available:

- Select other WCOBRA/TRAC-SB transient(s), which are less severe yet still have $PCT > PCT^{95\%}$.

• []^{a,c}

• []^{a,c}

• []^{a,c}

Table 33-6-1
Typical Superposition Test Calculations, Indian Point Unit 2

] a,c

Table 33-6-2
Sample Output from HOTSPOT-SB

J^{a,c}

Table 33-6-3
Rod Power Distribution

Table 33-6-4
Local Oxidation Fraction for Rods Operating at Lower Power, Large Break LOCA

L

Table 33-6-5
Rod Average Oxidation Fraction for Rods Operating at Lower Power
(Large Break LOCA)

[
] ^{a,c}

L

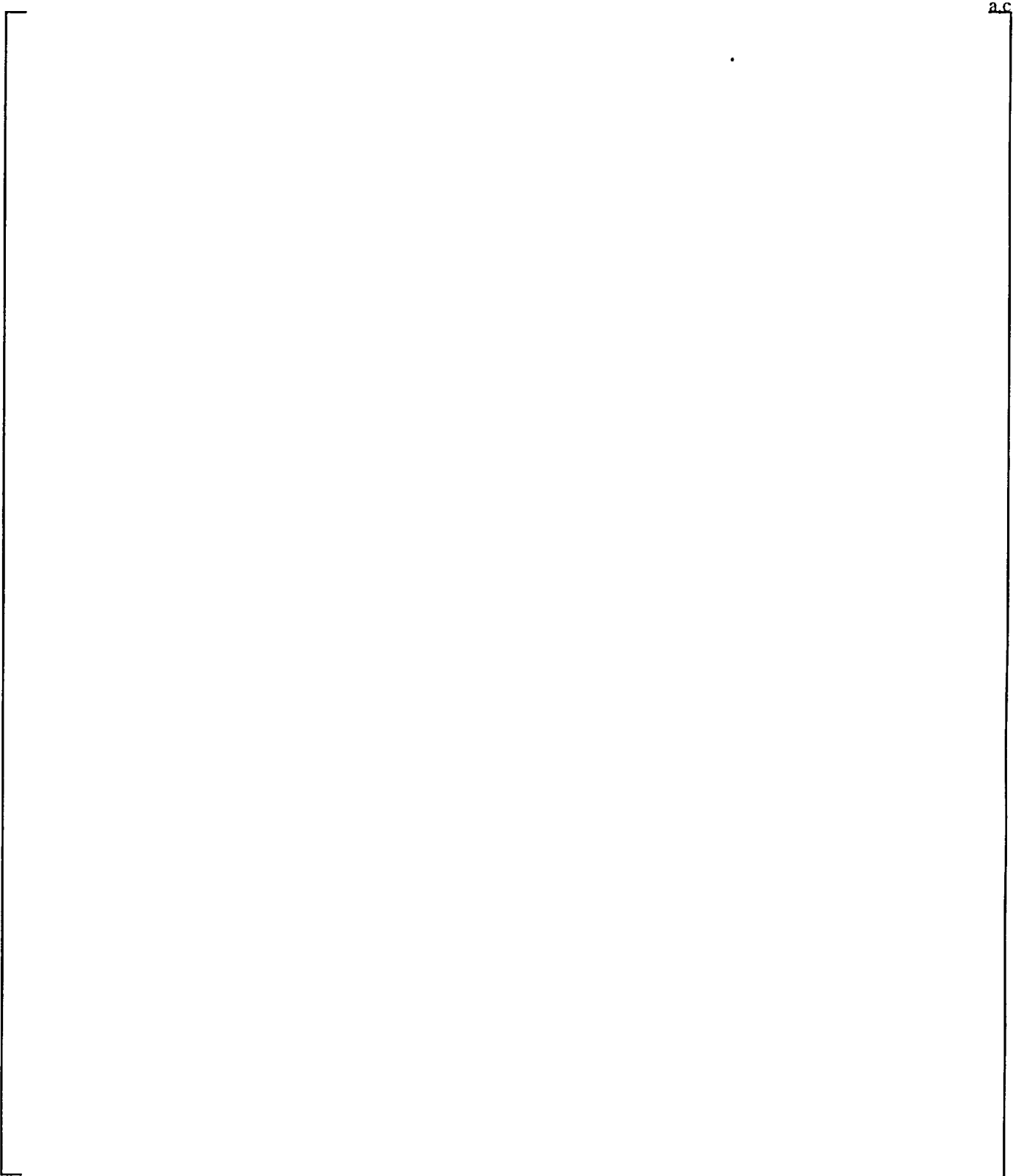


Figure 33-6-1. Superposition Prediction Compared to Calculated Results

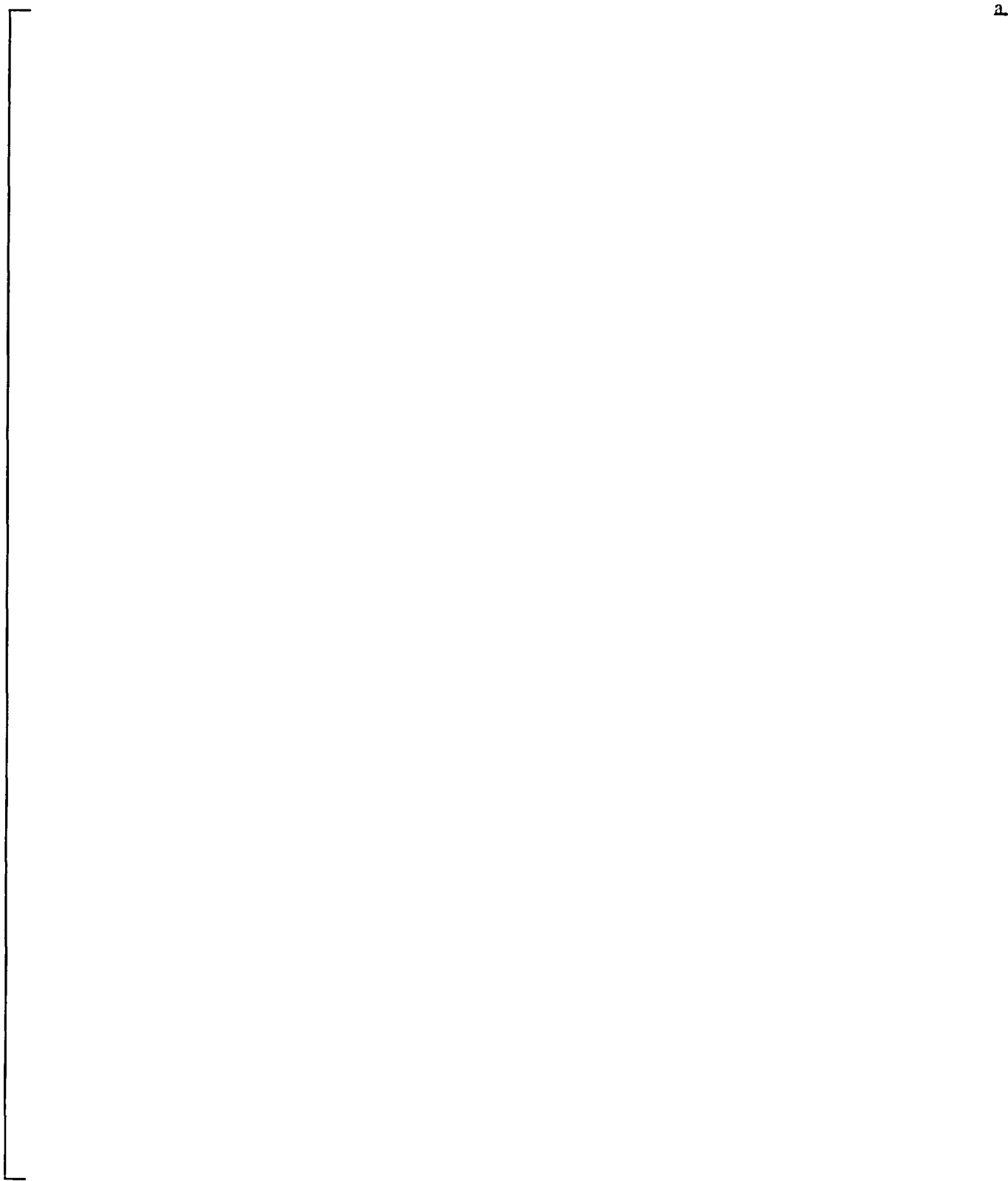


Figure 33-6-2. Final Superposition Result after Correction

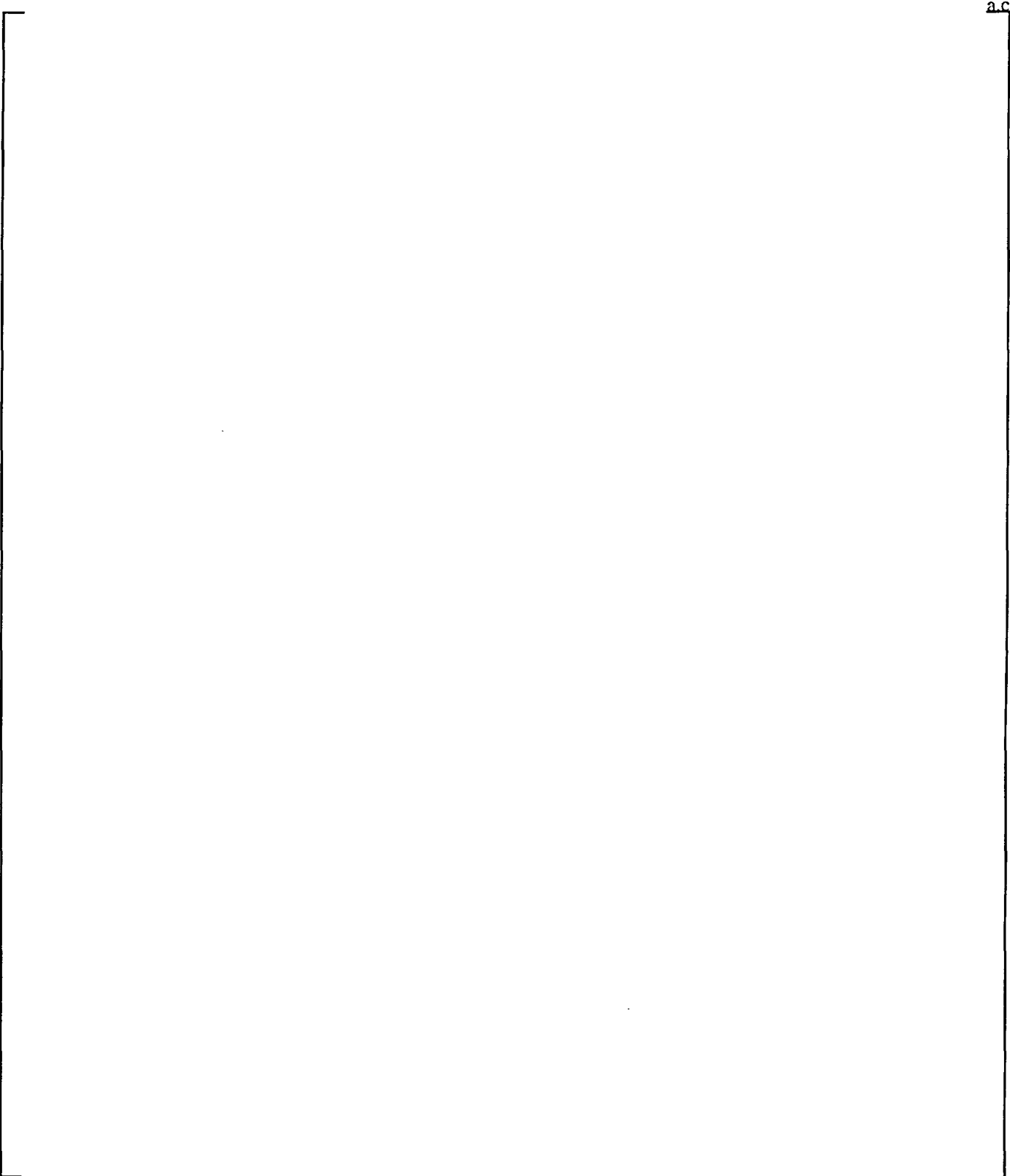


Figure 33-6-3. Flowchart of Uncertainty Determination Procedure

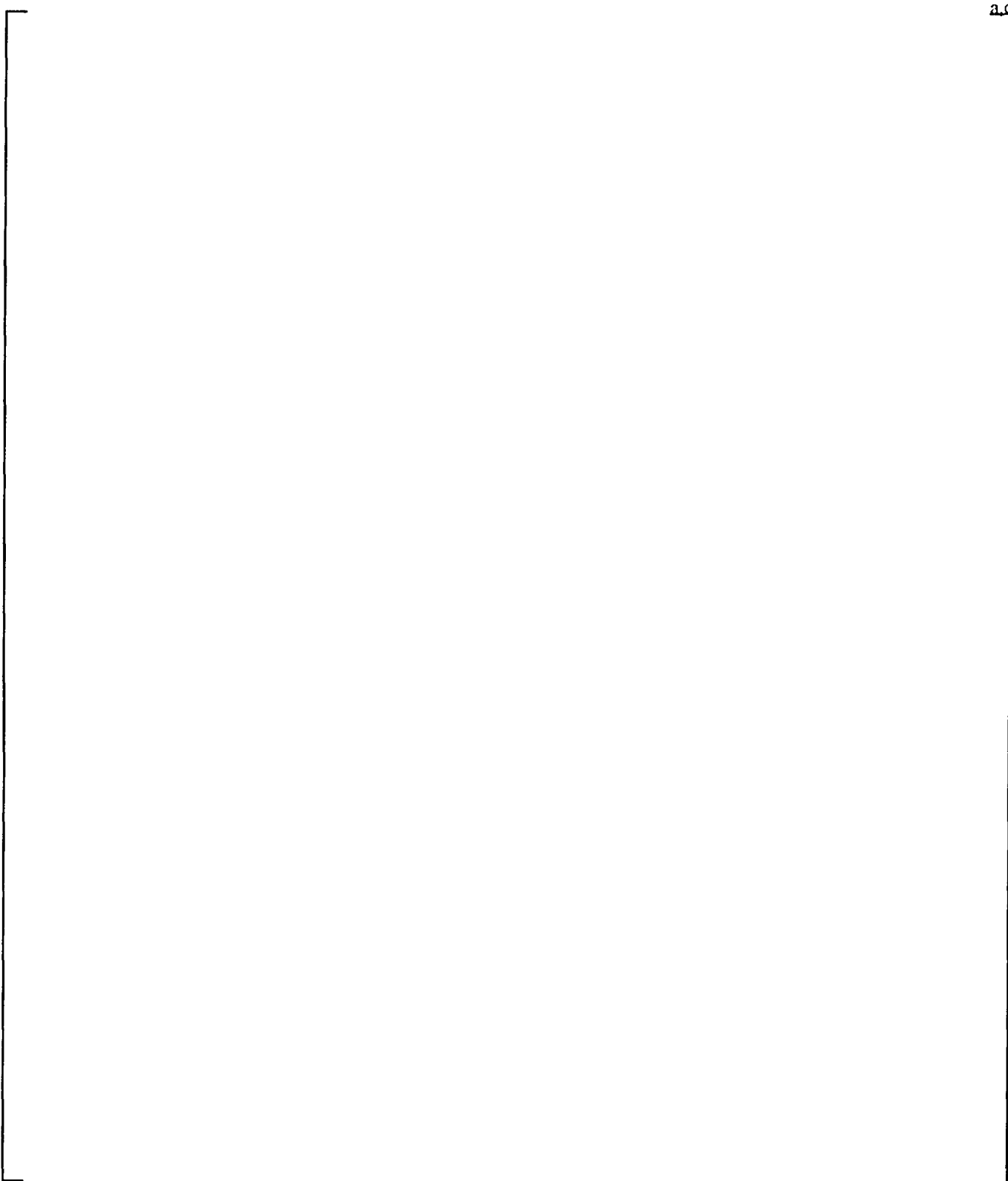


Figure 33-6-4. Comparison of Rod Power Census Envelope to Typical Core Design Data

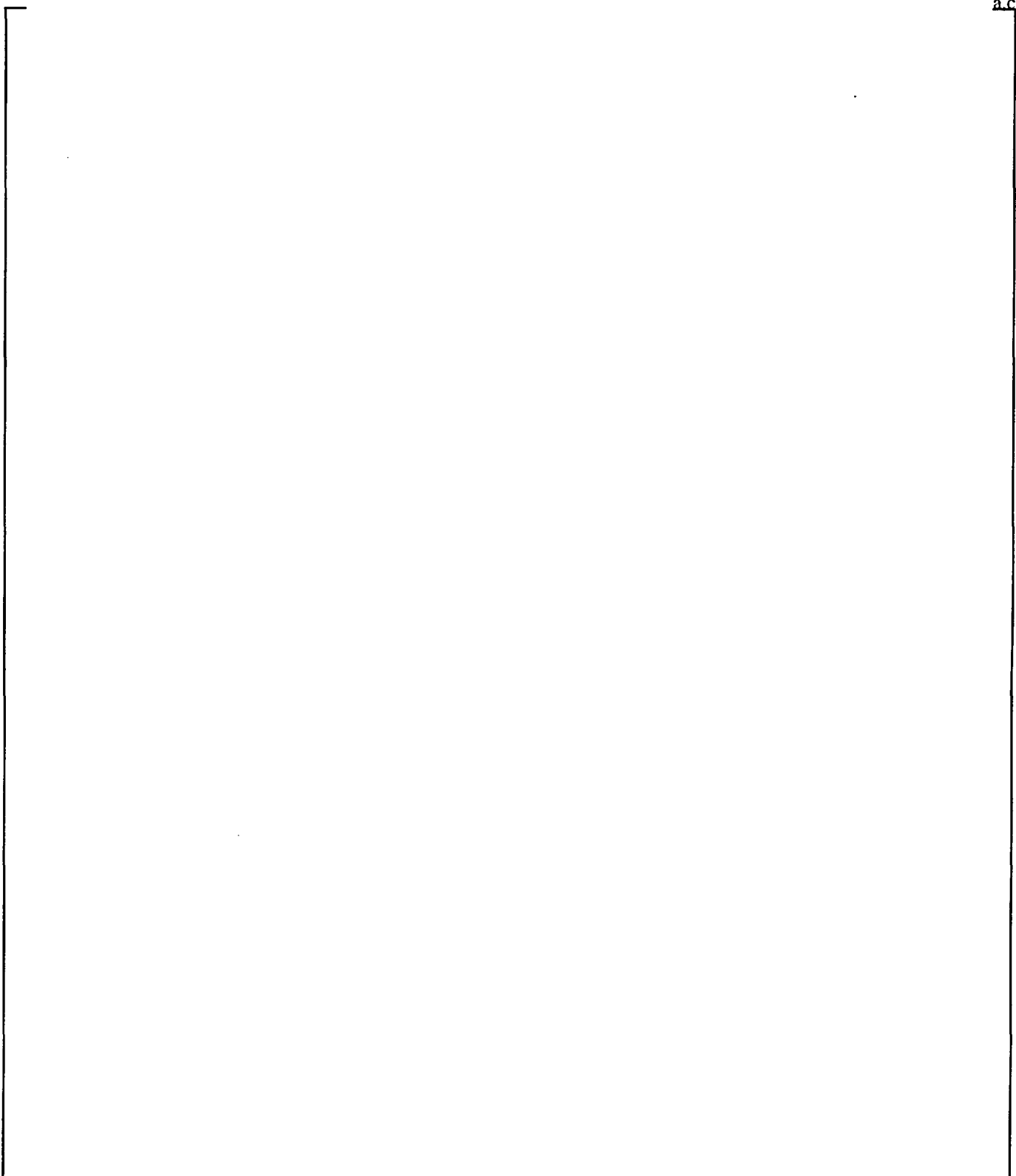


Figure 33-6-5. Local Average Oxidation Fraction for Lower Power Rods

3-7 References

ANSI/ANS 5.1-1979, 1978, "Decay Heat in Light Water Reactors," American Nuclear Society.

Bajorek, S. M., et al., 1998, "Code Qualification Document for Best Estimate LOCA Analysis Volume V: Quantification of Uncertainty," WCAP-12945-P-A, Vol. 5.

Shapiro, S. S., and Wilk, M. B., 1965, "An Analysis of Variance Test for Normality," Biometrika, 52, 3 and 4, pg 591.

SECTION 34

EXAMPLE PWR ANALYSIS

34-1 Introduction

In the following sections, the methodology described in Section 33 is implemented for an actual PWR to demonstrate the results produced by the methodology. The example is Indian Point Unit 2, which was also the plant used to develop the methodology.

34-2 Plant-Specific Results – Indian Point Unit 2

This section describes the results of the application of the best estimate small break LOCA methodology to Indian Point Unit 2, a four-loop Westinghouse plant with 15x15 fuel. The operating ranges and plant conditions outlined in these sections bound the planned operating range of the plant.

34-2-1 Reference Case Conditions

The best estimate methodology establishes changes in PCT due to changes in plant or model variables relative to a reference set of conditions (Section 33-3). The following paragraphs describe the assumptions in the key LOCA parameters for Indian Point Unit 2.

34-2-1-1 Plant Physical Description

- a) Dimensions: Nominal geometry is assumed. Nominal geometry input is accounted for in the data-based code uncertainty because experiments were also subject to thermal expansion and dimensional uncertainty effects. In addition, grid crushing due to seismic plus LOCA forces is not calculated to occur in the Indian Point Unit 2 core so the effect of distorted assembly geometry does not need to be analyzed.
- b) Flow Resistance: Best estimate values of loop flow resistance are assumed; no variations of the initial resistance are considered. [

]^{a,c}

- c) Pressurizer Location: The loop containing the pressurizer is assumed to be the broken loop; it was confirmed to be the limiting location in scoping studies presented in Section 28, Volume 3.
- d) Hot Assembly Location: The limiting location for the hot assembly identified in the WCOBRA/TRAC large break LOCA analysis is assumed. For Indian Point Unit 2, the hot assembly is located under a flow mixer (See Section 28).
- e) Hot Assembly Type: The hot assembly is a fresh reload assembly because it exhibits the highest linear heat rates and stored energy.
- f) SGTP Level: For the reference case, an SGTP level of 15 percent is assumed as the limiting value.

34-2-1-2 Plant Initial Operating Conditions

- Reactor Power
 - a) Initial Core Power: The core power assumed for the reference case is 100-percent power without measurement uncertainties. For the Indian Point Unit 2 analysis, the core power assumed (3216 MWt) is higher than the current licensed power, in anticipation of a future increase in licensed power. []^{a,c}
 - b) Hot Rod Peak Linear Heat Rate: The nominal hot rod peak linear heat rate is based []^{a,c}. Power shape 10 at that F_Q value (Figure 29-2-33, Section 29) is chosen as the reference case axial power distribution. Uncertainties in the peak linear heat rate due to transient variation and calculational uncertainties are accounted for in the local hot spot model uncertainty.
 - c) Hot Rod Average Linear Heat Rate: []^{a,c}

- d) Hot Assembly Average Linear Heat Rate: As also described in Section 33, the minimum difference between the power generated in the hot rod and that in the hot assembly average rod is conservatively assumed. Based on a study of current and anticipated fuel designs (discussed in Section 29), the hot assembly average rod is assumed to be []^{a,c} in power than the hot rod.
- e) Hot Assembly Peak Linear Heat Rate: Consistent with the average linear heat rates, the peaking factor used to calculate the peak linear heat rate generated in the hot assembly average rod is []^{a,c} than the value assumed in the hot rod.
- f) Axial Power Distribution: The power distribution represented by power shape 10 in Figure 29-2-33 (Section 29) is assumed for the reference case consistent with core design parameters *PBOT* and *PMID*. The Indian Point Unit 2 []^{a,c}.
- g) Low Power Region Relative Power (*PLOW*): Current and expected core designs for Indian Point Unit 2 result in a range of *PLOW* from 0.4 to 0.8. A *PLOW* of 0.4 is used in the reference case to obtain a high rod power level in the core average channels.
- h) Hot Assembly Burnup: BOL conditions in the hot assembly are assumed in the reference case. The fuel average temperatures for the hot rod and hot assembly rod are assumed to be at best estimate values for this burnup condition. Uncertainties in fuel temperature are accounted for in the local models uncertainty.
- i) Prior Operating History: The power distribution assumed to exist at the time of the LOCA is conservatively assumed to have existed since plant startup when determining fission product inventories.
- j) MTC: The maximum value specified in the Technical Specifications is assumed to conservatively estimate core reactivity and fission power.
- k) HFP Boron Concentration: A value typical of those used in current core designs at BOL conditions is assumed.

- Fluid Conditions

- a) Average Fluid Temperature (T_{avg}): The maximum expected value during normal full power operation, at the reference case SGTP level, is used for Indian Point Unit 2.

In future applications of this methodology to other plants, the nominal value will be used with sensitivity studies performed above and below the nominal value (Section 33). If a plant includes an operating window (that is, a range of normal operating temperatures), the limiting normal operating point will be identified through sensitivity studies.

The effect of uncertainties in this parameter is accounted for in the initial condition uncertainty.

- b) Pressurizer Pressure: The maximum expected value, including uncertainties (60 psia), is assumed for Indian Point Unit 2.
- c) Loop Flowrate: Nominal loop flow is assumed. Uncertainties in this value are not considered because the RCPs are tripped well in advance of the cladding temperature excursion during a small break LOCA.
- d) Upper Head Fluid Temperature (T_{uh}): The appropriate best estimate value of T_{uh} for the given T_{avg} value is assumed. Because variation in this parameter is quite small, uncertainties are not included.
- e) Pressurizer Level: The nominal value of pressurizer level is assumed. Because the pressurizer level is automatically controlled, as discussed in Section 30-2, uncertainties are small and not included.
- f) Accumulator Water Temperature: A nominal (midpoint) value within the range established for Indian Point Unit 2 is assumed with variations treated in the initial condition uncertainty.
- g) Accumulator Pressure: A nominal (midpoint) value of accumulator pressure is assumed with variations in pressure included in the initial condition uncertainty.

- h) Accumulator Water Volume: A nominal (midpoint) value of accumulator water volume is assumed with variations in volume included in the initial condition uncertainty.
- i) Accumulator Line Resistance (fL/D): A best estimate value of accumulator line frictional resistance is assumed.
- j) Accumulator Boron Concentration: The Technical Specification minimum value is assumed.

34-2-1-3 Accident Boundary Conditions

- a) Break Location: A break at the location where the SI delivery line enters the cold leg is assumed. Scoping studies have confirmed that the cold leg remains the limiting location for small break LOCA events.
- b) Break Type: Variations in break orientation (top, middle, and bottom) around the pipe perimeter at the limiting location are investigated, and the limiting position is selected. A break at the top of the cold leg of an SI delivery line is the limiting case.
- c) Break Size: A spectrum of areas is assumed for the cold leg break location, and the limiting size is used (Section 27, Volume 3). Variations in break size and in the critical flow model are, therefore, accounted for in a conservative way.
- d) Offsite Power: LOOP, consistent with the limiting case from the scoping results, is assumed.
- e) SI Flow: Minimum SI flow is assumed and is calculated using methods consistent with those currently used for Appendix K analysis. The scoping studies indicate that increased SI flow reduces PCT; this parameter is, therefore, bounded.
- f) TSI: Nominal (midpoint) values are assumed. Variations in TSI are accounted for in the initial condition uncertainty.

- g) SI Delay: Maximum values consistent with the limiting offsite power assumption are used.
- h) Containment Pressure: A value of 14.7 psia is used.
- i) Single Failure Assumption: The loss of a safety train (that is, the loss of an HHSI pump and an auxiliary feedwater pump) is assumed for the determination of pumped flowrates during the LOCA.

In future plant analyses, sensitivity studies may be performed to evaluate a less conservative set of assumptions.

- j) Rod Drop Time: Consistent with the current design basis for this plant, control rods are assumed to drop over a 2.4-second time interval during the small break LOCA.
- k) Steam Generator Secondary Safety Valve Setpoint: Nominal values are assumed. Variations are accounted for in the initial condition uncertainty. Indian Point Unit 2 is equipped with steam generator atmospheric relief valves, and they are modelled together with the main steam safety valves in WCOBRA/TRAC-SB.
- l) Auxiliary Feedwater Flow: Minimum values consistent with the limiting offsite power assumption are used.

34-2-2 Plant Operating Range

The PCT and its uncertainty developed by the best estimate methodology is valid for a range of plant operating conditions. Several parameters in the reference calculation are at nominal values. The range of variation of the operating parameters is accounted for in the uncertainty analysis by ensuring that in the Monte Carlo analysis the operating range is bounded.

Table 34-2-1 summarizes the value that the key LOCA parameters have in the reference case for Indian Point Unit 2. This case defines the reference nominal hot rod PCT ($NPCT_{000}$) used as the starting point in the Monte Carlo analysis as described in Section 33. The plant operating range limits over which the uncertainty evaluation is to be performed are also shown. The estimate of the PCT at 95-percent probability is considered to be valid over this range.

Table 34-2-2 presents the reference value of the plant variable, the nominal or midpoint operating value, and the operating range for the initial condition parameters. The power distribution variables are also shown for completeness. [

]^{a,c}

34-2-3 Confirmation of Reference Case Limiting Assumptions

Table 33-4-1, Section 33, indicates that several of the reference conditions are set to limiting values as verified on a plant-specific basis. For Indian Point Unit 2, the reference case assumptions were confirmed via calculations performed with WCOBRA/TRAC-SB investigating parameters such as the LOOP assumption and the SGTP level. The results are shown in Table 34-2-3. The assumptions used in the reference case shown in Table 34-2-3 were confirmed to be limiting.

34-2-4 Reference Case Results

Figures 34-2-1 to 34-2-5 show results from the reference case (3-inch cold leg break at the top of the pressurizer loop pipe, LOOP) calculated using WCOBRA/TRAC-SB. The x-axis of each of these figures is time in seconds. Figure 34-2-1 shows the nominal hot rod PCT. Figure 34-2-2 shows the cladding temperature elevation. When the core uncovers following loop seal clearance, the PCT transient begins at 1370 seconds. Core pressure (Figure 34-2-3) diminishes until it reaches 655 psia shortly after 1900 seconds and accumulator injection begins. This marks the end of heatup; refilling of the core (Figure 34-2-4) with accumulator water causes the overall core collapsed liquid level (solid line) and the hot assembly collapsed liquid level (dashed line) to increase, and the increase in heat transfer from the cladding to the core mixture allows the cladding to be significantly cooled and to quench. Figure 34-2-5 shows that the downcomer mass continues to increase once accumulator injection begins. Although a second reflood heatup may occur in some cases due to the fuel heat release causing accumulator injection to temporarily stop, in general this is not expected and does not occur for Indian Point Unit 2.

34-2-5 Initial Condition Uncertainty

The purpose of this uncertainty element is to capture the effect of variations in plant initial conditions (group ι in Table 33-2-3, Section 33).

Table 34-2-4 lists the PCT sensitivities for use in this uncertainty element to changes in plant variables based on sensitivity studies performed for Indian Point Unit 2. [

]^{a,c}

Using the information in Tables 34-2-3 and 34-2-4 and applying the methodology as described in Section 33-5-2-1, the results shown in Table 34-2-5 are obtained for the initial condition bias (η_{IC}) and uncertainty (σ_{IC}) for the Indian Point Unit 2 small break LOCA PCT.

34-2-6 Global Model Results

This step quantifies the effect on PCT of variations in the global model variables CD and $CYDG$ (listed in group β of Table 33-2-3, Section 33. The run matrix developed in Table 33-5-2, Section 33, was performed for Indian Point Unit 2 using WCOBRA/TRAC-SB. The reference case is run 09. [

]^{a,c}

Figures 34-2-6 through 34-2-9 plot the PCT results of cases involving variations in both *CD* and *CYDG* from their reference case values of 1.0 and 0.8 with the remaining conditions held constant. The x-axis in each of these figures is time in seconds. In each of these figures, the reference case is the solid line. [

]^{a,c}

Figures 34-2-8 and 34-2-9 plot the effect of variations in *CYDG* with *CD* reduced to 0.7. Increasing or decreasing the *CYDG* value has little impact on PCT at this *CD* value.

[

]^{a,c}

34-2-7 Local Model (Hot Spot) Results

The objective of these calculations is to quantify the effect on PCT of variations in local models listed as group γ in Table 33-2-3, Section 33. In contrast to the effect of plant conditions and global models, parametric variations and/or response surface fitting are not performed in the local model step. Instead, a direct Monte Carlo is performed using the HOTSPOT-SB computer code, which generates local variable uncertainty distribution for specific WCOBRA/TRAC-SB runs, as illustrated in Figure 33-2-5, Section 33. The information used to generate files of local fluid and power conditions from the WCOBRA/TRAC-SB run is described in Section 33-6-2-1, step 2; HOTSPOT-SB calculations are then performed. Output from HOTSPOT-SB for a global model matrix case is shown in Table 34-2-6. This output indicates that [

]^{a,c}

The best way to examine the effect of uncertainties of the local models is to plot, for a sample of the Monte Carlo trials, the calculated PCT versus the value of the random variable describing each model. If a strong correlation exists between the model variation and the PCT, there should be a discernable trend in the data points. [

]^{a,c}

34-2-8 Global Model Response Surface Results

The next step (Section 33-6-2-1, step 4) is to derive response surfaces which describe the difference between the hot spot PCT distribution average and the reference base case ($X_{0\beta}$) and the corresponding standard deviation ($\sigma_{0\beta}$). The data needed to develop these response surfaces are generated following the steps outlined in Section 33-6-2-1, step 4.

34-2-9 Local Model Effects for Plant Variations

[

]^{a,c}

Table 34-2-1

]a,c

Table 34-2-1 (Cont'd)
Reference Values and Plant Operating Range - Indian Point Unit 2

J^{a,c}

Table 34-2-1 (Cont'd)

Table 34-2-2
Reference Case, Nominal, and Range Values
for Plant Initial Operating Conditions

] a,c

Table 34-2-3
Reference Case Confirmatory Studies

Case	Assumption	Result (Change in PCT From Reference Value)
Offsite power availability	Reference: LOOP	
	OPA (RCPs operate until operator trips them)	-200°F
SGTP ⁽¹⁾	Reference: 15%	
	25%	-250°F

1. The scoping studies in Section 28, Volume 3, using WCOBRA/TRAC-SB showed that increasing SGTP to 25 percent resulted in a large reduction in PCT. As indicated in that section, the interactions among competing reactor coolant loops during loop seal clearance led to the clearing of two loop seals at the 25-percent SGTP level. No overriding phenomenon that led to this result could be established, and the behavior observed at 25-percent SGTP was characterized as a code uncertainty that leads to a large PCT effect for Indian Point Unit 2.

Table 34-2-4
Initial Condition Sensitivity Data for Indian Point Unit 2⁽¹⁾

1a,c

Table 34-2-5
Initial Condition Bias and Uncertainty
Indian Point Unit 2

[

]^{a,c}

Table 34-2-6
Typical HOTSPOT-SB Output for Core Boiloff Uncovery PCT

[

]^{a,c}

Table 34-2-7
Hot Spot Lookup Table

[
] ^{a,c}

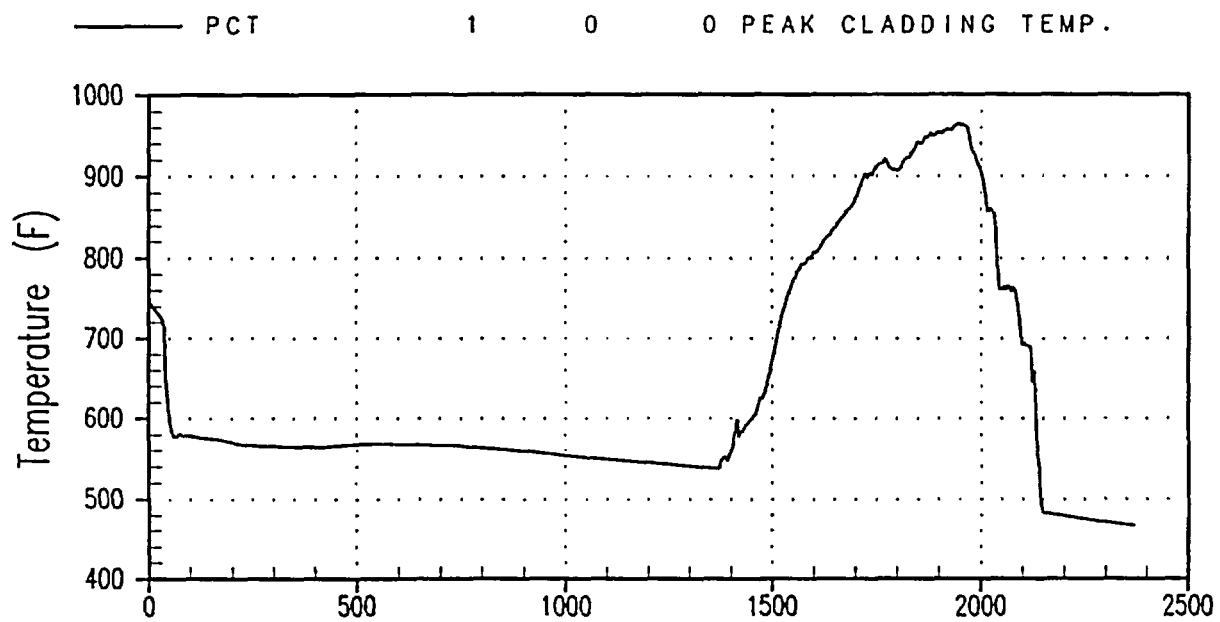


Figure 34-2-1. Nominal Hot Rod PCT

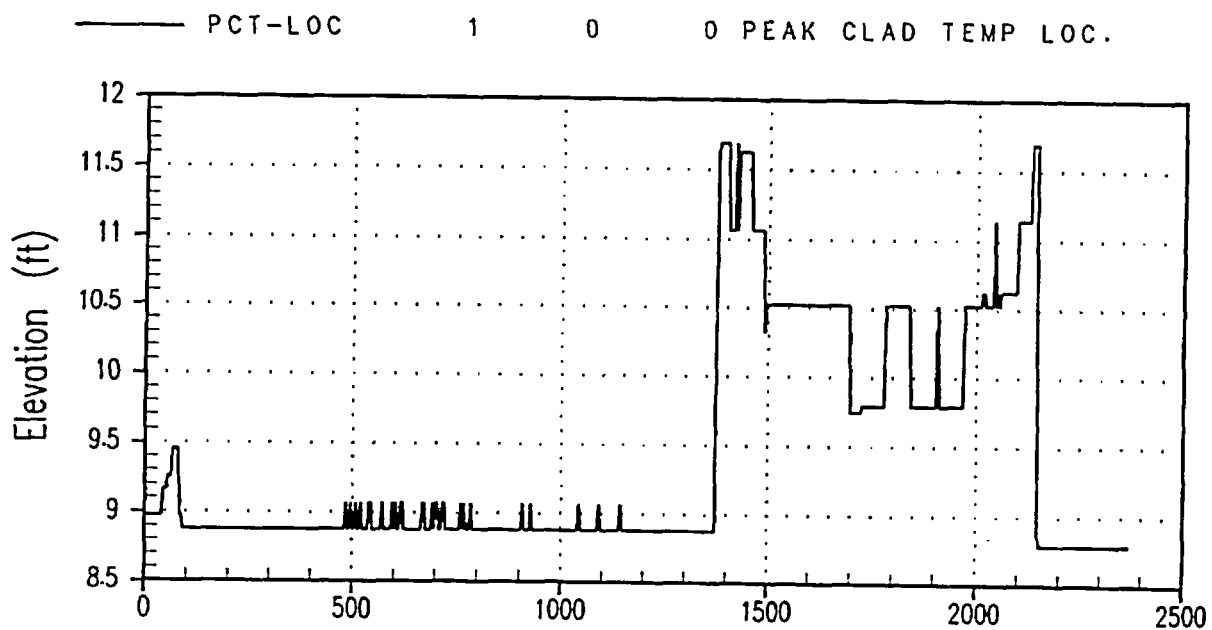


Figure 34-2-2. Nominal Hot Rod PCT Elevation

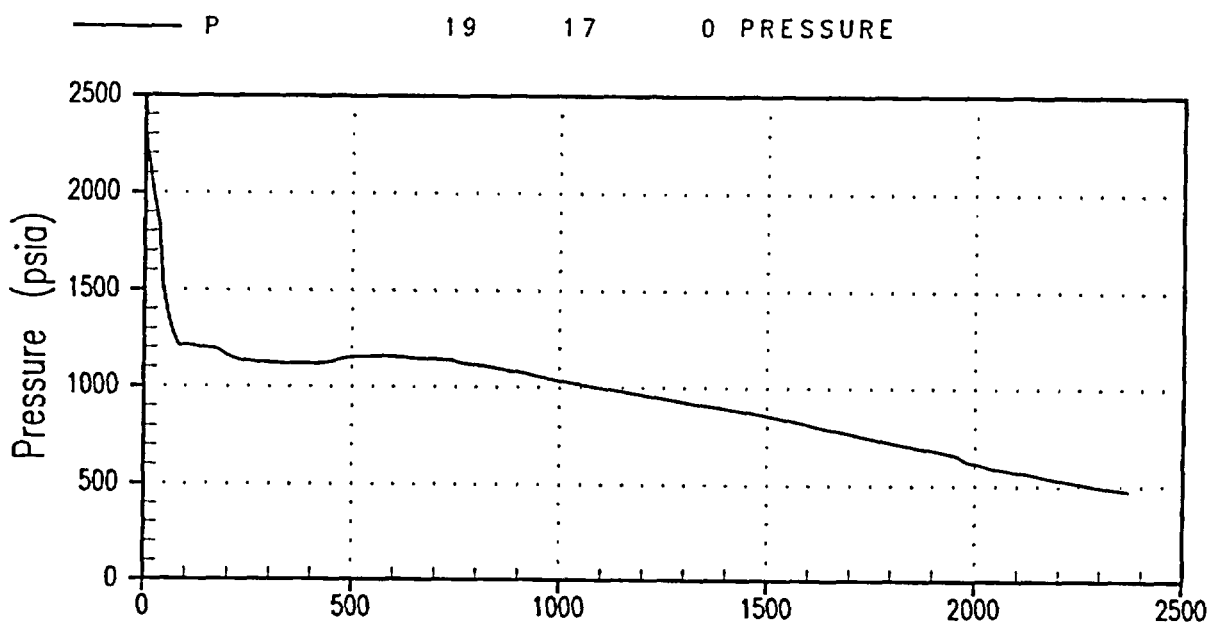


Figure 34-2-3. Core Pressure, 3-Inch Break Reference Case

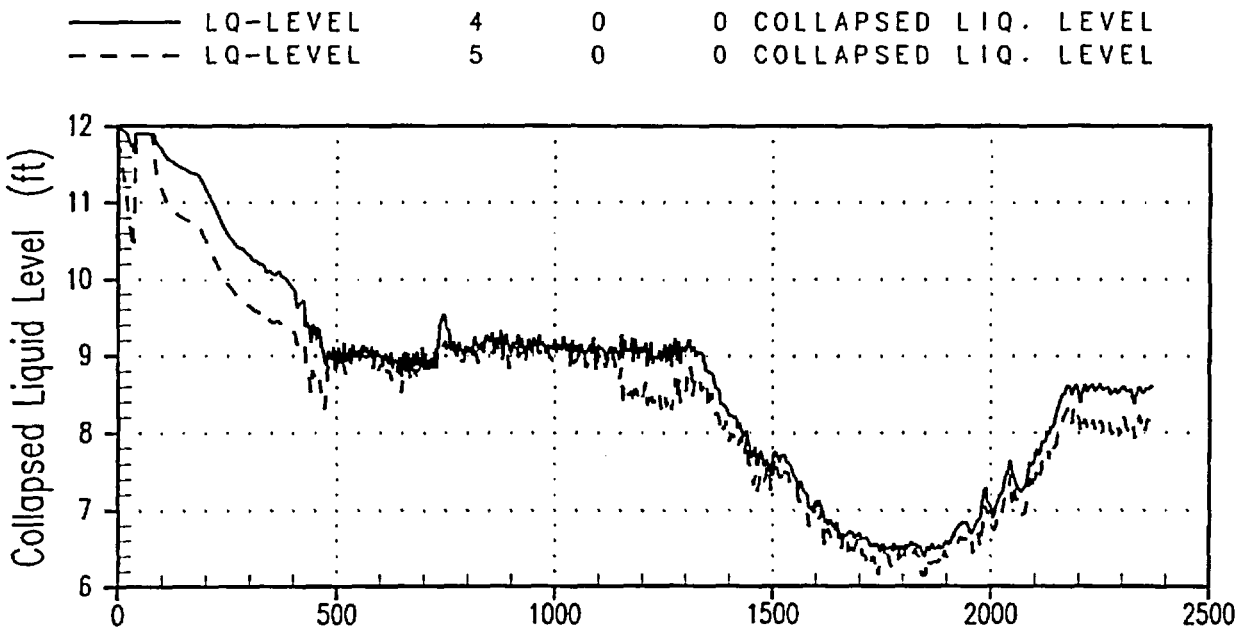


Figure 34-2-4. Core Collapsed Liquid Level, 3-Inch Break Reference Case

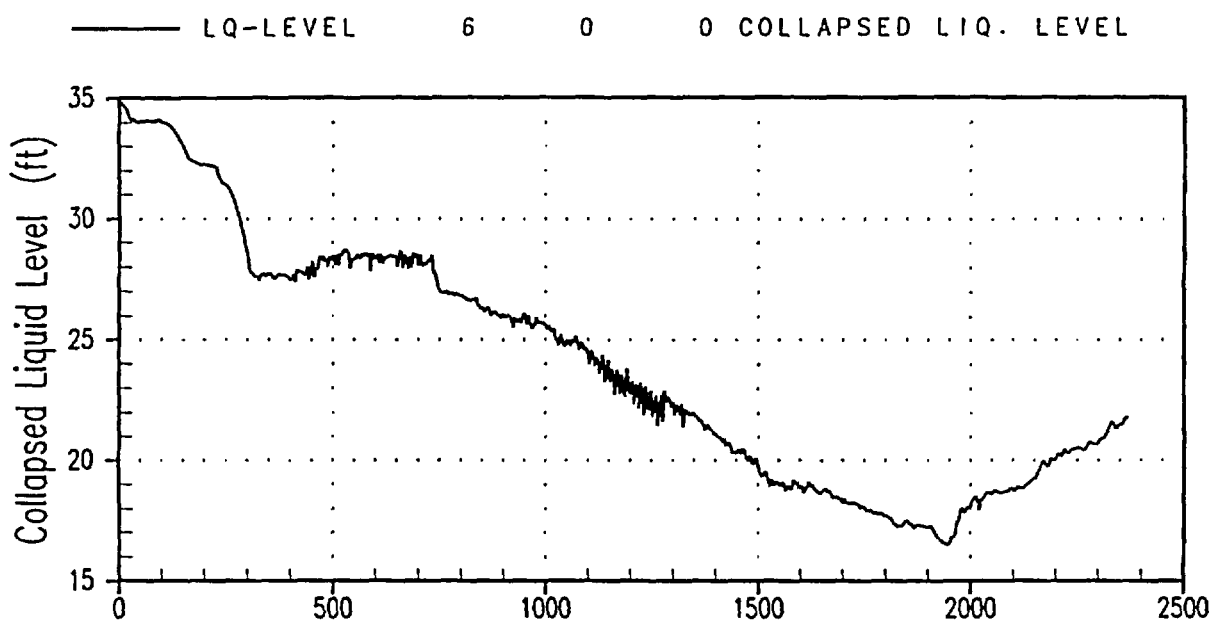


Figure 34-2-5. Downcomer Collapsed Liquid Level, 3-Inch Break Reference Case

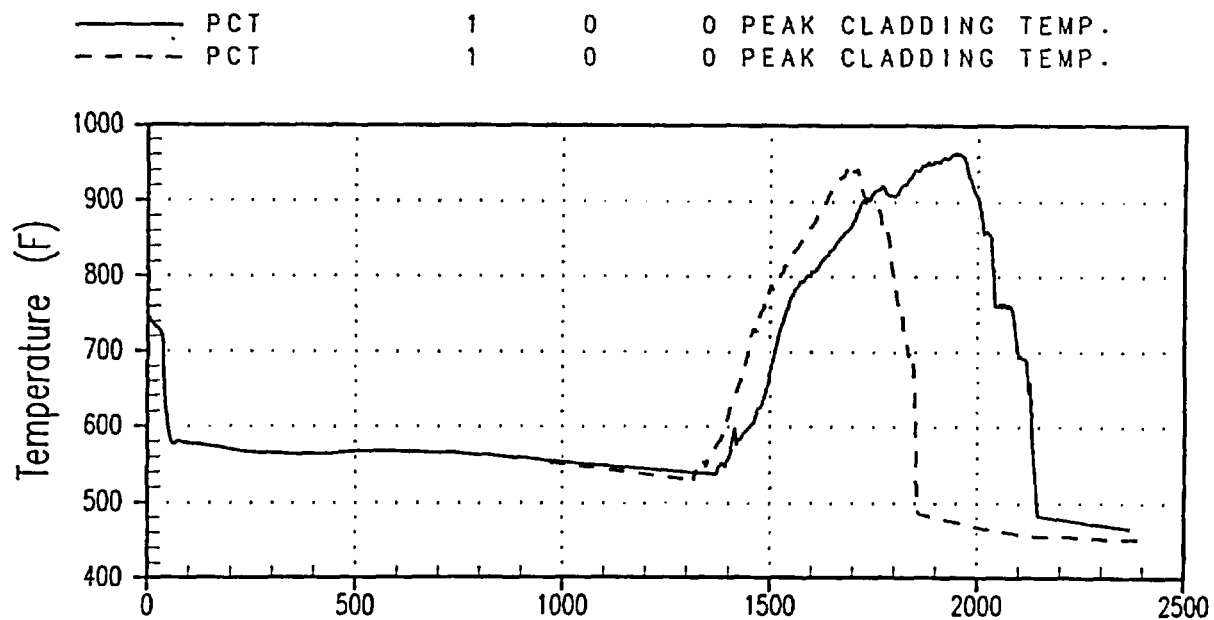


Figure 34-2-6. PCT Effect of Varying CYDG with CD = 1.15 (CYDG = 1.0)

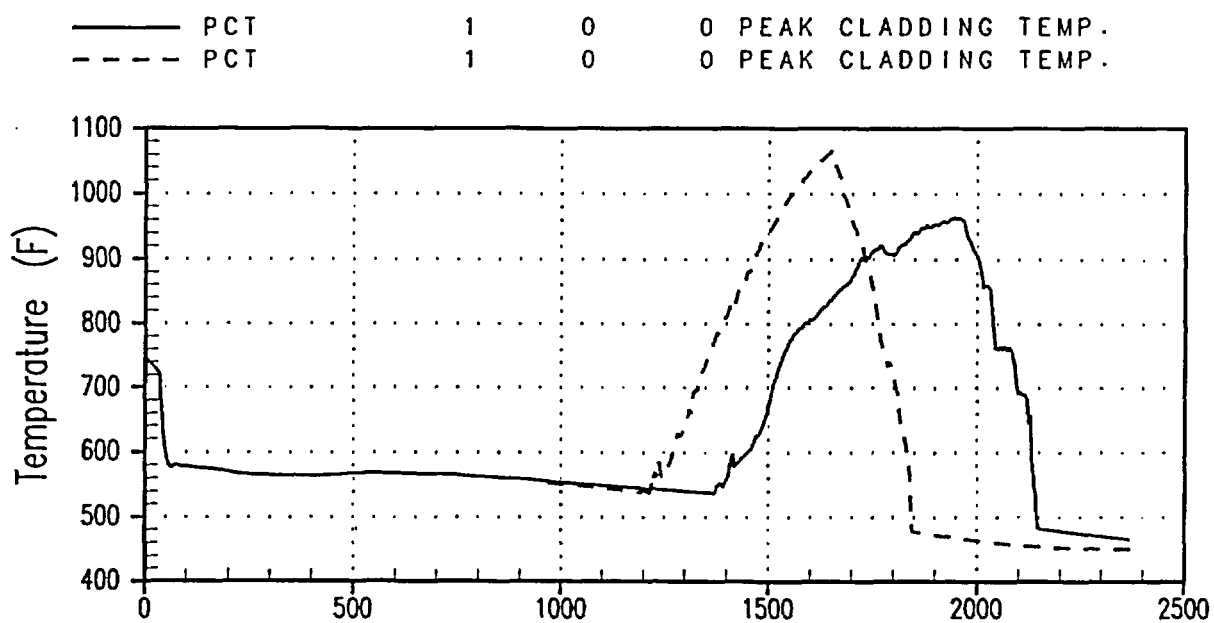


Figure 34-2-7. PCT Effect of Varying $CYDG$ with $CD = 1.15$ ($CYDG = 0.4$)

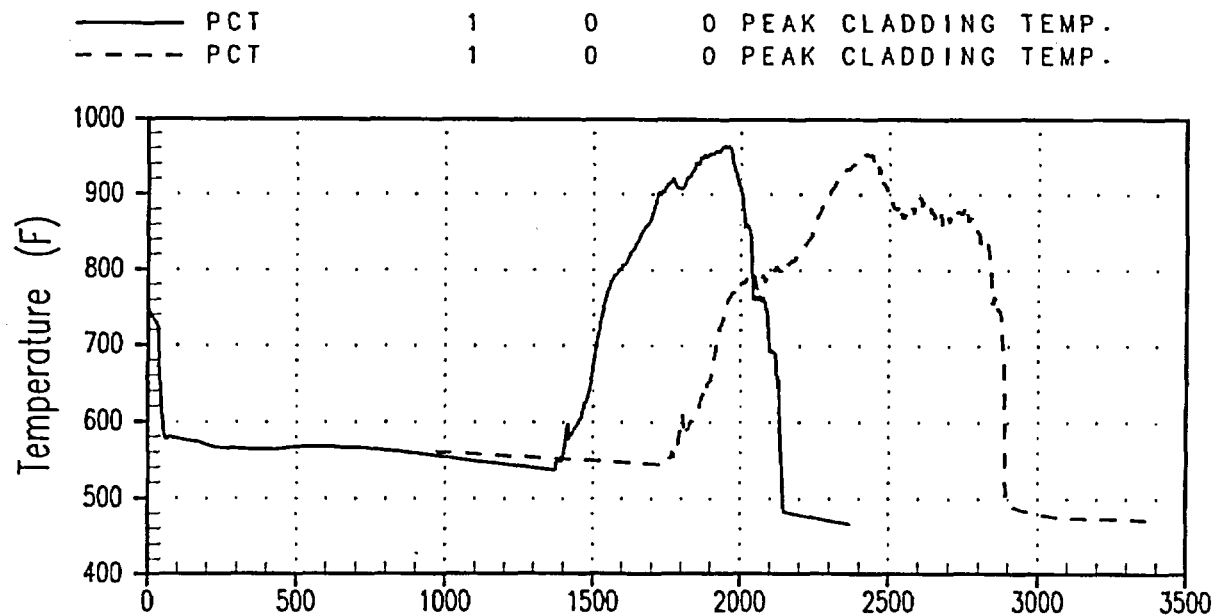


Figure 34-2-8. PCT Effect of Varying $CYDG$ with $CD = 0.7$ ($CYDG = 1.0$)

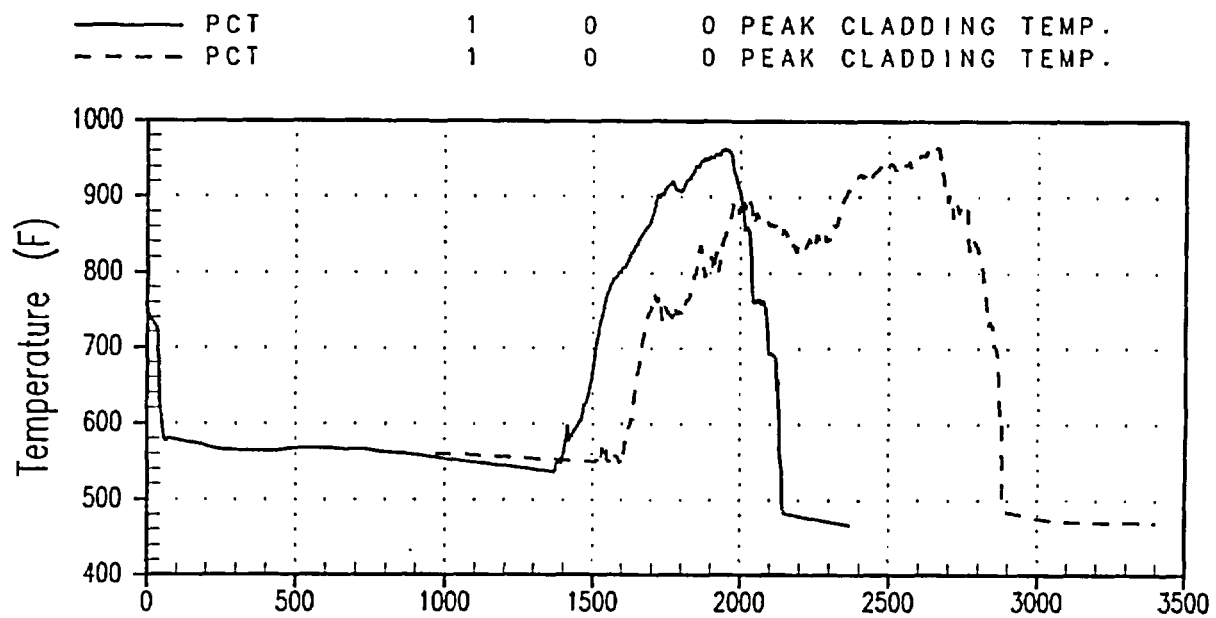


Figure 34-2-9. PCT Effect of Varying CYDG with CD = 0.7 (CYDG = 0.4)

34.3 Assessment of Total Uncertainty – Indian Point Unit 2

As previously discussed in Sections 27 and 28 (Volume 3), the loop seal steam venting behavior plays an important role in all cold leg small break LOCA transients that are large enough to deplete the RCS inventory to the point of yielding predominantly steam break flow. Depending on plant characteristics, the threshold break size for clearing multiple loop seals to vent steam to the break location may vary. For Indian Point Unit 2 this threshold size is the 3-inch equivalent diameter break; there is significant uncertainty as to which loop seal(s) will initially pass steam to the break location for this break size. [

]^{a,c}

The data generated in the previous section are used to assess total uncertainty in the final phase of the analysis. These steps are described in detail in Section 33-6-2-3 and are summarized below.

A series of [

]^{a,c} These runs will analyze variations in parameters from several of the uncertainty components and will be used to quantify the bias and uncertainty resulting from the superposition assumption (that is, the assumption that the major uncertainty components are independent). HOTSPOT-SB runs will be made for each of these WCOBRA/TRAC-SB calculations.

In the last step (Final MONTEC), the Monte Carlo simulation is repeated and includes the bias and uncertainty resulting from superposition corrections or the code uncertainty determined from data comparisons. The 95th percentile PCT from this PCT uncertainty distribution is considered to be the licensing basis PCT.

For Indian Point Unit 2, [

]^{a,c}

The final PCT uncertainty results are shown in Table 34-3-1.

The first section of the table provides the magnitude of the major contributors to uncertainty. The bias is expressed in terms of the average difference from the reference PCT. The average PCT change due to initial conditions is not a large contributor, as previously indicated.

[

]^{a,c}

A correction is then applied to the hot spot average PCT along with an additional uncertainty based on the estimated accuracy with which WCOBRA/TRAC-SB is able to predict [

]^{a,c}. Finally, the local hot spot PCT relative to the average is a measure of the average spread of individual hot rods around their average. The distribution is assumed to be symmetrical around *HPCT*, so the average is near zero, and is the result of uncertainty in local variables such as HTC and fuel relocation. The correction also increases this value according to Equation 32-2-14, Section 32.

The final uncertainty distribution PCT results are given in Table 34-3-2. This table lists the average PCT, its standard deviation, the 50th percentile (50 percent of all trials resulted in a PCT less than this value), and the 95th percentile (95 percent of all trials resulted in a PCT less than this value). The PCT at the 95-percent probability level is compared with the regulatory limit of 2200°F. Therefore, the new licensing basis PCT of 1328°F for Indian Point Unit 2, based on the limiting cold leg 3-inch equivalent diameter break, exhibits margin to the limit.

Table 34-3-1

]^{a,c}

Table 34-3-2
Monte Carlo Results for Indian Point Unit 2 PCT

Item	Temperature (°F)
[
] ^{a,c}

丁

丁

丁

SECTION 35

METHODOLOGY SUMMARY AND CONCLUSION

35-1 Introduction

In this section, the best estimate LOCA methodology, as described in this document, is compared against applicable regulatory criteria. In addition, modifications in associated analyses that use output from the LOCA analyses are discussed, as is the approach to plant and evaluation model changes.

35-2 Compliance with 10CFR50.46

This section identifies how the best estimate small break LOCA methodology described in this document and the Indian Point Unit 2 analysis comply with the Final Acceptance Criteria. The text in italics is from 10CFR50.46.

(a)(1)(I)

This section briefly outlines the requirements for an acceptable evaluation model and requires that demonstration be provided to show that the limits of 10CFR50.46 will be met with a high degree of probability. Additional details concerning these requirements are spelled out in Regulatory Guide 1.157 (USNRC, 1989). Compliance of the best estimate methodology with these requirements is addressed in detail in the next section.

(b)(1) Peak Cladding Temperature

The PCT at 95-percent probability is demonstrated, using the procedure described in Section 33-6-2, to remain below the limit of 2200°F for all small break LOCAs.

(2) Maximum Cladding Oxidation

The maximum cladding oxidation is verified, using the procedure described in Section 33-6-3-1, to remain below the regulatory limit of 17 percent of cladding thickness.

(3) Maximum Hydrogen Generation

The hydrogen generated in the core, as determined by estimating the total volume of cladding oxidized for the limiting conditions, is verified, using the procedure described in Section 33-6-3-2, to be less than the regulatory limit of 0.01 times the maximum theoretical amount.

(4) Coolable Geometry

Westinghouse reload cores are analyzed using plant-specific or bounding seismic and LOCA loads to confirm that the core remains coolable during the LOCA.

(5) Long-Term Cooling

Long-term cooling is dependent on the demonstration of continued delivery of cooling water to the core. The actions, automatic or manual, currently in place at these plants to maintain long-term cooling, remain unchanged.

35-3 Compliance with Regulatory Guide 1.157

This section identifies how the Westinghouse best estimate small break LOCA methodology complies with Regulatory Guide 1.157 (USNRC, 1989). Each item addresses an individual regulatory position from Regulatory Guide 1.157. The text in italics is from Regulatory Guide 1.157. Compliance assessment references are identified by numbers in parentheses and are listed at the end of each compliance assessment section as applicable. All other references are listed in Section 35-5.

REGULATORY POSITION: 1. BEST-ESTIMATE CALCULATIONS

The WCOBRA/TRAC-SB computer code used by Westinghouse for best estimate small break LOCA calculations is an improved version of the COBRA/TRAC code⁽¹⁾ originally developed and assessed by the NRC and its contractor as part of the NRC's best-estimate transient code development program. The models present in the WCOBRA/TRAC code version⁽²⁾ approved for best estimate large break LOCA analysis have been extended as necessary to enable the small break LOCA version to provide realistic calculations of phenomena important to the behavior of a PWR during a small break LOCA transient. These models have been assessed using

comparisons of code predictions with approximately 100 experiments in a number of separate-effects and integral-effects test facilities. These assessments have been supplemented in some cases by comparisons with other available models. The applicability of the WCOBRA/TRAC-SB models over the range of conditions expected during a PWR small break LOCA transient has been demonstrated by the use of a code validation matrix which covers, to the extent practical, those ranges of conditions.

Comparisons of WCOBRA/TRAC-SB calculations with data obtained from separate-effects and integral-effects tests have been used to determine the overall uncertainty and biases of the calculation, as recommended in Regulatory Position 1. The test simulations were also used to verify that important phenomena (for example, loop seal clearance and horizontal flow phenomena) are adequately predicted.

In some cases, the models used in WCOBRA/TRAC-SB include simplifications when a more detailed treatment is not warranted for small break LOCA calculations (for example,

[]^{a,c}). Assessment of model predictions of experimental data has indicated that the models intended to be best estimate perform effectively. The simplifications, conservatisms, and deficiencies of the WCOBRA/TRAC-SB computer code have been corrected, accounted for in the uncertainty analysis, or determined not to result in unrealistic calculations of important phenomena, as presented in Section 32.

References for Regulatory Position 1 Compliance Discussion

- (1) Thurgood, M. J., et al., 1983, "COBRA/TRAC - A Thermal-Hydraulics Code for Transient Analysis of Nuclear Reactor Vessels and Primary Coolant Systems," Vol. 1, PNL-4385, NUREG/CR-3046.
- (2) NRC letter to Westinghouse, "Acceptance for Referencing of the Topical Report, WCAP-12945(P), Westinghouse Code Qualification Document for Best-Estimate Loss-of-Coolant Analysis," June 28, 1996.

REGULATORY POSITION: 2. CONSIDERATIONS FOR THERMAL-HYDRAULIC
BEST-ESTIMATE CODES

2.1 Basic Structure of Codes

2.1.1 Numerical Methods

The overall numerical scheme used in WCOBRA/TRAC-SB is unchanged from that used in the best estimate COBRA/TRAC code originally developed and assessed by the NRC and its contractor. Westinghouse performed a substantial number of timestep and noding convergence studies, as described in Section 32, to finalize acceptable values for these parameters. Noding used for code validation against experimental data, and noding used for PWR calculations, were kept consistent to the extent practical to minimize the uncertainty introduced by noding. Nodalization studies of the ROSA integral-effects test facility were performed, and the variation in calculated results was included in the overall code uncertainty assessment.

2.1.2 Computational Models

WCOBRA/TRAC uses a two-fluid, three-field representation of flow in the vessel component.⁽¹⁾ The three fields are a vapor field, a continuous liquid field, and an entrained liquid drop field. Each field in the vessel uses a set of 3-D continuity, momentum, and energy equations, except that a single energy equation is used for the continuous liquid and entrained liquid drop fields.

[

]^{a,c}

[]^{a,c} are modelled using 1-D components. These components use a two-phase, five-equation drift flux formulation, which consists of two equations each for conservation of mass and energy, and a single equation for conservation of momentum.⁽²⁾ Appropriate constitutive relationships are used to obtain closure for the conservation equations.

Energy conduction equations are also used to calculate the time-dependent temperature distributions in the fuel rods,⁽³⁾ vessel component walls and internals,⁽⁴⁾ and walls of 1-D components.⁽⁵⁾

References for Regulatory Position 2.1.2 Compliance Discussion

- (1) Sections 2-2 and 2-3, Volume 1
- (2) Sections 2-4 and 2-5, Volume 1
- (3) Sections 7-2 through 7-5, Volume 1
- (4) Sections 7-2 and 7-6, Volume 1
- (5) Section 7-7, Volume 1

REGULATORY POSITION: 3. BEST-ESTIMATE CODE FEATURES

3.1 Initial and Boundary Conditions and Equipment Availability

Sensitivity studies were performed to identify the most limiting initial conditions expected over the life of the plant.⁽¹⁾ [

]^{a,c} in the overall calculational uncertainty assessment.⁽²⁾

The limiting break location was determined to be in a cold leg.⁽³⁾ A spectrum of break sizes in the cold leg are considered, and the limiting size is used in the scoping and sensitivity studies.

The PWR calculations consider the effect of the limiting single failure on ECCS performance,⁽⁴⁾ and scenarios both with offsite power only and with onsite power only are considered.⁽⁵⁾ The minimum SI flowrate and maximum SI delay times are used based on plant Technical Specification limits. The effect of variations in the initial conditions of the pumped SI water and the accumulators, within the ranges allowed by the plant Technical Specification limits, is also considered in the overall uncertainty assessment.⁽⁶⁾

References for Regulatory Position 3.1 Compliance Discussion

- (1) Section 30
- (2) Section 33
- (3) Section 28, Volume 3
- (4) Section 27, Volume 3, and Section 30
- (5) Section 27, Volume 3
- (6) Section 30

3.2 Sources of Heat During a Loss-of-Coolant Accident

3.2.1 Initial Stored Energy of the Fuel

The initial stored energy in the fuel is based on calculations performed with the Westinghouse PAD code, which is a detailed fuel rod design code whose models have been developed from, and benchmarked against, appropriate in-pile and out-of-pile data. This code has been reviewed and approved by the NRC.⁽¹⁾

3.2.1.1 Model Evaluation Procedure for Stored Energy and Heat Transfer in Fuel Rods

The Regulatory Guide specifies the following:

A model to be used in ECCS evaluations to calculate internal fuel rod heat transfer should:

- a. Be checked against several sets of relevant data, and*
- b. Recognize the effects of fuel burnup, fuel pellet cracking and relocation, cladding creep, and gas mixture conductivity.*

The initial stored energy in the fuel is based on calculations performed with the NRC-approved PAD code,⁽¹⁾ which has been checked against relevant in-pile and out-of-pile data, and which recognizes the effects of the specified parameters. The WCOBRA/TRAC fuel rod models include explicit modelling of [

]^{a,c}.

The HOTSPOT-SB code⁽³⁾ is used to account for uncertainties in the [

[
]^{a,c}.

3.2.1.2 Experimental Data for Stored Energy in Fuel Rods and Heat Transfer

The information provided previously addresses this recommendation. [
]^{a,c(1)}

References for Regulatory Position 3.2.1 Compliance Discussion

- (1) Weiner, R. A., et al., 1988, "Improved Fuel Performance Models for Westinghouse Fuel Rod Design and Safety Evaluations," WCAP-10851-P-A [PROPRIETARY].
- (2) Sections 7-3 and 7-4, Volume 1
- (3) Section 31-8

3.2.2 Fission Heat

Fission heat is calculated using a point kinetics model, which calculates shutdown reactivity on a best estimate basis. Details of the fission heat modelling are described in Section 8-3, Volume 1. The modelling is consistent with Regulatory Guide 1.157 (USNRC, 1989).

Credit is taken for control rod insertion in the Westinghouse best estimate small break LOCA methodology. It is conservatively assumed that the control rods insert with the specified delay time.

3.2.3 Decay of Actinides

The heat from radioactive decay of U-239 and Np-239 is calculated as described in Section 8-4, Volume 1. [
]^{a,c}

[

]^{a,c}

The treatment of the actinide decay heat source is considered to be in compliance with the regulatory guide, based on the previous discussion.

3.2.4 Fission Product Decay Heat

Fission product decay heat is calculated using the ANSI/ANS-5.1-1979 (American Nuclear Society, 1979) model, which is consistent with the Regulatory Guide recommendation.

3.2.4.1 Model Evaluation Procedure for Fission Product Decay Heat

The Q values and models for actinide decay heat are based on [

]^{a,c}

3.2.5 Metal-Water Reaction Rate

The metal-water reaction rate for zircaloy cladding is calculated using the Cathcart-Pawel model⁽¹⁾. A similar model is used for the advanced ZIRLO™ cladding material developed by Westinghouse. Uncertainties in the reaction rates calculated by these correlations are considered for the hot rod. If rod burst is calculated to occur, the reaction rates on the inner surface are calculated using the same models and uncertainties.

3.2.5.1 Model Evaluation Procedure for Metal-Water Reaction Rate

WCOBRA/TRAC-SB uses the Cathcart-Pawel model to calculate metal-water reaction for zircaloy cladding [

]^{a,c}

]^{a,c}.

Metal-water reaction rates for ZIRLO™ cladding [

]^{a,c}.

The WCOBRA/TRAC-SB calculation of the metal-water reaction rate includes consideration of preoxidation of the cladding as a result of normal operation, deformation during oxidation, and internal oxidation from steam following burst. The initial outer surface oxidation at the beginning of the transient is calculated by the Westinghouse PAD fuel rod design code and input to the WCOBRA/TRAC-SB and HOTSPOT-SB codes. The Regulatory Position 3.2.1.1 Compliance Discussion has an additional discussion of the use of swelling and burst models in WCOBRA/TRAC-SB and HOTSPOT-SB.

The WCOBRA/TRAC-SB models for metal-water reaction [

]^{a,c}.

References for Regulatory Position 3.2.5 Compliance Discussion

- (1) Cathcart, J. V., and Pawel, 1977, "Zirconium Metal-Water Oxidation Kinetics IV - Reaction Rate Studies," ORNL/NUREG-17, Oak Ridge National Laboratory, Oak Ridge, TN.

- (2) Cathcart, J. V., and Pawel, 1977, "Zirconium Metal-Water Oxidation Kinetics IV - Reaction Rate Studies," ORNL/NUREG-17, Oak Ridge National Laboratory, Oak Ridge, TN., page 67 and Figure 30.
- (3) Burman, D. L., 1990, "ZIRLO™ High Temperature Oxidation Tests," Appendix E to WCAP-12610, Westinghouse Electric Corporation, Pittsburgh, PA [PROPRIETARY].

3.2.6 Heat Transfer from Reactor Internals

Heat transfer from the piping, vessel walls, and vessel internal hardware is calculated in a best estimate manner. Heat transfer to guide tubes in the core is considered small and is not modelled in PWR calculations nor simulations of experiments.

In the simulations of experiments used to assess WCOBRA/TRAC-SB, heat transfer between structures and fluid was also included wherever important. Examples are as follows:

- LOFT: vessel wall, internals, and loop piping
- ROSA-IV: vessel wall, internals, and loop piping

3.2.7 Primary to Secondary Heat Transfer

Heat transfer between the primary and secondary sides is modelled [

]^{a,c}. The steam generator is assumed isolated at the initiation of the reactor trip during the transient, and auxiliary feedwater is modelled.

Simulated steam generators were used in the Semiscale, LOFT, and ROSA-IV integral test facilities. The WCOBRA/TRAC-SB analyses of experiments performed in these facilities explicitly modelled the simulated steam generators [

]^{a,c}

References for Regulatory Position 3.2.7 Compliance Discussion

- (1) Section 21, Volume 2
- (2) Section 20, Volume 2
- (3) Section 19, Volume 2

3.3 Reactor Core Thermal/Physical Parameters

3.3.1 Thermal Parameters for Swelling and Rupture of the Cladding and Fuel Rods

WCOBRA/TRAC includes models for swelling and rupture of the cladding. These models are dependent on the cladding temperature and the differential pressure across the cladding. The effects of fuel rod deformation are explicitly included in the models used to calculate [

]^{a,c}

The Regulatory Position 3.2.1.1 Compliance Discussion has an additional discussion of the use of swelling and burst models in WCOBRA/TRAC-SB and HOTSPOT-SB.

3.3.2 Other Core Thermal Parameters

The effect of the cladding change from alpha- to beta-phase is reflected in the cladding thermal and material properties. [

]^{a,c}

- (1) Donaldson, A. T., et al., 1982, "Biaxial Creep Deformation of Zircaloy-4 in the High Alpha Phase Temperature Range," TPRD/B.0100/N82, Central Electricity Generating Board - Berkeley Nuclear Laboratories, Berkeley, Gloucestershire, United Kingdom.
- (2) Donaldson, A. T., et al., 1985, "Biaxial Creep Deformation of Zircaloy-4 PWR Fuel Cladding in the Alpha, (Alpha + Beta) and Beta Phase Temperature Ranges," Journal of the British Nuclear Energy Society, pp. 83-89.

- (3) Donaldson, A. T., and Barnes, J. P., 1989, "Creep Behavior of ZIRLO Clad at Temperatures in the Alpha Phase Range, 873-973K, and in the Beta Phase Range, 1273-1373K," RD/B/6245/R89, Central Electricity Generating Board - Berkeley Nuclear Laboratories, Berkeley, Gloucestershire, United Kingdom [PROPRIETARY].
- (4) Donaldson, A. T., et al., 1989, "Creep Behavior of ZIRLO Clad at Temperatures in the Duplex Phase Range, 1048-1183K," RD/B/6304/R89, Central Electricity Generating Board - Berkeley Nuclear Laboratories, Berkeley, Gloucestershire, United Kingdom [PROPRIETARY].

3.4 Blowdown Phenomena

3.4.1 Break Characteristics and Flow

Break location studies have shown the limiting location to be in the cold leg.⁽¹⁾ The break spectrum studies for the cold leg consider a range of sizes, and uncertainties on the two-phase discharge flowrate are considered. This methodology is considered to be in compliance with Regulatory Position 3.1.

3.4.1.1 Model Evaluation Procedure for Discharge Flowrate

The WCOBRA/TRAC-SB calculation of critical flowrate considers the [

]^{a,c(2)}

Comparisons of this model to critical flow data obtained at a large number of test facilities – including the Marviken, Sozzi and Sutherland data, and the Amos and Shrock data – have been made to obtain uncertainties and modelling bias,⁽³⁾ and the range of applicability was established.

3.4.1.2 Experimental Data for Discharge Flowrate

The test data used to validate WCOBRA/TRAC-SB include a range of fluid conditions, pressures, and break nozzle geometries appropriate for small break LOCA.⁽³⁾ Comparisons with these data, and consideration of the resulting uncertainties and bias in the overall uncertainty methodology, result in conformance with the regulatory guide recommendations.

References for Regulatory Position 3.4.1 Compliance Discussion

- (1) Section 28, Volume 3
- (2) Section 4-8-2, Volume 1
- (3) Section 13, Volume 2

3.4.2 ECC Bypass

ECC penetration into the reactor vessel and core during a small break LOCA event is not an issue because when ECC injection occurs, the downcomer is partially full of water and no steam flows up the downcomer annulus to the break location. Therefore, Section 3.4.2 does not apply to small break LOCA events.

3.5 Noding Near the Break and ECCS Injection Point

In the PWR calculations, Westinghouse uses node sizes consistent, given the scales involved, with those used in the simulations of the experiments used to validate the break flow model and the condensation behavior at the ECCS injection point. This helps to ensure that the PWR calculations provide results with comparable accuracy as observed in the code validation.

3.6 Frictional Pressure Drop

The frictional pressure drops calculated in WCOBRA/TRAC are Re-dependent and account for two-phase flow effects.⁽¹⁾

3.6.1 Model Evaluation Procedure for Frictional Pressure Drop

The frictional pressure drop models were assessed by comparing the model to other correlations⁽²⁾ and by comparing the predicted pressure drop in complex geometries with measured data.⁽³⁾

[

]^{a,c}

[

]^{a,c}

3.6.2 Experimental Data for Frictional Pressure Drop

The information provided in Volume 2, Section 18, addresses this recommendation.

References for Regulatory Position 3.6 Compliance Discussion

- (1) Sections 4-2 and 4-7-2, Volume 1
- (2) Figures 4-10 through 4-13, Volume 1
- (3) Section 4-7-2, Volume 1
- (4) Section 20-3, Volume 2
- (5) Sections 2-2 and 2-3, Volume 1
- (6) Sections 2-4 and 2-5, Volume 1

3.7 Momentum Equation

The following effects are taken into account in the two-phase conservation of momentum equation:

- Temporal change in momentum. All momentum equations applied in the thermal-hydraulic network take into account the temporal change in momentum.^(1,2)
- Momentum convection. Both the vessel 3-D and 1-D component momentum equations include a complete description of momentum convection.^(1,2) [

]^{a,c}

- At the 1-D/3-D junction, [

]^{a,c}

- Area change momentum flux. Both the vessel and 1-D momentum equations are formulated to account for momentum changes resulting from area changes.^(1,2) The effect that the method of discretization has on these effects is recognized and taken into account.

- Momentum change due to compressibility. Both the 1-D and vessel momentum equations are formulated to account for the effects of phase compressibility on momentum flux.^(1,2)
- Pressure loss resulting from wall friction. The wall friction factor models used in the 1-D and vessel momentum equations use standard approaches which compare well with other models and correlations (Regulatory Position 3.6 Compliance Discussion).
- Pressure loss resulting from area changes. These losses are taken into account in conjunction with the area change momentum effect.
- Gravitational acceleration. Both vessel (3-D) and 1-D momentum equations take this effect into account.^(1,2)

The validity of the []^{a,c} is demonstrated in several ways:

- Comparisons between predictions and experiments at increasing scales, where 3-D effects would be expected to become more important
- Benchmarking of the PWR model during steady-state with experimentally determined vessel and loop pressure drops⁽⁴⁾
- Comparison with two-phase pressure drop experiments

References for Regulatory Position 3.7 Compliance Discussion

- (1) Sections 2-2 and 2-3, Volume 1
- (2) Sections 2-4 and 2-5, Volume 1
- (3) Section 4-7-4, Volume 1
- (4) Section 26-2, Volume 3

3.8 Critical Heat Flux

Regulatory Guide 1.157 states:

Best estimate models developed from appropriate steady-state or transient experimental data should be used in calculating critical heat flux (CHF) during loss-of-coolant accidents. The codes in which these models are used should contain suitable checks to ensure that the range of conditions over which these correlations are used are within those intended.

The CHF is calculated in the core using the Zuber pool boiling DNB correlation,⁽¹⁾ and the Biasi correlation for forced convection DNB.⁽²⁾ These correlations, and how they are programmed into WCOBRA/TRAC, are described in Section 6-2-4.⁽³⁾ The Biasi correlation consists of two separate expressions and depends on pressure, mass flux, quality, and hydraulic diameter. The Zuber correlation is applied only when the flowrate decreases to near zero and conditions approach those of pool boiling. The mass flux is checked to ensure that the [

]^{a,c}.

References for Regulatory Position 3.8 Compliance Discussion

- (1) Zuber, N., et al., 1961, "The Hydrodynamic Crisis in Pool Boiling of Saturated and Subcooled Liquids," International Developments in Heat Transfer, Int. Heat Transfer Conf., Boulder, Colorado, Part II, No. 27, pp. 23-236.

- (2) Biasi, L., et al., 1967, "Studies on Burnout, Part 3," Energia Nucleare, Vol. 14, No. 9, pp. 530-536.
- (3) Section 6-2-4, Volume 1
- (4) NUREG/CR-5069
- (5) Section 11-2, WCAP-12945
- (6) Section 14-1, WCAP-12945

3.9 Post-CHF Blowdown Heat Transfer

Concerning post-CHF blowdown heat transfer, Regulatory Guide 1.157 states:

Models of heat transfer from the fuel to the surrounding fluid in the post-CHF regimes of transition and film boiling should be best estimate models based on comparison to applicable steady-state or transient data. Any model should be evaluated to demonstrate that it provides acceptable results over applicable ranges. Best-estimate models will be considered acceptable provided their technical basis is demonstrated with appropriate data and analysis.

The models for transition and film boiling are described in Sections 6-2-5 and 6-2-8, Volume 1, respectively. The models for each regime are formulated to be mechanistic and are generally applicable to all phases of a LOCA transient. The models for each regime account for the effects of local void fraction and droplets, thermal radiation, thermal nonequilibrium, flowrate, wall heat flux, and liquid temperature. The models used for the phasic components of heat transfer for each of the regimes are similar to models used in other two-fluid codes such as RELAP and TRAC-PF1 and are referenced to correlations previously proposed for these regimes.

The models for heat transfer in the post-CHF period of a small break LOCA have been checked against several sets of experimental data that are prototypical of Westinghouse and other PWR fuel assemblies. The WCORBA/TRAC-SB heat transfer models were used to simulate several tests and predict cladding temperature histories in the ORNL⁽¹⁾ core uncover tests and INEL⁽²⁾ single-tube experiments.

The models and correlations used for post-CHF heat transfer to an uncovered core have done the following:

- Checked against acceptable sets of relevant data
- Recognized the effects of liquid entrainment and thermal radiation

Thus, they satisfy the Regulatory Guide concerning those criteria.

Regulatory Guide 1.157 also requires the following:

The uncertainties and bias of models or correlations used to calculate post-CHF heat transfer should be stated as well as the range of their applicability.

The uncertainties and biases of the models and correlations used to calculate post-CHF heat transfer during a small break LOCA are [

]^{a,c}

[

]^{a,c}.

References for Regulatory Position 3.9 Compliance Discussion

- (1) Section 15, Volume 2
- (2) Section 15, Volume 2
- (3) Section 32-5
- (4) Section 32-2

3.9.3 Post-CHF Heat Transfer from Uncovered Bundles

As indicated in the Regulatory Guide 1.157 text (USNRC, 1989), this regime is particularly important for small break LOCA. The heat transfer package programmed into WCOBRA/TRAC-SB is described in Section 6, Volume 1. The models and correlations used in WCOBRA/ TRAC-SB, and the techniques used to determine the phasic heat transfer contributions are similar, and in some cases identical, to those used in the NRC's best estimate codes such as COBRA, TRAC, and RELAP.

3.9.3.1 *Model Evaluation Procedures for Heat Transfer from Uncovered Rod Bundles*

Concerning the models and correlations used to calculate heat transfer from uncovered bundles, Regulatory Guide 1.157 states:

A correlation to be used in ECCS evaluations to calculate heat transfer from uncovered rod bundles should:

- a. *Be checked against an acceptable set of relevant data, and*
- b. *Recognize the effects of radiation, and of laminar, transition, and turbulent flows.*

Uncertainties and bias in the models and correlations used to calculate post-CHF heat transfer should be stated, as should the range of their applicability.

The effect of [

]^{a,c}

]^{a,c}

Regulatory Guide 1.157 provides some discussion on the acceptable form of correlations for turbulent convection:

The turbulent correlation may be of the general form:

$$Nu = A Re^m Pr^n$$

for higher Reynolds numbers (Re), where the coefficients A , m , and n are modifications from the basic Dittus-Boelter form and may be functions of other variables.

The WCOBRA/TRAC-SB relations for turbulent convection are of this form (Section 6, Volume 1). In addition, the distinction is made in the code between laminar and turbulent convection at low $Re^{(7)}$. This complies with the Regulatory Guide 1.157 direction that:

A distinction from, and transition to, laminar convection (i.e., $Re < 2000$) should be made, with a value of the laminar heat transfer for rod bundles that is appropriate for the applicable bundle geometry and flow conditions.

References for Regulatory Position 3.9.3 Compliance Discussion

- (1) Section 6-2-9, Volume 1
- (2) Sections 6-2-1 and 6-2-2, Volume 1
- (3) Section 6-2-4, Volume 1
- (4) Section 6-2-7, Volume 1
- (5) Section 6-2-3, Volume 1
- (6) Section 32-2, Volume 3
- (7) Section 6-2-9, Volume 1

3.10 Pump Modelling

The pump model in WCOBRA/TRAC-SB takes into account changes in pump rotor rotational speed as a result of changes in torque applied to the rotor from the fluid, pump rotor inertia, and resistance to rotation, if the power to the pump is lost.⁽¹⁾ If power to the pump is available, the pump is assumed to continue rotating at constant speed regardless of applied torque, as is a characteristic of the motor type. The interaction between the pump and the fluid is in two forms as follows:

- Torque applied by the fluid on the pump rotor
- Energy gained or lost by the fluid (in terms of pressure rise or loss) from the pump

The torque and pressure rise are provided as empirical curves relating these quantities to pump rotational speed, fluid volumetric flow, and fluid vapor fraction. The curves are based on single- and two-phase data obtained from tests using a scaled pump with similar specific speed.

Cases in which power to the pumps continues to be supplied, until manually tripped by the reactor operator, and where power to the pumps is lost are both analyzed as part of the

methodology, and the limiting case is used for subsequent uncertainty evaluations. In either case, the RCPs are tripped well before the PCT transient begins in a small break LOCA event.

[

]^{a,c}

References for Regulatory Position 3.10 Compliance Discussion

- (1) Section 9-4, Volume 1

3.11 Core Flow Distribution During Blowdown

The flow through the hot assembly is calculated directly from the WCOBRA/TRAC-SB conservation equations, and the effect of crossflow and cladding deformation is included.

[

]^{a,c}

3.12 Post-Blowdown Phenomena

3.12.1 Containment Pressure

Containment pressure is assumed to remain at 14.7 psia in the WCOBRA/TRAC-SB reference transient and in all other cases analyzed. This is conservative as the spilling SI delivery line for the break location at the top of the cold leg spills to the minimum backpressure.

3.12.2 Calculation of Post-Blowdown Thermal Hydraulics for Pressurized Water Reactors

The small break LOCA core uncover transient, which is similar to the reflood phase of the large break LOCA transient, is calculated on a best estimate basis, taking into consideration the thermal and hydraulic characteristics of the core, the ECC system performance, and important reactor systems. The distribution of water and steam in the reactor vessel is calculated directly from the WCOBRA/TRAC-SB conservation equations and appropriate constitutive relations. Assessment of the ability of WCOBRA/TRAC-SB to predict processes important in small break LOCA has been performed by comparison with test data from separate effects and integral systems tests.

3.12.2.1 Model Evaluation Procedures for Post-Blowdown Thermal-Hydraulics

The following lists the model evaluation procedures for post-blowdown thermal-hydraulics:

- Level Swell

During the PWR small break LOCA transient, the process of level swell is important. The level swell test simulations performed by Westinghouse were used to evaluate the ability of WCORBA/TRAC-SB to predict the axial distribution of voids during the reflood process.⁽¹⁾ These tests cover the range of conditions of interest during the reflood phase of a PWR. [

]^{a,c}

- Primary Coolant Pumps

As described in Section 2.7, Volume 3, cases in which the pump is both powered and not powered are considered in the methodology and the limiting case is taken into account.

- Carryover

The total fluid flow leaving the core exit is calculated directly from the WCORBA/TRAC-SB conservation equations and appropriate constitutive relations. WCORBA/TRAC-SB predictions of carryover influence the predictive capability of the code for single-effect and integral tests. The PWR modelling includes sufficient nodalization to capture the effects of cross-flow on carryover and the core fluid distribution during a small break LOCA.

- Upper Plenum Injection Plants

PWRs designed with upper plenum injection (UPI) deliver only the LHSI to the upper plenum. Therefore, the best estimate small break LOCA methodology used for UPI plants would be the same as presented herein.

- Upper Head Injection Plants

All domestic Westinghouse PWRs originally designed with upper head injection (UHI) have had these injection lines capped. These plants now rely on cold leg injection and are modelled as such. There are no special small break LOCA thermal-hydraulic phenomena associated with plants that have had their UHI lines capped.

- Accumulator Nitrogen

[

]^{a,c}

References for Regulatory Position 3.12.2 Compliance Discussion

- (1) Section 15, Volume 2

3.12.3 Steam Interaction with Emergency Core Cooling Water in Pressurized Water Reactors

Mixing of steam and subcooled water in the intact cold legs of a PWR is taken into account. Studies comparing predictions to the available data indicate that the overall degree of condensation is predicted reasonably well.⁽¹⁾

Interactions between steam and subcooled water in the loop piping were assessed by comparing WCORBA/TRAC-SB predictions with the condensation efficiency for horizontal stratified flow tests.⁽²⁾ The WCORBA/TRAC-SB interfacial heat transfer is ranged to account for uncertainties in these phenomena in the overall PWR uncertainty assessment.

References for Regulatory Position 3.12.3 Compliance Discussion

- (1) Section 14, Volume 2
- (2) Section 18, Volume 2

3.12.4 Post Blowdown Heat Transfer for Pressurized Water Reactors

This section of Regulatory Guide 1.157 (USNRC, 1989) provides guidance on validation for HTCs. In particular, it is stated that:

... the heat transfer calculations should be based on a best-estimate calculation of the fluid flow through the core, accounting for unique emergency core cooling systems.

In satisfying this requirement, integral test simulations are performed with WCOBRA/TRAC-SB to demonstrate the ability of the code to calculate phenomena under small break LOCA.^(1,2,3)

Regulatory Guide 1.157 also states:

The calculations should also include the effects of any flow blockage calculated to occur as a result of cladding swelling or rupture.

The models for swelling, rupture, and blockage are described in Section 7, Volume 1. The Regulatory Position 3.2.1.1 Compliance Discussion has an additional discussion of the use of swelling and burst models in WCOBRA/TRAC-SB and HOTSPOT-SB. The effects of hot assembly flow blockage calculated in WCOBRA/TRAC-SB are reflected in the local fluid conditions used in the HOTSPOT-SB calculations.

Also, Regulatory Guide 1.157 states:

Heat transfer calculations that account for two-phase conditions in the core during refilling of the reactor vessel should be justified through comparisons with experimental data. Best estimate models will be considered acceptable provided their technical basis is demonstrated through comparison with appropriate data and analysis.

The Westinghouse methodology [

]^{a,c}

Finally, the Regulatory Guide indicates several experimental tests that are useful for validation purposes:

The FLECHT-SEASET tests (Refs. 40, 45, and 46) should be considered when establishing an acceptable set of relevant data.

and:

The results from the 2D/3D program are particularly relevant.

The simulations used for bias and uncertainty determination are directly relevant to small break LOCA rather than to the large break LOCA experiments cited.

References for Regulatory Position 3.12.4 Compliance Discussion

- (1) Section 19, Volume 2
- (2) Section 20, Volume 2
- (3) Section 21, Volume 2

3.15 Special Considerations for Small-Break LOCA in PWRs

Regulatory Guide 1.157 (USNRC, 1989) notes that the phenomena associated with a small break LOCA event are significantly different from the phenomena during the large break LOCA. Changes in the distribution of liquid in the RCS at loop seal clearance have been identified as an important factor that impacts the core uncover during a small LOCA.^(1,2) [

]^{a,c}

Break flow may be greatly influenced by the location and specific geometry of the break.

The spectrum of breaks that identifies the reference case considers not only possible locations throughout the RCS, but also the effect of the break orientation around the pipe perimeter for the limiting cold leg location. The top orientation is identified as limiting because the specific geometry of a break at the top of the pipe includes the case in which the SI delivery pipe is severed, causing the pumped injection directed to the broken loop to spill to containment pressure.

The pump operation assumptions used in the calculations should be the most likely, based on operating procedures.....

The limiting assumption about the continued OPA is identified in the methodology and becomes the basis for the reference case small break LOCA. For Indian Point Unit 2 analyzed herein, the LOOP assumption is limiting; for a case with LOOP, the time at which pump operation ceases is determined by the plant electrical system design. The continued OPA may prove to be the limiting assumption for other PWRs. If this were true, the time at which the reactor operator acts to manually trip the RCPs would be variable within the context of the plant EOPs. A range of RCP trip times consistent with the operator action times identified for small break LOCAs by simulator training exercises will be analyzed for OPA-limited plants, and the uncertainty associated with continued RCP operation will be considered in the determination of the 95th percentile PCT.

The other phenomena identified in this section of Regulatory Guide 1.157 correspond to highly-ranked items in the PIRT in Section 1 of this document. The scoping studies have investigated the impact of variations in the prediction of these (and other) phenomena on calculated small break LOCA performance. The important phenomena, as identified for Indian Point Unit 2, have been considered in the propagation of uncertainty to calculate the 95th percentile PCT. The highly ranked PIRT phenomena will be carefully considered individually once again in any subsequent application of the best estimate small break LOCA methodology.

3.16 Other Features of Best-Estimate Codes

3.16.1 Completeness

The WCOBRA/TRAC-SB code used by Westinghouse for best estimate small break LOCA analyses is an extended version of the WCOBRA/TRAC code originally developed by Westinghouse in order to perform best estimate large break LOCA analysis. The models in the code are intended to provide realistic calculations of phenomena of importance to the behavior of a PWR during a small break LOCA transient. These models have been assessed using comparisons of code predictions with approximately 100 experiments in a number of separate effects test facilities and three integral test facilities (LOFT, ROSA-IV, and Semiscale).⁽¹⁾ The code validation matrix was selected to cover the range of conditions expected during a PWR small break LOCA transient to the extent practical. Uncertainty in the experimental data was considered in the overall uncertainty assessment.⁽²⁾

3.16.2 Data Comparisons

The WCOBRA/TRAC validation matrix is summarized in Tables 1-1 and 1-2 of Volume 1, Section 1. Comparisons of code predictions with important thermal-hydraulic parameters measured in these tests support the conclusion that realistic behavior is predicted and major biases do not exist in the models. The code uncertainty assessment includes the effects of uncertainties in the test data.

The methodology considers the need to range and/or bias each of the key parameters identified in the PIRT.⁽³⁾

References for Regulatory Position 3.16 Compliance Discussion

- (1) Table 1-1, Volume 1
- (2) Section 32-2
- (3) Section 1-4, Volume 1

4. ESTIMATION OF OVERALL CALCULATIONAL UNCERTAINTY

4.1 General

The Westinghouse approach to the overall calculational uncertainty has been to separate the uncertainties into two general classifications: the code and models uncertainty, and the plant conditions uncertainty. These two uncertainties are then combined to obtain the overall calculational uncertainty for the analysis.

The code and models uncertainty accounts for the uncertainty in predicting the important thermal-hydraulic phenomena identified in the PIRT and important modelling assumptions. This uncertainty was developed by performing a systematic assessment of the uncertainty associated with the prediction of break mass flowrate, stored energy and fuel rod behavior, core heat transfer, and core interfacial drag.⁽¹⁾ Estimates of the code biases and uncertainties for these parameters were based on comparisons with applicable separate effects and integral effects test data. Propagation of these uncertainties throughout the PWR transient was [

]^{a,c}.

The assessment of the thermal-hydraulic models in WCOBRA/TRAC-SB used a large number of test comparisons to ensure that estimates of the model uncertainties were well-founded and included potential scaling effects.

The plant uncertainty calculations account for the different possible operating conditions and accident initial conditions that the plant could experience. Parameters such as the worst break location, worst pressurizer location relative to the break, and worst onsite power availability condition are bounded because it is not possible to treat these conditions in a statistical fashion. Those code and model parameters that exhibit a minor impact on PCT are considered in the plant uncertainty calculation together with the plant initial and boundary conditions.⁽²⁾

Each component of the overall uncertainty is assessed on a plant-specific basis.

References for Regulatory Position 4.1 Compliance Discussion

- (1) Section 32
- (2) Section 33

4.2 Code Uncertainty

The best test of the overall accuracy of the computer code and the accuracy of individual models is to compare code predictions to data obtained from a wide range of experiments. Wherever possible, tests performed at full-scale or large-scale should be used to eliminate or minimize uncertainties associated with scalability. WCOBRA/TRAC-SB was used to simulate several different experiments that capture the small break LOCA phenomena at different scales. The WCOBRA/TRAC-SB validation matrix includes tests with different bundle sizes, rod arrays, lengths, power shapes, and grid types because the computer code has to model these effects for different plant designs and conditions.

One measure of the accuracy of the code uses the comparisons of the predicted and measured PCTs.⁽¹⁾ By selecting experiments with care and by comparing to data other than the measured cladding temperatures, it can be ensured that the PCT is reasonably predicted for the correct reasons. That is, the possibility of compensating errors being present can be investigated. An assessment of the possibility of compensating errors in WCOBRA/TRAC-SB has been performed. It is concluded that while compensating errors may exist, the net effect is a conservative prediction of a PWR LOCA transient.

The uncertainty associated with the experiments must also be considered when estimating the accuracy of the code using comparisons between predicted and measured temperatures. The effects of the data scatter are specifically treated in the uncertainty analysis.⁽¹⁾ An assessment of the test initial conditions was made by examining repeat tests.⁽²⁾ Noding used for code validation against experimental data and noding used for PWR calculations were kept consistent to the extent practical to minimize the uncertainty introduced by noding. Nodalization studies of the ROSA-IV integral effects test facility were performed, and the variation in calculated results was included in the overall code uncertainty assessment.⁽³⁾

While the available integral effects tests are useful for addressing the issues of scalability and compensating errors, there are insufficient data to address the potential for propagation of uncertainties as a LOCA transient progresses. A detailed study of uncertainty propagation requires that the effects be quantified using computer code calculations of a PWR LOCA transient. Westinghouse has developed a method similar to that used in the CSAU methodology,⁽⁴⁾ [

]^{a,c}.

References for Regulatory Position 4.2 Compliance Discussion

- (1) Section 32-2-1-4
- (2) Section 32-2-1-5
- (3) Section 32-2-1-2
- (4) Technical Program Group (TPG), 1989, "Quantifying Reactor Safety Margins: Application of Code Scaling, Applicability, and Uncertainty Methodology to a Large Break Loss of Coolant Accident," NUREG/CR-5249.

4.3 Other Sources of Uncertainty

4.3.1 Initial and Boundary Conditions and Equipment Availability

The treatment of important initial and boundary conditions and assumptions of the availability of important equipment are summarized in Table 33-4-1, Section 33.

4.3.2 Fuel Behavior

Uncertainties in the lead fuel rod initial conditions and behavior during the LOCA transient are explicitly accounted for. These uncertainties include hot rod peaking, gap conductance, fuel conductivity, cladding burst temperature, burst strain, fuel density after burst due to relocation, and metal-water reaction rates.⁽¹⁾ The treatment of fuel behavior in the Westinghouse methodology is considered to be more complete than that used in the CSAU methodology⁽²⁾ since [

]^{a,c}.

References for Regulatory Position 4.3.2 Compliance Discussion

- (1) Section 32-1
- (2) Technical Program Group (TPG), 1989, "Quantifying Reactor Safety Margins: Application of Code Scaling, Applicability, and Uncertainty Methodology to a Large Break Loss of Coolant Accident," NUREG/CR-5249.

4.3.3 Other Variables

Uncertainties in decay heat and break flowrate are included in the overall uncertainty assessment. The magnitude of the decay heat uncertainty was established using the pertinent small break LOCA value of ANSI/ANS-5.1-1979. This uncertainty [

]^{a,c}. The magnitude of the break flowrate uncertainty was established by comparing WCOBRA/TRAC-SB break flowrate predictions with test data from many experimental facilities, including the Marviken facility.⁽¹⁾ The metal-water reaction rate uncertainty is also considered as one of the fuel rod uncertainty parameters as noted in the Regulatory Position 4.3.2 Compliance Discussion.

References for Regulatory Position 4.3.3 Compliance Discussion

- (1) Section 32-4

4.4 Statistical Treatment of Overall Calculational Uncertainty

The overall calculational uncertainty is determined by combining the uncertainties in the code models and usage with uncertainties in plant initial conditions. [

]^{a,c(1)}

The best estimate small break LOCA methodology used by Westinghouse addresses the PCT, maximum cladding oxidation, maximum hydrogen generation, and coolable geometry criteria defined in 10CFR50.46(b)(1) through (b)(4). The PCT at the 95th percentile level is estimated as previously. The maximum cladding oxidation criterion and the maximum hydrogen generation criterion are verified as described in Section 33-6. Coolable geometry is demonstrated by ensuring that the PCT and maximum local oxidation criteria are satisfied.

The Westinghouse methodology used to satisfy the long-term cooling criterion defined in 10CFR50.46(b)(5) is unaffected by the use of best estimate techniques for the short-term transient calculation.

References for Regulatory Position 4.4 Compliance Discussion

- (1) Section 33

4.5 NRC Approach to LOCA Uncertainty Evaluation

The Westinghouse large break LOCA methodology is the first complete application of the CSAU methodology cited in Section 4.5 of Regulatory Guide 1.157 (USNRC, 1989). Its acceptance has been confirmed by the NRC⁽¹⁾ and the ACRS.⁽²⁾ The Westinghouse small break

LOCA methodology uses many of the same techniques, including an enhanced version of the WCOBRA/TRAC computer code.

References for Regulatory Position 4.5 Compliance Discussion

- (1) Letter, R. C. Jones (USNRC) to N. J. Liparulo (Westinghouse), "Acceptance for Referencing of the Topical Report WCAP-12945(P), Westinghouse Code Qualification Document for Best Estimate Loss of Coolant Analysis," June 28, 1996.
- (2) Letter, T. S. Kress (ACRS Chairman) to S. A. Jackson (USNRC Chairman), "Westinghouse Best-Estimate Loss-of-Coolant Accident Analysis Methodology," April 19, 1996.

35-4 Plant and Evaluation Model Changes and Their Impact on Analysis

Changes in the configuration of the plant may occur following the safety analysis. In particular, minor changes in fuel configuration, and calculated steady-state and transient peaking factors occur with each reload. Changes in the evaluation model may also be necessary. The following sections describe the steps taken and the criteria used in making decisions with the licensee concerning the evaluation of plant and model changes, the reporting of these changes, and the extent of reanalysis.

35-4-1 Plant Changes

Minor changes in plant configuration often occur during normal operation. These changes are typically evaluated by the licensee under the criteria of 10CFR50.59. In many cases, Westinghouse is asked to perform a technical evaluation so that the licensee can determine whether the change results in an unreviewed safety question. The technical evaluation involves several steps, including the evaluation of the effect of the change on the safety analysis key results (in the case of LOCA, the PCT). Usually, this is done by examining prior sensitivity studies from previous analyses for similar plants. Sometimes, a calculation is performed using the evaluation model for the specific plant being evaluated. If the estimated effect of the change, when added to the current licensing basis PCT, still meets the limit of 10CFR50.46(b), then the change will be deemed not to constitute an unreviewed safety question (other criteria must also

be met unrelated to the results of the evaluation model). If this conclusion is made, then the change can be implemented without prior review and approval by the NRC.

In the best estimate methodology, the changes that may affect the PCT are those identified as key LOCA parameters. The operating range of the plant identified in Section 34 constitutes the region within which the estimated 95-percent probability PCT applies. Therefore, operation within this region will not cause the PCT to exceed the 10CFR50.46 limits. In some cases, the operating range exceeds the limits placed on plant operation by the Technical Specifications. If a change is contemplated in a Technical Specification still within the limits identified by the operating range, then a safety evaluation will conclude that no change to the PCT will occur (because a Technical Specification change is involved, other regulatory requirements must be met, however). If the change causes the operating range to exceed the range specified for the parameter, then a safety evaluation will include a change in PCT resulting from the wider range, using the procedures outlined in Section 34. For example, if a wider range in accumulator pressure is desired for Indian Point Unit 2, a sensitivity study will be performed, a new range will be incorporated into Table 34-2-2, and a new initial condition uncertainty will be calculated using the procedure in Section 33. In some cases, sufficient information may exist from similar plants to allow an estimate of the change to be made without a plant-specific analysis. Fuel changes that normally occur during reloads, and which do not include changes in Technical Specifications, may also be evaluated and implemented in this manner.

Plant changes in which a reanalysis involving a recalculation of the reference transient and several points in the response surface may be necessary are those involving significant changes in core power, ECCS flow, or in the power distribution factors, which cause these parameters to fall outside the range of the operating range identified in Section 34.

If a change occurs in a parameter that is bounded, then the effect of the change will be included as a bias to the reference transient calculation.

It may happen that a plant change significantly affecting the LOCA results, but that did not appear on the key LOCA parameters list, is found. In this case, the change will be evaluated in the same way as other changes, but the parameter will also be included on the LOCA parameters list. This is considered to result in a change in the evaluation model, and reports will be filed through the licensee, as required by 10CFR50.46(a)(3)(I).

35-4-2 Evaluation Model Changes

The following is considered to make up the evaluation model described in this report. Any change in the following is considered to result in a change to the evaluation model, under 10CFR50.46:

- The models and correlations in WCOBRA/TRAC-SB (Any change to these models is considered a change to the evaluation model.)
- The procedures described in Section 26, Volume 3, for constructing an input model of a PWR
- The procedures described in Section 33 for evaluating the individual and overall calculational uncertainty
- The uncertainties and assumed distributions for the parameters included in the overall calculational uncertainty, and described in Section 32

The following are not considered part of the evaluation model, and could be changed and implemented through the 10CFR50.59 process described previously:

[

]^{a,c}

]^{a,c}

If a change to the evaluation model is made, an estimate of the effect of the change will be made by [

]^{a,c}. As a confirmation of the continued

validity of the code and model uncertainty, an appropriate subset of the code assessment matrix will also be reanalyzed. Any potential effect on the results of Section 32 will be factored into the overall assessment of the effect of the evaluation model change.

35-5 References

American Nuclear Society, 1979, "American National Standard for Decay Heat Power in Light Water Reactors," ANSI/ANS-5.1-1979.

USNRC, 1989, "Regulatory Guide 1.157: Best-Estimate Calculations of Emergency Core Cooling System Performance."